PETROPHYSICS

By: Mohammad Hossein Saberi
Mh.saberi@aut.ac.ir

- Petrophysics
    1. Reservoir Characterization
    2. Well Logging
    3. Well Correlation
    4. Software- Geolog

- Mid Term Exam

- 1 Presentation

Reference Books

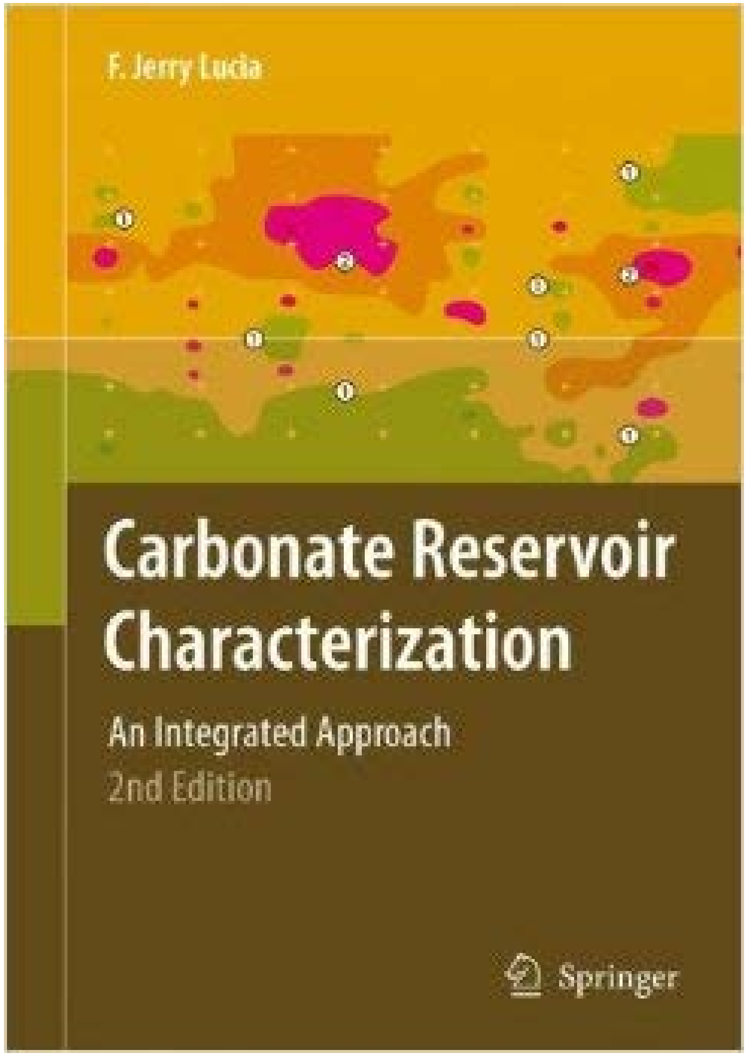

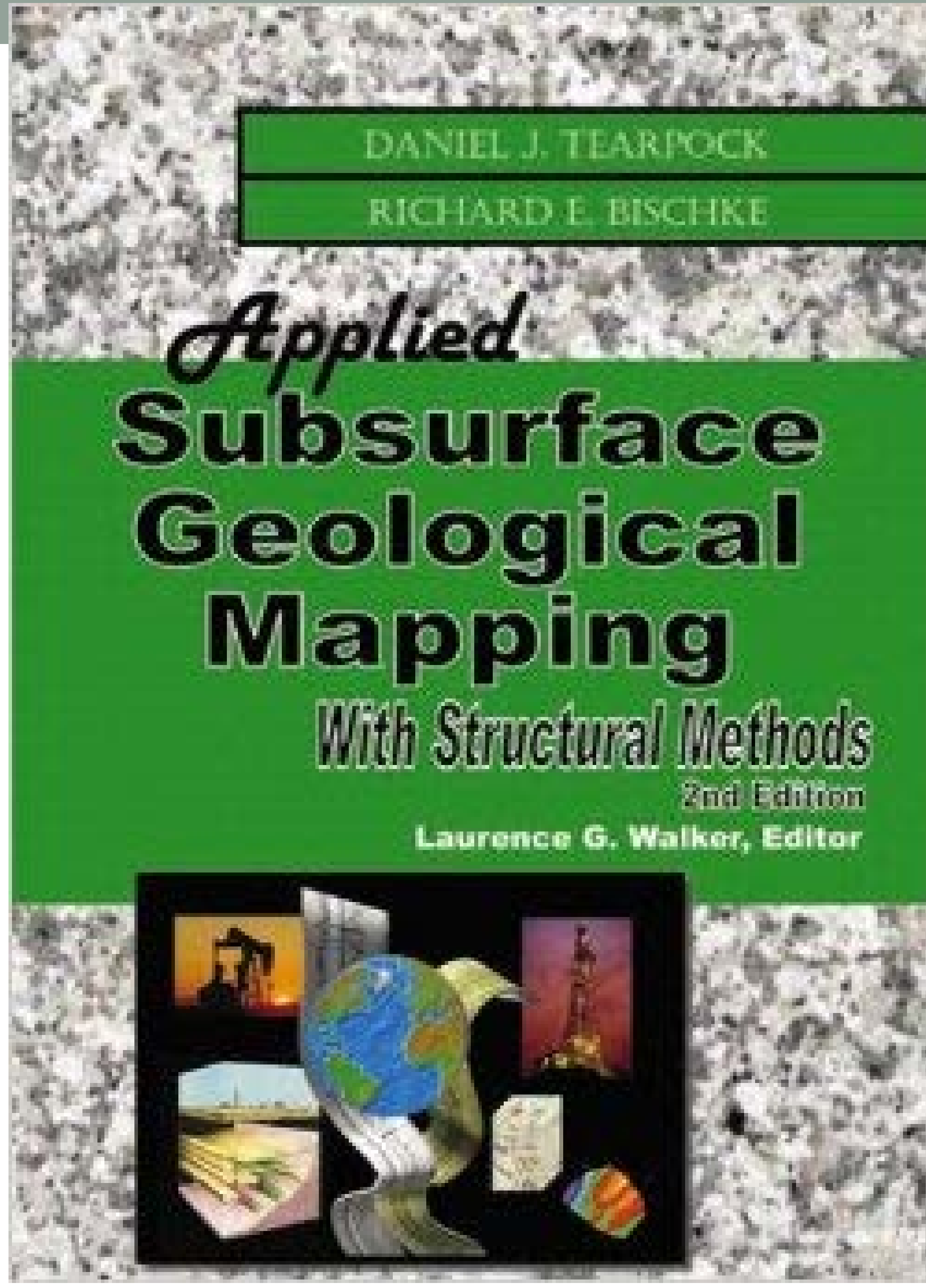
DANIEL J. TEARPOCK
RICHARD E. BISCHKE
Applied
Subsurface
Geological
Mapping
With Structural Methods
2nd Edition
Laurence G. Walker, Editor

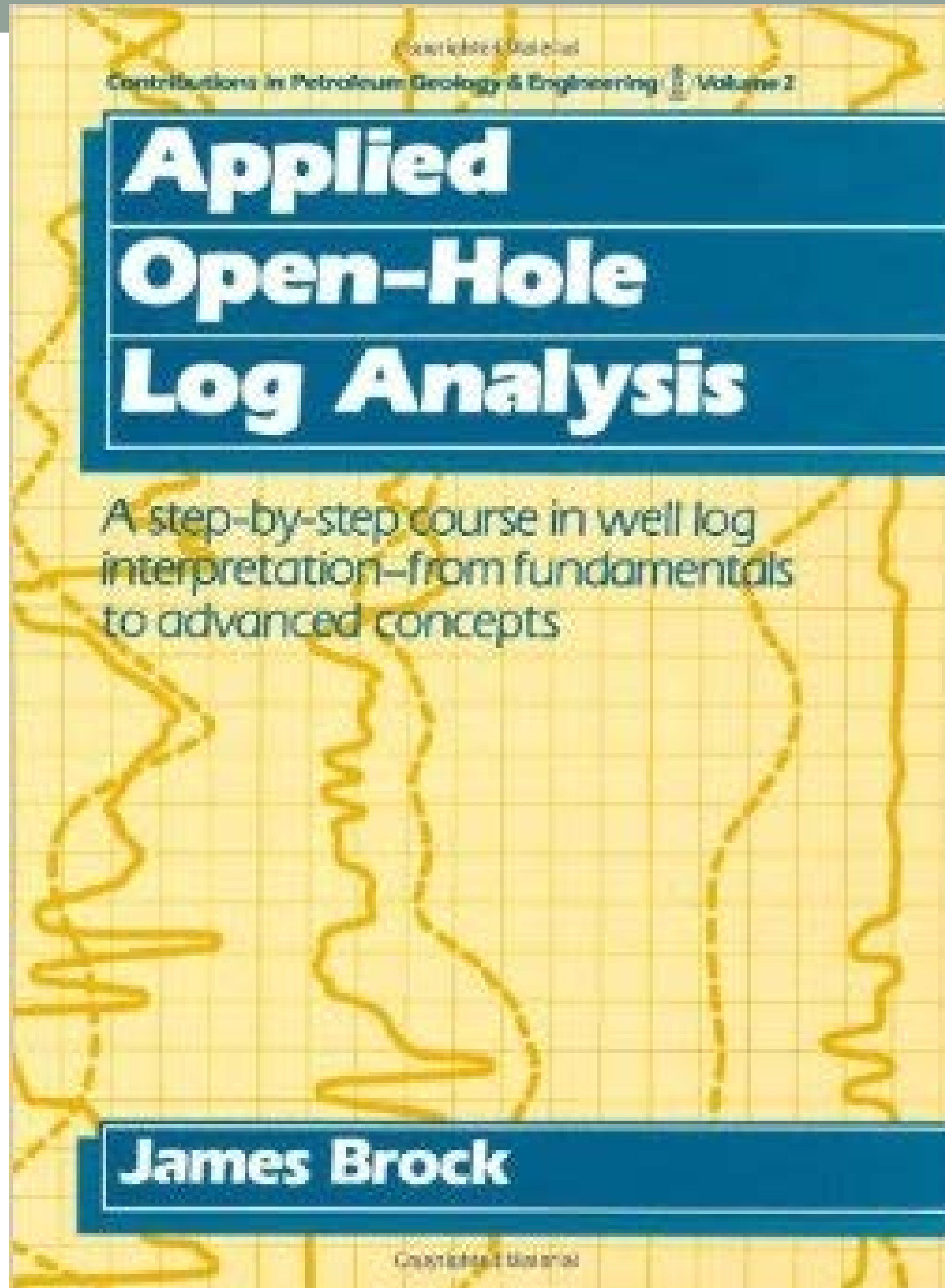
Copyrighted Material
Contributions in Petroleum Geology & Engineering Volume 2
Applied Open-Hole Log Analysis
A step-by-step course in well log interpretation–from fundamentals to advanced concepts
James Brock
Copyrighted Material

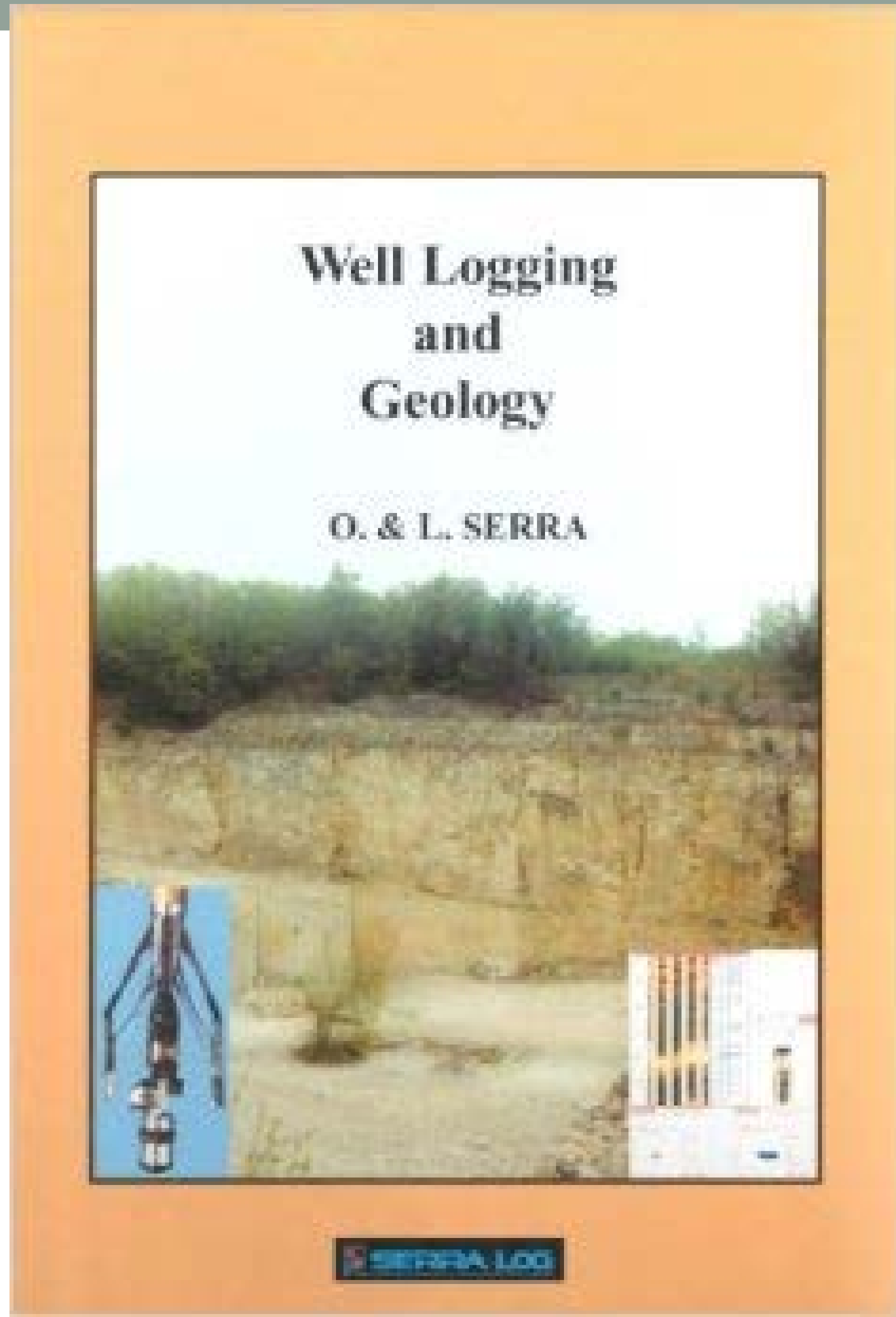
Well Logging
and
Geology
O. & L. SERRA
SERRA LOG

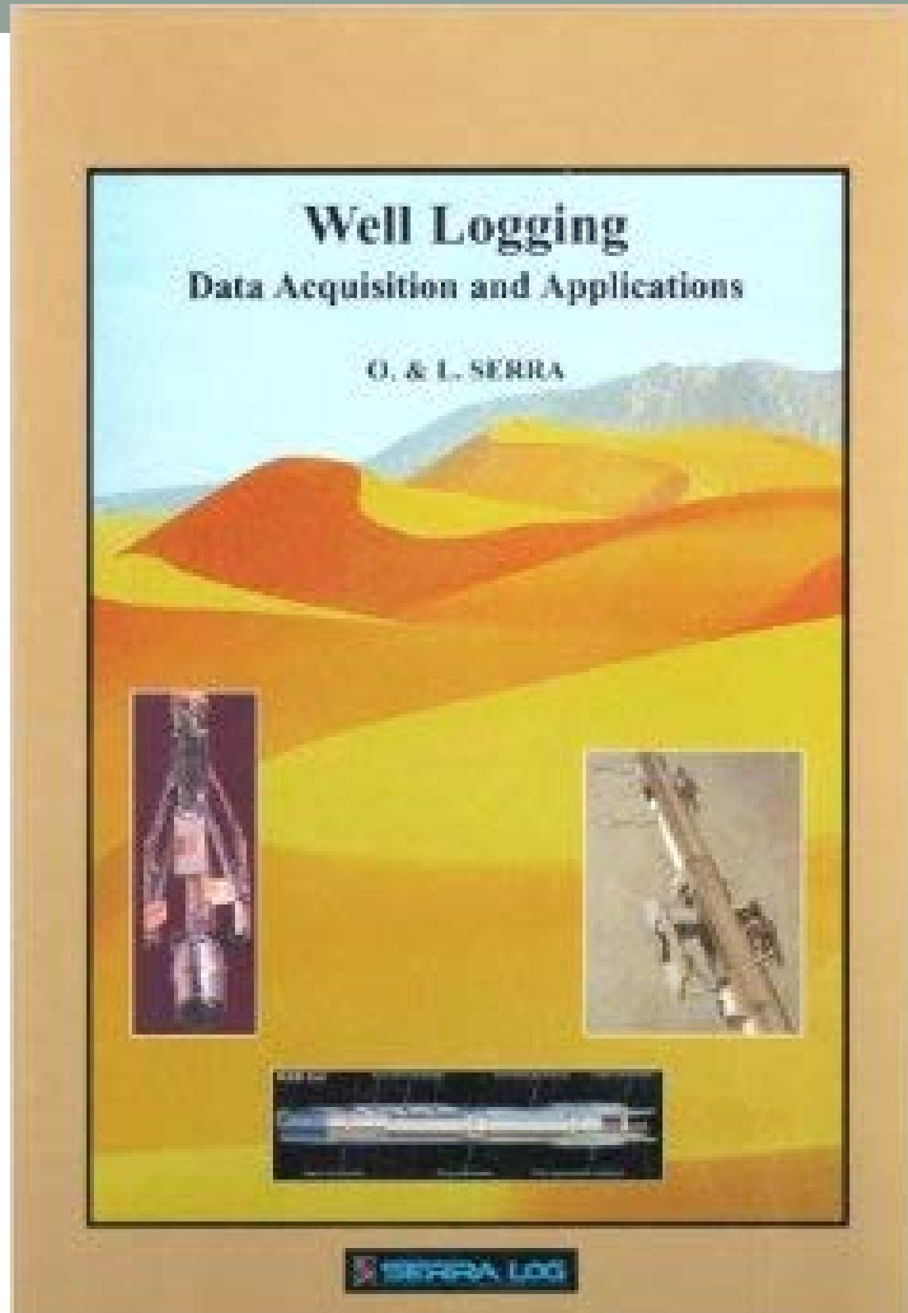
Well Logging
Data Acquisition and Applications
O. & L. SERRA
SERRA LOG

Reservoir Characterization

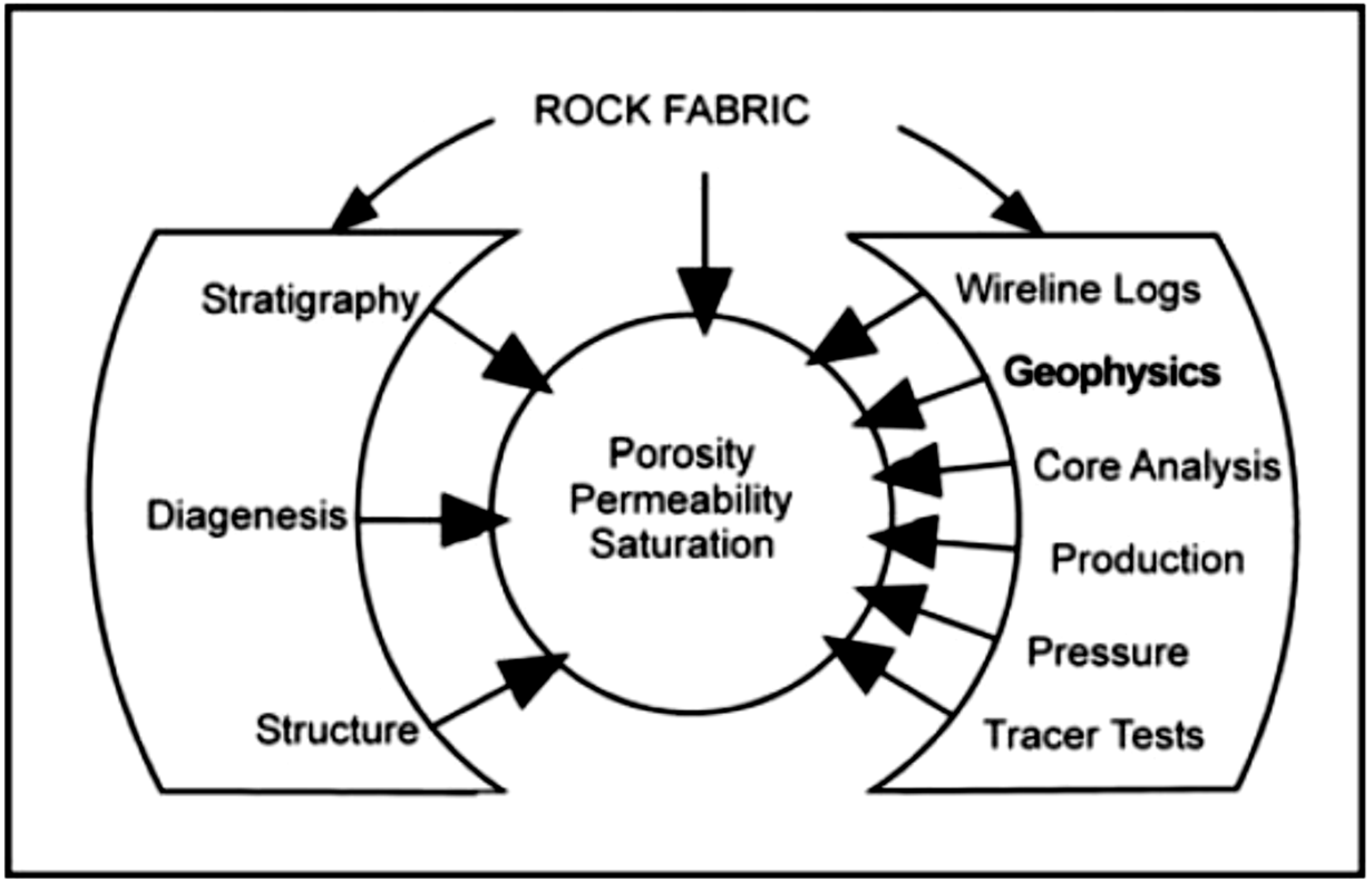

Petrophysical Evaluation:

- **Reservoir Geological Analysis**
- **Routine Core Analysis (RCAL)**
- **Special Core Analysis (SCAL)**
- **Wire line log Interpretation**

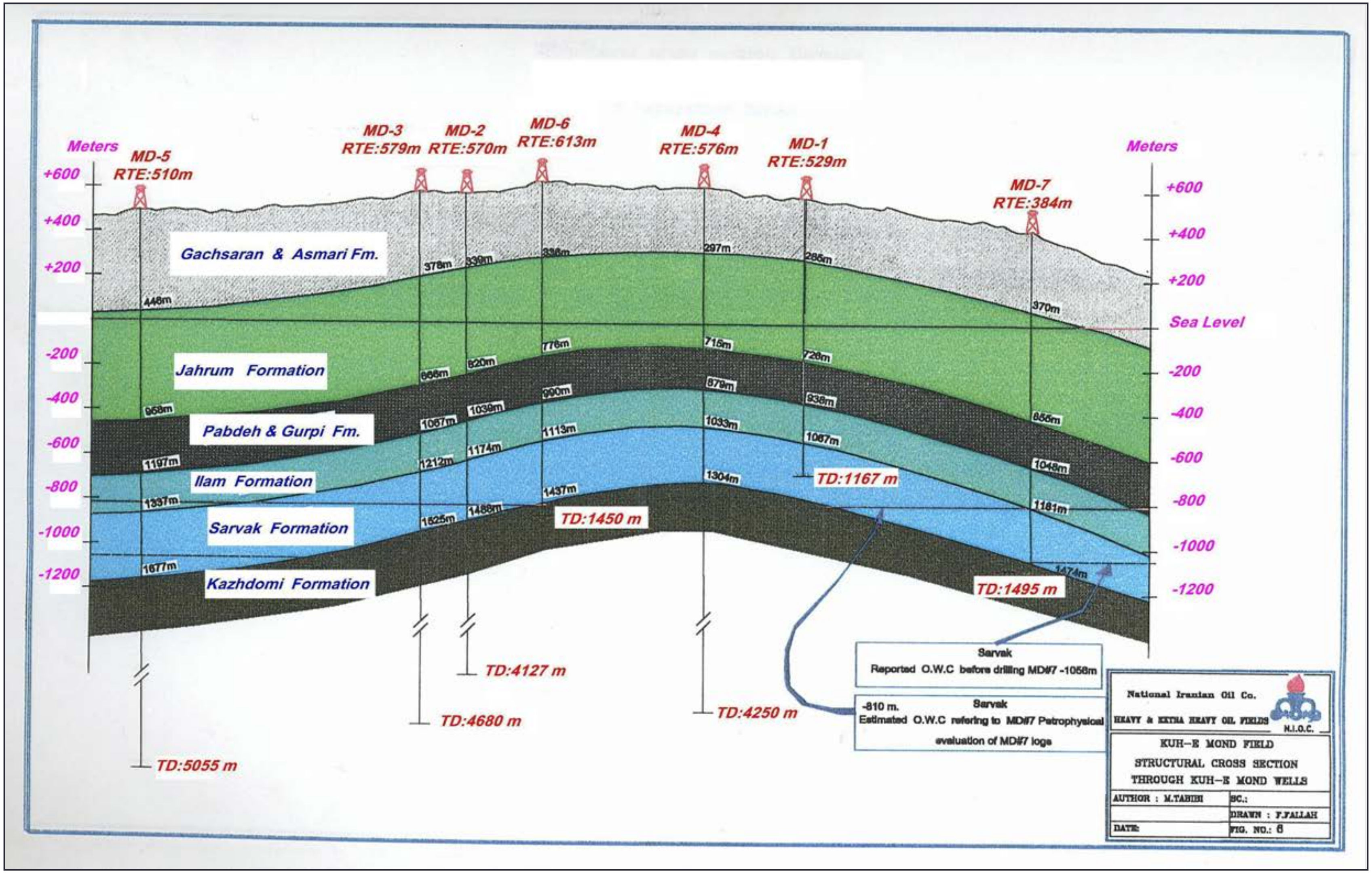

Meters
MD-5
RTE:510m
MD-3
RTE:579m
MD-2
RTE:570m
MD-6
RTE:613m
MD-4
RTE:576m
MD-1
RTE:529m
MD-7
RTE:384m
Meters
+600
+400
+200
Sea Level
-200
-400
-600
-800
-1000
-1200
Gachsaran & Asmari Fm.
Jahrum Formation
Pabdeh & Gurpi Fm.
Ilam Formation
Sarvak Formation
Kazhdomi Formation
TD:1167 m
TD:1450 m
TD:1495 m
TD:4127 m
TD:4680 m
TD:4250 m
TD:5055 m
Sarvak
Reported O.W.C before drilling MD#7 -1056m
-810 m.
Sarvak
Estimated O.W.C refering to MD#7 Petrophysical evaluation of MD#7 logs
National Iranian Oil Co.
HEAVY & EXTRA HEAVY OIL FIELDS
N.I.O.C.
KUH-E MOND FIELD
STRUCTURAL CROSS SECTION
THROUGH KUH-E MOND WELLS
AUTHOR : M.TABIBI
SC.:
DRAWN : F.FALLAH
DATE:
FIG. NO.: 6

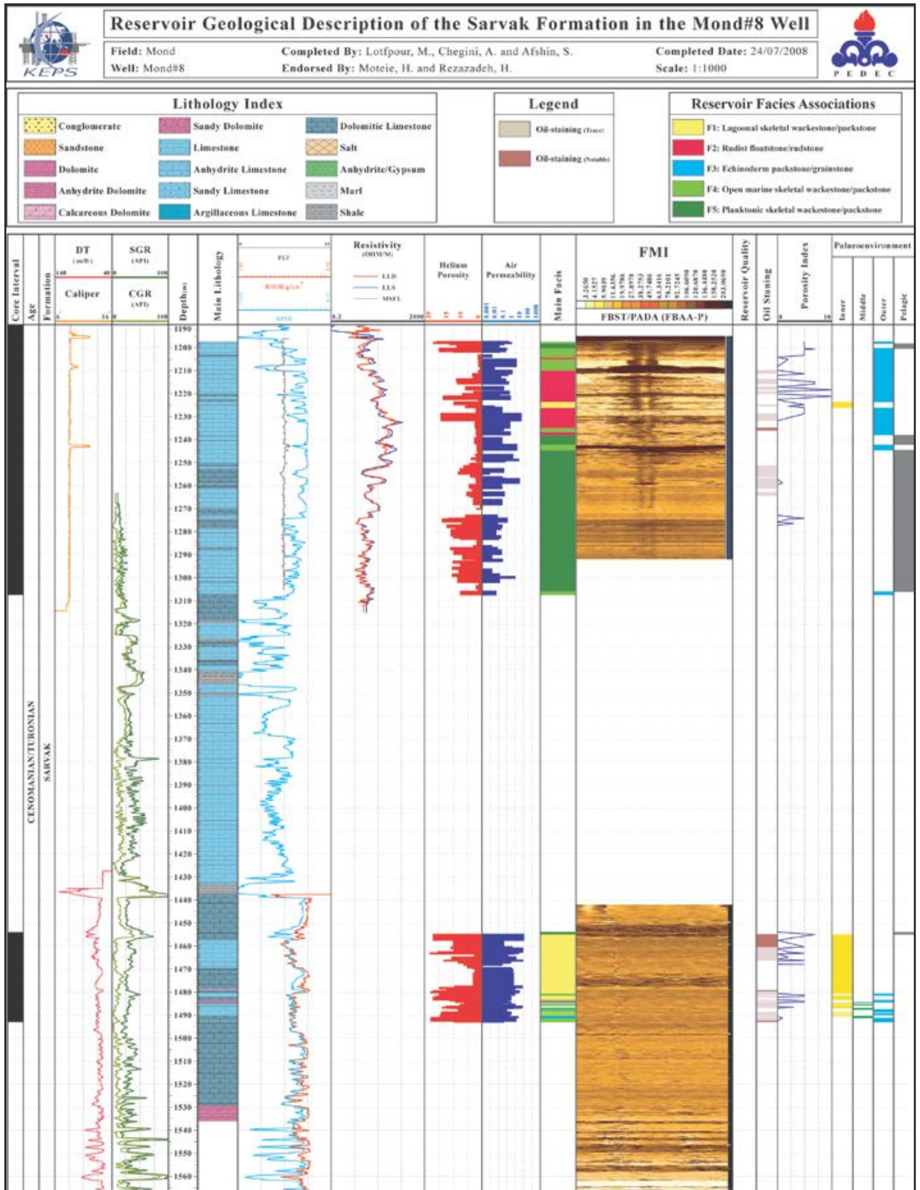
Reservoir Geological Description of the Sarvak Formation in the Mond#8 Well
Field: Mond
Well: Mond#8
Completed By: Lotfpour, M., Chegini, A. and Afshin, S.
Endorsed By: Moteie, H. and Rezazadeh, H.
Completed Date: 24/07/2008
Scale: 1:1000
KEPS
PEDEC
Lithology Index
Conglomerate
Sandstone
Dolomite
Anhydrite Dolomite
Calcareous Dolomite
Sandy Dolomite
Limestone
Anhydrite Limestone
Sandy Limestone
Argillaceous Limestone
Dolomitic Limestone
Salt
Anhydrite/Gypsum
Marl
Shale
Legend
Oil-staining (Trace)
Oil-staining (Notable)
Reservoir Facies Associations
F1: Lagoonal skeletal wackestone/packstone
F2: Rudist floatstone/rudstone
F3: Echinoderm packstone/grainstone
F4: Open marine skeletal wackestone/packstone
F5: Planktonic skeletal wackestone/packstone
Core Interval
Age
Formation
DT
SGR
Caliper
CGR
Depth
Main Lithology
Resistivity
LLD
LLS
MSFL
Helium Porosity
Air Permeability
Main Facies
FMI
FBST/PADA (FBAA-P)
Reservoir Quality
Oil Staining
Porosity Index
Palaeoenvironment
Inner
Middle
Outer
Pelagic
CENOMANIAN/TURONIAN
SARVAK

Sedimentology and reservoir geological study of the Upper Dalan and Kangan Formations in the South Pars Field, Persian Gulf

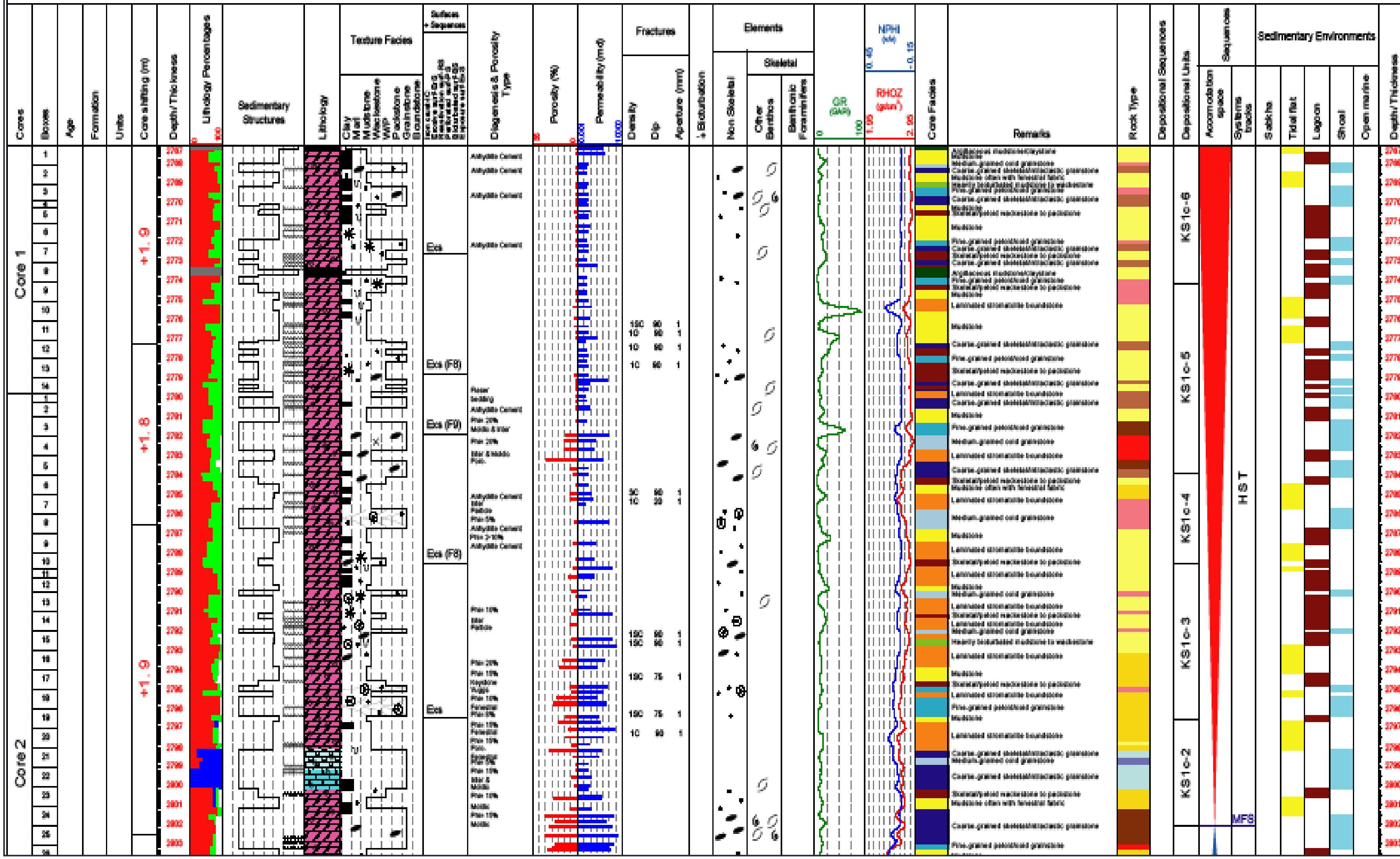

Differences between carbonate and siliciclastics reservoirs

Porosity

- Vuggy porosity common in carbonates, rare in clastics
- Microporosity common in carbonates
- High proportion of non-effective porosity in carbonates

Permeability

- High contrasts in permeability common in carbonates
- Link between porosity and permeability is not straightforward in carbonates and is difficult to predict

Petrophysical Rock Properties

- **Porosity**:

$$Porosity = \frac{\text{Pore volume}}{\text{Bulk volume}} = \frac{\text{Bulk volume - Mineral volume}}{\text{Bulk volume}}$$

- Effective and Non-Effective
- Visual method and laboratory (Boyle’s Law) measurements

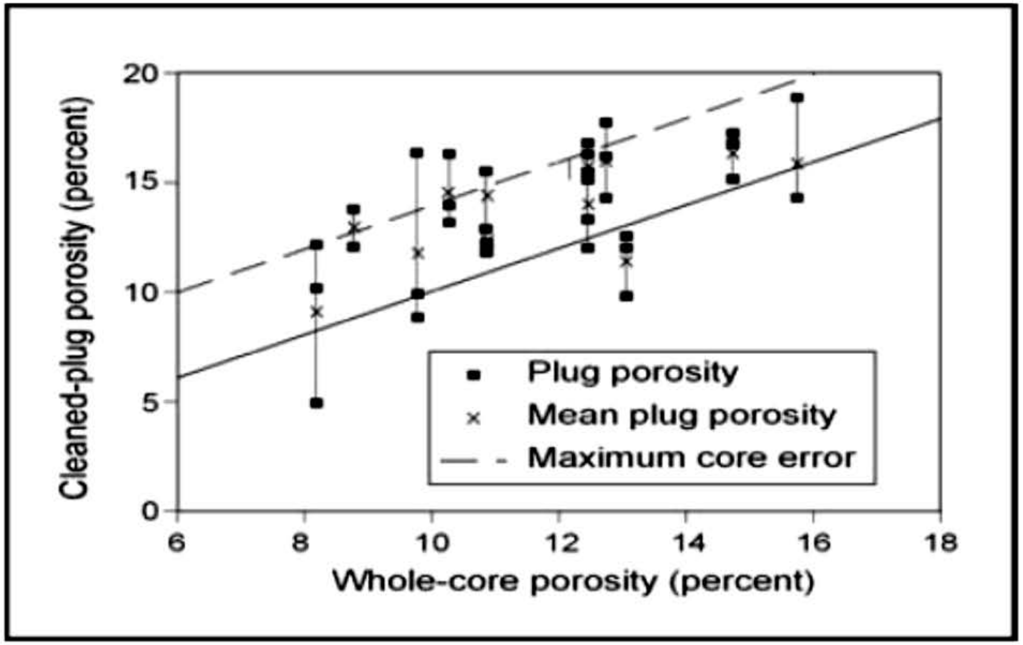

Fig. 1.1. Plot of whole-core porosity values versus porosity values of plug samples taken from the whole-core samples and recleaned. Whole-core porosity is too small by 0 – 4 porosity percent

- Porosity measurements should be made at in situ stress conditions because carbonate rocks are compressible, and porosity decreases with increasing effective stress. The common laboratory method is to increase confining pressure while maintaining a constant pore pressure. The resulting decrease in porosity is normally very small (2%) in Paleozoic and many Mesozoic reservoirs, and porosity measurements at ambient conditions are usually adequate (Harari et al. 1995). Porosity values of all high-porosity carbonates, however, should be checked for porosity loss with increasing confining pressure.

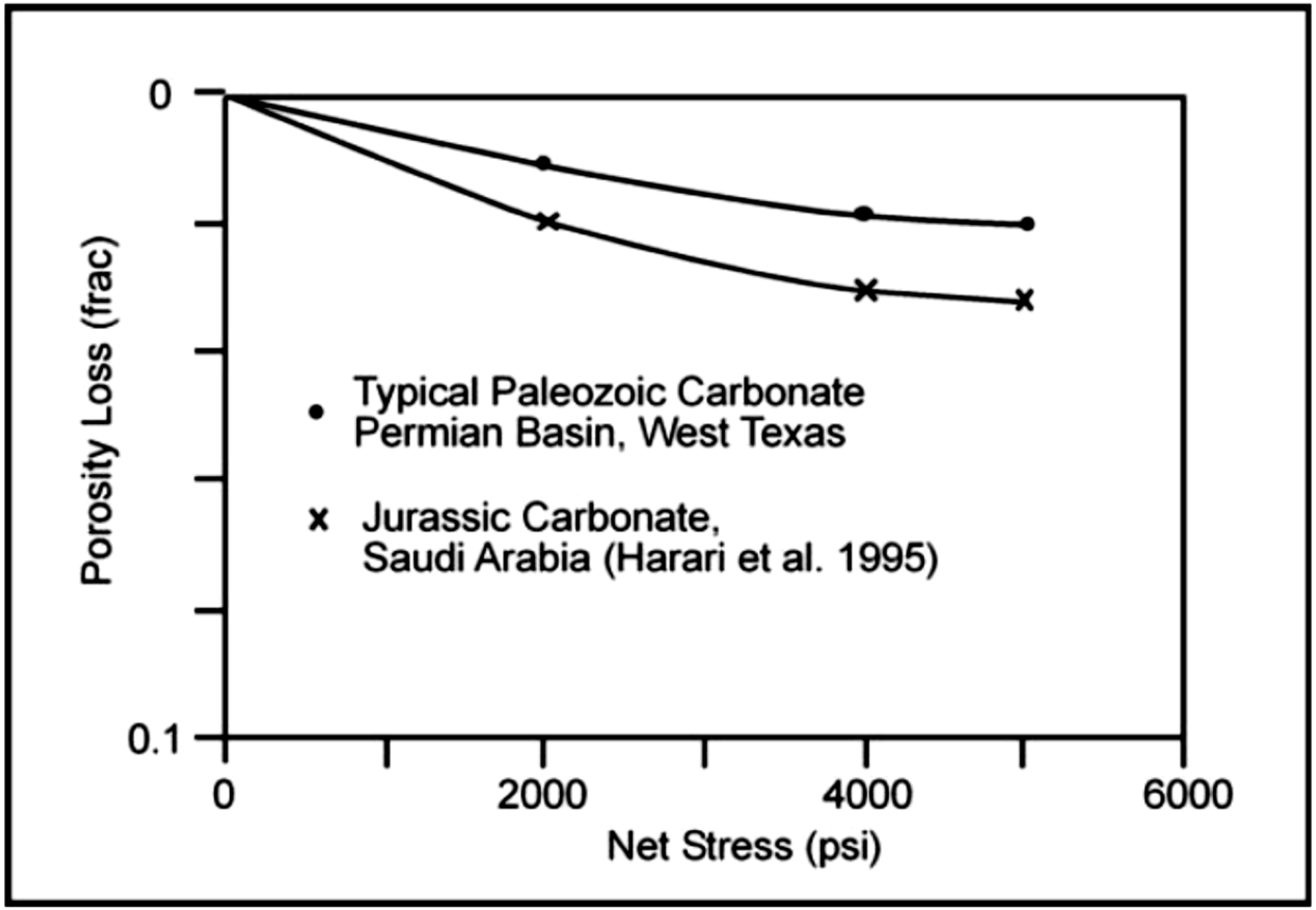

Fig. 1.2. Effect of confining pressure on porosity in Paleozoic and Jurassic carbonate reservoirs. Porosity loss is defined as confined porosity/unconfined porosity

- In carbonate sediment the shape of the grains and the presence of intragrain porosity as well as sorting have a large effect on porosity.

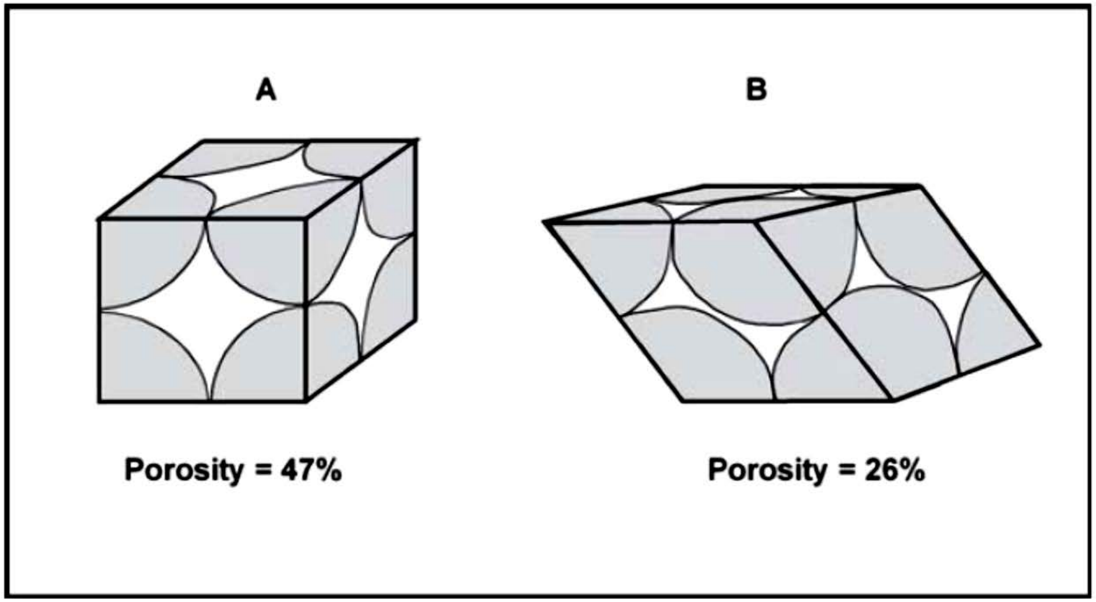

Fig. 1.3. Comparison of porosity in **(A)** cubic packed spheres and **(B)** rhombohedral-packed spheres. The porosity is a function of packing, and pore size is controlled by the size and packing of spheres

- # Permeability:

$$\text{Darcy's Law:} \quad Q = A\left(\frac{k}{\mu}\right)\left(\frac{\Delta P}{L}\right), \tag{3}$$

where Q is rate of flow, k is permeability, μ is fluid viscosity, $(\Delta P)/L$ is the potential drop across a horizontal sample, and A is the cross-sectional area of the sample. Permeability is a rock property, viscosity is a fluid property, and $\Delta P/L$ is a measure of flow potential.

- Normally, either air or brine is used as a fluid and, when high rates of flow can be maintained, the results are comparable. At low rates, air permeability will be higher than brine permeability. This is because gas does not adhere to the pore walls as liquid does, and the slippage of gases along the pore walls gives rise to an apparent dependence of permeability on pressure. This is called the Klinkenberg effect, and it is especially important in low-permeability rocks.

- Permeability is a vector and scalar quantity. Horizontal permeability varies in different directions, and vertical permeability is commonly less than horizontal permeability.
- A measure of permeability can be obtained from production tests using pressure buildup analyses. The pressure in the well is drawn down by production, the well is shut in, and the rate of pressure increase is measured. The rate of pressure increase is a function of the effective permeability of the reservoir. The effective, average permeability of the interval tested is calculated using the following equation:

$$\text{Slope (psi/log cycle)} = 162.6(q\mu B_o/kh),$$

- where *q* is the flow rate in stock-tank-barrels/day, μ = viscosity in centipoises, Bo is reservoir-barrels/stock-tank-barrels, *k* is permeability in millidarcys, and *h* is the net reservoir interval in feet.

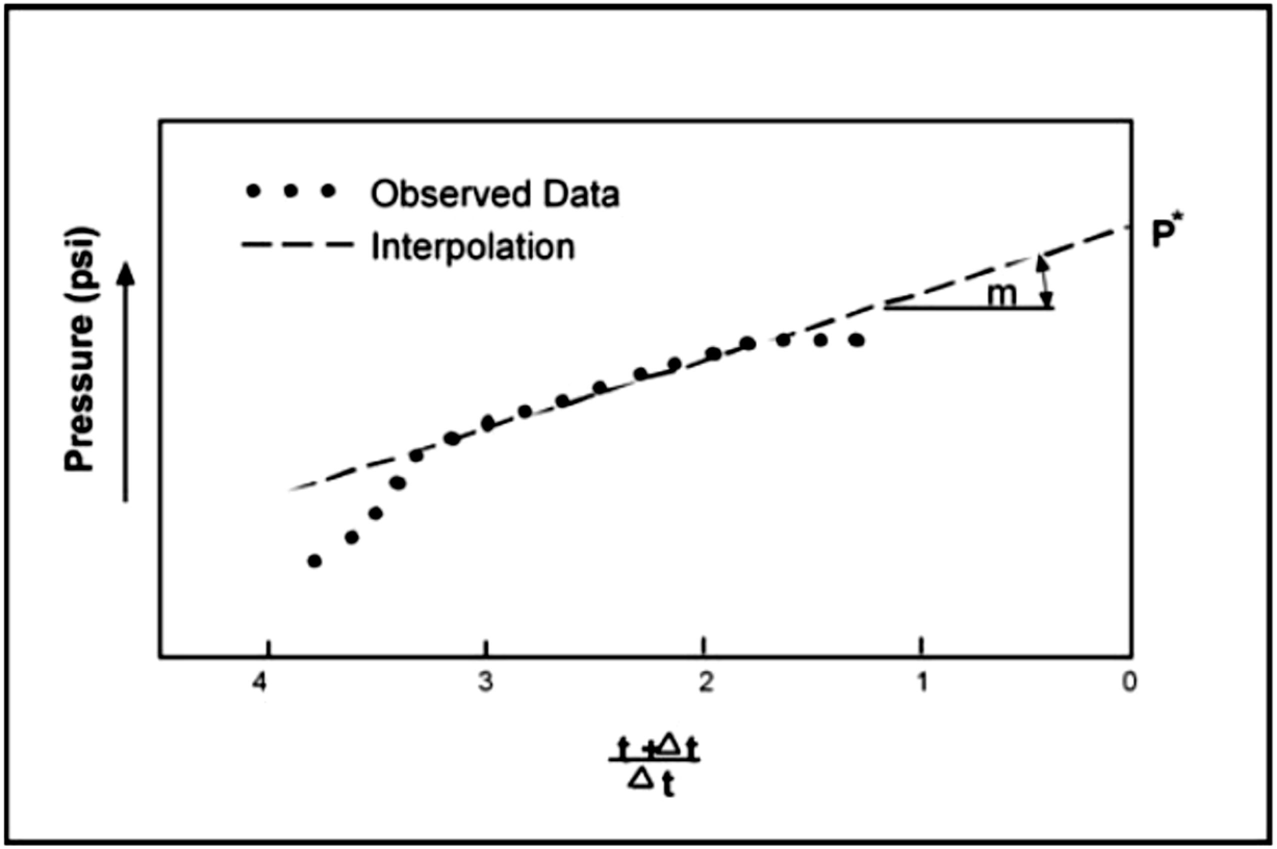

Fig. 1.6. Typical Horner pressure buildup plot (after Dake 1978). The slope of the line is a function of permeability-feet (kh)

- It is common practice to estimate permeability using simple porosity permeability transforms developed from core data. However, porosity permeability cross plots for carbonate reservoirs commonly show large variability , demonstrating that factors other than porosity are important in modeling permeability. These equations illustrate that the size and distribution of pore space, or pore-size distribution, is important along with porosity in estimating permeability. In general it can be concluded that there is no relationship between porosity and permeability in carbonate rocks unless pore-size distribution is included.

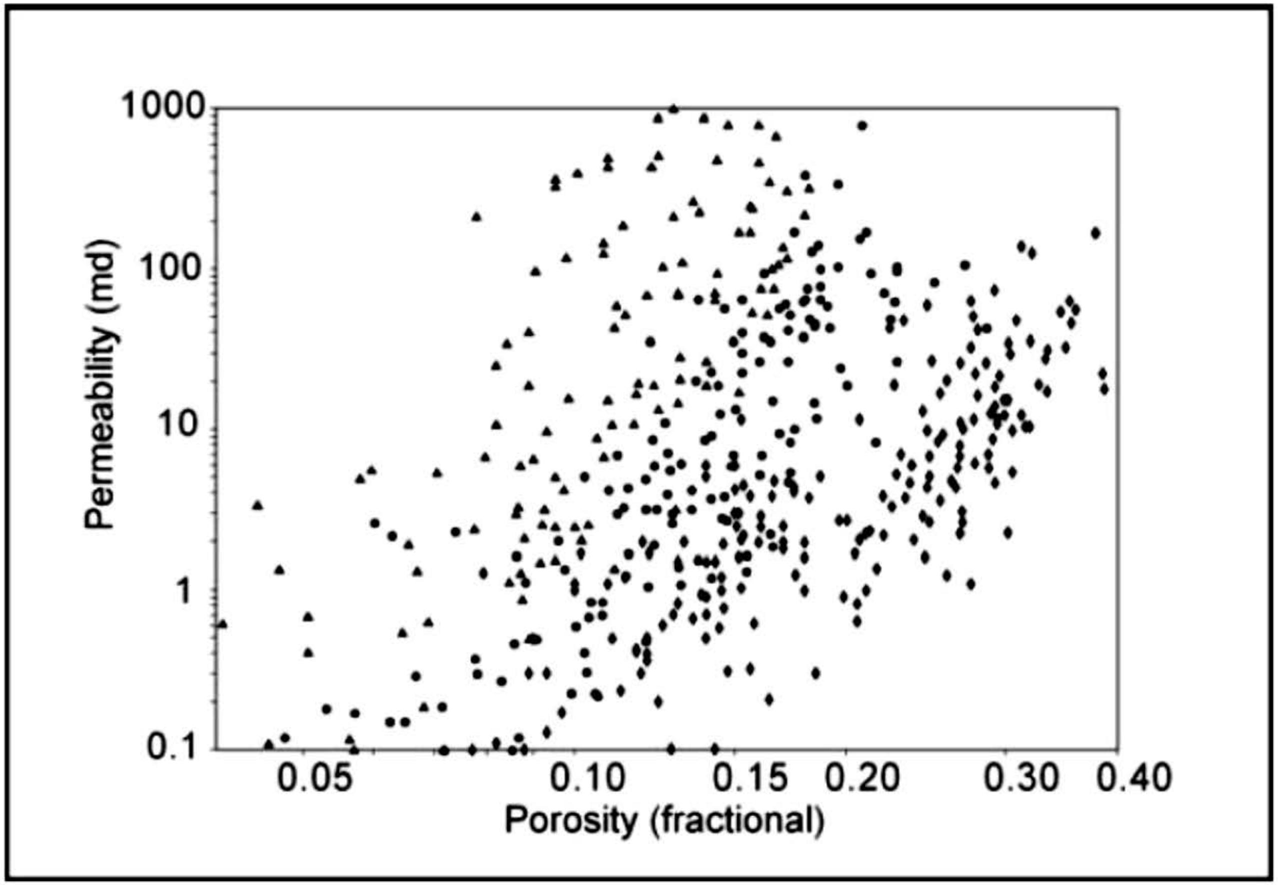

Fig. 1.7. Plot of porosity and permeability for carbonate rocks, illustrating that there is no relationship between porosity and permeability in carbonate rocks without including pore-size distribution

- **wettability:**

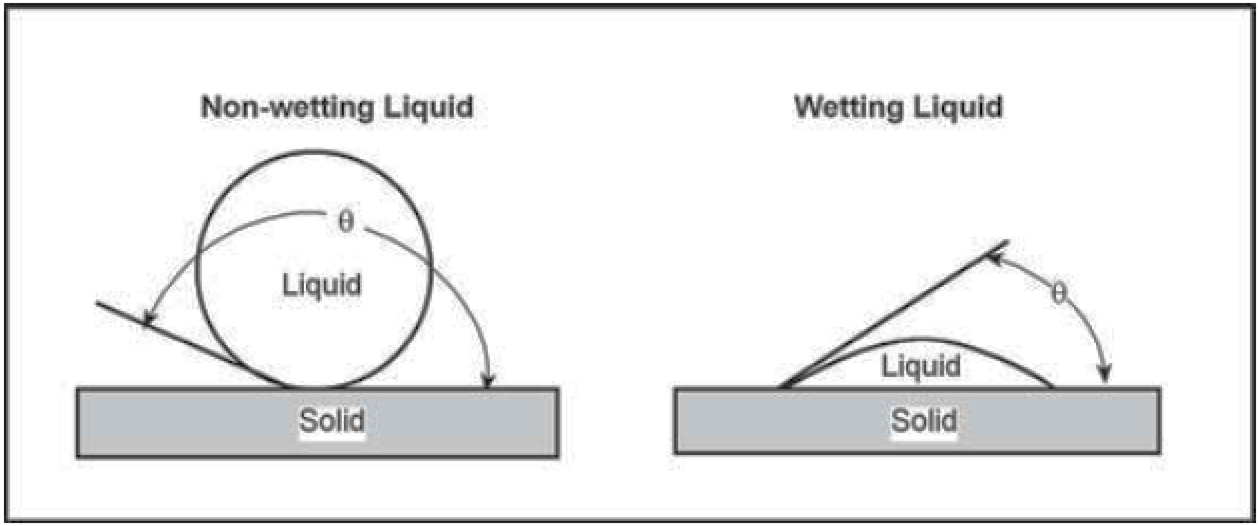

Fig. 1.10. Adhesive forces and the definition of wettability. If the adhesive forces are less than cohesive forces, ($\theta > 90^o$), the liquid is said to be nonwetting. If adhesive forces are greater than cohesive forces, ($\theta < 90^o$), the liquid is said to be the wetting phase

- Hydrocarbon saturation in a reservoir is related to pore size as well as capillary pressure and capillary forces. For oil to accumulate in a hydrocarbon trap and form a reservoir, the surface tension between water and oil must be exceeded. This means that the pressure in the oil phase must be higher than the pressure in the water phase. If the pressure in the oil is only slightly greater than that in the water phase, the radius of curvature will be large and the oil will be able to enter only large pores. As the pressure in the oil phase increases, the radius of curvature decreases and oil can enter smaller pores

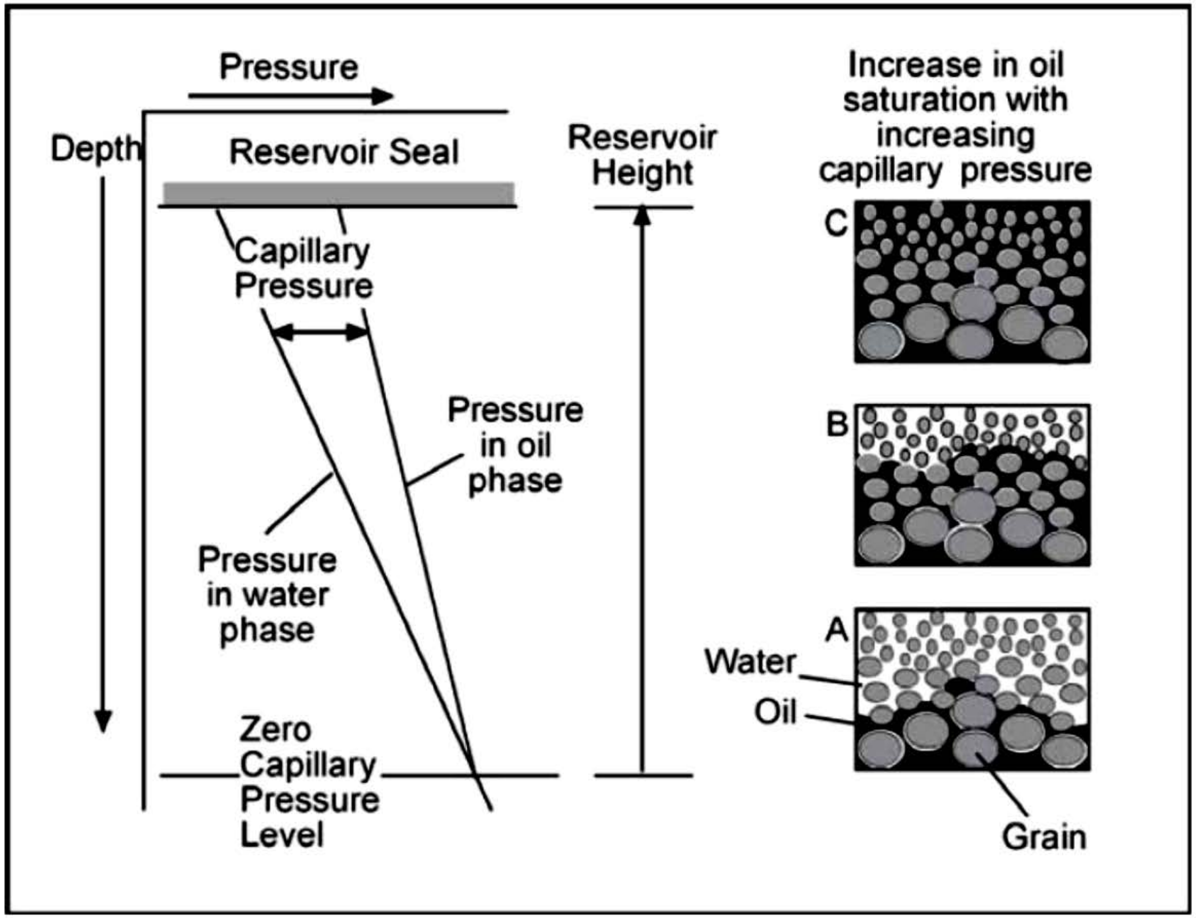

Fig. 1.14. Diagram showing smaller pores being filled with a non-wetting fluid (oil) displacing a wetting fluid (water) as capillary pressure increases linearly with reservoir height. Pore size is determined by grain size and sorting. **(A)** Only the largest pores contain oil at the base of the reservoir. **(B)** Smaller pores are filled with oil as capillary pressure and reservoir height increase. **(C)** Smallest pores are filled with oil toward the top of the reservoir

- The pressure in the water phase depends upon the degree to which the fluid column is connected to the Earth’s surface. In an open system, the fluid pressure is equal to depth times the density of the fluid and is called hydrostatic. The hydrostatic pressure gradient is about 0.434 psi/ft; overburden pressure equals the weight of the overburden sediment and has a gradient of about 1 psi/ft. Deviations from hydrostatic pressure, abnormal pressures, occur when the formation fluid is confined and cannot equilibrate with surface pressure.

- Over pressuring is the most common abnormal pressure and is produced by (1) compaction during rapid burial, (2) tectonic compression, and (3) hydrocarbon generation and migration (Osborne and Swarbrick 1997). In extreme cases, fluid pressures can equal and even exceed overburden pressures. Uncommonly, pressures can be lower than hydrostatic. Under pressure is often related to erosional unloading that results in an increase in pore volume due to the elastic rebound of the sediment as the overburden is reduced (Bachu and Underschultz 1995).

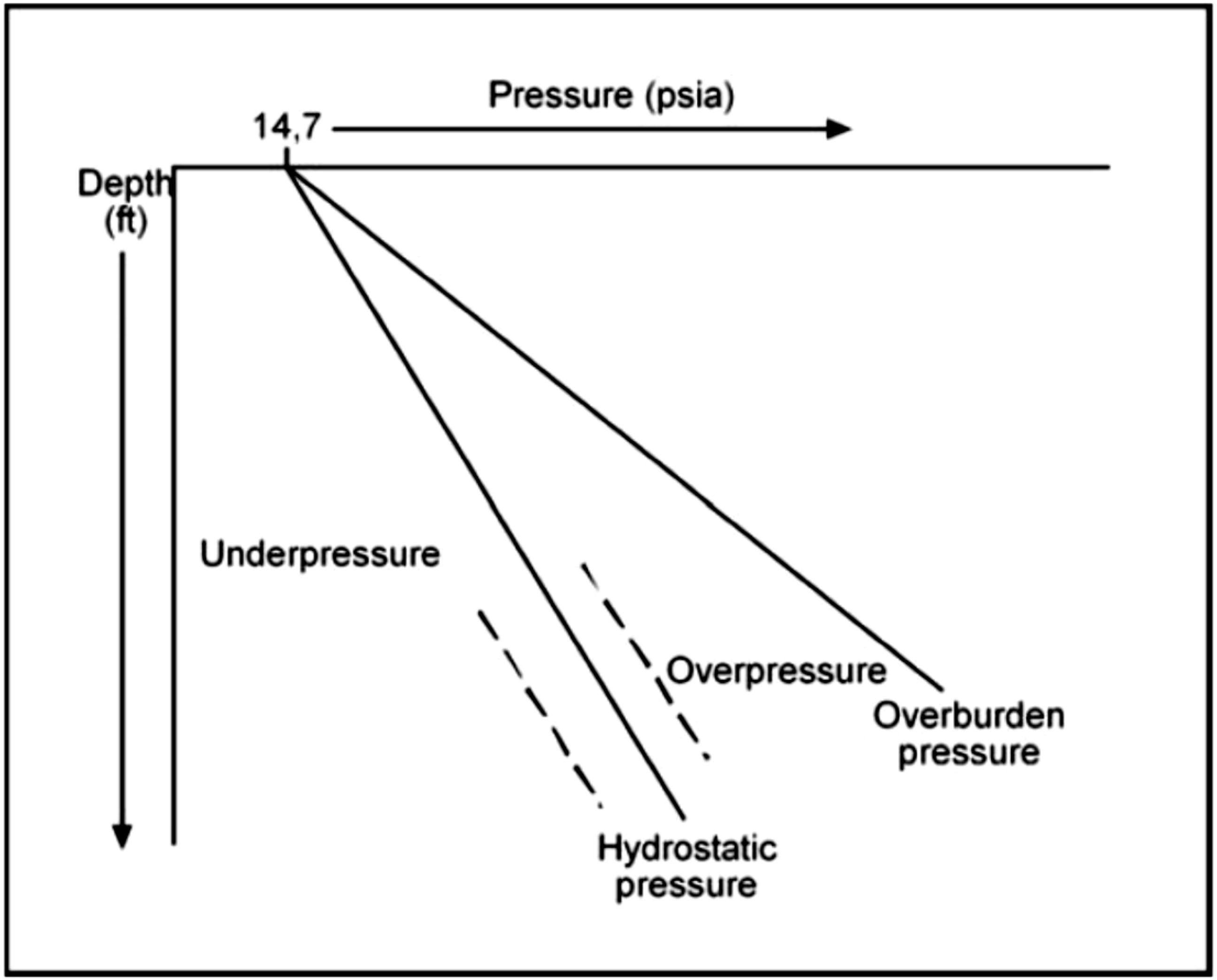

Fig. 1.16. Diagram illustrating overburden, normal hydrostatic, and abnormal over- and underpressure regimes. (After Dake 1978)

- **Relative Permeability:**
- *Relative permeability* is simply the permeability measured at a specific fluid saturation expressed as a fraction of the total or absolute permeability. *Absolute permeability* is the permeability of a rock that is 100% saturated with a single fluid.

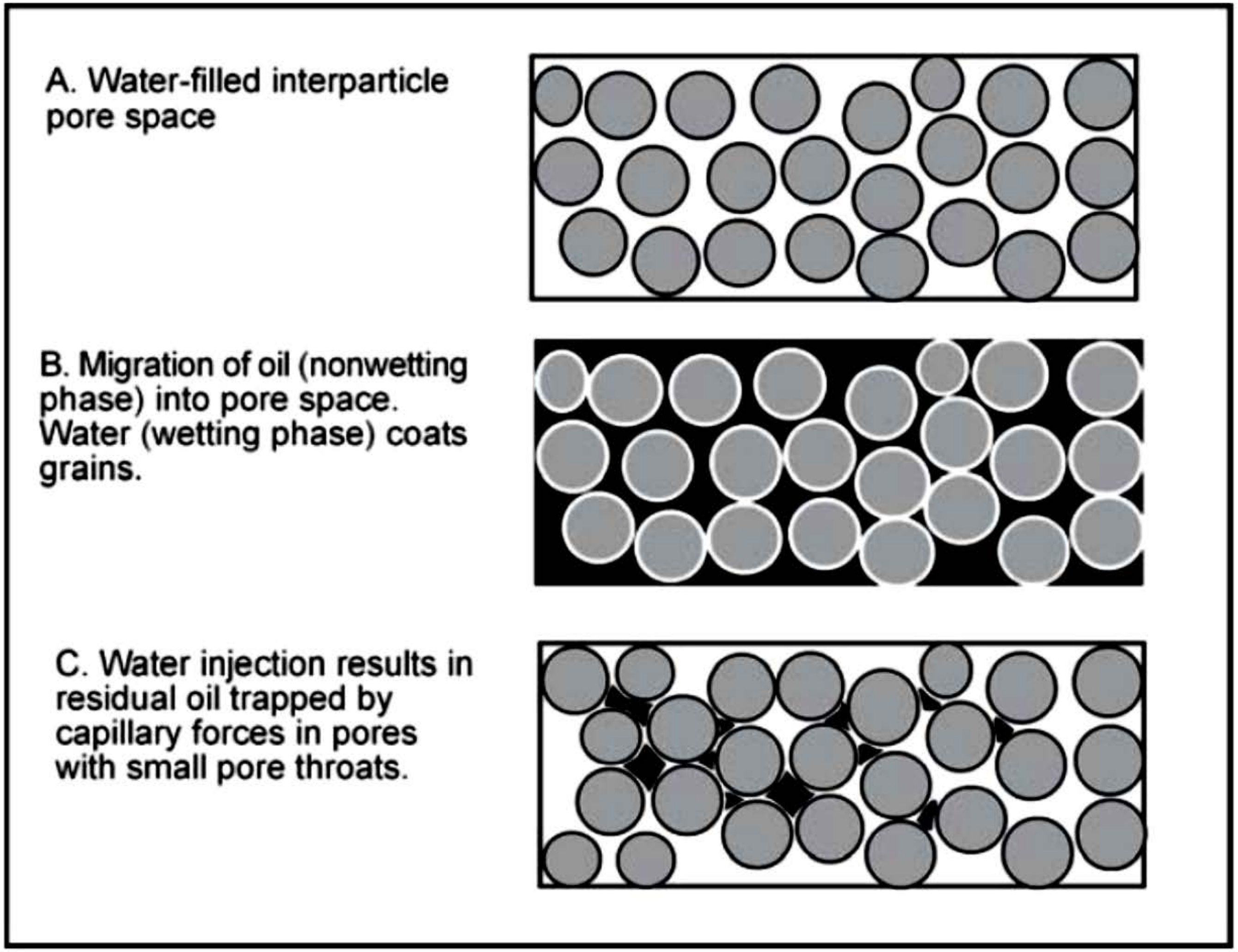

Fig. 1.17. Diagram of oil and water distribution in a water-wet rock under three conditions: **(A)** 100% water saturation, **(B)** injection of a nonwetting fluid (oil), and **(C)** injection of a wetting fluid (water)

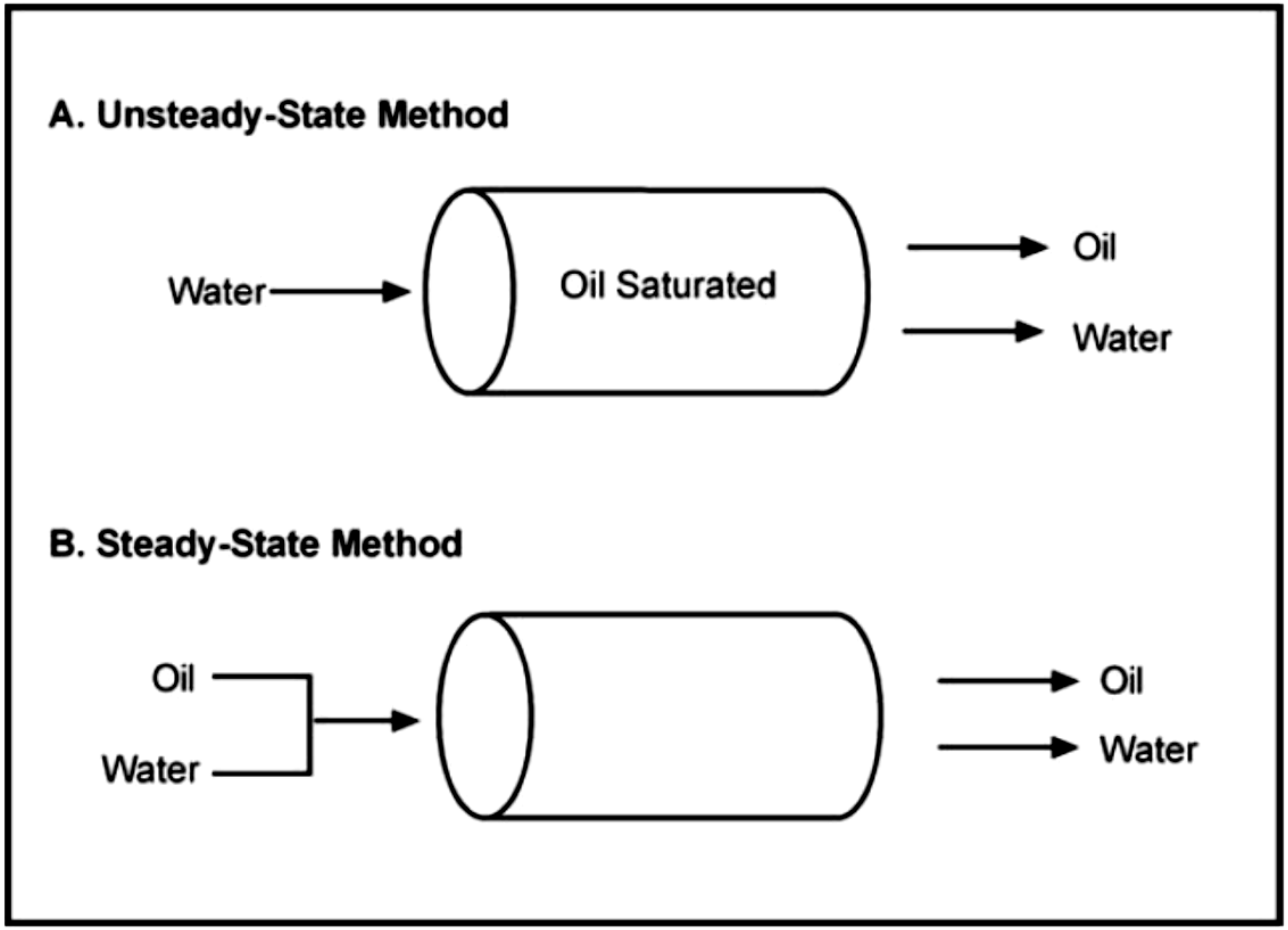

Fig. 1.19. Illustration of unsteady-state and steady-state methods of measuring two-phase oil and water relative permeability

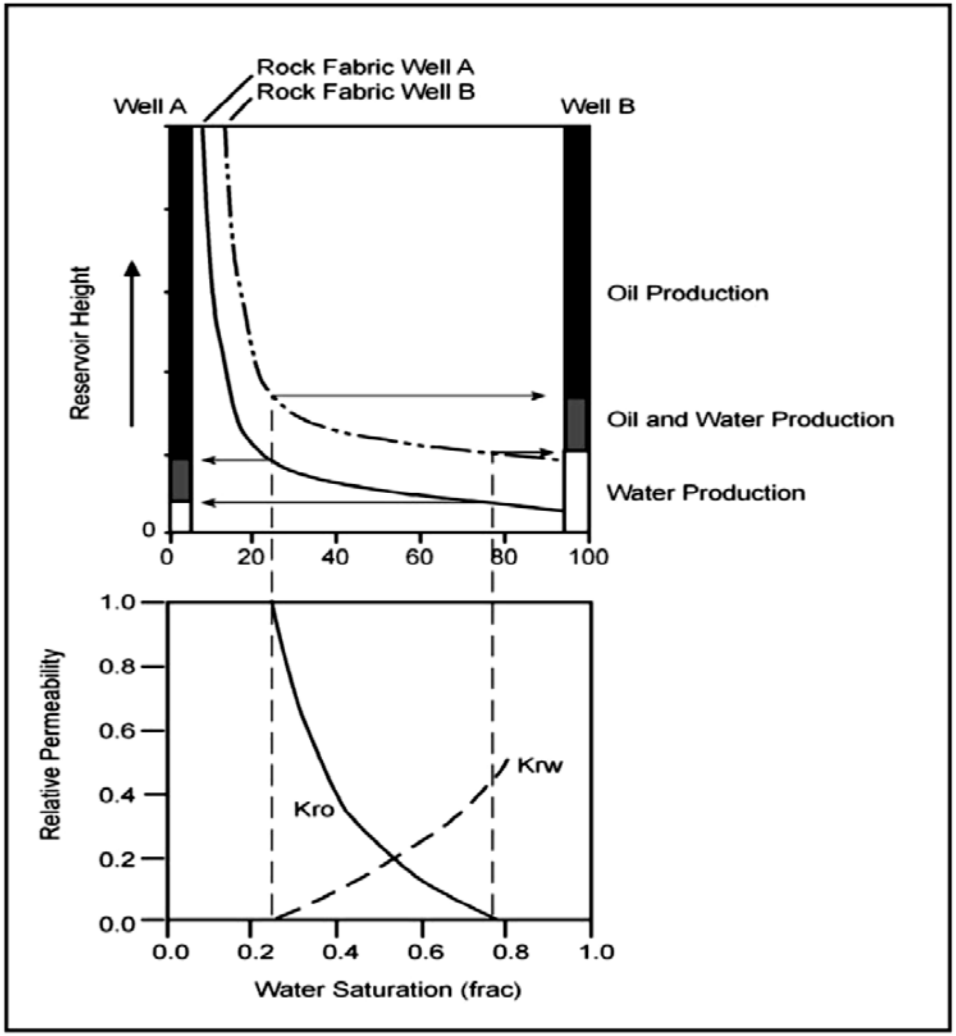

Fig. 1.20. Simplified illustration showing the relationship between relative permeability to oil and water, capillary pressure converted to reservoir height, water saturation, and pore size. The effect of pore size is illustrated by considering two capillary pressure curves **(rock-fabric A, rock-fabric B)** from carbonate rocks with different pore-size distributions. The change in pore size results in the possibility of intervals where (1) clean oil is produced from rock-fabric A and oil and water from rock-fabric B , and (2) oil and water is produced from rock-fabric A and water from B

Rock-Fabric Classification

Carbonate rock textures: Dunham classification

Depositional texture recognizable					Depositional texture not recognizable
Original components not bound together during depositon				Original components were bound together	
Contains mud (clay and fine-size carbonate)			Lacks mud and is grain supported		
Mud - supported		Grain - supported			
Less than 10% grains	More than 10% grains				
Mudstone	Wackestone	Packestone	Grainstone	Boundstone	Crystalline

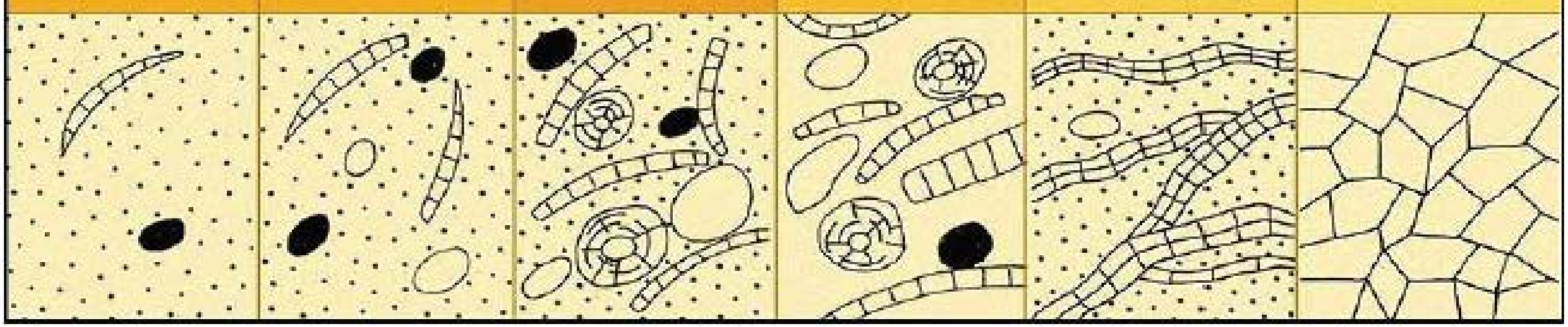

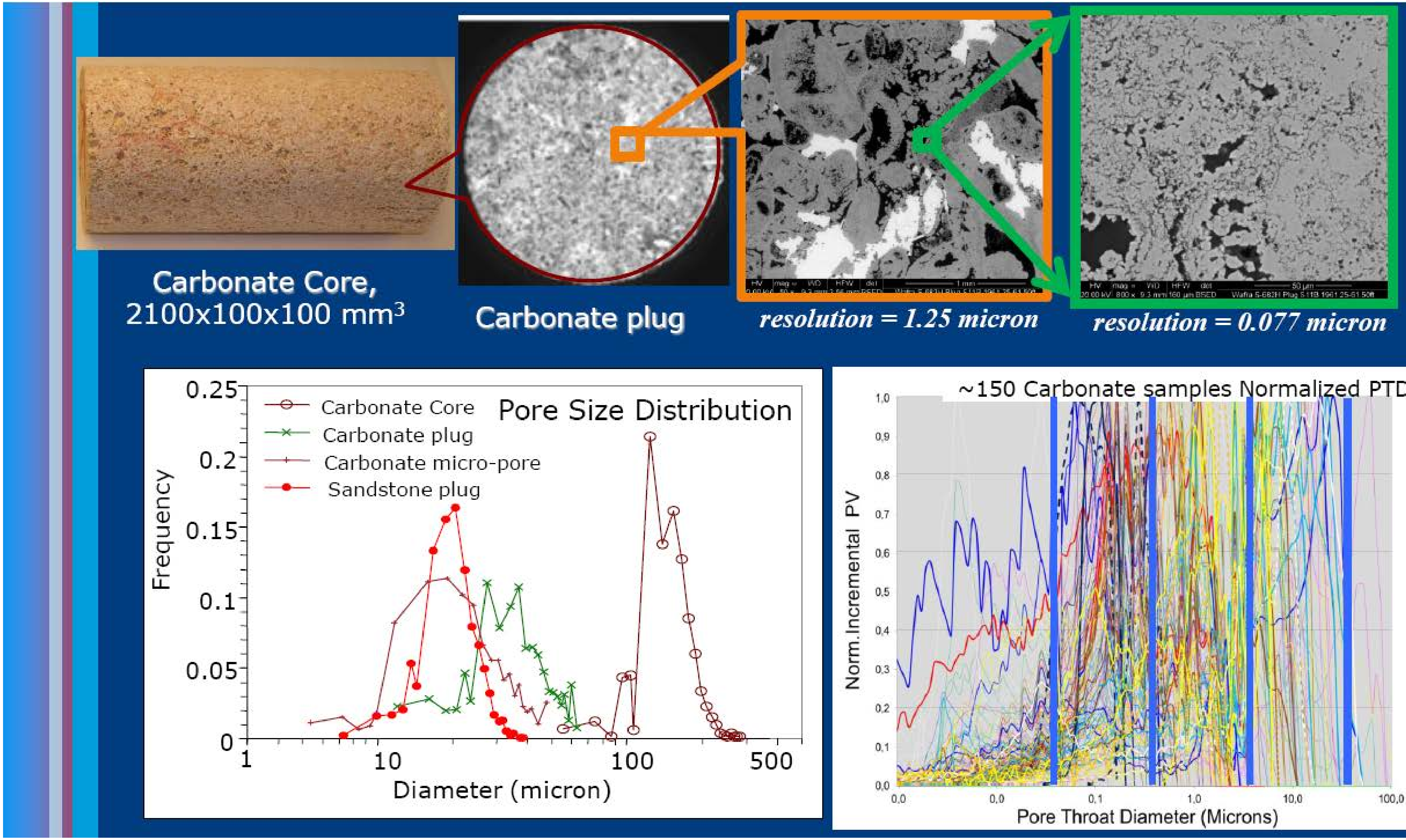
Carbonate Core,
2100x100x100 mm³
Carbonate plug
resolution = 1.25 micron
resolution = 0.077 micron
Pore Size Distribution
Carbonate Core
Carbonate plug
Carbonate micro-pore
Sandstone plug
Frequency
Diameter (micron)
~150 Carbonate samples Normalized PTD
Norm.Incremental PV
Pore Throat Diameter (Microns)

Pore Throat Size Classes

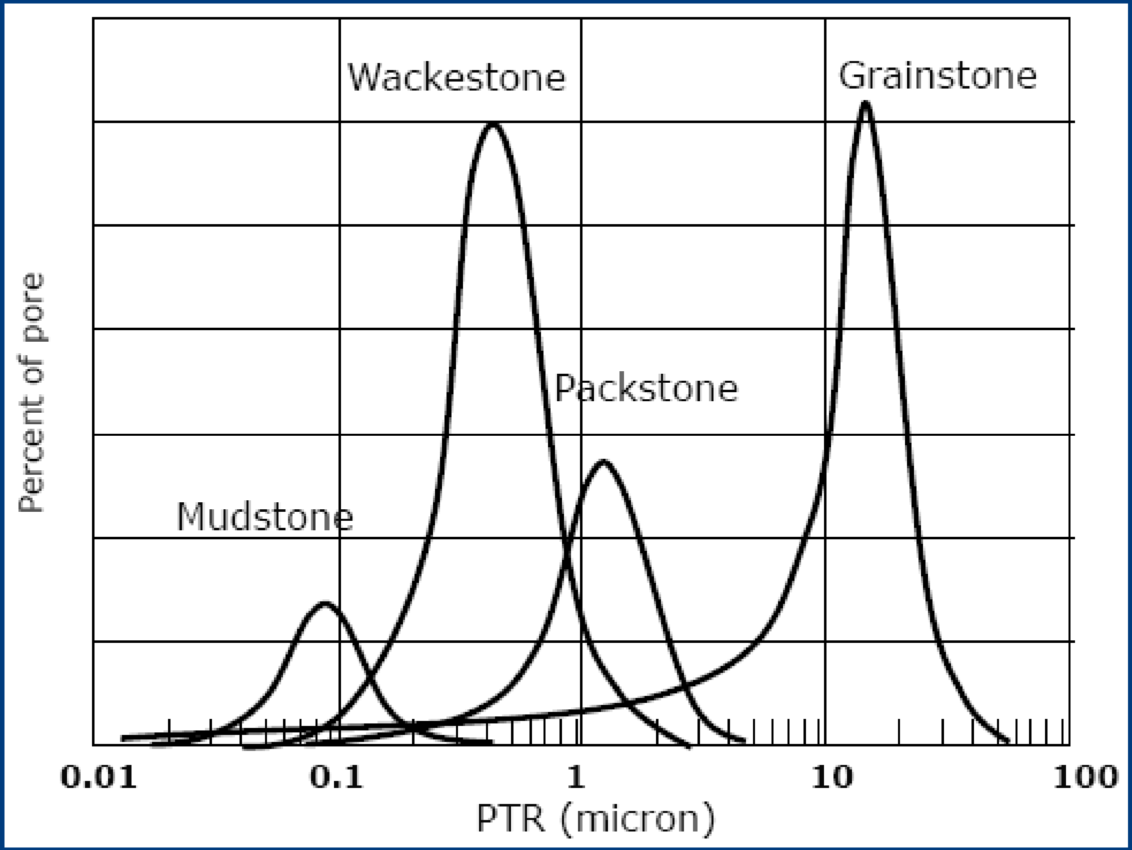

Macropores 1: Pore Throat size > 10 microns

Macropores 2: Pore Throat size between 4 and 10 microns

Mesopore 1: Pore Throat size between 1 and 4 microns

Mesopore 2: Pore Throat size between 0.3 and 1 micron

Micropore: Pore Throat size <0.3 micron

After Marzouk et al. (1995)

Core Based Pore Observation Tools

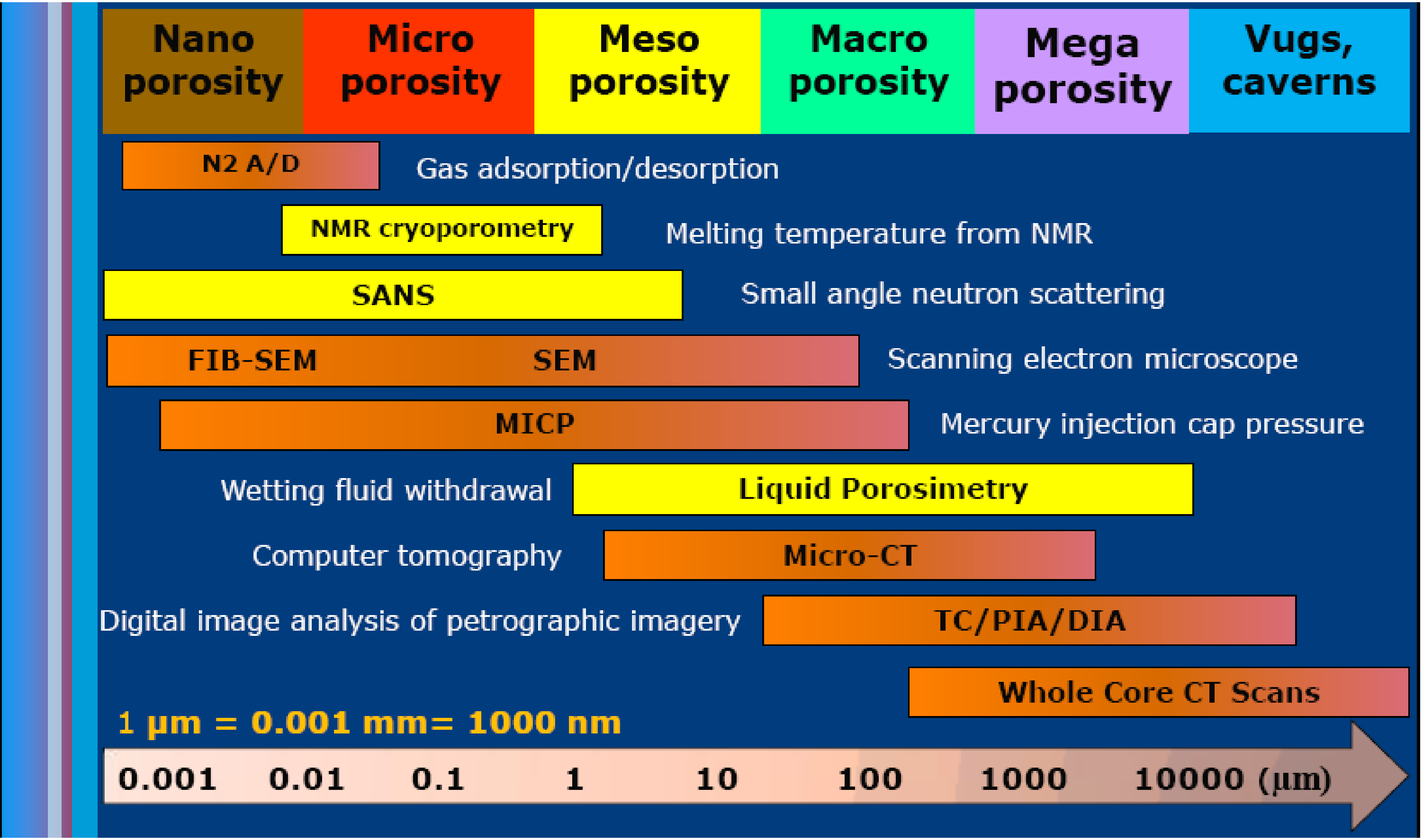

Porosity classification System

- Classic pore type classification systems mostly observational
- Archie (1952) – textural/petrophysical with 12 pore types
- Choquette and Pray (1970) – definitions of pore types genetic/depositional with 15 pore types
- Lucia (1983, 1995, 1999) – rock fabric/petrophysical with 18 pore types
- Lønøy (2006) – modified Choquette Pray pore size with 20 pore types
- Marzouk, Tazenaki, Suzuki (1998), Clerke et al. (2008) – MICP based

Idealized Carbonate Porosity Types

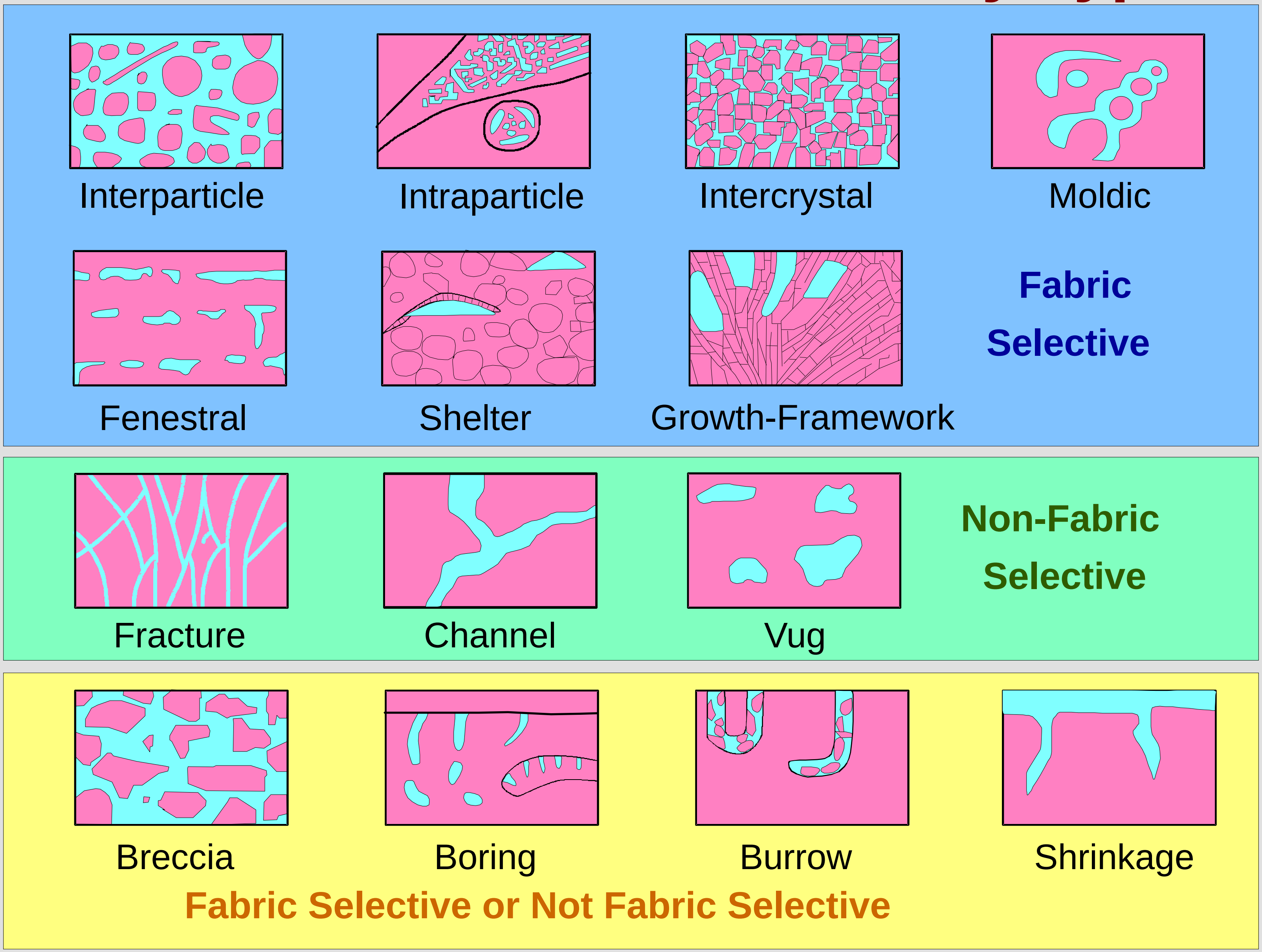

(modified from Choquette and Pray, 1970)

Pore type Classifications

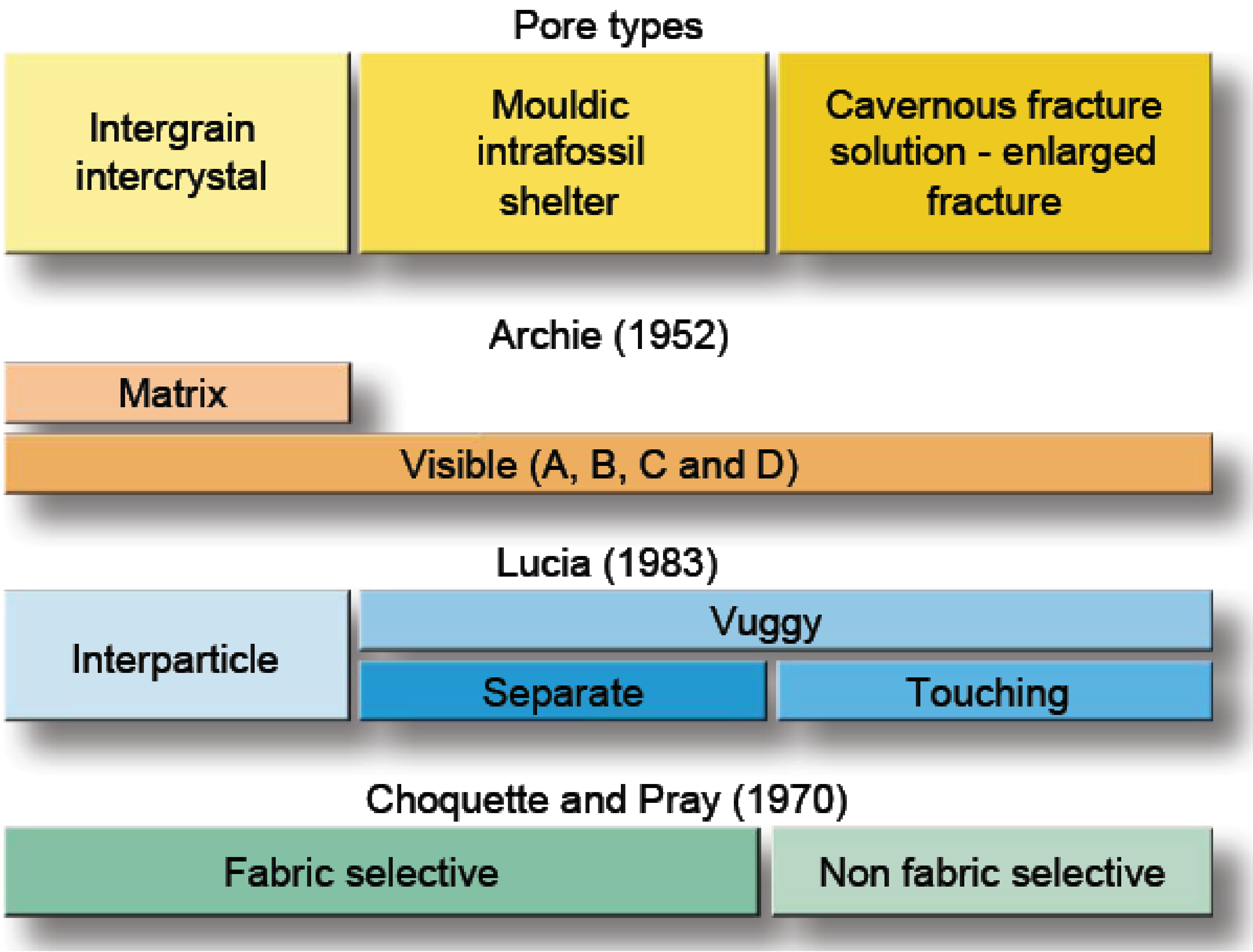

Carbonate Diagenesis

"The diagenesis of carbonate sediments encompasses all the processes which affect the sediments after deposition until the realms of incipient metamorphism at elevated temperatures and pressures."

Diagenetic processes include:

- Cementation
- Micritisation
- Neomorphism
- Dissolution
- Compaction / fracturing
- Dolomitisation

Term	Abbreviations: Lucia	Abbreviations: Choquette and Pray (1970)
Interparticle	IP	BP
Intergrain	IG	-
Intercrystal	IX	BC
Vug	VUG	VUG
Separate Vug	SV	-
Moldic	MO	MO
Intraparticle	WP	WP
Intragrain	WG	-
Intracrystal	WX	-
Intrafossil	WF	-
Intragrain microporosity	$ig\mu\phi$	-
Shelter	SH	SH
Touching Vug	TV	-
Fracture	FR	FR
Solution-enlarged fracture	SF	CH*
Cavernous	CV	CV
Breccia	BR	BR
Fenestral	FE	FE

*Channel.

Classification of Interparticle Pore Space

- In the absence of vuggy porosity, pore-size distribution in carbonate rocks can be described in terms of particle size, sorting, and interparticle porosity.
- Lucia (1983) showed that particle size can be related to mercury capillary displacement pressure in nonvuggy carbonates with more than 0.1 md permeability, suggesting that particle size describes the size of the largest Pores. Whereas the displacement pressure characterizes the largest pores sizes, the shape of the capillary pressure curve characterizes the smaller pore sizes and is dependent on interparticle porosity (Lucia 1983).

- The **petrophysical properties** of interparticle porosity are related to **particle size**, **sorting** and **interparticle porosity**. Grain size and sorting of grains and micrite is based on Dunham’s classification, modified to make it compatible with petrophysical considerations. Instead of dividing fabrics into grain support and mud support, fabrics are divided into grain-dominated and mud-dominated. The important attributes of grain-dominated fabrics are the presence of open or occluded intergrain porosity and a grain-supported texture. The important attribute of mud-dominated fabrics is that the volume between the grains is filled with mud even if the grains appear to form a supporting framework.

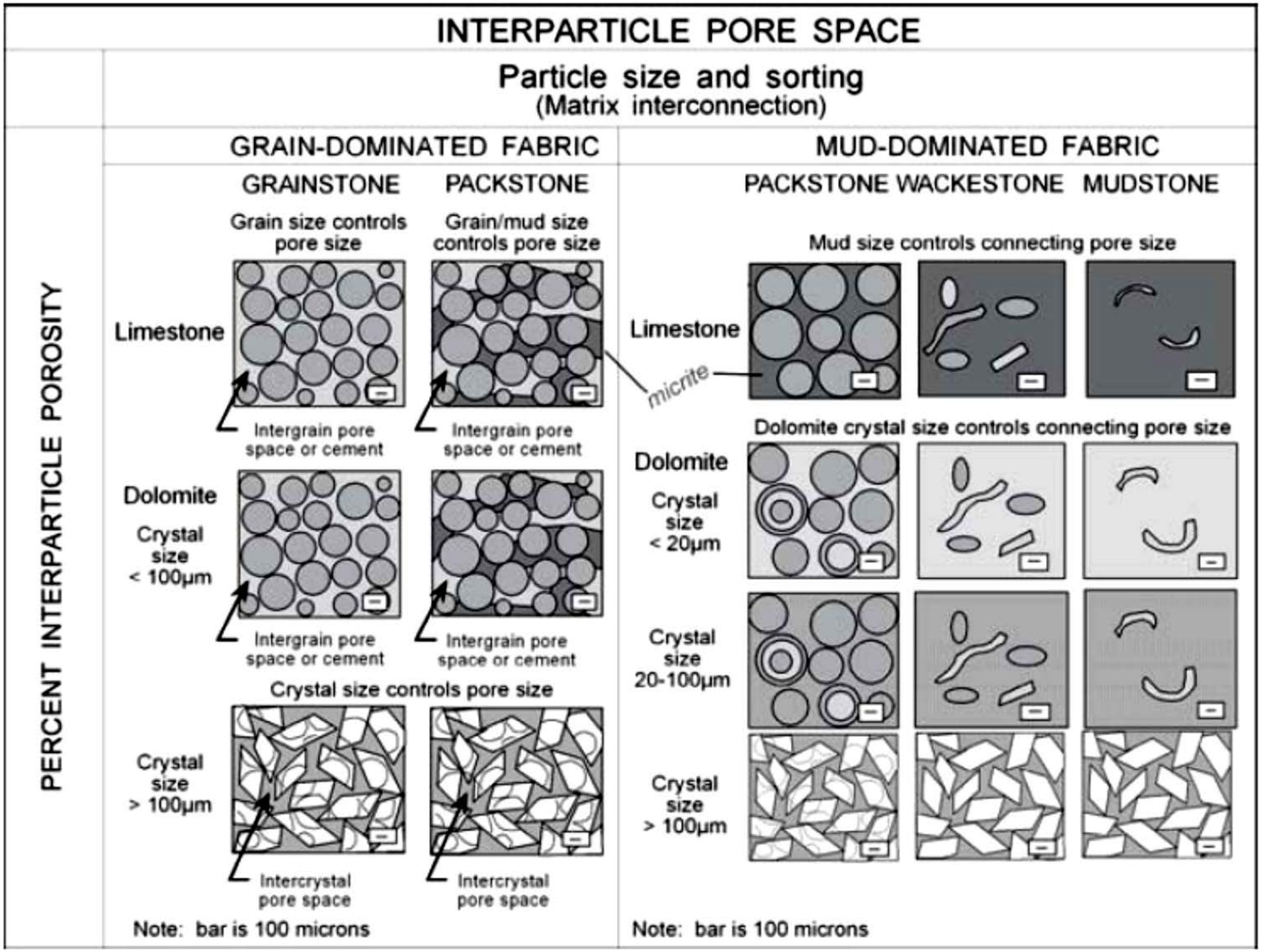
INTERPARTICLE PORE SPACE
Particle size and sorting
(Matrix interconnection)
GRAIN-DOMINATED FABRIC
MUD-DOMINATED FABRIC
GRAINSTONE
PACKSTONE
PACKSTONE WACKESTONE MUDSTONE
Grain size controls pore size
Grain/mud size controls pore size
Mud size controls connecting pore size
PERCENT INTERPARTICLE POROSITY
Limestone
Limestone
micrite
Intergrain pore space or cement
Intergrain pore space or cement
Dolomite crystal size controls connecting pore size
Dolomite
Dolomite
Crystal size < 100µm
Crystal size < 20µm
Intergrain pore space or cement
Intergrain pore space or cement
Crystal size 20-100µm
Crystal size controls pore size
Crystal size > 100µm
Crystal size > 100µm
Intercrystal pore space
Intercrystal pore space
Note: bar is 100 microns
Note: bar is 100 microns

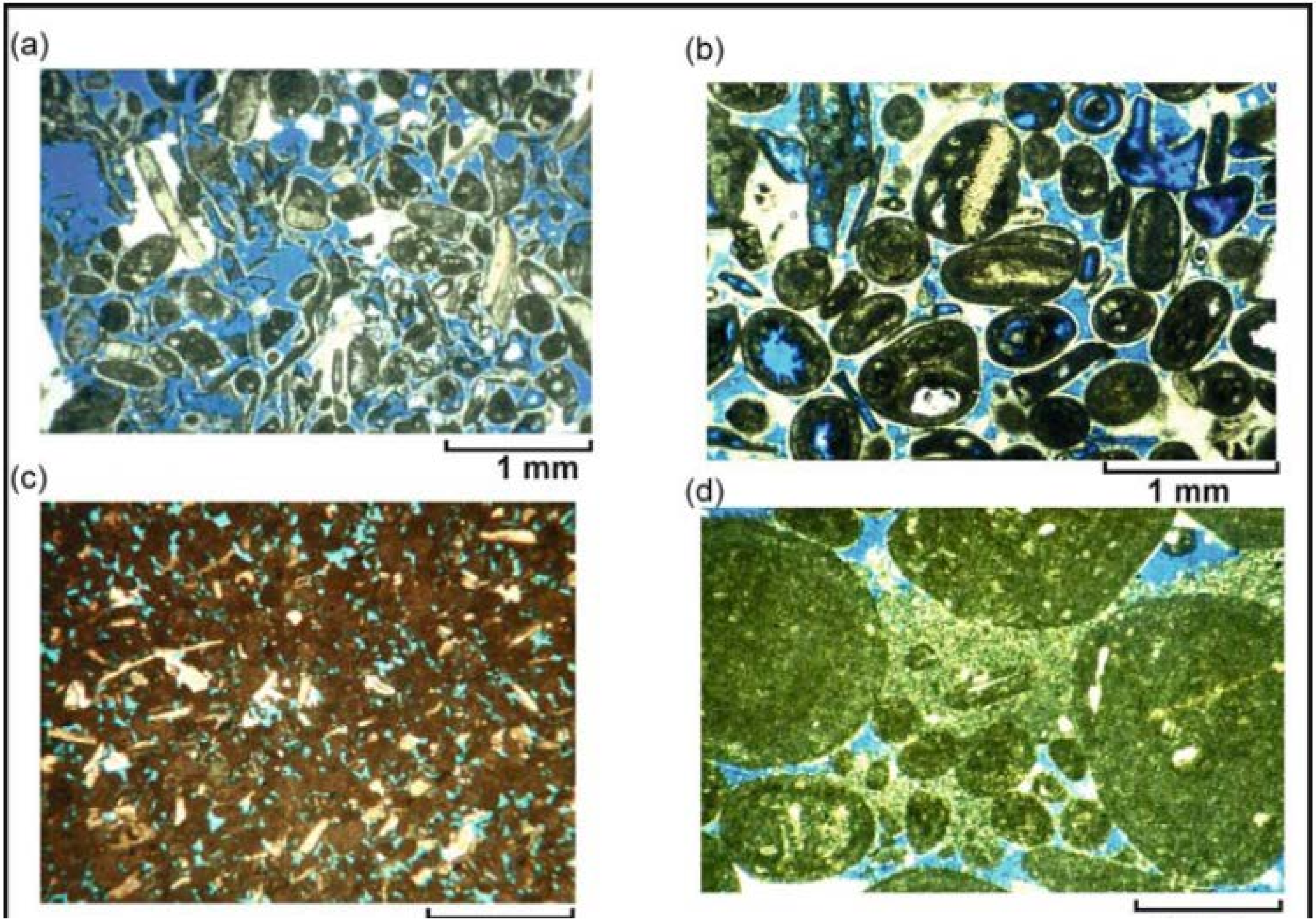
(a)
(b)
1 mm
1 mm
(c)
(d)

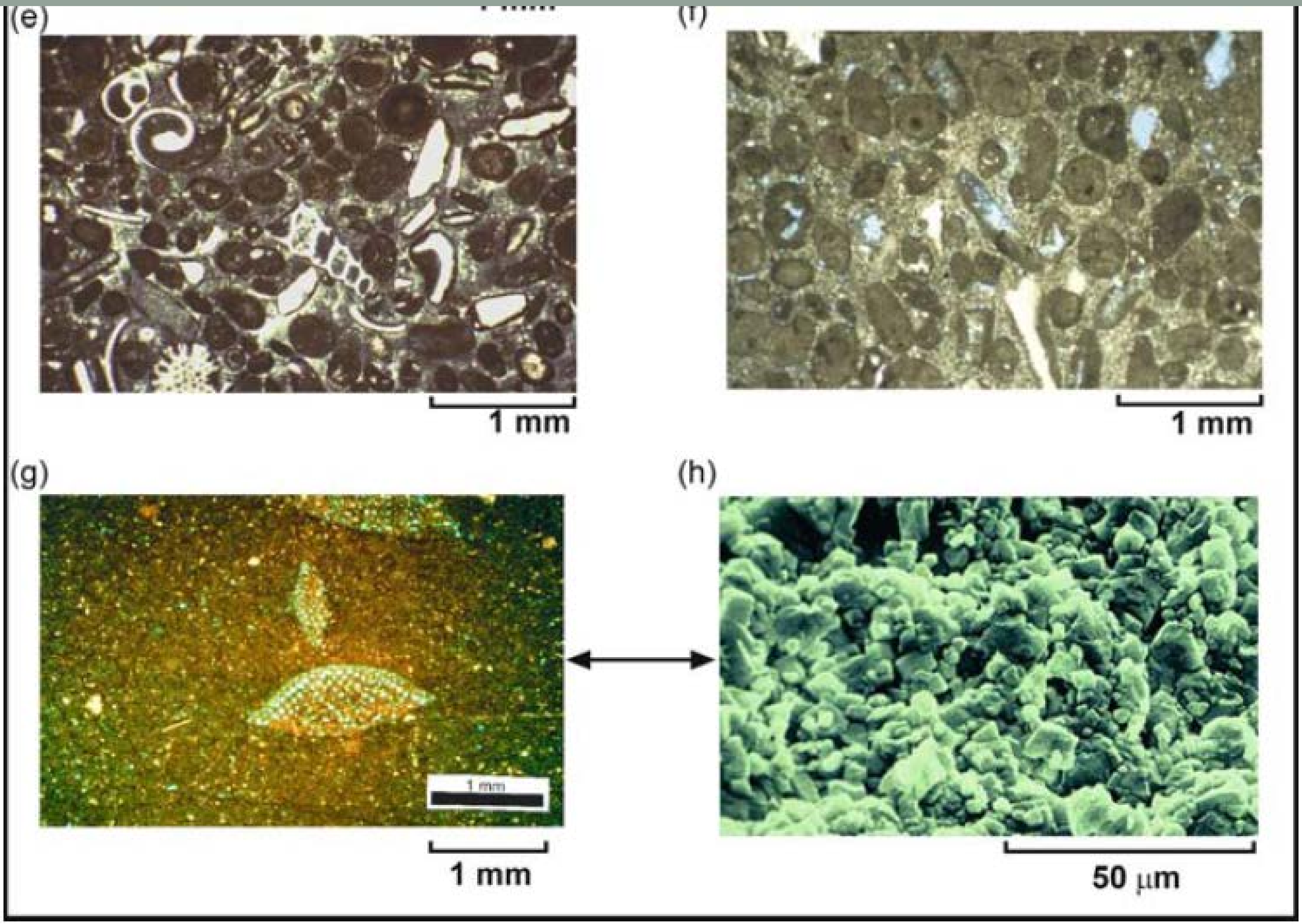

Fig. 2.8. Examples of nonvuggy limestone rock fabrics. **(a)** Grainstone. **(b)** Grainstone with some separate-vug pore space. **(c)** Grain-dominated packstone. **d)** Large grain grain-dominated packstone. **(e)** Mud-dominated packstone. **(f)** Mud-dominated packstone with some separate-vug pore space. **(g)** Wackestone with microporosity. **(h)** Scanning electron microscope photo of microporosity in a wackestone

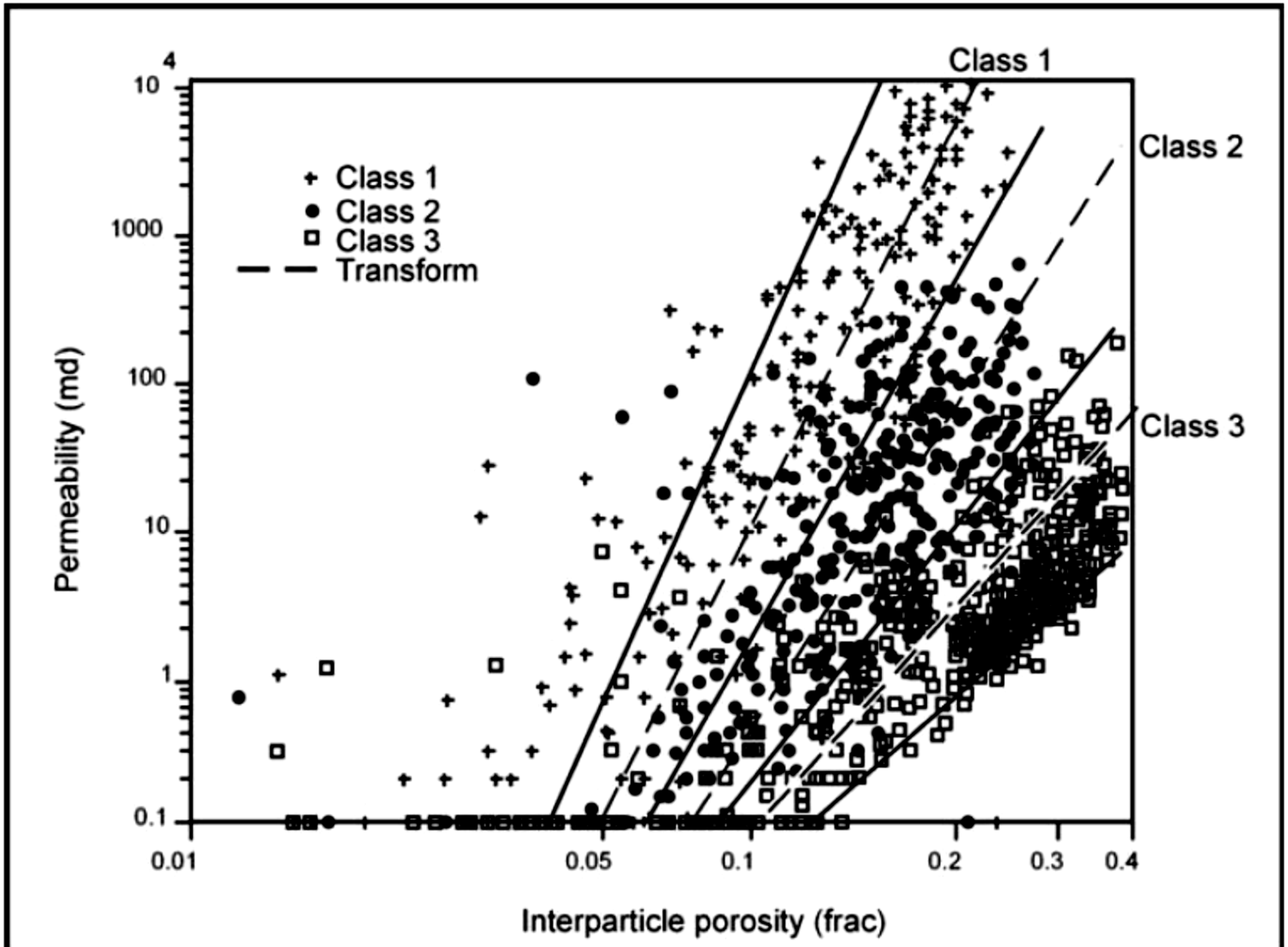

Class 1
Class 2
Class 3
Class 1
Class 2
Class 3
Transform
Permeability (md)
10^4
1000
100
10
1
0.1
0.01
0.05
0.1
0.2
0.3
0.4
Interparticle porosity (frac)

- Permeability and saturation characteristics of interparticle porosity can be grouped into three rock-fabric/petrophysical classes. Class 1 is composed of grainstones, dolograinstones, and large crystalline dolostones. Class 2 is composed of grain-dominated packstones, fine to medium crystalline graindominated dolopackstones, and medium crystalline mud-dominated dolostones. Class 3 is composed of mud-dominated limestone and fine crystalline mud-dominated dolostones.

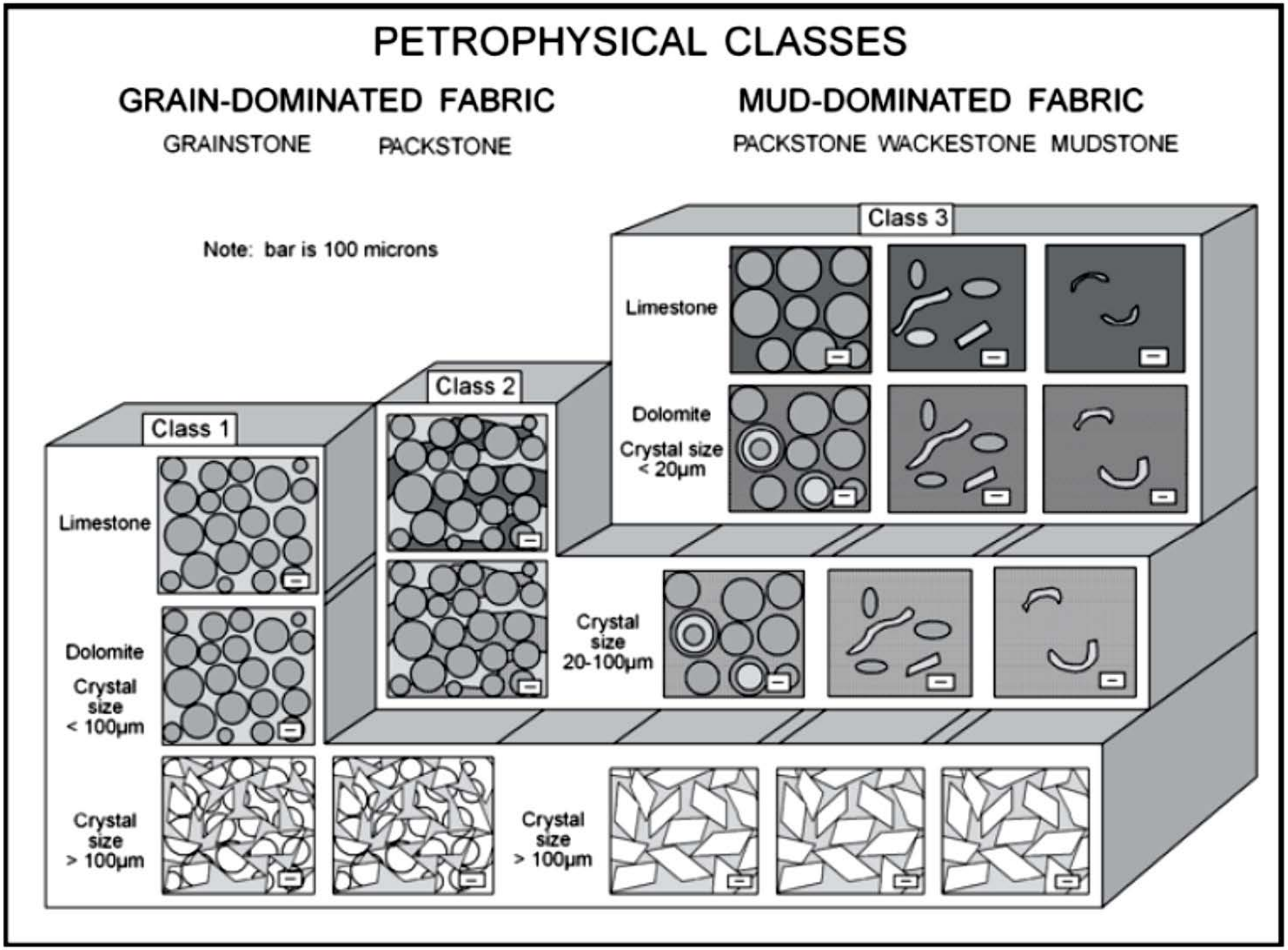
PETROPHYSICAL CLASSES
GRAIN-DOMINATED FABRIC
GRAINSTONE
PACKSTONE
MUD-DOMINATED FABRIC
PACKSTONE WACKESTONE MUDSTONE
Note: bar is 100 microns
Class 3
Limestone
Dolomite
Crystal size
< 20µm
Class 2
Class 1
Limestone
Dolomite
Crystal
size
< 100µm
Crystal
size
20-100µm
Crystal
size
> 100µm
Crystal
size
> 100µm

Class 1 - Grainstones, dolograinstones, and large crystalline dolostones.

$$k = \left(45.35 \times 10^{8}\right)\phi_{ip}^{8.537}$$

$$Sw_i = 0.02219 \times H^{-0.316} \times \phi^{-1.745}$$

Class 2 - Grain-dominated packstones, fine and medium crystalline grain-dominated dolopackstones, and medium crystal mud-dominated dolostones.

$$k = \left(2.040 \times 10^{6}\right)\phi_{ip}^{6.38}$$

$$Sw_i = 0.1404 \times H^{-0.4.07} \times \phi^{-1.440}$$

Class 3 - Mud-dominated limestones and fine crystalline mud-dominated dolostones.

$$k = \left(2.884 \times 10^{3}\right)\phi_{ip}^{4.275}$$

$$Sw_i = 0.6110 \times H^{-0.505} \times \phi^{-1.210}$$

Vuggy Porosity

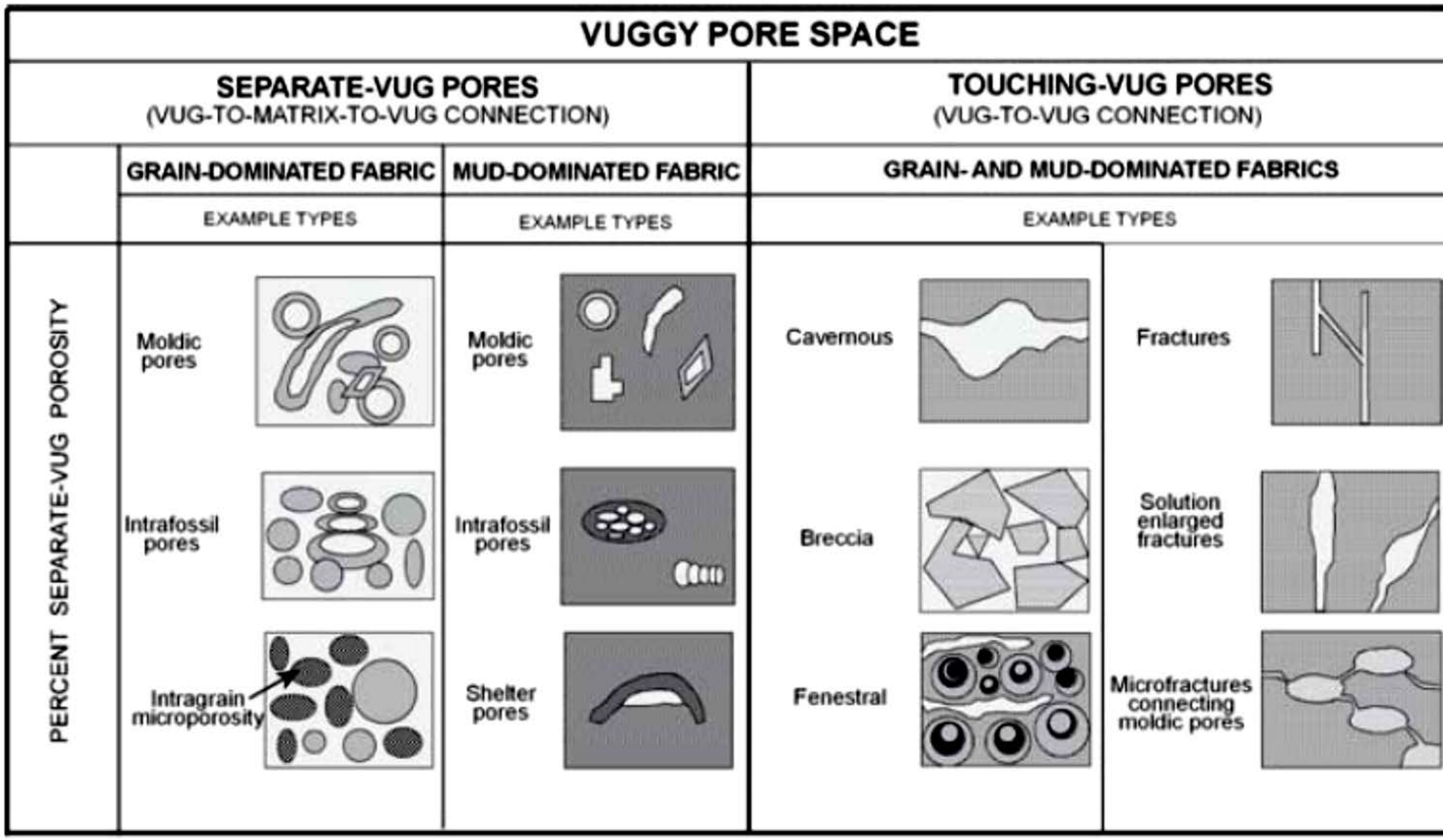

Separate-Vug

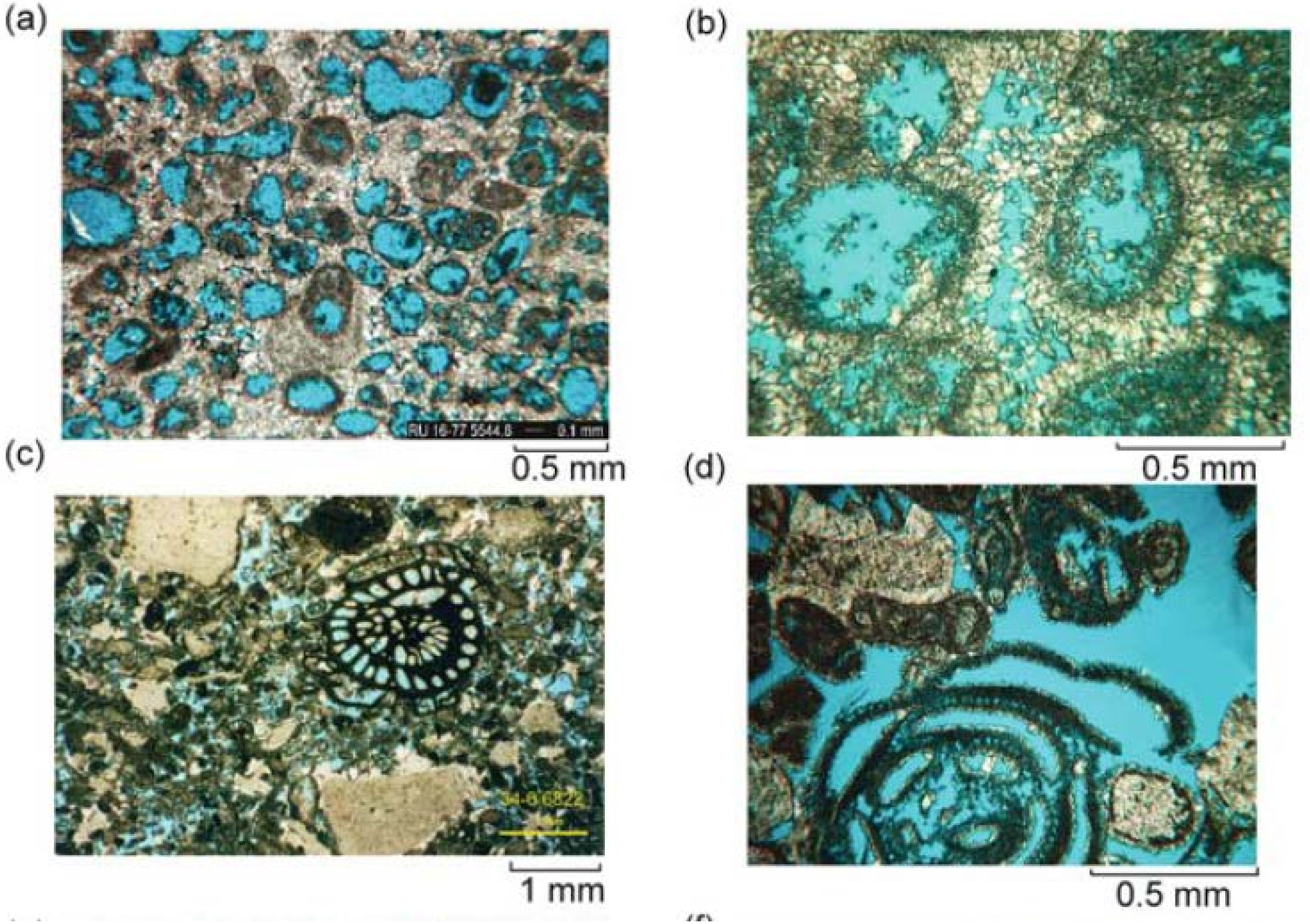

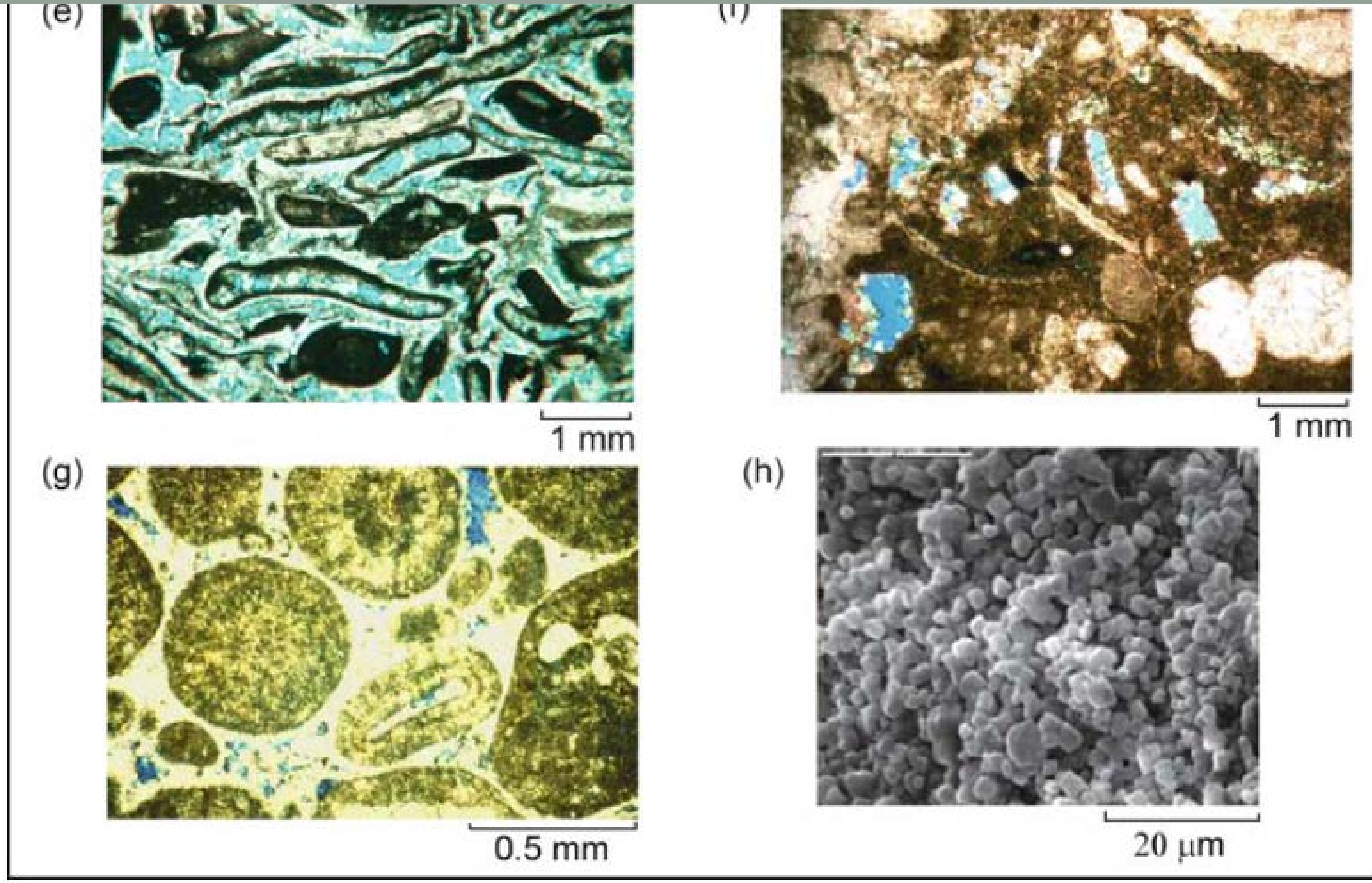

Fig. 2.20. Examples of separate-vug pore types. **(a)** Oomolds in oomoldic grainstone. **(b)** Oomolds and intergrain pore space in a grainstone. **(c)** Intrafossil pore space in a fusulinid grain-dominated packstone. **(d)** Intrafossil pore space in a foram with a large opening to interparticle pore space. **(e)** Skeletal grain molds in moldic skeletal grainstone. **(f)** Grain molds in a wackestone. **(g)** Ooid grainstone with intragrain microporosity. **(h)** Scanning electron photomicrograph of intragrain microporosity showing micropores in a 5-micron rhombic calcite matrix

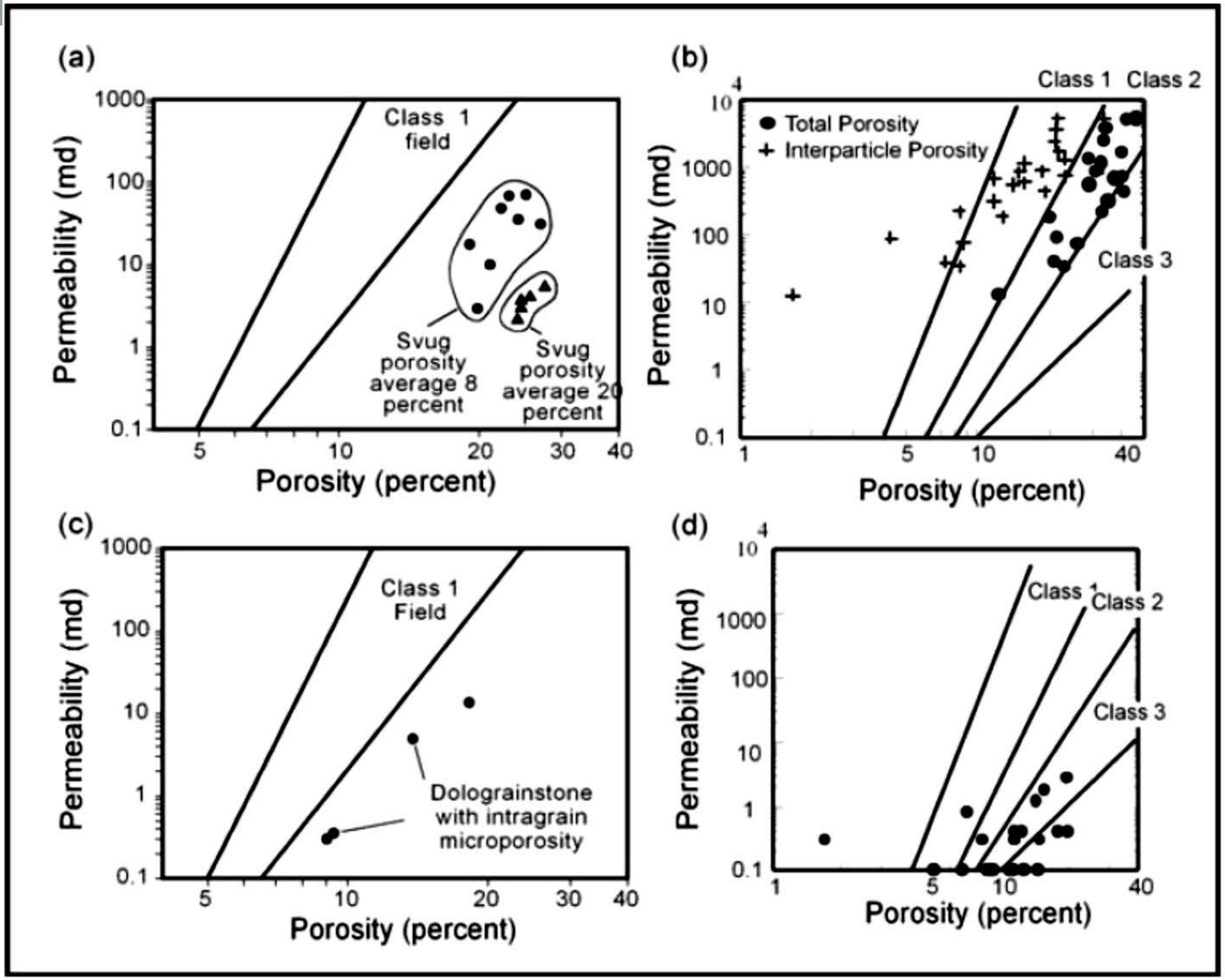

Fig. 2.21. Cross plot illustrating the effect of separate-vug porosity on air permeability. **(a)** Grainstones with separate-vug porosity in the form of grain molds plot to the right of the grainstone field in proportion to the volume of separate-vug porosity. **(b)** Grainstones with intrafossil and intragrain microporosity plot in the class 2 field when plotted against total porosity. **(c)** Dolograinstones with intragrain microporosity plot in the class 2 field. **(d)** Grainstones with intragrain microporosity plot in the class 3 field

- The addition of separate-vug porosity to interparticle porosity increases total porosity but does not significantly increase permeability. Therefore, it is important to determine interparticle porosity by subtracting separate-vug porosity from total porosity and using interparticle porosity to estimate permeability. The effect of separate vugs on permeability and initial water saturation depends upon the size of the pores connecting the intra- and intergrain pore space. Large separate vugs are normally filled with hydrocarbons above the transition zone. Intragrain microporosity will contain significant amounts of capillary-bound water within the transition zone, resulting in water-free production of hydrocarbons from intervals with high initial water saturations. The transition zone for grainstones with large volumes of separate vugs will be greater than that expected for a nonvuggy grainstone.

Touching Vug

(a)

(b)

(d)

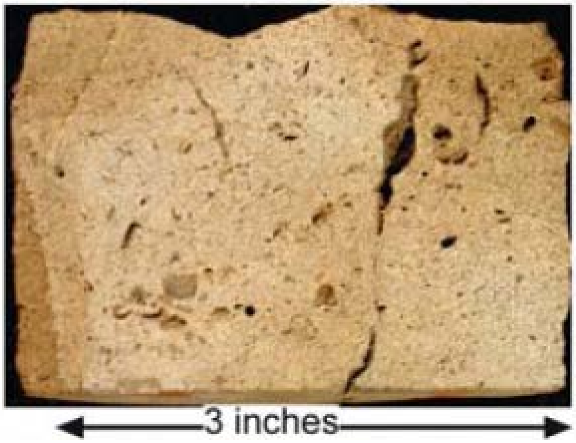

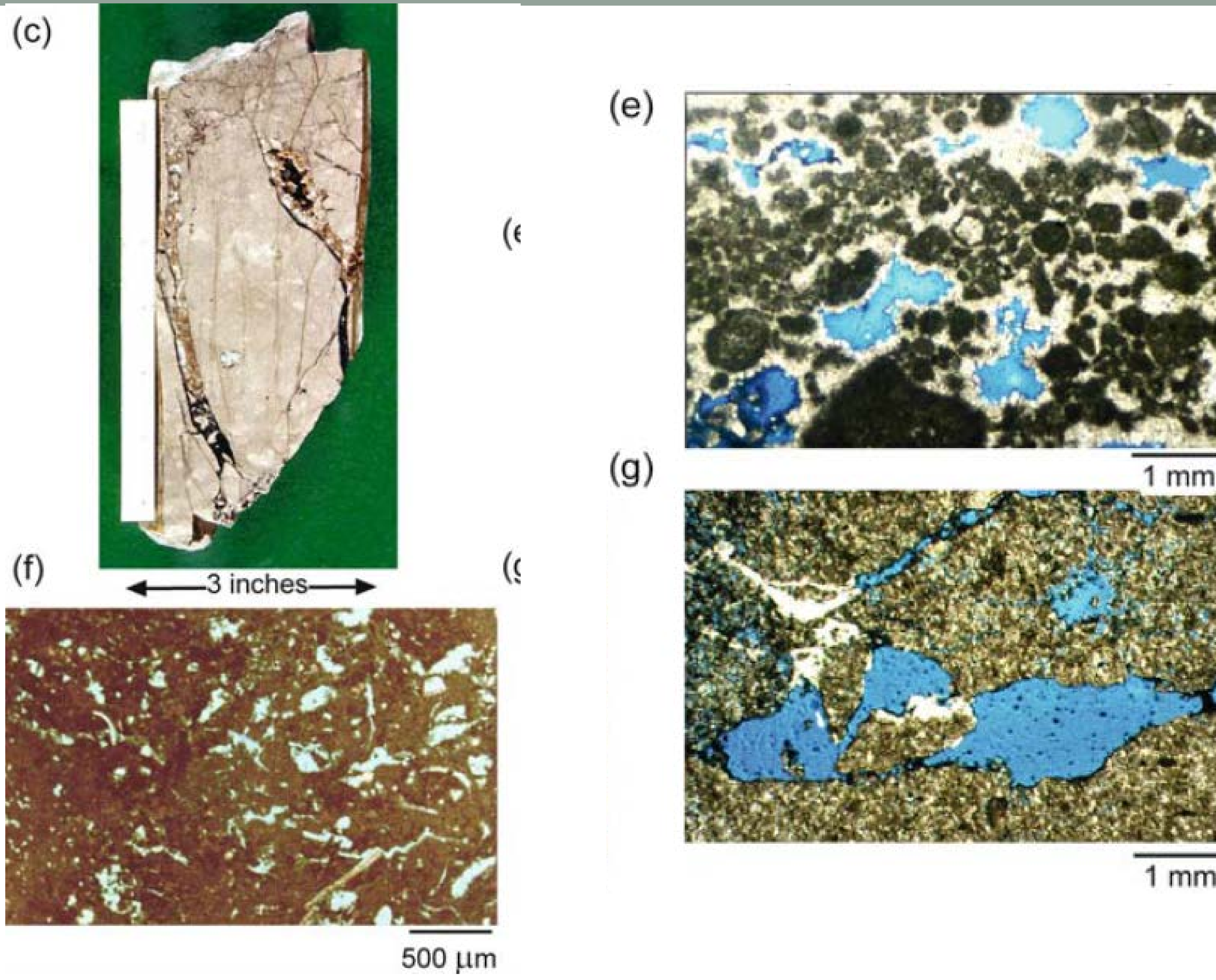
(c)
3 inches
(e)
1 mm
(g)
1 mm
(f)
500 µm

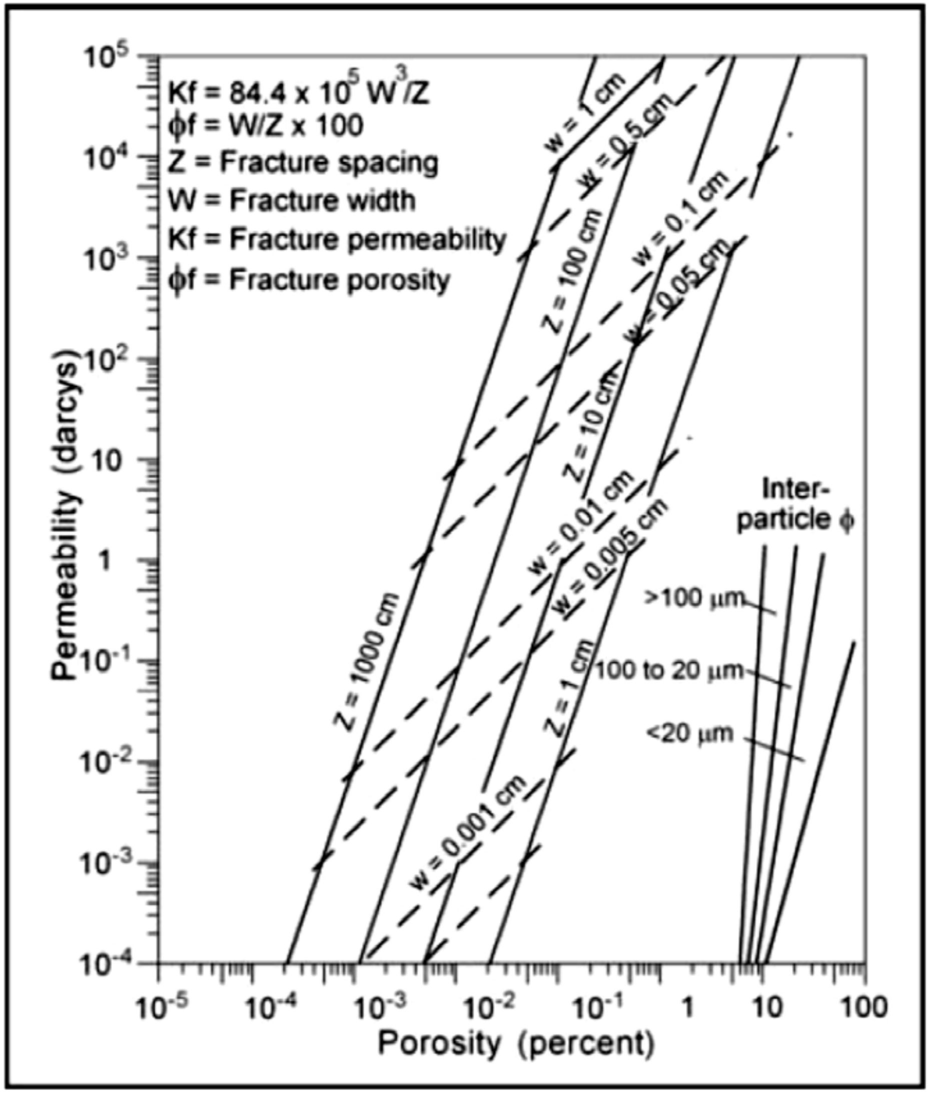

Kf = 84.4 x 10^5 W^3/Z
ϕf = W/Z x 100
Z = Fracture spacing
W = Fracture width
Kf = Fracture permeability
ϕf = Fracture porosity
w = 1 cm
w = 0.5 cm
w = 0.1 cm
w = 0.05 cm
w = 0.01 cm
w = 0.005 cm
w = 0.001 cm
Z = 1000 cm
Z = 100 cm
Z = 10 cm
Z = 1 cm
Inter-
particle ϕ
>100 µm
100 to 20 µm
<20 µm
Permeability (darcys)
Porosity (percent)

- Touching-vug pore systems cannot be related to porosity but are related to the geometry of fracture pore space, large vugs, and collapse breccia. These pore systems are normally larger than the well bore and cannot be adequately studied using cores. Small touching-vug systems formed by microfractures and grain dissolution connecting grain molds can be characterized by core measurements. These systems enhance permeability 5x to 10x over that expected from matrix permeability.

Making Sense of Carbonate Pore Systems

Making sense of carbonate pore systems

Arve Lønøy

AUTHOR

Arve Lønøy ~ *Norsk Hydro Oil & Energy, Sandsliveien 90, N-5049 Sandsli, Bergen, Norway; arve.lonoy@hydro.com*

Arve Lønøy received a Cand. Real. degree in carbonate sedimentology from the University of Bergen in 1981. He has since then worked as a research geologist on carbonate sedimentology and, to a lesser extent, siliciclastic petrography in the Norsk Hydro Research Center. His main work on carbonates has been on Paleozoic carbonates of the Arctic (Norway, Canada, and Russia) and the Mesozoic of western Africa and the Middle East.

Based on empirical data, mostly from Europe and the Middle East, a new pore-type classification system has been developed. The new system not only uses elements from existing pore-type classification systems, but also introduces many new elements. The new pore-type system includes 20 pore-type classes that show a predictable relation between porosity and permeability. It combines sedimentologic and diagenetic features with flow-related properties, and reservoir-critical parameters can thus be predicted using sedimentologic and diagenetic models.

Table 1. Porosity-Permeability Coefficients of Determination (R^2) for the Lucia (1983, 1995, 1999) and Choquette and Pray (1970) Classification Systems*

Pore Type	R^2
Lucia (1983, 1995, 1999) Classification System	
Interparticle, class 3	0.68
Interparticle, class 2	0.62
Interparticle, class 1	0.79
Vuggy, separate	0.86
Vuggy, touching	0.45
Choquette and Pray (1970) Classification System	
Interparticle	0.70
Intercrystalline	0.50
Moldic	0.88
Intraparticle	0.86
Vuggy	0.50

*Using samples from the present study.

Table 2. New Porosity Classification System*

Pore Type	Pore Size	Pore Distribution	Pore Fabric	R^2
Interparticle	Micropores (10–50 μm)	Uniform	Interpartide, uniform micropores	0.88
		Patchy	Interpartide, patchy micropores	0.79
	Mesopores (50–100 μm)	Uniform	Interpartide, uniform mesopores	0.86
		Patchy	Interpartide, patchy mesopores	0.85
	Macropores (>100 μm)	Uniform	Interpartide, uniform macropores	0.88
		Patchy	Interpartide, patchy macropores	0.87
Intercrystalline	Micropores (10–20 μm)	Uniform	Intercrystalline, uniform micropores	0.92
		Patchy	Intercrystalline, patchy micropores	0.79
	Mesopores (20–60 μm)	Uniform	Intercrystalline, uniform mesopores	0.94
		Patchy	Intercrystalline, patchy mesopores	0.92
	Macropores (>60 μm)	Uniform	Intercrystalline, uniform macropores	0.80
		Patchy	Intercrystalline, patchy macropores	
Intraparticle			Intrapartide	0.86
Moldic	Micropores (<10–20 μm)		Moldic micropores	0.86
	Macropores (>20–30 μm)		Moldic macropores	0.90
Vuggy			Vuggy	0.50
Mudstone microporosity	Micropores (<10 μm)		Tertiary chalk	0.80
			Cretaceous chalk	0.81
		Uniform	Chalky micropores, uniform	0.96
		Patchy	Chalky micropores, patchy	

*Partly based on Choquette and Pray (1970) and Lucia (1983, 1995, 1999). Porosity-permeability coefficients of determination (R^2) are based on samples from the present study.

- the new classification scheme was to incorporate the observation of Lucia (1983) that pore size is a primary factor in understanding porosity-permeability relationships. Whereas Lucia recognized the control of pore size on porosity permeability relationships, his classification scheme uses grain size (of particles or crystals) instead of pore size as the primary means of pore class division (i.e., his interparticleclasses1, 2, and3). In this study, direct description of pore size was used (instead of particle or crystal size). This is in part because of the range of sorting observed in many samples that made classification of particle size problematic and partly because later cements commonly act to occlude pore space, making the relation of pore size to grain size indirect. The result of incorporating pore size into the systemwas a further increase in the R2.

- Important modifications include the addition of uniform and patchy porosity distribution and the incorporation of mudstone microporosity made to achieve high R2 values.
- In this Article, Thin-section porosity was impregnated with bluedyed epoxy for visualization of pore types. Helium porosity and air permeability (Klinkenberg corrected) were measured on horizontal and a few vertical plugs.

The main differences between the new carbonate pore system and those of Choquette and Pray (1970) and Lucia (1983, 1995, 1999) are as follows:

- Porosity distribution is a major new element in the classification.
- Lucia's subdivision of interparticle porosity has been partly incorporated into the new classification system, but is now based on pore size instead of grain size and sorting.
- Lucia's three interparticle pore-type classes and Choquette and Pray's interparticle and intercrystalline porosity types have been subdivided into 12 new classes (6 interparticle and 6 intercrystalline).
- Micromoldic and macromoldic pores are differentiated.
- A new pore-type category, consisting of four pore types, is introduced: mudstone microporosity.

The new classification system combines sedimentologic and diagenetic features with flow-related properties, and reservoir-critical parameters can thus be predicted using sedimentologic and diagenetic models.

The new classification system is based on three main elements: pore type, pore size, and pore distribution. Age is an important factor for some of the mudstone micropore classes.

Pore Type

Six main pore types are identified: interparticle, intercrystalline, vuggy, intraparticle, moldic, and mudstone microporosity (Table 2). The first five pore types are almost identical to those defined by Choquette and Pray (1970), whereas the last one is new.

Pore Size

Lucia (1983, 1995, 1999) realized that pore-size distribution controls permeability and is related to rock fabric. Therefore, he used average particle size and sorting to differentiate between different interparticle pore-type classes. The term "particle" was used as a general term for grains (multicrystalline particles) and crystals (single-crystal particles) (Lucia, 1983).

Interparticle pore diameters and size distributions were measured on the reference samples shown in Figure 1a–c. Micropores have a dominant pore diameter in the 10–60-μm range (70% of the pores). Mesopores have a dominant pore diameter of 40–100 μm, although approximately 30% of the pores are in the 100–300-μm range. Macropores are generally larger than 100 μm in diameter (approximately 75% of the pores). Interparticle pore-size groups may thus be defined by 10–50 (micropores), 50–100 (mesopores), and greater than 100 μm (macropores). Porosity with dominant pore diameters less than 10 μm is classified as mudstone microporosity.

Intercrystalline micropores are commonly 10–20 μm in diameter, whereas mesopore diameters mostly are in the 20–60-μm range. Intercrystalline macropores have diameters larger than 60 μm.

Moldic micropore diameters are typically less than 10–20 μm, although they occasionally can be larger. Moldic macropores are larger than 20–30 μm.

Figure 1. Thin-section micrographs showing samples with a predominance of interparticle porosity, some of which are solution enlarged. Minor intraparticle and moldic pores are present, but interparticle pores predominate

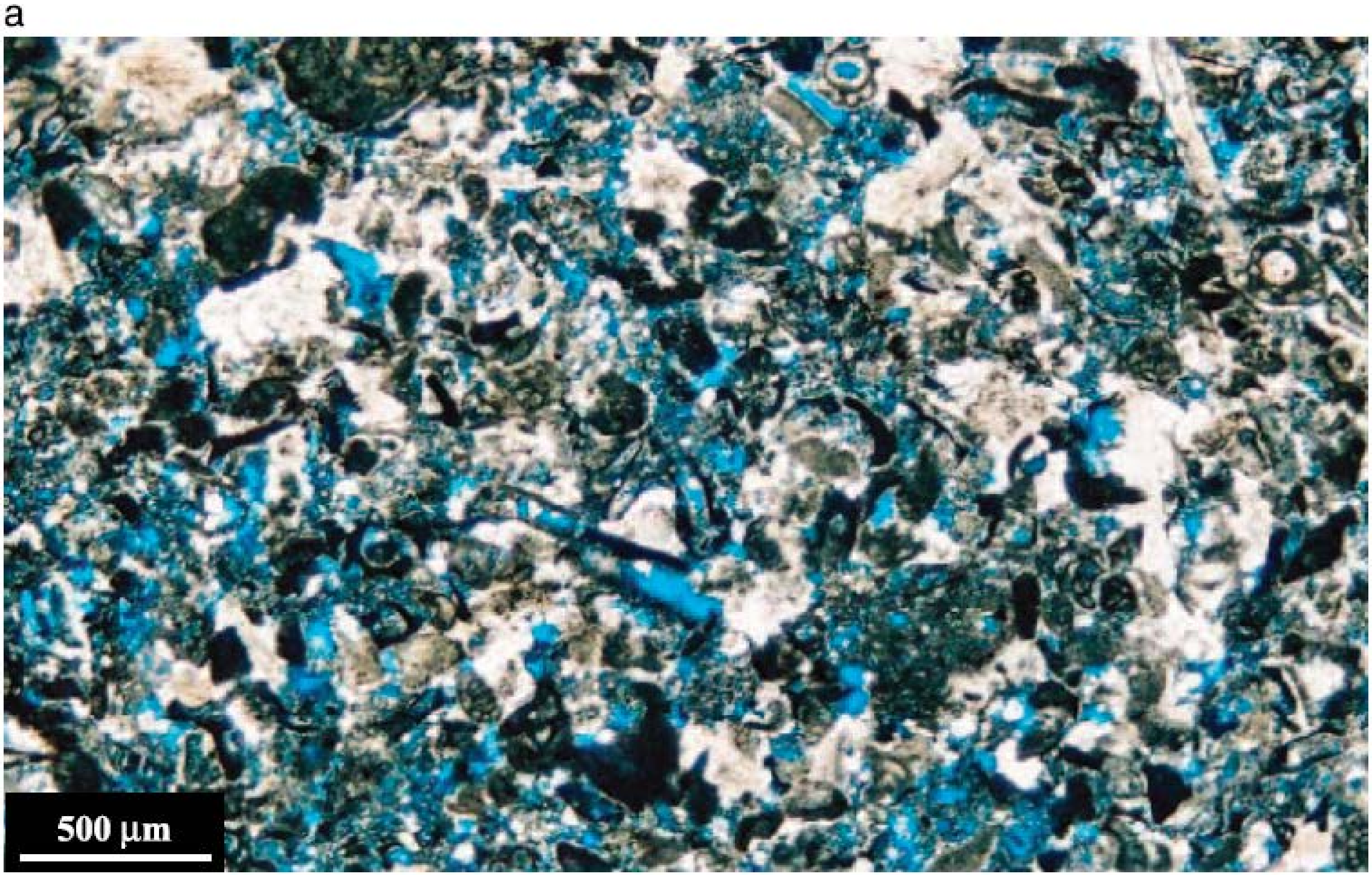

Microporosity (10–50 mm pore diameter) with uniform porosity distribution, f = 17.6%, k = 0.84 md;

b

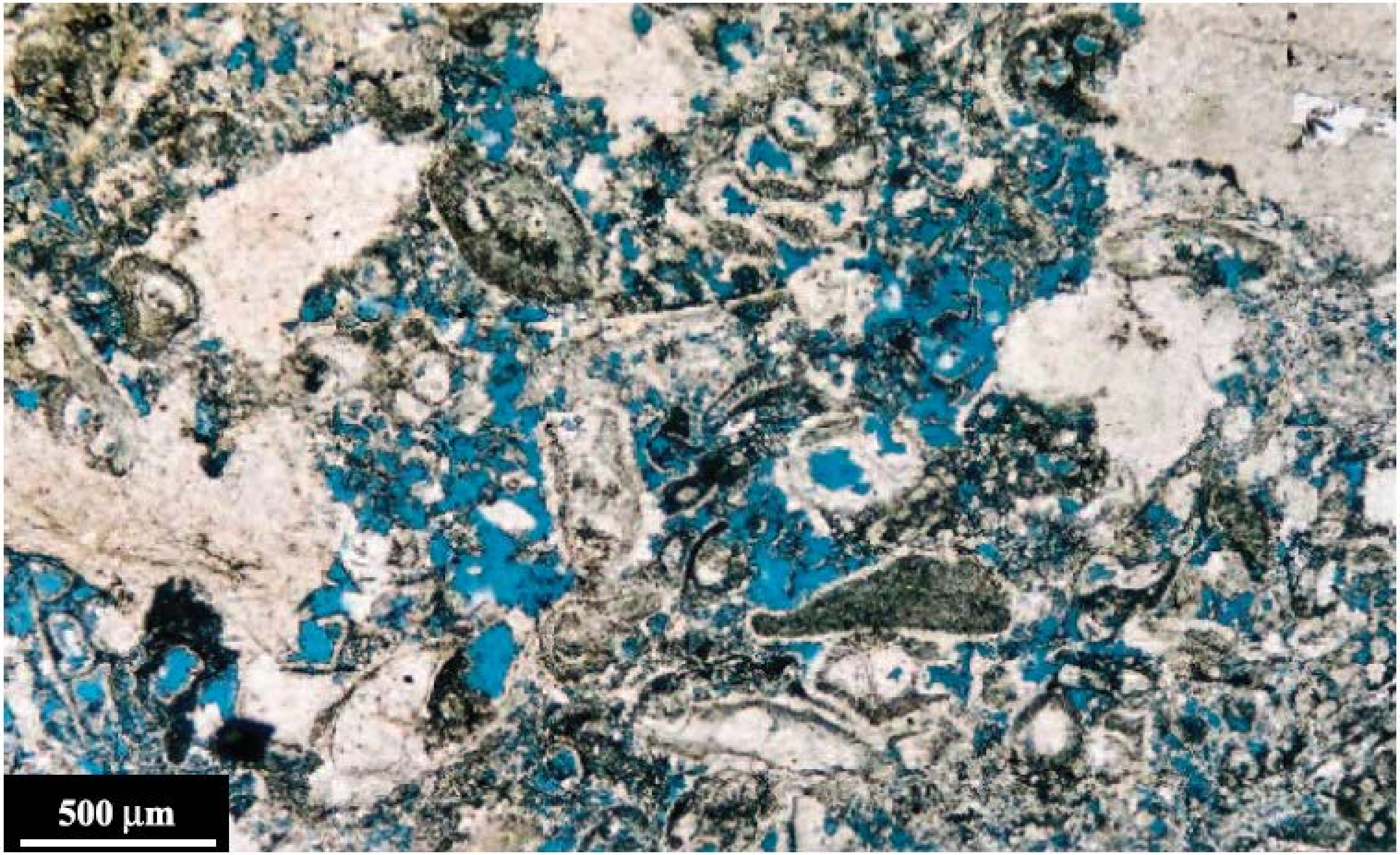

mesoporosity (50–100 mm pore diameter) with uniform porosity distribution, f = 19.3%, k = 9.47 md;

c

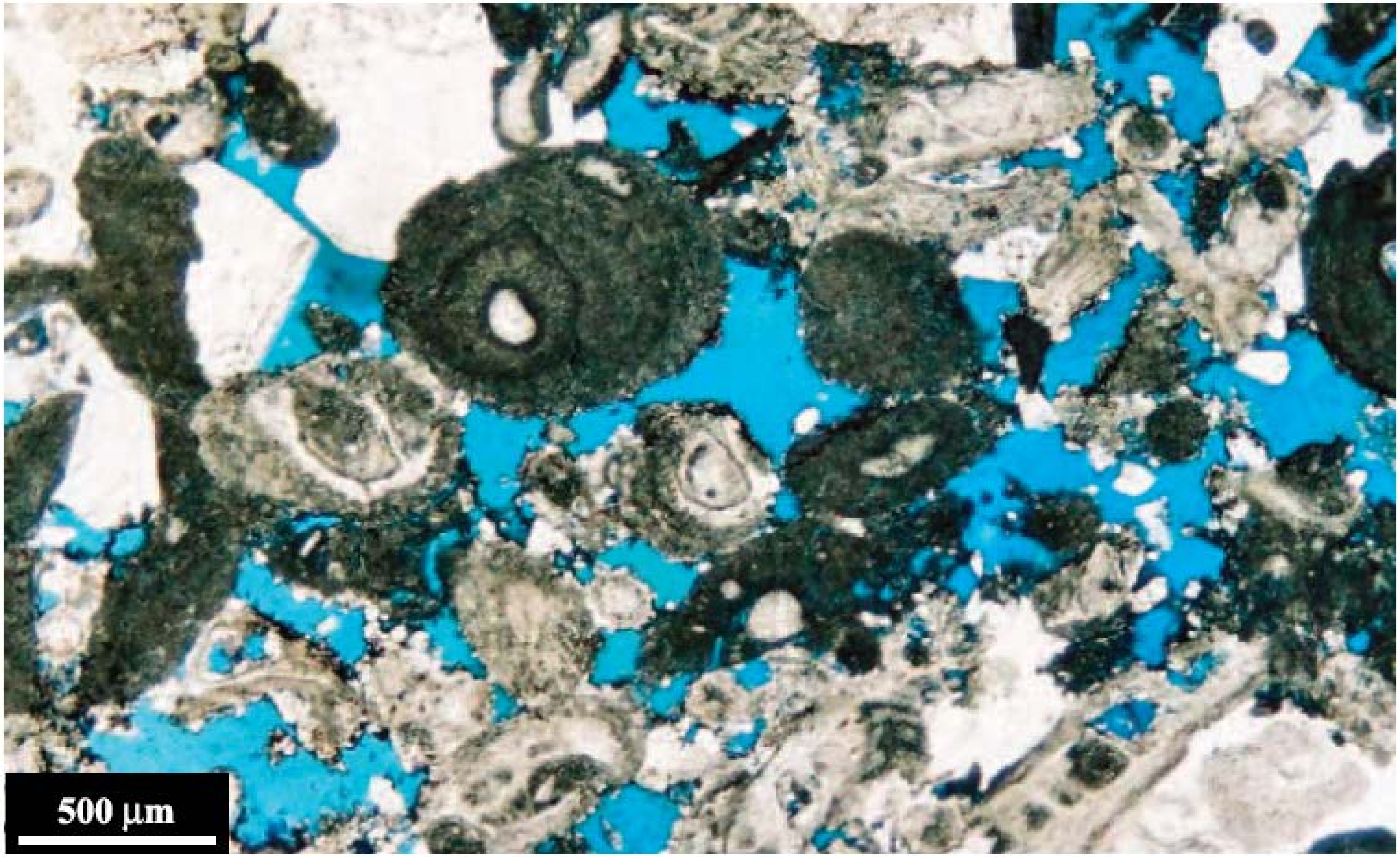

Macroporosity (>100 mm pore diameter) with uniform porosity distribution, f = 15.3%, k = 132 md;

d

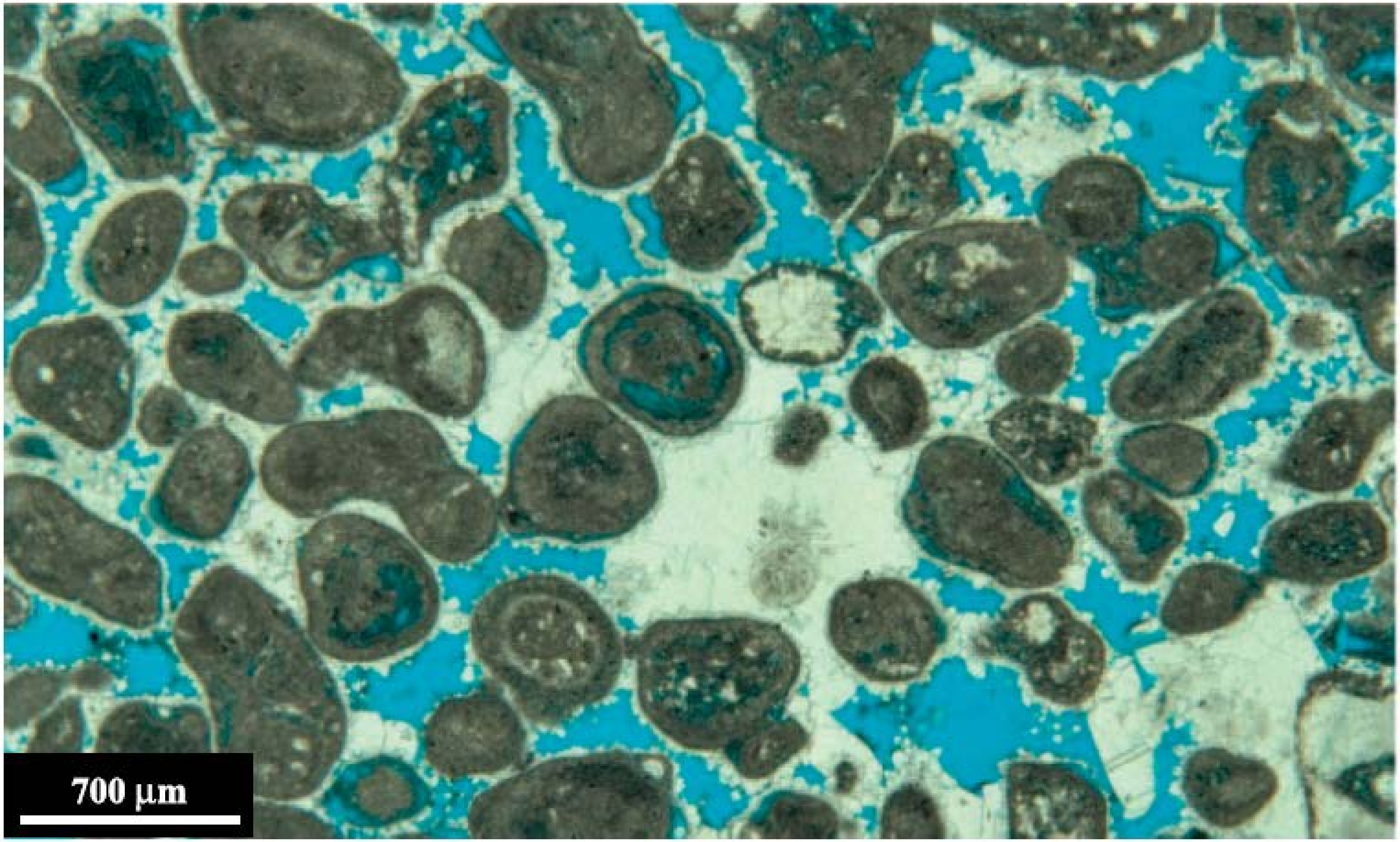

macroporosity (>100 mmpore diameter) with uniform porosity distribution and porelining calcite cement, f = 9.7%, k = 0.465 md.

Pore Distribution

Porosity distribution is a new element in pore-type classification and has a significant effect on porosity-permeability relationships (also noted by Lucia et al., 2004a, b). The distribution of interparticle pores, intercrystalline pores, and mudstone micropores has been visually classified as either uniform or patchy.

At similar porosities, a patchy porosity distribution is observed to yield significantly higher permeability than uniform porosity distribution. The reason for this is that the porosity is concentrated over a smaller volume and the pore system is better connected than for an equivalent, uniformly distributed pore volume. Furthermore, a patchy porosity distribution is often related to secondary dissolution with slight corrosion of pore throats, and this process also tends to favor connected pores.

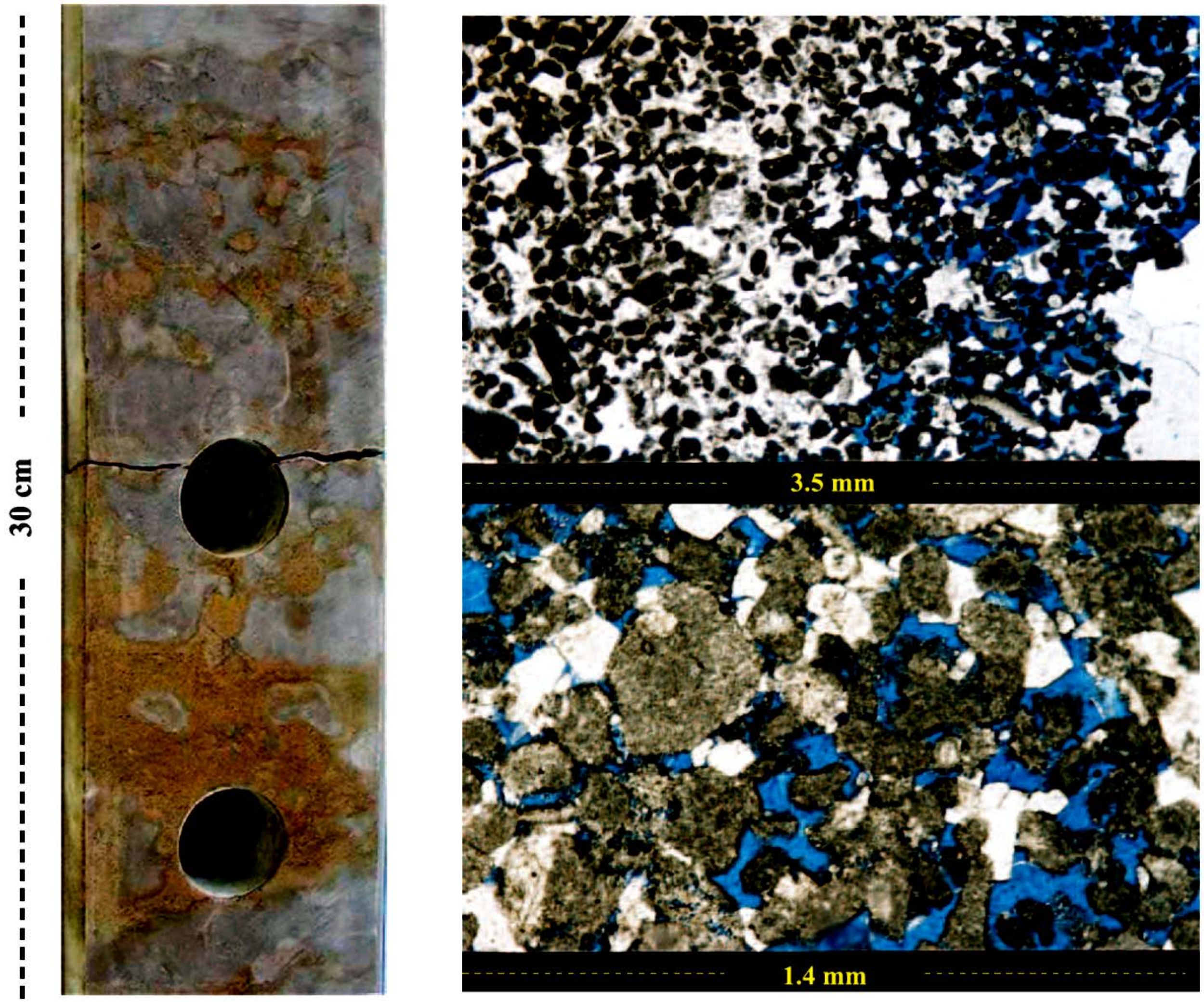

Figure 2. Example of patchy interparticle mesoporosity (50–100 μm pore diameter) in Devonian rocks from Russia. Left: core slab showing patchy pore distribution related to differential dissolution. Tight, calcite-cemented areas are gray; porous, oil-stained areas are brown. Right: thin-section photomicrographs showing patchy interparticle mesopores related to differential dissolution of cements. Lower photomicrograph is a close-up showing patchy porosity at a larger scale. Note the abundance of rhombohedral pore outlines, which are indicative of dissolution. Calcite cements are white. Both photomicrographs were taken under plane-polarized light.

PORE-TYPE DEFINITIONS

Interparticle Porosity:

- Choquette and Pray (1970) defined interparticle porosity as porosity occurring between grains (intergrain). Lucia (1983) extended the term “interparticle” to also include pore spaces between crystals (intercrystal). This redefinition thus included both the interparticle and intercrystalline porosity types of Choquette and Pray (1970). However, the results of this study show that the petrophysical properties of intergrain and intercrystal pores are different.

- Interparticle pores are normally associated with medium- to high-energy depositional settings in the studied data set, such as rimmed, platform-margin shoals, distally steepened ramp-margin shoals, inner-rampfringing shoals, middle-ramp barrier shoals, local platforminterior shoals, gravity-driven flow deposits, beaches, wash-over fans, and others. Micropores and mesopores occur within grain-supported textures composed of extremely small bioclastic fragments, where larger interparticle pores have been partially occluded by cement, or within poorly sorted grainstones. Micropores also occurwithin recrystallized mud of mud-lean packstones. Macropores are most common in moderately to well sorted, high-energy grainstones.

Intercrystalline Porosity:

- Intercrystalline porosity is the porosity between crystals that may be of either primary or secondary origin (Choquette and Pray, 1970). All intercrystalline pores included in the studied data set are secondary in origin and occur between crystals that have grown more or less in place by calcite recrystallization or dolomitization.

a

microporosity (10–20 mm pore diameter) with uniform porosity distribution, f = 18.1%, k = 0.476 md;

b

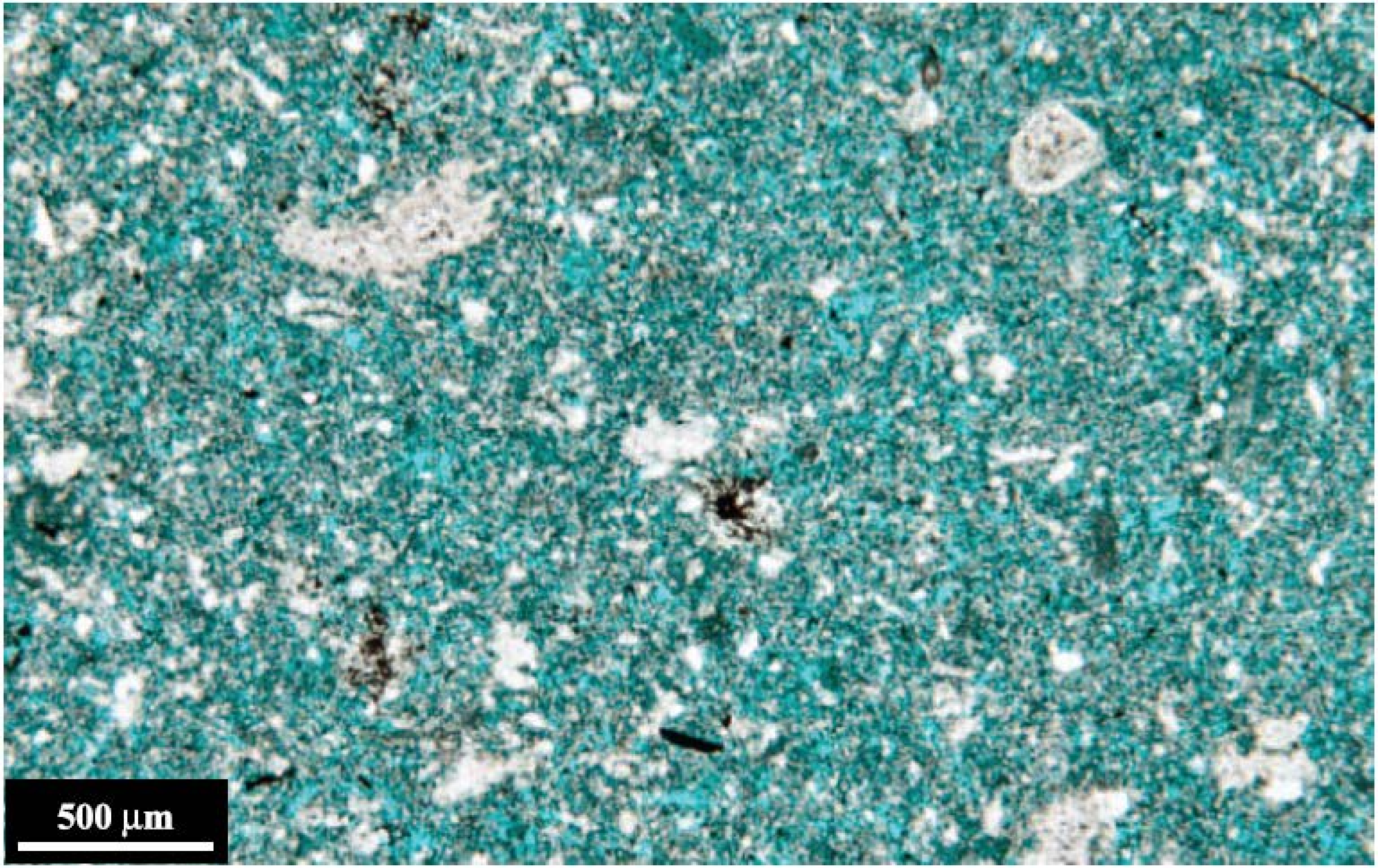

Mesoporosity (20–60 mm pore diameter) with uniform porosity distribution, f = 19.3%, k = 4.93 md;

c

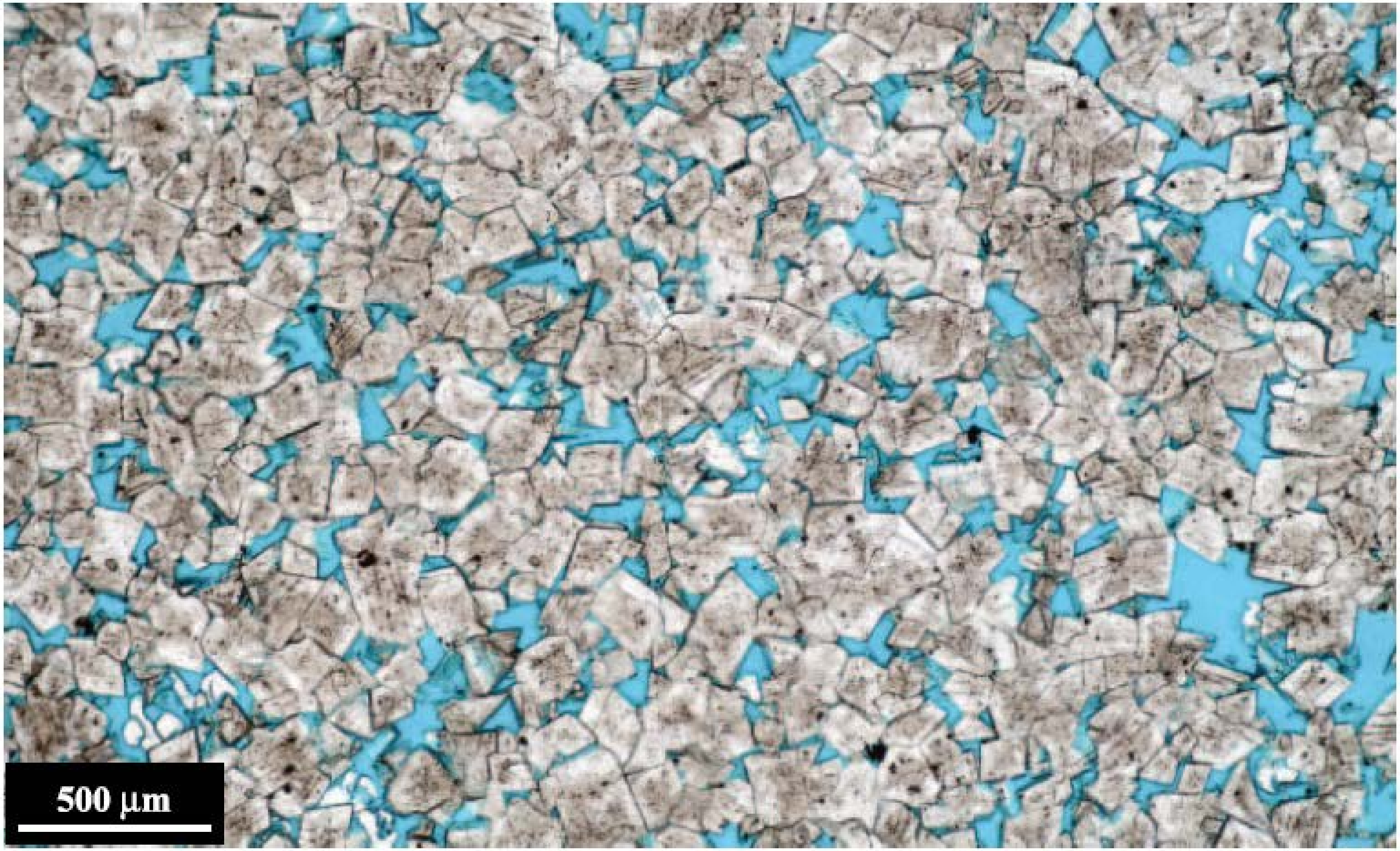

macroporosity (>60 mm pore diameter) with uniform porosity distribution, f = 11.0%, k = 16.7 md;

d

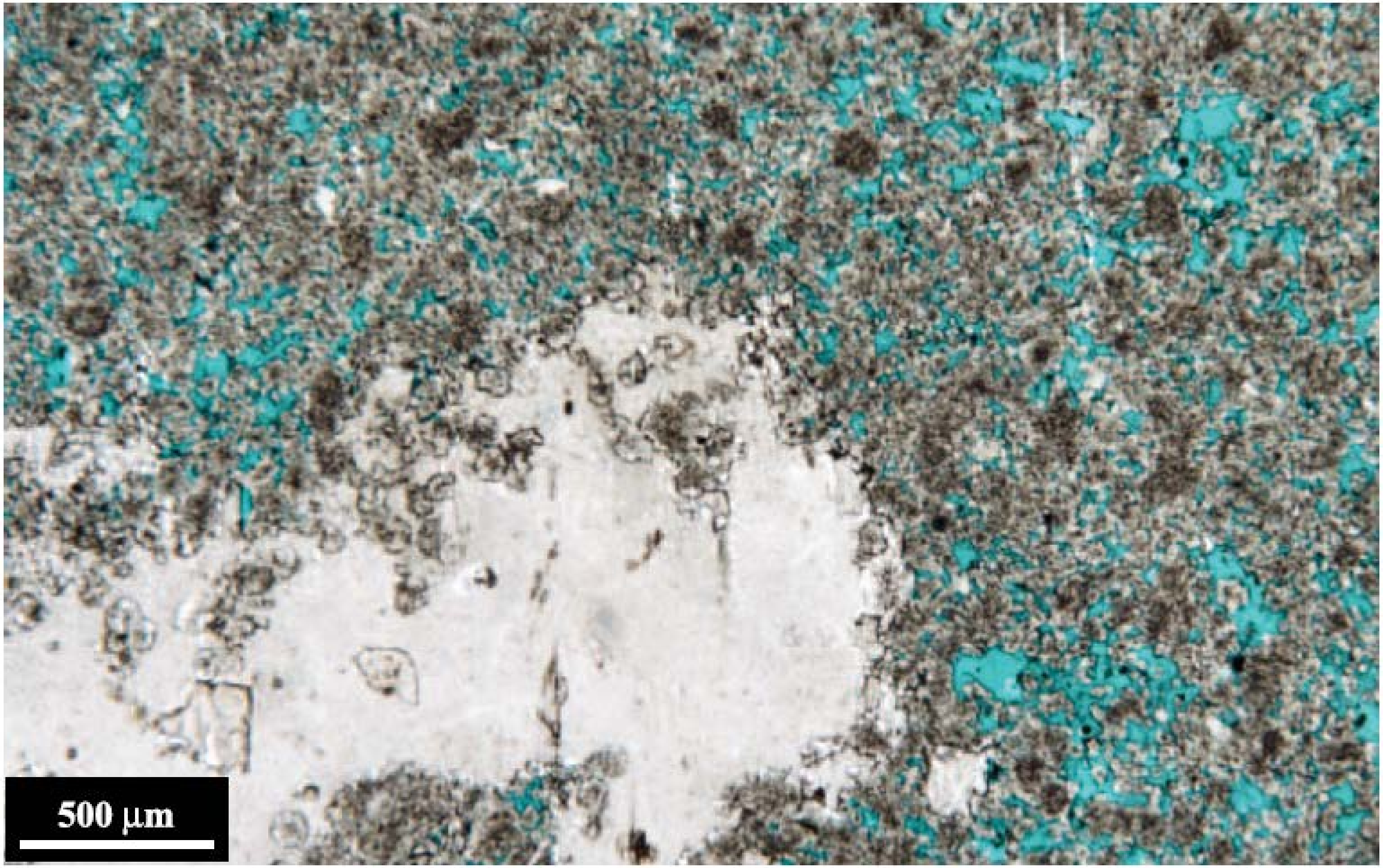

Mesoporosity (20–60 mm pore diameter) with patchy porosity distribution related to gypsum cementation (white); f = 12.1%, k = 16.0 md.

Mudstone Microporosity:

- Mudstone micropores have extremely small pore sizes, commonly a few micrometers in diameter. Individual pores cannot be seen with a standard petrographic microscope.
- Chalk micropores are primary in origin and occur between grains of planktonic calcareous algae (coccospheres) or their component crystal plates (coccoliths). Chalky micropores are not related to chalk, but the pore structure is similar. These pores occur between recrystallized mud particles and may be formed either during early meteoric leaching or deeper burial diagenesis (Pittman, 1971; Budd, 1989; Moshier, 1989). The pores typically form in low-energy, muddy, platform-interior facies.

- Four natural classes of mudstone microporosity exist in the database: (1) Tertiary chalk, (2) Cretaceous chalk, (3) chalky micropores with uniform distribution, and (4) chalky micropores with patchy distribution. The distinction between Tertiary and Cretaceous chalks is important because a general decrease in the size of calcareous nannoplankton across the Cretaceous–Tertiary boundary (Macleod et al., 1997) corresponds to a decrease in reservoir quality in Tertiary chalks (Hardman, 1983).

a

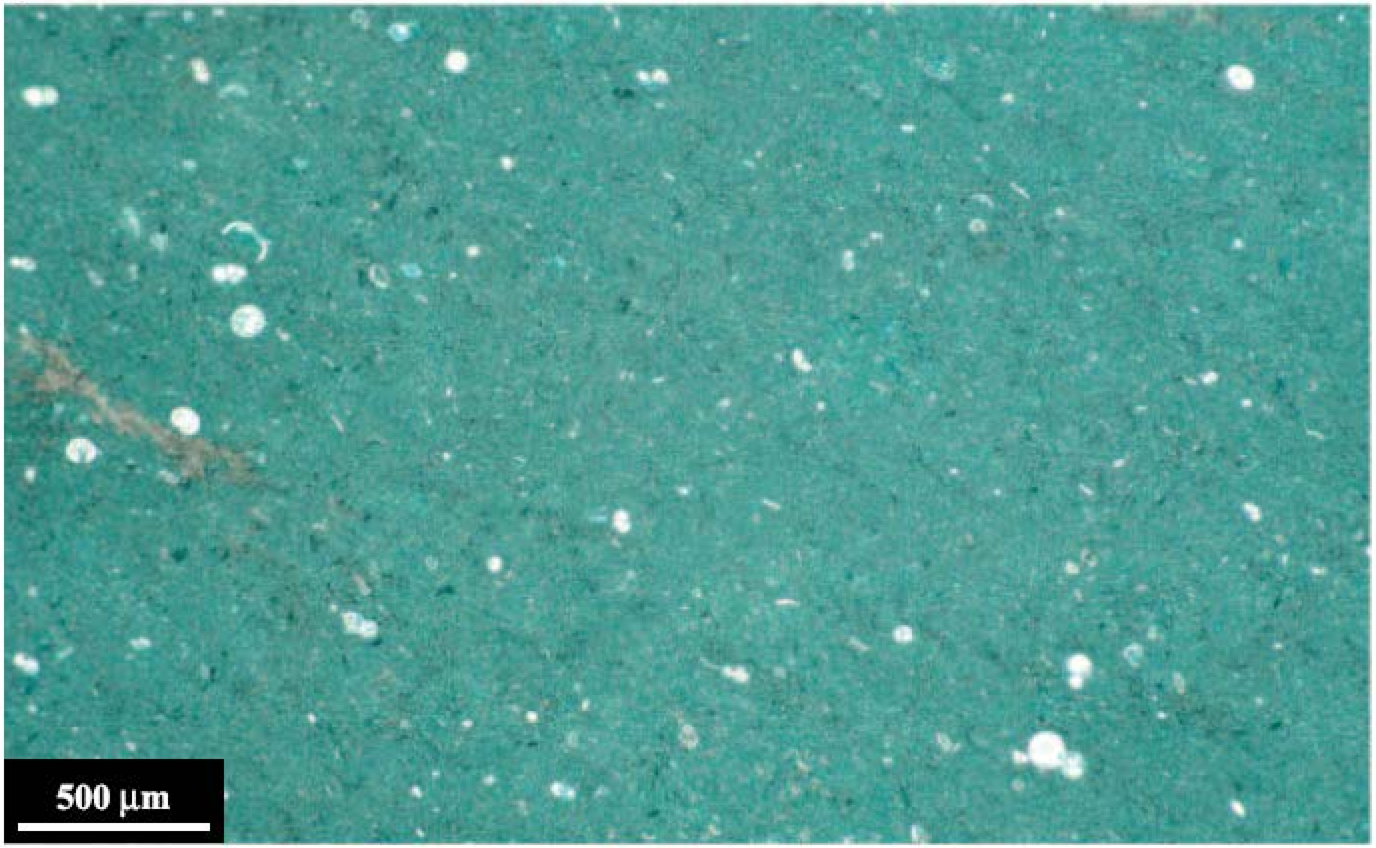

chalk, f = 25.4%, k = 0.734 md;

b

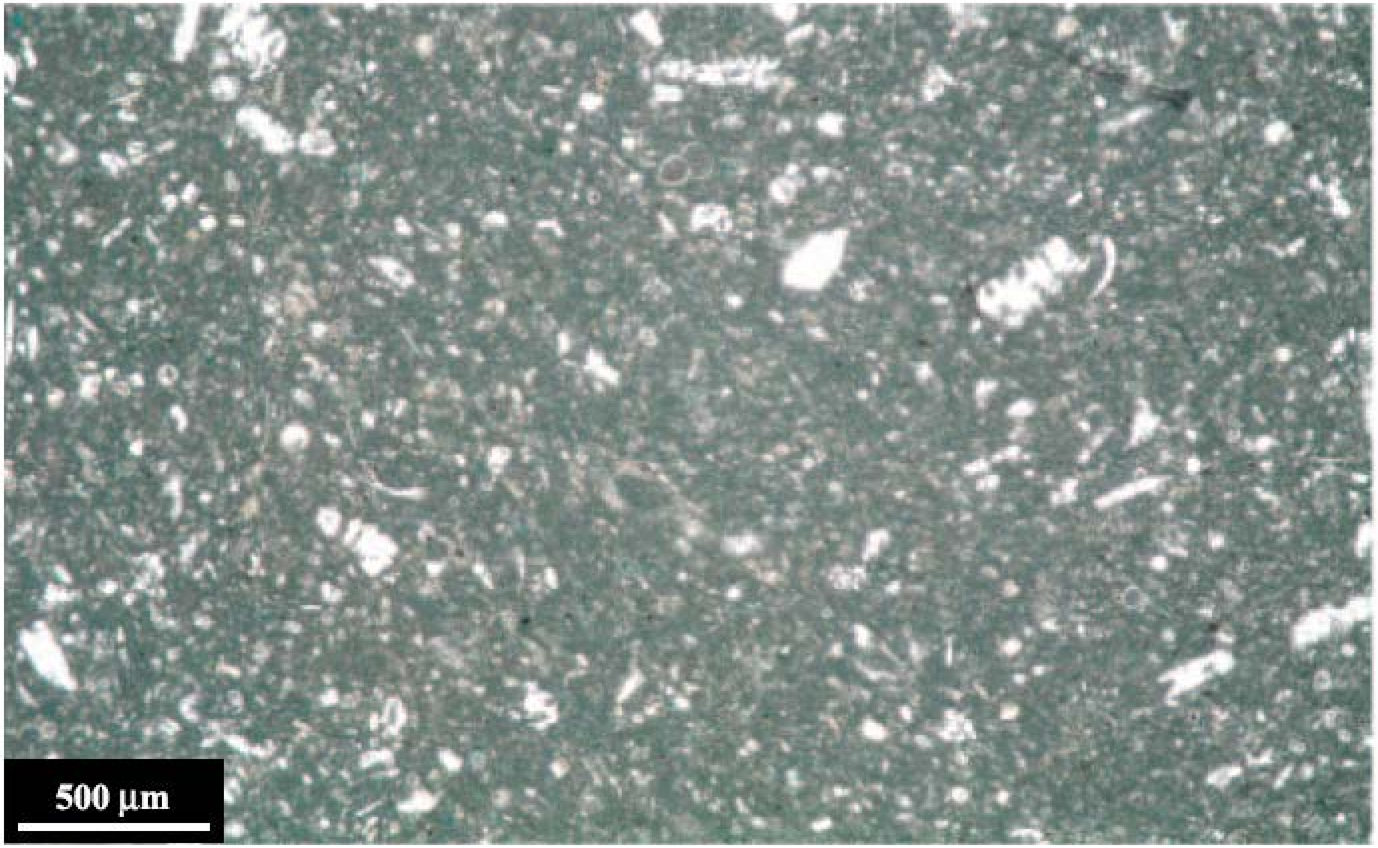

chalky microporosity, f = 4.9%, k = 0.01 md;

c

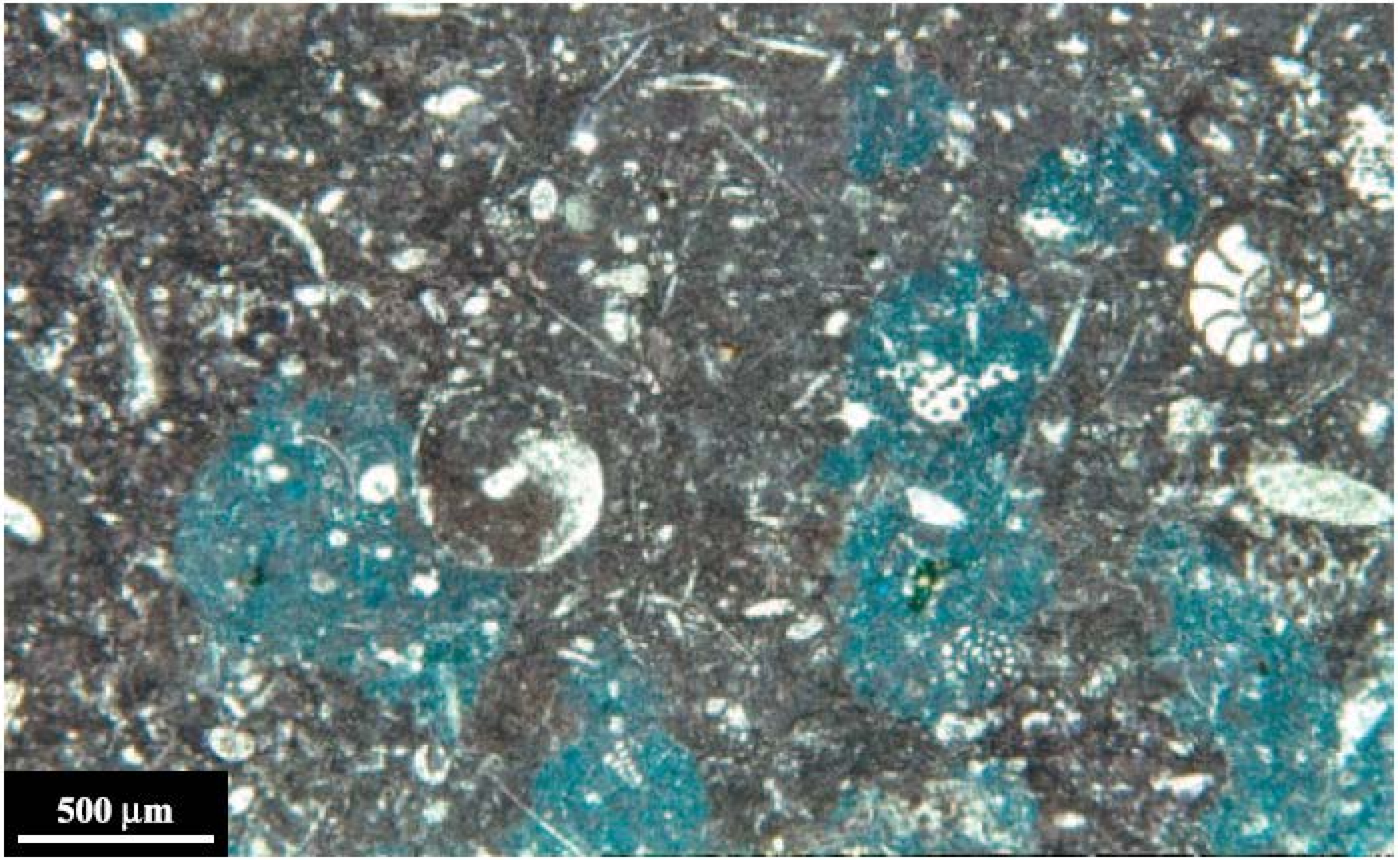

patchily distributed chalky microporosity, no porosity, or permeability measurements are available. Individual pores are too small to be seen, but porosity can be discerned because of impregnation with blue-dyed epoxy.

Moldic Porosity:

- Moldic pores are secondary pores formed by the selective, complete, or partial dissolution and recrystallization of grains or crystals. This definition is slightly modified from Choquette and Pray (1970) by including pores formed by partial dissolution and recrystallization. A distinctive difference in solubility between grains and/or crystals and the surrounding matrix is commonly needed and is commonly related to mineralogical differences (Moore, 2001).

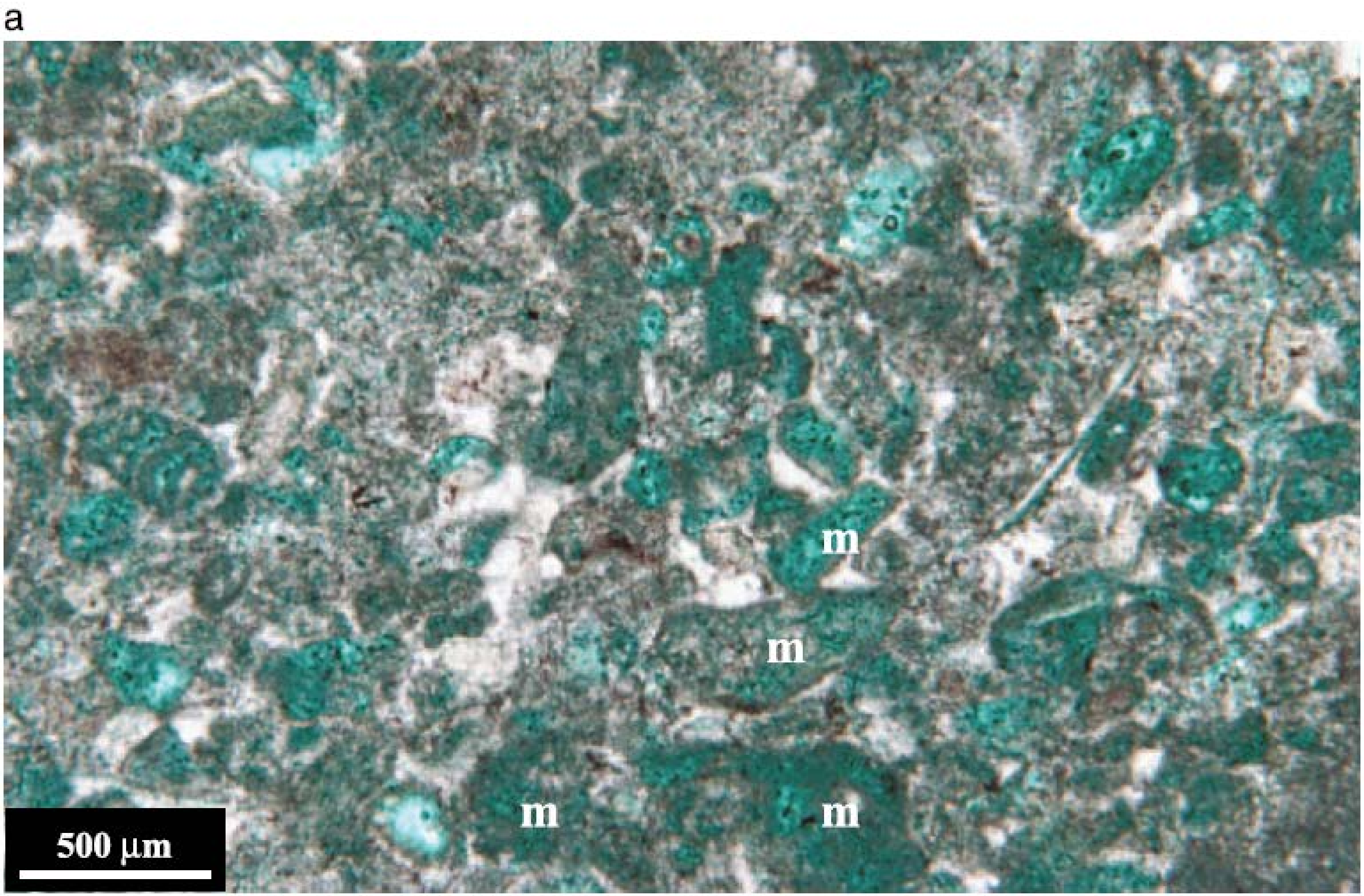

microporosity, f = 21.7%, k = 3.45md;
Some of the moldic micropores are marked by m

b

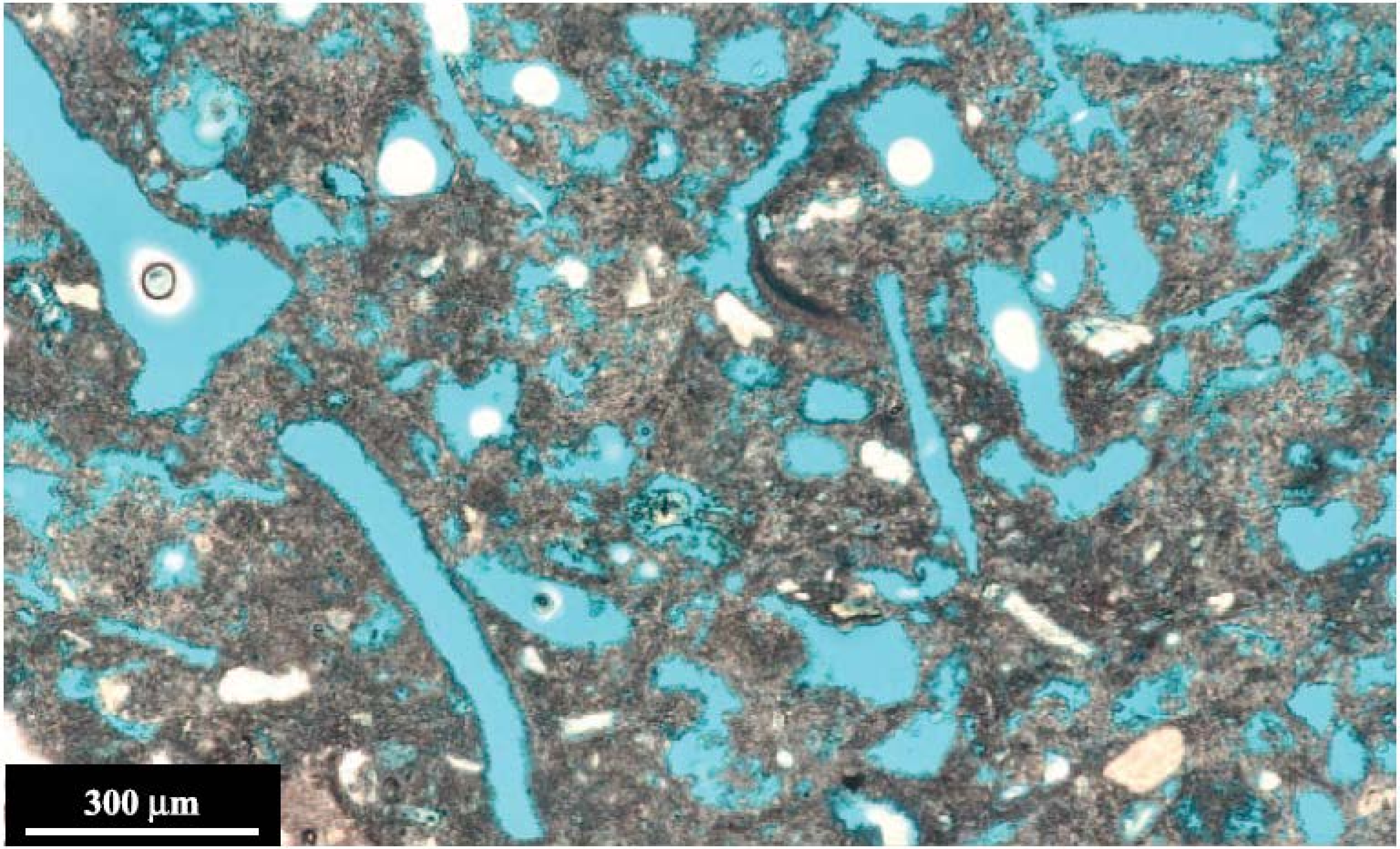

macroporosity, f = 24.74%, k = 35.2 md.

Intraparticle Porosity:

- Intraparticle pores are pore spaces occurring within grains, either of primary origin or formed through the decay of organic material in carbonate skeletons. A skeletal wall will therefore enclose, at least partly, most intraparticle porosity.

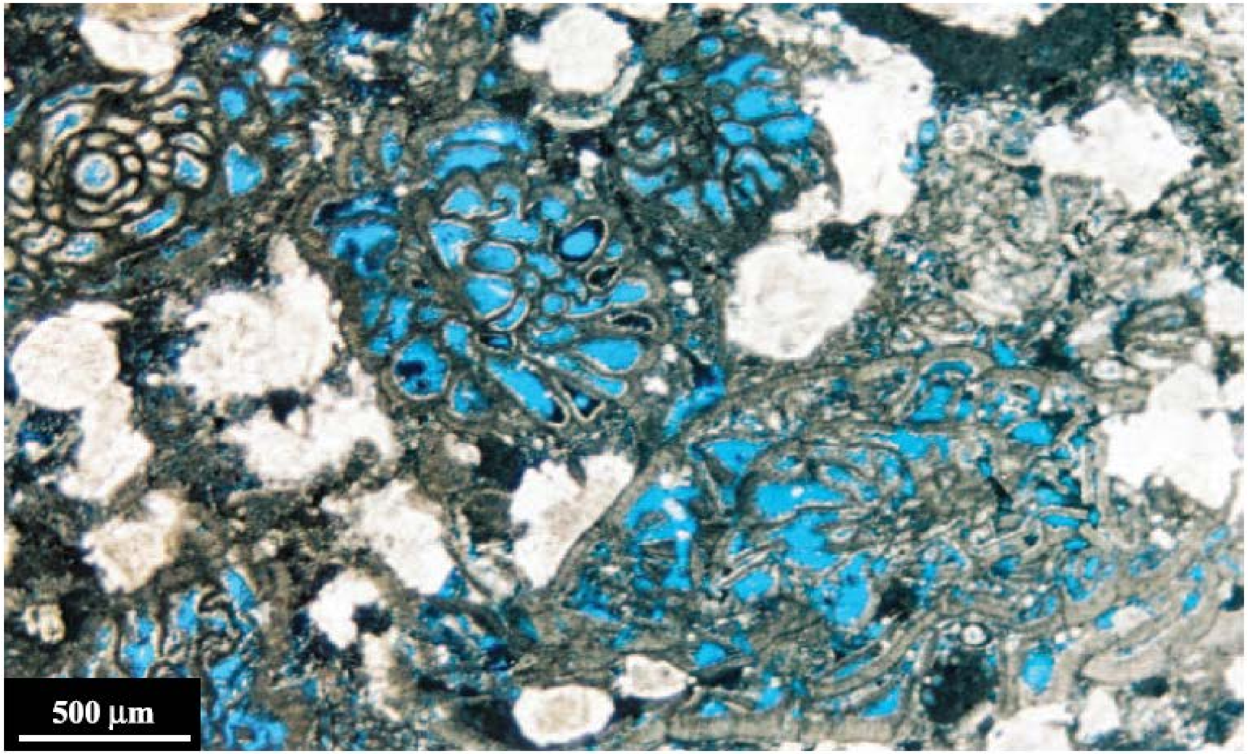

intraparticle porosity in fusulinid foraminifera. f = 16.0%, k = 1.25 md.

Vuggy Porosity:

- The definition of vuggy porosity in this article follows the definition of Choquette and Pray (1970). Vuggy pores are secondary solution pores that are not fabric selective (i.e., the pores cut across grains and/or cement boundaries). The pores are of irregular size and shape and may or may not be interconnected. Many vugs are solution-enlarged molds where the outlines of the precursor grains are poorly defined.

- Vuggy porosity (as defined by Choquette and Pray, 1970) is formed by the dissolution of cement, matrix, and grains. This typically occurs under the influence of near-surface meteoric waters (Loucks and Handford, 1992; Saller et al., 1994), but may also be related to deep-burial fluids (Moore and Druckman, 1981; Choquette and James, 1987; Moore and Heydari, 1993). Meteoric diagenesis is commonly associated with sea level low stands and subaerial exposure surfaces in humid climates (Loucks and Hand ford, 1992; Saller et al., 1994). Deep-burial dissolutionmay be related to hydrocarbon maturation and shale dewatering (Moore, 1989). Fluid-migration pathways, such as fractures and faults, are the main controls on vuggy porosity distribution during deep burial.

Core slabs showing vuggy porosity. Plug-derived porosities and permeabilities are strongly dependent on the location of core plugs because of the large vug sizes.

POROSITY-PERMEABILITY RELATIONSHIPS

- Porosity-permeability crossplots are used for predicting permeability from porosity or vice versa. Borehole porosity can be estimated from wire-line logs, but apart from the nuclear magnetic resonance log, there is no log that measures permeability. Therefore, it is common practice to establish porosity-permeability relationships through core analysis and then estimate permeability where cores do not exist using porosity logs and core derived porosity-permeability relationships. This method works well when there is a simple relationship between porosity and permeability, as in many sandstone reservoirs. In carbonate reservoirs, however, the porosity-permeability relationship is very complex because of the great variability of pore types.

Interparticle Pore-Type Classes:

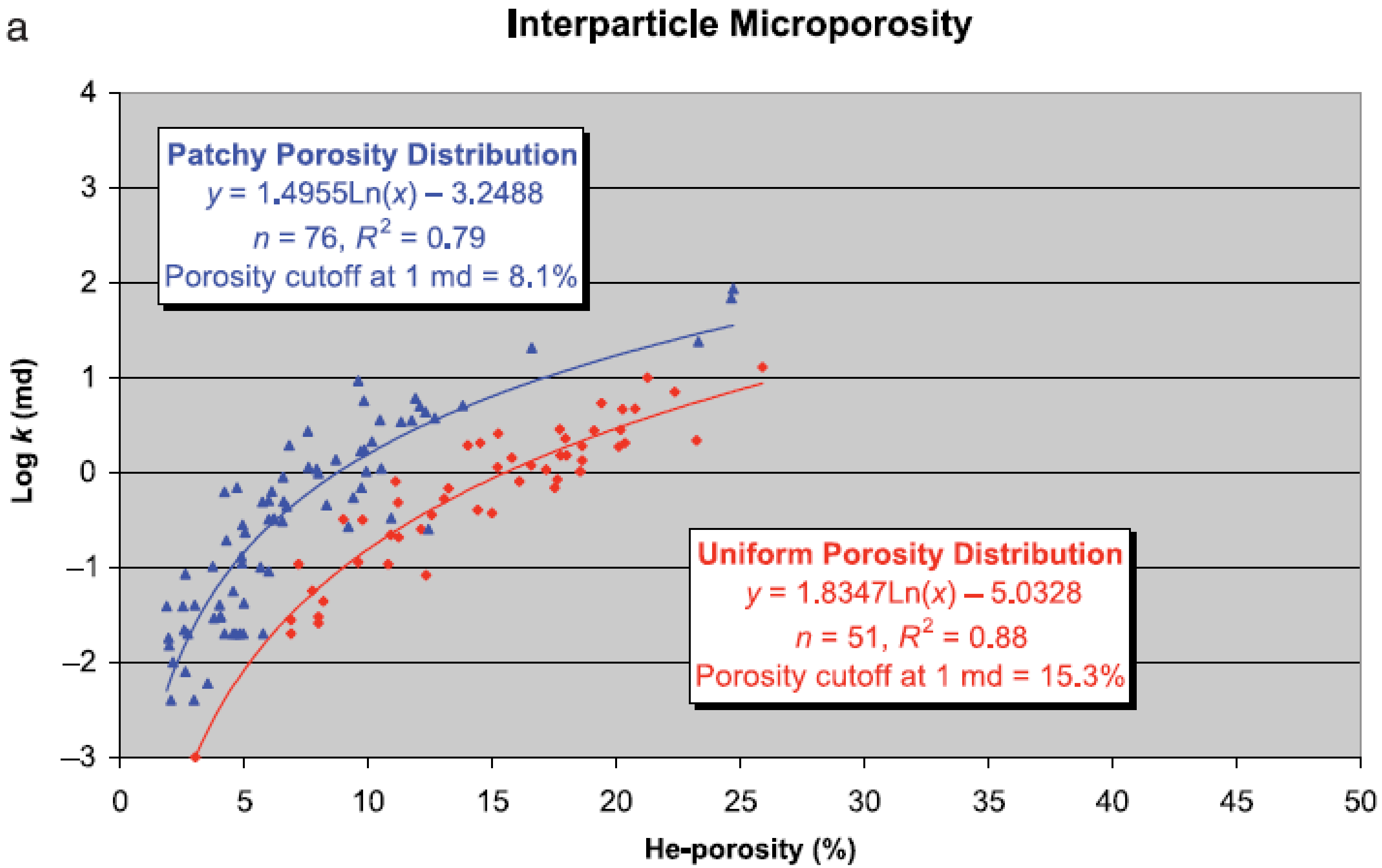

Interparticle micropores (10–50 mm pore diameter);

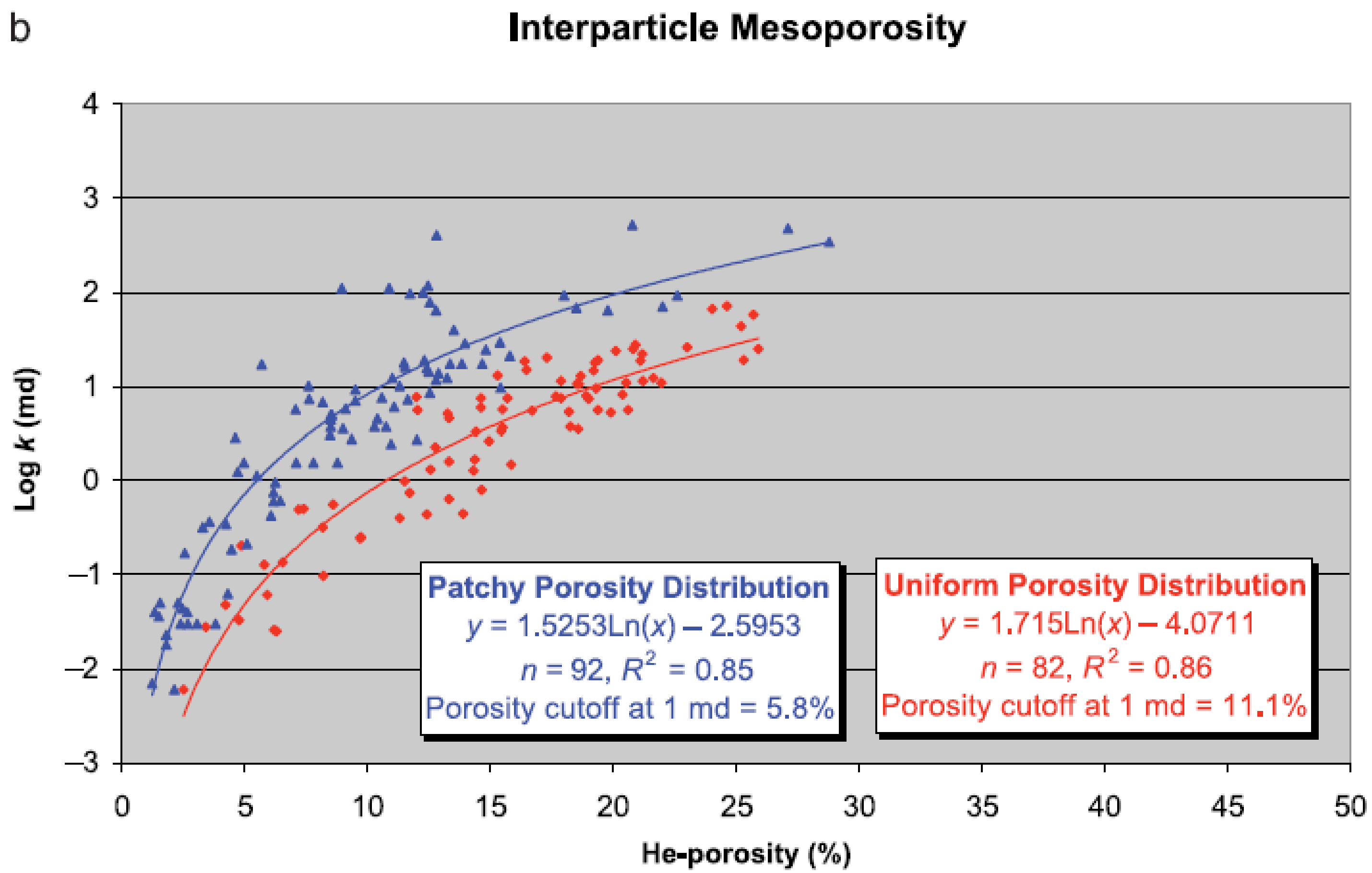

interparticle mesopores (50–100 mm pore diameter);

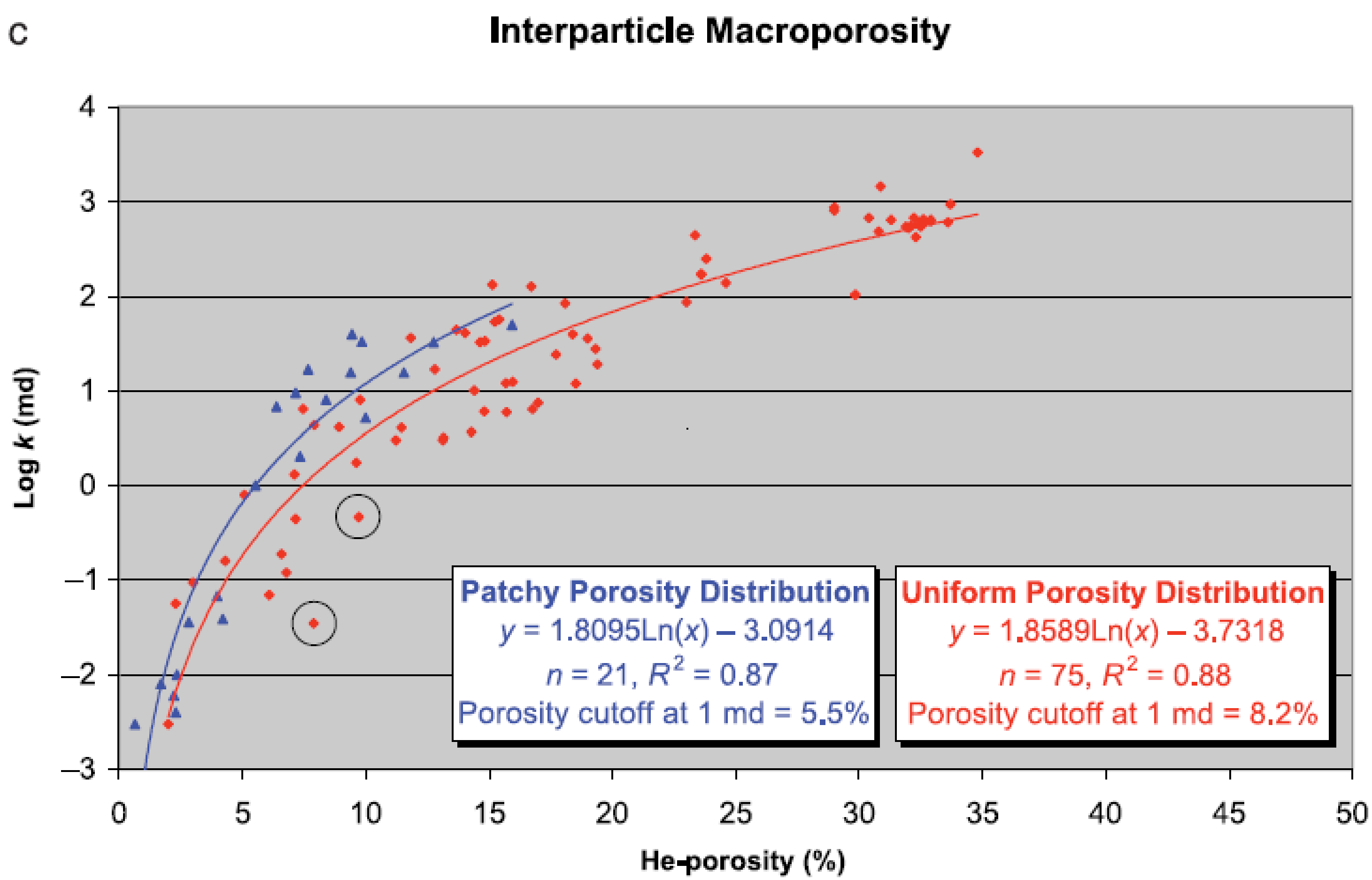

interparticle macropores (>100 mm pore diameter);

- If 1md is used as the critical flow parameter, the porosity cutoff for interparticle microporosity (10–50-mm pore diameter) is reduced from 15.3% at uniform porosity distribution to 8.1%, when the porosity is patchily distributed. Similarly, for meso- (50–100-mm pore diameter) and macroporosity (>100-mm pore diameter), the porosity cutoff is reduced from 11.1 to 5.8 and 8.2 to 5.5%, respectively, for the corresponding 1-md permeability.

- Intercrystalline Pore-Type Classes:

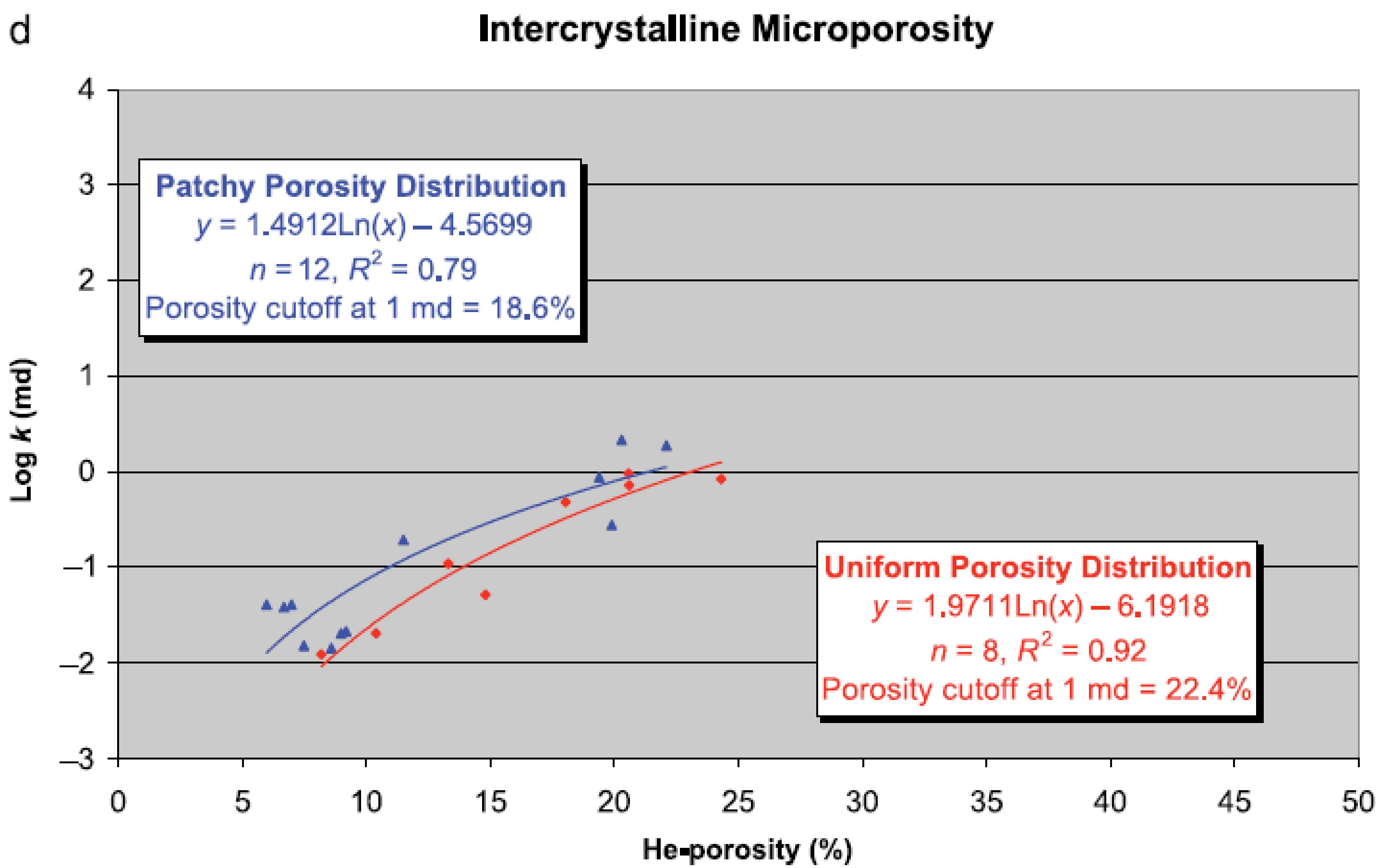

Intercrystalline micropores (10–20 mm pore diameter);

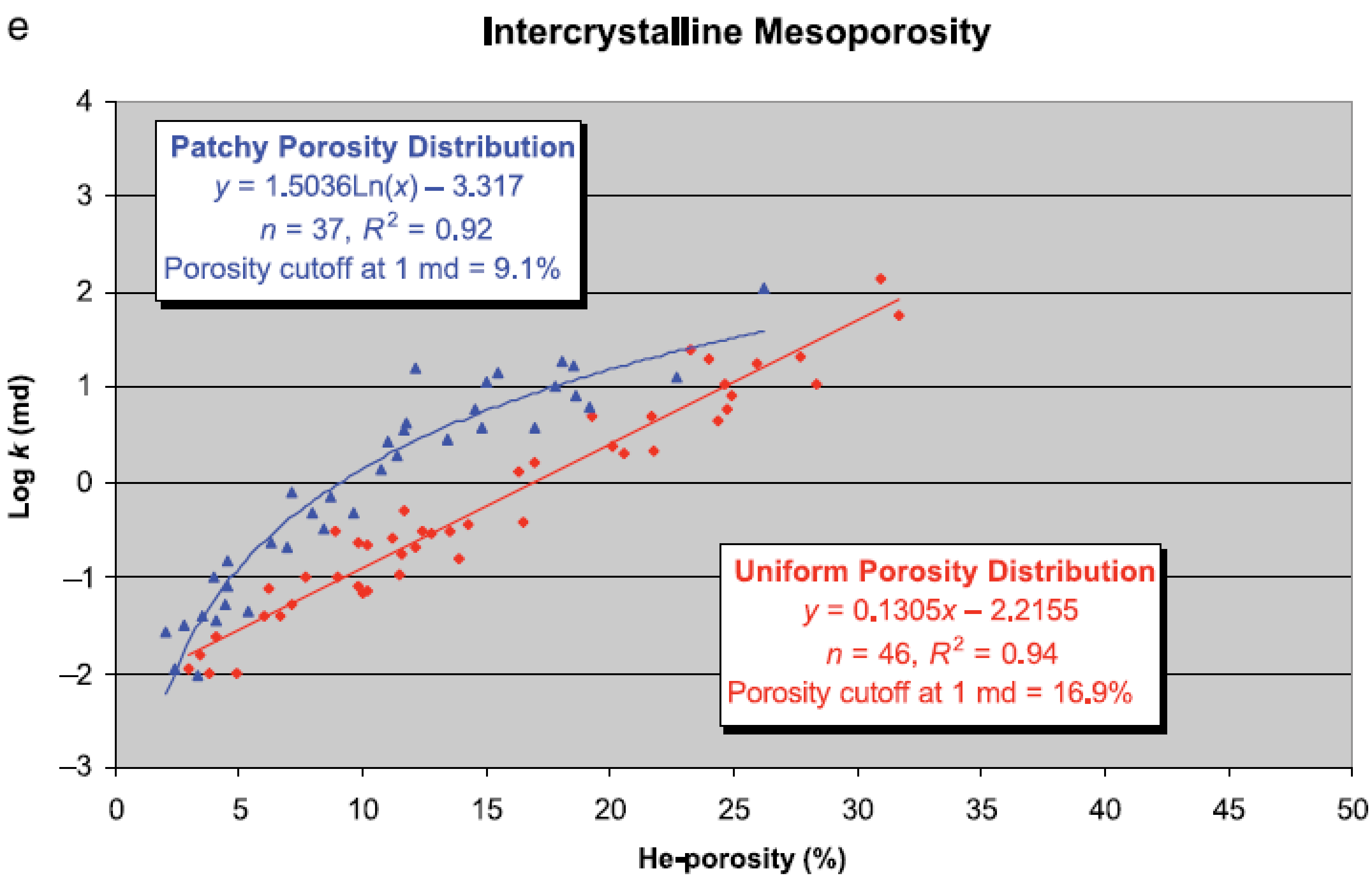

intercrystalline mesopores (20–60 mm pore diameter);

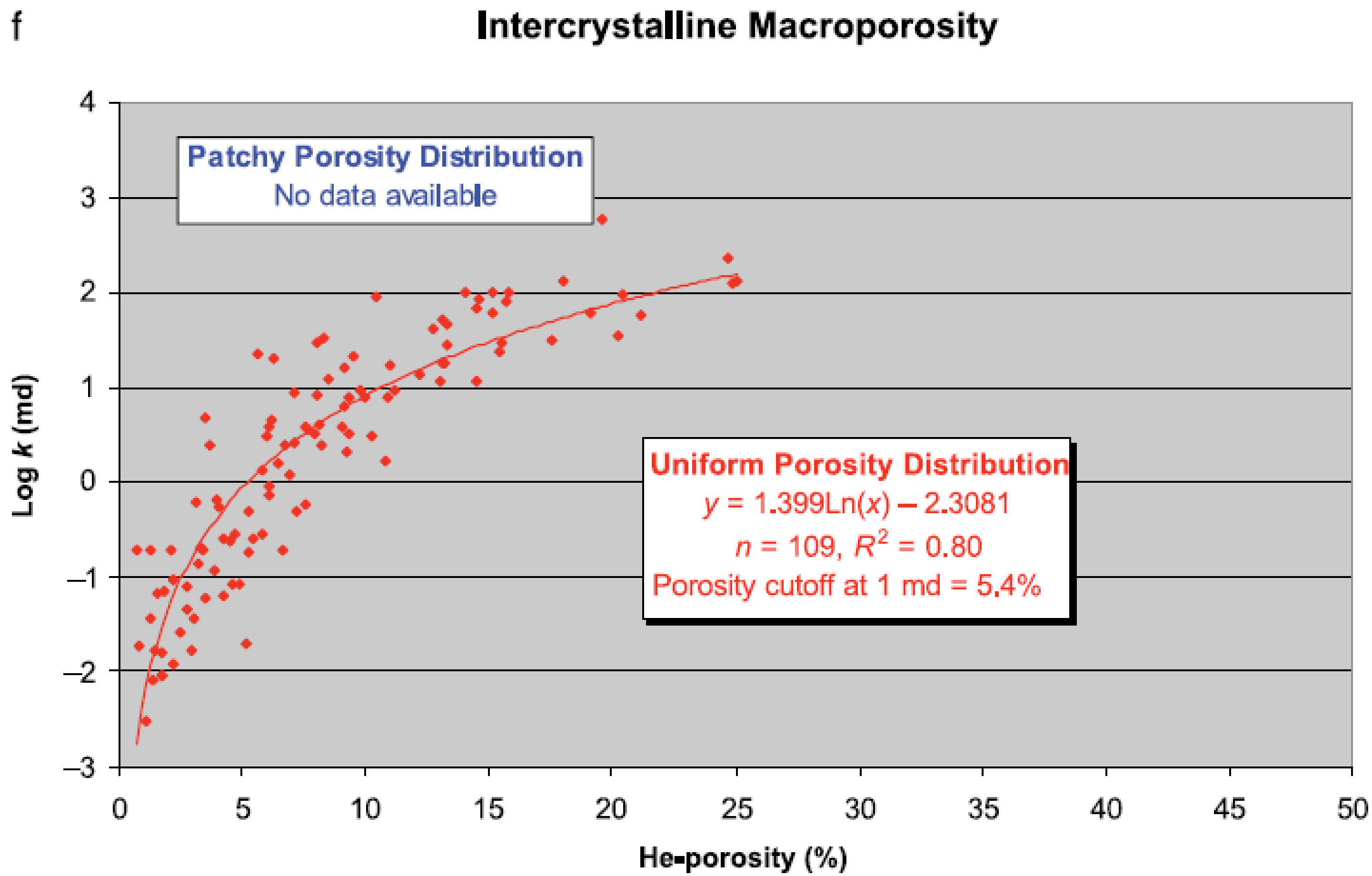

intercrystalline macropores (>60 mm pore diameter).

- As for interparticle pores, pore size and porosity distribution have a clear control on k/f. A significant increase in k/f exists when pore size increases and/or porosity distribution becomes patchier. If 1 md is used as the critical flow parameter, the porosity cutoff for intercrystalline microporosity (10– 20-mm pore diameter) is reduced from 22.4% at uniform porosity distribution to 18.6%, when the porosity is patchily distributed. Similarly, for mesoporosity (20–60-mm pore diameter), the porosity cutoff is reduced from 16.9 to 9.1%. Uniformly distributed macroporosity (>60-mm pore diameter) has a porosity cutoff of 5.4%.

- Mudstone Micropore Classes:

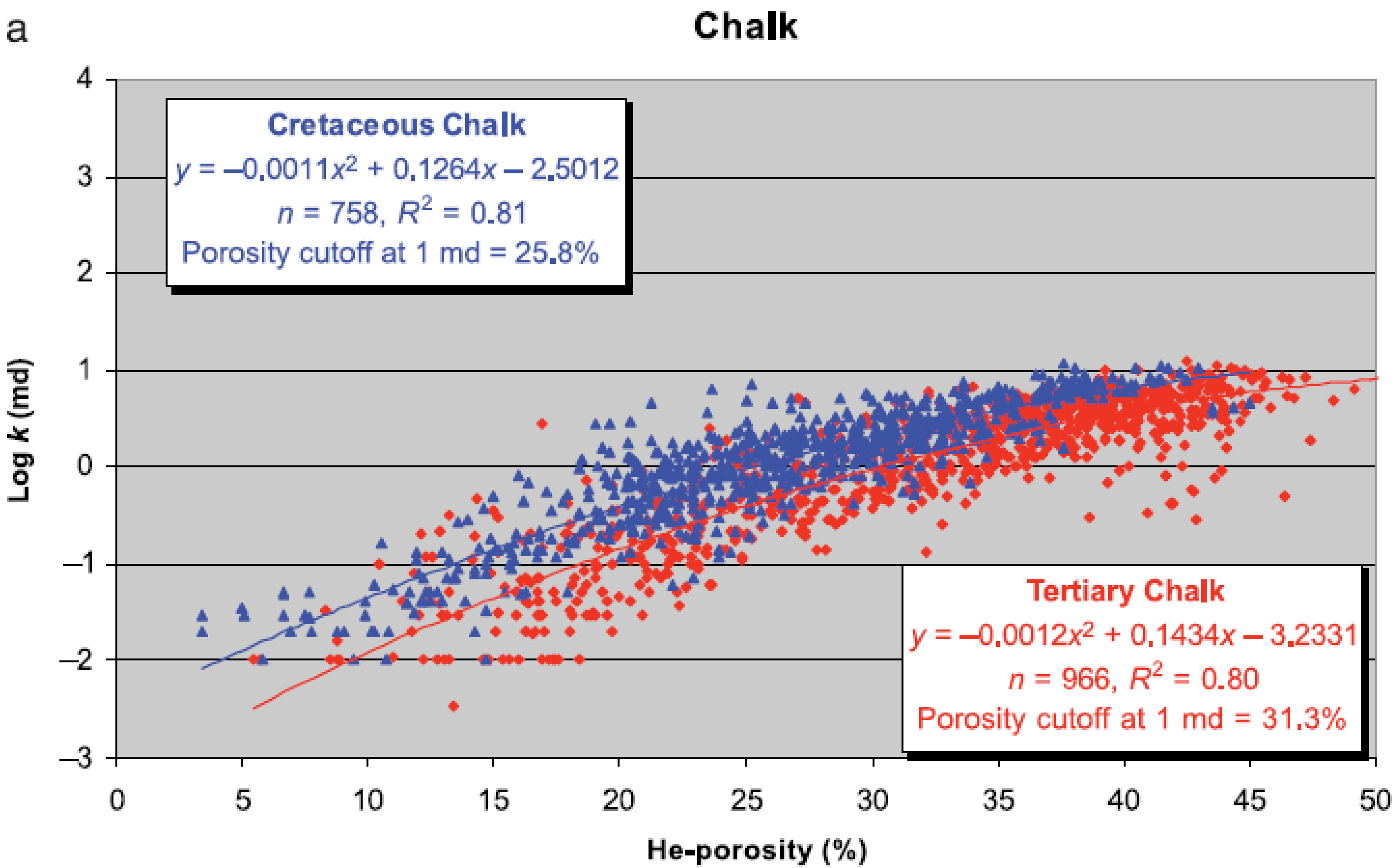

chalk

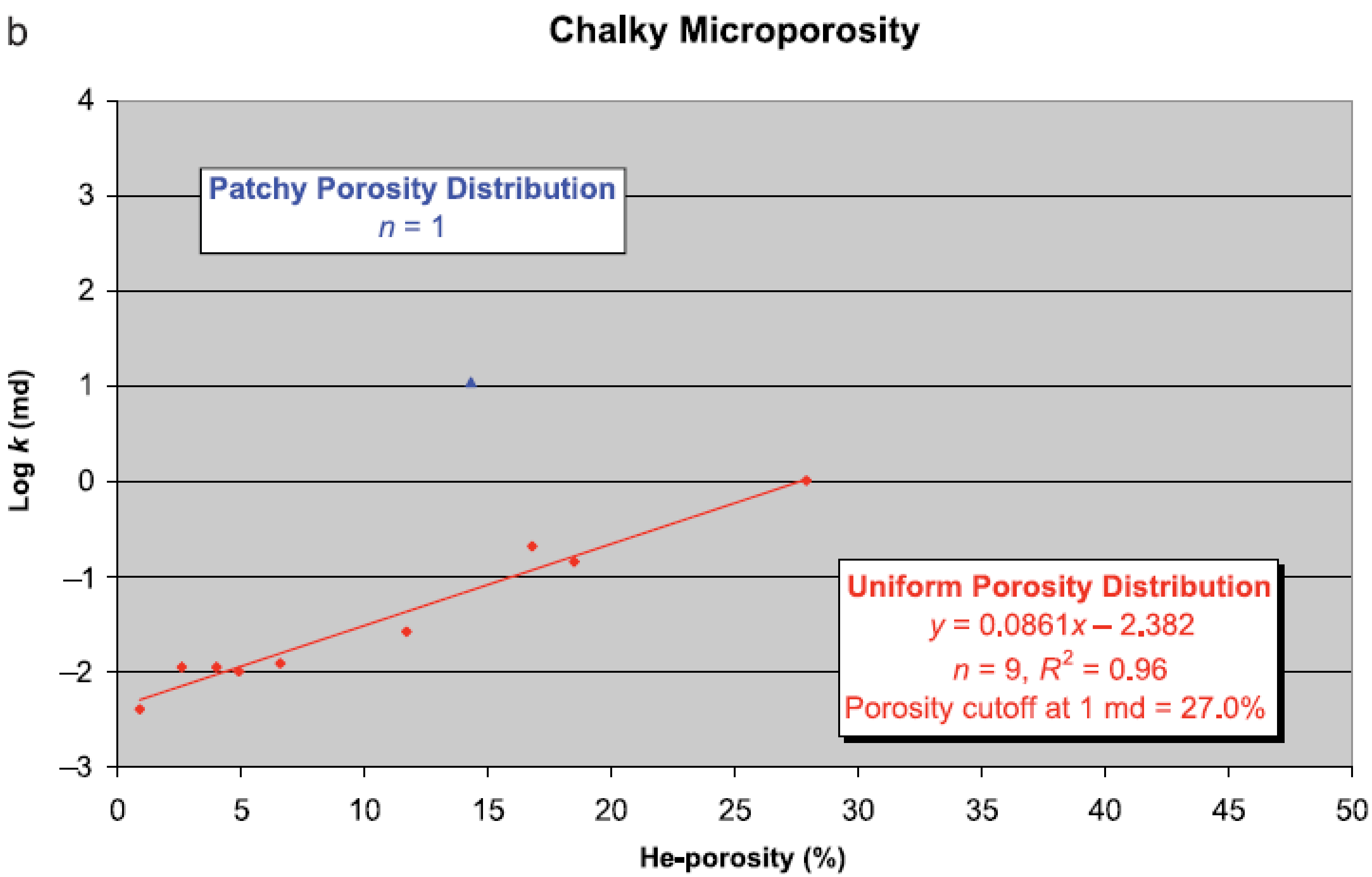

chalky micropores

- If 1 md is used as the critical flow parameter, the porosity cutoff is 25.8% for Cretaceous chalk, 31.3% for Tertiary chalk, and 27.0% for chalky microporosity with uniform distribution. The only sample with patchy distribution of chalky micropores shows a significantly higher k/f than for samples with a uniform porosity distribution

• Moldic Pore-Type Classes:

c

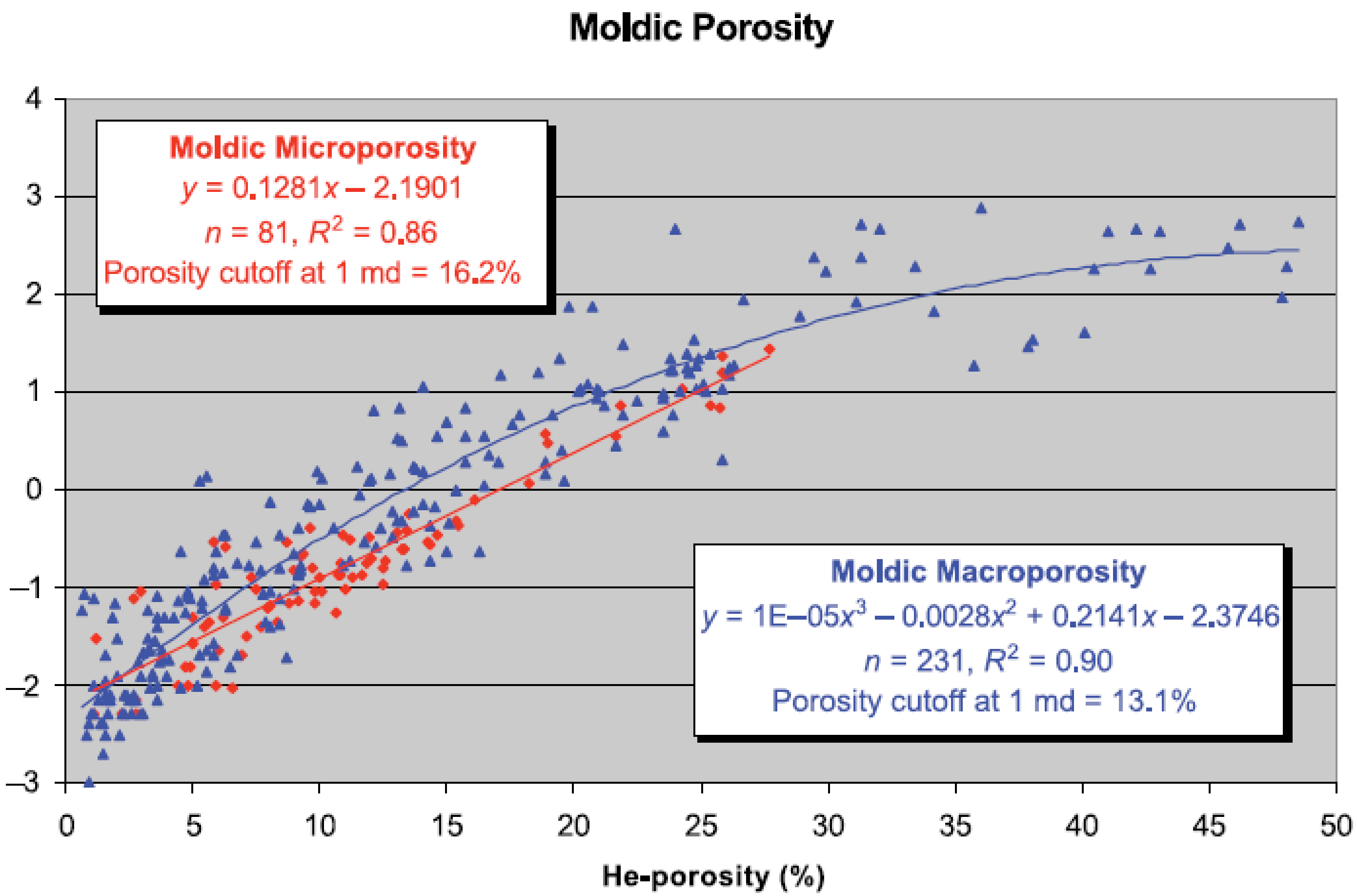

moldic pores,

- If 1 md is used as the critical flow parameter, the porosity cutoff is 13.1% for macropores and 16.2% for micropores. Differences in k/f for the two pore-type classes result from a slight overall reduction in pore-throat diameters, as confirmed by mercury capillary-pressure measurements, and is probably related to the presence of intramold matrix in moldic micropores.

Intraparticle Porosity:

- If 1md is used as the critical flow parameter, the porosity cutoff is 14.1%.

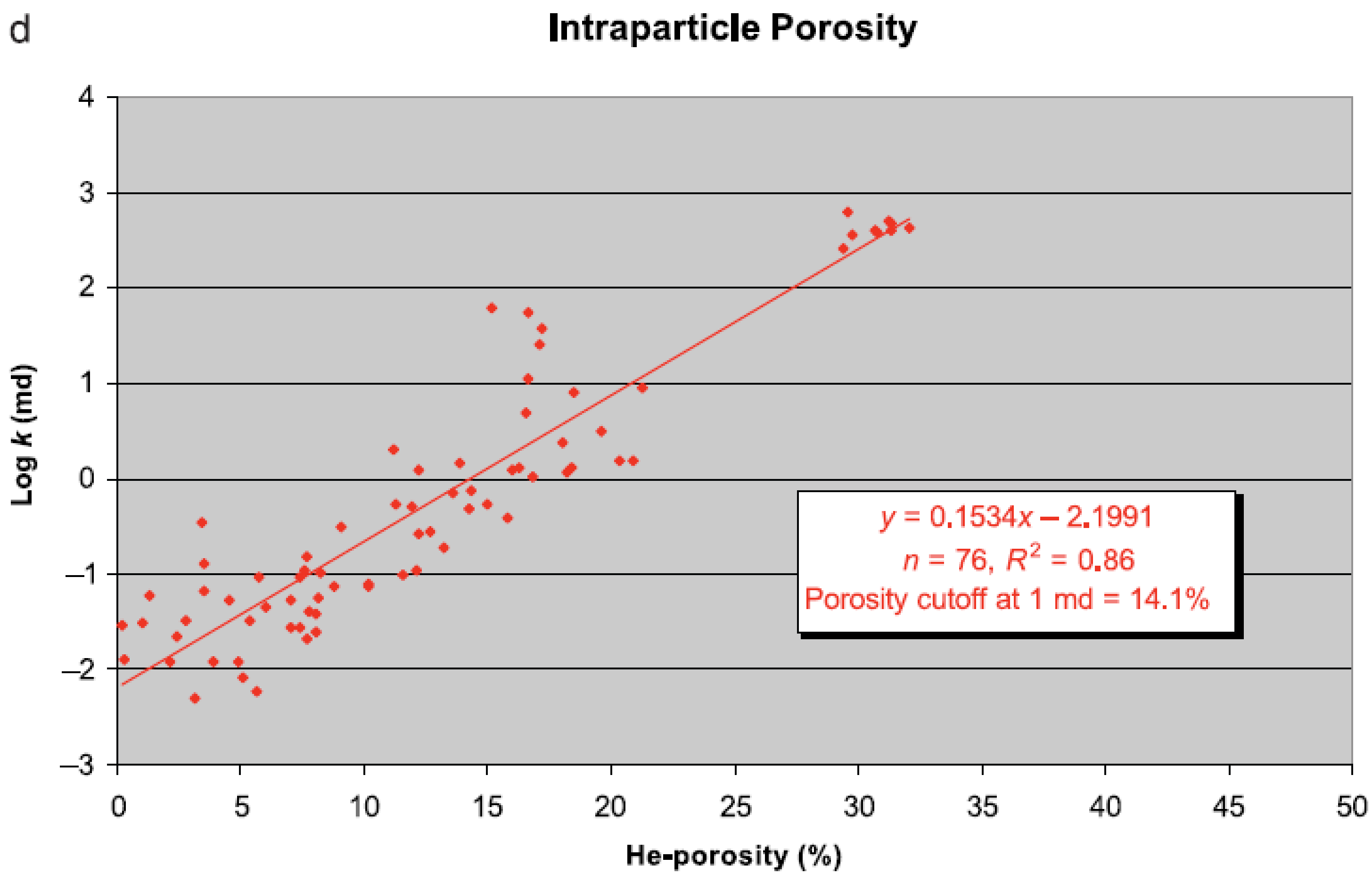

Vuggy Porosity:

e

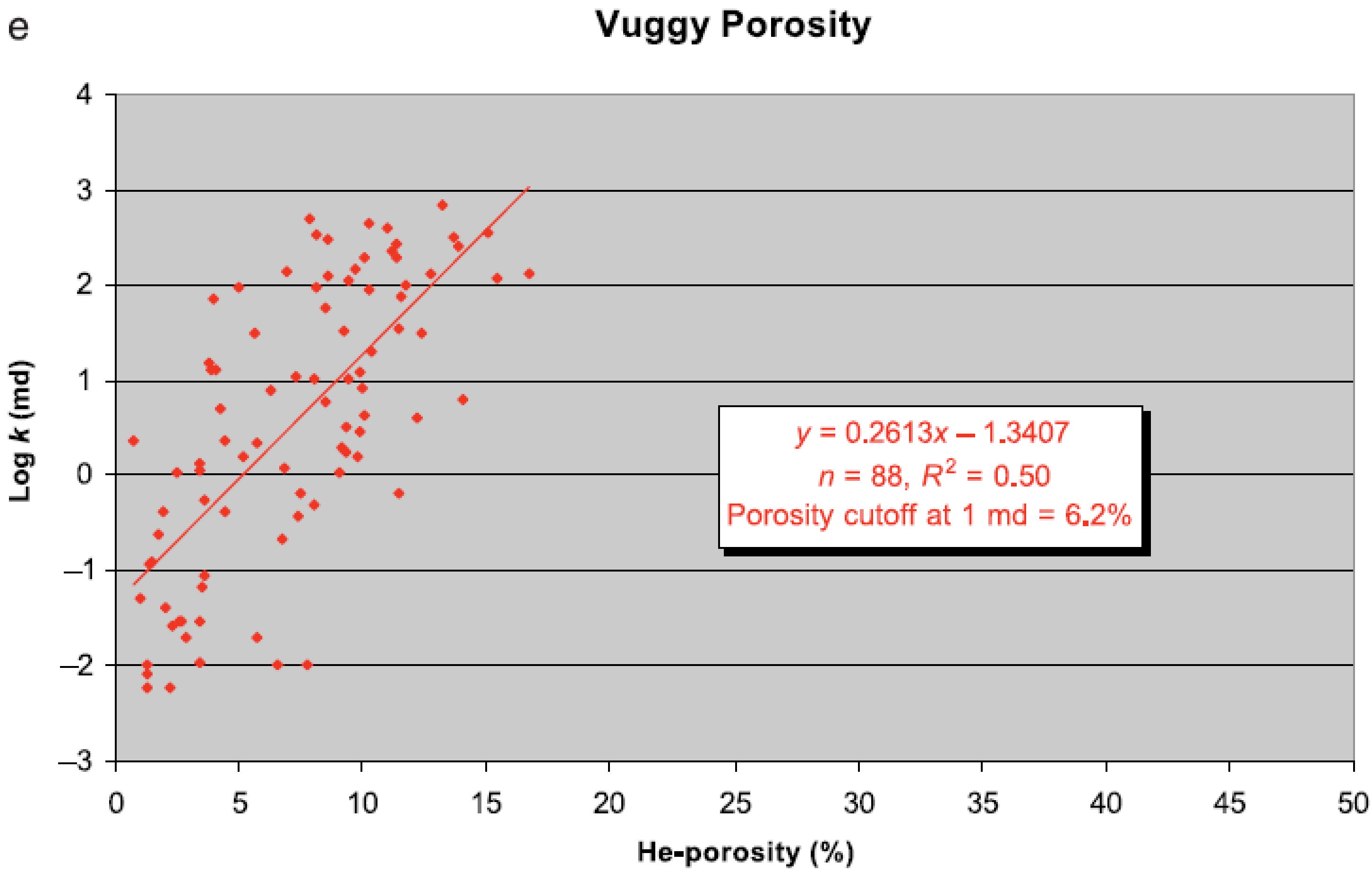

vuggy pores.

- If 1 md is used as the critical flow parameter, the porosity cutoff is 6.2%. The poor relationship between porosity and permeability is most likely related to a low sample-to vug size ratio (many vugs are more than 1 cm [0.4 in.] in diameter). It may also be argued that the scatter in data points results from a variable degree of connectivity between the vugs, but such an explanation could not be confirmed by the present data set.

Comparison to Other Classification Systems

1. The effect of patchy porosity distribution on the porosity-permeability relationship
2. The split between interparticle and intercrystal porosity (as in Choquette and Pray, 1970) and the introduction of mudstone microporosity
3. The use of pore-size differentiation instead of particle size and sorting differentiation (samples in the studied data set show widely different pore sizes within each of Lucia’s, 1995, 1999, interparticle classes because of the variable extent of interparticle and intercrystalline cementation and allochem sorting)

Table 2. New Porosity Classification System*

Pore Type	Pore Size	Pore Distribution	Pore Fabric	R^2
Interparticle	Micropores (10–50 μm)	Uniform	Interpartide, uniform micropores	0.88
		Patchy	Interpartide, patchy micropores	0.79
	Mesopores (50–100 μm)	Uniform	Interpartide, uniform mesopores	0.86
		Patchy	Interpartide, patchy mesopores	0.85
	Macropores (>100 μm)	Uniform	Interpartide, uniform macropores	0.88
		Patchy	Interpartide, patchy macropores	0.87
Intercrystalline	Micropores (10–20 μm)	Uniform	Intercrystalline, uniform micropores	0.92
		Patchy	Intercrystalline, patchy micropores	0.79
	Mesopores (20–60 μm)	Uniform	Intercrystalline, uniform mesopores	0.94
		Patchy	Intercrystalline, patchy mesopores	0.92
	Macropores (>60 μm)	Uniform	Intercrystalline, uniform macropores	0.80
		Patchy	Intercrystalline, patchy macropores	
Intraparticle			Intrapartide	0.86
Moldic	Micropores (<10–20 μm)		Moldic micropores	0.86
	Macropores (>20–30 μm)		Moldic macropores	0.90
Vuggy			Vuggy	0.50
Mudstone microporosity	Micropores (<10 μm)		Tertiary chalk	0.80
			Cretaceous chalk	0.81
		Uniform	Chalky micropores, uniform	0.96
		Patchy	Chalky micropores, patchy	

*Partly based on Choquette and Pray (1970) and Lucia (1983, 1995, 1999). Porosity-permeability coefficients of determination (R^2) are based on samples from the present study.

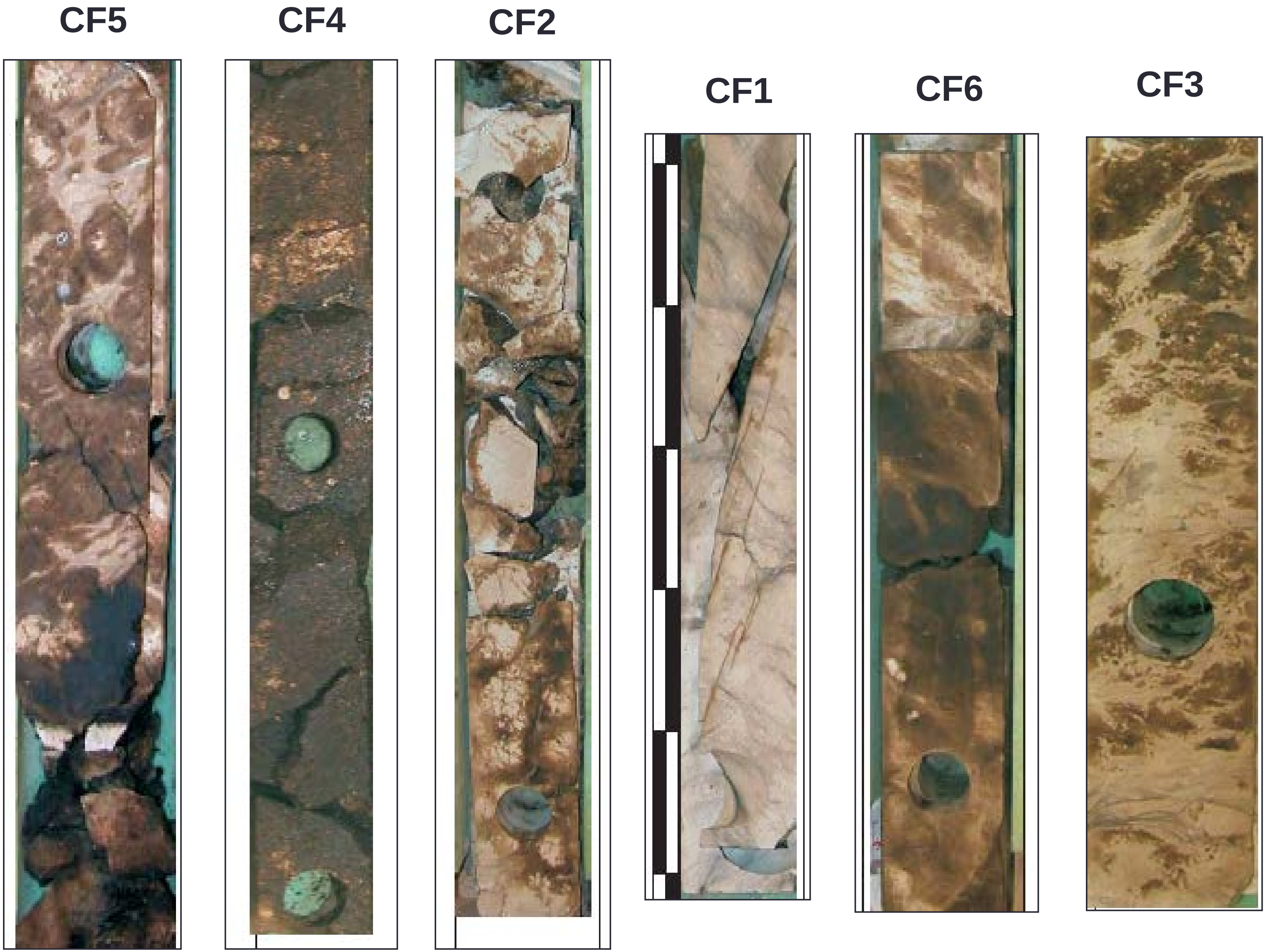
CF5
CF4
CF2
CF1
CF6
CF3

Primary porosity in the carbonate reservoir

Non-porous carbonate facies

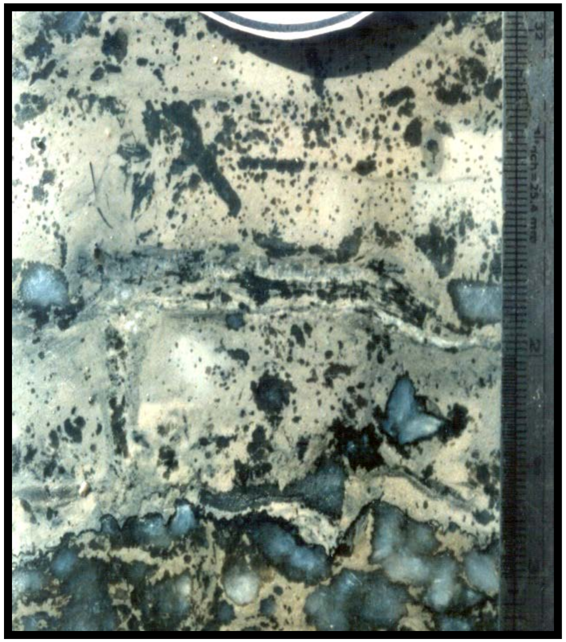


0.5 mm

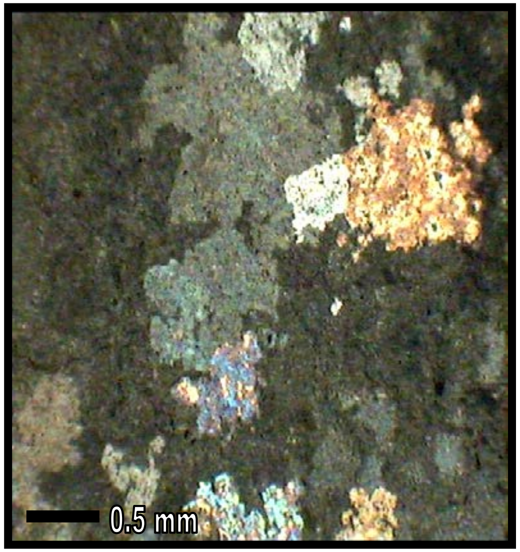
0.5 mm

Porosity Types in the carbonates

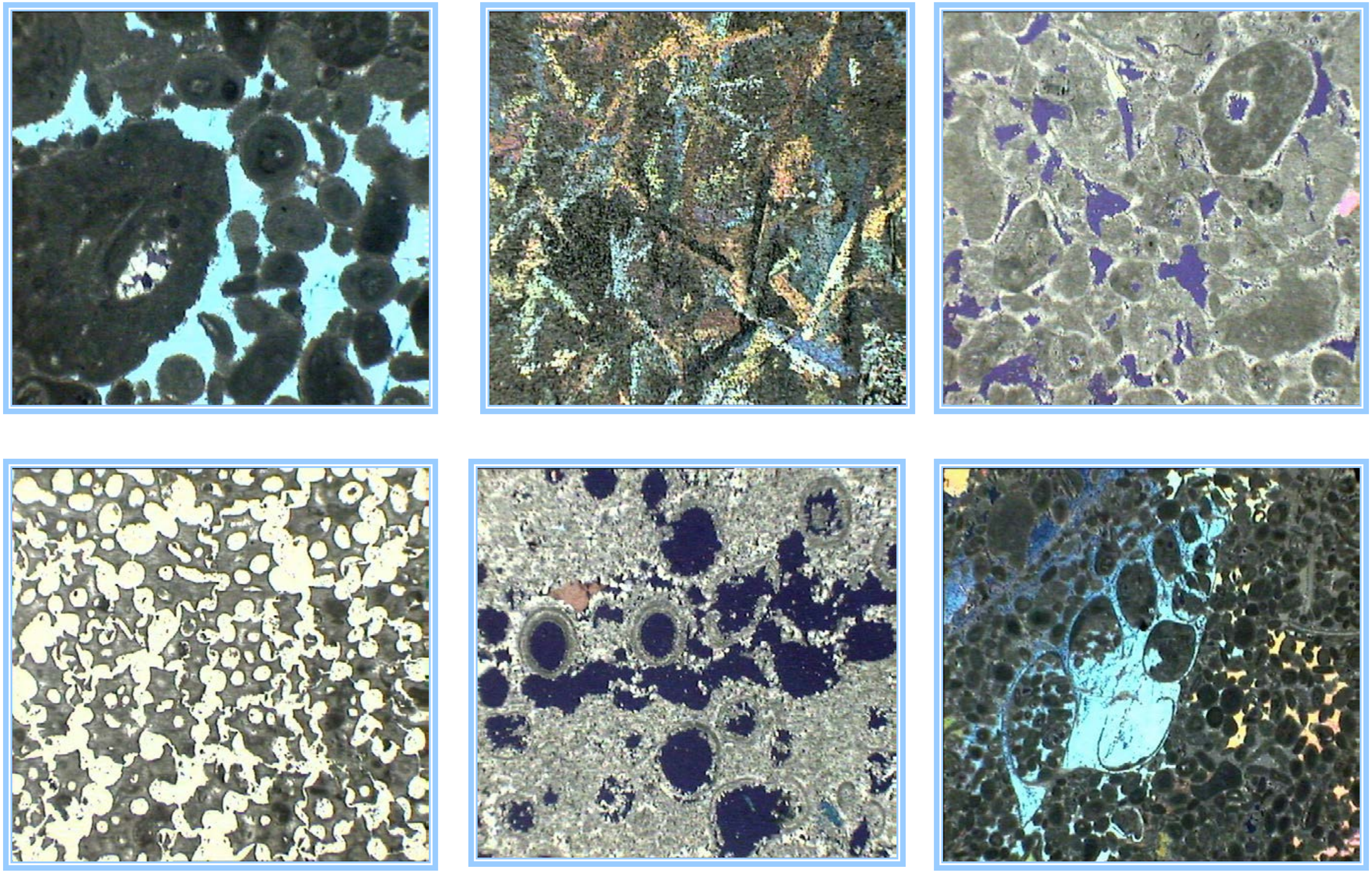

Diagenetic impact on the porosity

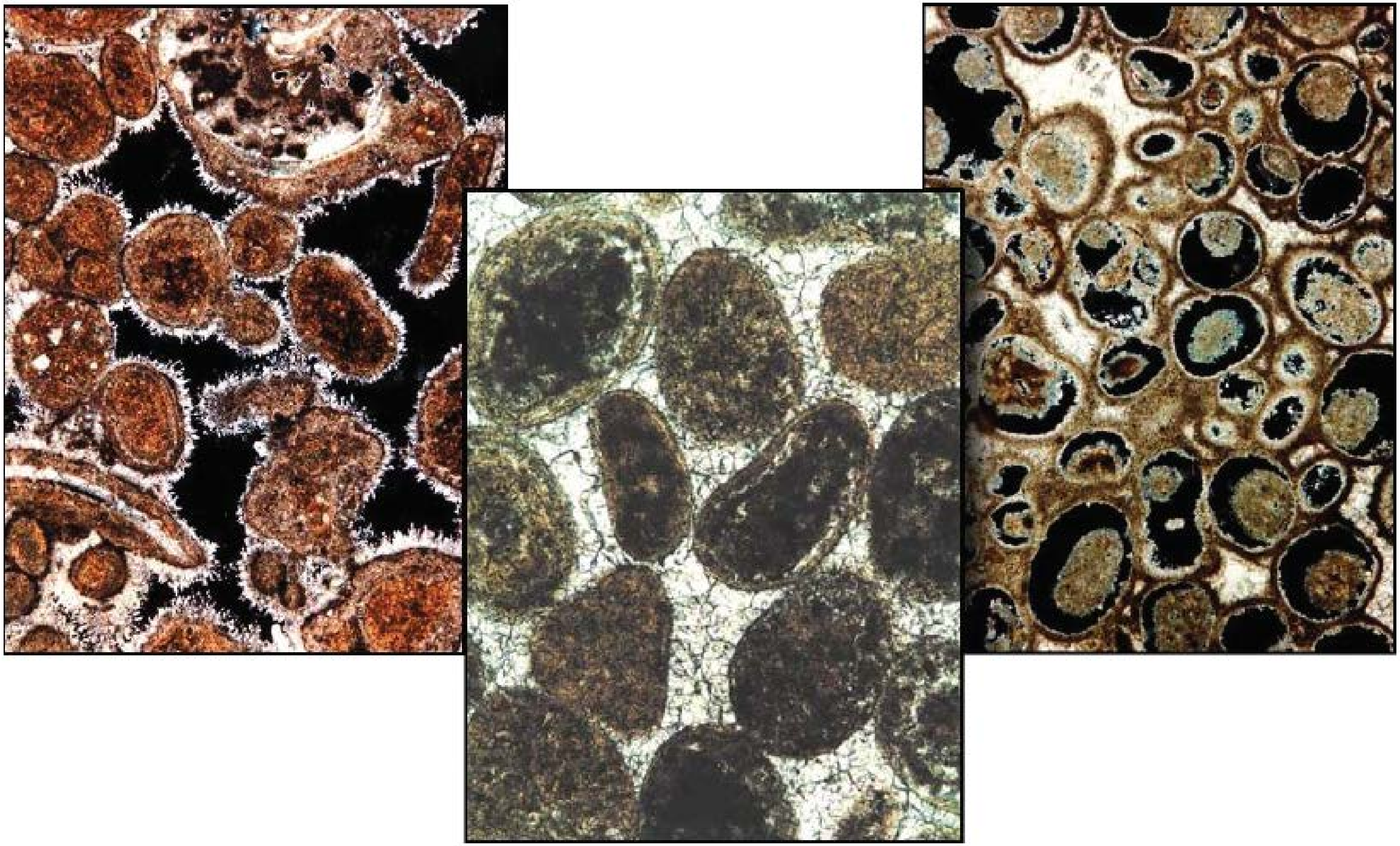

Carbonate pore types: Intraparticle porosity

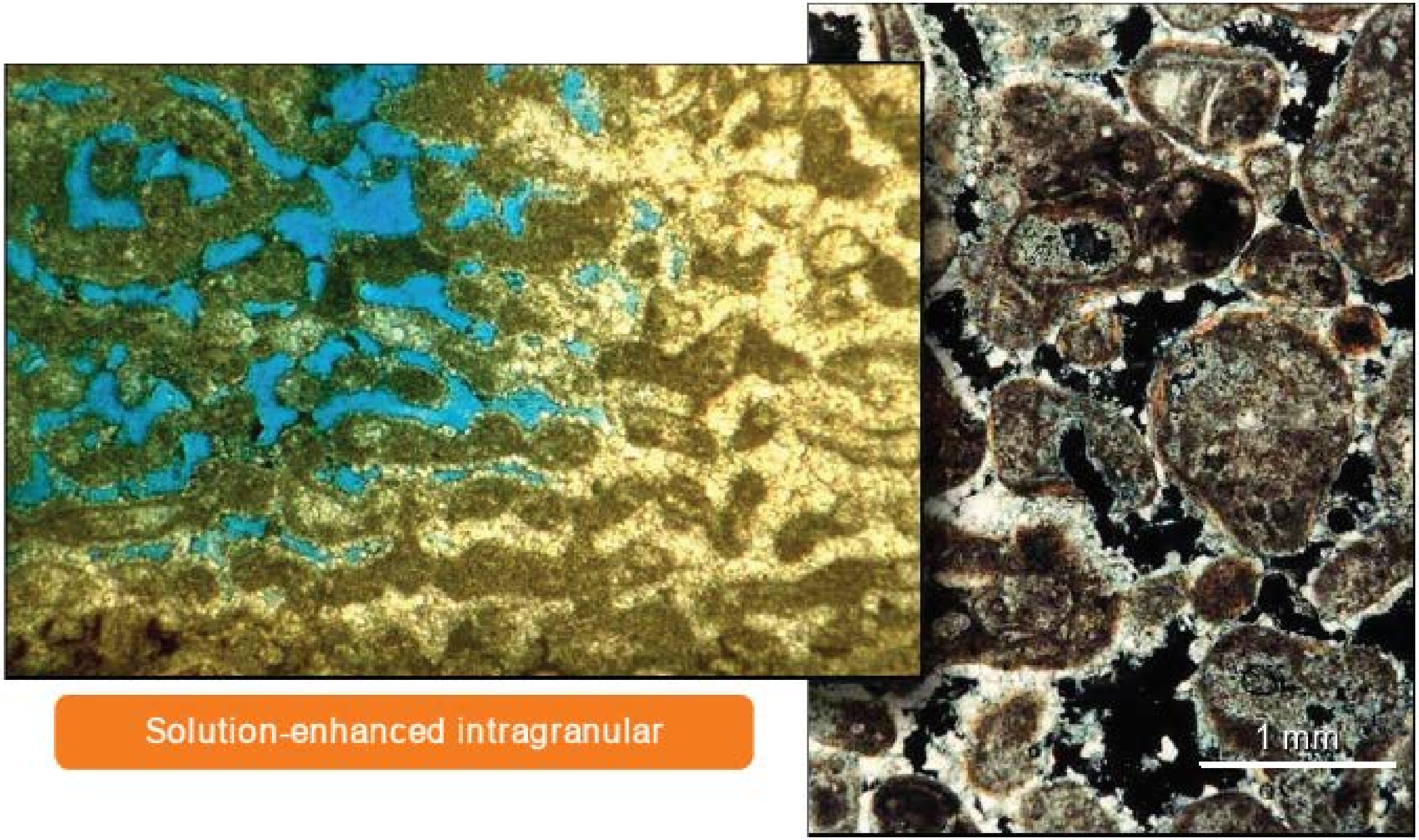

Solution-enhanced intragranular

Solution-enhanced intergranular

Carbonate pore types: Moldic porosity

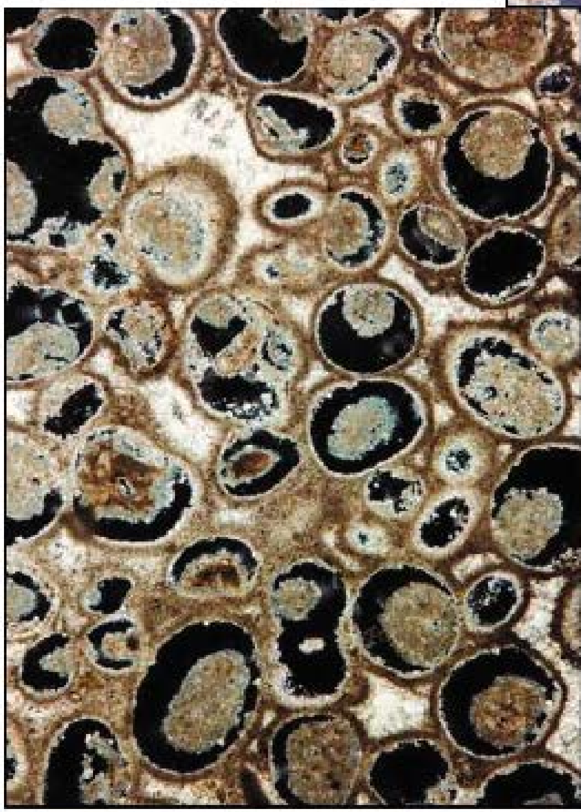

Ooid mouldic

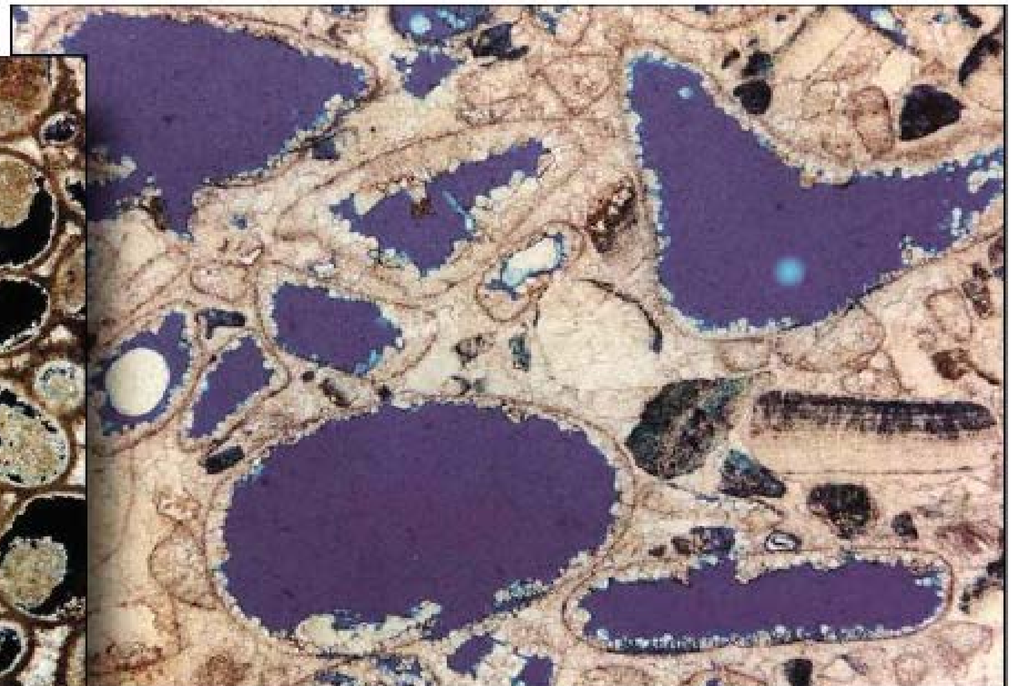

Skeletal mouldic

Carbonate pore types: Intercrystalline

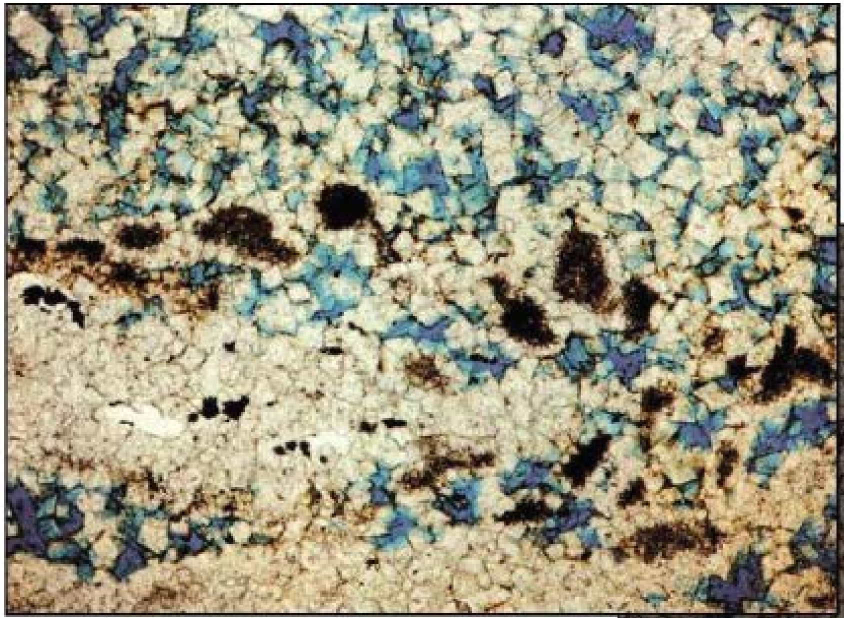

Dolomitic Intercrystalline

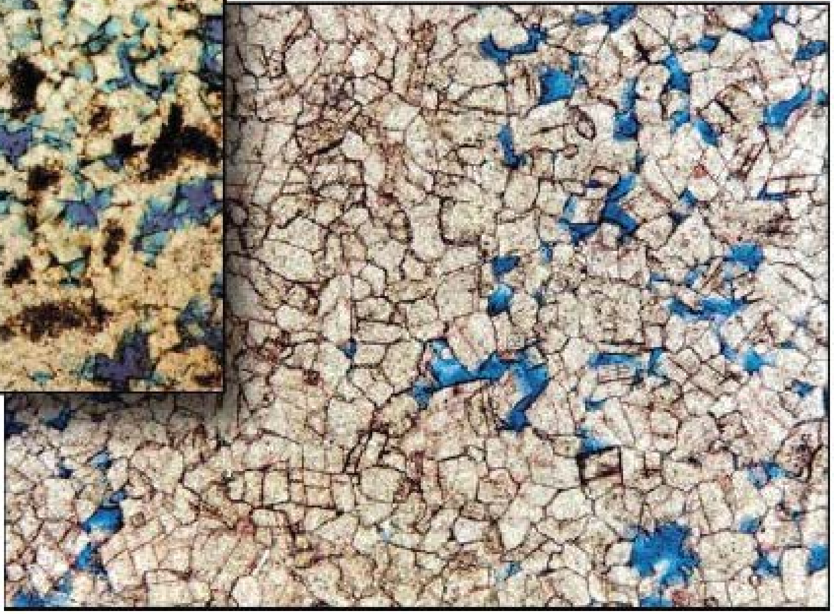

Dolomitic Intercrystalline

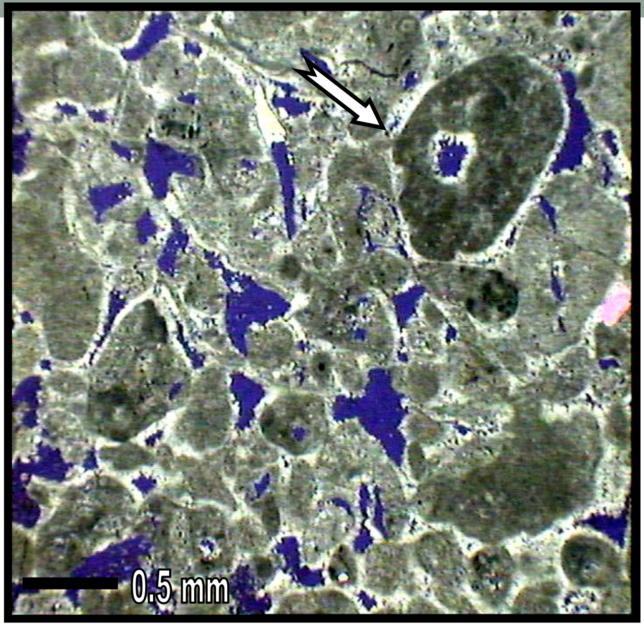
0.5 mm

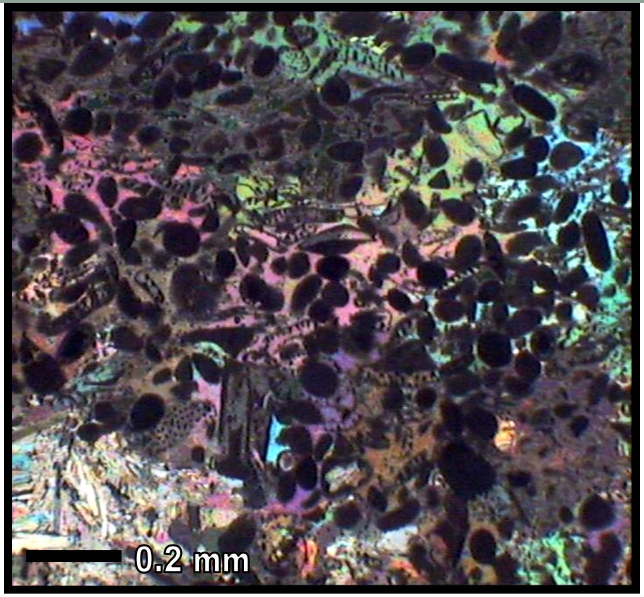
0.2 mm

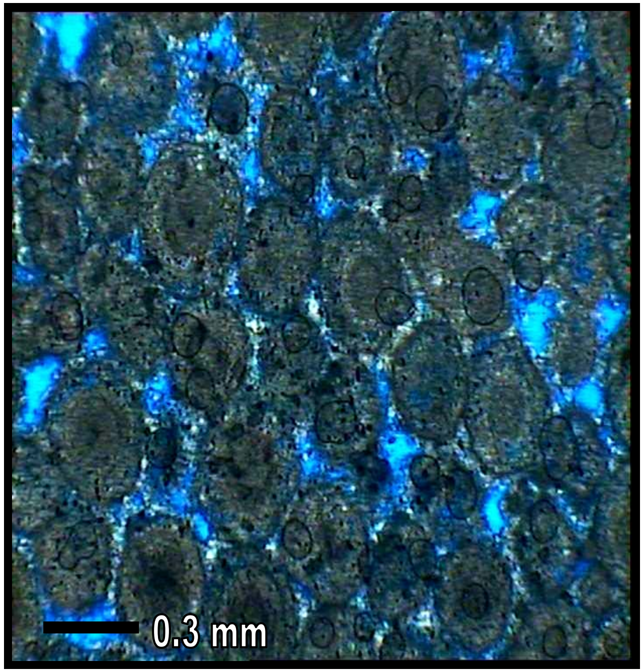
0.3 mm

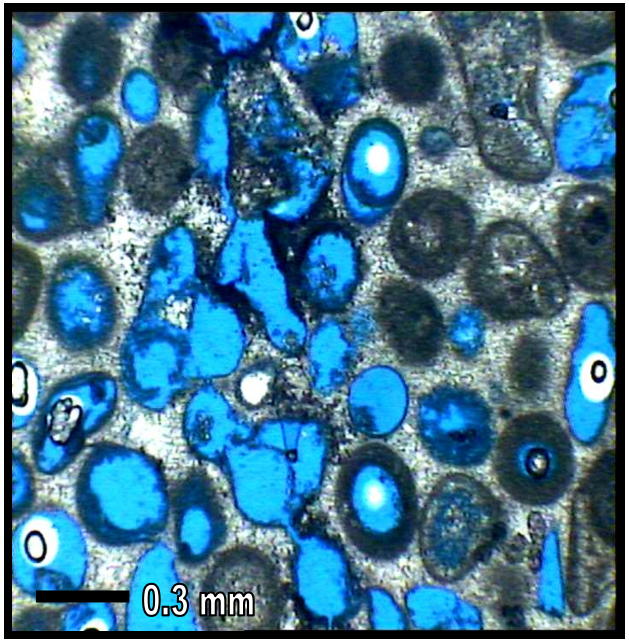
0.3 mm

Sandstone reservoir with intergranular porosity

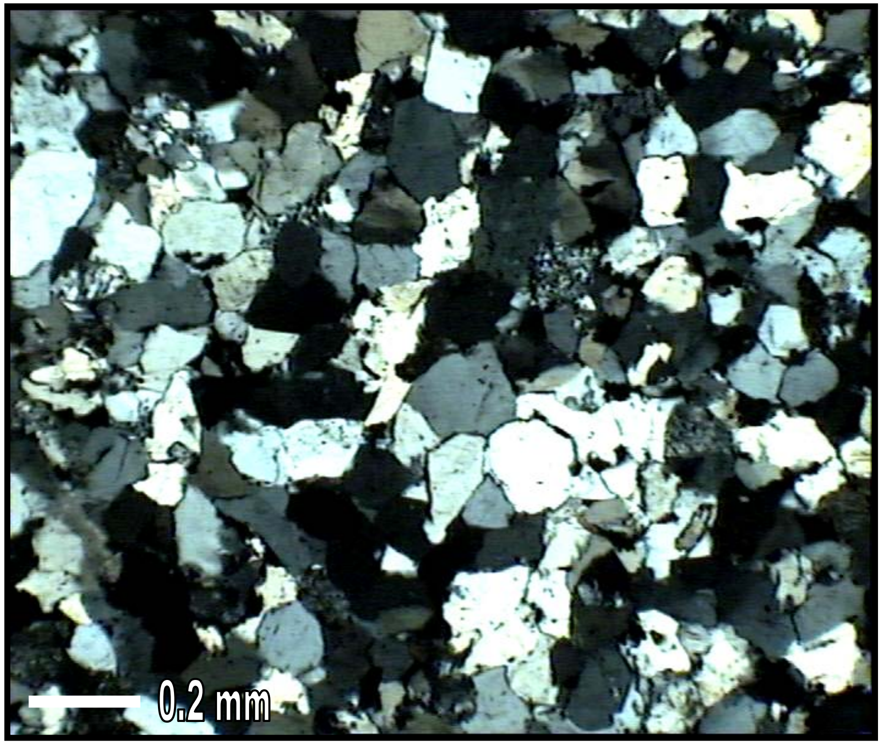

Reservoir Facies Classification

F1: Massive anhydrite and pervasive anhydrite plugging

F2: Dolomitic mudstone often with fenestral fabric.

F3: Stromatolite boundstone oftan with microbial communities.

F4: Lime skeletal / peloid wackestone to packstone

F5: Medium-grained ooid grainstone with oomoldic porosity.

F6: Coarse - grained skeletal grainstone with interparticles porosity.

F7: Fine-grained peloid / ooid grainstone.

F8: Intra formational conglomerate.

F9: Heavily bioturbated mudstone.

F10: Fossiliferous mudstone / wackestone.

F11: Dark argillaceous mudstone with lamination.

F12: Thrombolite boundstone.

Reservoir Characterization

Core facies	No.	Helium Porosity (%)				Air Permeability (mD)			
		MAX	MEAN	MIN	Std. Dev.	MAX	MEAN	MIN	Std. Dev.
CF1	9	3.56	0.90	0.13	1.07	0.782	0.154	0.045	0.236
CF2	160	24.22	4.52	0.10	5.11	158.692	5.467	0.019	18.748
CF3	15	15.12	3.19	0.67	4.06	15.172	2.722	0.028	4.479
CF4	180	24.30	5.98	0.01	6.24	108.512	5.622	0.001	14.879
CF5	179	36.32	15.79	0.21	9.02	242.815	11.297	0.010	28.535
CF6	135	32.86	9.44	0.11	7.60	213.197	8.274	0.019	23.955
CF7	195	36.64	10.15	0.06	9.86	346.693	17.412	0.023	51.922
CF8	6	9.99	5.06	0.90	3.74	42.134	7.132	0.043	17.147
CF9	53	26.66	7.57	1.23	7.55	80.529	6.039	0.002	15.461
CF10	13	15.75	5.27	0.16	4.75	24.195	5.256	0.043	9.072
CF11	0	-	-	-	-	-	-	-	-
CF12	5	1.26	1.07	0.73	0.21	0.116	0.063	0.037	0.031

Reservoir Characterization on the carbonate reservoir

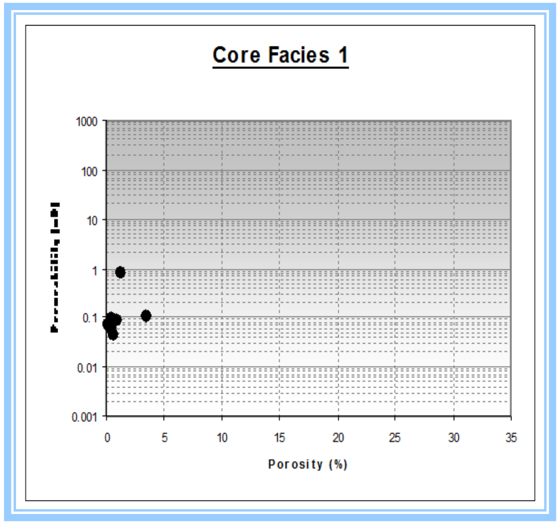

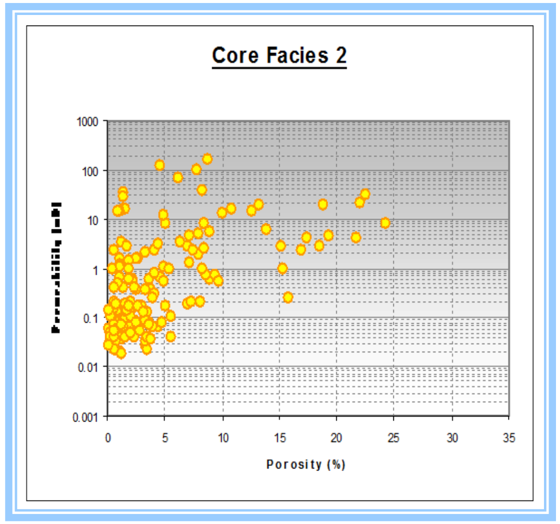

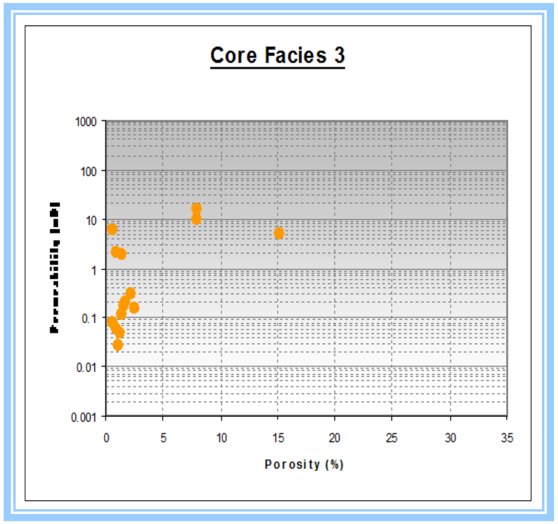

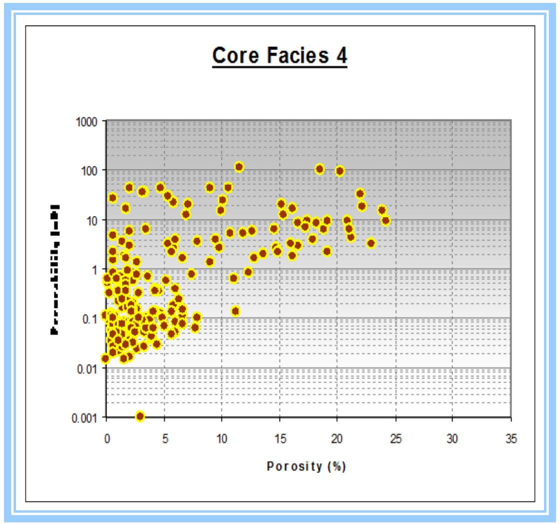

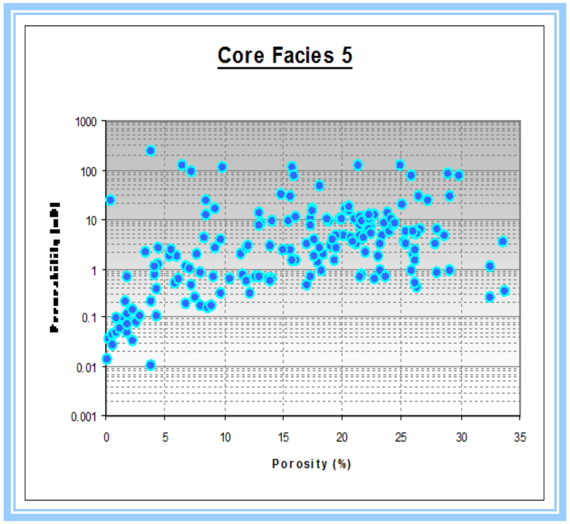

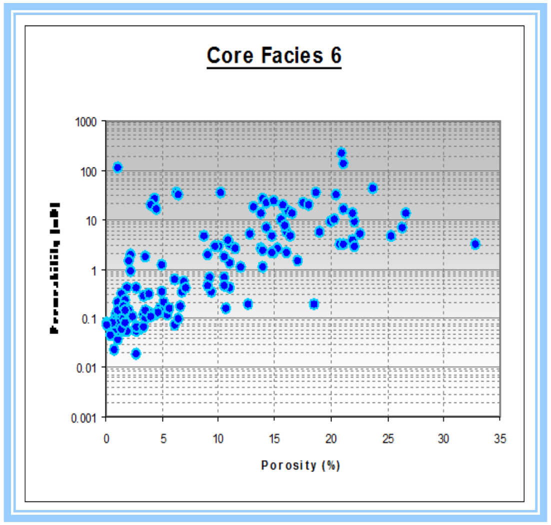

Reservoir Rock Typing

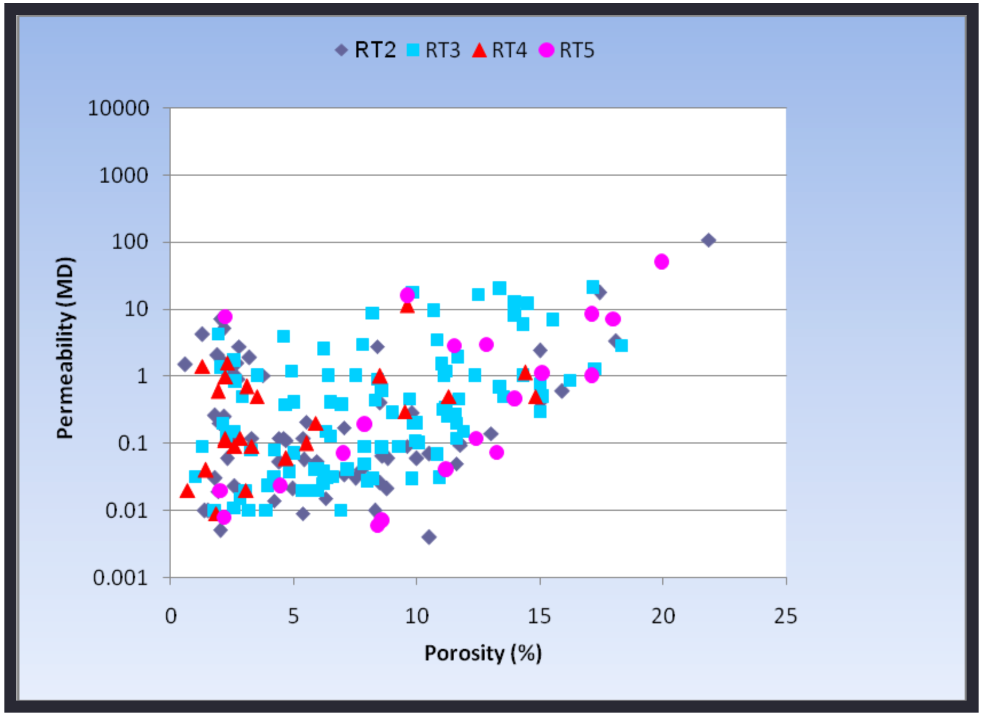

RT1: Argillaceous mudstone/claystone

RT2: Lime bioclastic mud-dominated wackestone

RT3: Lime bioclastic grain-dominated packstone/grainstone

RT4: Lime coarse grain Rudist dominated wackestone/packstone

RT5: Dolomitized bioclastic mud-dominated wackestone/packstone

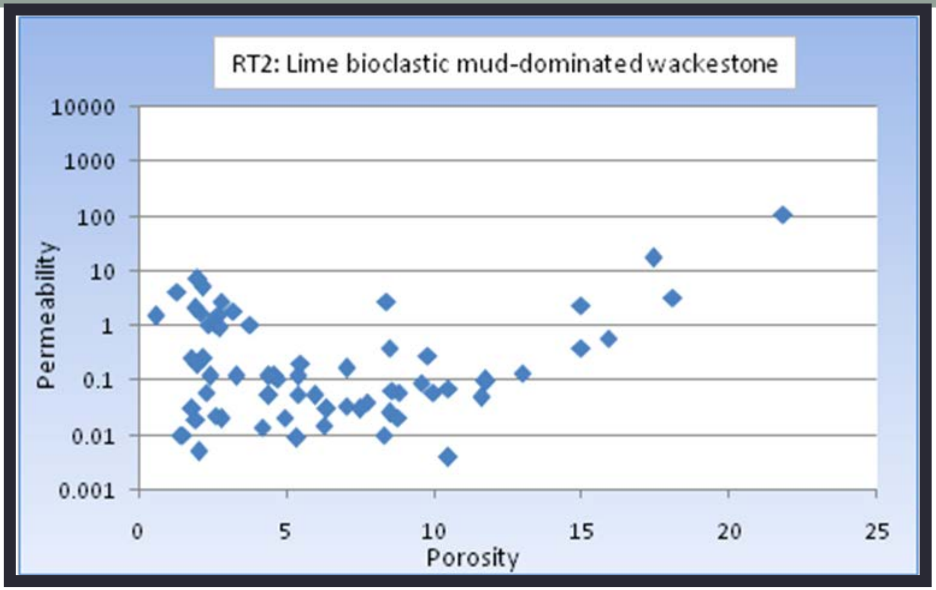
RT2: Lime bioclastic mud-dominated wackestone
10000
1000
100
10
1
0.1
0.01
0.001
Permeability
0
5
10
15
20
25
Porosity

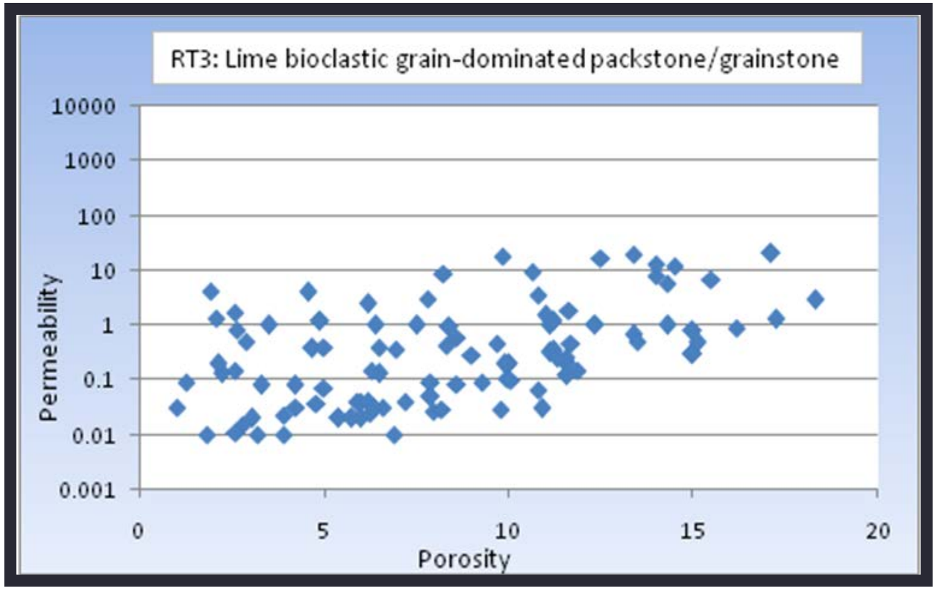
RT3: Lime bioclastic grain-dominated packstone/grainstone
10000
1000
100
10
1
0.1
0.01
0.001
Permeability
0
5
10
15
20
Porosity

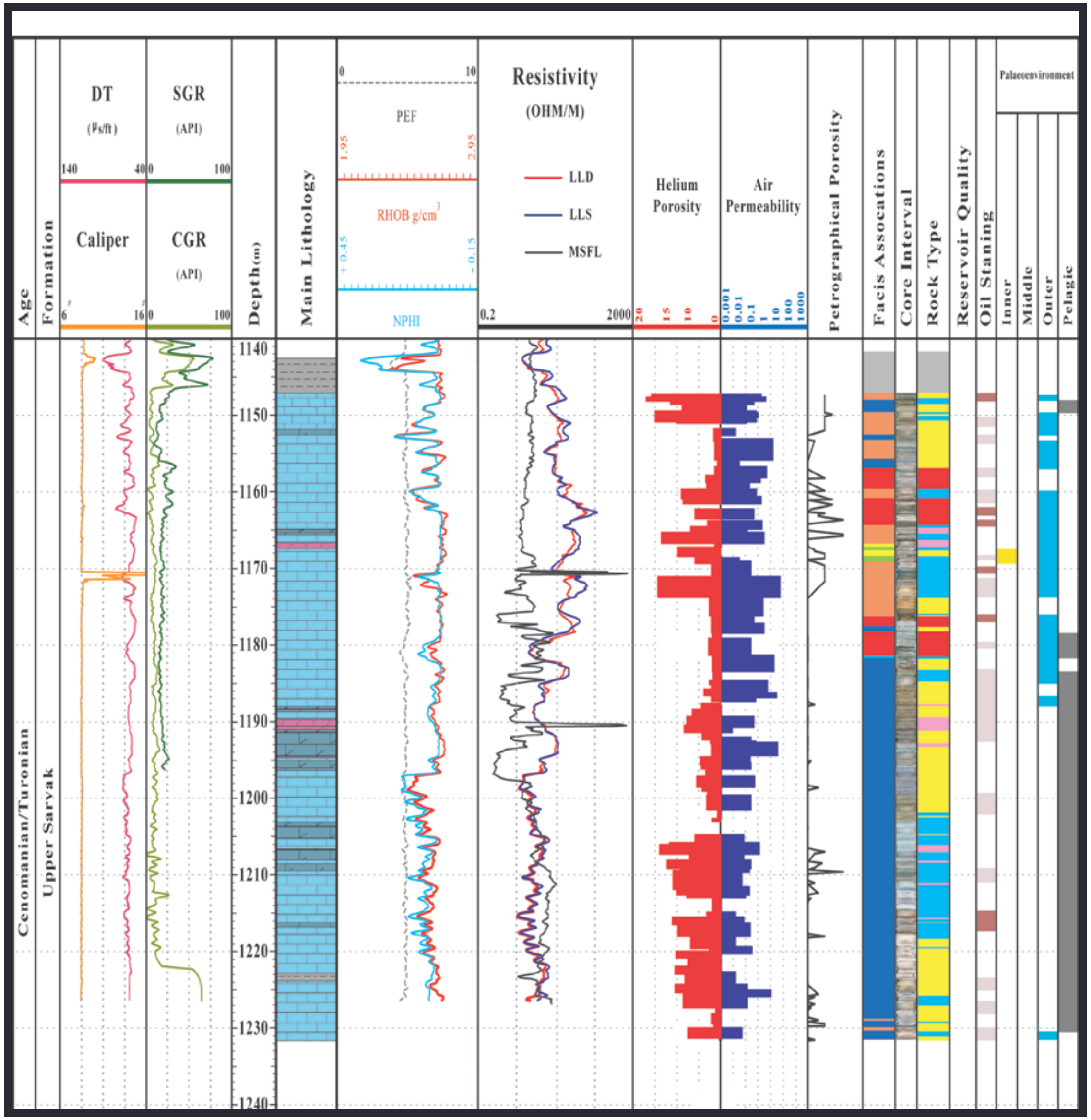

Reservoir Rock Type

- RT1: Argillaceous mudstone/claystone
- RT2: Lime bioclastic mud-dominated wackestone
- RT3: Lime bioclastic grain-dominated packstone/grainstone
- RT4: Lime coarse grain Rudist dominated wackestone/packstone
- RT5: Dolomitized bioclastic mud-dominated wackestone/packstone

Facies Associations

- F1: Lagoonal skeletal wackestone
- F2: Lagoonal skeletal packstone
- F3: Fine to medium-grained peloid/skeletal packstone/grainstone
- F4: Medium-grained Rudist/Echinoderm wackestone/packstone
- F5: Coarse-grained Rudist/Sponge floadstone/Rudstone
- F6: Planktonic skeletal wackestone/packstone
- F7: Argillaceous mudstone/claystone

Petrophysical correlation across the Field

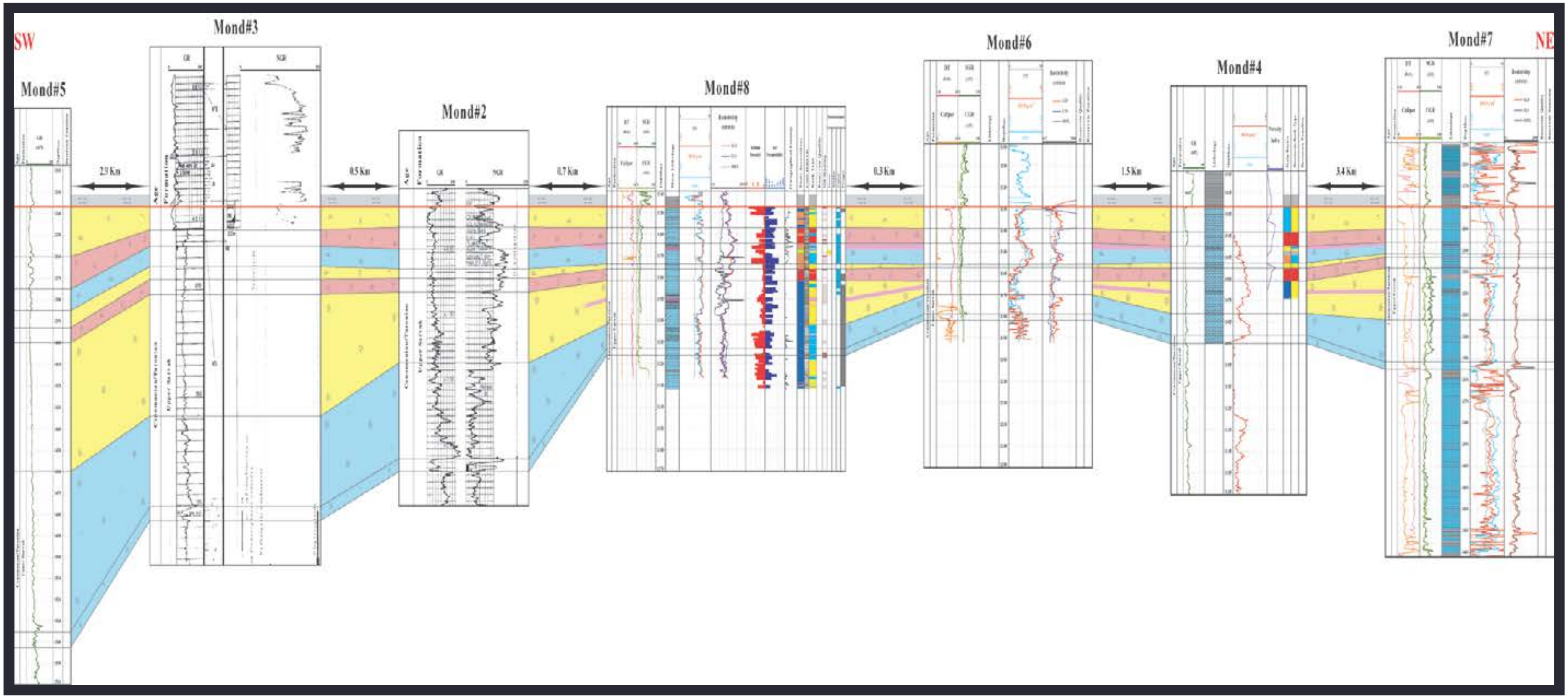

Well Logging

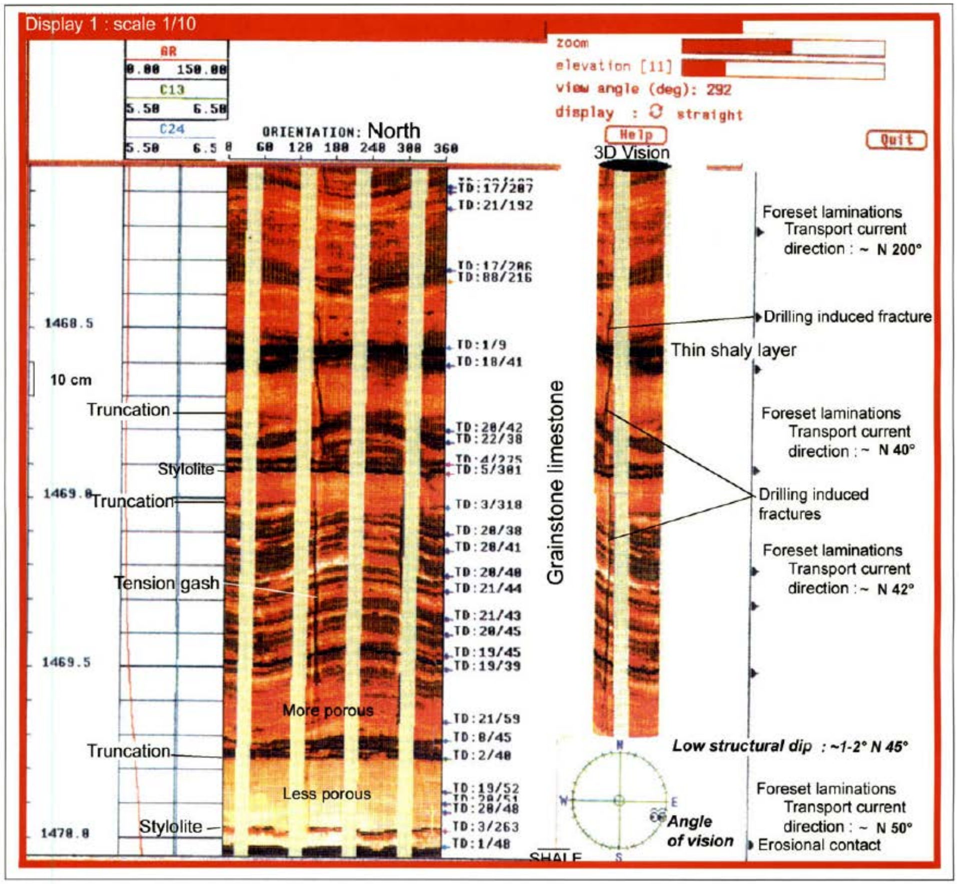

Figure 1-8a - Example of borehole wall images and its interpretation in terms of depositional units, texture, sedimentary structures and dip data.

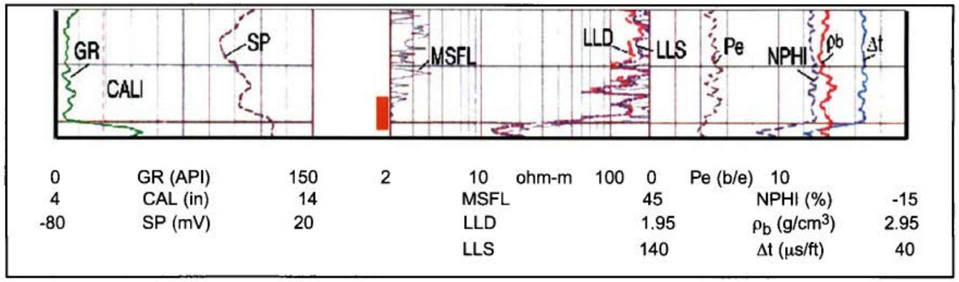

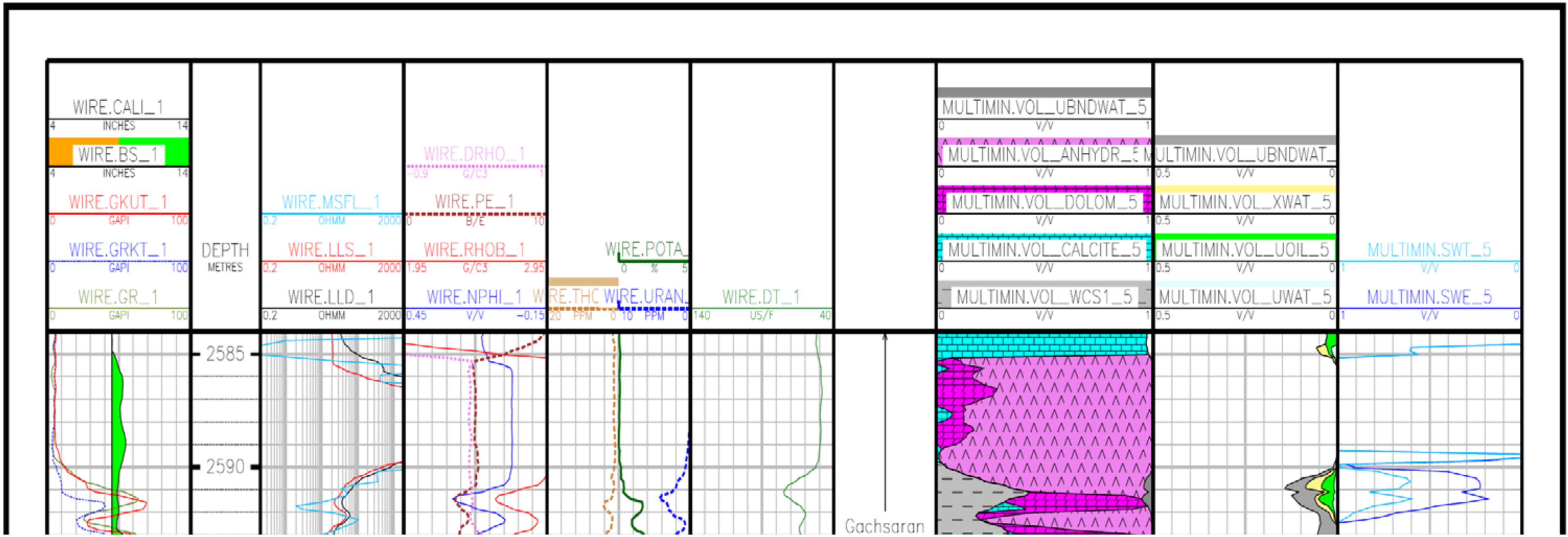

WIRE.CALI_1
4 INCHES 14
WIRE.BS_1
4 INCHES 14
WIRE.GKUT_1
0 GAPI 100
WIRE.GRKT_1
0 GAPI 100
WIRE.GR_1
0 GAPI 100
DEPTH
METRES
2585
2590
WIRE.MSFL_1
0.2 OHMM 2000
WIRE.LLS_1
0.2 OHMM 2000
WIRE.LLD_1
0.2 OHMM 2000
WIRE.DRHO_1
-0.9 G/C3 1
WIRE.PE_1
0 B/E 10
WIRE.RHOB_1
1.95 G/C3 2.95
WIRE.NPHI_1
0.45 V/V -0.15
WIRE.POTA_
0 % 5
WIRE.THC
20 PPM 0
WIRE.URAN_
10 PPM 0
WIRE.DT_1
140 US/F 40
Gachsaran
MULTIMIN.VOL_UBNDWAT_5
0 V/V 1
MULTIMIN.VOL_ANHYDR_5
0 V/V 1
MULTIMIN.VOL_DOLOM_5
0 V/V 1
MULTIMIN.VOL_CALCITE_5
0 V/V 1
MULTIMIN.VOL_WCS1_5
0 V/V 1
MULTIMIN.VOL_UBNDWAT_
0.5 V/V 0
MULTIMIN.VOL_XWAT_5
0.5 V/V 0
MULTIMIN.VOL_UOIL_5
0.5 V/V 0
MULTIMIN.VOL_UWAT_5
0.5 V/V 0
MULTIMIN.SWT_5
1 V/V 0
MULTIMIN.SWE_5
1 V/V 0

General Processes Used For Recording Physical Parameters

Natural or spontaneous phenomena

Basic equipment : a single detector (passive system)

- Natural gamma radioactivity
  - Total
  - Spectrometry
- Spontaneous potential
- Temperature - Bottom hole temperature
- Formation pressure
- Borehole diameter
- Borehole deviation

Physical properties measured by inducing from the formation a response to an excitation

Basic equipment : source or emitter + detector (s)

- Resistivity
  - Long-spacing devices
    - non-focused
    - focused
  - Short-spacing devices
    - non-focused
    - focused
  - Ultra-long spacing devices
- Conductivity
- Dielectric constant (electromagnetic propagation)
- Magnetic susceptibility
- Total magnetic field
- Electronic density
- Photoelectric index
- Neutron interactions
  - Epithermal neutron absorption
  - Thermal neutron absorption
  - Induced γ ray spectrometry by inelastic collisions
  - Induced γ ray spectrometry by thermal neutron absorption
  - Induced γ ray spectrometry by thermal neutron activation
  - Thermal neutron decay time
- Relaxation time of proton spin (nuclear magnetic resonance)
- Acoustic velocity
- Acoustic-signal amplitude
- Well seismics
- Formation dip - Dipmeter
- Borehole imagery
  - electric
  - ultrasonic

Basic of Logging

- Depth of investigation
- Vertical Resolution

Depth Of Investigation Of Logging Tools

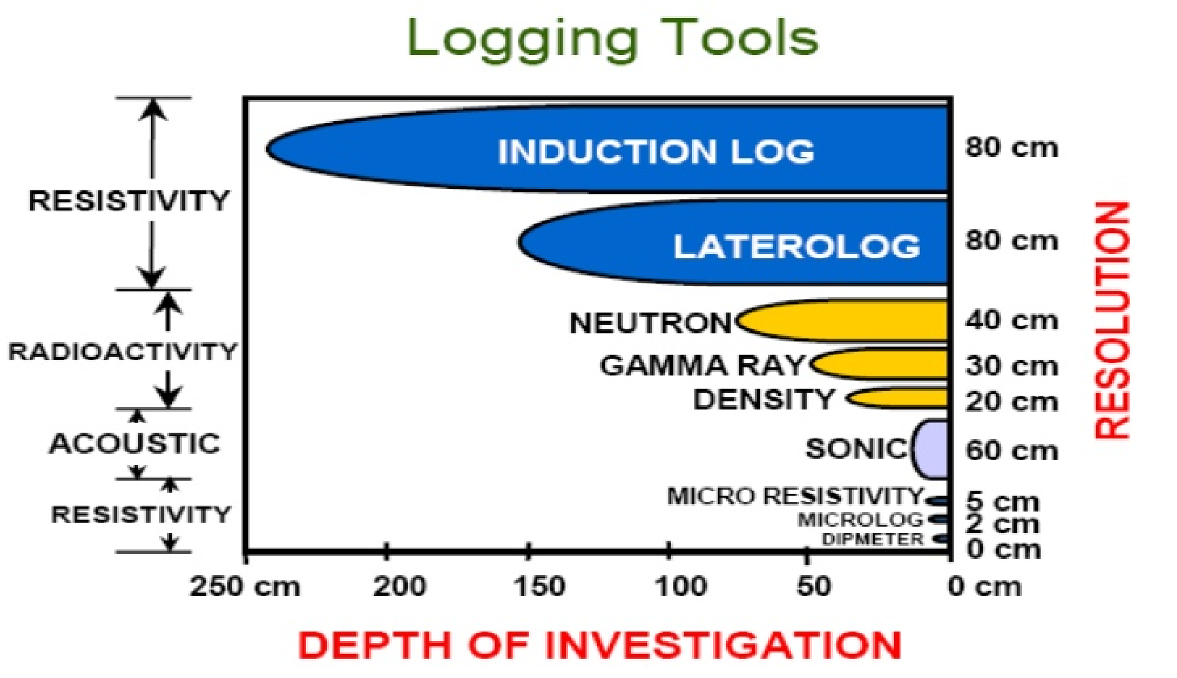

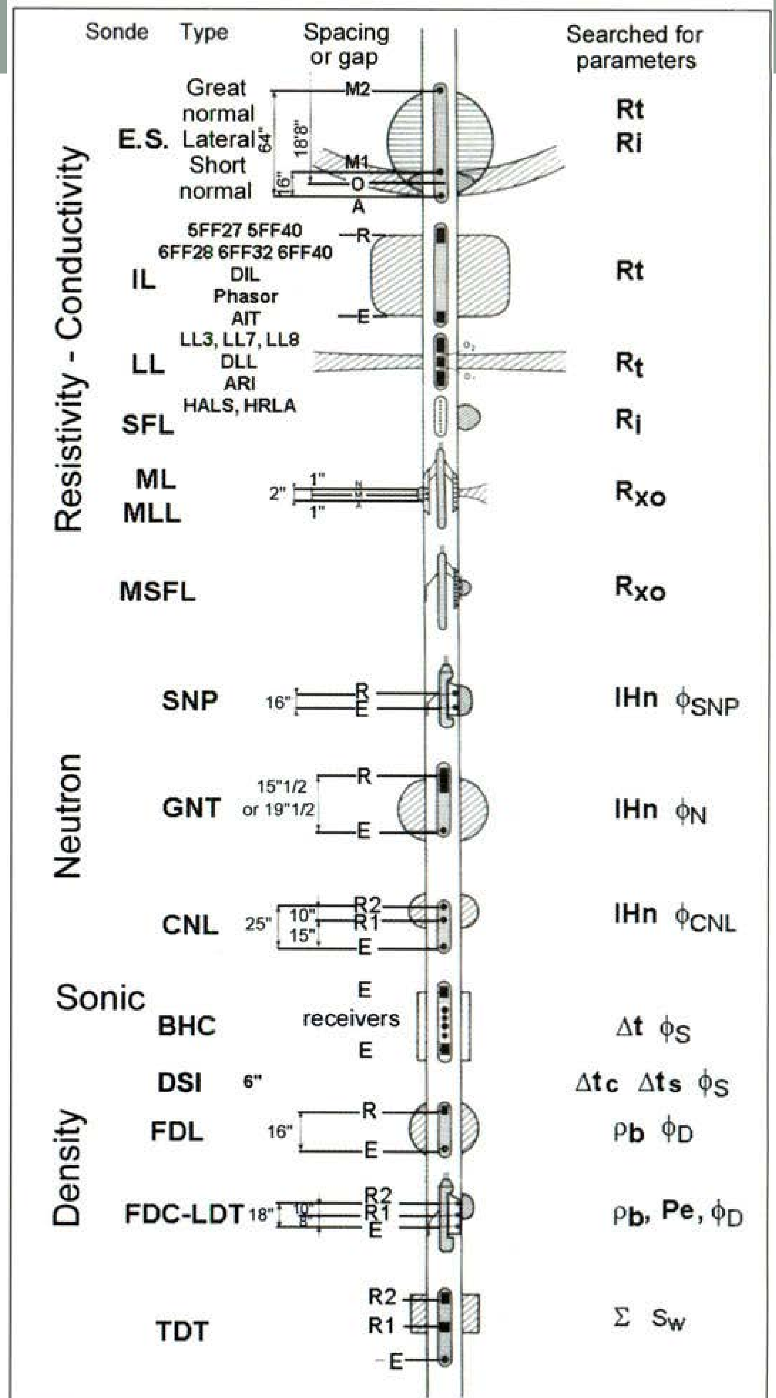
Sonde
Type
Spacing or gap
Searched for parameters
Resistivity - Conductivity
E.S.
Great normal
Lateral
Short normal
64"
18'8"
16"
M2
M1
O
A
Rt
Ri
IL
5FF27 5FF40
6FF28 6FF32 6FF40
DIL
Phasor
AIT
R
E
Rt
LL
LL3, LL7, LL8
DLL
ARI
HALS, HRLA
Rt
SFL
Ri
ML
MLL
2"
1"
1"
Rxo
MSFL
Rxo
Neutron
SNP
16"
R
E
IHn ϕSNP
GNT
15"1/2
or 19"1/2
R
E
IHn ϕN
CNL
25"
10"
15"
R2
R1
E
IHn ϕCNL
Sonic
BHC
E
receivers
E
Δt ϕS
DSI
6"
Δtc Δts ϕS
Density
FDL
16"
R
E
ρb ϕD
FDC-LDT
18"
10"
8"
R2
R1
E
ρb, Pe, ϕD
TDT
R2
R1
E
Σ Sw

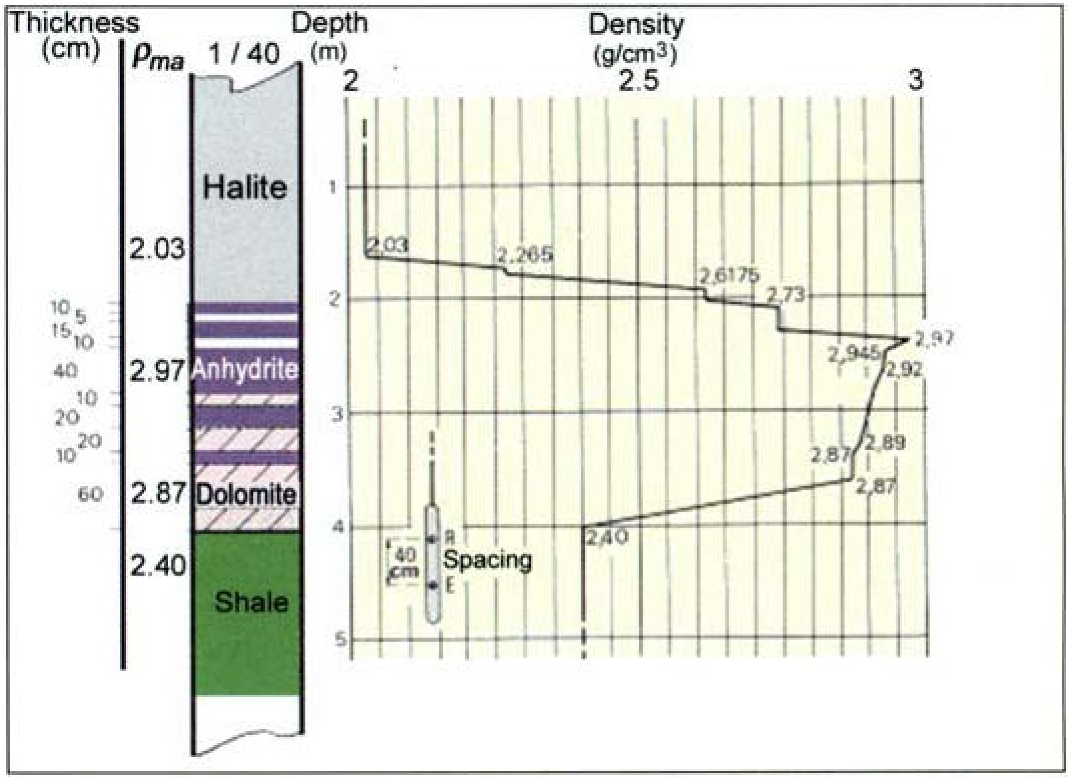

Thickness (cm)
ρ_{ma}
1 / 40
Depth (m)
Density (g/cm3)
2
2.5
3
Halite
2.03
Anhydrite
2.97
Dolomite
2.87
Shale
2.40
10
5
15
10
40
10
20
20
10
60
1
2
3
4
5
2,03
2,265
2,6175
2,73
2,97
2,945
2,92
2,89
2,87
2,87
2,40
40 cm
Spacing
R
E

Intrinsic vertical resolution of Schlumberger tools (completed from Allen *et al.*, 1988, and Theys, 1991).

Measurement	Vertical resolution	Sampling rate	Remarks
SP	6-10 ft	6 in.	Only if salinity contrast
Phasor Induction			
deep	84 - 96 in.	6 in.	
medium	60 - 72 in.		
enhanced	36 in.		
SFL	30 in.	6 in.	
AIT	18 in.	6 in	1, 2 or 4 ft Gives an image of the invasion
Laterolog			
DLL	28 in.	6 in.	
ARI	8 in.	0.5 in.	Gives an electrical image
HALS	8 - 16 in.	0.5 in.	Gives an electrical image
Microlog			
Microinverse	2 - 4 in.	2 in.	The measure is not focalized
Micronormal	4 in.		
MicroSFL	2 - 3 in.	2 in.	Focalized
Dipmeter - Imagery			
HDT	0.5 in.	0.2 in.	
SHDT	0.4 in.	0.1 in.	
FMS	0.2 in.	0.1 in.	Gives an electrical image
FMI	0.2 in.	0.1 in.	Gives an electrical image
EPT			
Transit time	2 in.	2 or 0.4 in.	
Attenuation	2 in.	2 or 0.4 in.	Shale indicator
Litho-density			
Density	15 in.	6 or 2 in.	
enhanced	4 in.		
Pe	2 in.		
Neutron			
Porosity	15 in.	6 or 2 in.	
resolution matched	24 in.		
enhanced	12 in.		
CMR	6 in.	6 in.	Estimation of porosity, permeability, pore size
TDT	6 - 66 in.*		
Gamma ray			
Standard	8 - 12 in.	6 in.	
Spectroscopy	8 - 12 in.		Measures Th, U and K
Sonic			
Standard	48 in.	6 in.	
BHC	24 in.		
Six-inch Δt	6 in.	1.2 in	
DSI	6 in.		Measures compressional shear & Stoneley wave velocity

* depends on the time constant and the depth interval on which the mean value is computed.

Table 2-4
Recommended maximum logging speeds.

Measurement		Maximum logging speed (ft/min)	Maximum logging speed (m/min)
SP		100	30
Induction		83	25
Laterolog		50	15
Rxo measurement		33	10
Neutron	TC = 2 sec	30	9
GR	TC = 3 sec	20	6
Density	TC = 4 sec	15	4.5
TDT			
Spectrometry		15	4.5
Sonic Transit time		60	18
Attenuation		35	10
Dipmeter		50	15
Imagery		15	4.5

- **Data Transmission:**

1. Cable transmission
2. Mud pulse telemeter

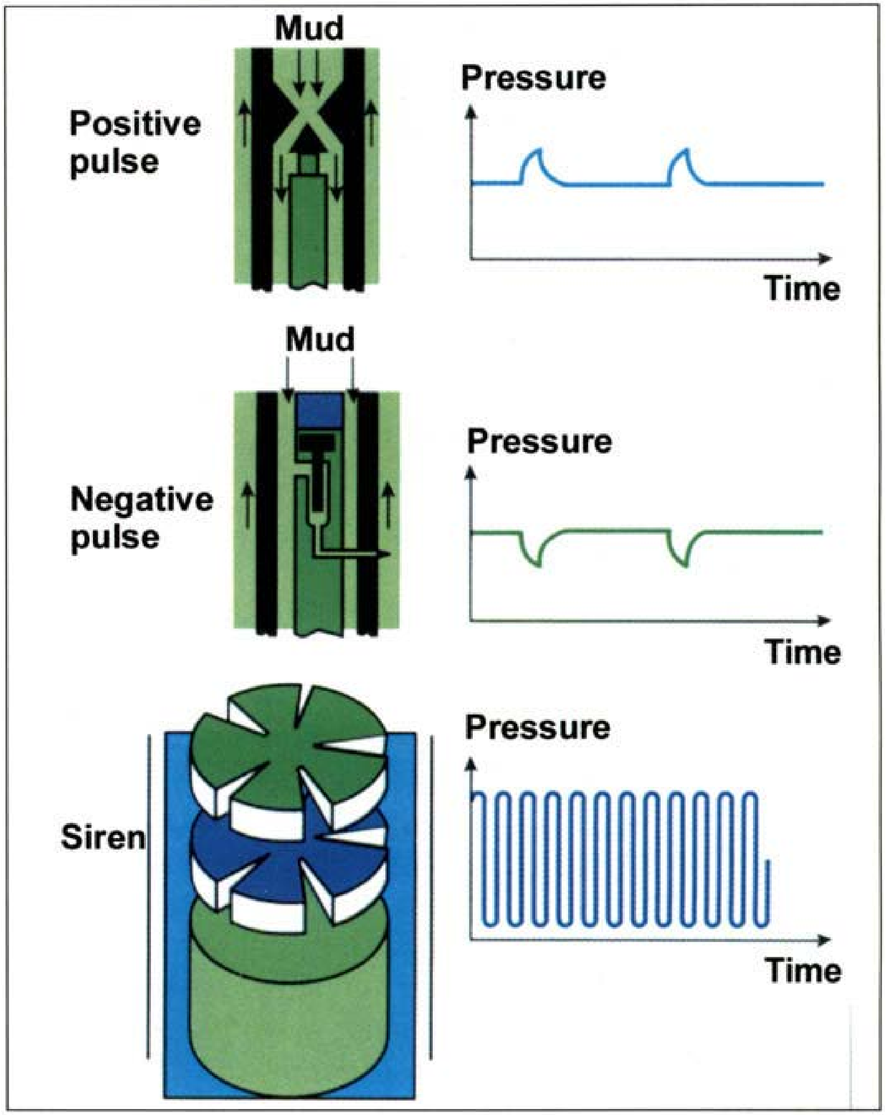


Fixed-mount Pulser
Retrievable Pulser with Stinger

Caliper Logs

What Do They Measure?

Size and shape of a recently drilled hole.

How Do They Work?

- Mechanical arms record hole size
- Hydraulic systems with calibrated potentiometers.

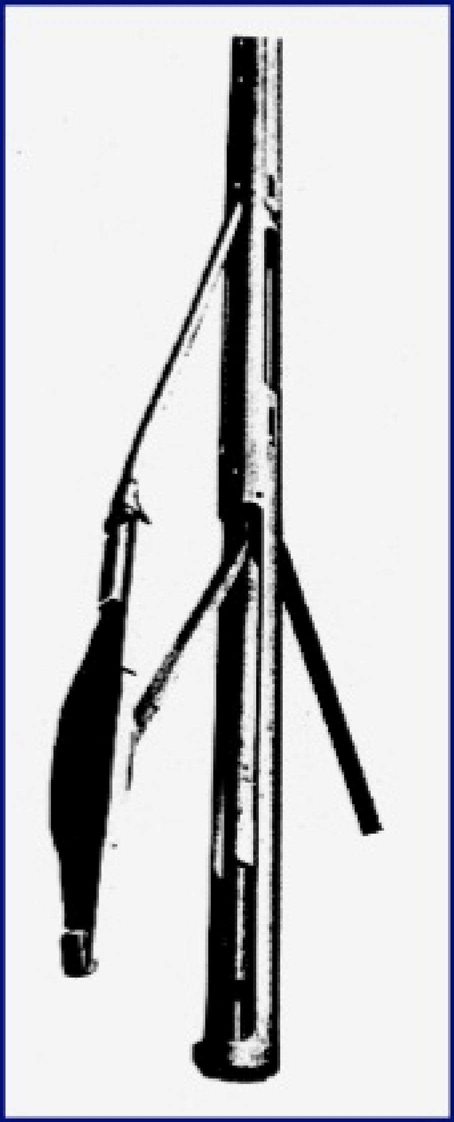

How Are They Used?

- Hole size used to correct other logs
- Hole volume for cementing
- Lithologic information
  - washouts indicative of formation properties
- Stress field from hole break-out

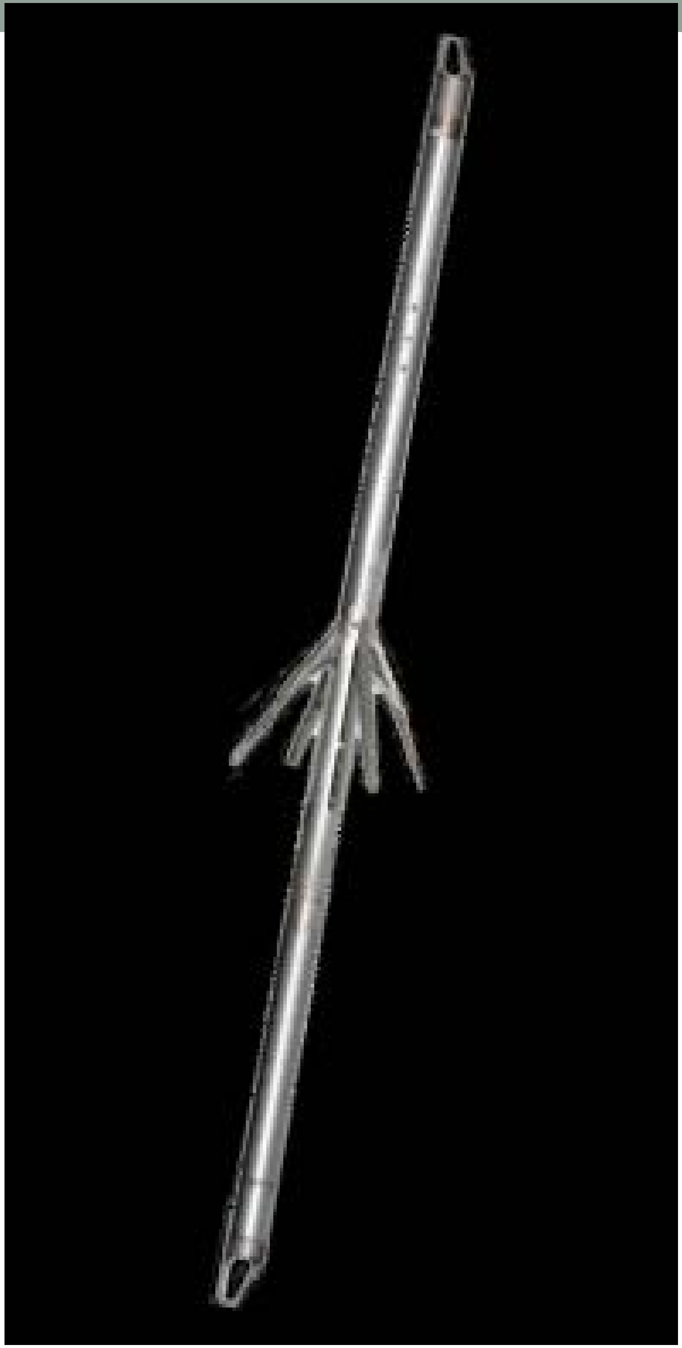

Generalities On Nuclear Measurements

Principle of the different nuclear logging techniques

Measurement principle
Natural radioactivity Natural gamma (γ) radioactivity (total) Natural gamma (γ) ray spectroscopy
Radiation induced by neutron bombardment Spectroscopy of γ rays emitted by the activation of oxygen: $^{16}O(n,p)^{16}N(\beta^-)$ $^{16}O^*(\gamma = 6.13\ MeV)^{16}O$ or the activation of a wide range of elements
Spectroscopy of γ rays emitted from fast neutron interactions (mainly inelastic): e.g.: $^{16}O(n,n'\ \gamma = 6.13\ MeV)^{16}O$, $t_{1/2} = 1.7 \times 10^{-11}$ sec
Spectroscopy of γ rays emitted by thermal neutron capture
Epithermal neutron density at a fixed distance from a high-energy neutron source Thermal neutron density at a fixed distance from a high-energy neutron source, by: (a) detection of neutrons themselves (b) detection of gamma rays arising from capture of the thermal neutrons
Decay rate of the thermal neutron population. The thermal neutron density is sampled at two different times between neutron bursts, by detecting the capture gamma rays.

Compton scattering of gamma rays Gamma rays emitted from a source are scattered by the formation. The count-rate of those reaching the detector is function of the formation density.
Photoelectric absorption of low energy gamma rays Low-energy gamma absorption and measurement of the photoelectric absorption index of the formation, related to the lithology.
Decay of proton spin precession induced by a strong magnetic field Protons are caused to precess about the local Earth magnetic field by a strong DC magnetic pulse. This precession decays with a time characteristic of the formation fluids, porosity and pore size.

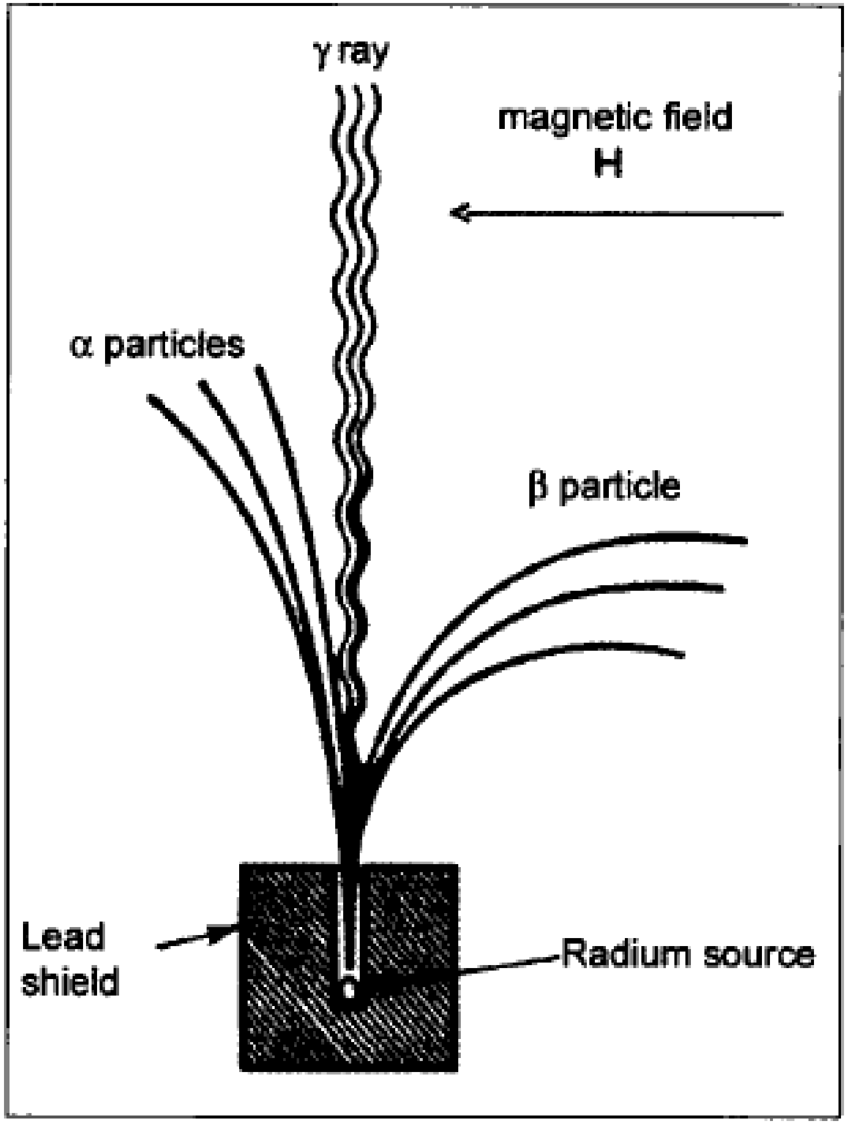

Figure 10-1 - The three types of radiation. Only the gamma ray is not deviated by a magnetic field as it is not charged.

- ***α* –radiation:** An *α* -particle may be emitted from an atomic nucleus during radioactive decay. It is positively charged and has two protons and two neutrons. It is physically identical to the nucleus of the helium atom. By *α* -emission the element of atomic number Z is transformed into an element of atomic number Z - 2 and the number of nucleons decreases from **A** to **A** - **4.**
- **β particles:** β particles are high-energy, high-speed electrons or positrons emitted by certain types of radioactive nuclei such as potassium-40. The beta particles emitted are a form of ionizing radiation also known as beta rays

- **ɣ-radiation: ɣ**-radiation may be considered as an electromagnetic wave similar to visible light or X-rays, or as a particle or photon. Gamma rays are electromagnetic radiations emitted from an atomic nucleus during radioactive decay. These radiations are characterized by wave lengths in the range of 10^{-9} to 10^{-11} cm, equivalent to frequencies ranging from 10^{19} to 10^{21} sec-1

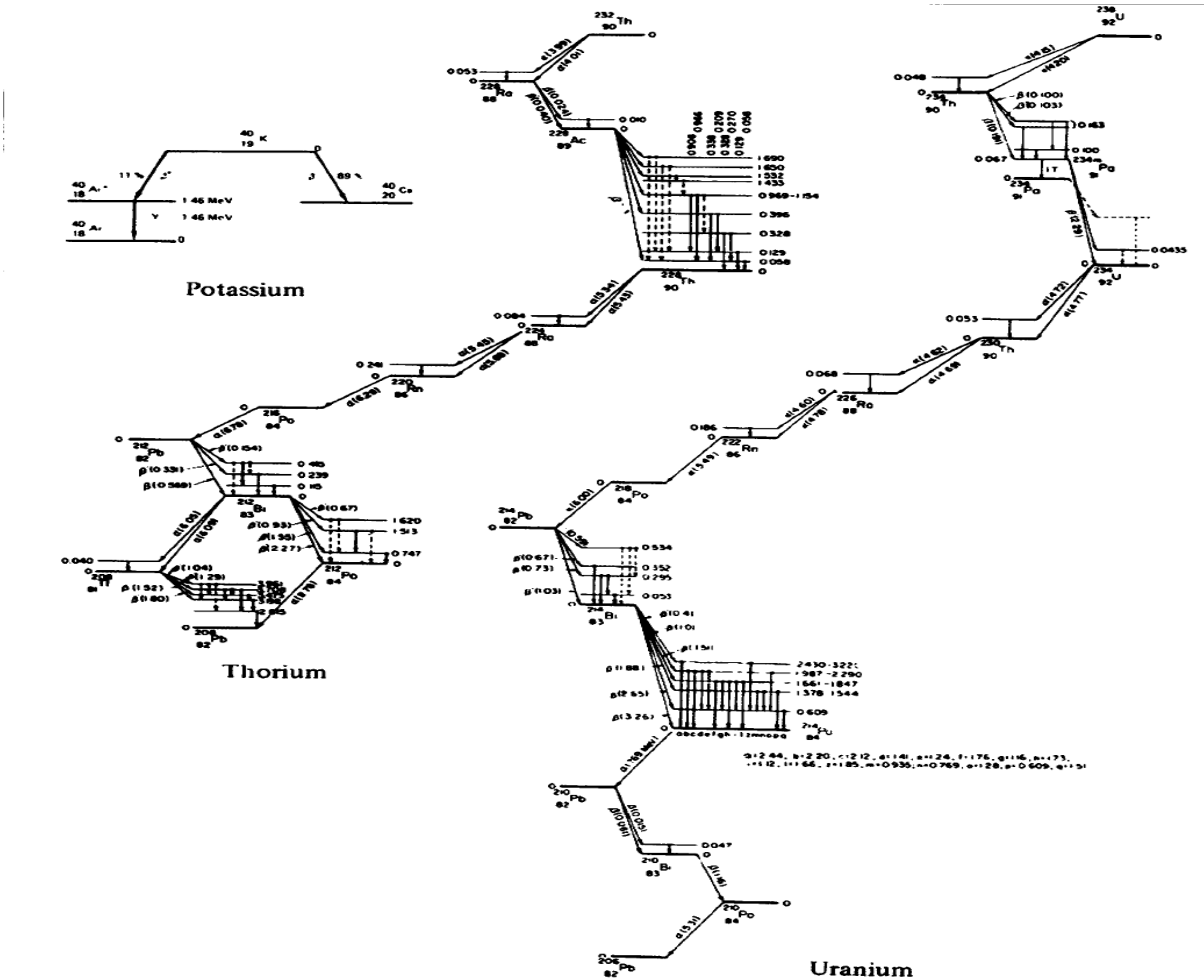
Potassium
Thorium
Uranium

Pair production

- When the photon energy is above the threshold value of 1.022 MeV, the interaction of photon and matter leads to pair production, it means the production of a negatron (or negative electron) and a positron (or positive electron) each with an energy of 0.51 1 MeV

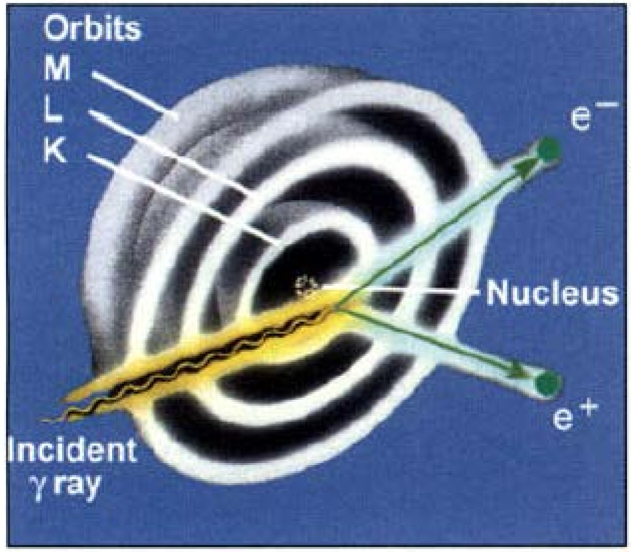

Figure 9-5 - Schematic o pair production at a nucleus (courtesy of Schlumberger).

Compton scattering

- When the incident photon collides with an electron its energy is divided between the kinetic energy E = mv2 given to the electron ejected from its atom with initial velocity v and a photon "scattered" in a direction making an angle with the original incident direction (energy is between1.022 MeV and 150 KeV).
- This type of reaction is called Compton scattering and it is the reaction figuring mainly in density measurements. The scattering effect is sensitive to the electron density of the formation (number of electrons per unit volume). The macroscopic cross section in a material consisting of atoms of mass **A,** and atomic number ***Z,*** is expressed by:

$$\Sigma_{Co} = \sigma_{Co} (N_{Av}/A) \rho_b Z \quad (9\text{-}5)$$

where:

Σ_{Co} is the macroscopic Compton cross section

σ_{Co} is the Compton cross section

N_{Av} is the Avogadro's number (6.022×10^{23} mol^{-1})

ρ_b the material density.

Z represents the number of electrons per atom.

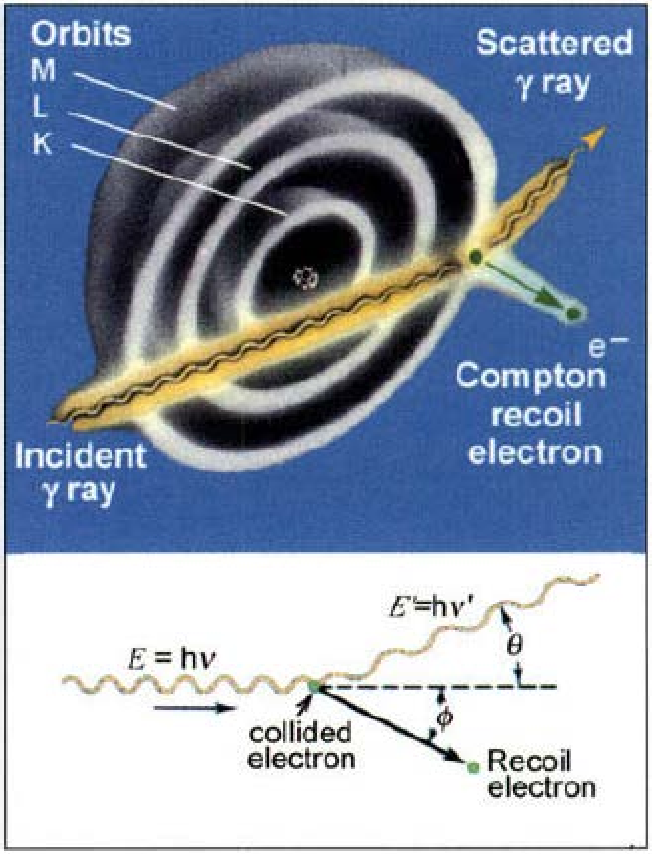

Figure 9-7 - Schematic of the Compton process. Geometrical relations in the Compton process. (courtesy of Schlumberger).

Photoelectric effect

- In the course of a collision with an electron a photon loses part of its initial energy and for a certain energy level it can transfer all its remaining energy to the electron in the form of kinetic energy. The electron is ejected from its atom and the photon disappears. The gamma ray is absorbed (energy is less than 150 KeV).
- The microscopic cross-section of this reaction, Ƭ, has been found to be related to the atomic number of the target atom, Ƭ, and the energy of the incident gamma ray, Eɣ, by the following relation:

$$\tau_{\text{atom}} = 12.1\ [(Z)^{4.6} / (E_\gamma)^{3.15}]$$

The unit is the barns / atom

- The photoelectric effect is highest when the gammaray energy is small and the atomic number of the element high. For the most abundant rocks composing the Earth's crust, it becomes the dominant process for gamma ray energies below about 100 keV. It is at the origin of a measurement that is sensitive to the average atomic number of the formations and so to the lithology.

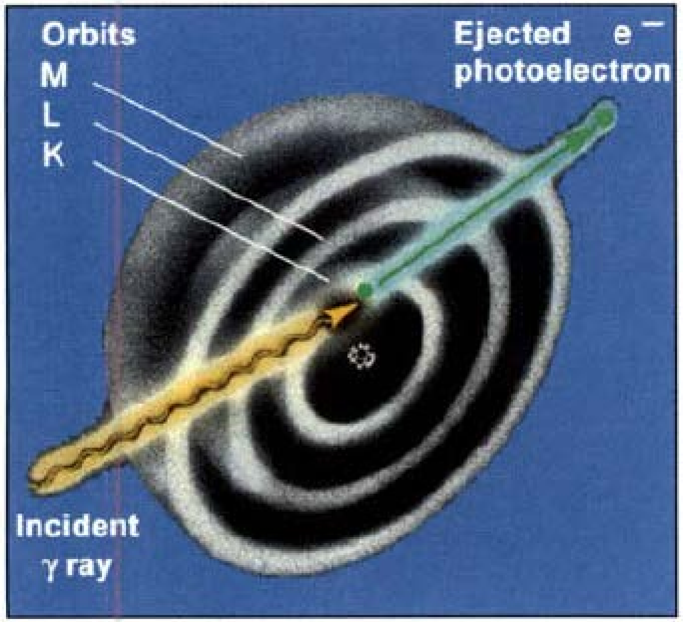

Figure 9-8 - Schematic of the photoelectric process (courtesy of Schlumberger).

Neutron radiation

- Neutron radiation is a kind of ionizing radiation which consists of free neutrons. A result of nuclear fission or nuclear fusion, it consists of the release of free neutrons from atoms, and these free neutrons react with nuclei of other atoms to form new isotopes, which, in turn, may produce radiation.

Neutron energy	Energy range
0.0–0.025 eV	Cold neutrons
0.025 eV	Thermal neutrons
0.025–0.4 eV	Epithermal neutrons
0.4–0.6 eV	Cadmium neutrons
0.6–1 eV	EpiCadmium neutrons
1–10 eV	Slow neutrons
10–300 eV	Resonance neutrons
300 eV–1 MeV	Intermediate neutrons
1–20 MeV	Fast neutrons
> 20 MeV	Relativistic neutrons

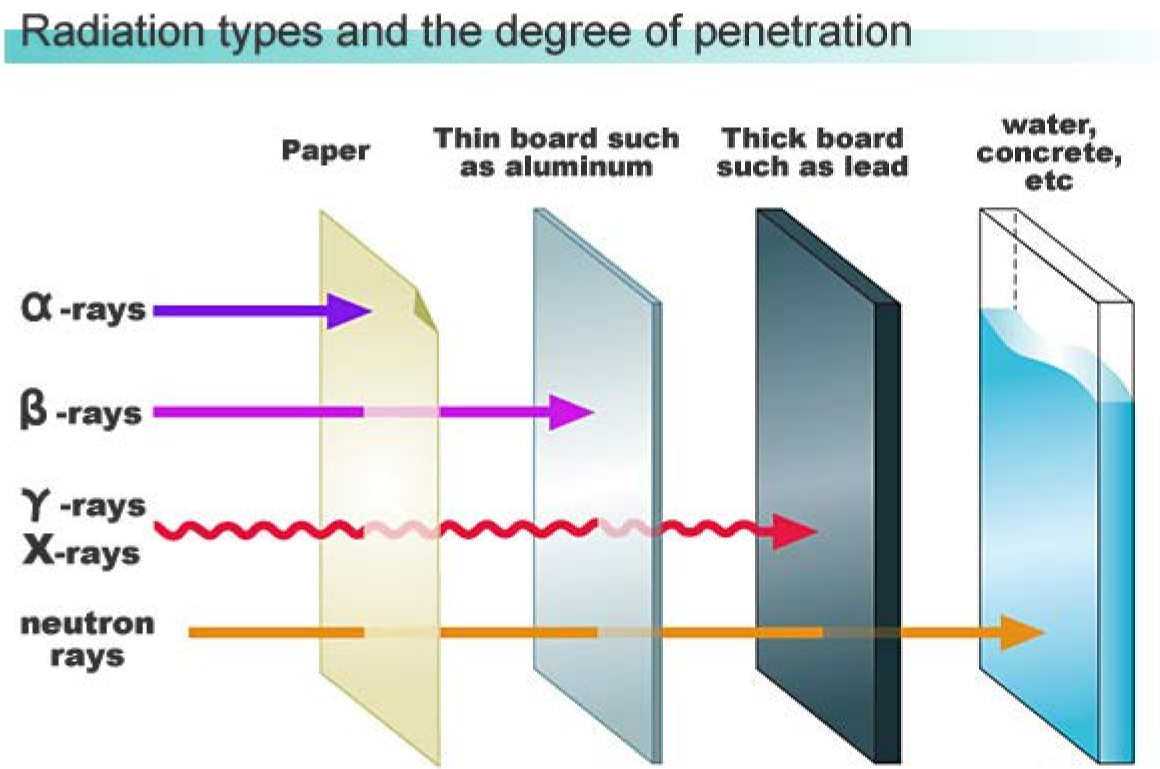
Radiation types and the degree of penetration
Paper
Thin board such as aluminum
Thick board such as lead
water, concrete, etc
α -rays
β -rays
γ -rays
X-rays
neutron rays

Minerals and rocks containing radioactive elements

Main radioactive elements

Element	Isotope	Percentage of the total element (%)	Emissions α	Emissions β	Emissions γ	Half life (year)	Relative abundance in Earth's crust (ppm)
Primeval natural gamma -ray emitters							
Potassium	^{40}K	0.0118		1	1	1.3×10^{9}	2.5
Uranium [d]	^{235}U	0.72	8[d]	5[d]	a	7.1×10^{8}	0.02
Secondary gamma-ray emitters by their daughters							
Uranium series	^{238}U	99.27	8[d]	6[d]	b	4.5×10^{9}	3
Thorium series	^{232}Th		7[d]	5[d]	b	1.4×10^{10}	12

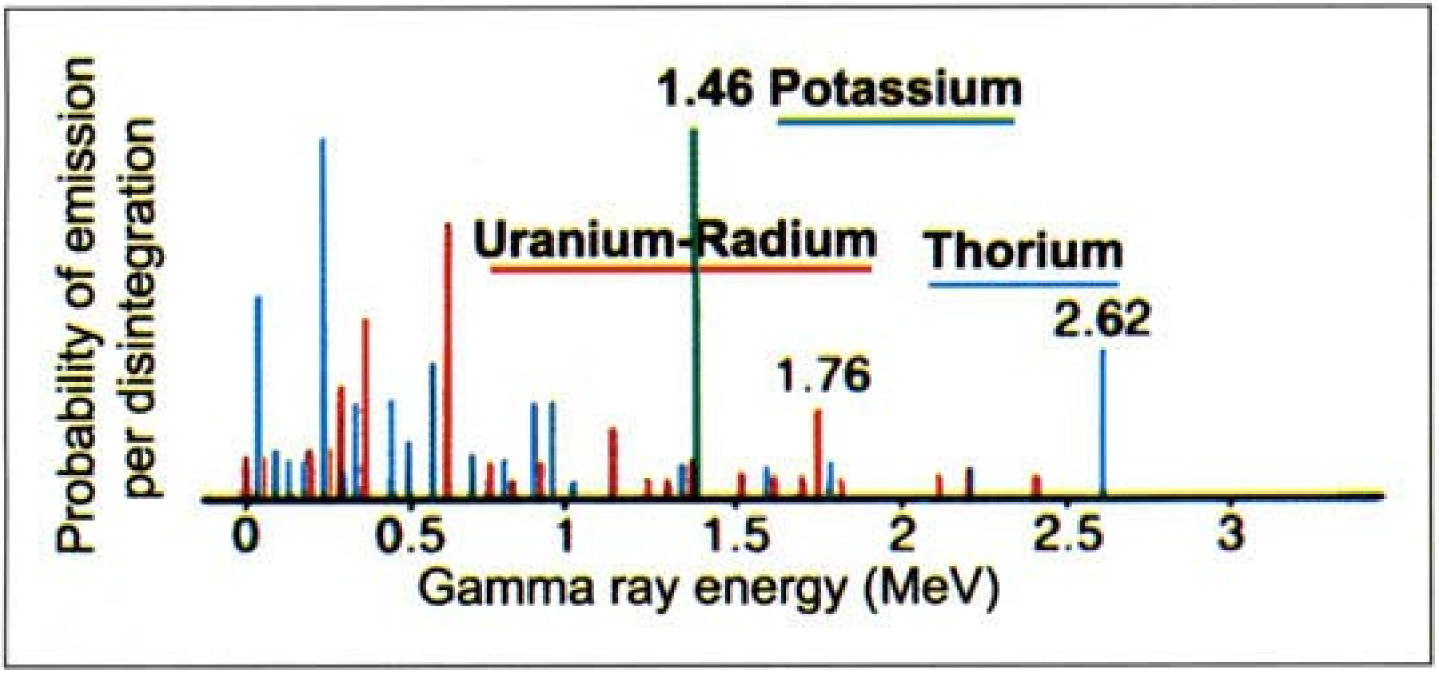
1.46 Potassium
Uranium-Radium
Thorium
2.62
1.76
Probability of emission
per disintegration
0
0.5
1
1.5
2
2.5
3
Gamma ray energy (MeV)

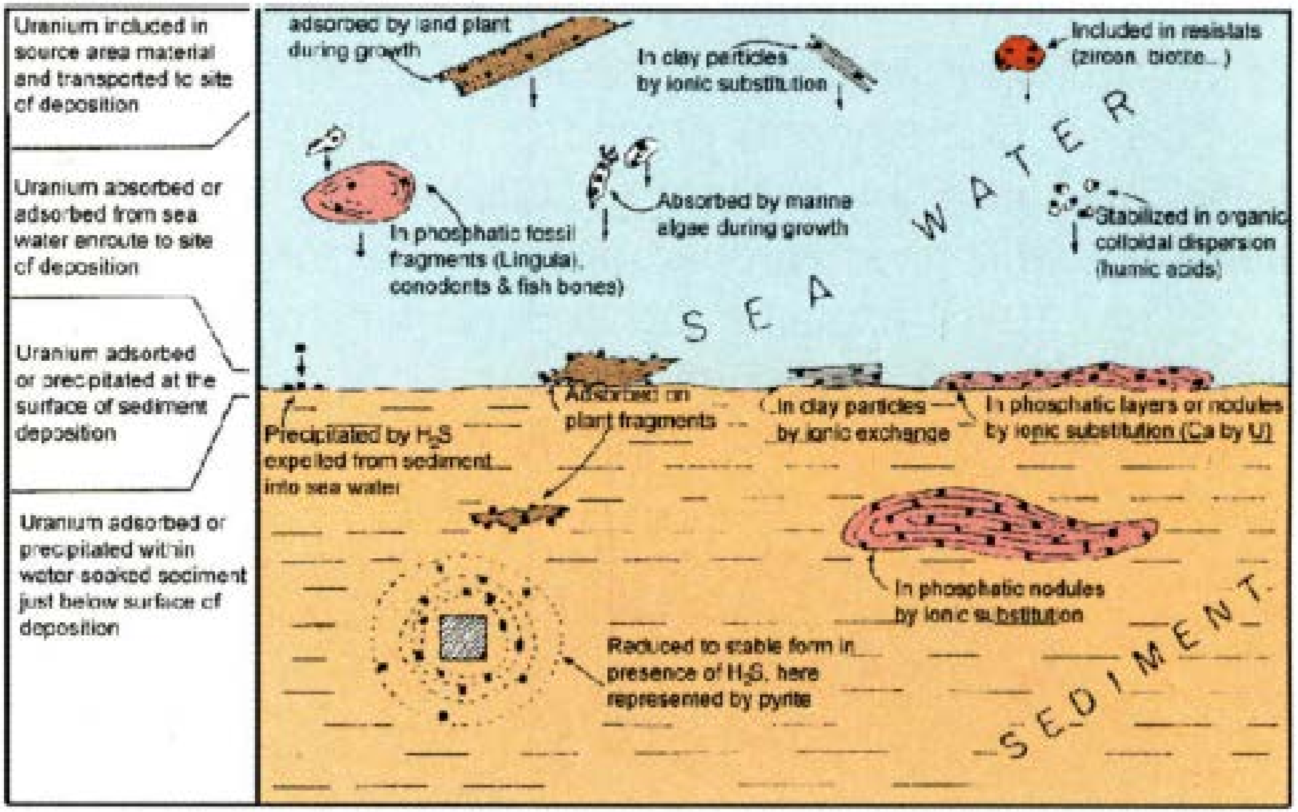

Figure 10-10 - Diagramatic sketch showing possible association and time of emplacement of uranium with common constituents of marine black shales. Uranium is represented by black squares (from Swanson, 1960).

Total Natural Radioactivity Measurement

- The measurement of the total natural radioactivity of the formations crossed by a well is known as the gamma ray log.
- The gamma-ray sonde contains generally one detector of scintillation-counter type. This type of counter is more efficient than the Geiger-Mueller counters previously used in older tools. Its dimension is shorter allowing a better vertical resolution.
- The detector records all the gamma rays emitted by the formation above some practical lower energy limit (on the order of 100 keV).

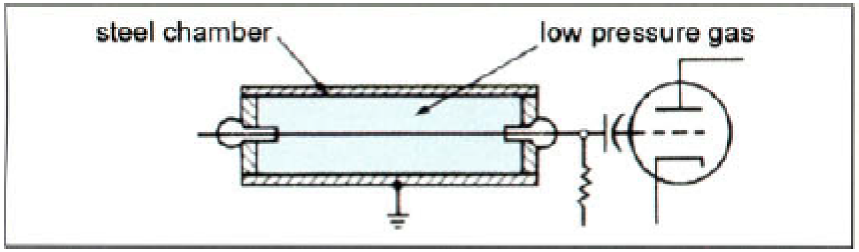

Figure 9-11 - Typical ionization chamber.

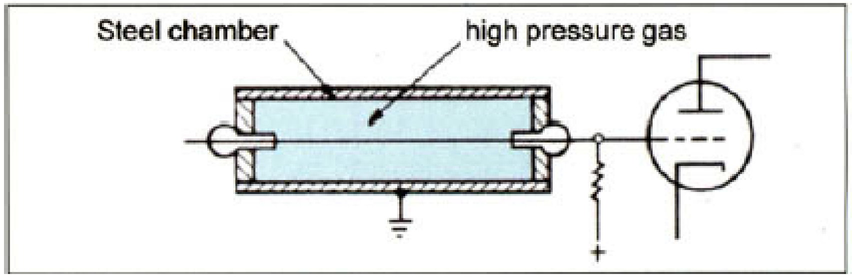

Figure 9-10 - Typical Geiger-Mueller counter.

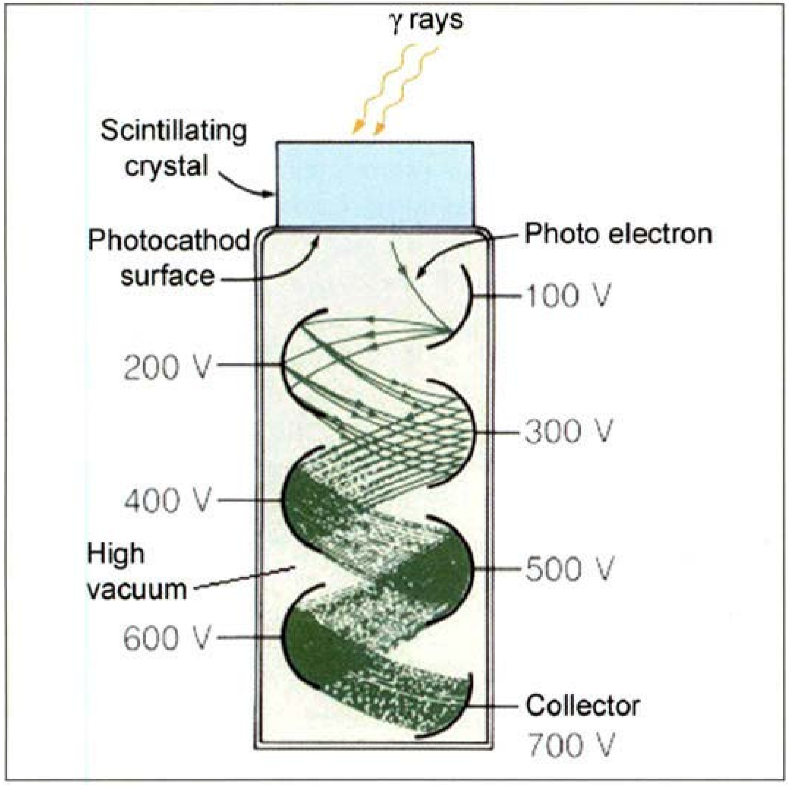

- Any gamma-ray flux generated in a formation at a distance x from the borehole wall must cross the thickness x of this formation of density and a thickness h of the hole filled of mud of density ρ_m before reaching the detector. From this fact it is easy to understand that the borehole environment will affect the GR measurement. In addition, one must take into account that the mud can itself be radioactive due to its content in bentonite and sometimes in KCl, and in barite which makes the mud denser. Consequently, to evaluate the actual radioactivity of the formation corrections for borehole influence must be previously achieved.

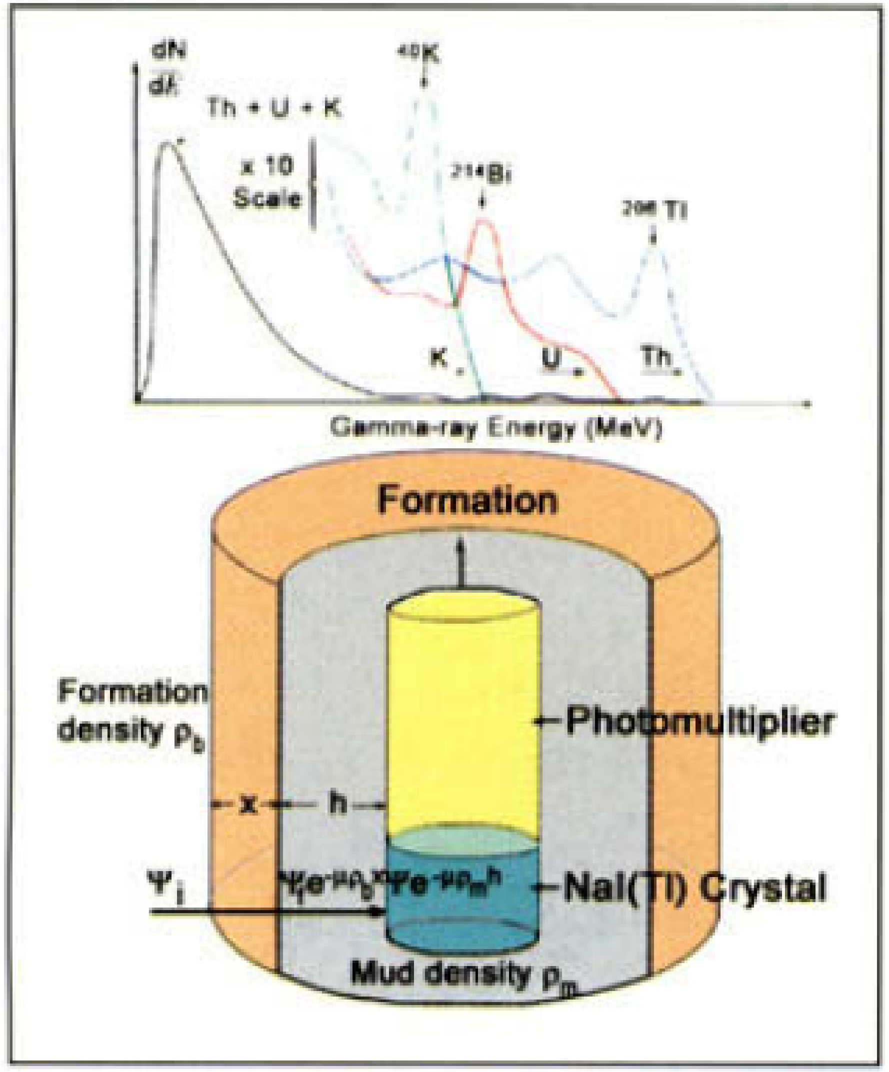

Figure 11-2 - The initial gamma-ray flux, Ψ_i, generated at distance x from the borehole wall and crossing a section h in the borehole filled by non-radioactive mud of density ρ_m has a reduced intensity when reaching the detector located in the well . The total spectrum recorded is reproduced on the top.

- Units:
- The global radioactivity was originally expressed in µg Ra equivalent /tonne. Now the unit is the A.P.I. (for American Petroleum Institute).
- The definition of the API unit comes from an artificially radioactive formation, constructed at the Houston University (see further the paragraph on Calibrations) to simulate about twice the radioactivity of a shale. This artificial formation contains approximately **4%** of potassium, 24 ppm of thorium and 12 ppm of uranium (Belknap ***eta/.,*** 1959). This mixture generates 200 API units.

- **Depth of investigation:**
- Gamma rays are absorbed or attenuated by the medium through which they travel, particularly when their energy is low or the medium dense. Consequently, a natural gamma-ray tool only detects radiation originating from a relatively small volume surrounding the detector.
- Consequently, one can speak about a geometrical factor and compute for each lithology type a radius of investigation.
- **Vertical resolution:**
- Vertical resolution is equal to the diameter of the "sphere“ of investigation, and varies accordingly with formation and densities, and gamma-ray energies.

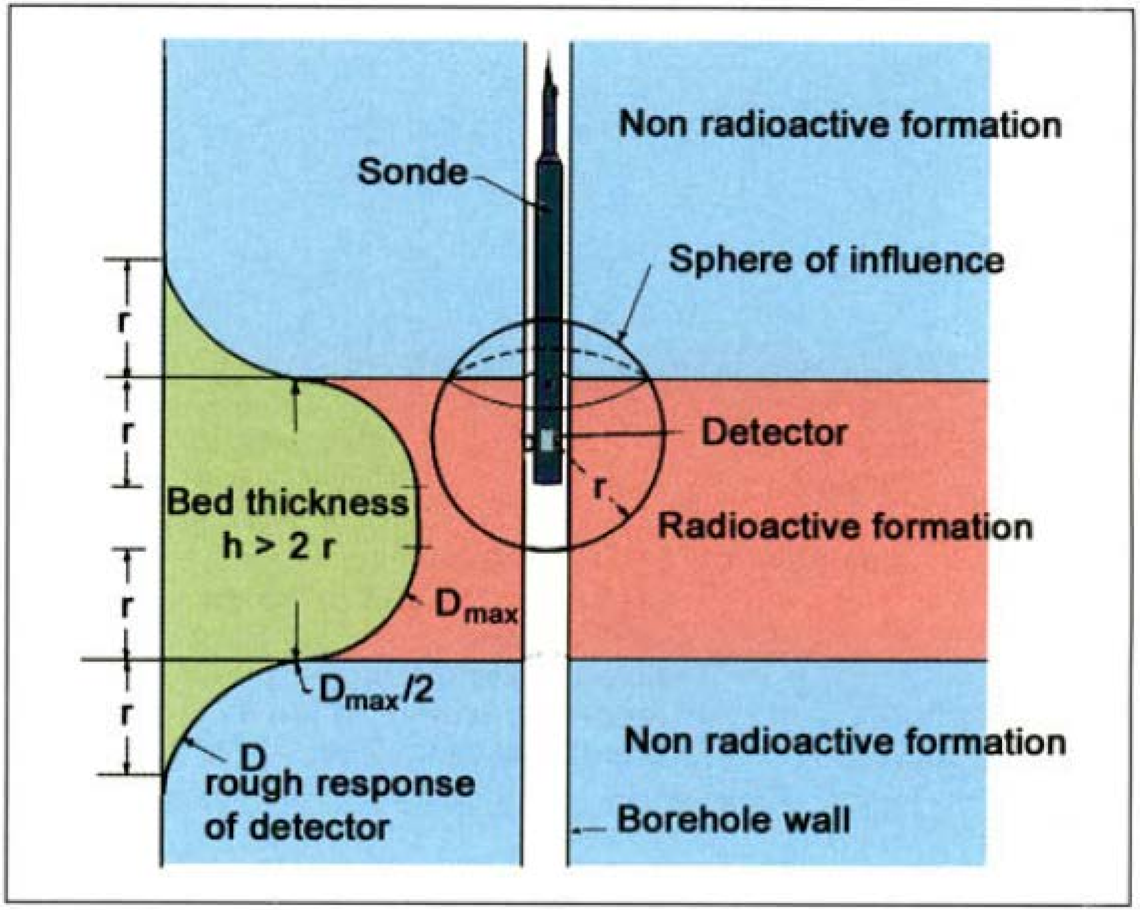

Figure 11-8 - Sphere of influence for a detector compared to the bed thickness, and shape of the curve (adapted from Hallenburg, 1973).

- **Factors affecting the gamma-ray response:**

1. Statistical variations
2. Logging speed
3. Hole condition effects
    1. Hole fluid
    2. Tubing. casina etc.
    3. Cement
    4. Bed thickness

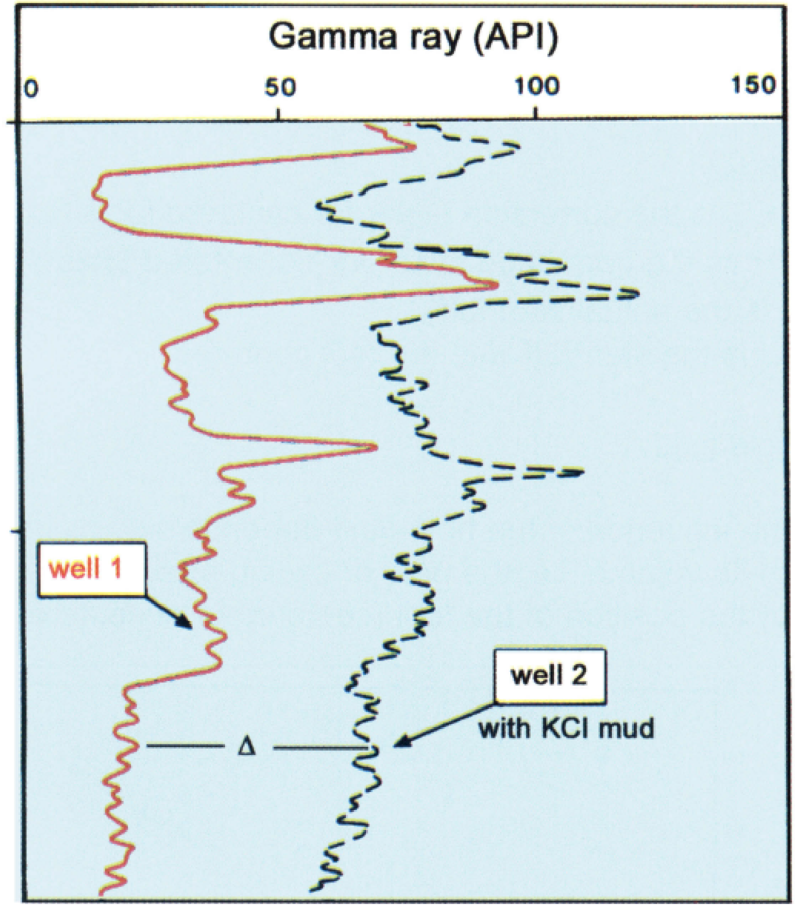

Figure 11-12 - Example illustrating the influence of mud with KCl on the gamma ray measurement. Well 2 is situated 3 km apart from well 1. The curve shape allows the correlation of formations between wells. The difference, Δ, between the two readings is approximately equal to 50 API. This difference is less important in front of more radioactive peaks due probably to non invasion of the shale beds

(adapted from Rider, 1986).

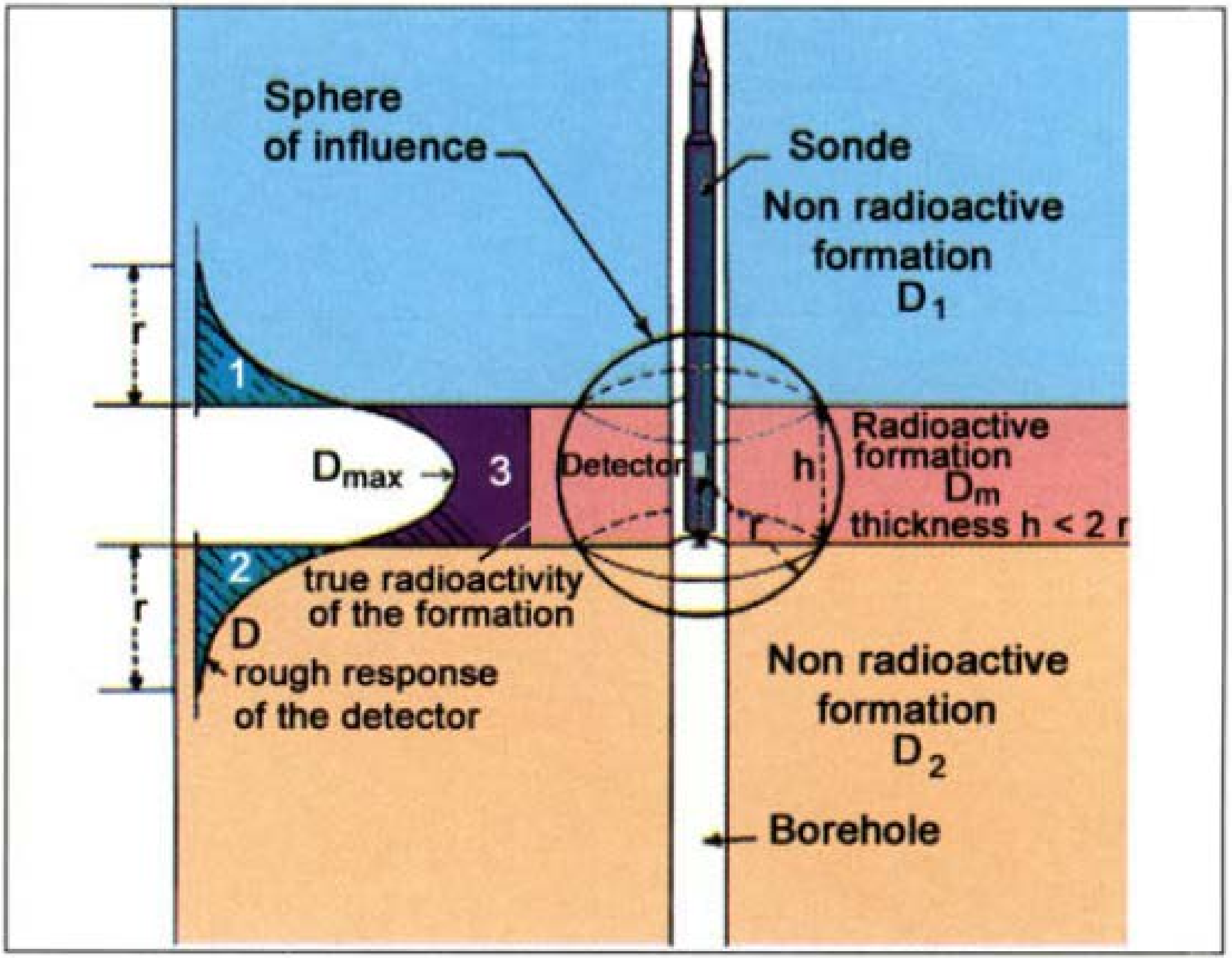

Figure 11-13 - Response in a thin bed (from Hallenburg, 1973).

Applications of the total Gamma-Ray

Applications	Qualitative	Quantitative	Knowing
Petrophysics	"Clean" formations	Computation of V_{sh} Location of testing Location of perforations	GR_{min} and GR_{max}
Geology	**Lithology**: shaly formations feldspathic sandstones glauconitic sandstones potassium salts Radioactive silts Uranium ores **Sedimentology**: Facies determination Sequences Grain size evolution **Stratigraphy**: Correlations Unconformity detection Transgressions **Tectonics**: Overturned series Reverse or thrust fault detection **Core and fluid sampling**	Shale percentage Potassium percentage 15 API # 1% K	GR_{min} and GR_{max} Combination with other log data

- Lithology determination:
- The gamma-ray measurement is essentially used to detect shale beds especially if SP curve is not useful. Evaporites can also be detected and their potassium content evaluated using charts. In first approximation 15 API corresponds to 1% of In combination with other log data, such as resistivity, neutron, density and sonic, one can determine the main lithologies. Silty formations can be recognized as soon as the gamma-ray curve is compared to other logs.

- Sedimentology:
- The gamma-ray curve can reflect typical grain size evolutions with depth - fining or coarsening up sequences - which may reflect typical facies as illustrated by Figure. This application requires a calibration on core data (cf. Chapters 3 to 5 of Well Logging and Geology from O.& L. Serra, 2003).

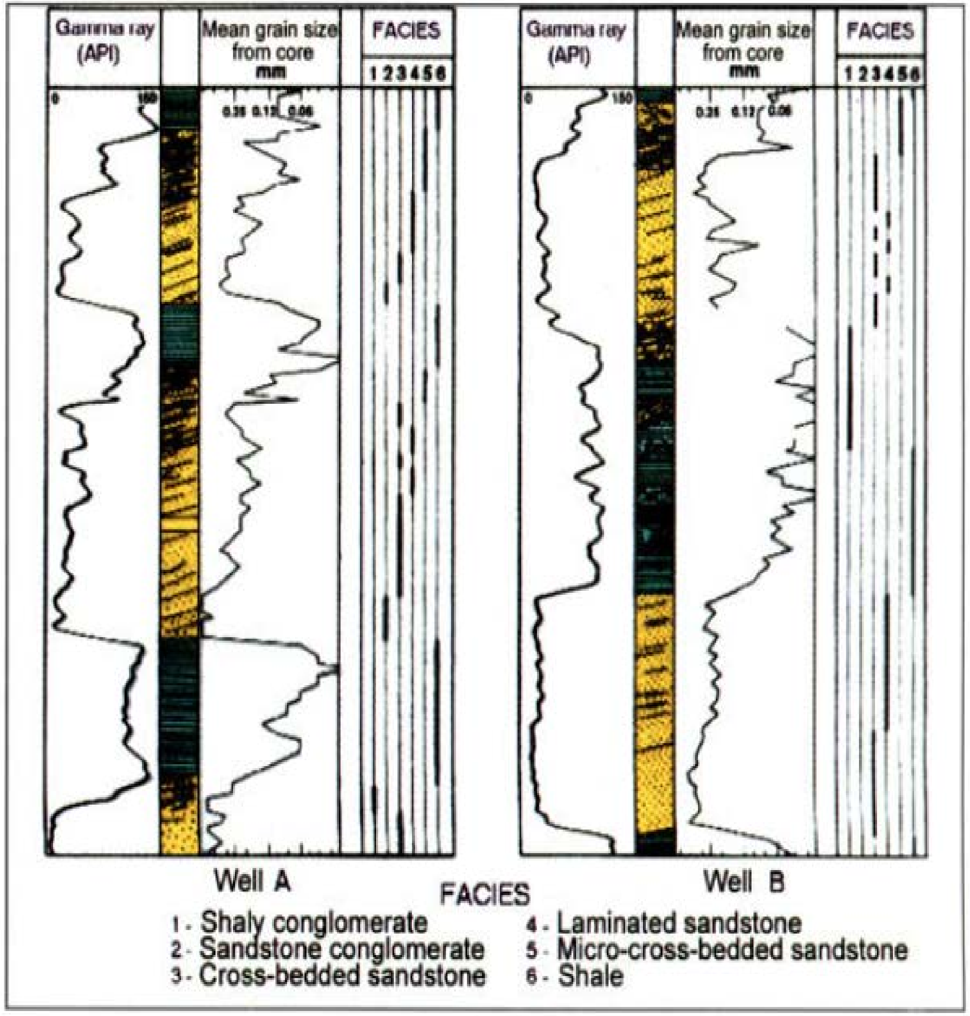

- Well-to-well correlations:
- Correlations between wells are better achieved and accurate using gamma-ray curves. This is linked to the fact that the gamma ray measurement is practically not affected by change in porosity or fluid content

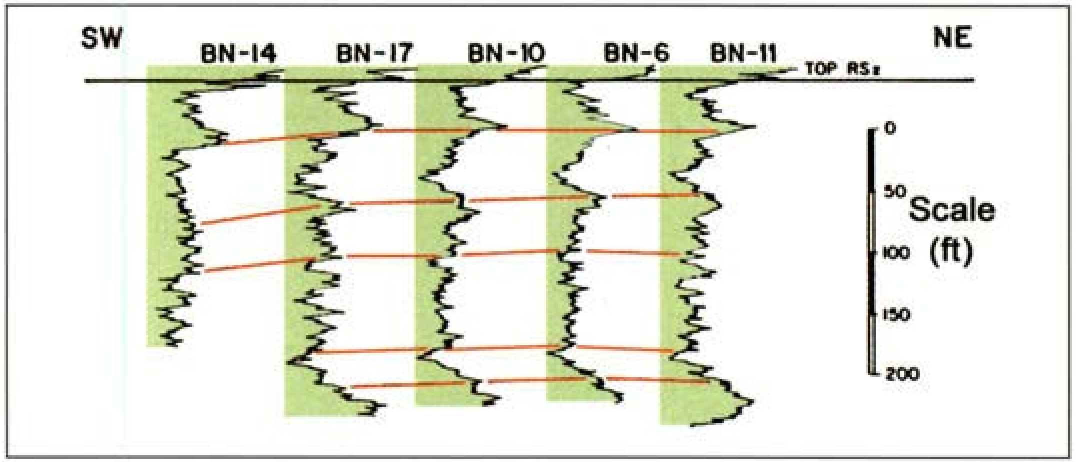

- Detection of unconformities or transgressions:
- **A** sudden important change in the gamma-ray value may indicate either an unconformity or a transgression (cf. Chapter 11 of Well Logging and Geology, 0. & L. Serra, 2003).

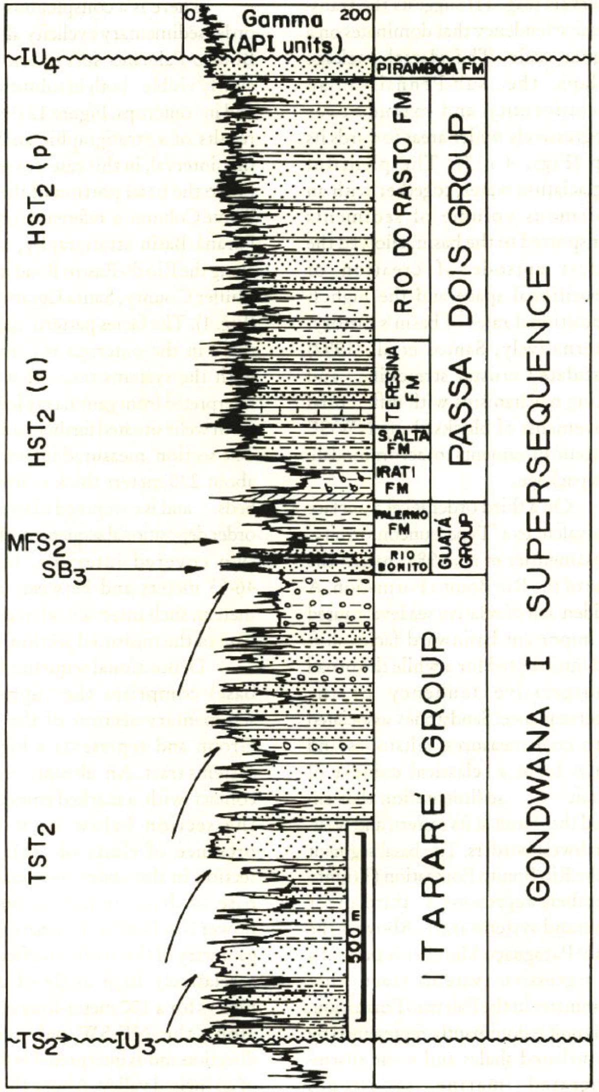

Figura 11 - Gamma and lithologic profiles showing a subsurface section of the Gondwana I supersequence. Location on Fig. 14. Legends: see Fig. 6.

- Tectonic applications:
- As just mentioned above, the gamma -ray curves are not affected by the fluid and porosity and when analyzed carefully they allow the detection of overturned or repeat intervals (cf. Chapter 8 of Well Logging and Geology, 0. & L. Serra, 2003).

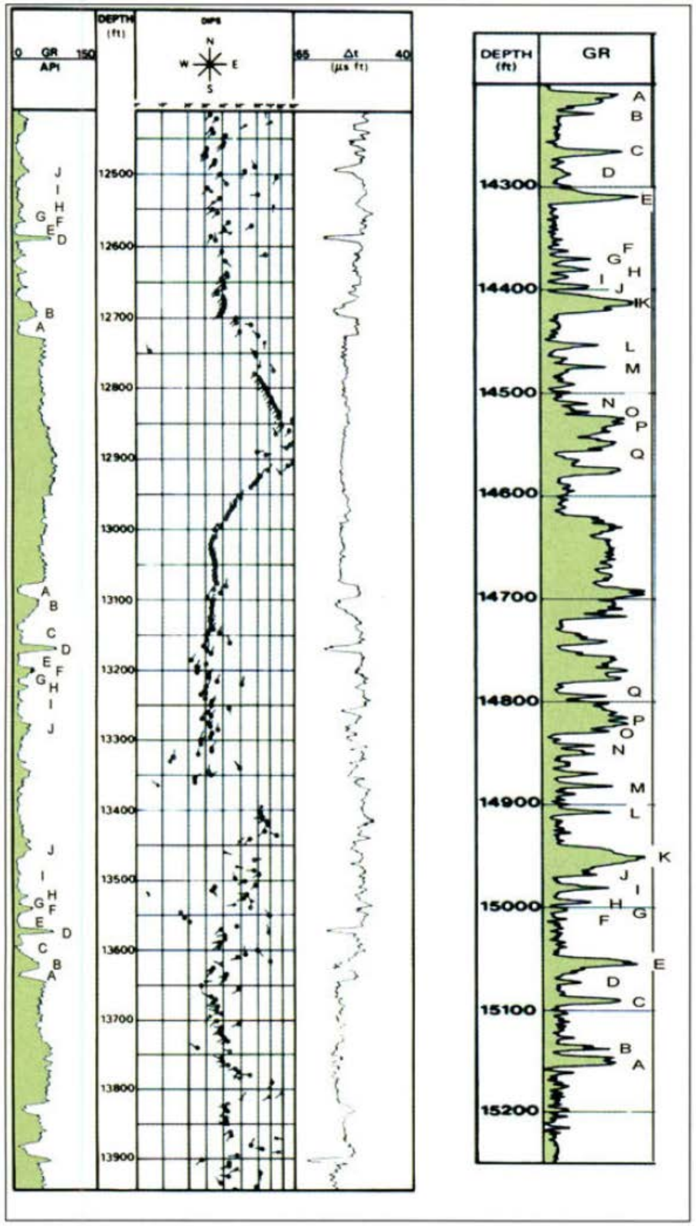

Figure 11-19 - Two examples of overturned folds very well detected thanks to gamma-ray curve analysis. The repeated peaks are indicated by letters (courtesy of Schlumberger).

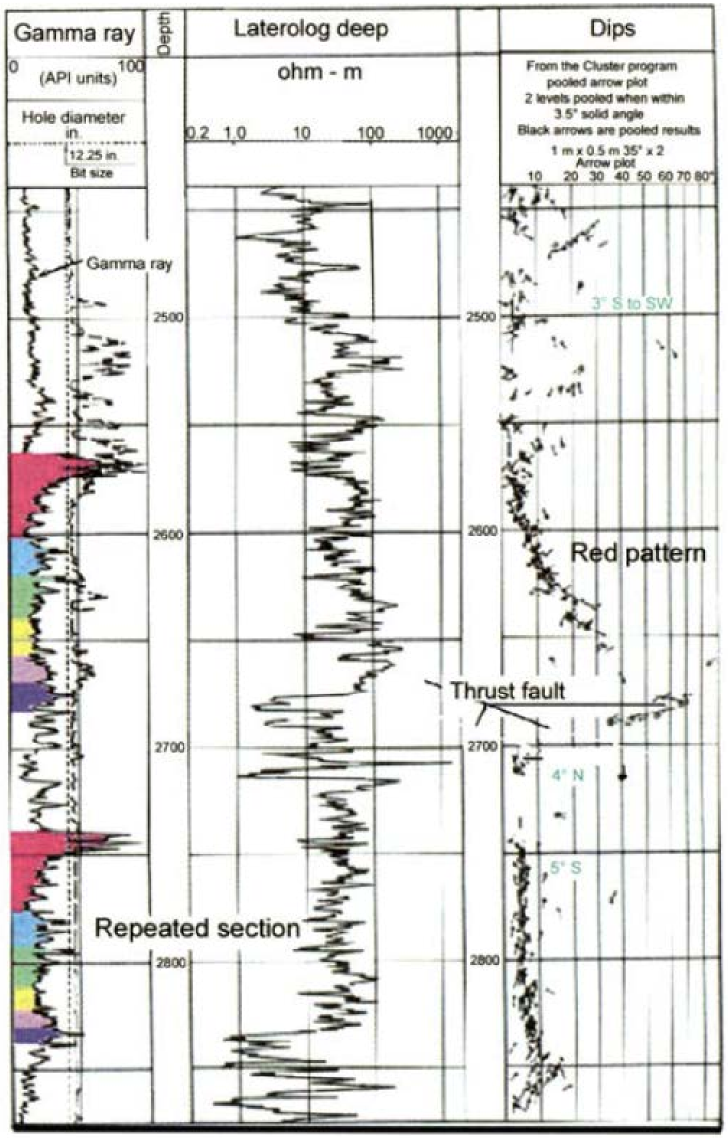

Figure 11-20 - Example of reverse fault perfectly detected by analysis of the gamma-ray curve (from Schlumberger, Well Evaluation Conference, Iran, 1976).

- Estimation of shale fraction of reservoir rocks:
- In sedimentary rocks, shales are the most common radioactive rocks (if we ignore potassium salts), with the radiation arising primarily from the clay fraction. To a reasonable approximation we can consider that the GR level is related to shaliness by:

$$V_{sh} < (V_{sh})_{GR} = [(GR - GR_{min})/(GR_{sh} - GR_{min})] \quad (11\text{-}17)$$

- It must be understood that the GR response may include radioactivity from sources other than shale, for instance from orthoclase, microcline or micas often present in chemically immature sandstones, or from heavy radioactive mienrals such as zircon and monazite. For this reason, the right side of the equation is an upper limit to Vsh. Relationships between gamma-ray values and shale content must be adapted to typical formations or calibrated on core data

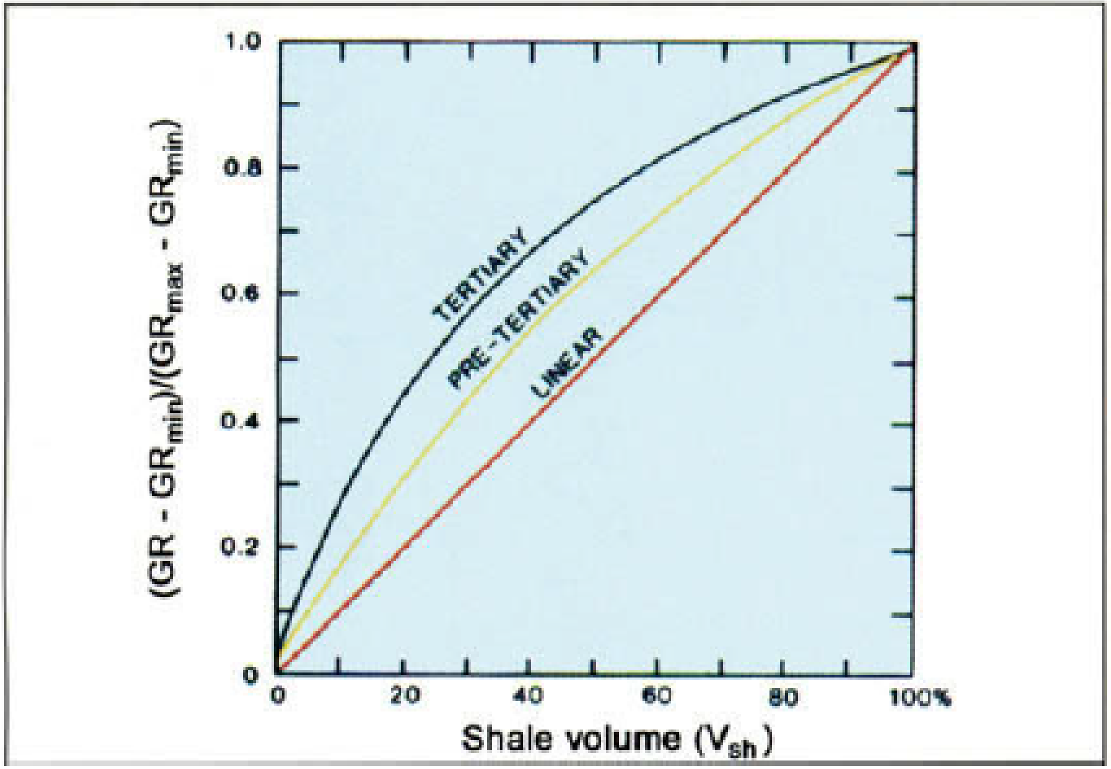

Figure 11-21 - Evaluation of the shale content from the gamma-ray values as a function of the age of the shaly formations (from Dresser Atlas document).

- **Depth control of sampling, perforating and testing equipment**:
- Positioning wireline testers, sidewall core sampling, or perforations is better achieved using gamma ray curves in open holes, or even through tubing or casing.
- **The evaluation of injection profiles:**
- The gamma ray is sometimes used in connection with radioactive tracers operations.

Natural Gamma Ray Spectrometery Tool (NGT)

- The gamma rays emitted by the three decay series have a number of discrete energies. In Figure are shown the three corresponding theoretical gamma-ray emission spectra. Each spectrum characterizes a decay series, each series has a spectral "signature" that enables its presence to be discerned.

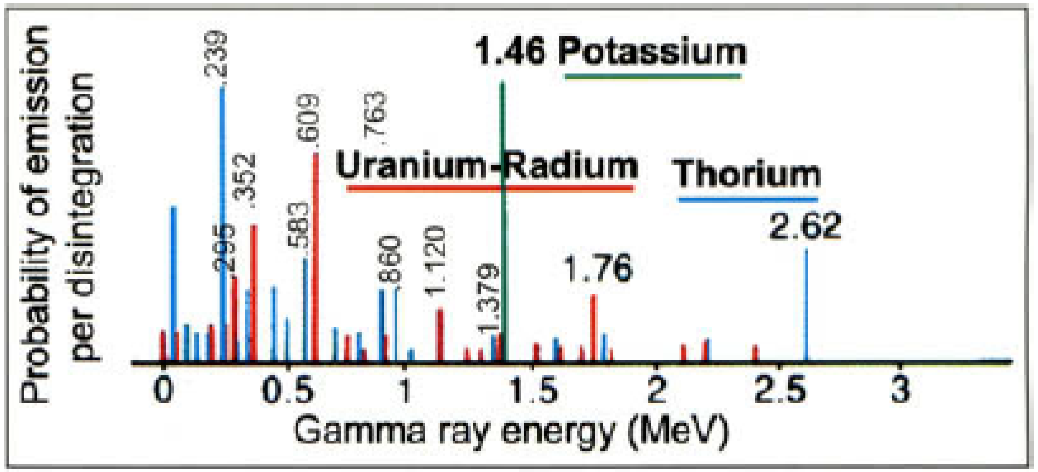

- To obtain a quantitative evaluation of thorium, uranium and potassium from an analysis of the total energy distribution, it is helpful to divide the spectrum into two regions:
    1. the high-energy region, with the three main peaks: Thallium 208TI at 2.62 MeV (from the 232Th family), Bismuth 214Bi at 1.76 MeV (from the 23811 family), and Potassium 40K at 1.46 MeV;
    2. the low-energy region, covering the energy range of the gamma rays resulting from Compton scattering in the formation, plus lower-energy emissions from the thorium and uranium series.

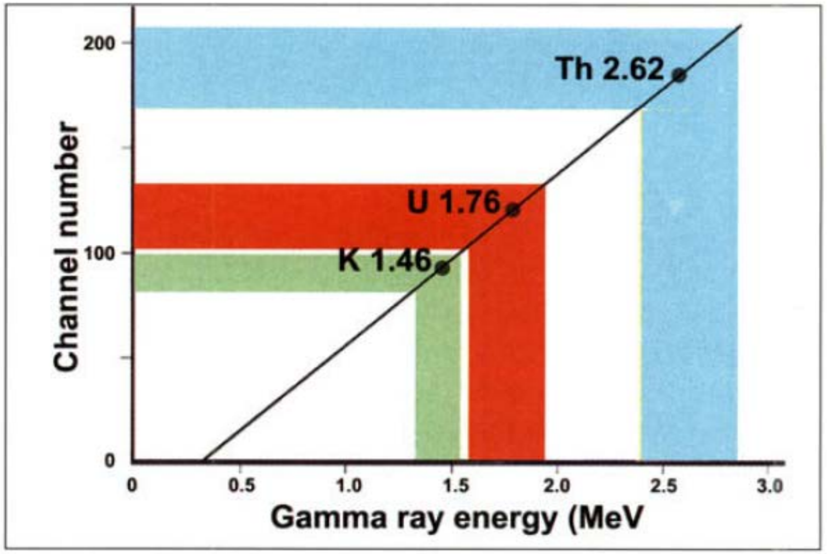

- The Schlumberger Natural Gamma ray Spectrometry tool (NGS or NGT) uses five windows.

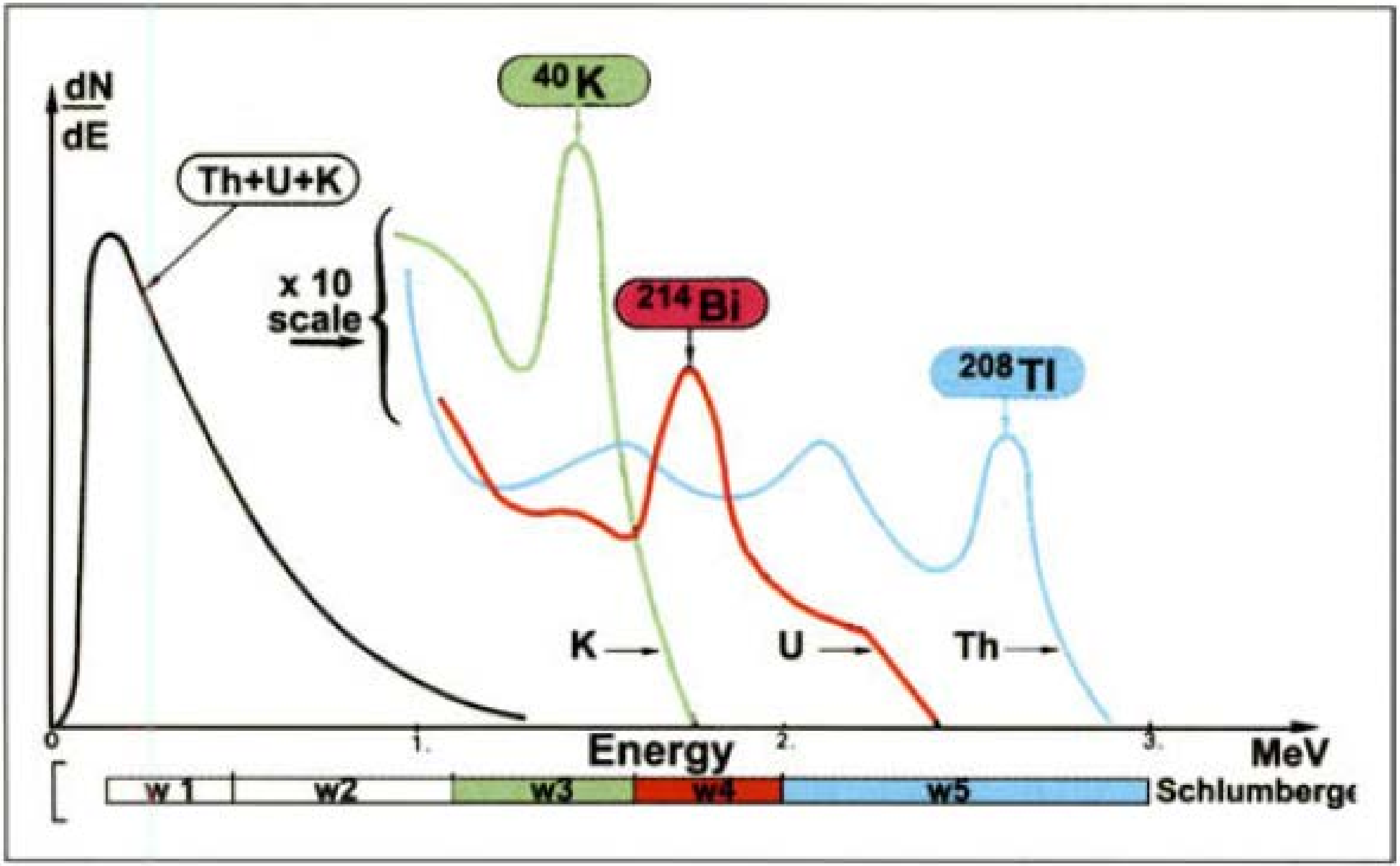

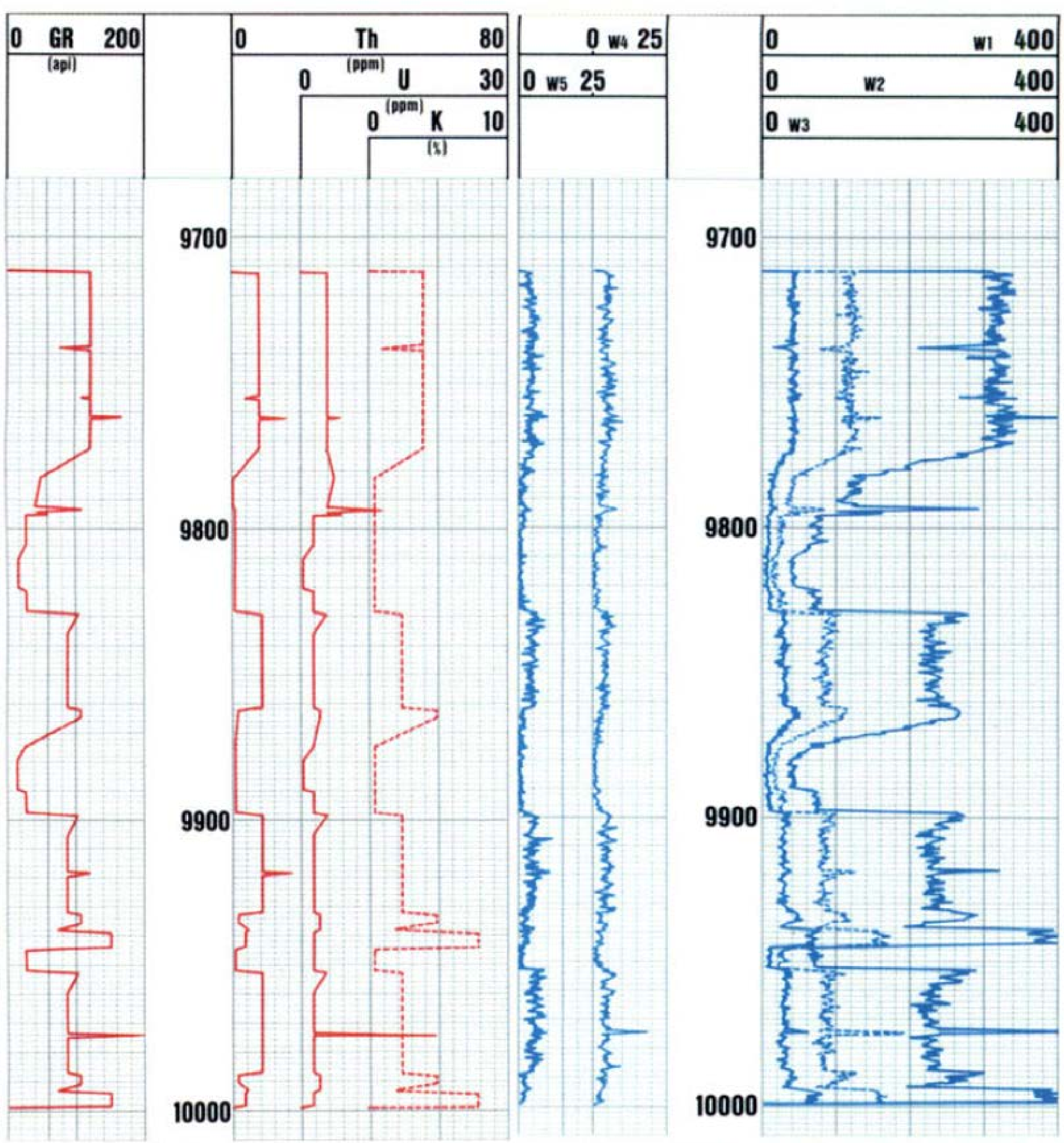
0 GR 200
(api)
0 Th 80
(ppm)
0 U 30
(ppm)
0 K 10
(%)
0 w4 25
0 w5 25
0 w1 400
0 w2 400
0 w3 400
9700
9800
9900
10000
9700
9800
9900
10000

- **Depth of investigation:**
- The depth of investigation depends not only on hole size, mud-density and formation bulk density, but on the energies of the gamma rays themselves Higher-energy radiation can reach the detector from deeper in the formation.

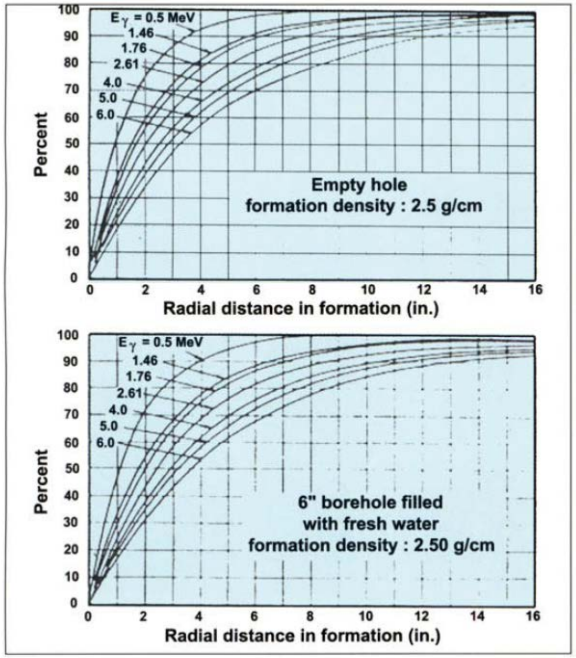

- Vertical resolution:
- In average, for 90% of the signal, it corresponds to approximately three times the size of the detector crystal, so close to 36 in. But, once again it depends on the rock density and the energy of the gamma ray. Enhancement techniques can be used to improve the vertical resolution. In that case one can expect a vertical resolution close to 18 in.

- **Environmental and other effects on the measurement:**

1. Time constant (vertical smoothing), logging speed, dead time
2. The borehole
3. Tool position
4. Casing
5. Bed thickness

Applications

Application	Qualitative		Quantitative	Knowing
Petrophysics	Separation between shaly formations and radioactive reservoirs		Computation of the shale content Computation of the percentage of the minerals composing the rocks	Th_{min}, K_{min}, Th_{max}, K_{max}. The mineralogical model and the logging parameters of the minerals - Other log data.
Geology	Lithology	Lithological type Nature of radioactive minerals	Mineral admixture	The mineralogical model and the logging parameters of the minerals - Other log data.
	Sedimentology	Clay type Facies Environment	Clay mineral admixture	The mineralogical model and the logging parameters of the minerals - Other log data.
	Geochemical	Source-rock evaluation		Uranium percentage in source-rock.
	Stratigraphy	Correlations Unconformities		
	Tectonics	Repeated formations Overturned formations		

- **Lithology:**
- 1- Evaporitic environment:
- Differentiate between shales and potassium salts; these last minerals having a much higher potassium content than the clay minerals, and no thorium content since thorium is insoluble and can be considered as an indicator of detrital origin. So in front of potassium evaporates, the Th curve will be flat and near zero while the K curve will show a high percentage of potassium and a shape generally very similar to that of the total gamma ray, at least if at the same time the uranium curve is flat and near zero (showing little organic material in the rock)

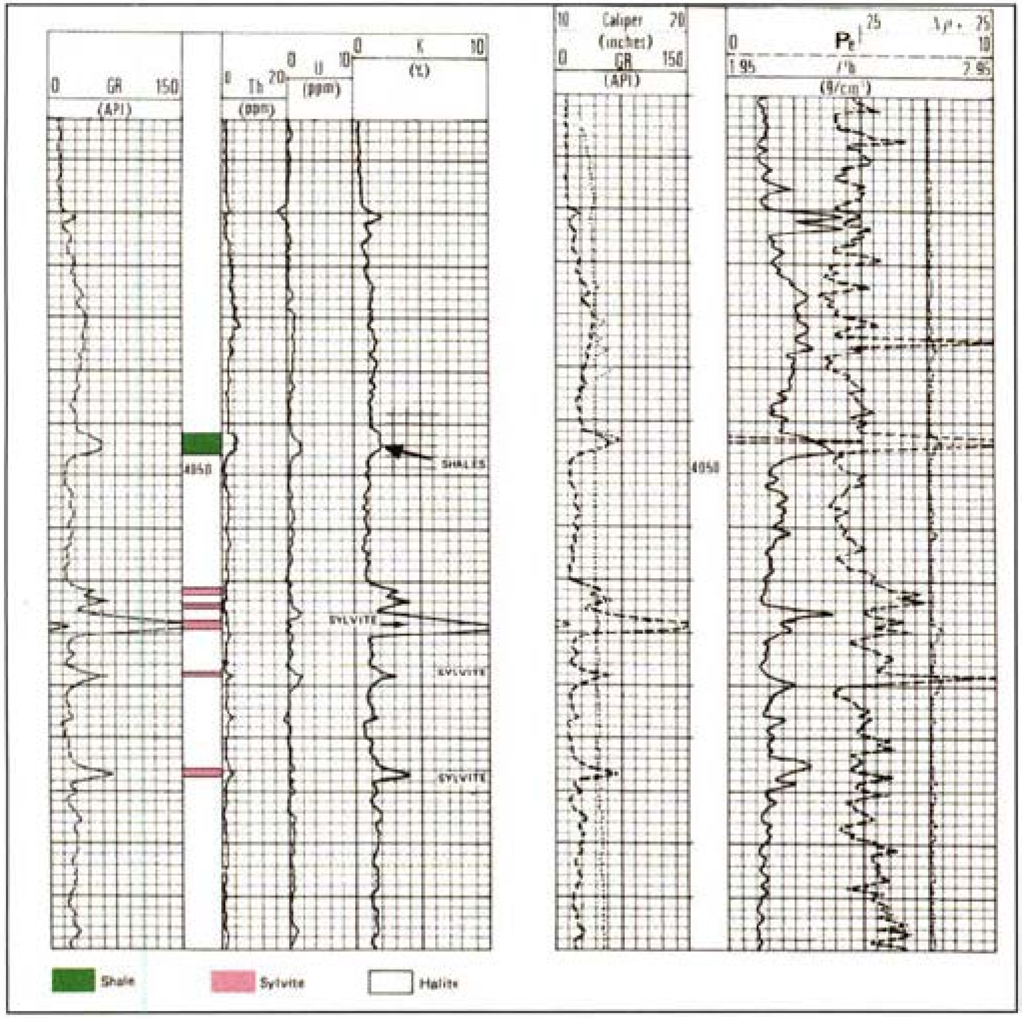

Figure. 12-26 - Example of response in evaporite. Observe at 4065 the high potassium value (higher than 10%). It indicates the existence of sylvite in this halite interval. The sylvite presence is confirmed by the value of Pe in the uncaved zone.

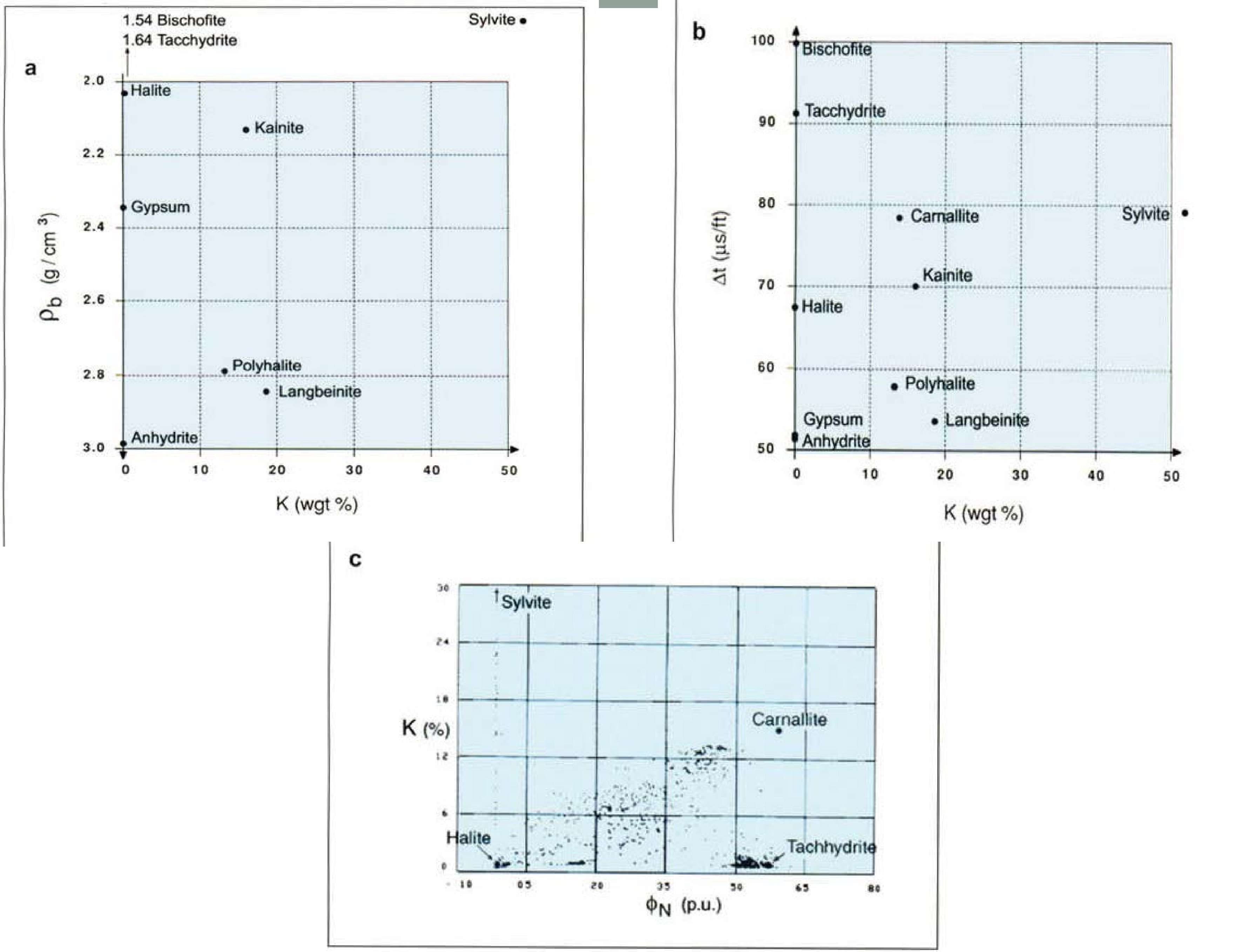
a
1.54 Bischofite
1.64 Tacchydrite
Sylvite
Halite
Kainite
Gypsum
Polyhalite
Langbeinite
Anhydrite
ρ_b (g / cm^3)
2.0
2.2
2.4
2.6
2.8
3.0
0
10
20
30
40
50
K (wgt %)
b
Bischofite
Tacchydrite
Carnallite
Sylvite
Kainite
Halite
Polyhalite
Gypsum
Anhydrite
Langbeinite
Δt (μs/ft)
100
90
80
70
60
50
0
10
20
30
40
50
K (wgt %)
c
Sylvite
Carnallite
Halite
Tachhydrite
K (%)
ϕ_N (p.u.)

- 2- Sand-shale series:
- Very often pure clean sands or sandstones exhibit very low radioactivity; because their thorium, uranium and potassium contents are very low too. They correspond to orthoquartzites.
- But sometimes sands or sandstones contain significant percentages of clay, are radioactive. In these cases, To compute a better shale percentage by using the shale indicators derived from the thorium or the potassium, or from their sum (CGR):

$$(V_{sh})_{Th} = (Th - Th_{min}) / (Th_{sh} - Th_{min})$$
$$(V_{sh})_{K} = (K - K_{min}) / (K_{sh} - K_{min})$$
$$(V_{sh})_{CGR} = (CGR - CGR_{min}) / (CGR_{sh} - CGR_{min})$$

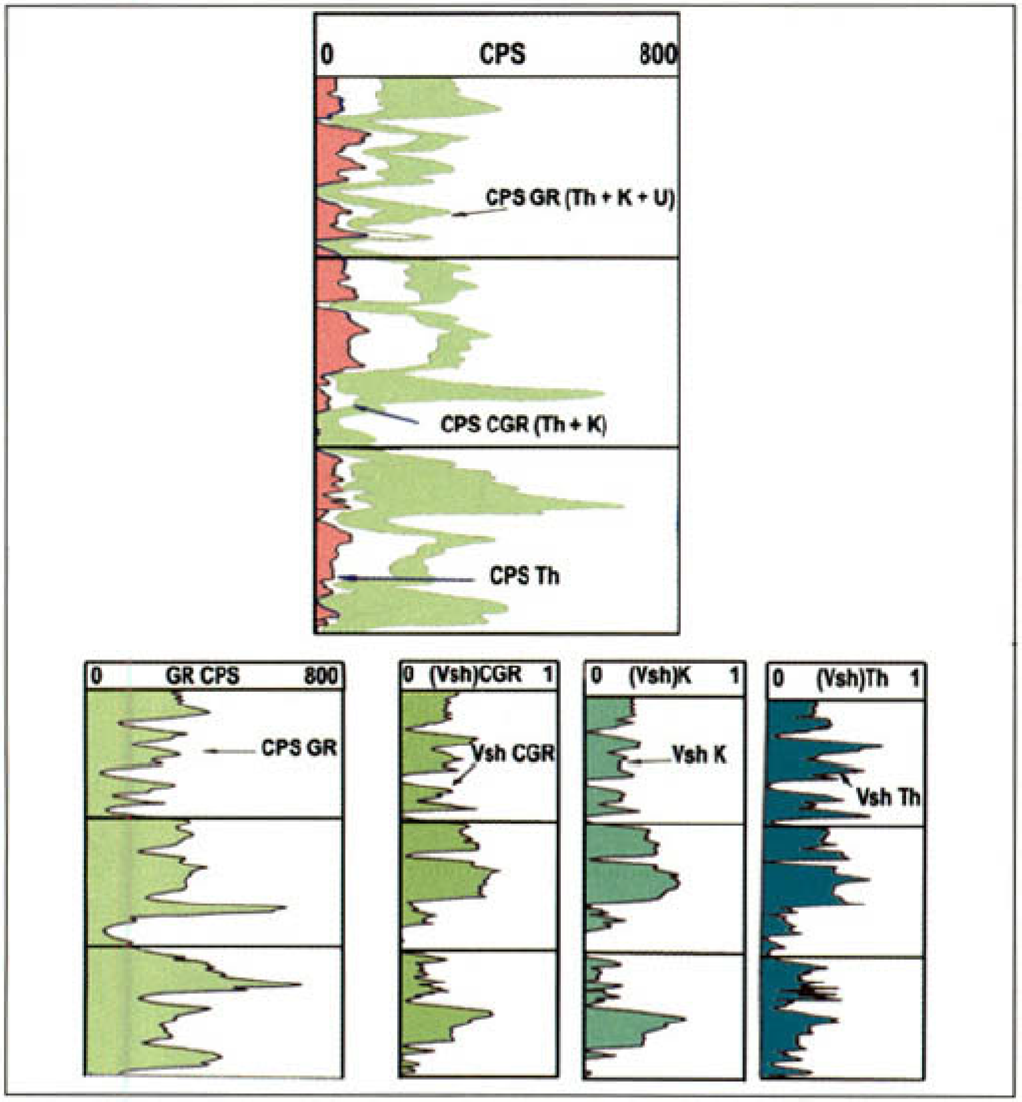

Figure 12-29 - (a) Formation response due to thorium, thorium and potassium; thorium, potassium and uranium. (b) Comparison of the three shale indicators with the total gamma ray (from Serra et al., 1980).

- *3- Feldspathic sandstones or arkoses:*
- They will show some potassium content – dependent on the feldspar percentage in the sands - due to the high percentage of potassium in feldspars.
- 4- *Heavy minerals within sandstones:*
- Very often heavy minerals like zircon, allanite, monazite, and sphene are thorium and uranium-bearing, which give rise to some radioactivity in pure sandstones. This case is easy to recognize because the potassium level is enerally very low, only the thorium and uranium curves being active. Consequently, this type of sandstone shows a very high Th/K ratio. At the same time **ρb** and the apparent matrix density (**ρ** ma)a generally increase owing to th denser minerals present.

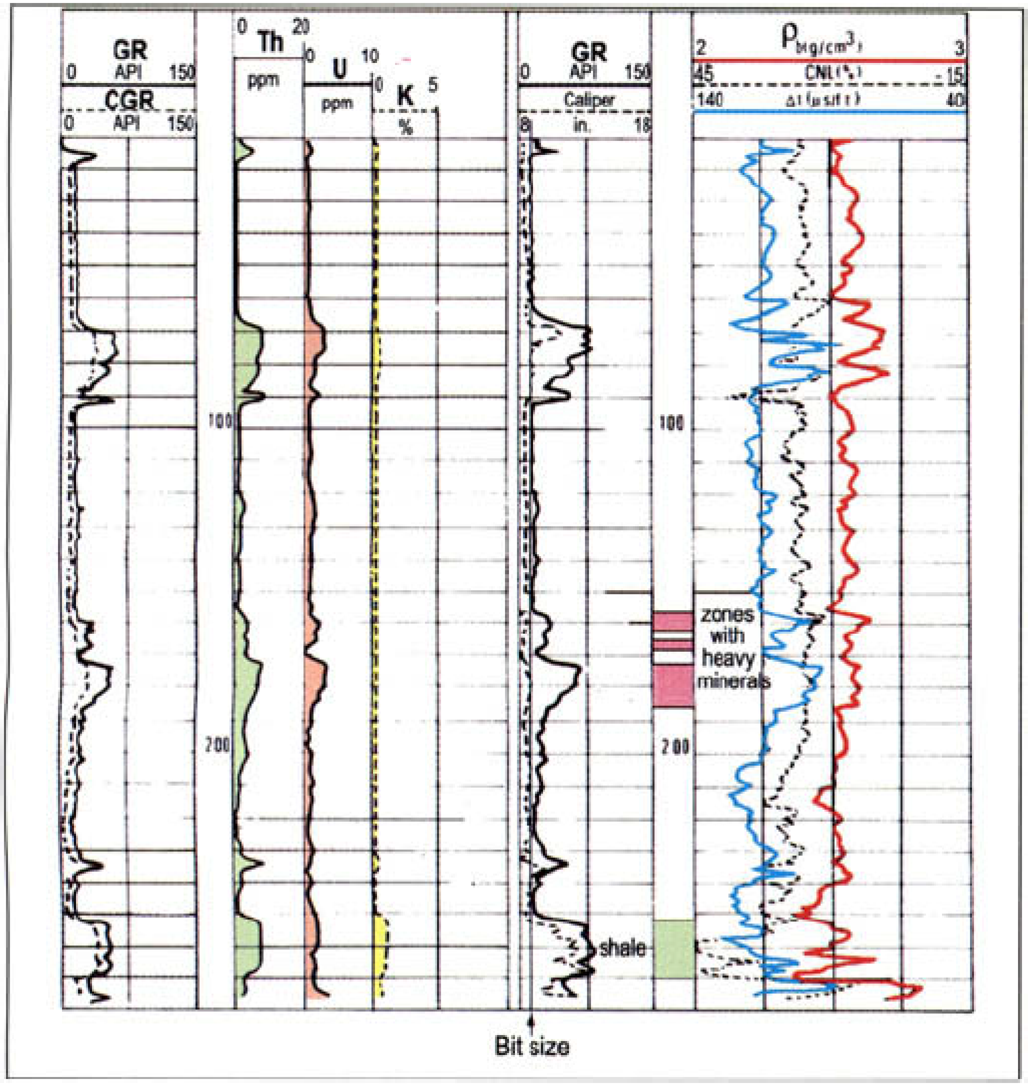

Figure 12-36 - Example of heavy mineral influence on thorium and uranium. Observe the very low potassium content and the increase of density while neutron does not change.

- *5- Shaly sands and sandstones:*
- The combination of NGS and LDT* data (P, or Uma) allows the determination of the clay mineral types present within the sands.

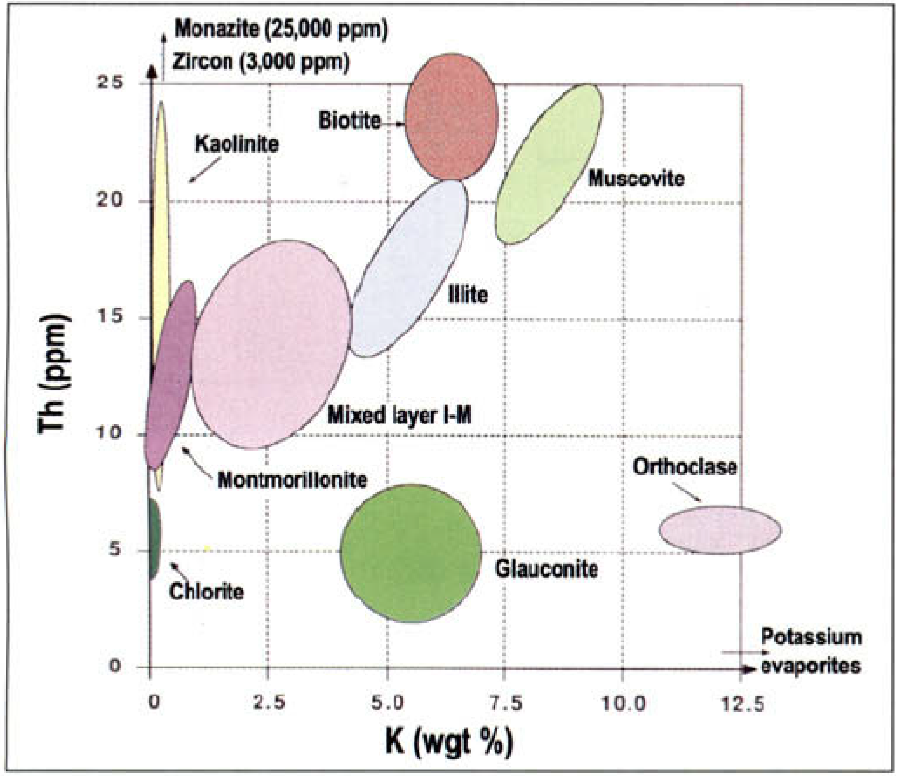

Figure 12-37 - Thorium vs potassium cross-plot with the position of the main radioactive minerals. These minerals are represented by ellipses to indicate that their elemental composition can vary in relation with the importance of the weathering.

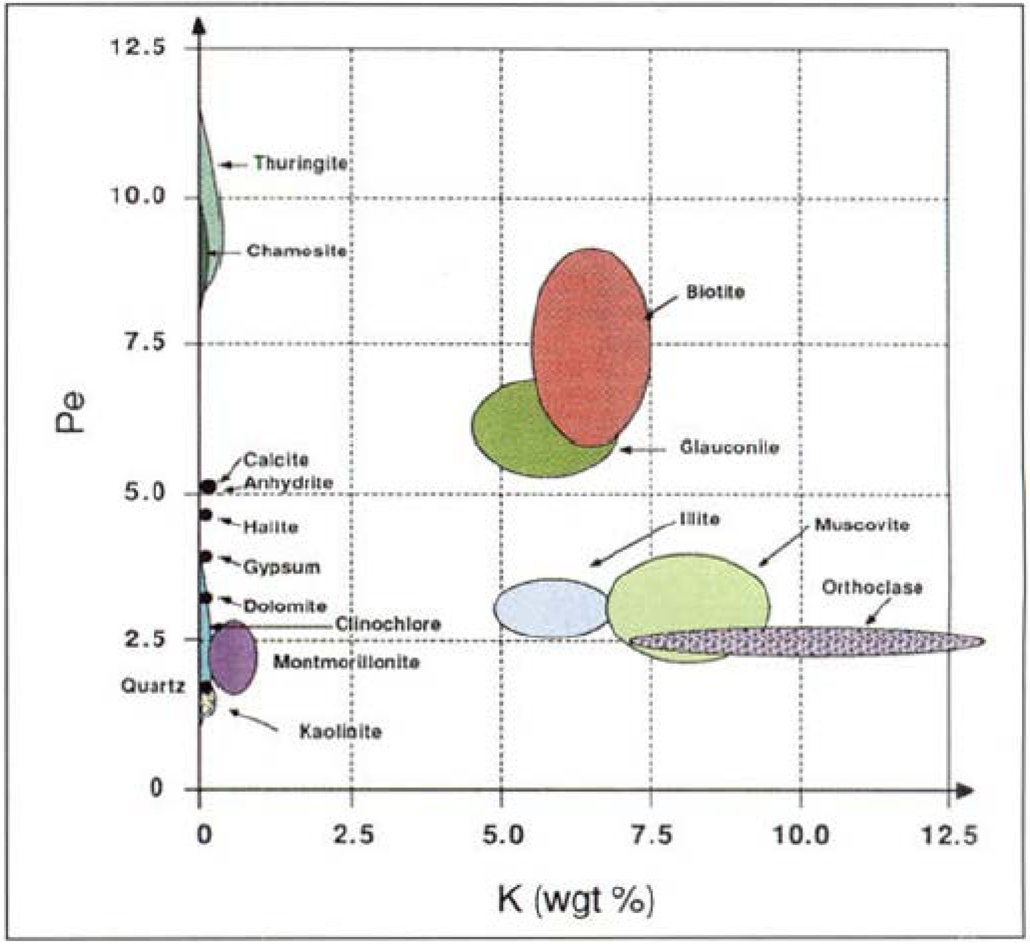

Figure 12-38 - Pe vs potassium with the position of the main minerals.

- 6- Carbonate series:
- In these rocks the standard gamma ray is very often a poor clay indicator, because the observed radioactivity is not related to clay content of the rock, but to the presence of uranium. In a pure carbonate of a chemical origin, the thorium will be absent, since it is insoluble. So, if the spectrometry measurement shows a carbonate level with thorium and potassium near zero this corresponds to a pure carbonate. If at the same time the uranium is zero too, this carbonate was precipitated in an oxidizing environment

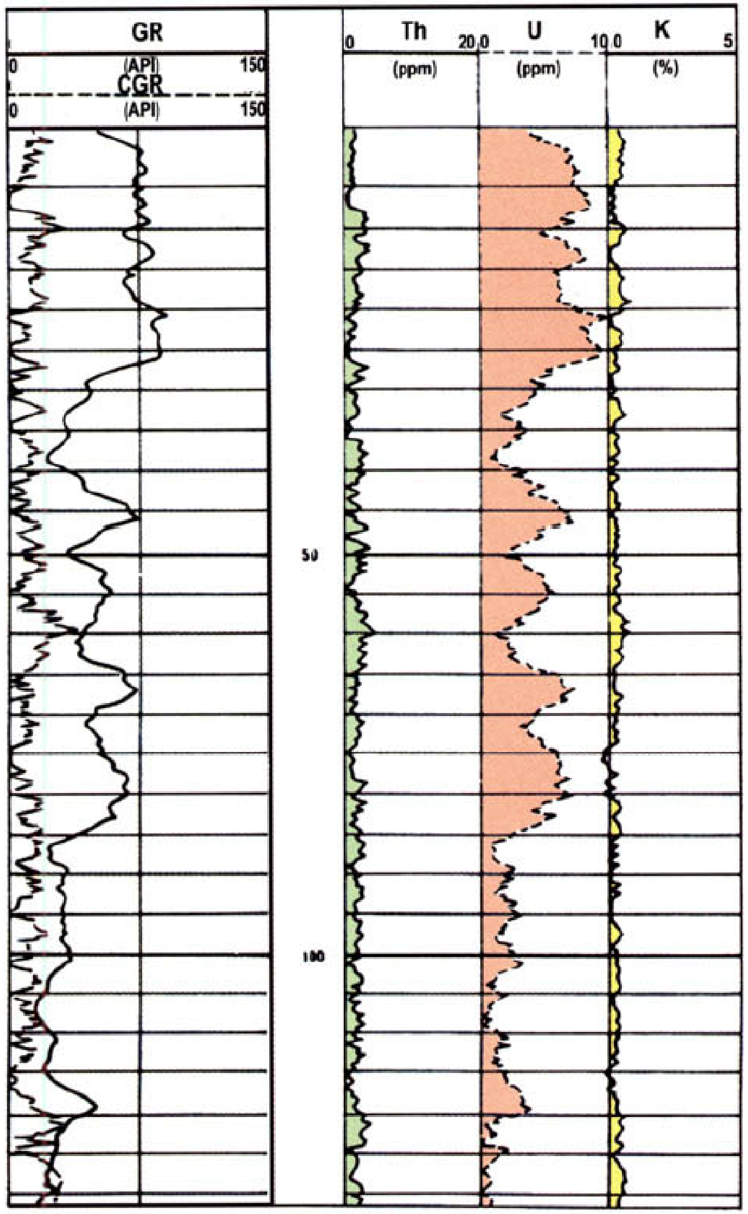

Figure 12-40 - Example of NGS response in a carbonate series showing that the radioactivity is mainly due to uranium. The thorium/uranium ratio is in many place lower than 2.

- If the levels show a variable percentage of uranium, the corresponding carbonate can either have been deposited in a reducing environment (restricted), generally favorable also to the conservation of organic material and to its transformation into hydrocarbon; or, if it is compact (low porosity) it corresponds to a carbonate with stylolites, in which impurities such as uranium, organic matter and even clay minerals, are concentrated. Peaks of uranium can also correspond to phosphate-bearing levels. If Th and K are present with uranium, this indicates the presence of clays in the carbonate (clayey carbonates to mark). If K is present with or without uranium it can correspond to a carbonate of algal origin or a carbonate with glauconite.

- Well-to-well correlations:
- As the gamma ray, the natural radioactivity spectrometry is very usefull for correlations either of facies or chronostratigraphic. Particularly, peaks on thorium curves are often used for well to well correlations. as they correspond generally to volcanic ashes (or bentonitic levels) and, consequently, can be considered as deposited at exactly the same time over a wide area (Lock & Hoyer, 1971).

- Detection **of** unconformities:
- Abrupt changes in the mean thorium/potassium ratio are generally indicative of important variations in the proportion of radioactive minerals which occur when there are changes in geological conditions of deposition. These correspond to unconformities.

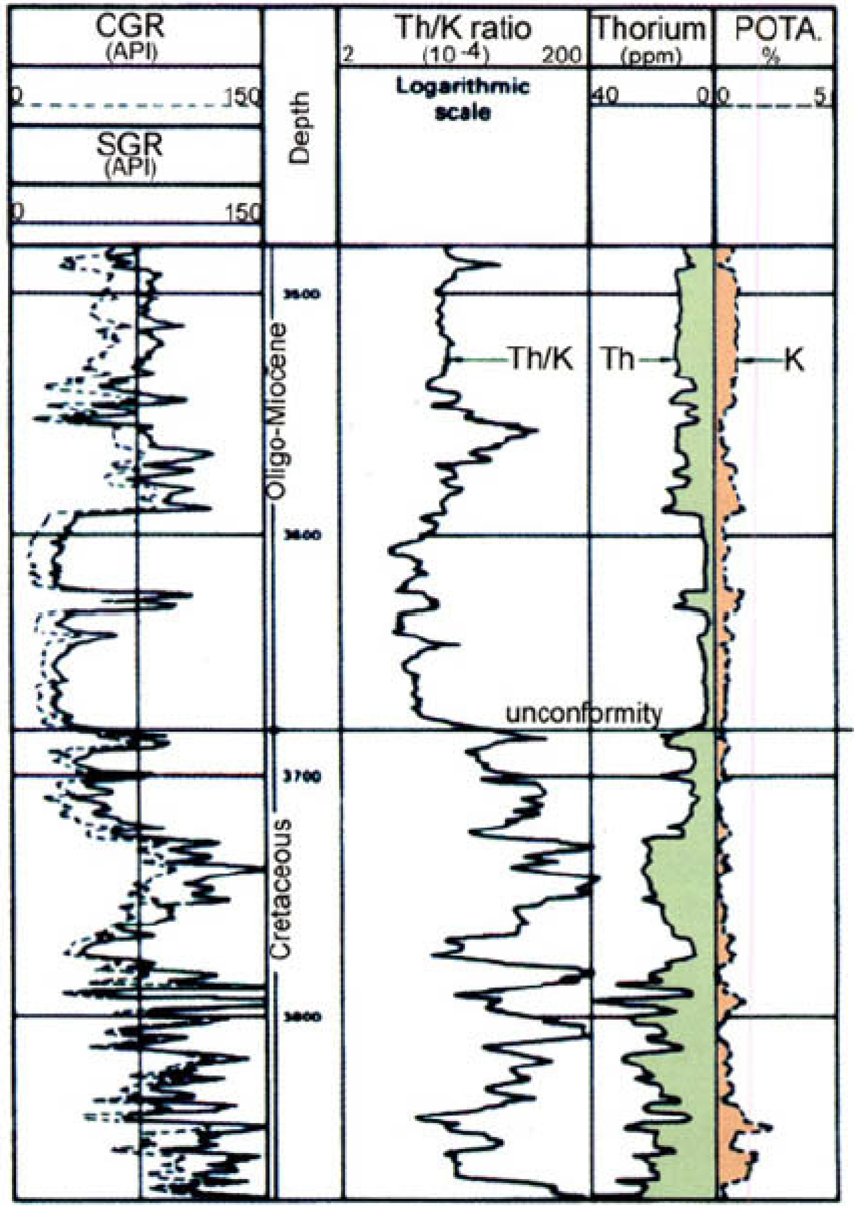

Figure 12-41 - Unconformity detected by the NGS and not easily seen on other logs (from WEC, Venezuela, 1980).

- **Fracture and stylolite detection:**
- In reducing conditions the circulation of hydrothermal or underground waters in fractures may cause precipitation of the uranium salt, uraninite. So fractures can be recognized by peaks of uranium. The presence of fractures must be confirmed by other methods because uranium is often associated with stylolites: during compaction, insoluble impurities (clay minerals, organic matter, iron oxides ...) are often concentrated in very thin layers called stylolites, which can also give radioactive peaks

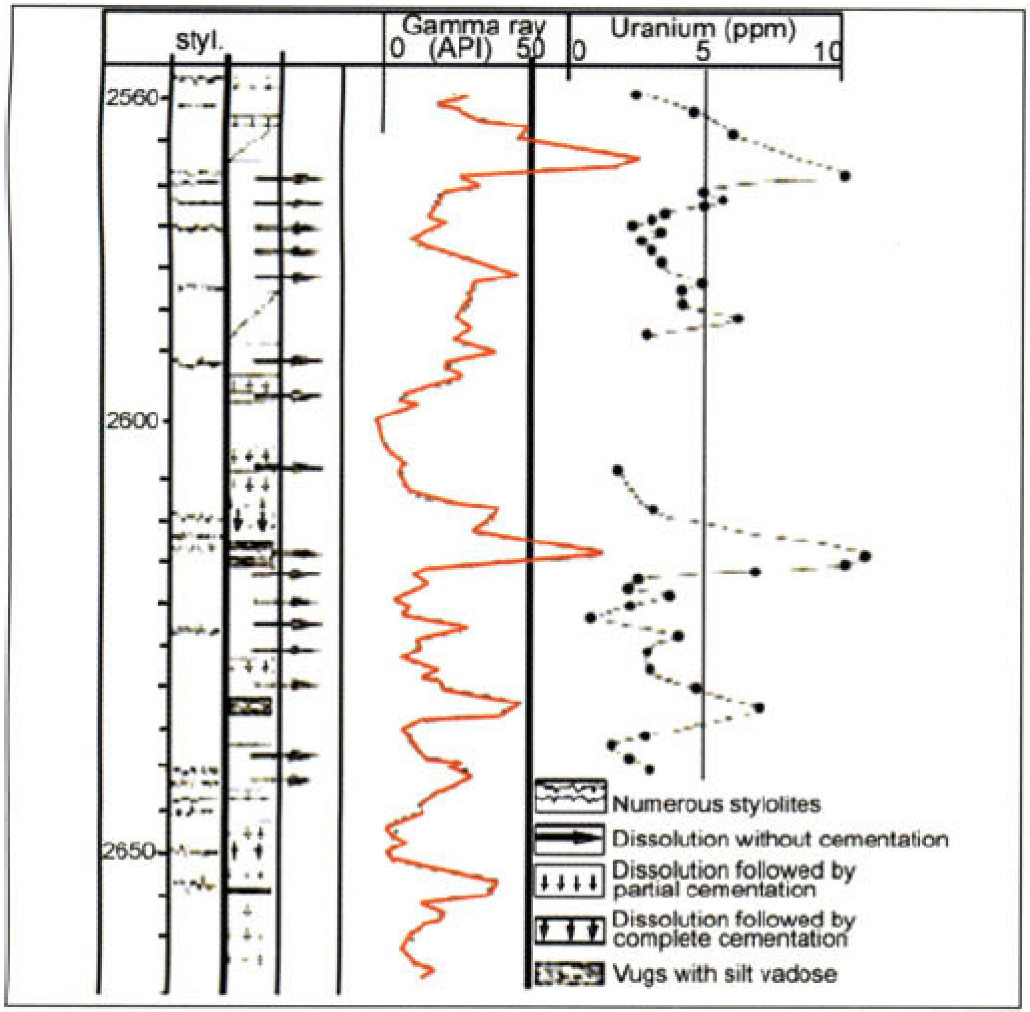

Figure 12-42 - Example of stylolites detected by uranium peaks confirmed by measurements realized on core (from Hassan et al., *1976).*

- Igneous rock recognition:
- Except for syenite, most of the intrusive igneous rocks show a Th/U ratio close to 4. Deviations from this value seem to indicate weathering effects during which uranium is dissolved and eliminated by rain and running waters; or oxidizing conditions before crystallization of magma; or intrusions of basic igneous rocks.

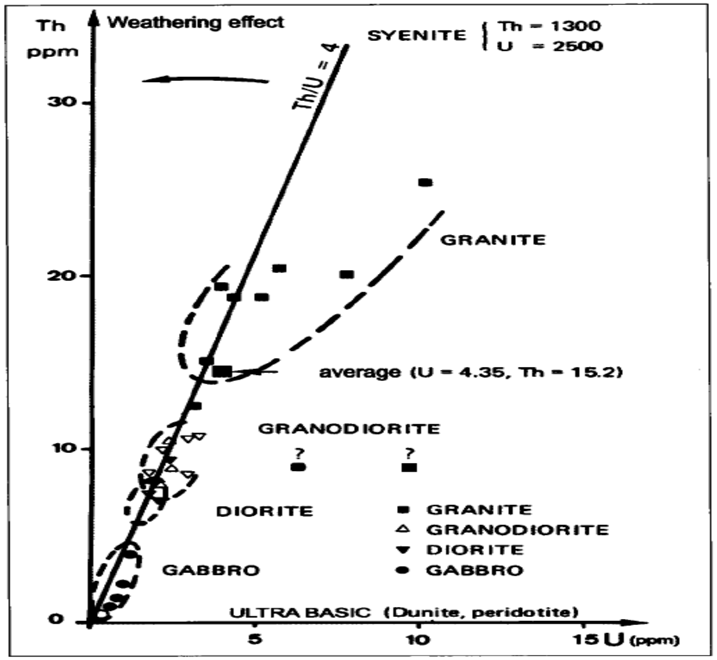

Figure 12-46 - Thorium vs uranium cross-plot for the main igneous rocks.

- **Diagenesis:**
- Under compaction, montmorillonite is transformed into illite, passing through an intermediate mixed-layer illitemontmorillonite phase (Hassan *et al.*, 1976). This results in a decrease of the Th/K ratio with depth. In undercompacted shales this trend will be reversed.

Logging & source rock

- در اين جا ما مي خواهيم پتانسيل هيدروكربن زايي حوضه رسوبي را آناليز كنيم.
- اين آناليز با مشخص كردن محل سنگ منشا و ارزيابي خواص ژئوشيميايي آن آغاز مي شود.
- معمولا سنگ هاي مادر شيلي مي باشند و متاسفانه نمي توان از آنها core تهيه كرد ولي side wall core مي توان تهيه كرد كه نقاط اطلاعاتي است و طيف اطلاعاتي نمي باشد.
- در ادامه ما به بررسي راه هاي گوناكوني كه توسط logging براي رسيدن به سنگ مادر داريم مي پردازيم.

The carbolog method

- این تکنيك در سال 1989 توسط carpenter و همكاران ابداع شد.
- این روش ، روشي سريع و با كيفيت مي باشد.
- این روش نياز دارد كه براي هر حوضه رسوبي به طور جداگانه كاليبره شود.

The uranium concentration

- محيط احيايي كه براي تبديل مواد آلي به نفت لازم است ، محيطي مناسب هم براي تجمع اورانيوم مي باشد.
- وجود باكتري و اسيد هوميك باعث مي شود كه يون هاي محلول اورانيوم به مواد نامحلول تبديل شود.
- بر اساس كارهاي افراد بسياري يك سري نمودار براي مشخص كردن مقدار مواد آلي براساس مقدار اورانيوم پيشنهاد شده كه در زير آنها را مشاهده مي كنيد.

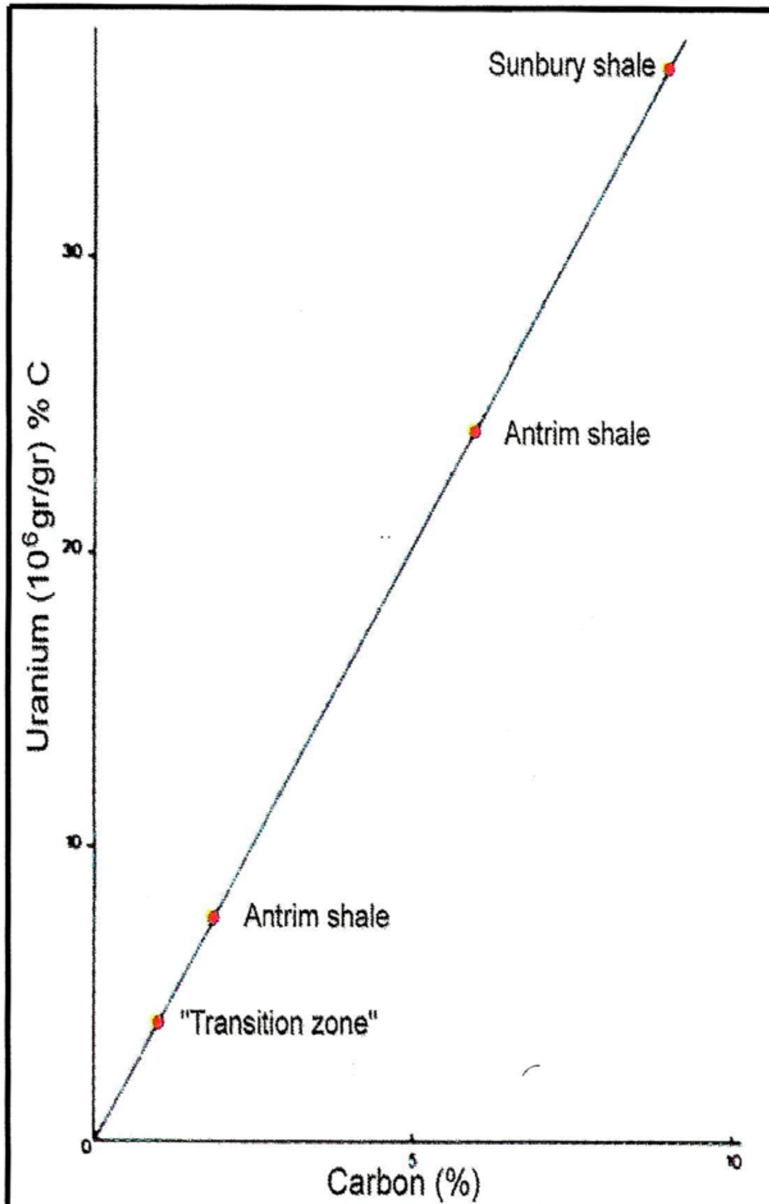

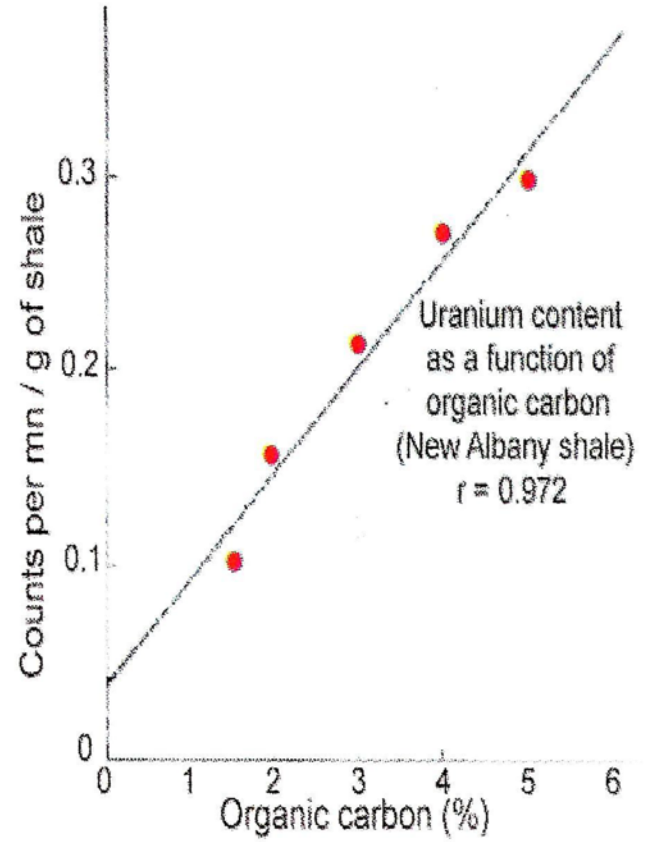

Relation between uranium and organic carbon in sedimentary rocks (from Beers & Goodman, 1944).

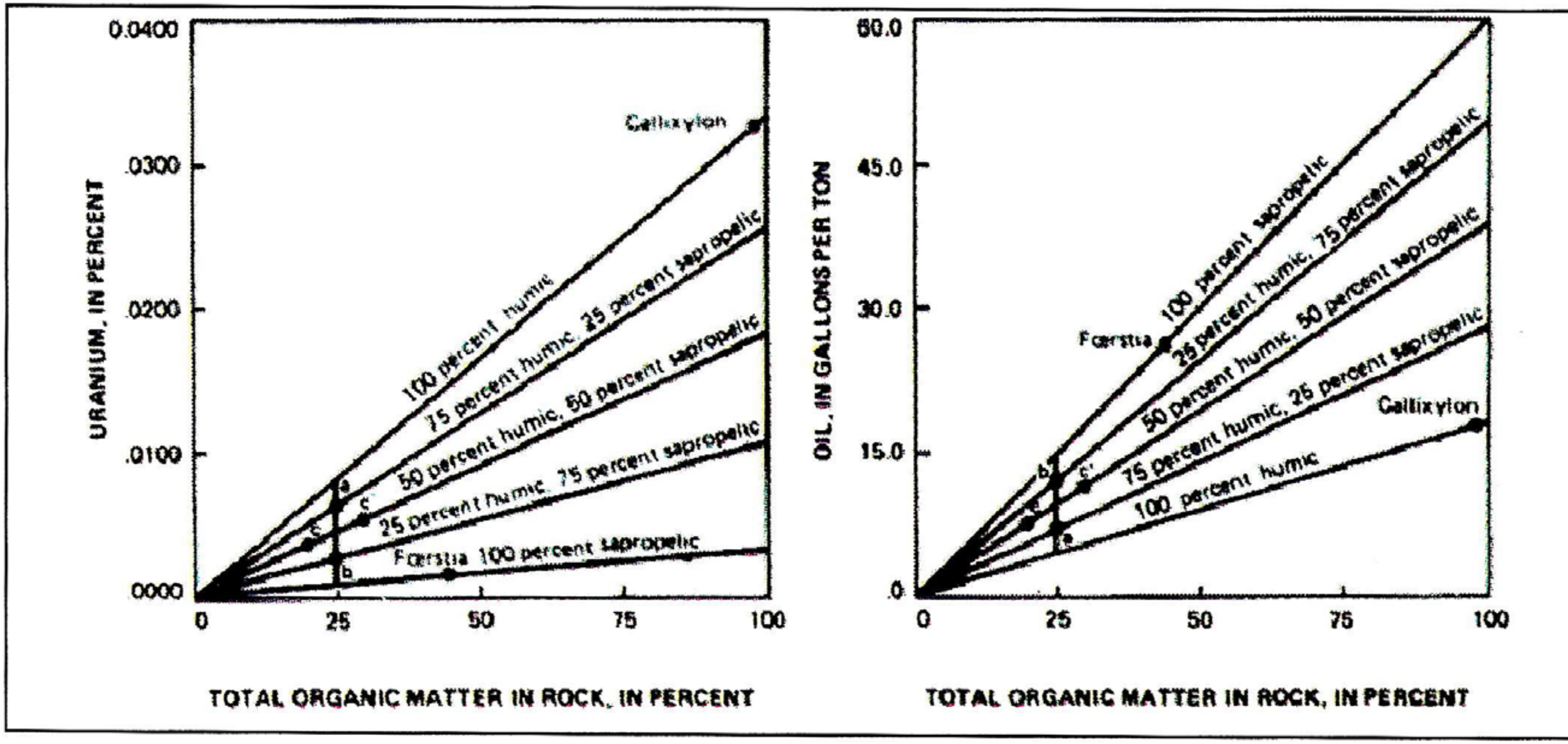

On the left: diagram showing possible relation of uranium content to total organic matter as controlled by the proportion of humic and sapropelic material making up the organic matter. On the right: oil yield of a marine black shale as a function of the total organic matter (from Swanson, 1960).

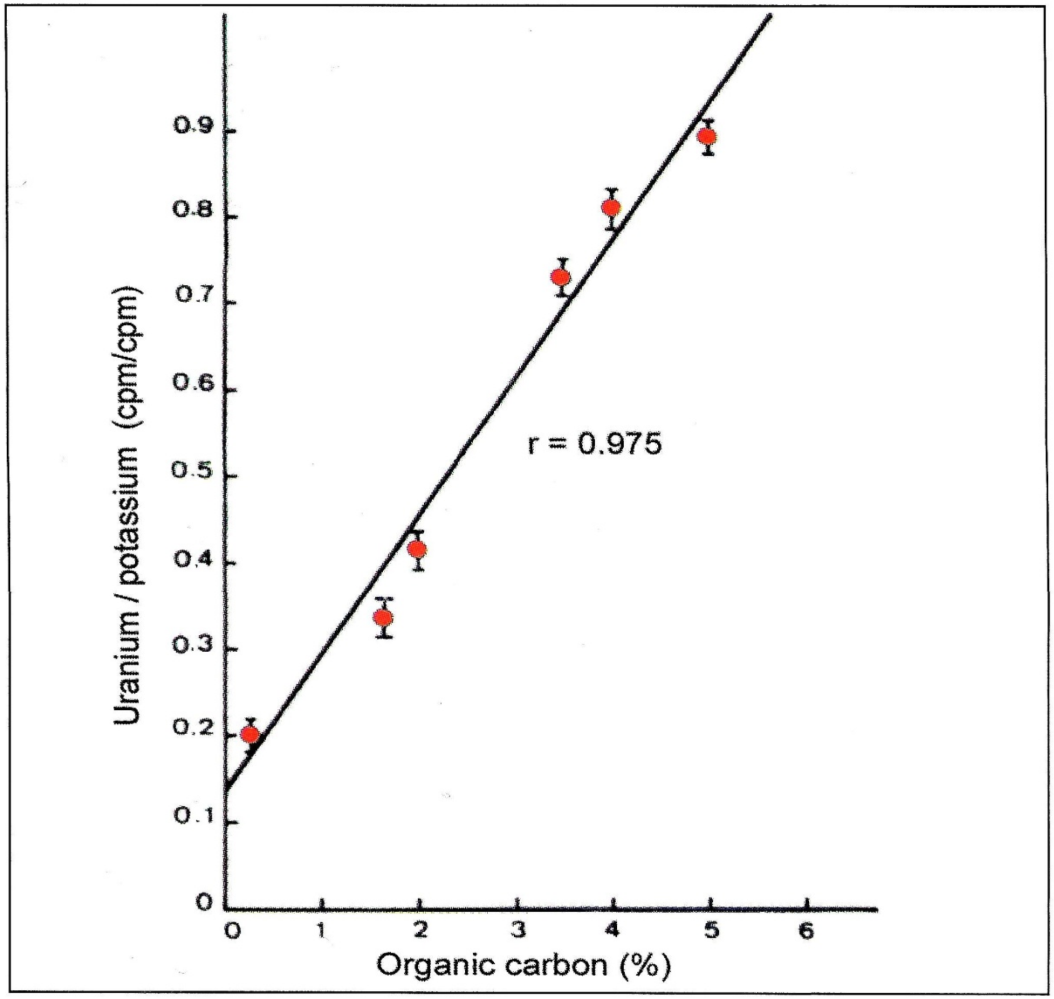

Relation between uranium (expressed as a uranium/potassium ratio) and organic carbon (from Supernaw et al., 1978).

- علاوه بر اين مي توان در روي نمودارها گفت كه مقادير بالاي اورانيوم نشانه ي سنگ منشا مي باشد.

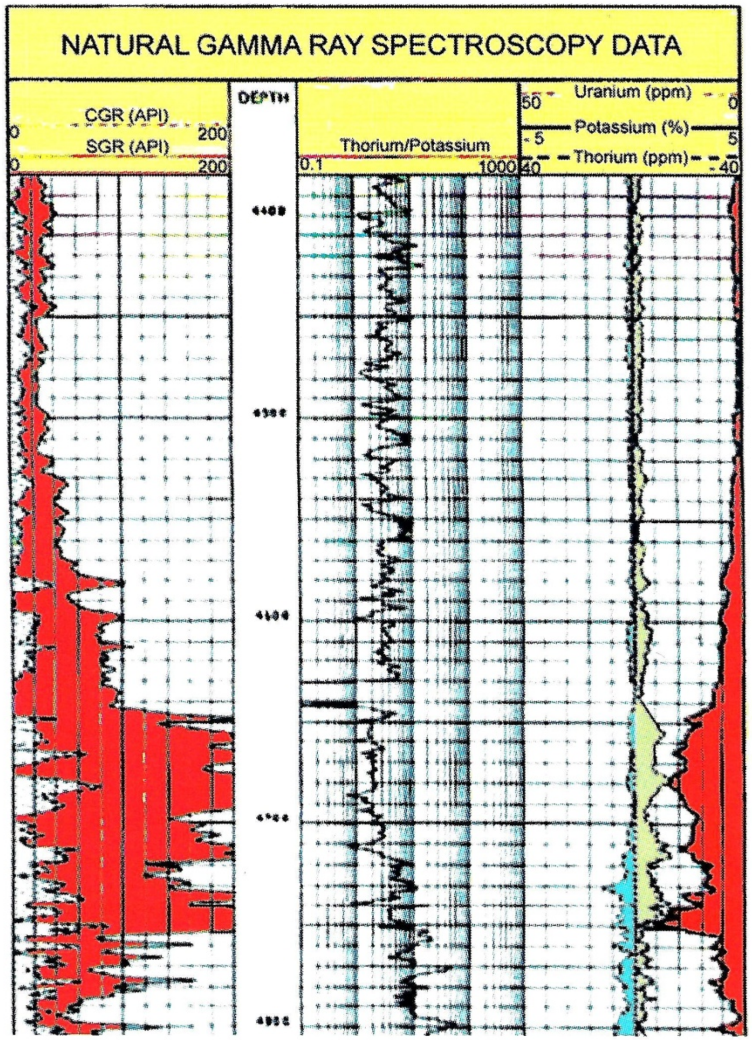

Example of formation very rich in uranium as shown by the natural gamma ray spectrometry data. It may correspond to a potential source rock (courtesy of Schlumberger).

The ΔlogR method

- این متد توسط ژئولوژیست هاي Exxon پیشنهاد شد.
- این نمودار ترکیبي از نمودار صوتي و نمودار مقاومت مي باشد که نتایج با توجه به Level of organic metamorphism units(LOM) تفسیر مي شود.
- نمودار ΔlogR وقتي حاصل مي شود که نمودار صوتي را در مقیاس لگاریتمي رسم کرده و در همان ستون نودار مقاومت را به صورت خطي رسم کرده ، حال جدایش بین این دو نمودار ، نمودار ΔlogR مي باشد.
- مناطقي که این دو نمودار روي هم قرار بگیرند(base line) ناحیه ي non – source مي باشد.
- مقدار ΔlogR از رابطه ي زیر محاسبه مي شود.

$$\Delta \log R = \log_{10} (R/R_{\text{base line}}) + 0.025(\Delta t - \Delta t_{\text{base line}})$$

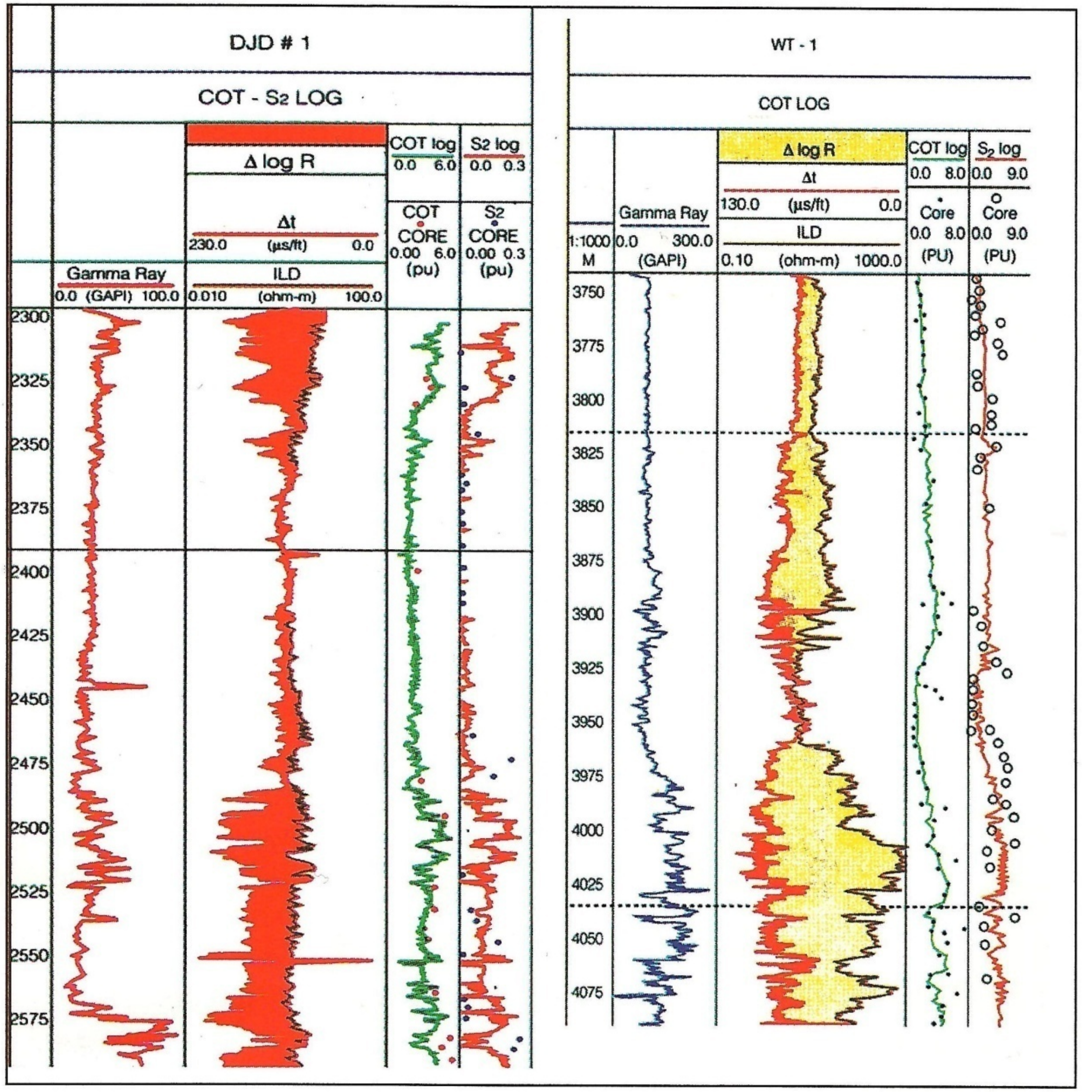

Two example of Δ log R, TOC and S_2 curves determined on 2 wells of Algeria (from Malla & Baci, 1995).

- براي مشخص كردن TOC از نمودار ΔlogR بايد مقدار LOM مشخص باشد.
- براي يافتن LOM نياز به دانستن Ro داريم و با دانستن Ro مي توان توسط نمودار زير LOM را بدست آورد.
- مقدار Ro را توسط آزمايشگاه بدست مي آوريم و يا توسط ابزار nuclear fission trace بدست آورد.
- براي مقادير مختلف LOM داريم:

0 to 7.5 : immature

7.5 to 11.5 : oil phase

> 11.5 : gas phase

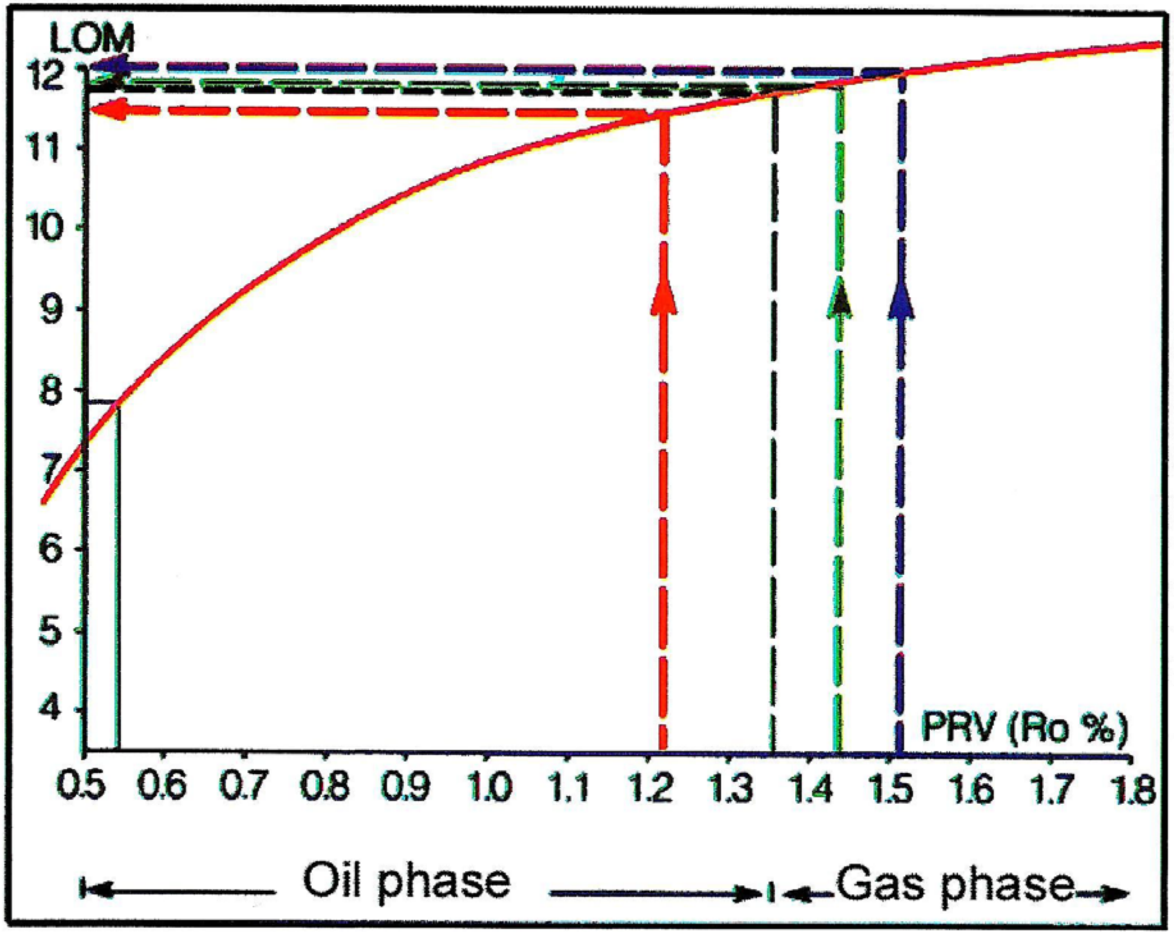

The value of LOM, determined from measured PRV equivalents for well DJD-1, was calculated at 11.5 (from Malla & Baci, 1995).

• با دانستن ΔlogR و LOM ، TOC از نمودار زير بدست مي آيد.

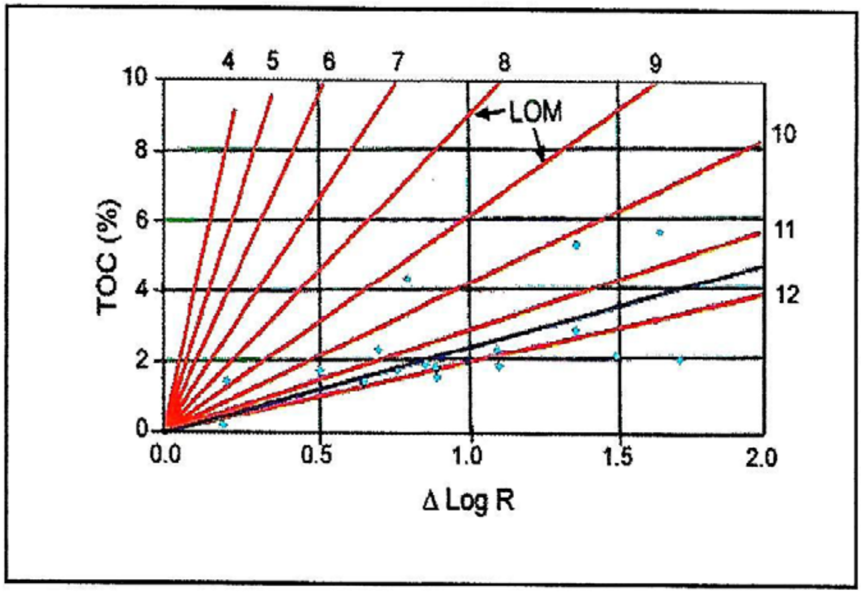

Chart to allow the determination of TOC from Δ log R separation and LOM (from Malla & Baci, 1995).

• پارامتر hydrocarbon generation potential(S2) را مي توان از نمودار زير بدست آورد.

Determination of S_2 from TOC and LOM for type II (oil-prone) kerogen (from Malla & Baci, 1995).

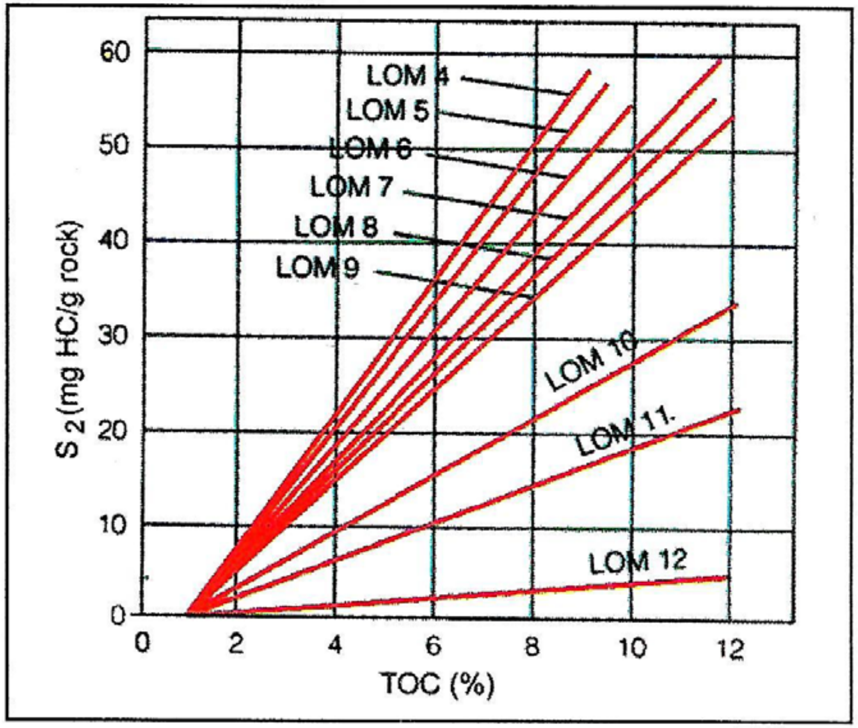

Method based on cross - plot

- اين روش بر اساس اثر مواد آلي بر واكنش ابزار نسبت به موادآلي بنا نهاده شده است.
- مواد آلي هادي نمي باشند ، در نتيجه باعث افزايش ماومت مي شوند.
- دانسيته مواد آلي بين 0.95 تا 1.05 است و با دانسيتهي سنگ ها متفاوت است.
- زمان عبور مواد آلي حدود 180 ميكرو ثانيه است.
- واكنش نسبت به نوترون در مواد آلي حدود 67 p.u مي باشد ولي در مينرال هاي شيل كمتر از 50 p.u مي باشد.
- حضور مواد آلي باعث افزايش GR مي شود.
- حال به ارائه ي cross – plot ها ي پيشنهادي مي پردازيم.

- Autric و Dumesnil در سال 1985 از نمودار صوتي ويا گاما بر حسب مقاومت نمودارهاي زير را پيشنهاد كردند.

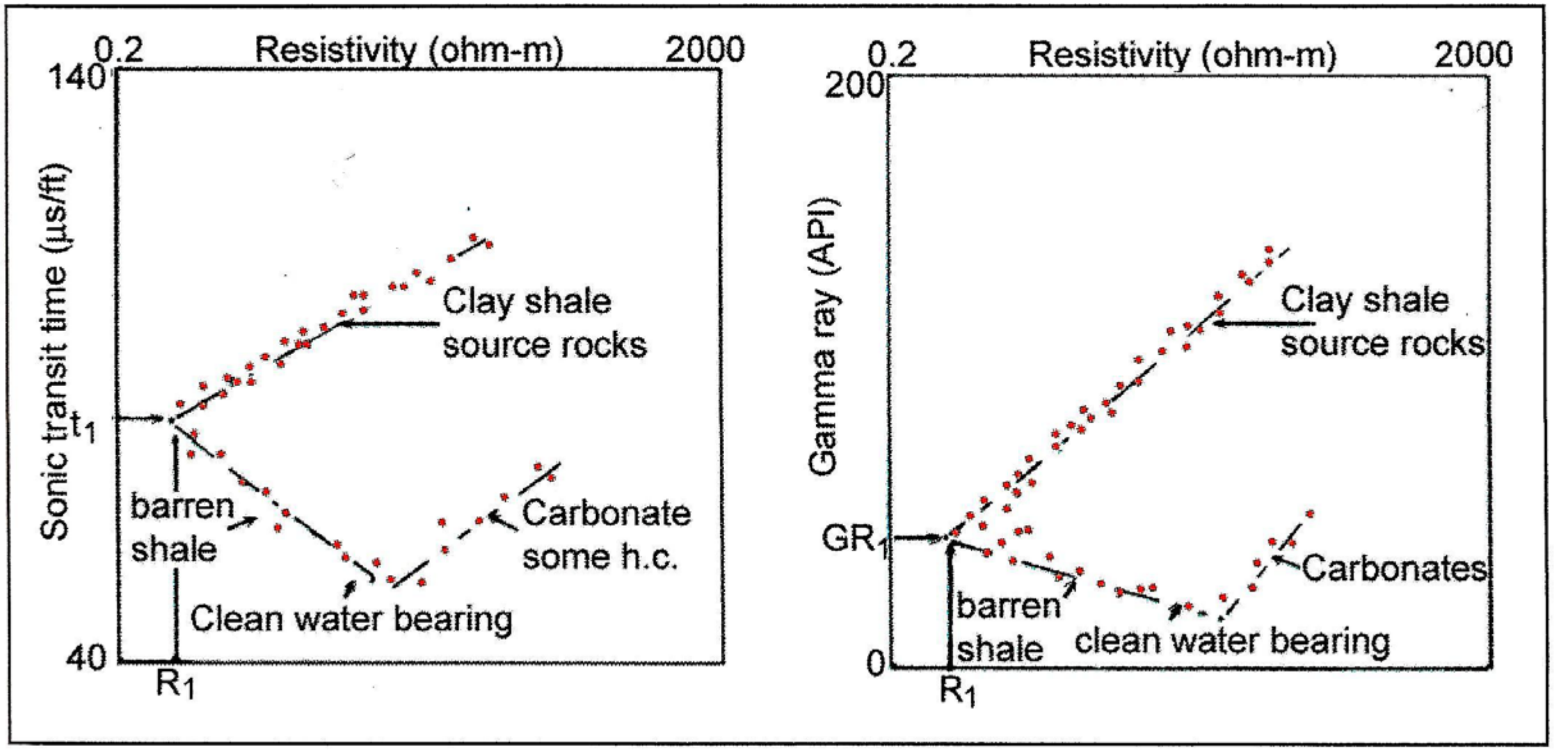

Characterization of source rocks by cross-plots combining sonic transit time and resistivity (left diagram), or gamma ray and resistivity (right diagram) (from Autric & Dumesnil, 1985).

• Meyer و Nederlof در سال 1984 نمودارهاي زير را پيشنهاد كردند.

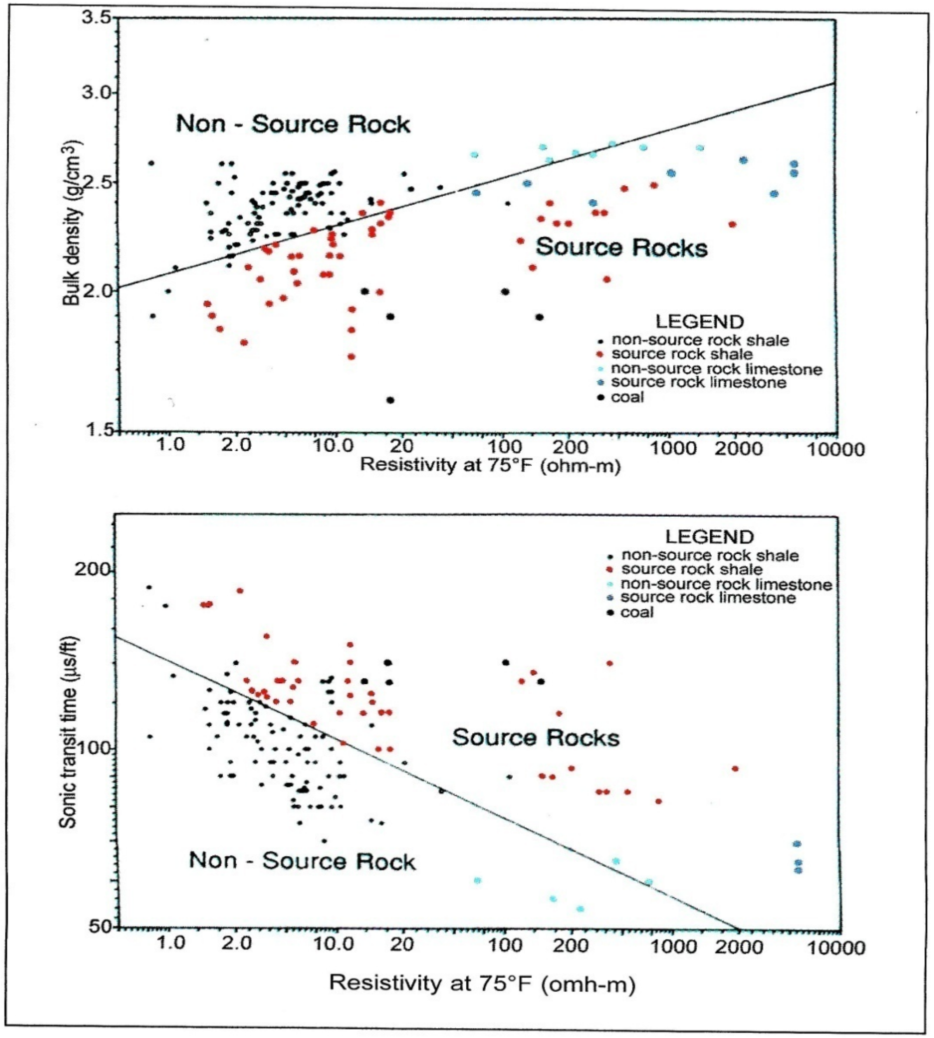

Bulk density-resistivity cross-plot and sonic-resistivity cross-plots allowing the identification of source rocks (from Meyer & Nederlof, 1984).

Method based on nuclear mesurment

- اين روش براساس محاسبه ي C/O مي باشد.
- رفتار هر عنصر در برخورد نوترون پر انرژي با خودش متفاوت مي باشد و بر اين اساس مي توان كربن و هيدروژن موجود در سازند را بر اين اساس مشخص كرد.
- در زير اين واكنش را براي چند عنصر مشاهده مي كنيد.

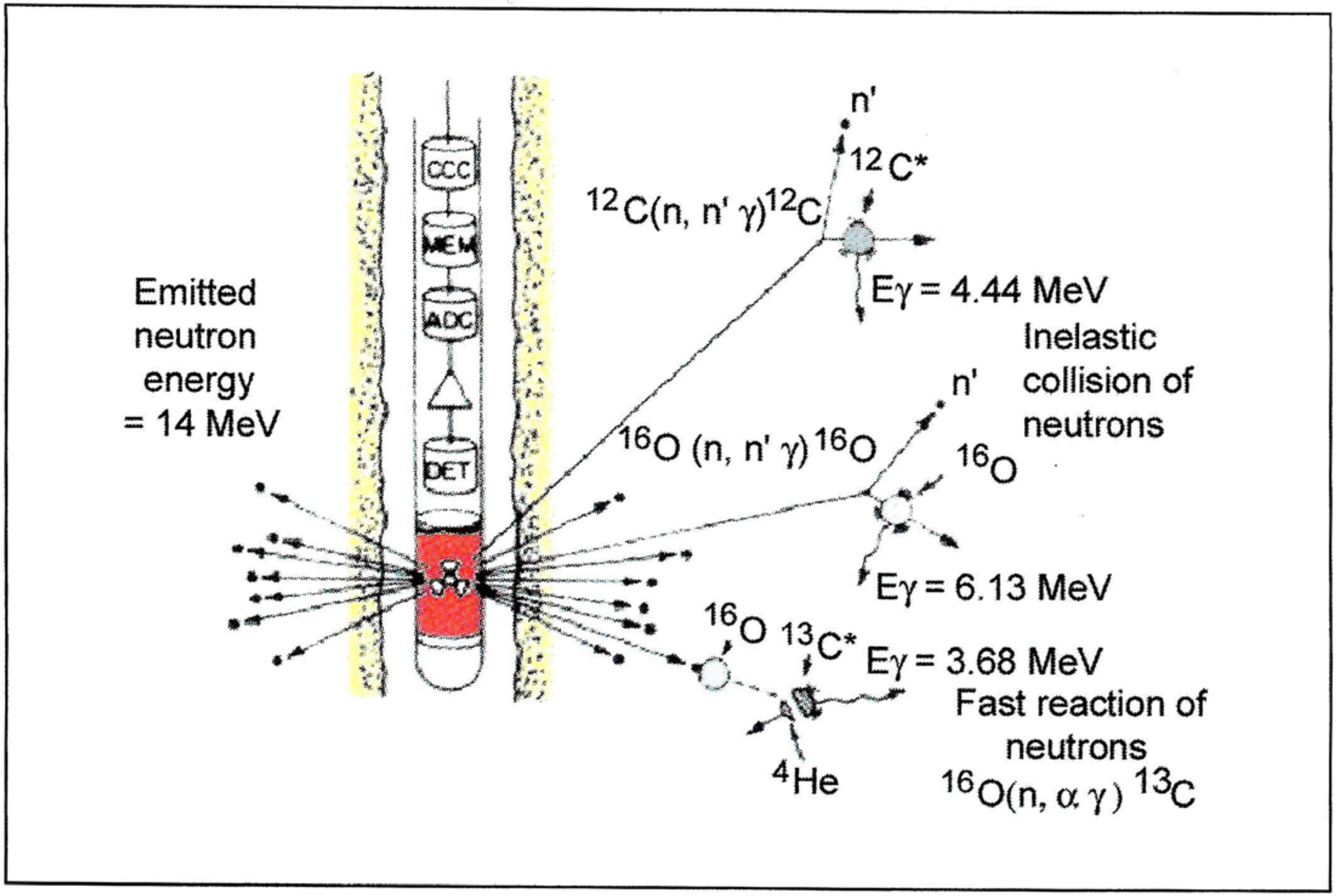

Example of interactions between high energy neutrons and C and O atoms (courtesy of Schlumberger).

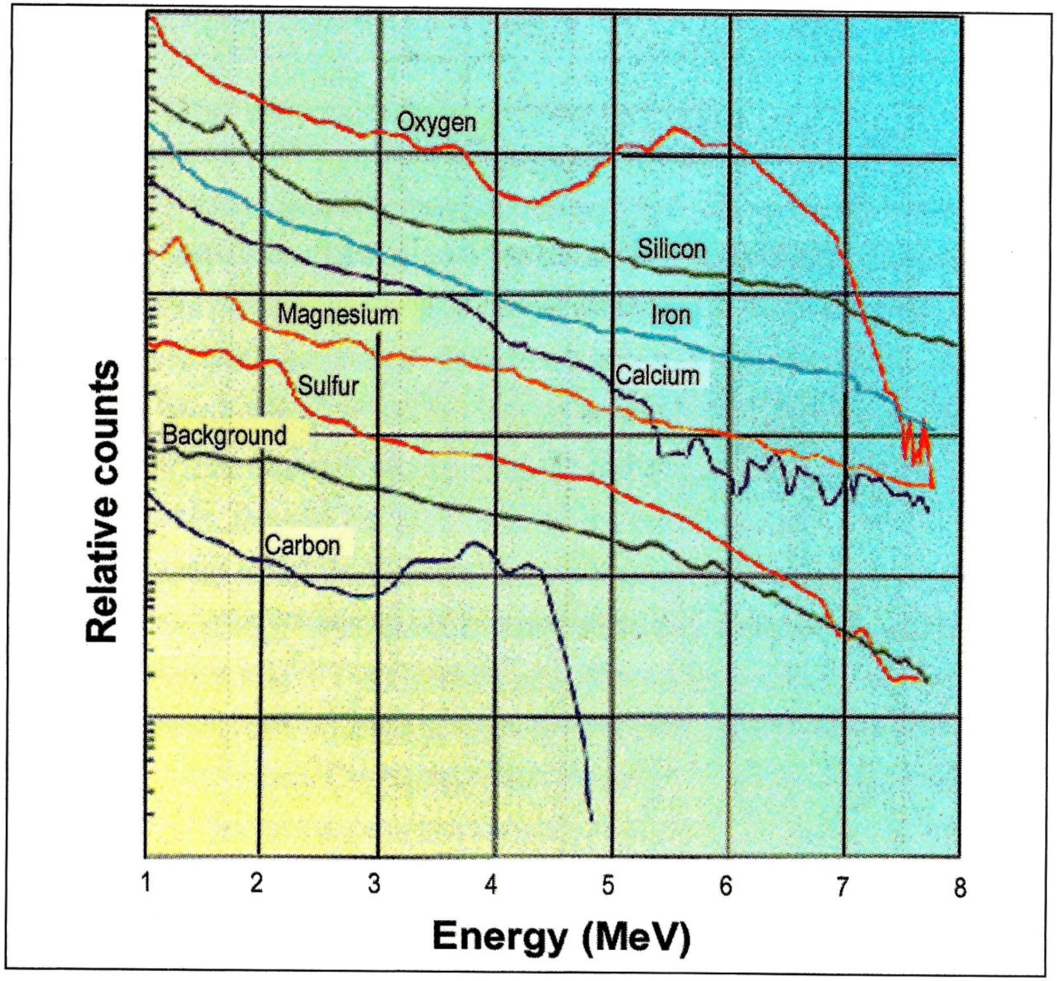

Typical Inelastic collision spectrum. Observe the peaks of Oxygen and Carbon. They are more characteristic and so can be easily detected by window energy detection collimated around these peaks (courtesy of Schlumberger).

- اين روش توسط Herron در سال 1986 بيان شد و براي يافتن total organic carbon بايد دو موضوع زير را اصلاح كرد.

1. مقدار O موجود در سنگ ، اين موضوع راحت حل مي شود در صورت اين كه ليتولوژي به طور كامل شناخته شده باشد.
2. اصلاح كربن غير آلي موجود در سازند همانند كربن كلسيت يا دولوميت.

- با اصلاح دو موضوع بالا مي توان به راحتي كربن آلي موجود در سازند را مشخص كرد.
- در شكل زير اين موضوع را براي نمونه اي مشاهده مي كنيد و نتايج را با نتايج core مقايسه كرده ايم . مشاهده مي كنيد كه اين نتايج بسيار به هم نزديك مي باشد.
- اين روش نياز به كاليبره شدن توسط نتايج core را ندارد ، ولي متاسفانه هزينه ي زيادي دارد درنتيجه خيلي استفاده نمي شود.

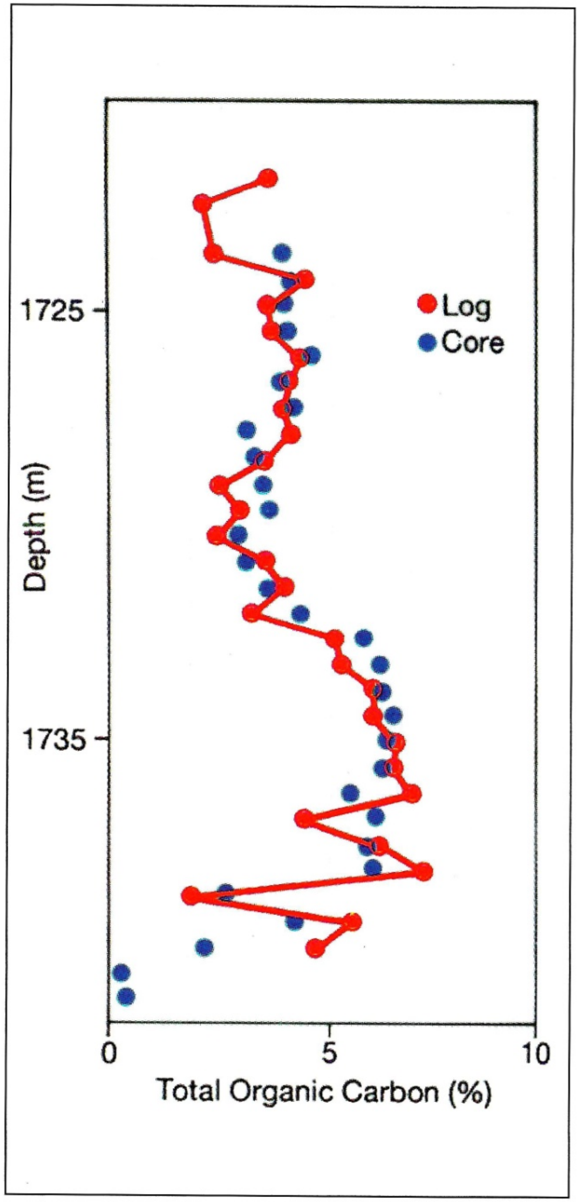

Evaluation of the organic carbon content through the measurement of the carbon-oxygen ratio (from Herron et al.*, 1988).*

Neutron Log

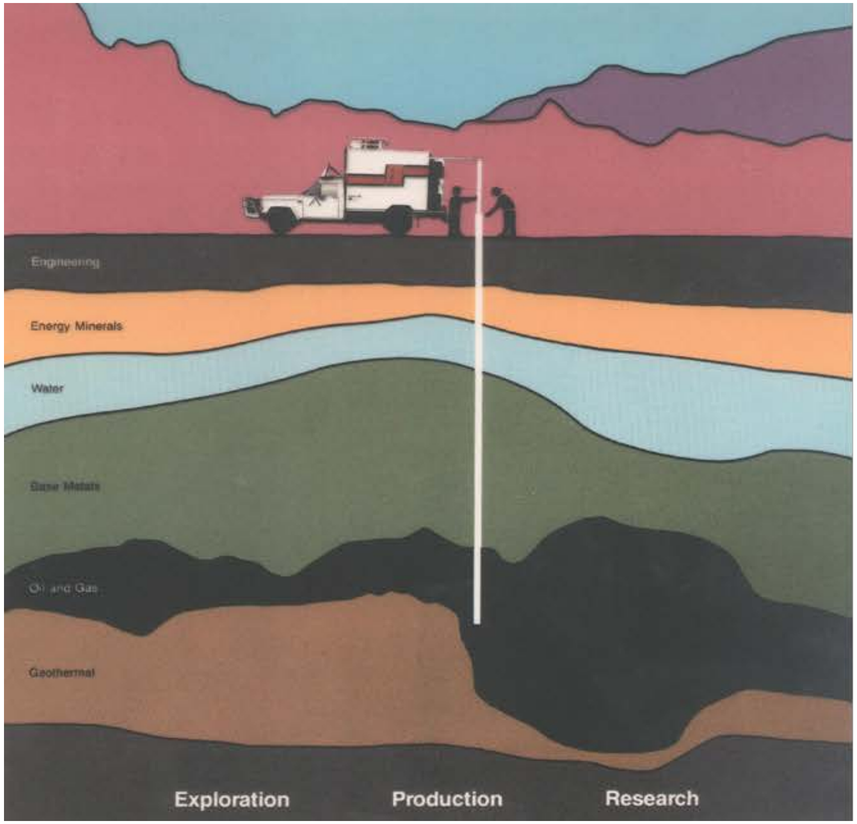
Engineering
Energy Minerals
Water
Base Metals
Oil and Gas
Geothermal
Exploration
Production
Research

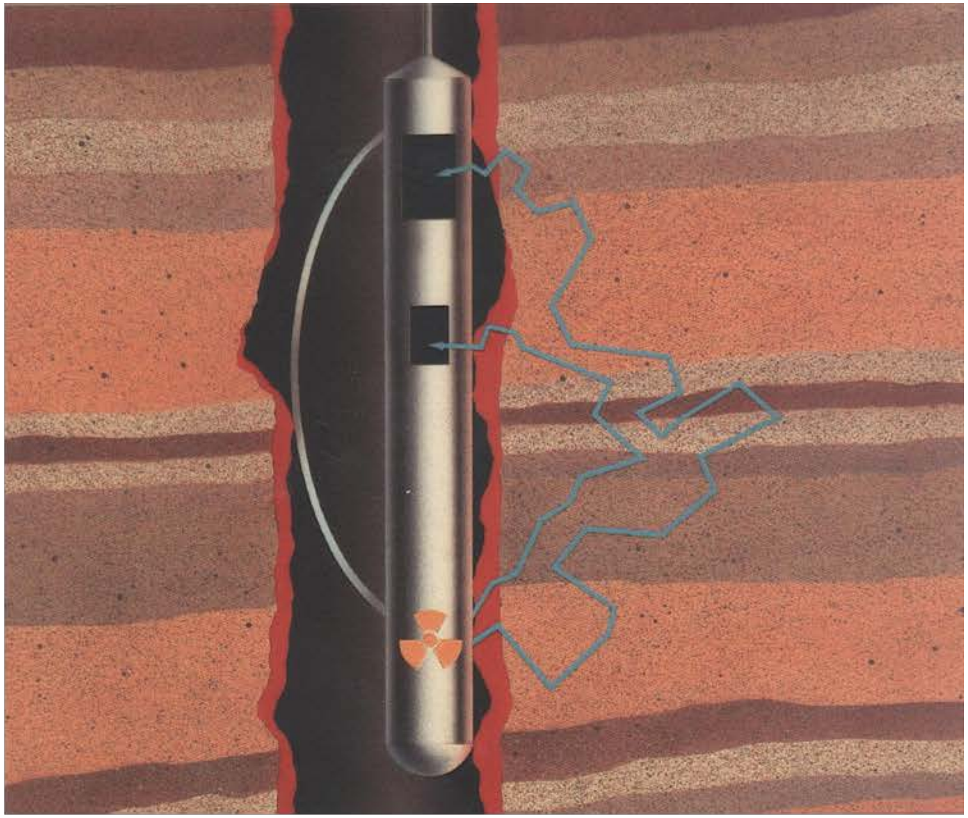

Definition

Neutron tools were the first logging instruments to use radioactive sources for determining the porosity of the formation. After the later introduction of the gamma-gamma density tool, the neutron measurement was applied in conjunction with the density porosity reading in order to recognize and correct for effects of shale and gas.

Neutron tool response is dominated by the concentration of hydrogen atoms in the formation. In clean reservoirs containing little or no shale, the neutron log response will provide a good measure of formation porosity if liquid-filled pore spaces contain hydrogen, as is the case when pores are filled with oil or water (hydrogen index =1). By contrast, when logging shaly or gas-bearing formations, a combination of Neutron and Density readings will often be required for accurate porosity assessment.

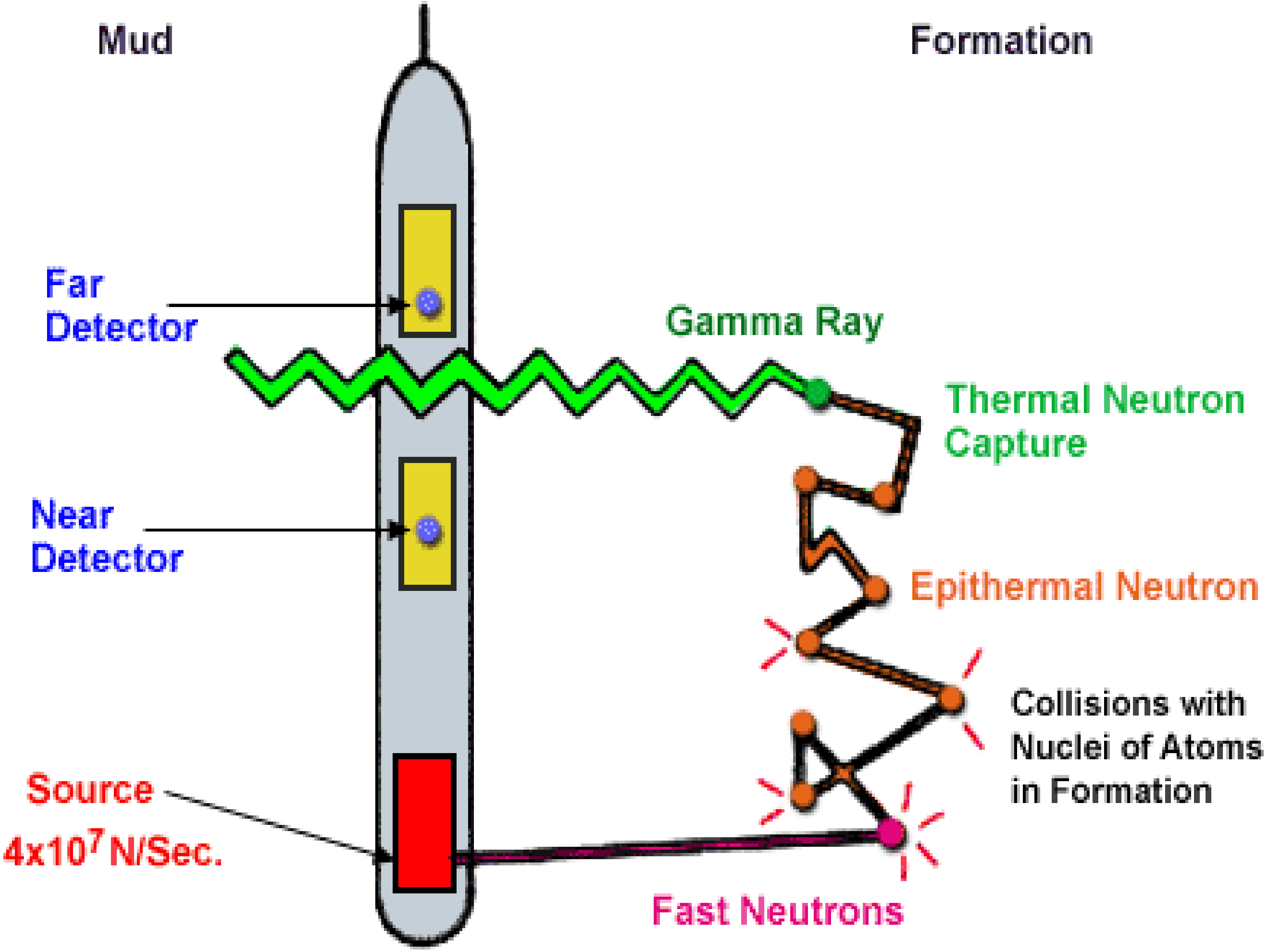

Generalized Neutron Logging Tool illustrates a typical neutron logging tool.

Basic Principles

The electrically neutral neutron has a mass that is practically identical to that of the hydrogen atom. The neutrons that are emitted from a neutron source have a high energy of several million electron volts (MeV). After emission, they collide with the nuclei within the borehole fluid and formation materials. With each collision, the neutrons loose some of their energy. The largest loss of energy occurs when the neutrons collide with hydrogen atoms. The rate at which the neutrons slow-down depends largely on the amount of hydrogen in the formation.

With each collision the neutrons slow down, until the neutrons reach a lower (epithermal) energy state and then continue to lose energy until they reach an even lower (thermal) energy state of about 0.025 eV. At this energy the neutrons are in thermal equilibrium with other nuclei in the formation. At thermal speeds, the neutrons will eventually be captured by a nucleus. When a nucleus captures a thermal neutron, a gamma ray (called a gamma ray of capture)is emitted to dissipate excess energy within the atom.

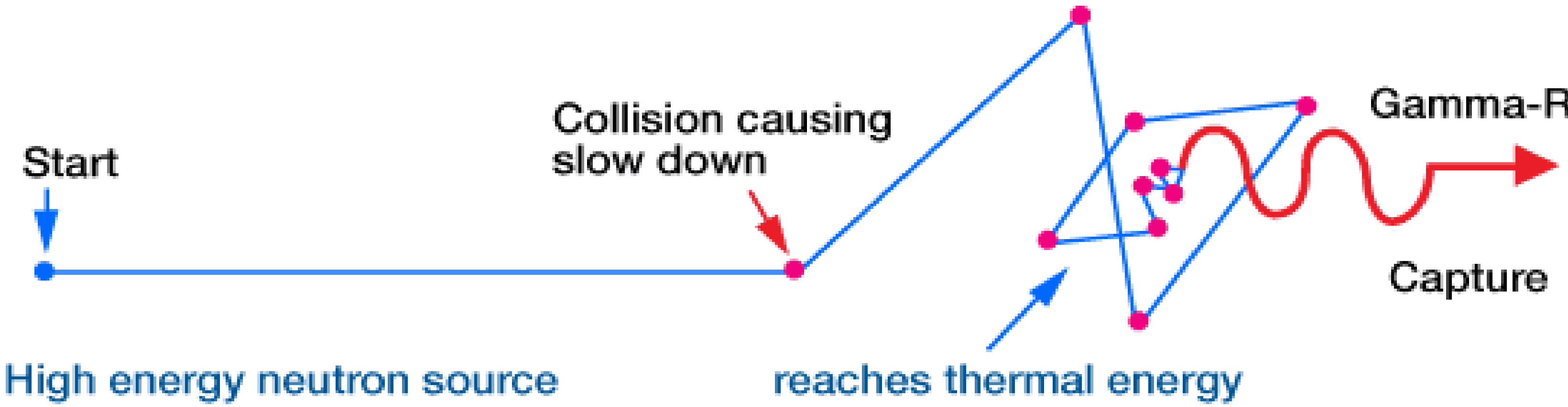

Emission, Traveling and Collisions of a Neutron in a Formation

The amount of energy lost at each collision depends on the relative mass of the target nucleus, and the scattering cross section. (At the nuclear level, the term *cross section* is defined as the effective area within which a neutron must pass in order to interact with an atomic nucleus. Such interactions are typically classified either as neutron capture or as neutron scatter. The cross-section is a probabilistic value dependent on the nature and energy of the particle, as well as the nature of the capturing or scattering nucleus.

Depending on the type of tool being used, either the gamma rays emitted after neutron capture, the epithermal neutrons or the thermal neutrons will be counted.

The principles of neutron logging are summarized below:

· A neutron source emits a continuous flux of high-energy neutrons.

· Collisions with formation nuclei reduce the neutron energy -thereby slowing it down.

· At thermal energy levels (approximately 0.025 eV), neutrons are captured.

· Neutron capture results in an emission of gamma rays.

· Depending on the type of tool, the detector measures the slowed down neutrons and/or emitted gamma rays.

Neutron logging devices contain one or more detectors and a neutron source that continuously emits energetic (fast) neutrons.

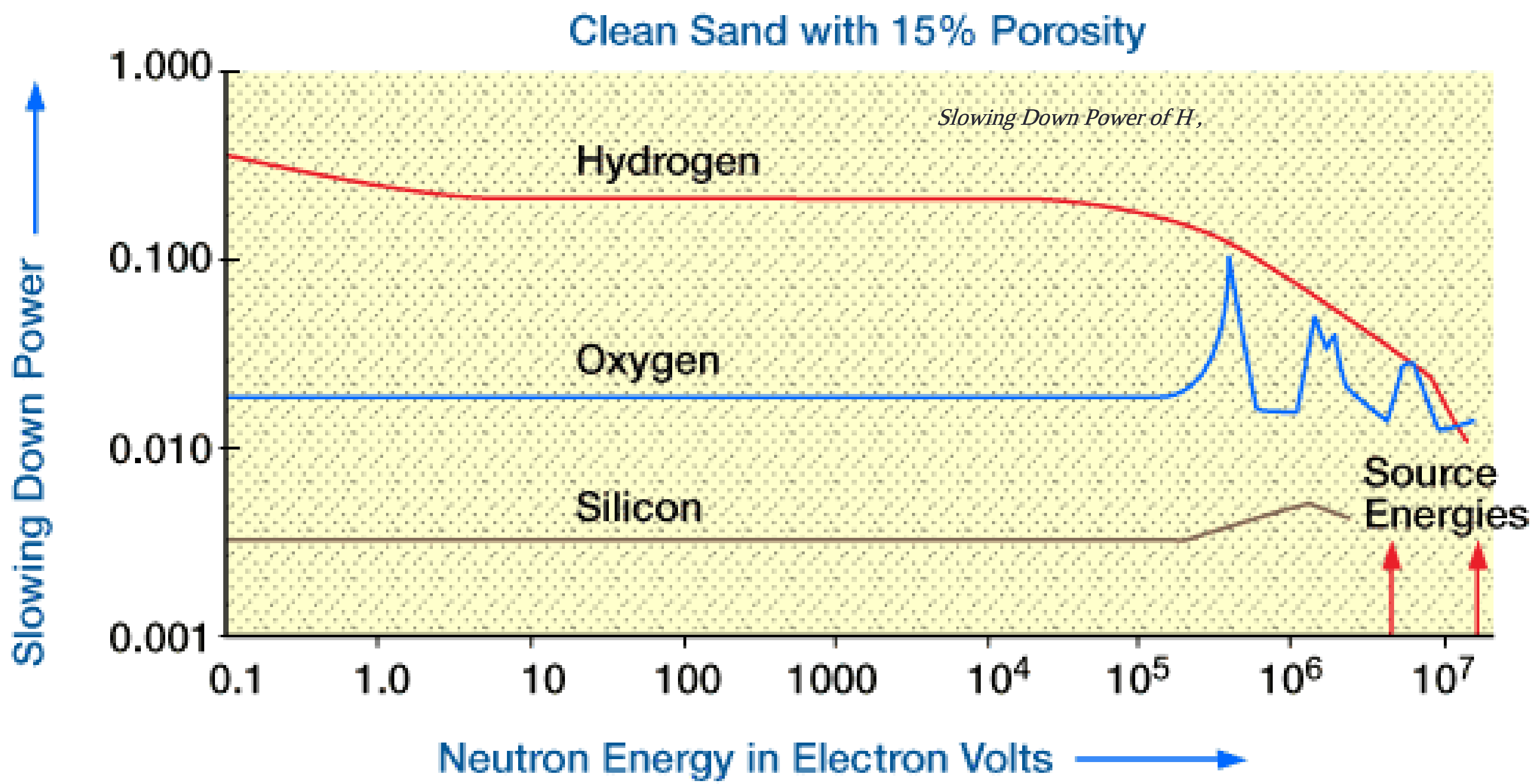

Slowing down power of H, O, SI for different neutron energies

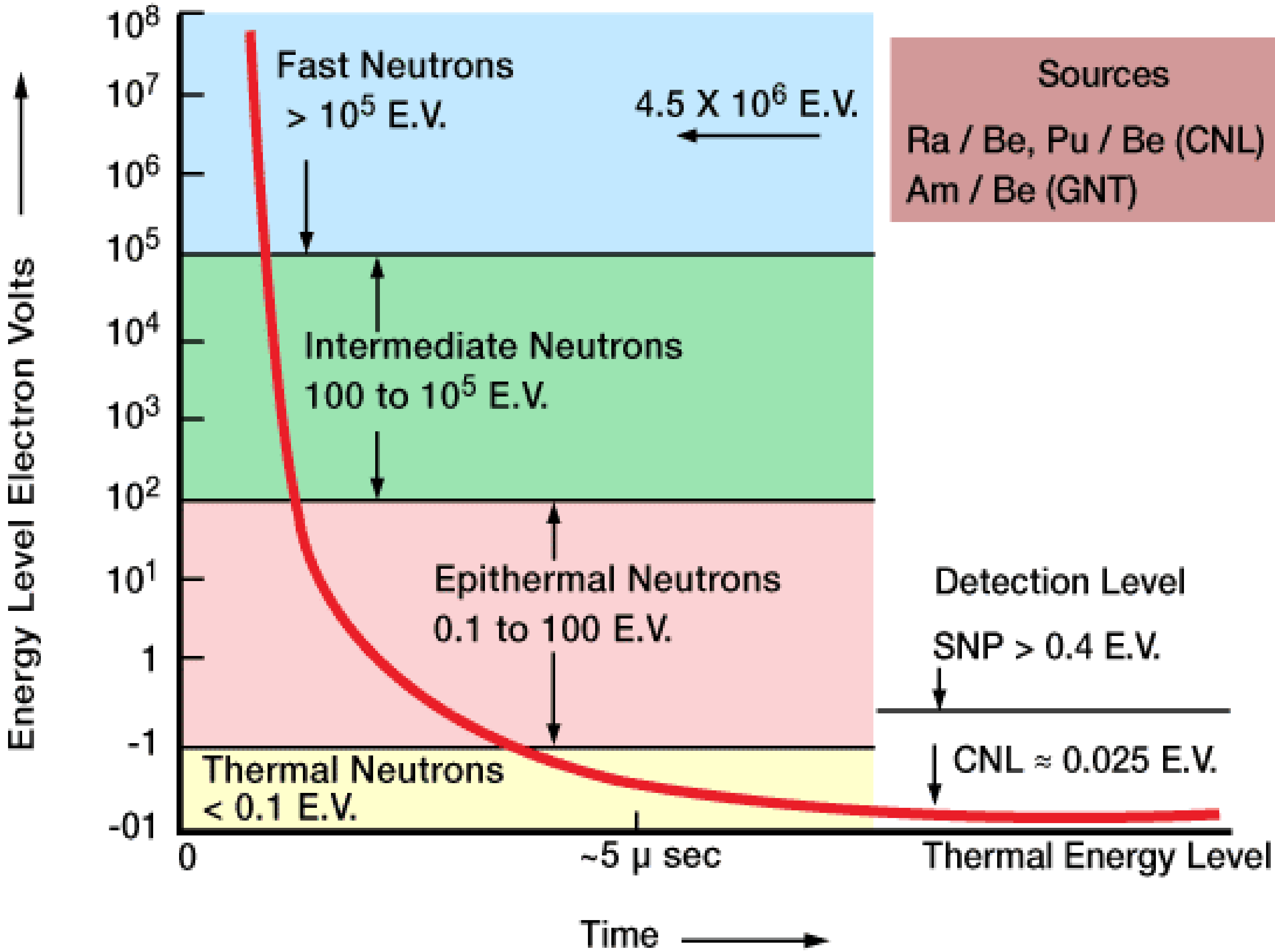

Neutron energy level versus time after leaving the source illustrates the slow down process

Porosity (or the hydrogen index) can be determined by measuring epithermal or thermal neutron populations, or by measuring capture gamma rays, or any combination thereof.
Neutron logs that detect epithermal neutrons are referred to as *sidewall neutron* logs. By contrast, the compensated neutron log, in widespread use today, detects thermal neutrons, using two neutron detectors to reduce borehole effects. Single thermal neutron detector tools, of poorer quality, are also available in many areas of the world.

Capture gamma rays are used for porosity determination, and logs of this type are referred to as *neutron-gamma* logs. The responses of these devices are dependent upon such variables as porosity, lithology, hole size, hole rugosity, fluid type, and temperature.

Compensated and sidewall logs use corrections from their electronic panels to account for some of these variables, while neutron-gamma logs require departure curves (provided in chart books) to make corrections.

NEUTRON POROSITY EQUIVALENCE CURVES
SIDEWALL NEUTRON POROSITY LOG (SNP)
MAY ALSO BE USED FOR GNT NEUTRON LOGS

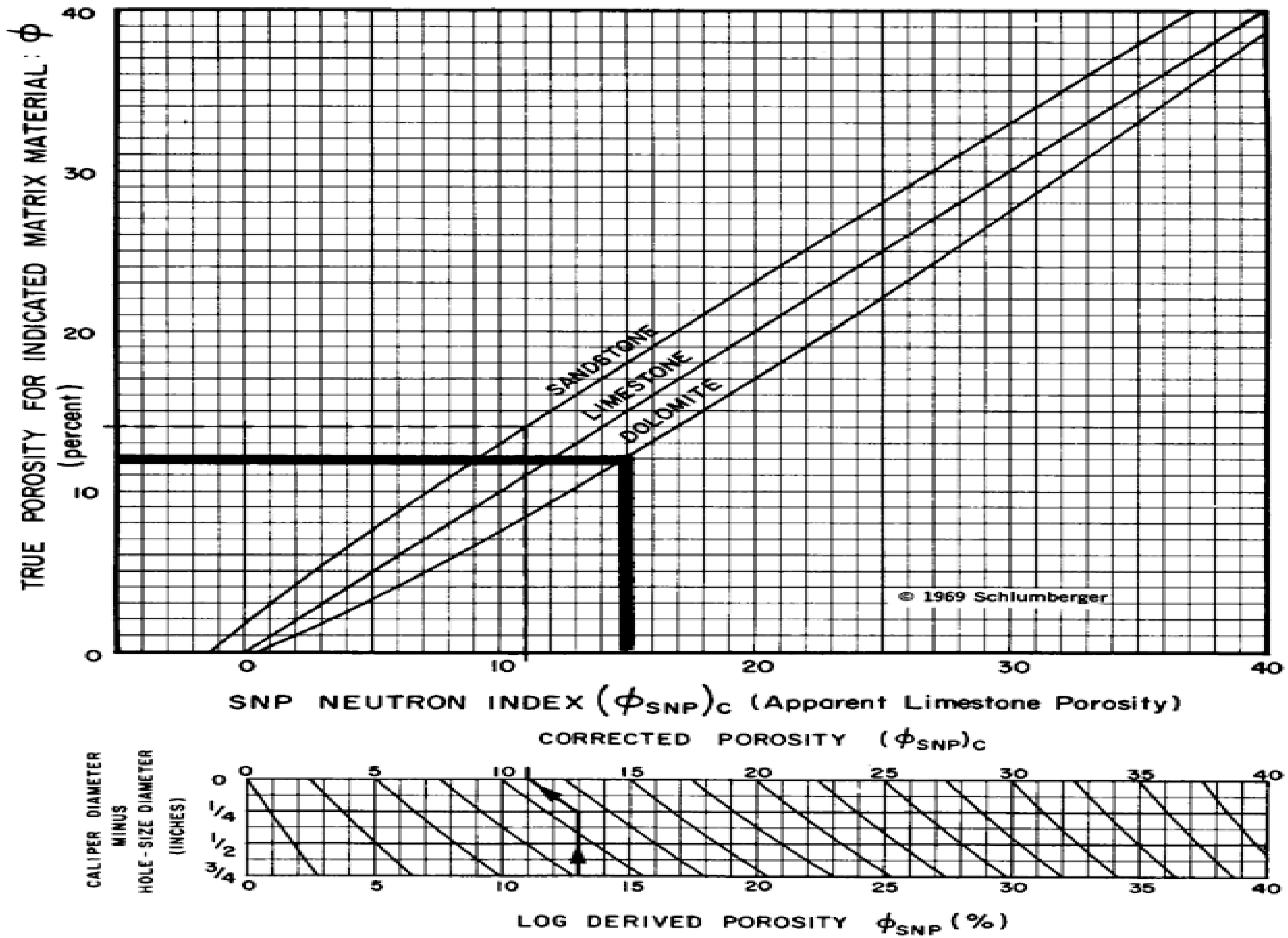

NEUTRON LOGGING APPLICATIONS

Neutron tools are used primarily to determine:

· porosity, usually in combination with the density tool

· gas detection, usually in combination with the density tool, but also with a sonic tool

· shale volume determination, in combination with the density tool

· lithology indication, again in combination with the density log and/or sonic log

· formation fluid type.

Depending on the device, these applications may be made in either open or cased holes. Additionally, because neutrons are able to penetrate steel casing and cement, these logs can be used for depth tie-in as well as providing information on porosity and hydrocarbon saturations in cased holes

Density log

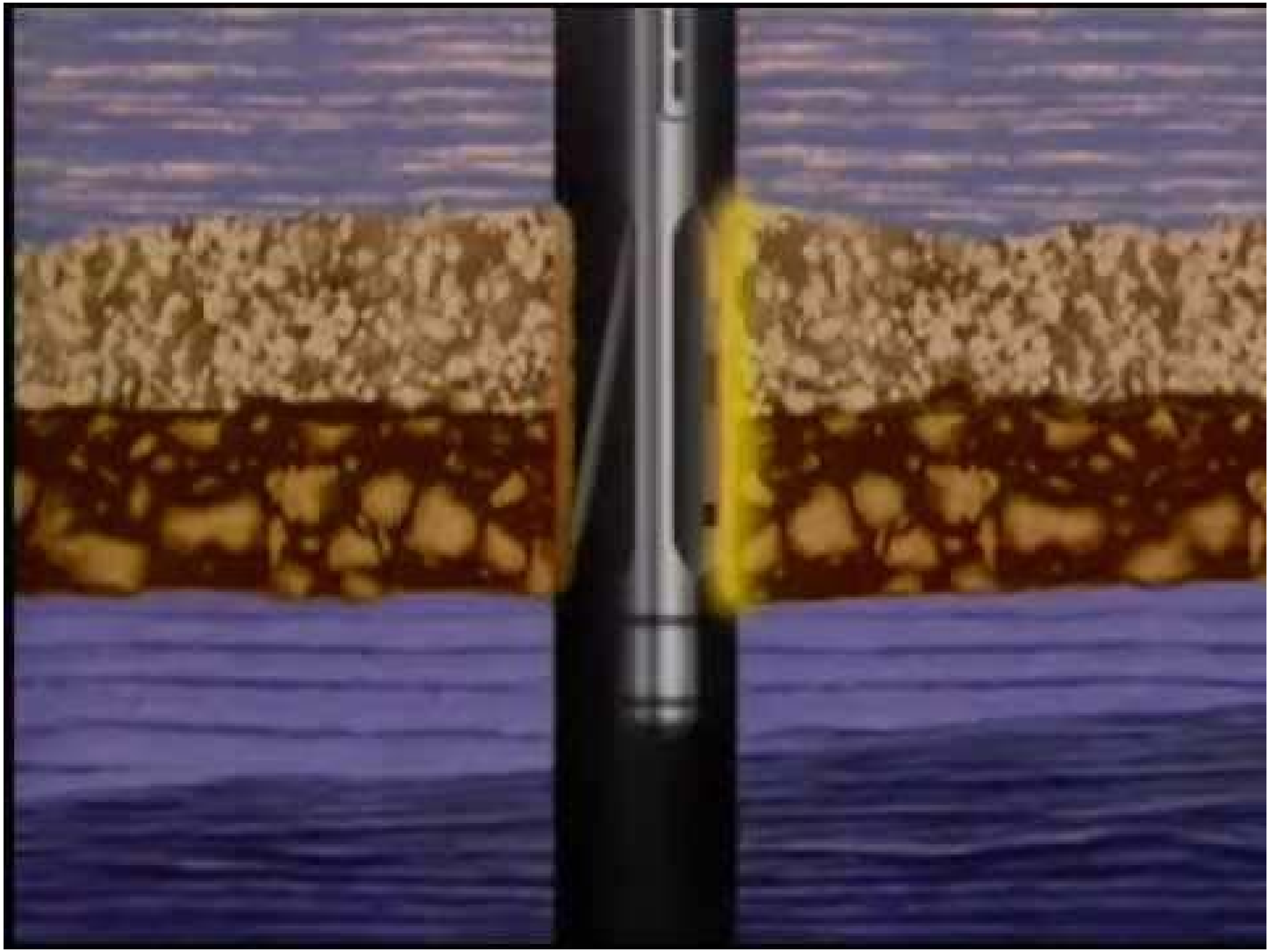

Density Log

The formation density log is a porosity log that measures ***electron density*** of a formation.

The density logging device is a contact tool which consists of a medium-energy gamma ray source that emits gamma rays into a formation. The gamma ray source is either Cobalt-60 or Cesium-137.

A density derived porosity curve is sometimes presented in tracks #2 and #3 along with the bulk density and correction curve . The most frequently used scales are a range of 2.0 to 3.0 gm/cc or 1.95 to 2.95 gm/cc across two tracks. Track #1 contains a gamma ray log and caliper

Formulation bulk density is a function of matrix density, porosity, and density of the fluid in the pores (salt, mud, fresh mud, or hydrocarbons). Density is one of the most important pieces of data in formation evaluation. In the majority of the wells drilled, density is the primary indicator of porosity. In combination with other measurements, it may also be used to indicate lithology and formation fluid type.

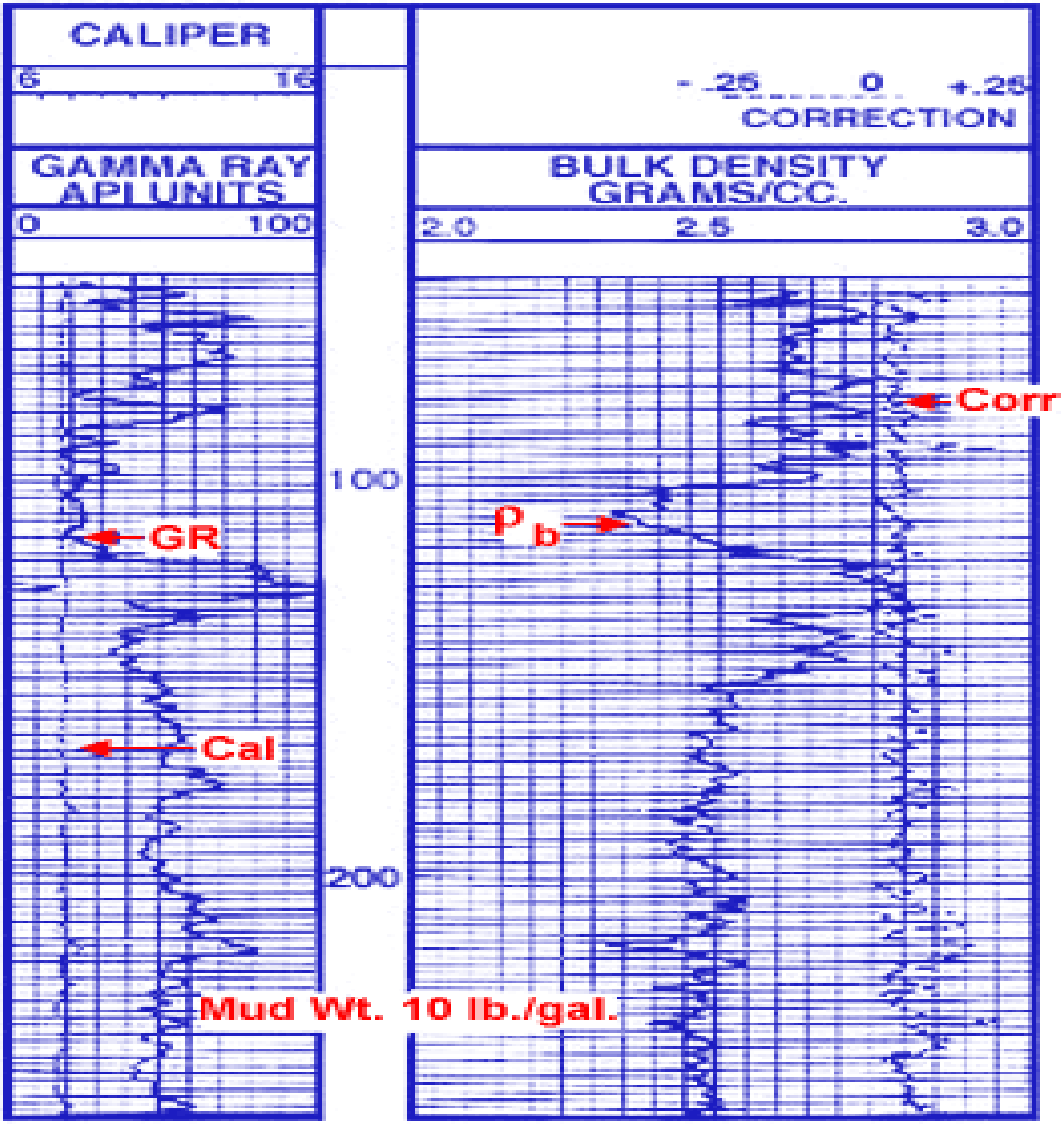

Courtesy Schlumberger Well Services

The tool can be used by itself, but is typically run in combination with other tools, such as the compensated neutron and resistivity tools. The formation density skid device ,*Schematic of the Dual-Spacing Formation Density Logging Device (FDC*) carries a gamma ray source and two detectors, referred to as the short-spacing and long-spacing detectors

The tool employs a radioactive source which continuously emits gamma rays. These pass through the mudcake and enter the formation, where they progressively lose energy until they are either completely absorbed by the rock matrix or they return to one the two gamma ray detectors in the tool

Dense formations absorb many gamma rays, while low-density formations absorb fewer. Thus, high-count rates at the detectors indicate low-density formations, whereas low count rates at the detectors indicate high-density formations .For example, in a thick anhydrite bed the detector count rates are very low, while in a highly washed-out zone of the hole, simulating an extremely low-density formation, the count rate at the detectors is extremely high.

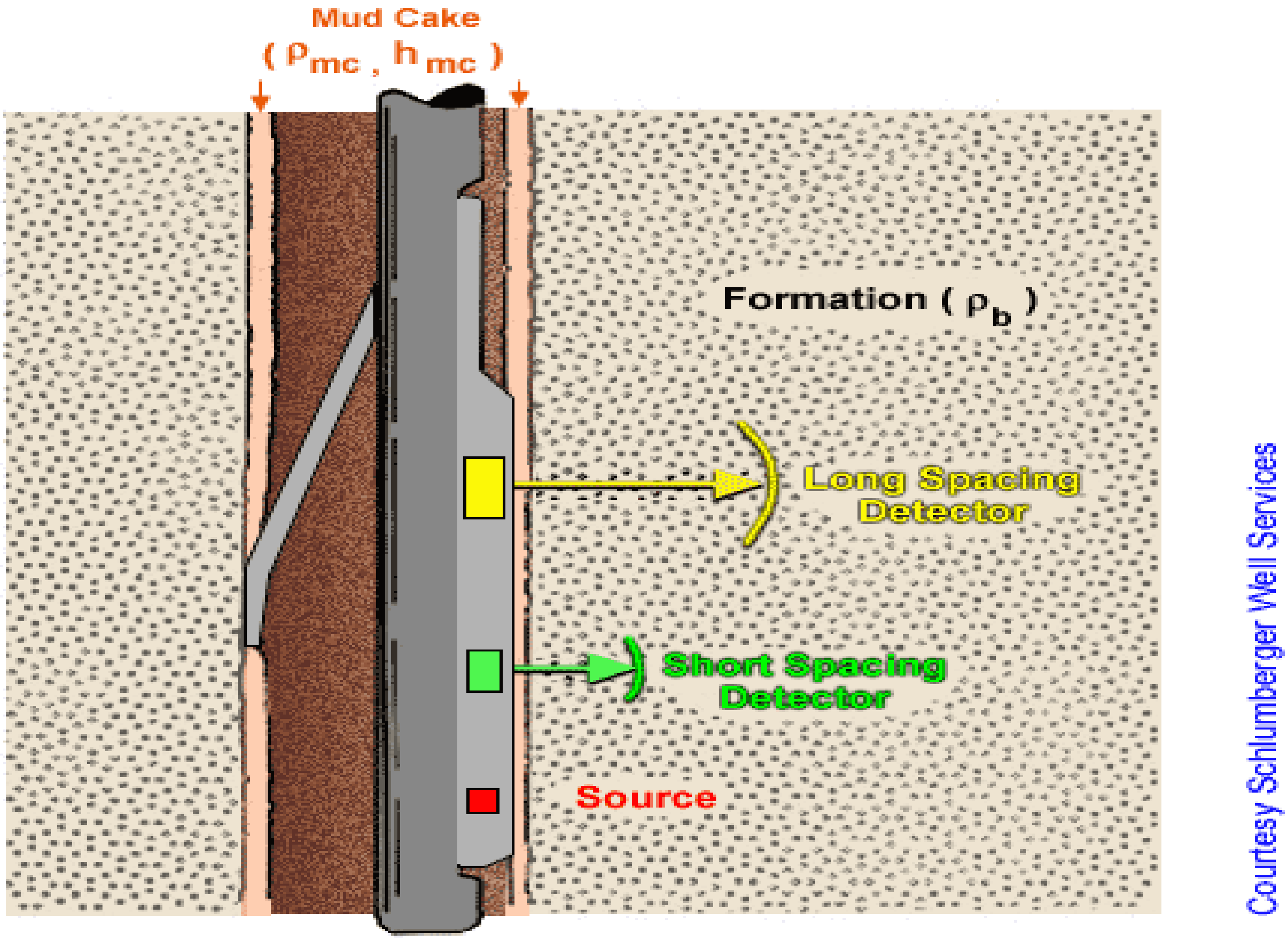

This tool is a contact-type tool; i.e., the skid device must ride against the side of the borehole to measure accurately.

Gamma rays can react with matter in three distinct manners:

· *Photoelectric effect,* where a gamma ray collides with an electron, is absorbed, and transfers all of its energy to that electron. In this case, the electron is ejected from the atom.

· *Compton scattering,* where a gamma ray collides with an electron orbiting some nucleus. In this case, the electron is ejected from its orbit and the incident gamma ray loses energy.

· *Pair production,* where a gamma ray interacts with an atom to produce an electron and positron. These will later recombine to form another gamma ray.

Photoelectric interaction can be monitored to find the lithology-related parameter, Pe. For the conventional density measurement, only the Compton scattering of gamma rays is of interest. Conventional logging sources do not emit gamma rays with sufficient energies to induce pair production, therefore pair production will not be a topic of this discussion.

To determine density porosity, either by chart or by calculation, the matrix density and type of fluid in the borehole must be known. The formula for calculating density porosity is:

$$\Phi = \frac{\rho_{ma} - \rho_b}{\rho_{ma} - \rho_f}$$

Where invasion of formation is shallow, low density of the formation's hydrocarbon will increase density porosity. Oil does not significantly affect density porosity, but gas does (gas affect). Hilchie (1978) suggests using a gas density of 0.7 gm/cc for fluid density (p**f**) in the density porosity formula if gas density in unknown.

The density log gives reliable porosity values, provided the borehole is smooth, the formation is shale-free, and the pore space does not contain gas. In shaly formations and/or gas-bearing zones, it is necessary to refine the interpretative model to make allowances for these additions or substitutions to the rock system.

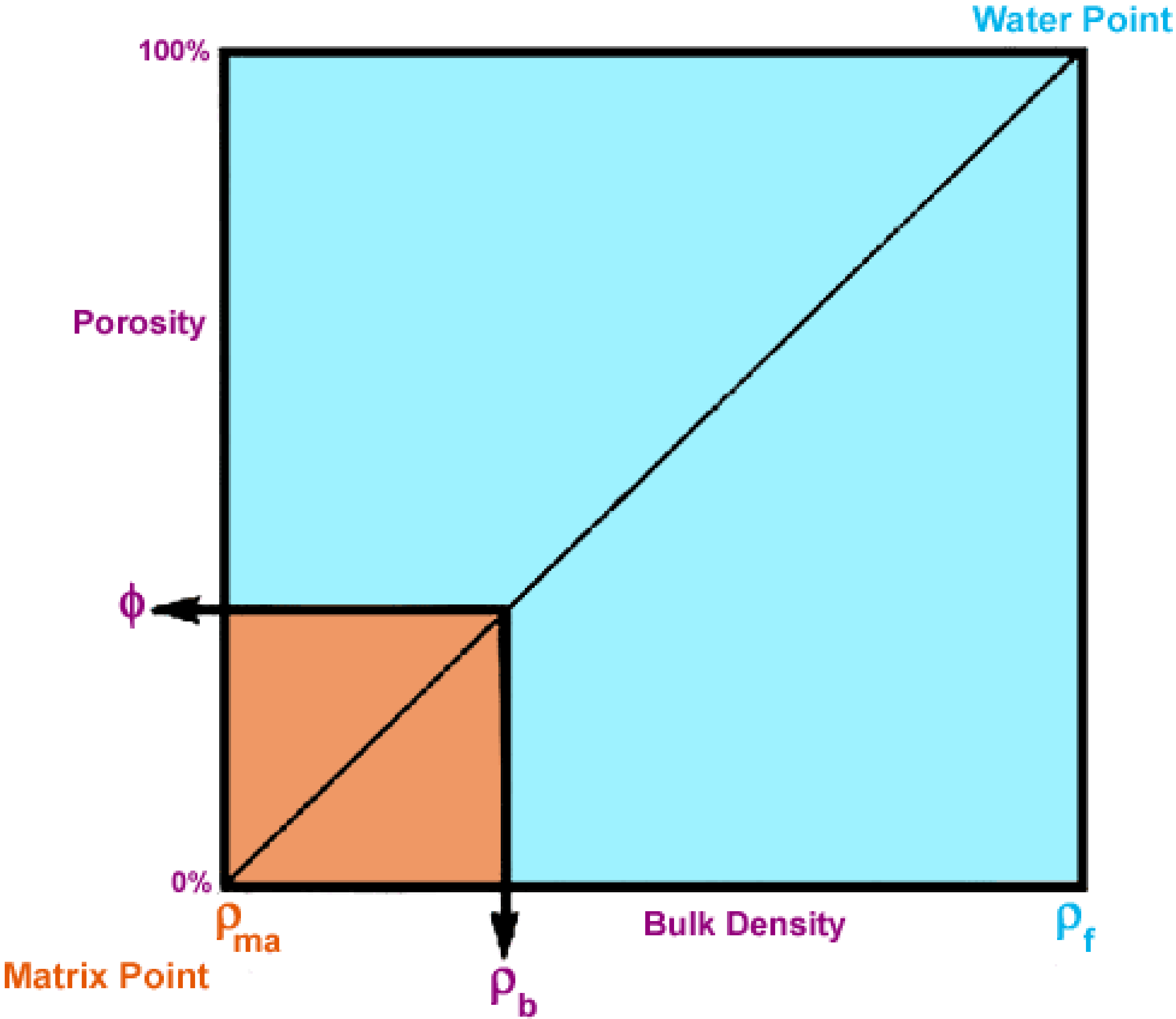
Water Point
100%
Porosity
ϕ
0%
ρma
Matrix Point
ρb
Bulk Density
ρf

LITHOLOGIC DENSITY TOOL

The Pe, or lithodensity log, run with the lithodensity tool (LDT), is another version of the standard formation density log. In addition to the bulk density (rb), the tool also measures the **photoelectric absorption index (Pe)** of the formation. This new parameter enables a lithological interpretation to be made without prior knowledge of porosity.

The photoelectric effect occurs when a gamma ray collides with an electron and is absorbed in the process, so that all of its energy is transferred to the electron. The probability of this reaction taking place depends upon the energy of the incident gamma rays and the type of atom. The photoelectric absorption index of an atom increases as its atomic number, Z, increases.

$$Pe = (0.1 \cdot Z_{eff})^{3.6}$$

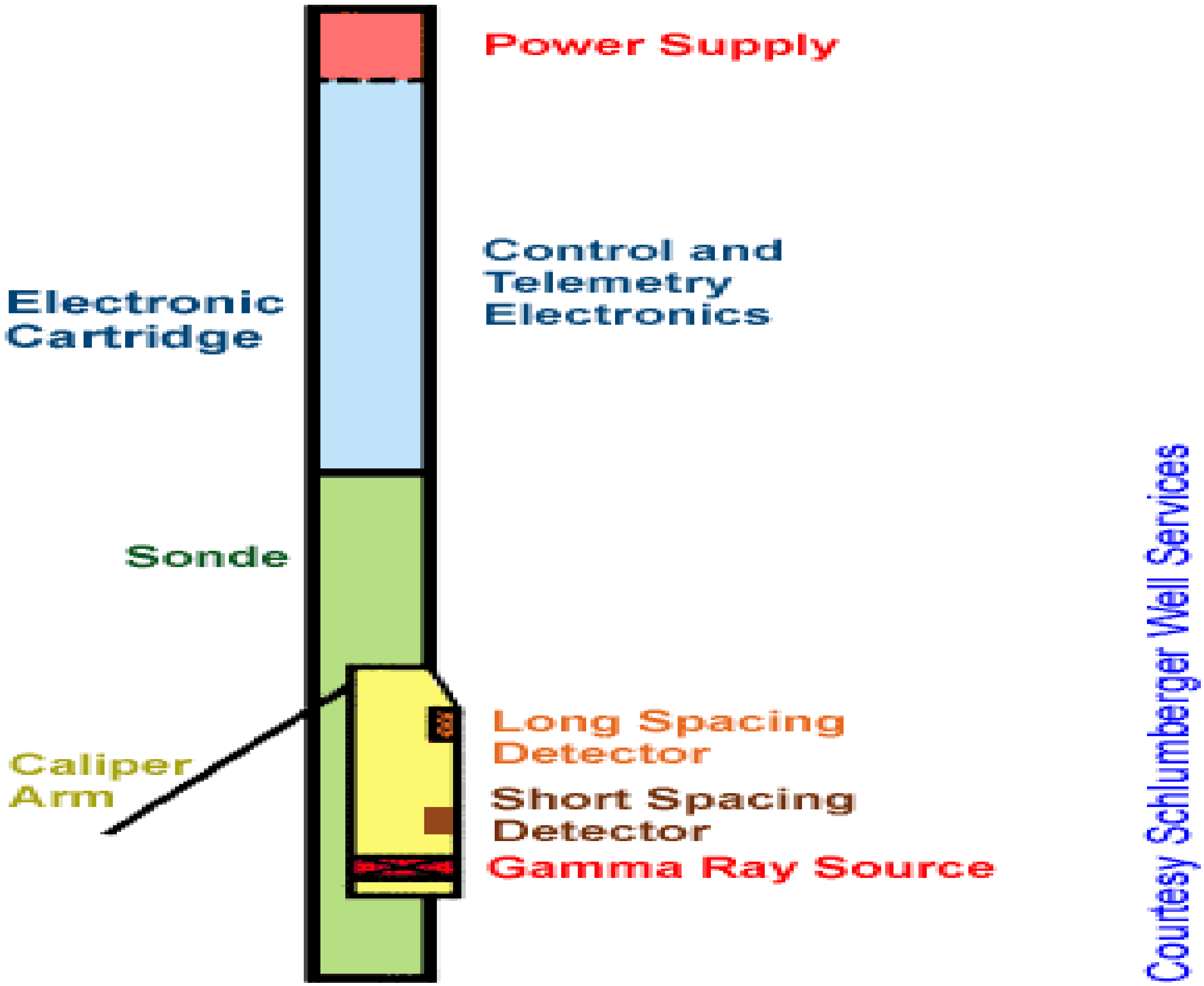

Power Supply
Electronic Cartridge
Control and Telemetry Electronics
Sonde
Caliper Arm
Long Spacing Detector
Short Spacing Detector
Gamma Ray Source
Courtesy Schlumberger Well Services

The lithodensity tool is similar to a conventional density logging device, and uses a skid containing a gamma ray source and two gamma ray detectors held against the borehole wall by a spring-actuated arm. Gamma rays are emitted from the tool and are scattered by the formation, losing energy until they are absorbed via the photoelectric effect.

At a finite distance from the source, there is a gamma ray energy spectrum as shown in in the figure given below. Variation in Gamma Ray Spectrum for Formations of Different Densities. This Figure also shows that an increase in the formation density results in a decrease in the number of gamma rays detected over the whole spectrum.

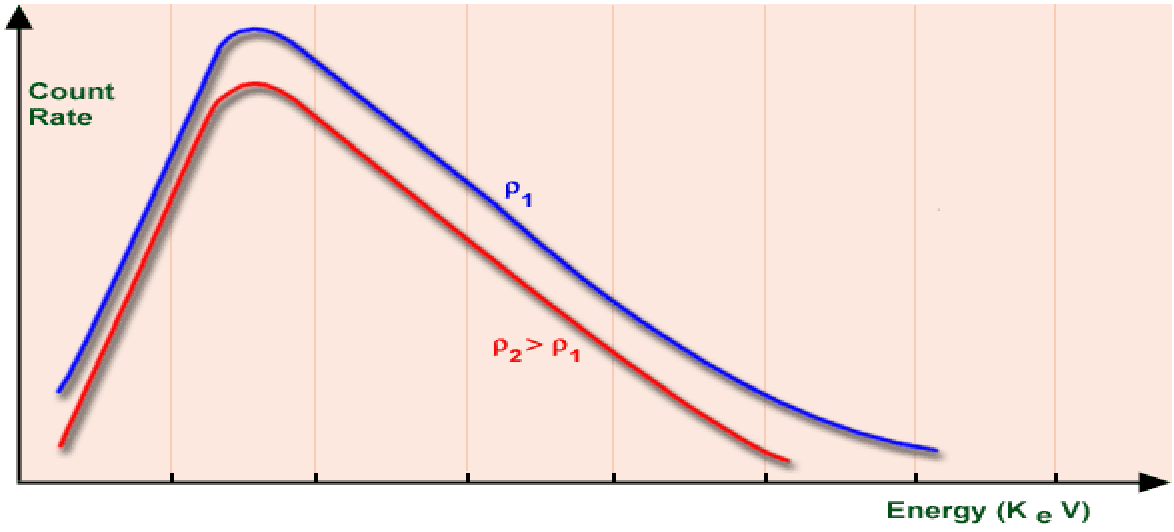

Courtesy Schlumberger Well Services

For formations of constant density but different photoelectric absorption coefficients, the gamma ray spectrum is only altered at lower energies, as indicated in the next figure .

Observing the gamma ray spectrum, we notice that region H only supplies information relating to the density of the formation, whereas region L provides data relating to both the electron density and the Pe value. By comparing the counts in the energy windows H and L, the Pe can be measured. The gamma ray spectrum at the short spacing detector is only analyzed for a density measurement, which is used to correct the formation density determined from the long spacing spectrum for effects of mud-cake and rugosity.

The photoelectric absorption coefficient is virtually independent of porosity, there being only a slight decrease in the coefficient as the porosity increases. Similarly, the fluid content of the formation has little effect. Simple lithologies, such as pure sandstone and anhydrite, can be read directly from logs using Pe curves. Look for the following readings in the most commonly occurring reservoir rocks and evaporites.

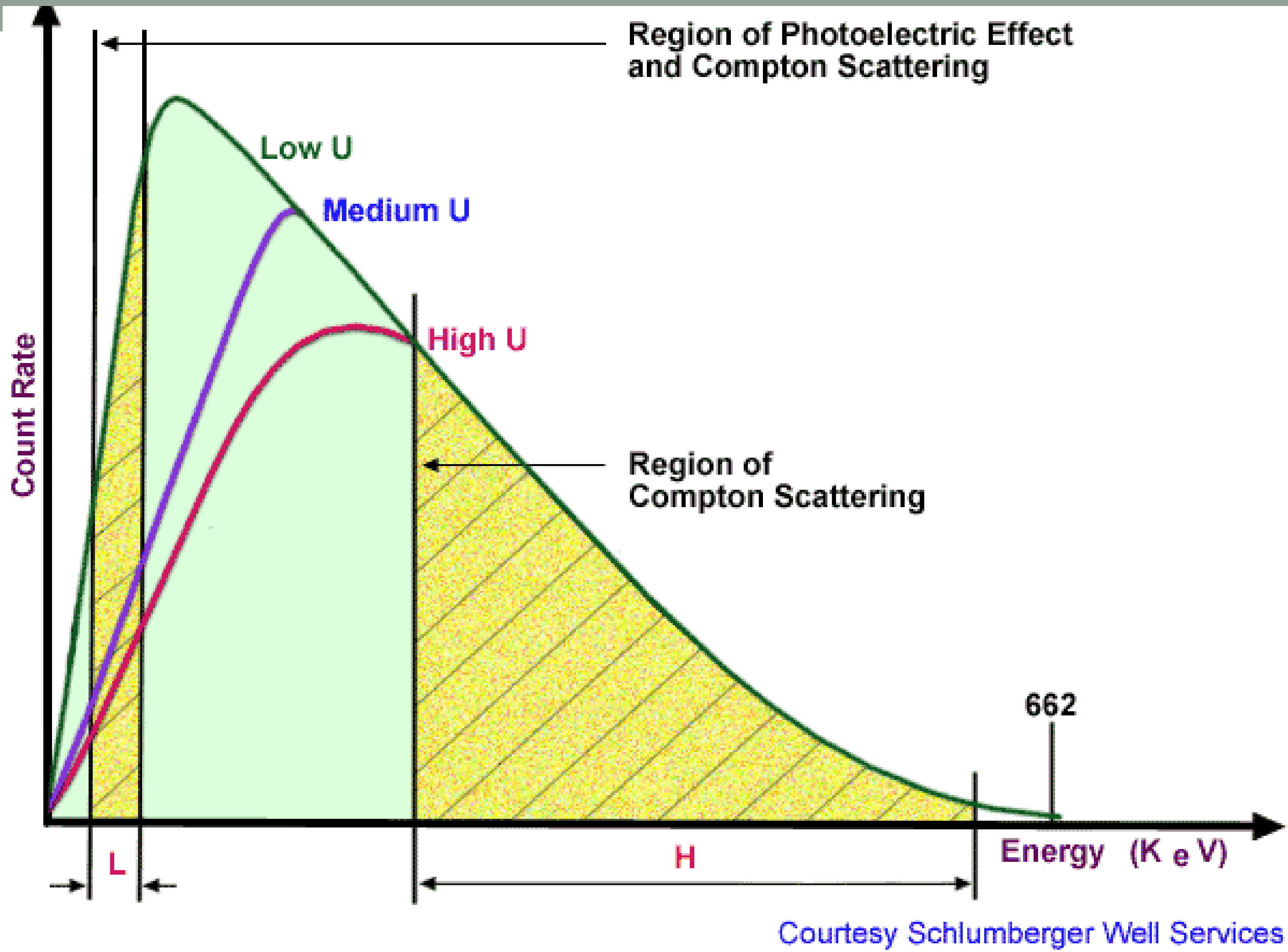
Region of Photoelectric Effect
and Compton Scattering
Low U
Medium U
High U
Count Rate
Region of
Compton Scattering
662
L
H
Energy (K e V)
Courtesy Schlumberger Well Services

Material	Pe
Sand	1.81
Shale	3-4
Limestone	5.08
Dolomite	3.14
Salt	4.65
Anhydrite	5.05

Application of density log

It can assist the geologist to: (1) identify evaporite minerals, (2) detect gas-bearing zones, (3) determine hydrocarbon density, and (4) evaluate shaly sand reservoirs and complex lithologies.

Sonic Log

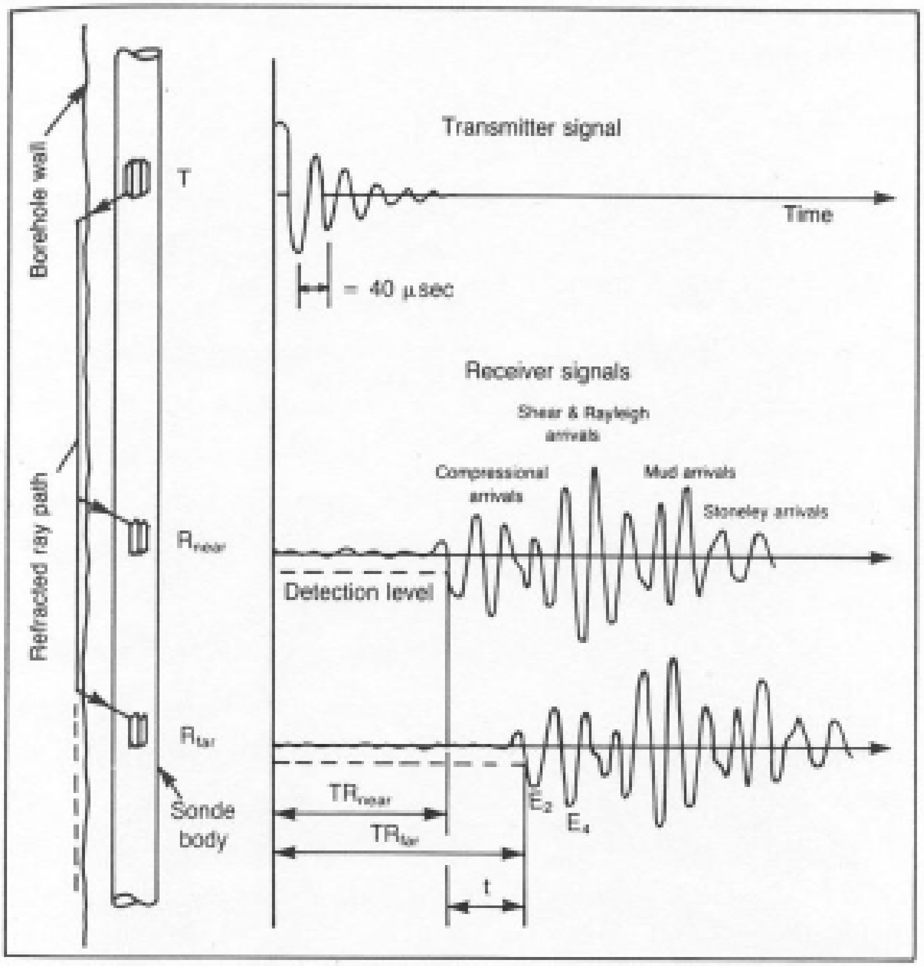

Basic Sonic logging system (courtesy Schlumberger. © SPE)

Uses

1) **Determine porosity of reservoir rock**

2) Improve correlation and interpretation of seismic records

3) Identify zones with abnormally high pressures

4) Assist in identifying lithology

5) Estimate secondary pore space

6) Indicate mechanical integrity of reservoir rocks and formations that surround them (in conjunction with density data)

7) Estimate rock permeability

Principle

Transmitter emits sound waves

Receivers pick up and record the various waves

Measure the first arrival of the compressional wave

Travel time is the difference in arrival of the compressional wave at the receivers

(1', 2', 3' Sonic)

$\Delta t = (t2 - t1)/Ls$

where Ls is span between receivers.

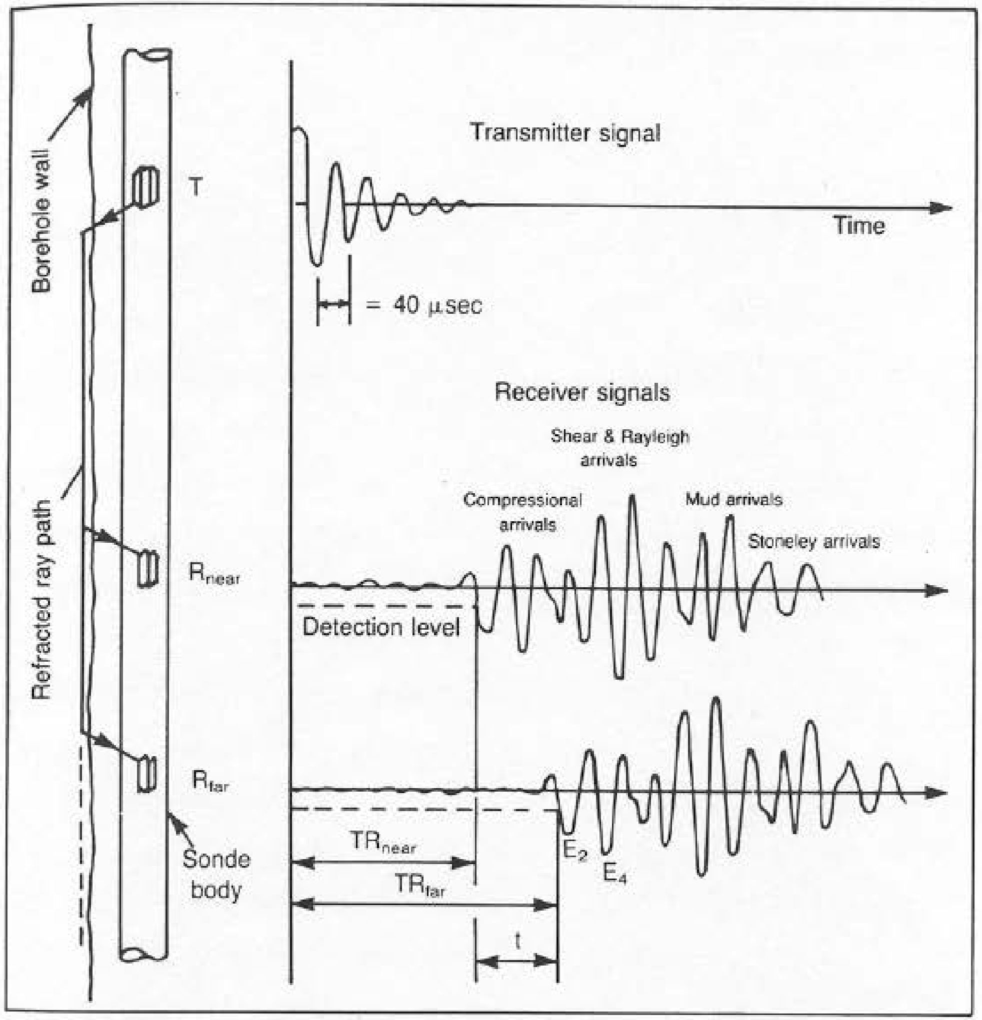

Basic Sonic logging system (courtesy Schlumberger, © SPE)

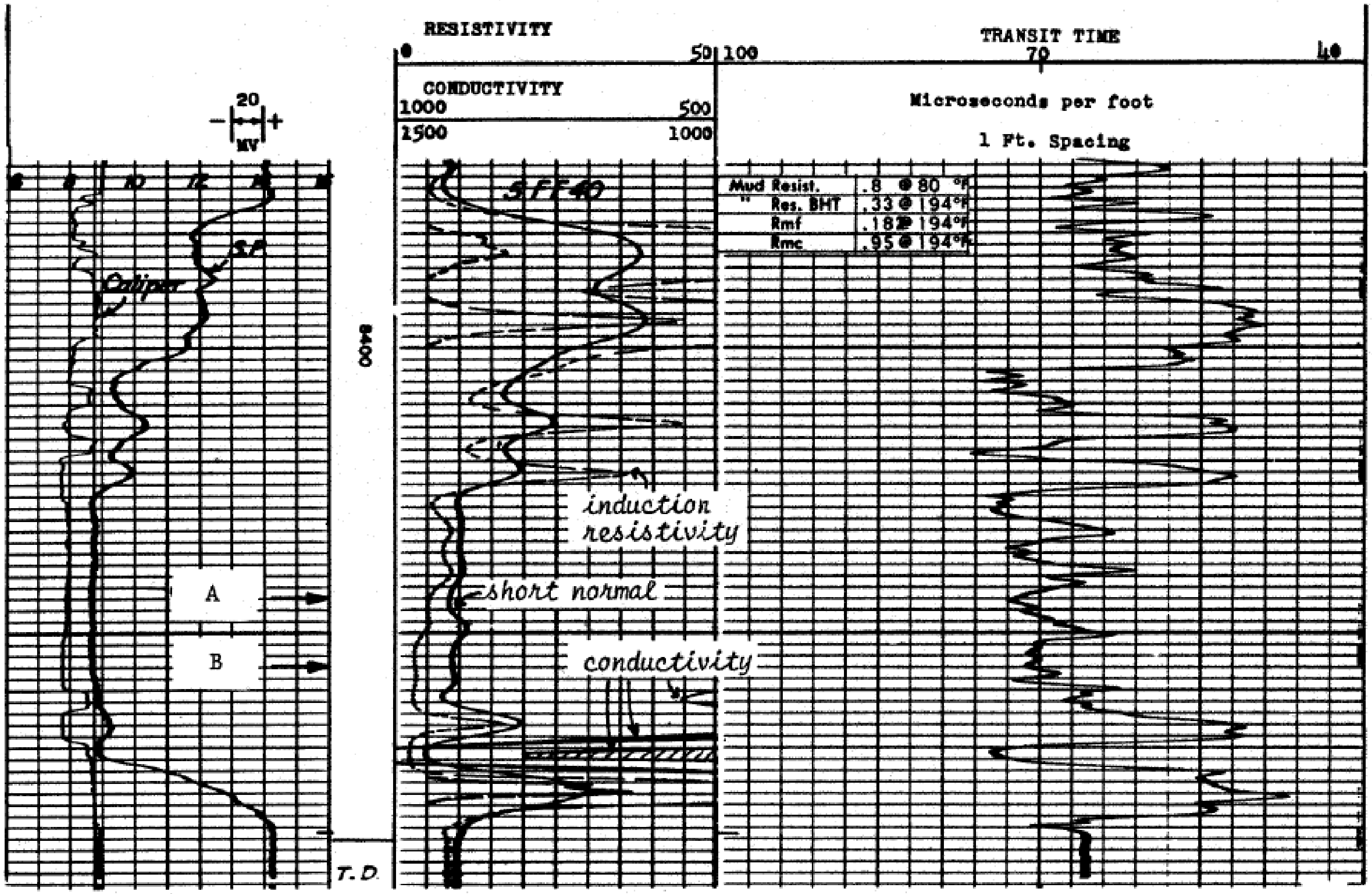
RESISTIVITY
0
50
CONDUCTIVITY
1000
500
1500
1000
TRANSIT TIME
100
70
40
Microseconds per foot
1 Ft. Spacing
20
MV
Mud Resist. .8 @ 80 °F
" Res. BHT .33 @ 194°F
Rmf .18 @ 194°F
Rmc .95 @ 194°F
SFF40
SP
Caliper
8400
induction resistivity
short normal
conductivity
A
B
T.D.

Vertical Resolution

Span

- defined as distance between receivers
- determines vertical resolution, h ~ span

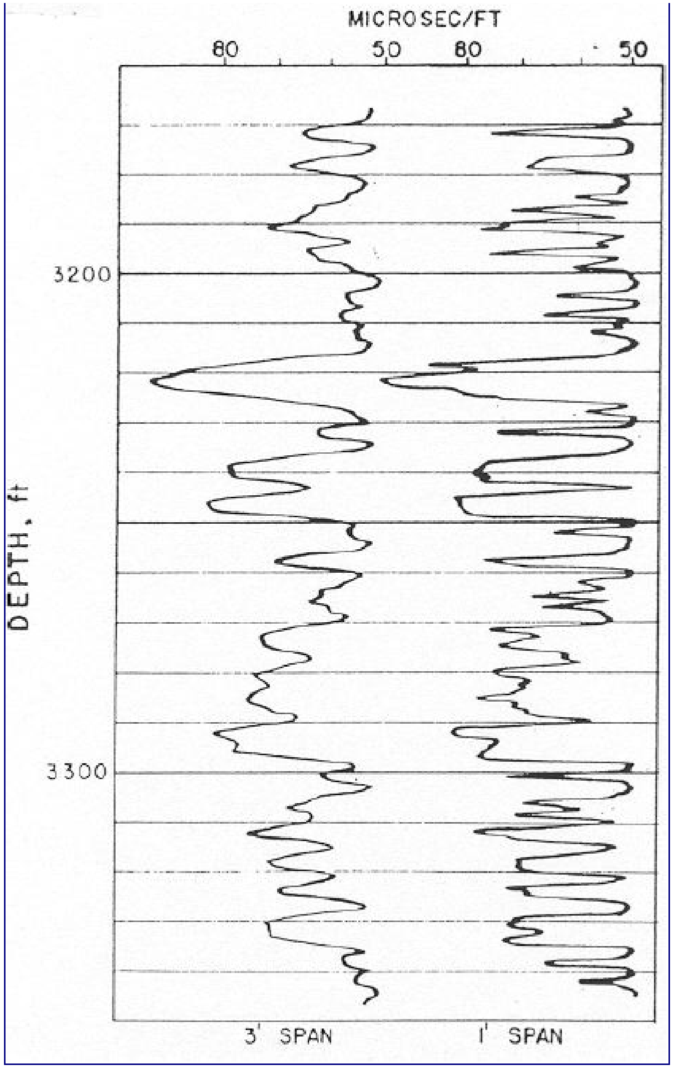

3 and 1-ft spacing sonic logs recorded in a west texas well (Bassiouni, 1994)

Lateral Resolution

Depth of investigation

- varies with wavelength, λ, which is related to formation velocity, v, and tool frequency, f. $\lambda = v/f$
- Depth of investigation, Di ~ 3 λ
- Rule of thumb, 0.75 to 3.75 ft.
- indirectly related to T-R spacing

Critical T-R Spacing

- short enough for pulse to be detected
- long enough to allow 1st arrival to be compressional wave and not mud wave
- f(standoff, v_{mud}/v_{fm})
- borehole enlargement effects

Cycle Skipping

<u>Cause:</u> Dampening of first arrival at far receiver

<u>Effect:</u>

Sonic curve shows spiking or an abrupt change towards a higher travel time

<u>Occurs in:</u>

- Unconsolidated formations (particularly gas bearing);
- fractured formations;
- transmitter weak and/or receiver poor

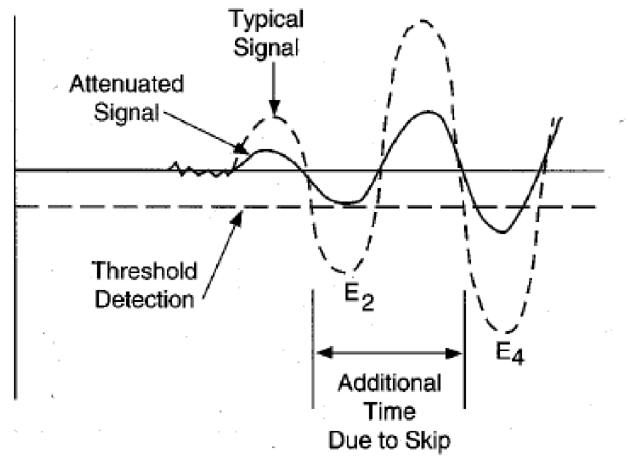

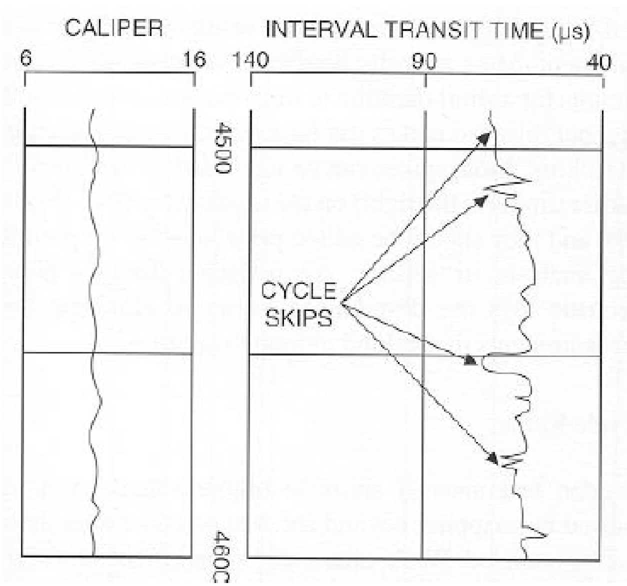

Types

- Basic Sonic (obsolete)
- **BHC - borehole compensated sonic (most common)**
- LSS - Long spaced sonic
- Array Sonic or Full Waveform Sonic
- Dipole Shear Imager (DSI)

Basic Sonic Log

- One transmitter and two or three receivers, T-R1-R2 -R3
- Borehole and sonde tilt problems

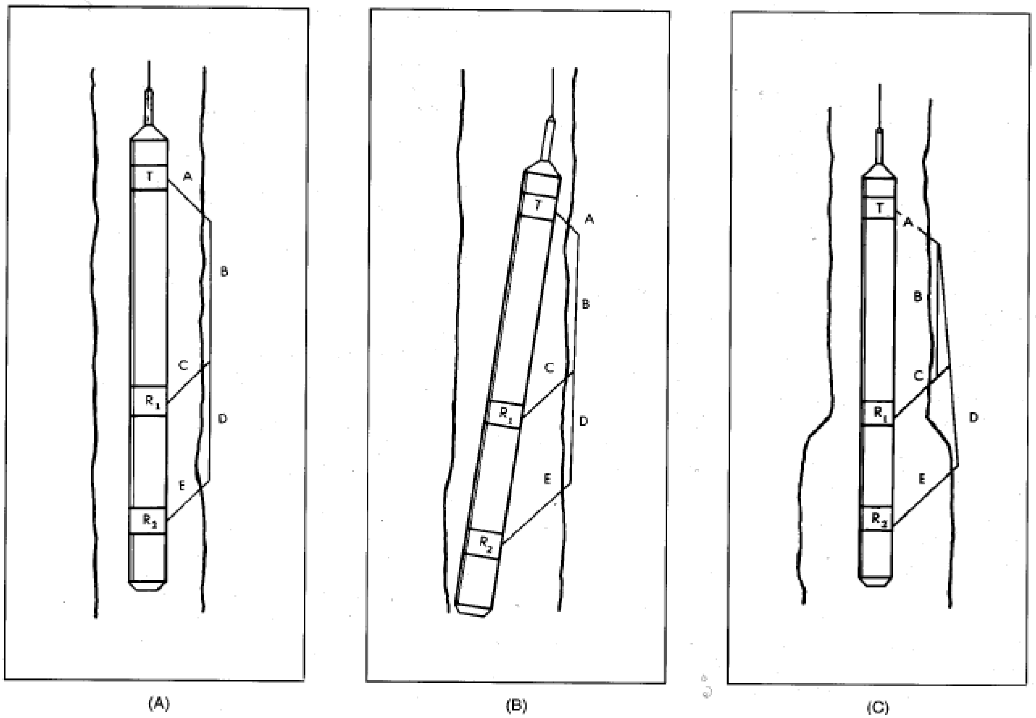

Single transmitter, two-receiver configuration
Western Atlas (1993)

Example-Borehole enlargement Effects

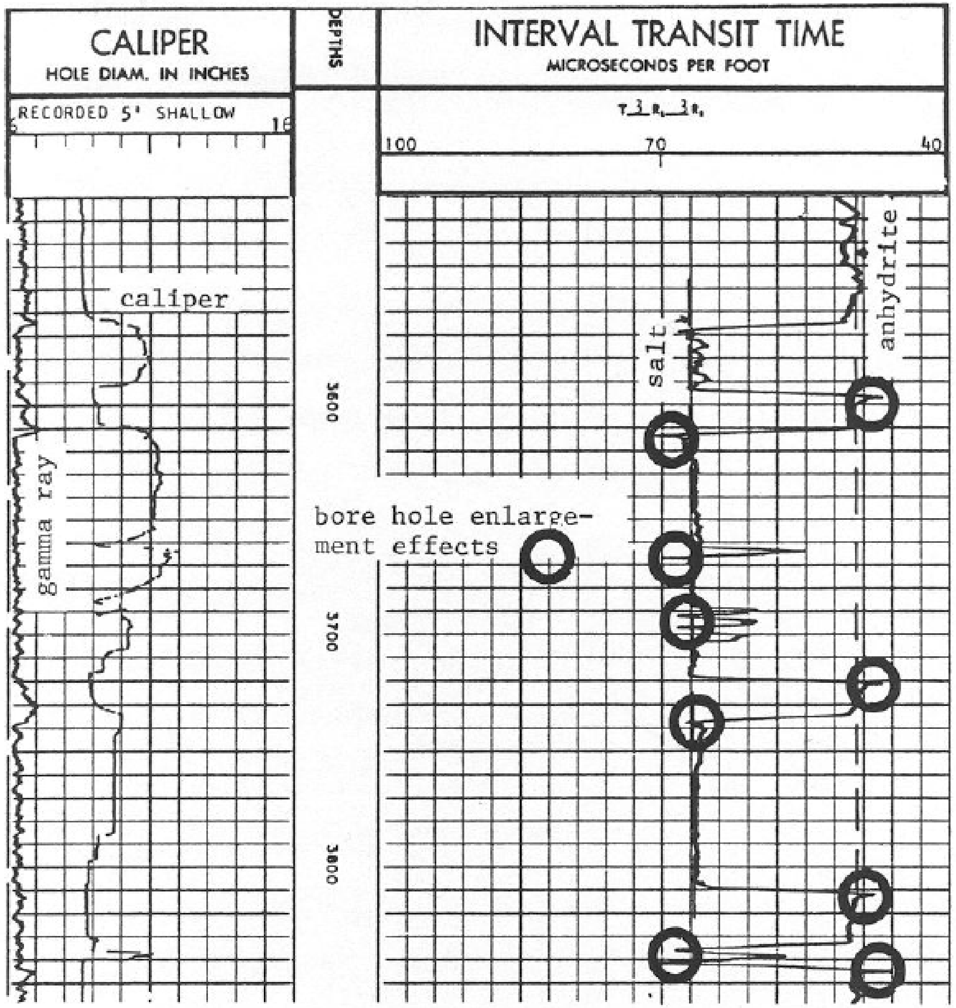

West Texas acoustic log
Hilchie (1978)

Borehole compensated Sonic (BHC)

- Automatically compensates for borehole effects and sonde tilt
- System of upper and lower transmitters bounding two sets of receivers.

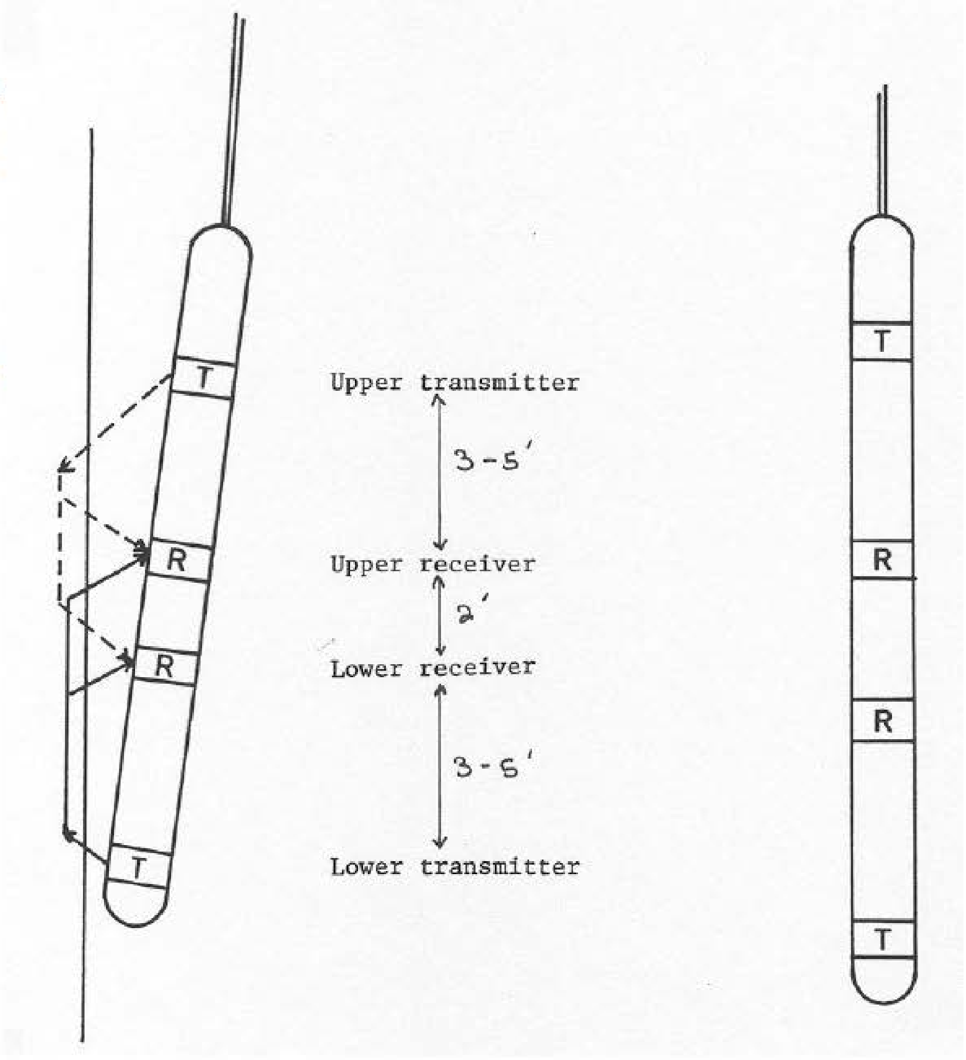

Comparison of BHC with Basic Sonic

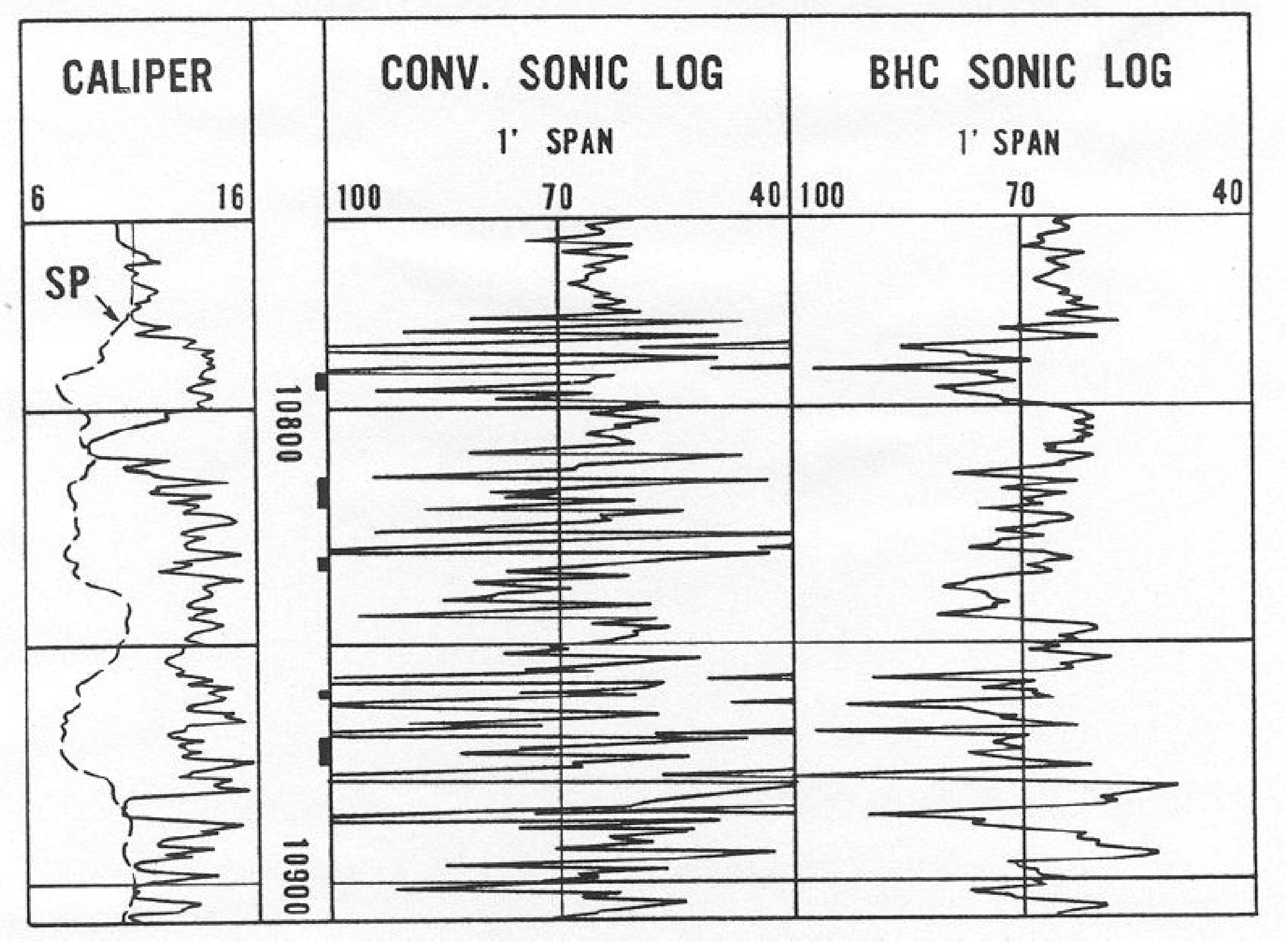

Porosity

Wyllie Eq. - linear time averaged relationship

$$\Delta t = \frac{\sum \frac{L_f}{L}}{V_f} + \frac{\sum \frac{L_{ma}}{L}}{V_{ma}}$$

– empirically determined

– for clean and consolidated sandstones

– uniformly distributed small pores

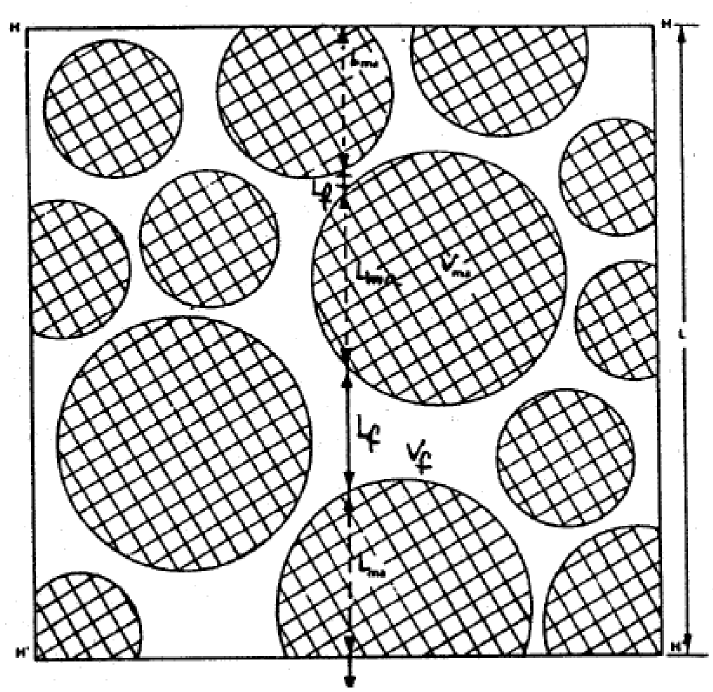

Wyllie Equation

$$\phi = \frac{\Delta t_{log} - \Delta t_{ma}}{\Delta t_f - \Delta t_{ma}}$$

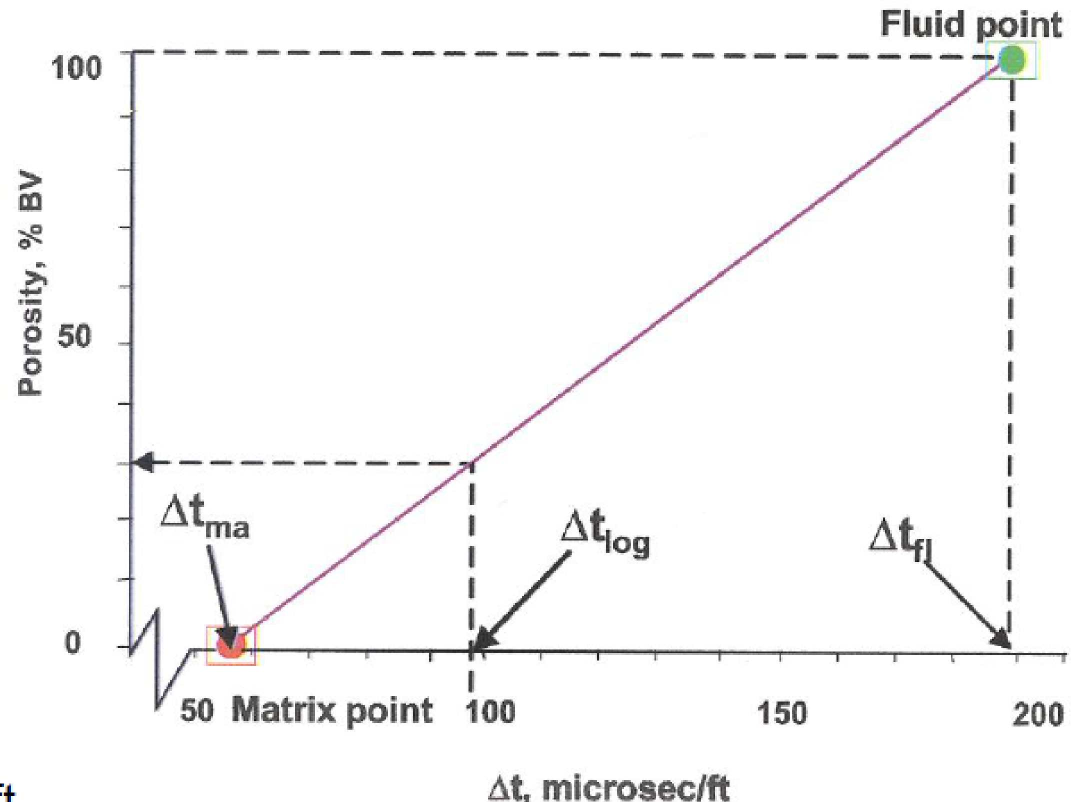

Δt_{ma}, μsec/ft	
ss	55.5
lms	47.6
dol	43.5
Anhy	50.0

Δt_f, μsec/ft	
fresh	189
salt	185

Porosity – uncompacted sands

Evidence: when Δt_{log} > 100 microsec/ft in overlying shale

Result: Estimated porosity too high

Correction: Observed transit times are greater in uncompacted sands; thus apply empirical correction factor, Cp

$$\phi = \frac{t_{log} - t_{ma}}{t_f - t_{ma}} \frac{1}{C_p}$$

Estimate Cp from overlying shale zone

$$C_p = c \frac{\Delta t_{sh}}{100}$$

where the shale compaction coefficient, c , ranges from $0.8 < c < 1.3$.

Porosity – uncompacted sands-Fluid Effect

- Sonic primarily independent of fluid type
- Know lithology, can calculate porosity
- Fluid Effect in high porosity formations with high HC saturation. Correct by:

$$\text{oil}: \quad \phi_{corr} = 0.9 * \phi_s$$

$$\text{gas}: \quad \phi_{corr} = 0.7 * \phi_s$$

- Apply after compaction correction.

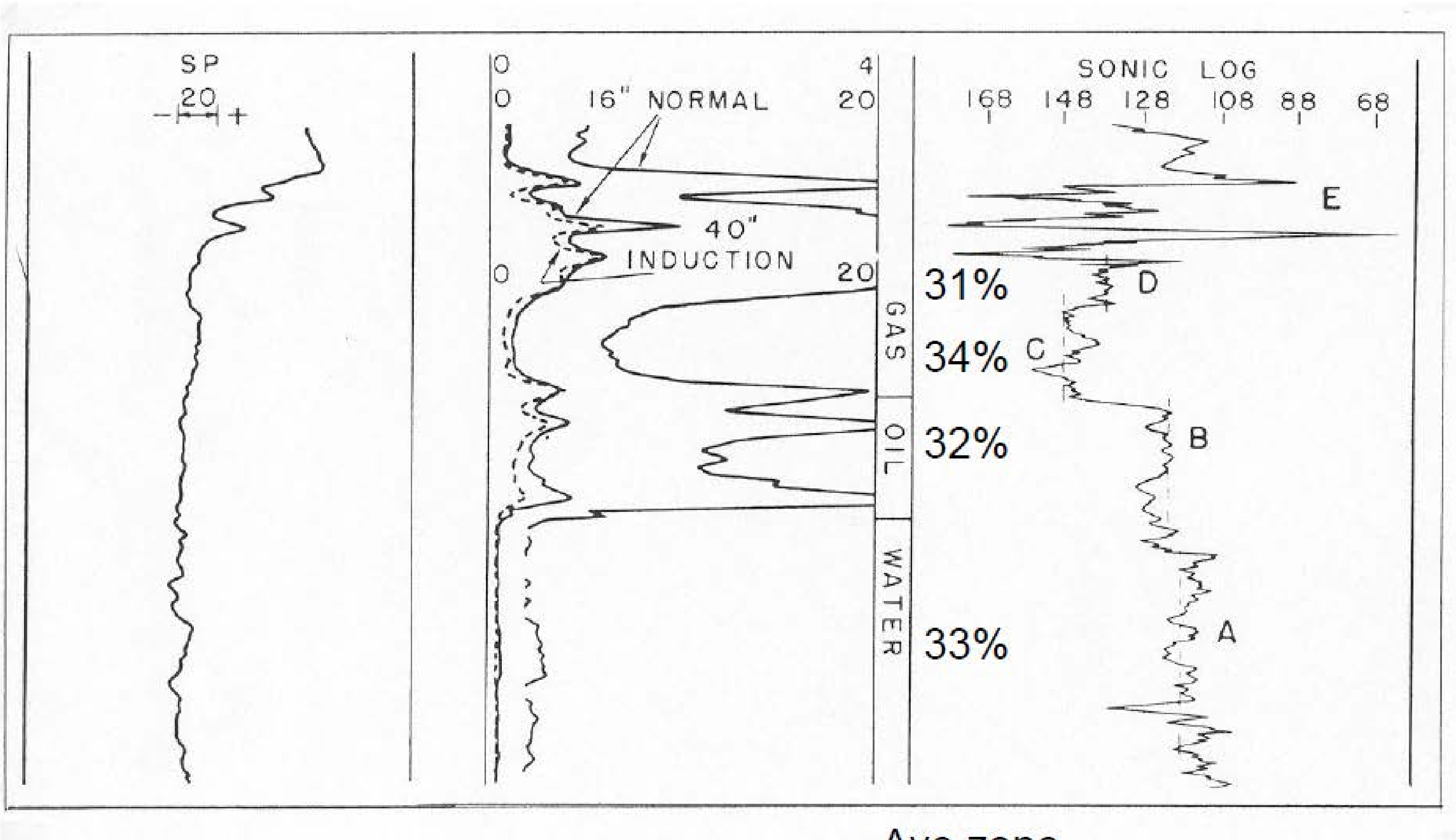

Cp = 1.44…from overlying shale

Ave zone
Core ϕ

Transit time - porosity transform (Raymer-Hunt)

- based on field observation
- yields slightly greater porosity in the 5 to 25% range
- does not require compaction correction

$$\phi = C\frac{t_{log} - t_{ma}}{t_{log}}$$

Where

C ranges from 0.625 to 0.700

Typical value used in practice is C = 0.67

C = 0.6 for gas-saturated formations

Δt_{ma}, μsec/ft	
Ss	56.0
Lms	49.0
Dolo	44.0

Porosity comparison

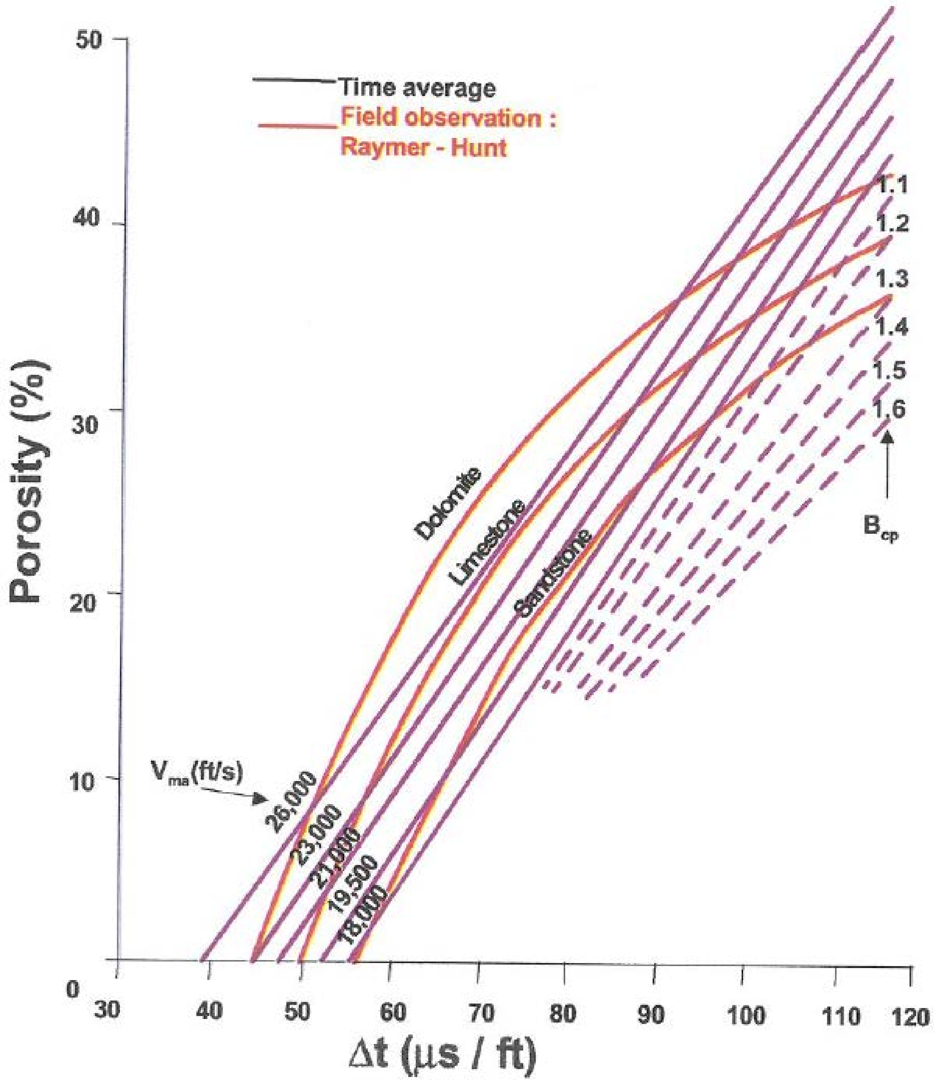

Secondary Porosity

- Sonic ignores secondary porosity; i.e, vugs and fractures
- Result: Measured transit time < than would be calculated for given porosity
- Estimate Secondary porosity by:

$$\phi_2 = \phi_t - \phi_s$$

- Alternative: Develop specific empirical relationships for heterogeneous systems

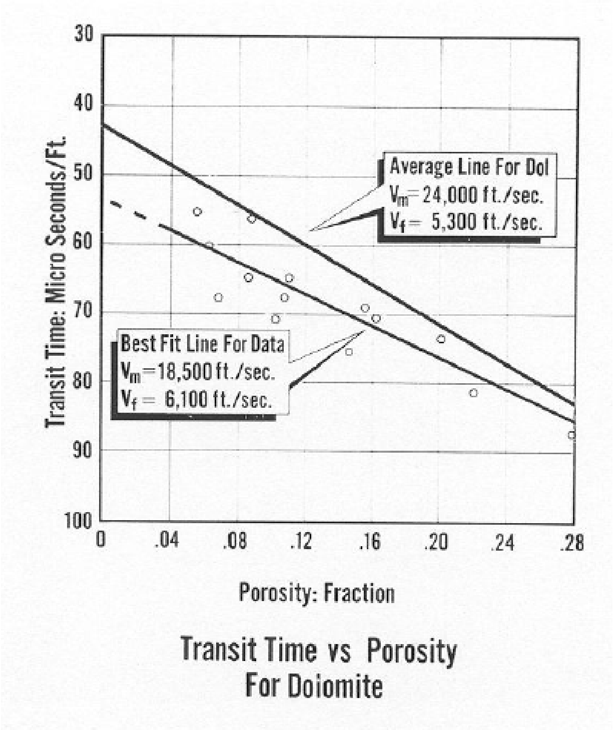

<u>Example of Porosity – Velocity Correlation in Dolomite</u>
The example illustrates travel times which are consistently greater than predicted by the "time-average equation". (Corelab)

Combination Neutron Density Log

The Combination Neutron-Density Log is a combination porosity log. Besides its use a porosity device, it is also used to determine lithology and to detect gas-bearing zones. The Neutron-Density Log consists of neutron and density curves recorded in tracks #2 and #3 and a caliper and gamma ray log in track #1.

Where an ***increase*** in density porosity occurs along with a ***decrease*** in neutron porosity in a gas-bearing zone, it is called ***gas effect.*** Gas effect is created by gas in the pores. Gas in the pores causes the density log to record too high a porosity (i.e. gas in lighter than oil or water), and causes the neutron log to record too low a porosity (i.e. gas has a lower concentration of hydrogen atoms than oil or water). The effect of gas on the Neutron-Density Log is a very important log response because it helps a geologist to detect gas-bearing zones.

Qualitative Interpretation
V/s
Quantitative Interpretation

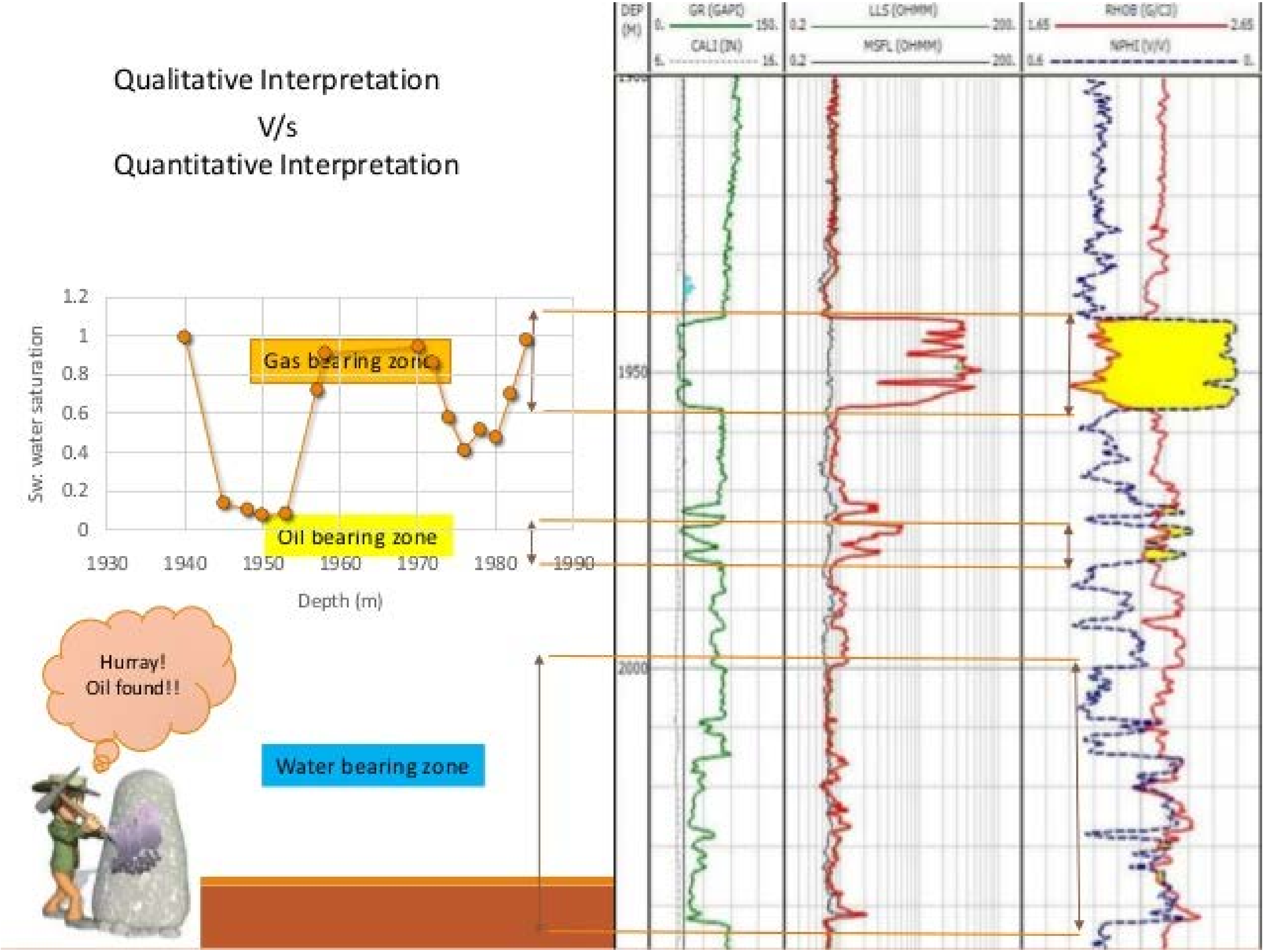

Gas Bearing Formation Interpretation

- **<u>Effect of gas on neutron log response</u>**
  - lower hydrogen content than calibrated value, thus higher count rate resulting in low ϕ_a.
  - Shale effect is opposite to the gas effect, makes detection extremely difficult

- **<u>Effect of gas on density log response</u>**
  - presence of gas reduces bulk density, resulting in a high apparent porosity.
  - shale effect can increase or decrease bulk density, dependent on shale's bulk density.

- **<u>Effect of gas on sonic log response</u>**
  - increase in sonic log porosity in poorly-consolidated sands.
  - not quantitative or predictable

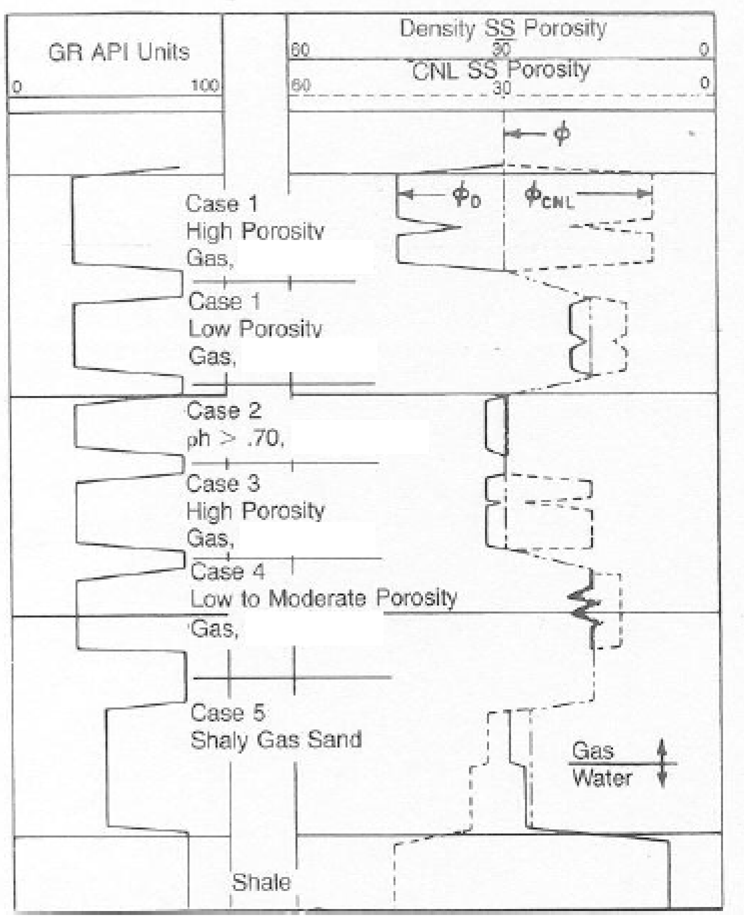

Type I: mirror image, gas crossover
(both FDC and CNL investigate same Saturation profile)

Type II: asymmetric gas crossover

Type III: Shaly gas sand

Idealized example of saturation effects on density and neutron logs. (Helander,1983)

Density – neutron log illustrating Type I gas effect (Hilchie, 1978)

- deep invasion, or
- Extremely shallow invasion

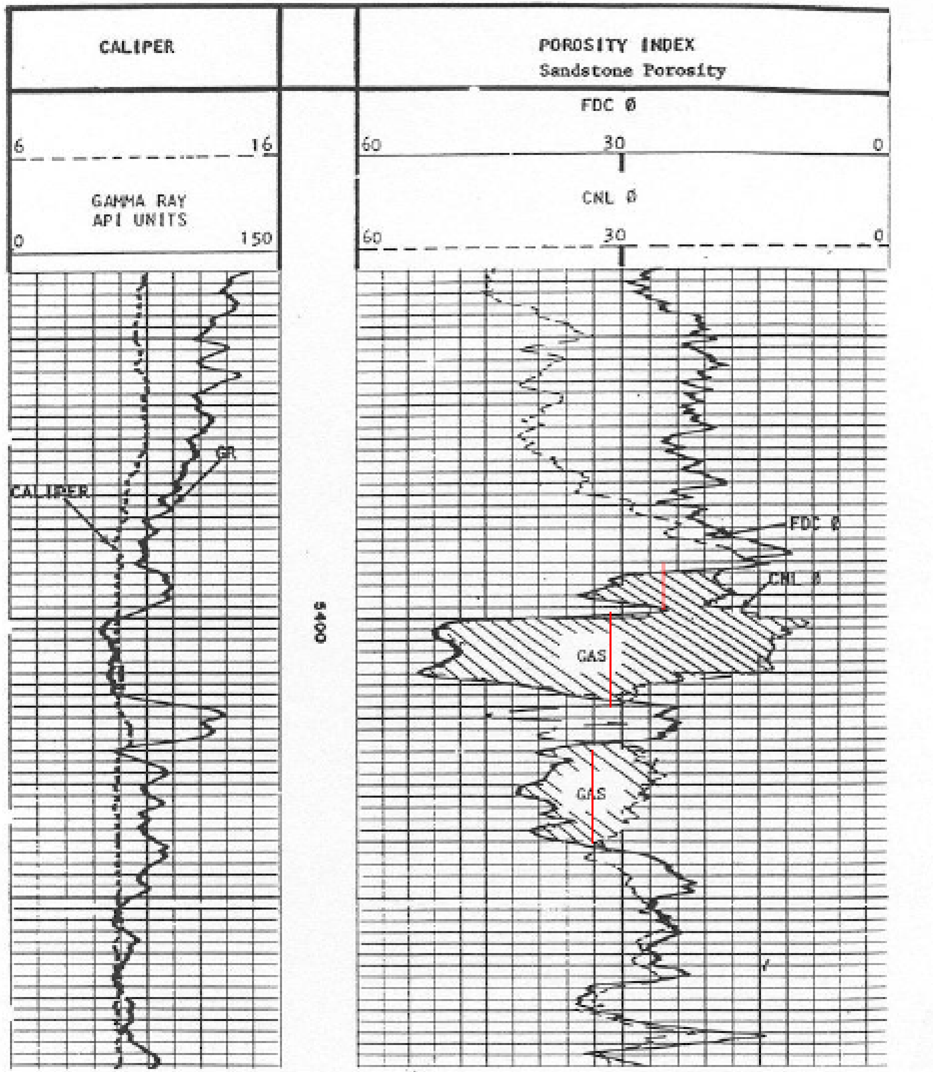

Density – neutron log illustrating the effect of shallow to moderate invasion. (Type II)
(Bassiouni, 1994)

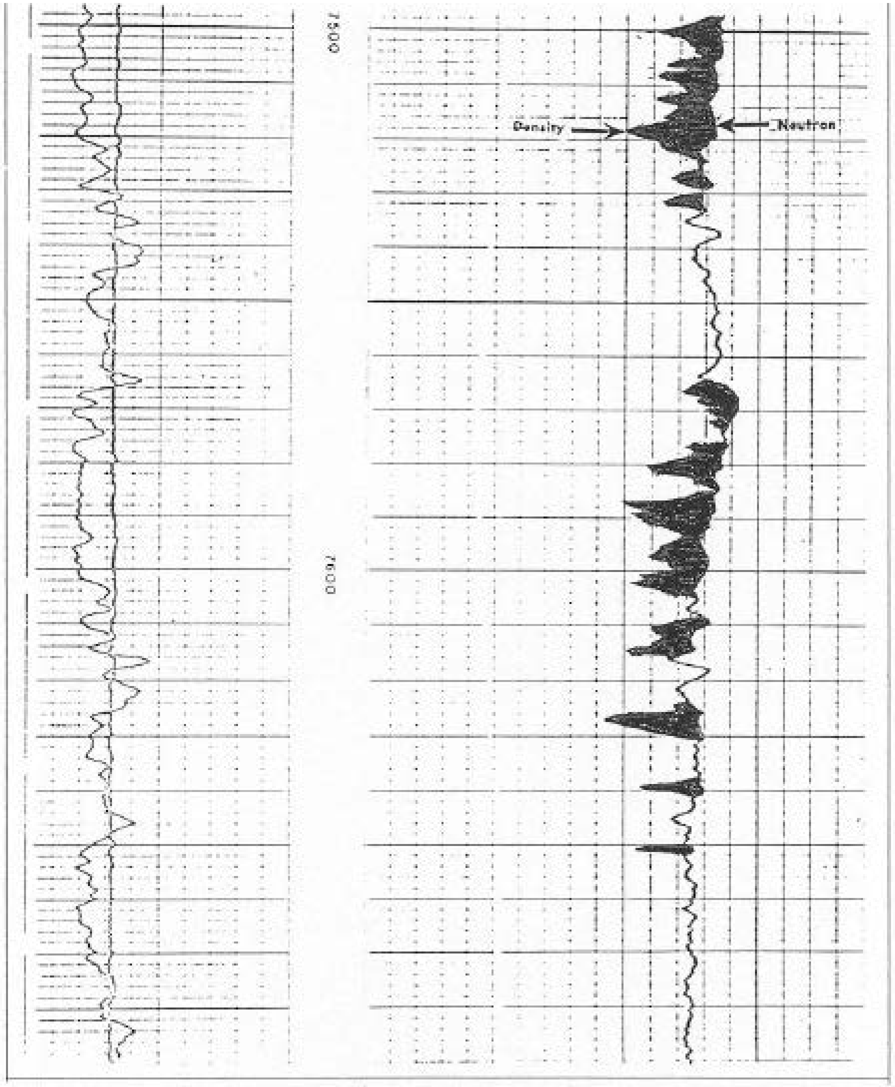

Density – neutron log illustrating a gas-bearing shaly sand. (Type III) (Hilchie, 1978)

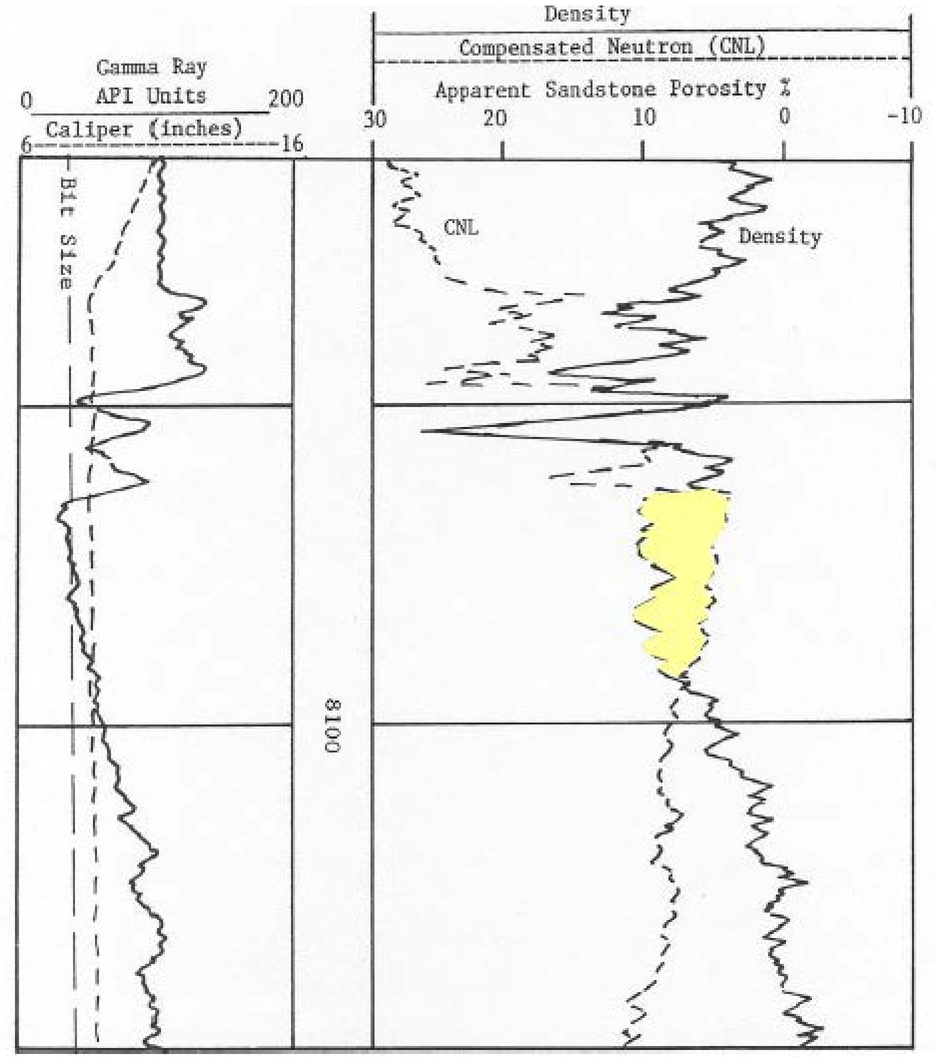

The gamma ray log measures the natural radiation of a formation, and primarily functions as a lithology log. It helps differentiate shales (high radioactivity) form sands, carbonates, and anhydrites (low radioactivity). The neutron log is a porosity device that is used to measure the amount of hydrogen in a formation. The density log is a porosity device that measures electron density. When these three logs are used together (i.e. Combination Gamma Ray Neutron-Density log), lithologies can be determined.

M-N* Lithology Plot

The M-N* plot requires a sonic log along with neutron and density logs. The sonic log is a porosity log that measures interval transit time. A sonic log, neutron log, and density log are all necessary to calculate the lithology dependent variables M* and N*. M* and N* values are essentially independent of matrix porosity (sucrosic and intergranular).

MID* Lithology Plot

The MID* (Matrix Identification) plot, like the M-N* is a crossplot technique which helps identify lithology and secondary porosity. Also, like M-N* plot, the MID* plot requires data from neutron, density, and sonic logs.

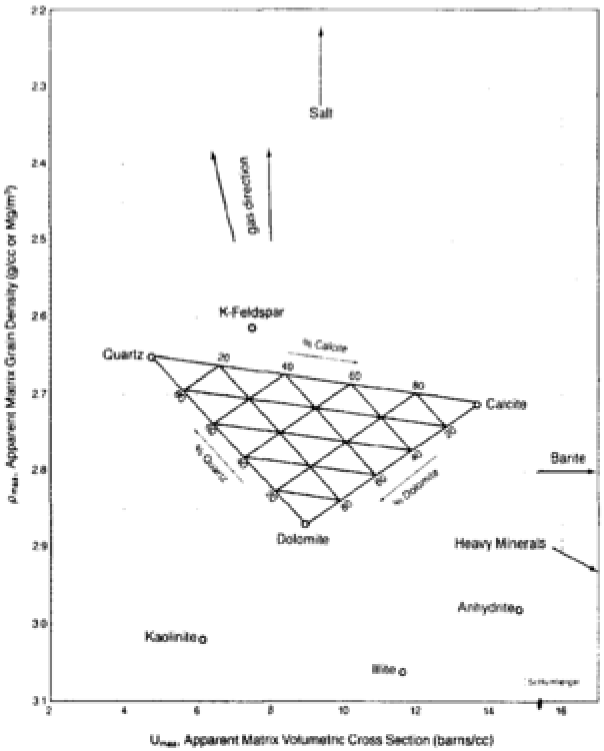
Salt
gas direction
K-Feldspar
Quartz
% Calcite
Calcite
% Quartz
% Dolomite
Barite
Dolomite
Heavy Minerals
Anhydrite
Kaolinite
Illite
ρ_{maa}, Apparent Matrix Grain Density (g/cc or Mg/m³)
U_{maa}, Apparent Matrix Volumetric Cross Section (barns/cc)

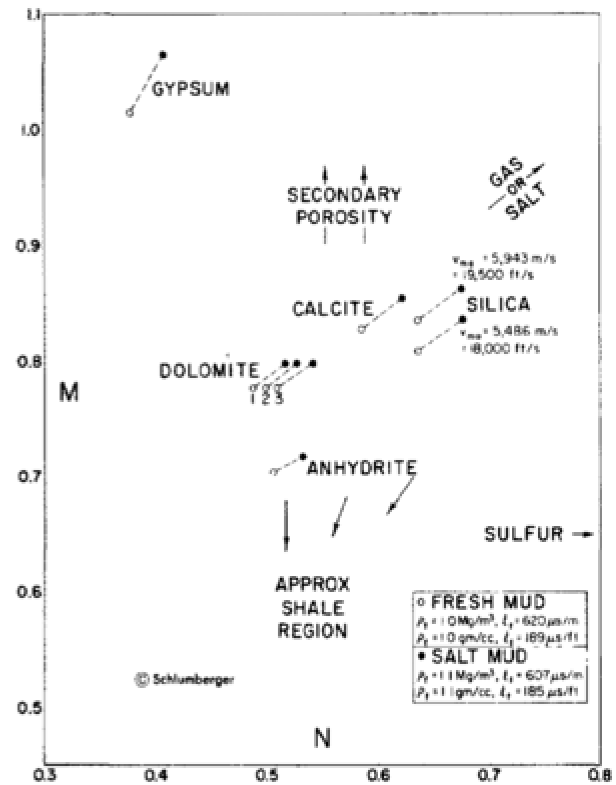
GYPSUM
SECONDARY
POROSITY
GAS
OR
SALT
CALCITE
SILICA
DOLOMITE
1 2 3
M
ANHYDRITE
SULFUR
APPROX
SHALE
REGION
FRESH MUD
SALT MUD
© Schlumberger
N

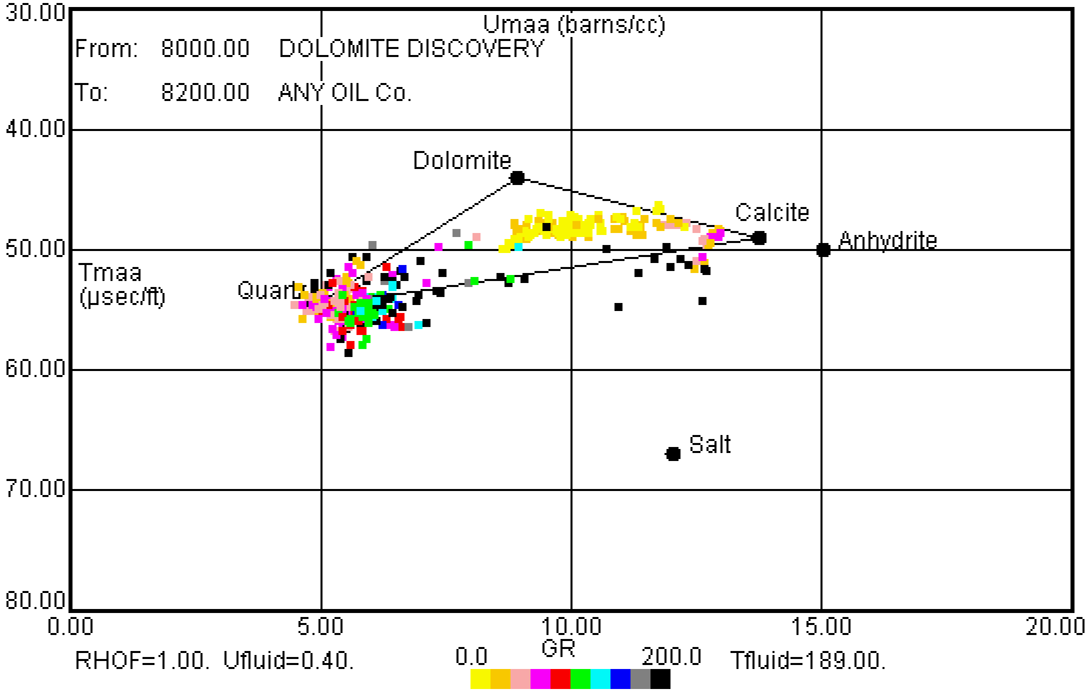
Umaa (barns/cc)
From: 8000.00 DOLOMITE DISCOVERY
To: 8200.00 ANY OIL Co.
Dolomite
Calcite
Anhydrite
Tmaa
(μsec/ft)
Quartz
Salt
30.00
40.00
50.00
60.00
70.00
80.00
0.00
5.00
10.00
15.00
20.00
RHOF=1.00. Ufluid=0.40.
0.0
GR
200.0
Tfluid=189.00.

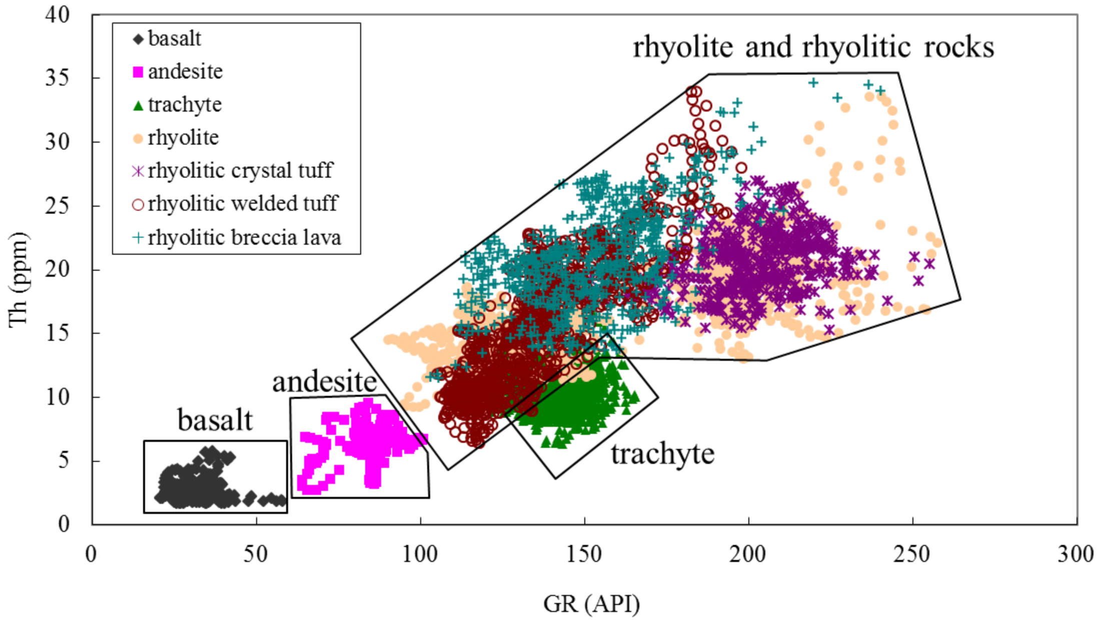
basalt
andesite
trachyte
rhyolite
rhyolitic crystal tuff
rhyolitic welded tuff
rhyolitic breccia lava
rhyolite and rhyolitic rocks
andesite
basalt
trachyte
Th (ppm)
GR (API)
0
5
10
15
20
25
30
35
40
0
50
100
150
200
250
300

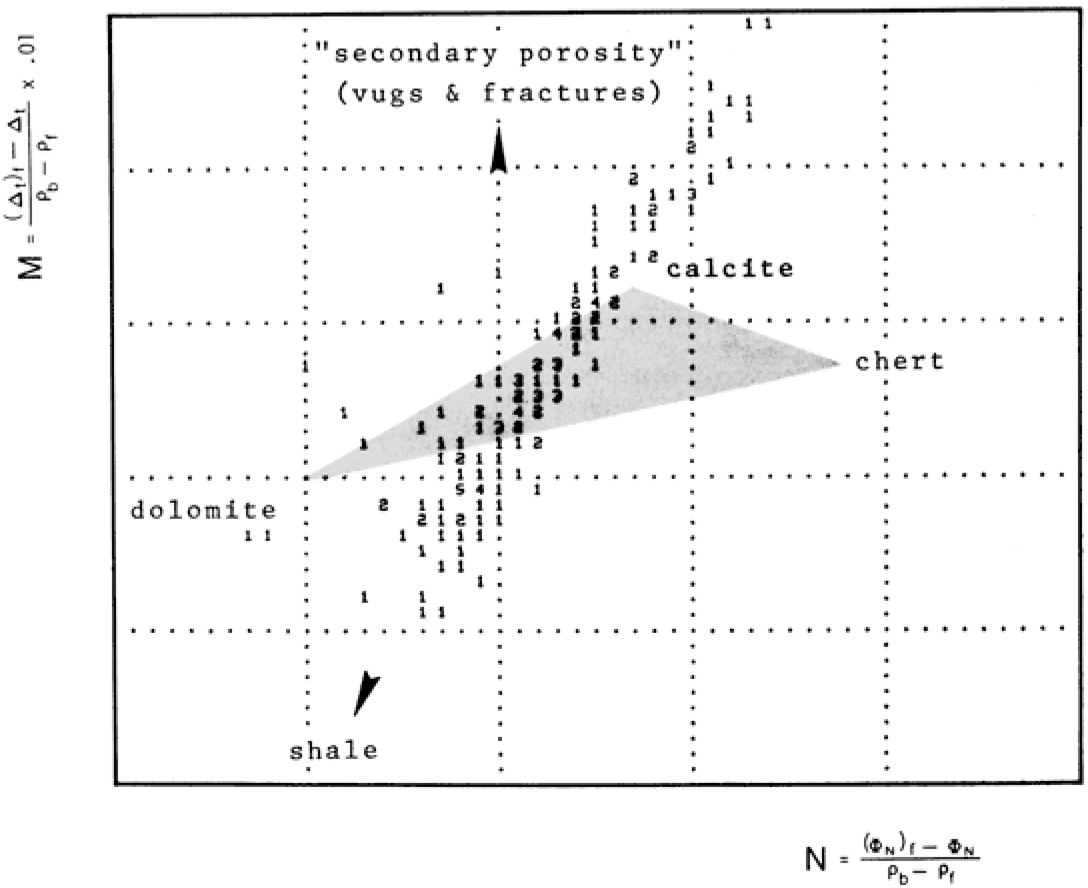

"secondary porosity"
(vugs & fractures)
calcite
chert
dolomite
shale
$M = \frac{(\Delta_t)_f - \Delta_t}{\rho_b - \rho_f} \times .01$
$N = \frac{(\Phi_N)_f - \Phi_N}{\rho_b - \rho_f}$

POROSITY DETERMINATION FROM LOGS

OPENHOLE LOG EVALUATION

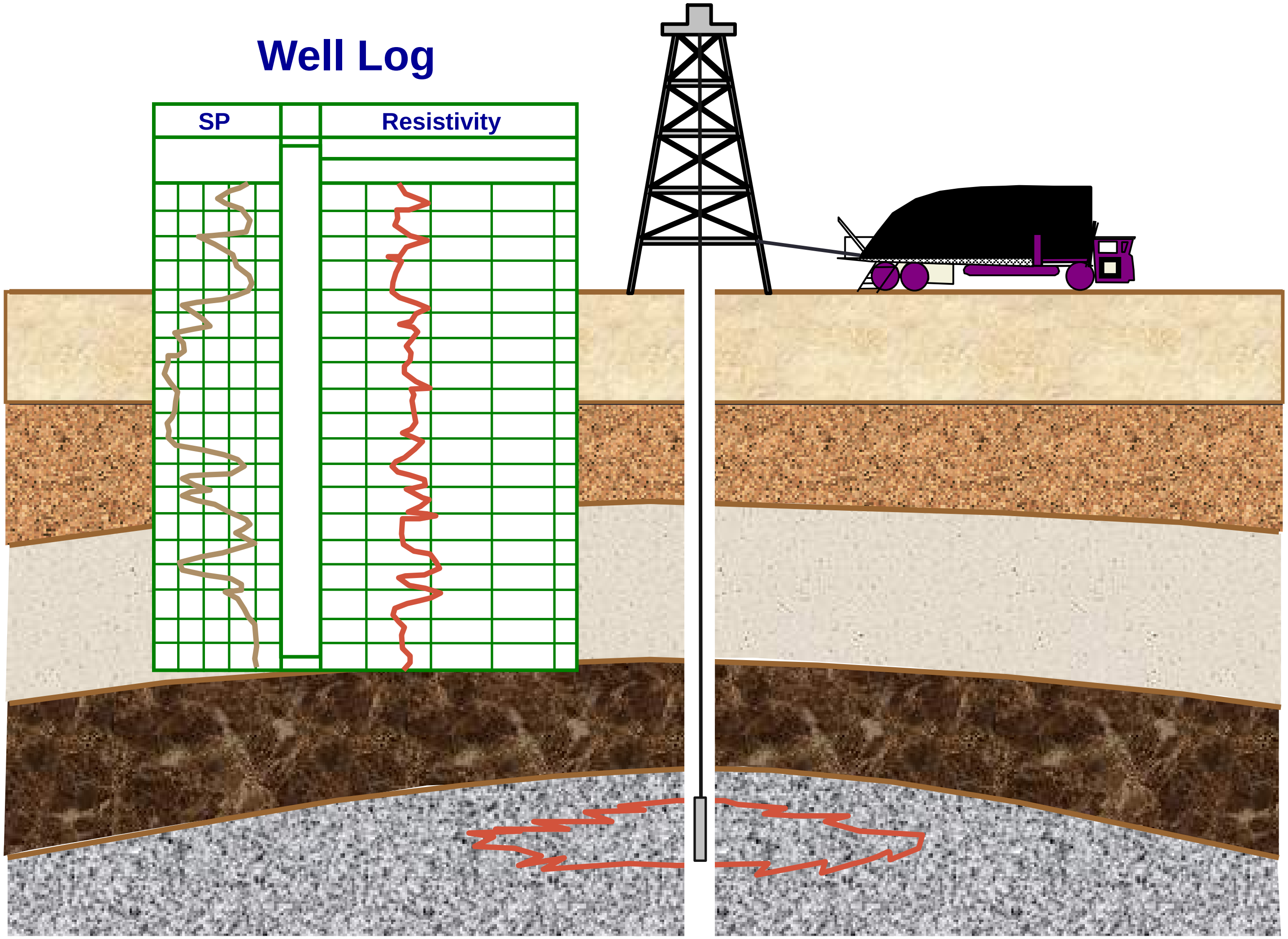

POROSITY DETERMINATION BY LOGGING

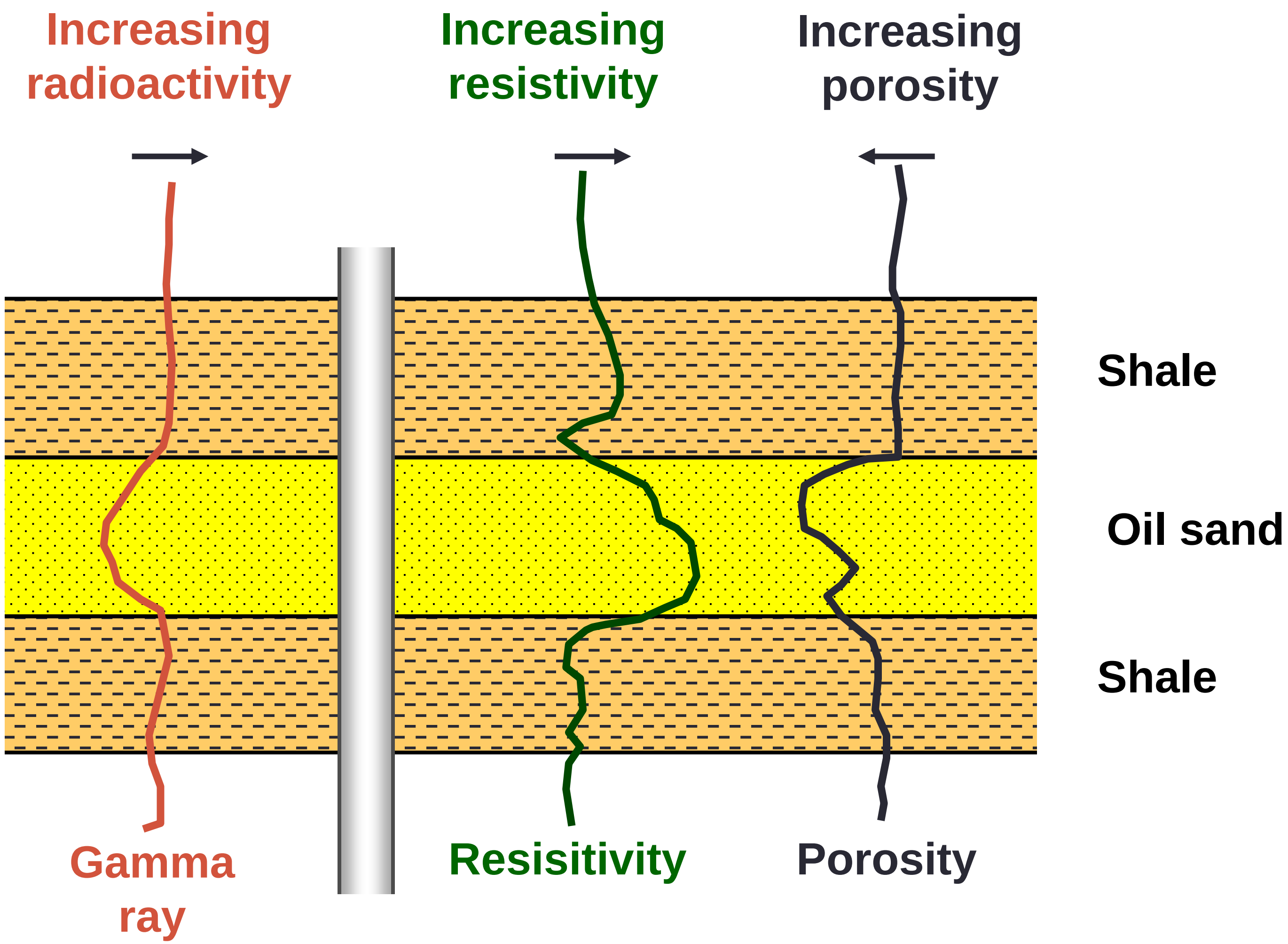

POROSITY LOG TYPES

3 Main Log Types

- Bulk density
- Sonic (acoustic)
- Compensated neutron

These logs do not measures porosity directly. To accurately calculate porosity, the analyst must know:
•Formation lithology
• Fluid in pores of sampled reservoir volume

DENSITY LOGS

- Uses radioactive source to generate gamma rays
- Gamma ray collides with electrons in formation, losing energy
- Detector measures intensity of back-scattered gamma rays, which is related to electron density of the formation
- Electron density is a measure of bulk density

DENSITY LOGS

- Bulk density, ρ_b, is dependent upon:
  - Lithology
  - Porosity
  - Density and saturation of fluids in pores
    - Saturation is fraction of pore volume occupied by a particular fluid (intensive)

DENSITY LOG

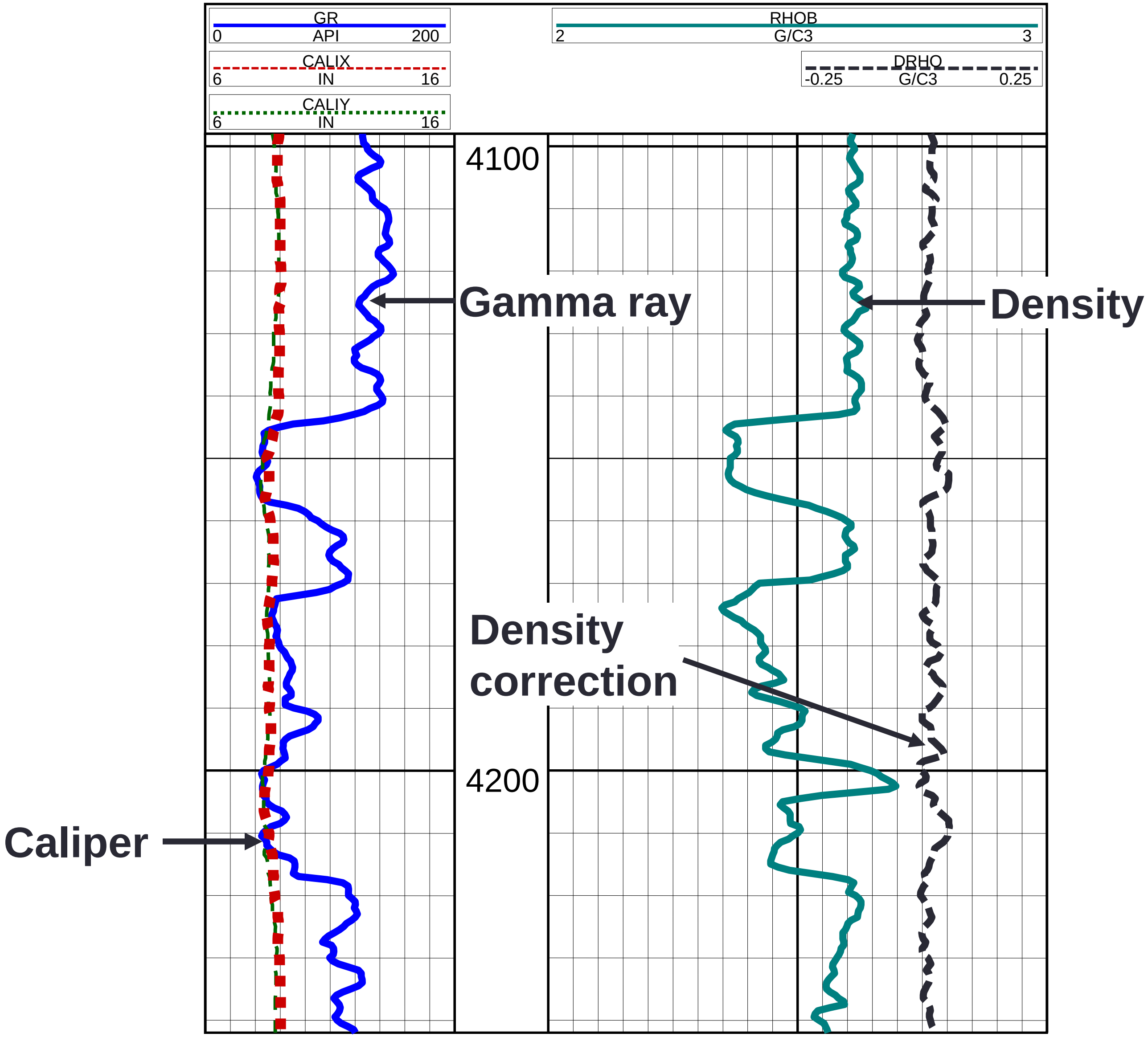
GR
0 API 200
CALIX
6 IN 16
CALIY
6 IN 16
RHOB
2 G/C3 3
DRHO
-0.25 G/C3 0.25
4100
4200
Gamma ray
Density
Density correction
Caliper

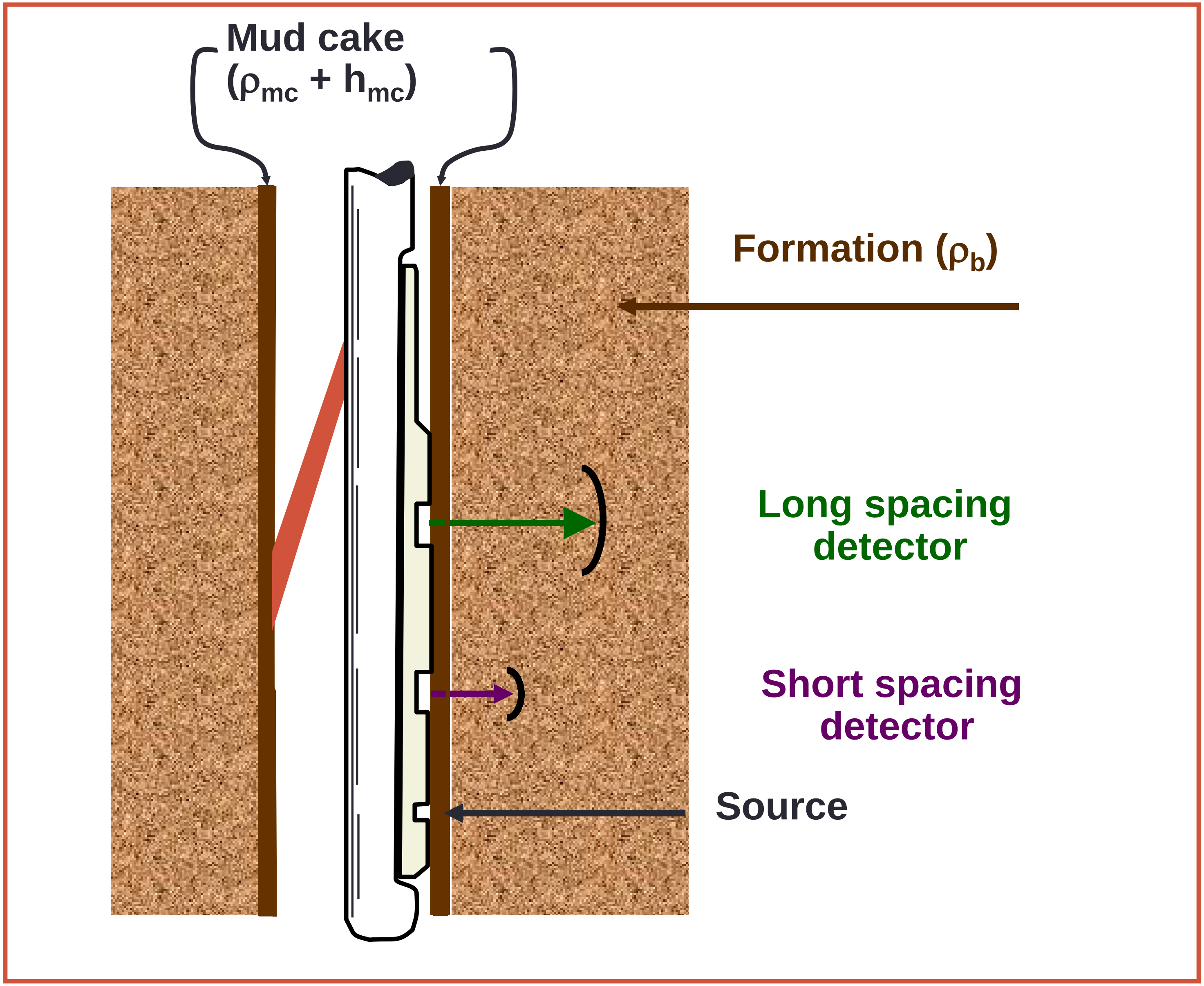

Mud cake
(ρmc + hmc)
Formation (ρb)
Long spacing detector
Short spacing detector
Source

BULK DENSITY

$$\rho_b = \underbrace{\rho_{ma}(1-\phi)}_{\text{Matrix}} + \underbrace{\rho_f\,\phi}_{\text{Fluids in flushed zone}}$$

- Measures electron density of a formation
- Strong function of formation bulk density
- Matrix bulk density varies with lithology
  - **Sandstone 2.65 g/cc**
  - **Limestone 2.71 g/cc**
  - **Dolomite 2.87 g/cc**

POROSITY FROM DENSITY LOG

Porosity equation

$$\phi = \frac{\rho_{ma} - \rho_b}{\rho_{ma} - \rho_f}$$

Fluid density equation

$$\rho_f = \rho_{mf} S_{xo} + \rho_h (1 - S_{xo})$$

We usually assume the fluid density (ρ_f) is between 1.0 and 1.1. If gas is present, the actual ρ_f will be < 1.0 and the calculated porosity will be too high.

ρ_{mf}	is the mud filtrate density, g/cc
ρ_h	is the hydrocarbon density, g/cc
S_{xo}	is the saturation of the flush/zone, decimal

DENSITY LOGS

Working equation (hydrocarbon zone)

$$\rho_b = \phi S_{xo} \rho_{mf} + \phi (1 - S_{xo}) \rho_{hc}$$

$$+ V_{sh} \rho_{sh} + (1 - \phi - V_{sh}) \rho_{ma}$$

ρ_b	=	Recorded parameter (bulk volum
$\phi S_{xo} \rho_{mf}$	=	Mud filtrate component
$\phi (1 - S_{xo}) \rho_{hc}$	=	Hydrocarbon component
$V_{sh} \rho_{sh}$	=	Shale component
$1 - \phi - V_{sh}$	=	Matrix component

DENSITY LOGS

- If minimal shale, $V_{sh} \approx 0$
- If $\rho_{hc} \approx \rho_{mf} \approx \rho_f$, then
- $\rho_b = \phi \, \rho_f - (1 - \phi) \, \rho_{ma}$

$$\phi = \phi_d = \frac{\rho_{ma} - \rho_b}{\rho_{ma} - \rho_f}$$

ϕ_d = Porosity from density log, fraction

ρ_{ma} = Density of formation matrix, g/cm^3

ρ_b = Bulk density from log measurement, g/cm^3

ρ_f = Density of fluid in rock pores, g/cm^3

ρ_{hc} = Density of hydrocarbons in rock pores, g/cm^3

ρ_{mf} = Density of mud filtrate, g/cm^3

ρ_{sh} = Density of shale, g/cm^3

V_{sh} = Volume of shale, fraction

S_{xo} = Mud filtrate saturation in zone invaded by mud filtrate,

BULK DENSITY LOG

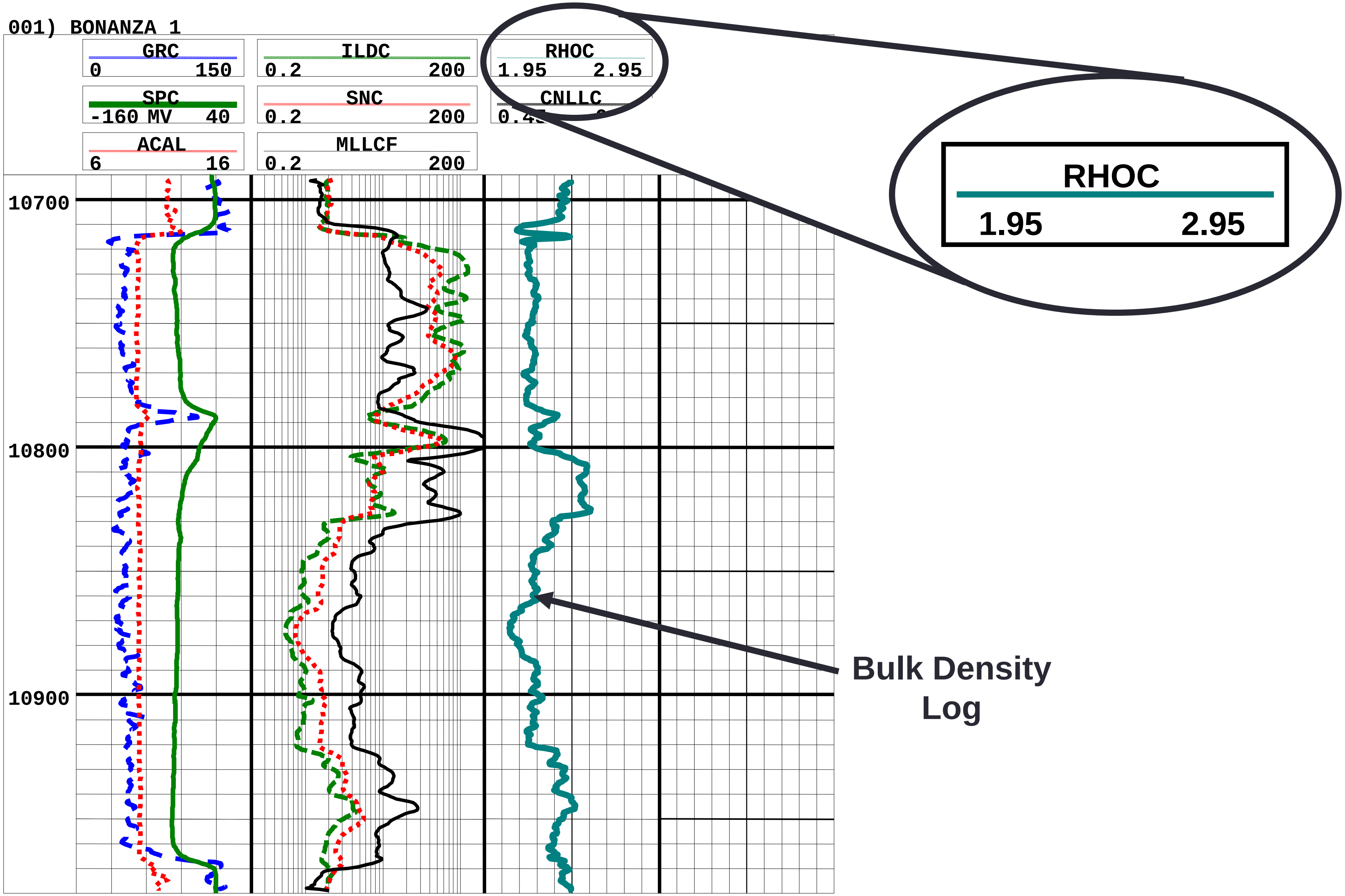

NEUTRON LOG

- Logging tool emits high energy neutrons into formation
- Neutrons collide with nuclei of formation's atoms
- Neutrons lose energy (velocity) with each collision

NEUTRON LOG

- The most energy is lost when colliding with a hydrogen atom nucleus
- Neutrons are slowed sufficiently to be captured by nuclei
- Capturing nuclei become excited and emit gamma rays

NEUTRON LOG

- Depending on type of logging tool either gamma rays or non-captured neutrons are recorded
- Log records porosity based on neutrons captured by formation
- If hydrogen is in pore space, porosity is related to the ratio of neutrons emitted to those counted as captured
- Neutron log reports porosity, calibrated assuming calcite matrix and fresh water in pores, if these assumptions are invalid we must correct the neutron porosity value

NEUTRON LOG

Theoretical equation

$$\phi_N = \phi\, S_{xo}\, \phi_{Nmf} + \phi\left(1 - S_{xo}\right)\phi_{Nhc}$$

$$+ V_{sh}\, \phi_{sh} + \left(1 - \phi - V_{sh}\right)\phi_{Nma}$$

ϕ_N = Recorded parameter

$\phi\, S_{xo}\, \phi_{Nmf}$ = Mud filtrate portion

$\phi\,(1 - S_{xo})\, \phi_{Nhc}$ = Hydrocarbon portion

$V_{sh}\, \phi_{Nsh}$ = Shale portion

$(1 - \phi - V_{sh})\, \phi_{Nhc}$ = Matrix portion where ϕ = True porosity of rock

ϕ_N = Porosity from neutron log measurement, fraction

ϕ_{Nma} = Porosity of matrix fraction

ϕ_{Nhc} = Porosity of formation saturated with hydrocarbon fluid, fraction

ϕ_{Nmf} = Porosity saturated with mud filtrate, fraction

V_{sh} = Volume of shale, fraction

S_{xo} = Mud filtrate saturation in zone invaded by mud filtrate, fraction

POROSITY FROM NEUTRON LOG

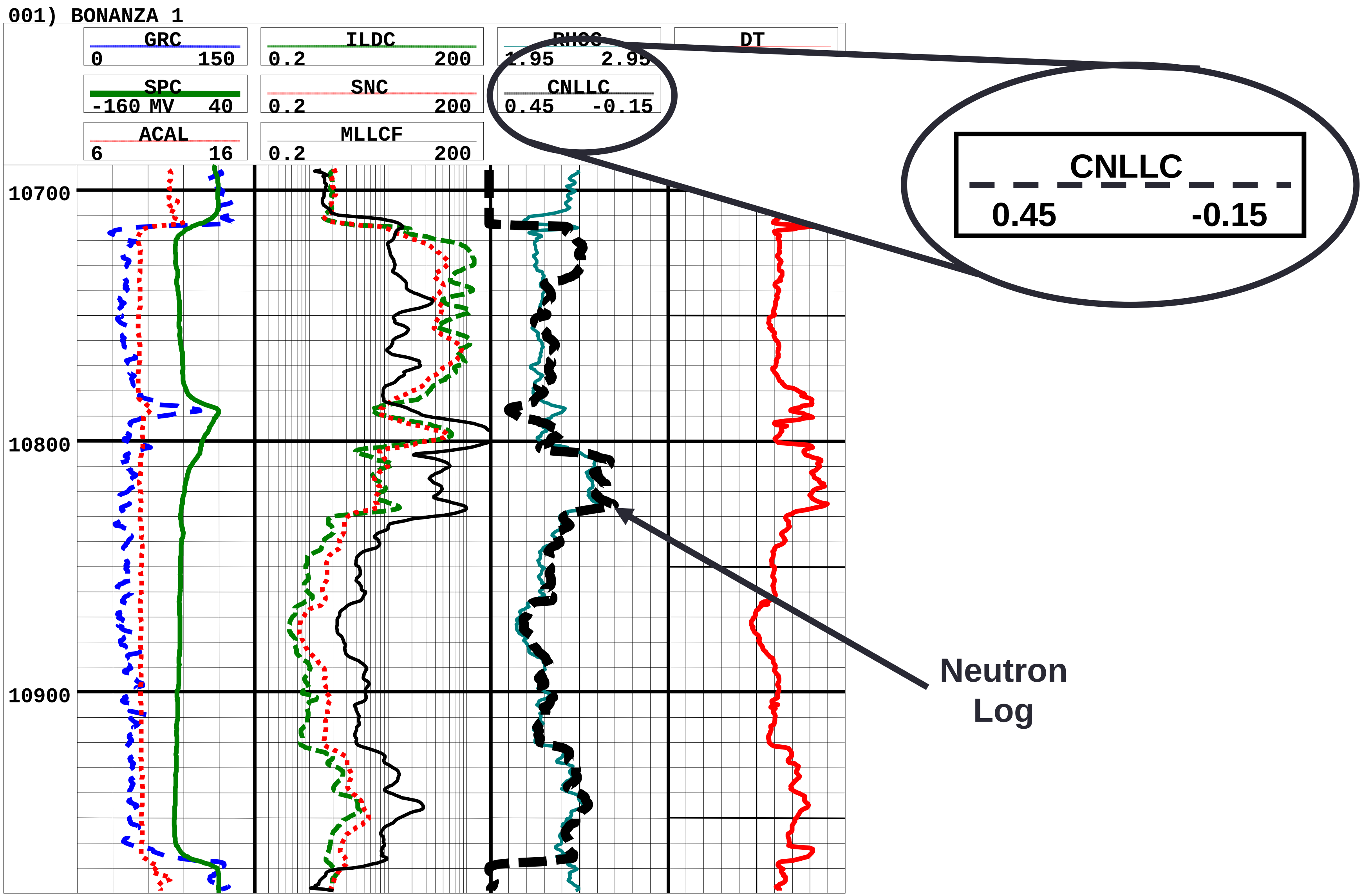

ACOUSTIC (SONIC) LOG

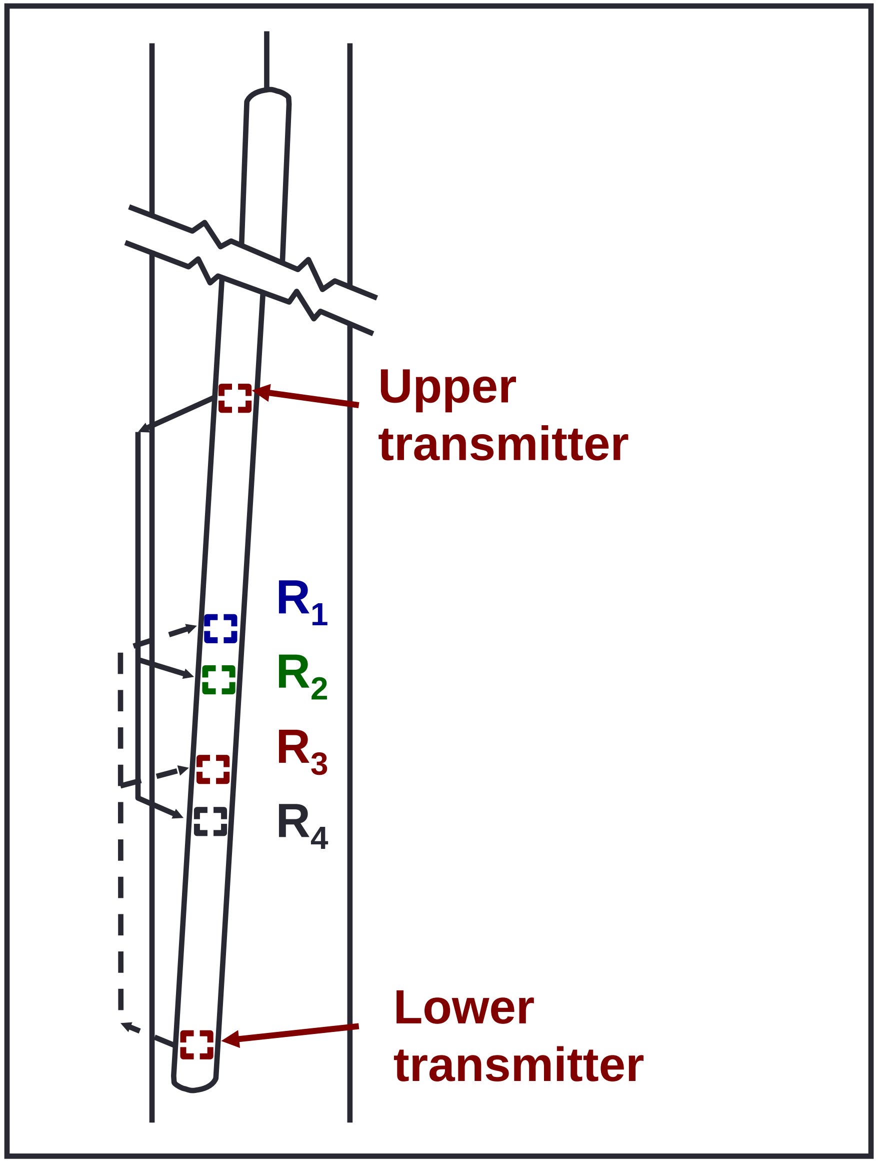

- Tool usually consists of one sound transmitter (above) and two receivers (below)
- Sound is generated, travels through formation
- Elapsed time between sound wave at receiver 1 vs receiver 2 is dependent upon density of medium through which the sound traveled

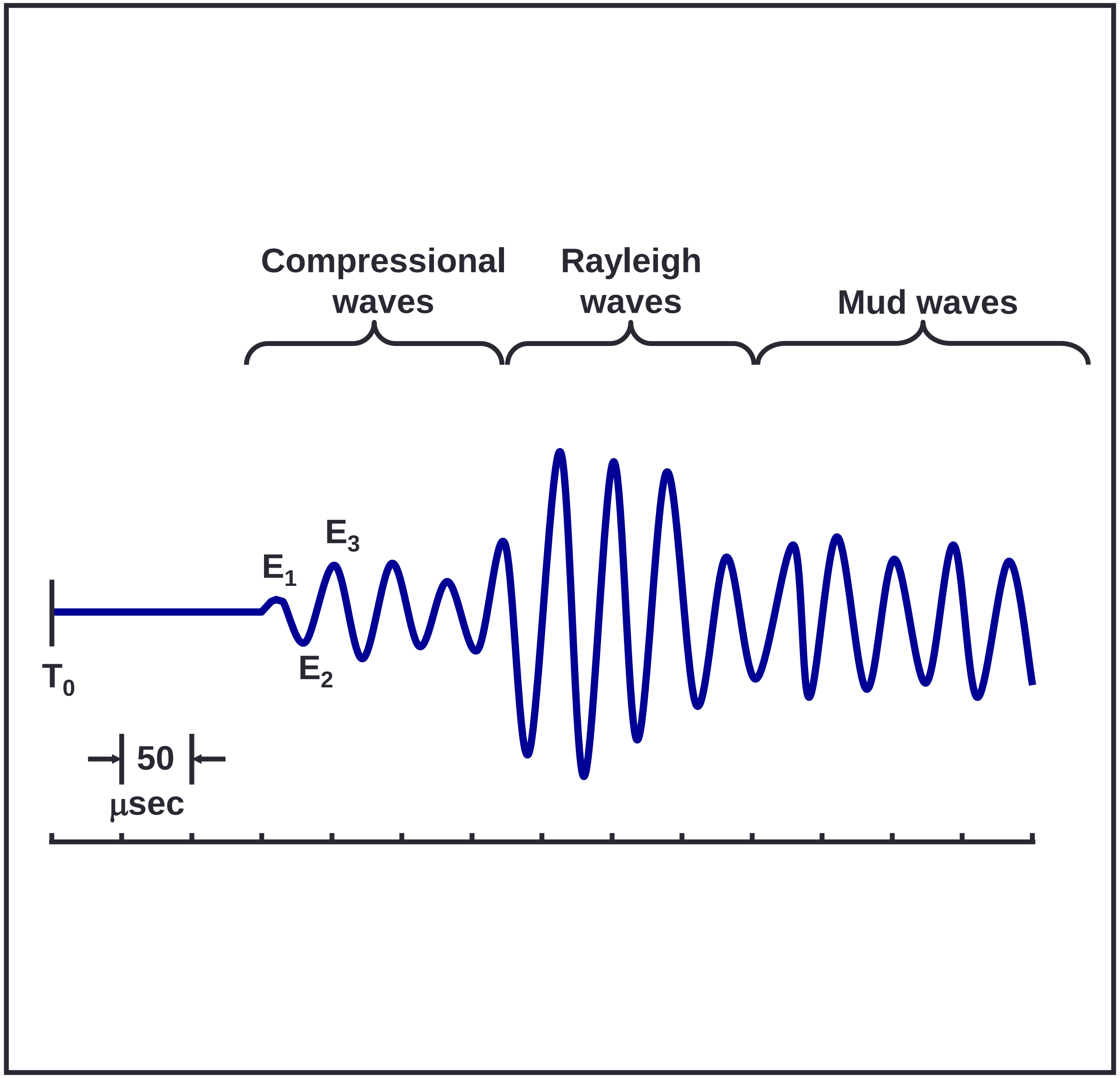
Compressional waves
Rayleigh waves
Mud waves
E1
E2
E3
T0
50
µsec

COMMON LITHOLOGY MATRIX TRAVEL TIMES USED

Lithology	Typical Matrix Travel Time, Δt_{ma}, μsec/ft
Sandstone	55.5
Limestone	47.5
Dolomite	43.5
Anydridte	50.0
Salt	66.7

ACOUSTIC (SONIC) LOG

Working equation

$$\Delta t_L = \phi S_{xo} \Delta t_{mf} + \phi (1 - S_{xo}) \Delta t_{hc}$$

$$+ V_{sh} \Delta t_{sh} + (1 - \phi - V_{sh}) \Delta t_{ma}$$

Δt_L	=	Recorded parameter, travel time read from log
$\phi S_{xo} \Delta t_{mf}$	=	Mud filtrate portion
$\phi (1 - S_{xo}) \Delta t_{hc}$	=	Hydrocarbon portion
$V_{sh} \Delta t_{sh}$	=	Shale portion
$(1 - \phi - V_{sh}) \Delta t_{ma}$	=	Matrix portion

ACOUSTIC (SONIC) LOG

- If $V_{sh} = 0$ and if hydrocarbon is liquid (i.e. $\Delta t_{mf} \approx \Delta t_f$), then
- $\Delta t_L = \phi\, \Delta t_f + (1 - \phi)\, \Delta t_{ma}$

or

$$\phi_s = \phi = \frac{\Delta t_L - \Delta t_{ma}}{\Delta t_f - \Delta t_{ma}}$$

ϕ_s = Porosity calculated from sonic log reading, fraction

Δt_L = Travel time reading from log, microseconds/ft

Δt_{ma} = Travel time in matrix, microseconds/ft

Δt_f = Travel time in fluid, microseconds/ ft

ACOUSTIC (SONIC) LOG

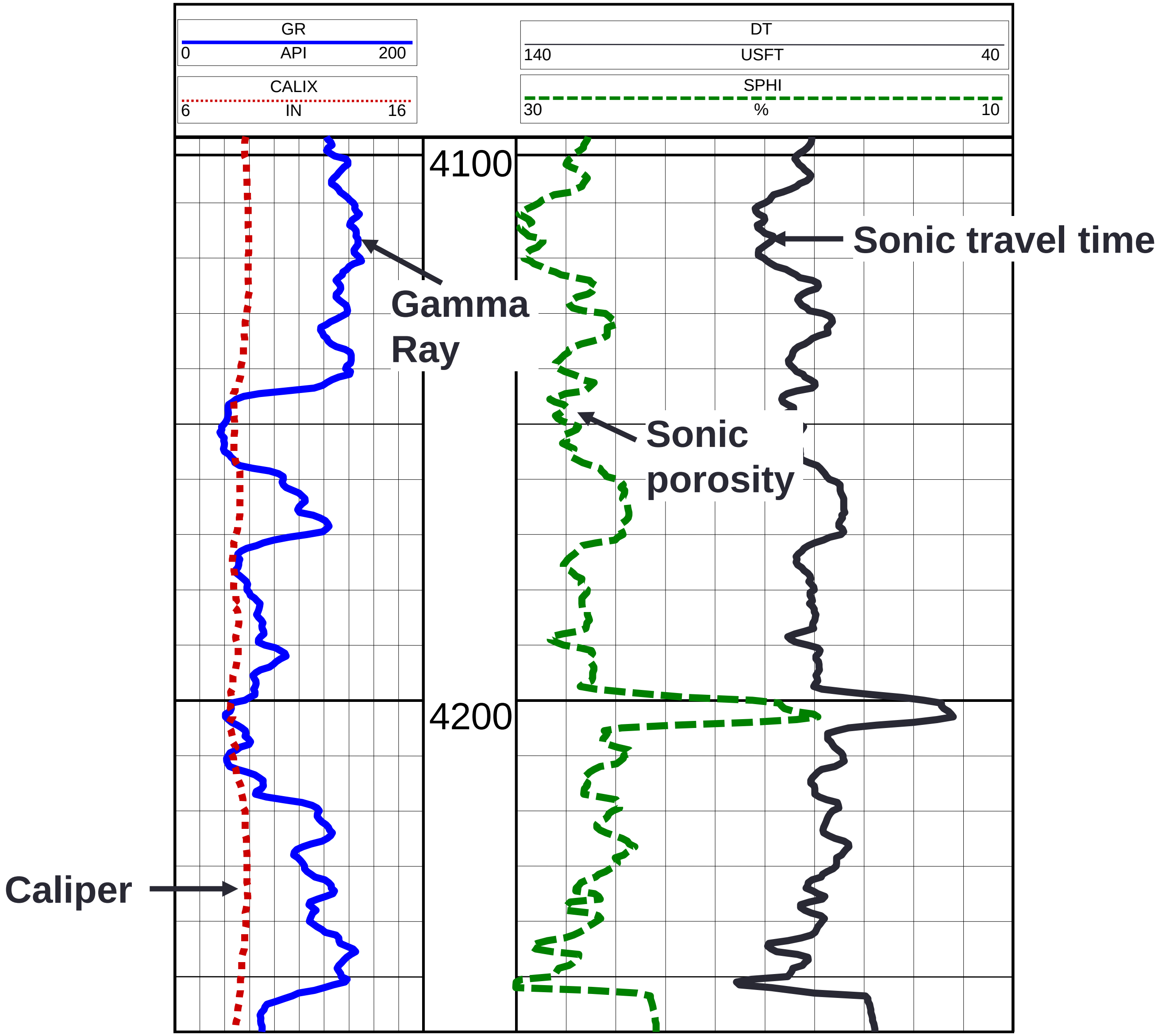

SONIC LOG

The response can be written as follows:

$$t_{log} = t_{ma}\left(1 - \phi\right) + t_f\ \phi$$

$$\phi = \frac{t_{log} - t_{ma}}{t_f - t_{ma}}$$

t_{log} = log reading, μsec/ft

t_{ma} = the matrix travel time, μsec/ft

t_f = the fluid travel time, μsec/ft

ϕ = porosity

SONIC LOG

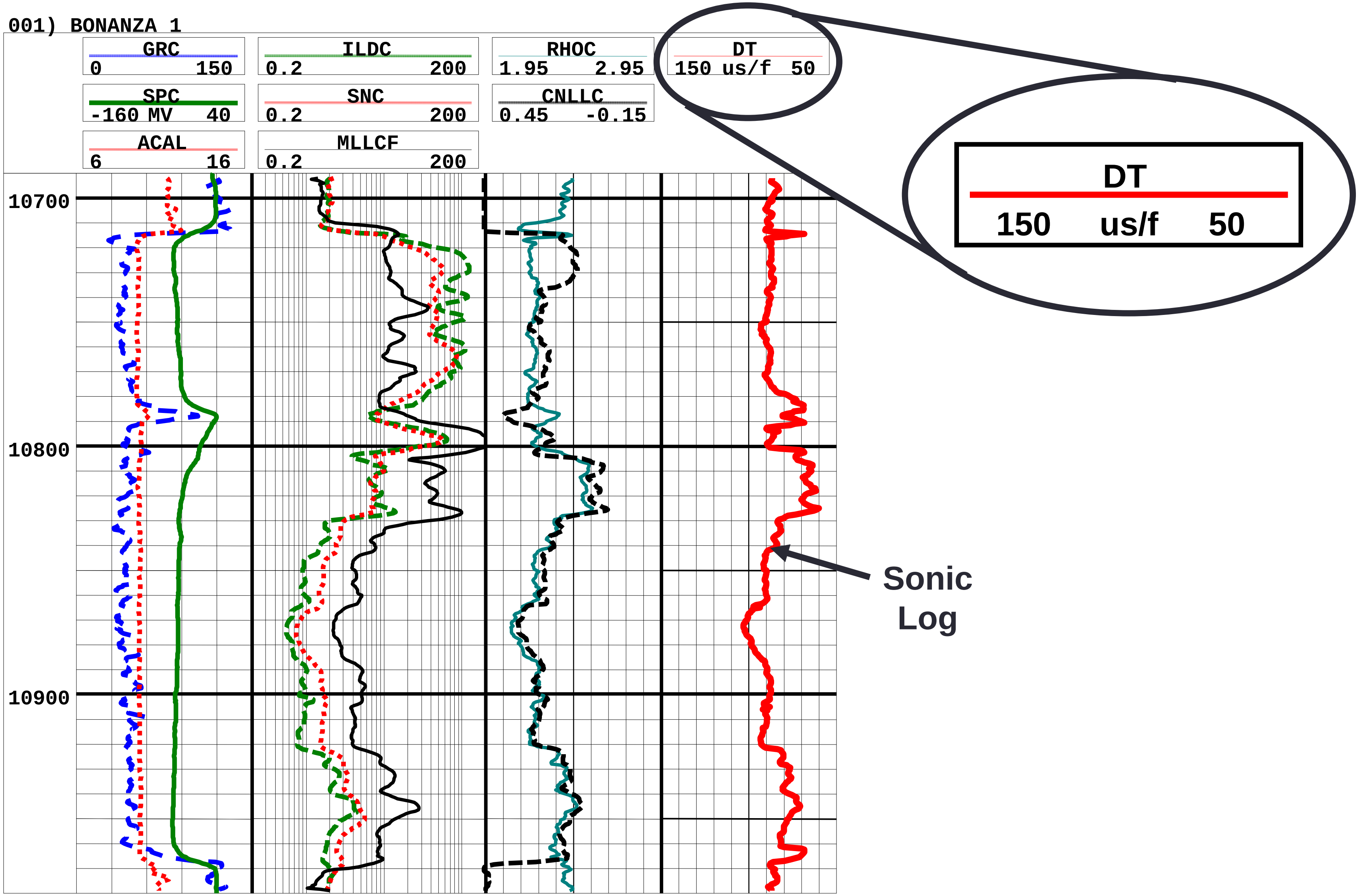

001) BONANZA 1
GRC
0 150
ILDC
0.2 200
RHOC
1.95 2.95
DT
150 us/f 50
SPC
-160 MV 40
SNC
0.2 200
CNLLC
0.45 -0.15
ACAL
6 16
MLLCF
0.2 200
10700
10800
10900
DT
150 us/f 50
Sonic Log

EXAMPLE

Calculating Rock Porosity Using an Acoustic Log

Calculate the porosity for the following intervals. The measured travel times from the log are summarized in the following table.

At depth of 10,820', accoustic log reads travel time of 65 μs/ft.

Calculate porosity. Does this value agree with density and neutron logs?

Assume a matrix travel time, Δt_m = 51.6 μsec/ft. In addition, assume the formation is saturated with water having a Δt_f = 189.0 μsec/ft.

EXAMPLE SOLUTION SONIC LOG

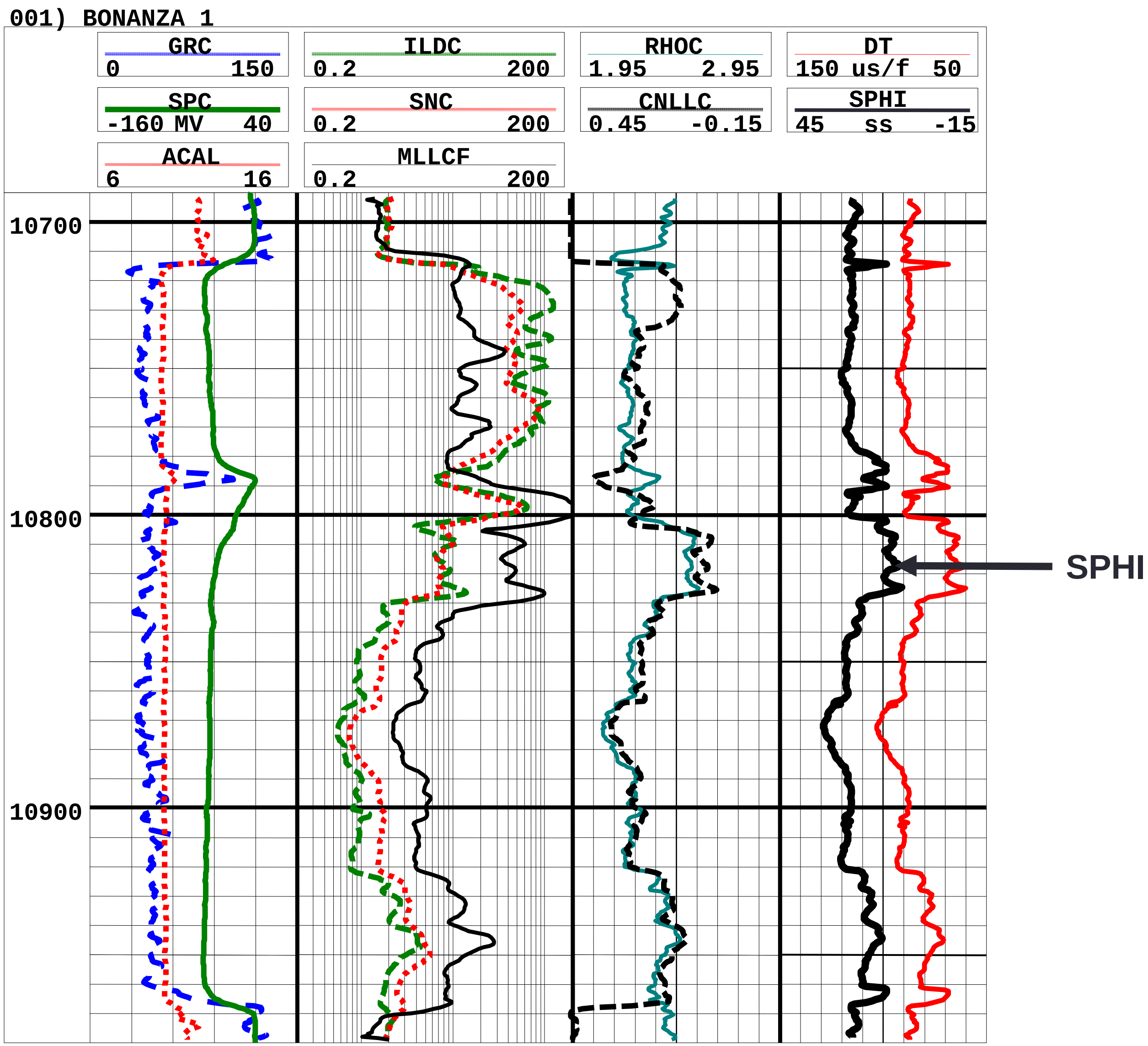

FACTORS AFFECTING SONIC LOG RESPONSE

- Unconsolidated formations
- Naturally fractured formations
- Hydrocarbons (especially gas)
- Rugose salt sections

RESPONSES OF POROSITY LOGS

The three porosity logs:

- Respond differently to different matrix compositions
- Respond differently to presence of gas or light oils

Combinations of logs can:

- Imply composition of matrix
- Indicate the type of hydrocarbon in pores

GAS EFFECT

- Density - ϕ is too high
- Neutron - ϕ is too low
- Sonic - ϕ is not significantly affected by gas

ESTIMATING POROSITY FROM WELL LOGS

Openhole logging tools are the most common method of determining porosity:

- Less expensive than coring and may be less risk of sticking the tool in the hole
- Coring may not be practical in unconsolidated formations or in formations with high secondary porosity such as vugs or natural fractures.

If porosity measurements are very important, both coring and logging programs may be conducted so the log-based porosity calculations can be used to calibrated to the core-based porosity measurements.

Influence Of Clay-Mineral Distribution On Effective Porosity

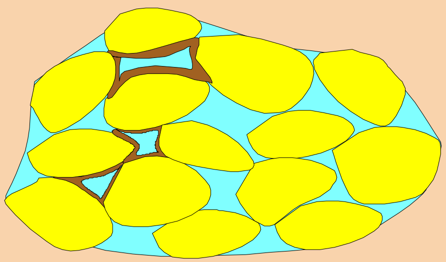

Dispersed Clay
- Pore-filling
- Pore-lining
- Pore-bridging

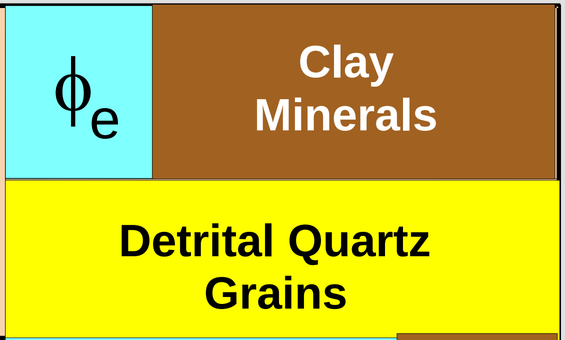

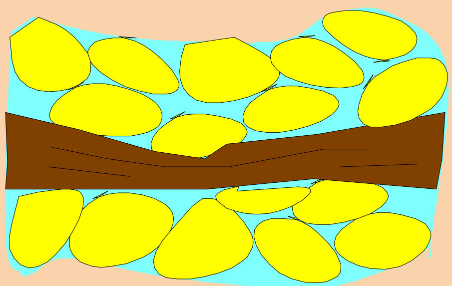

Clay Lamination

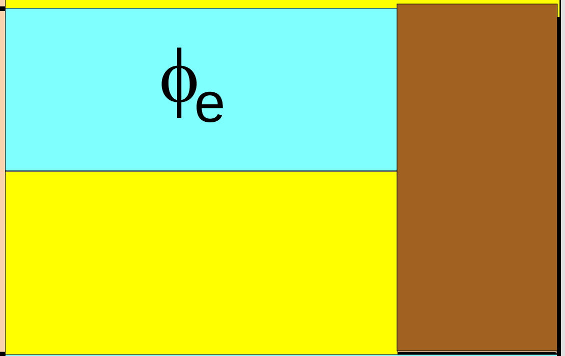

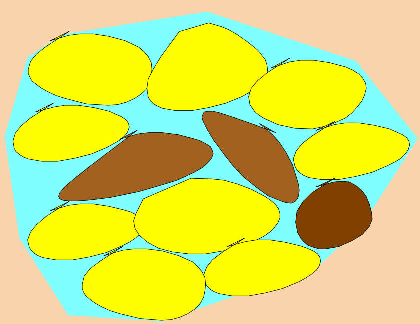

Structural Clay
(Rock Fragments, Rip-Up Clasts, Clay-Replaced Grains)

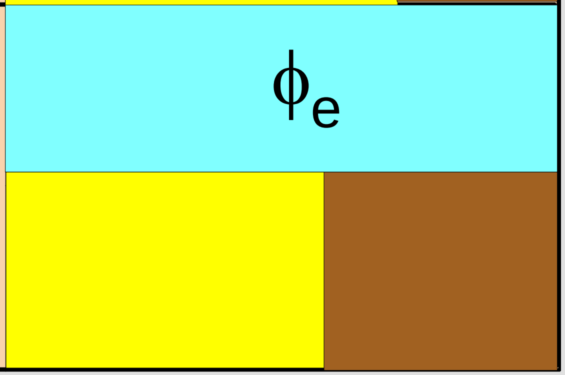

GEOLOGICAL AND PETROPHYSICAL DATA USED TO DEFINE FLOW UNITS

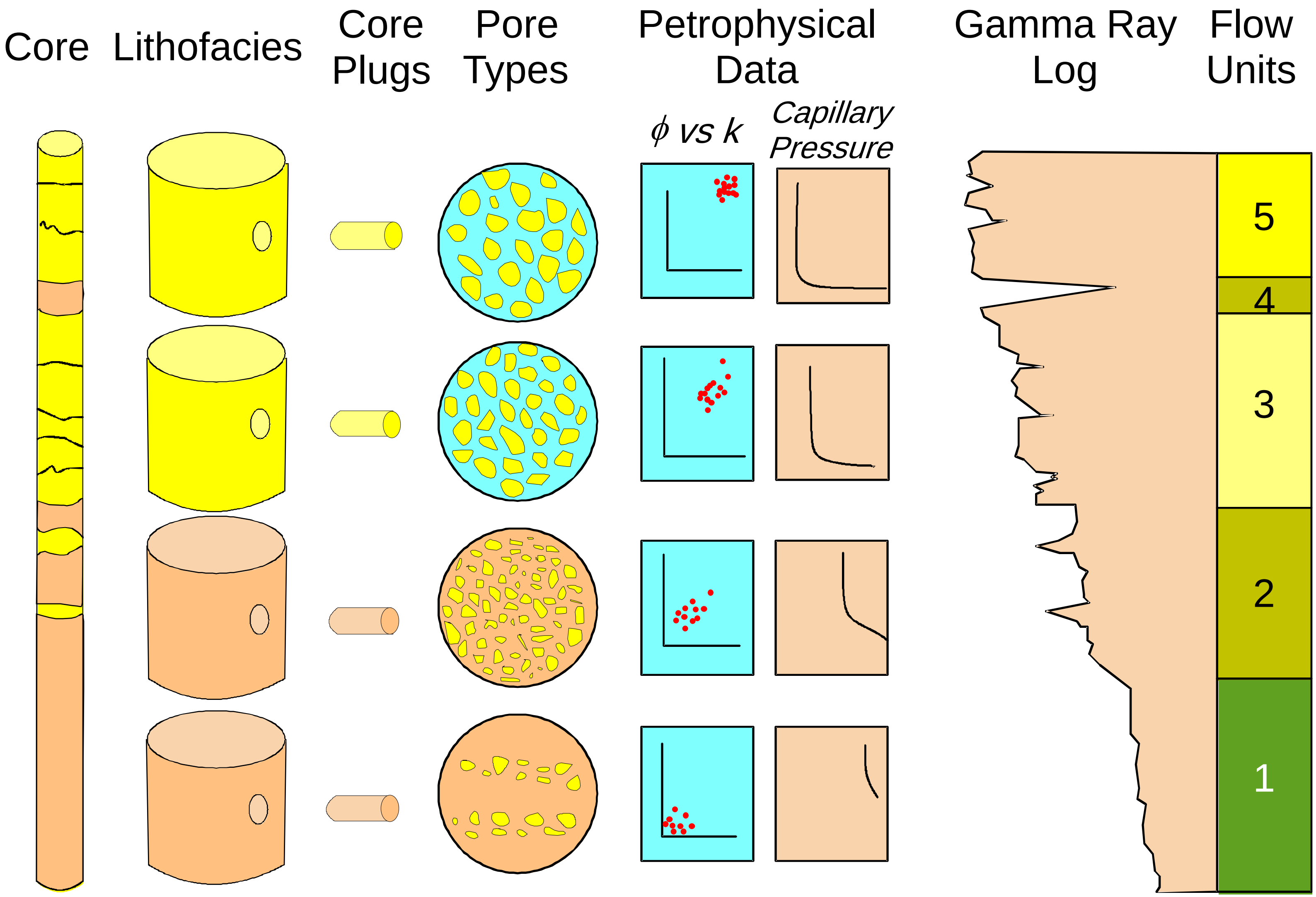

Schematic Reservoir Layering Profile in a Carbonate Reservoir

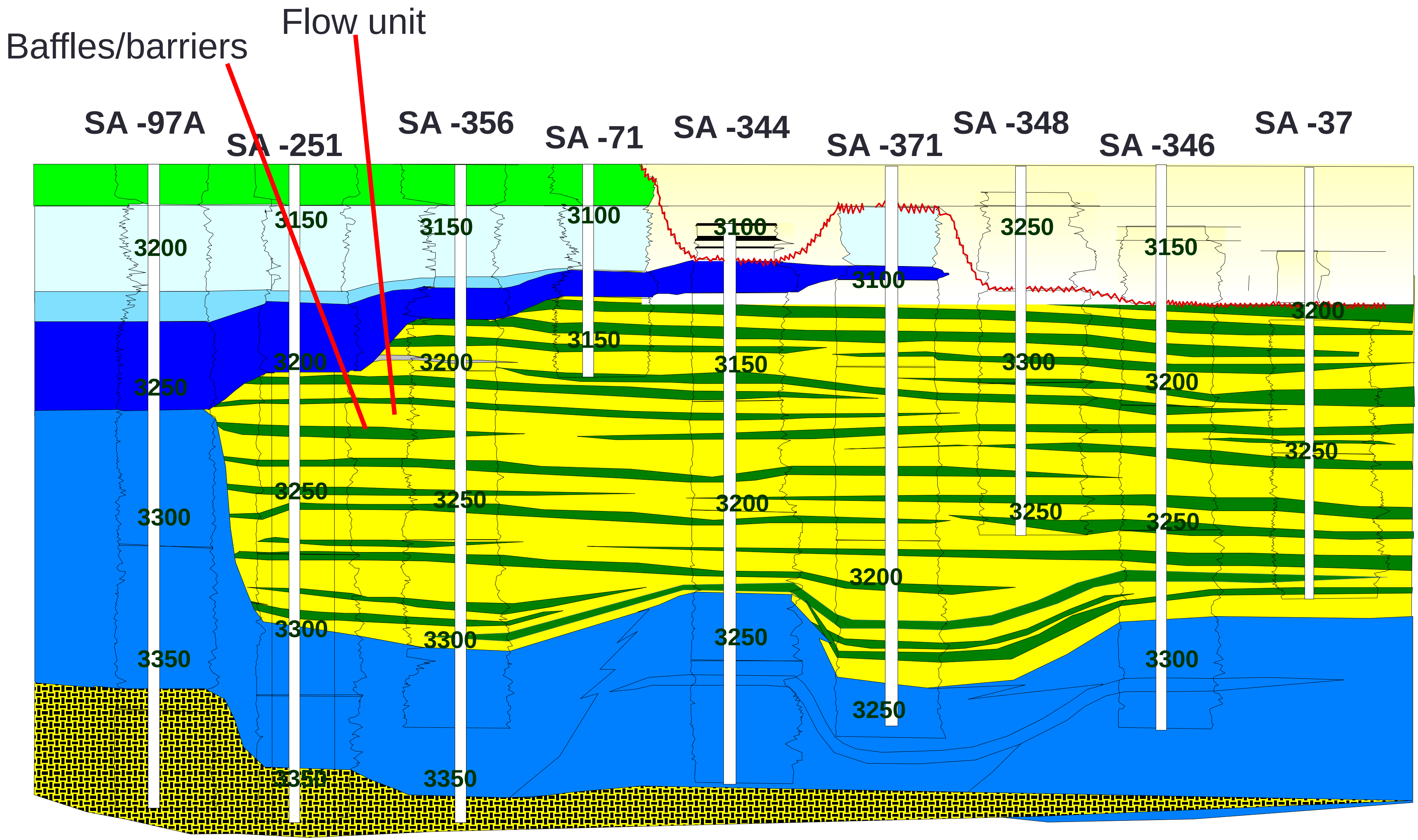

From Bastian and others

Resistivity Log

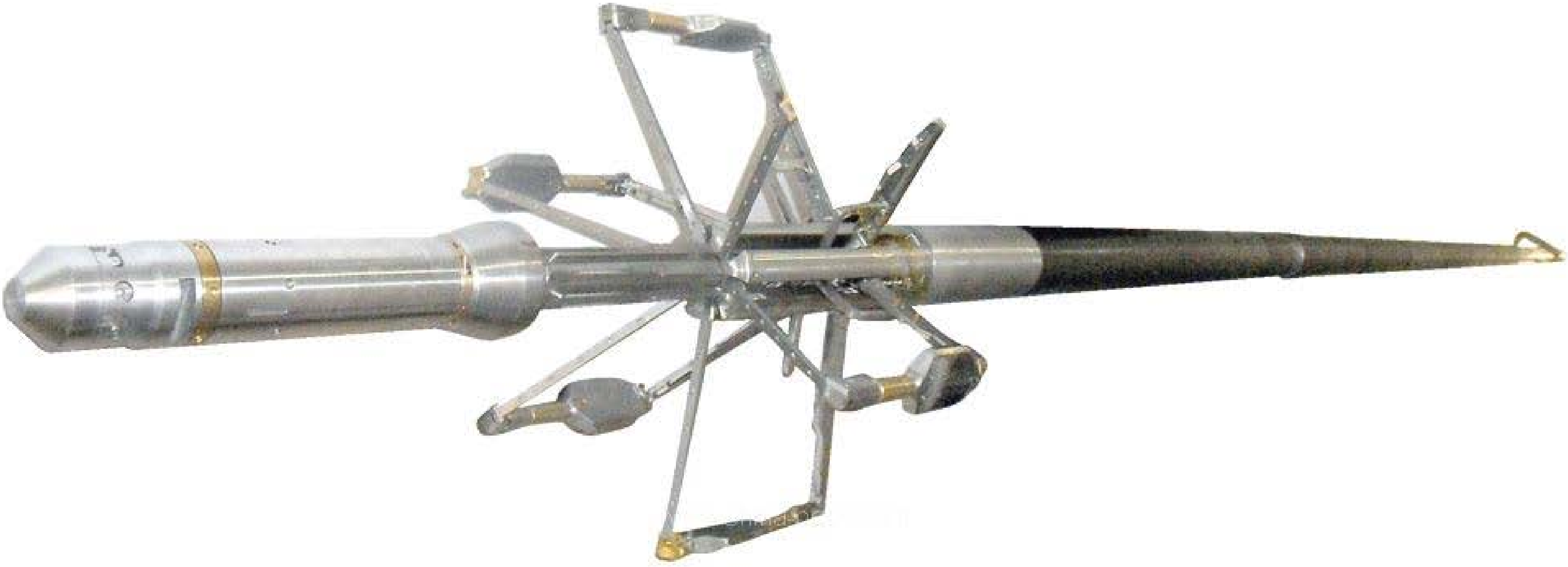

- Resistivity logging is a method of well logging that works by characterizing the rock or sediment in a borehole by measuring its electrical resistivity. Resistivity is a fundamental material property which represents how strongly a material opposes the flow of electric current. In these logs, resistivity is measured using 4 electrical probes to eliminate the resistance of the contact leads. The log must run in holes containing electrically conductive mud or water.
- Resistivity logging is sometimes used in mineral exploration (especially exploration for iron and potassium) and water-well drilling, but most commonly for formation evaluation in oil- and gas-well drilling. Most rock materials are essentially insulators, while their enclosed fluids are conductors. Hydrocarbon fluids are an exception, because they are almost infinitely resistive. When a formation is porous and contains salty water, the overall resistivity will be low. When the formation contains hydrocarbon, or contains very low porosity, its resistivity will be high. High resistivity values may indicate a hydrocarbon bearing formation.

- Usually while drilling, drilling fluids invade the formation, changes in the resistivity are measured by the tool in the invaded zone. For this reason, several resistivity tools with different investigation lengths are used to measure the formation resistivity. If water based mud is used and oil is displaced, "deeper" resistivity logs (or those of the "virgin zone") will show lower conductivity than the invaded zone. If oil based mud is used and water is displaced, deeper logs will show higher conductivity than the invaded zone. This provides not only an indication of the fluids present, but also, at least qualitatively, whether the formation is permeable or not.

- **Basics about the Resistivity:**

- Resistivity measures the electric properties of the formation,
- Resistivity is measured as, R in W per m,
- Resistivity is the inverse of conductivity,
- The ability to conduct electric current depends upon:
    - The **Volume** of water,
    - The **Temperature** of the formation,
    - The **Salinity** of the formation

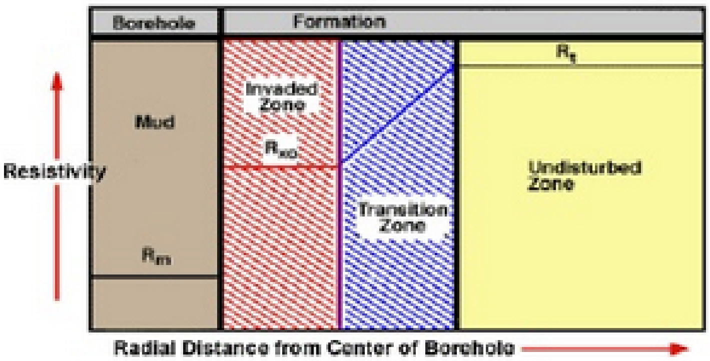

The Resistivity Log:

Resistivity logs measure the ability of rocks to conduct electrical current and are scaled in units of ohm-meters.

The Usage:

Resistivity logs are electric logs which are used to:

Determine Hydrocarbon versus Water-bearing zones,
Indicate Permeable zones,
Determine Resisitivity Porosity.

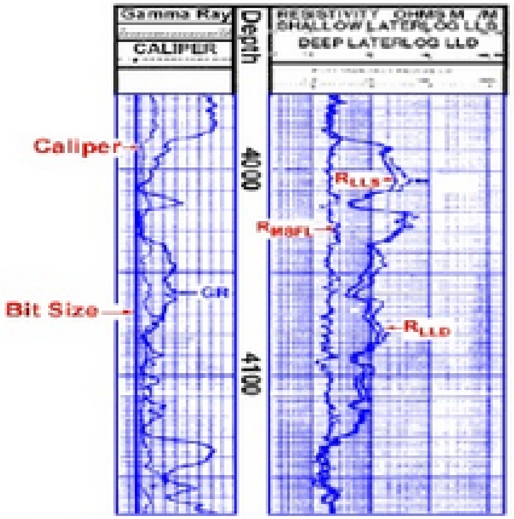

Resistivity Logging

There are two types of resistivity logging tools:

- Laterolog tools send a current from electrodes on the logging tool, through the formation, to a return electrode located either at surface or downhole.
  - Laterolog tools need a conductive path between the logging tool and the formation
- Induction tools generate current loops in the formation and measure the strength of the electromagnetic signal created by these current loops.
  - Induction tools do not require a conductive path in the borehole. They work in oil-base muds and air-filled holes.

Basic Resistivity tool types

Laterolog Logging Tools

Induction Logging Tools

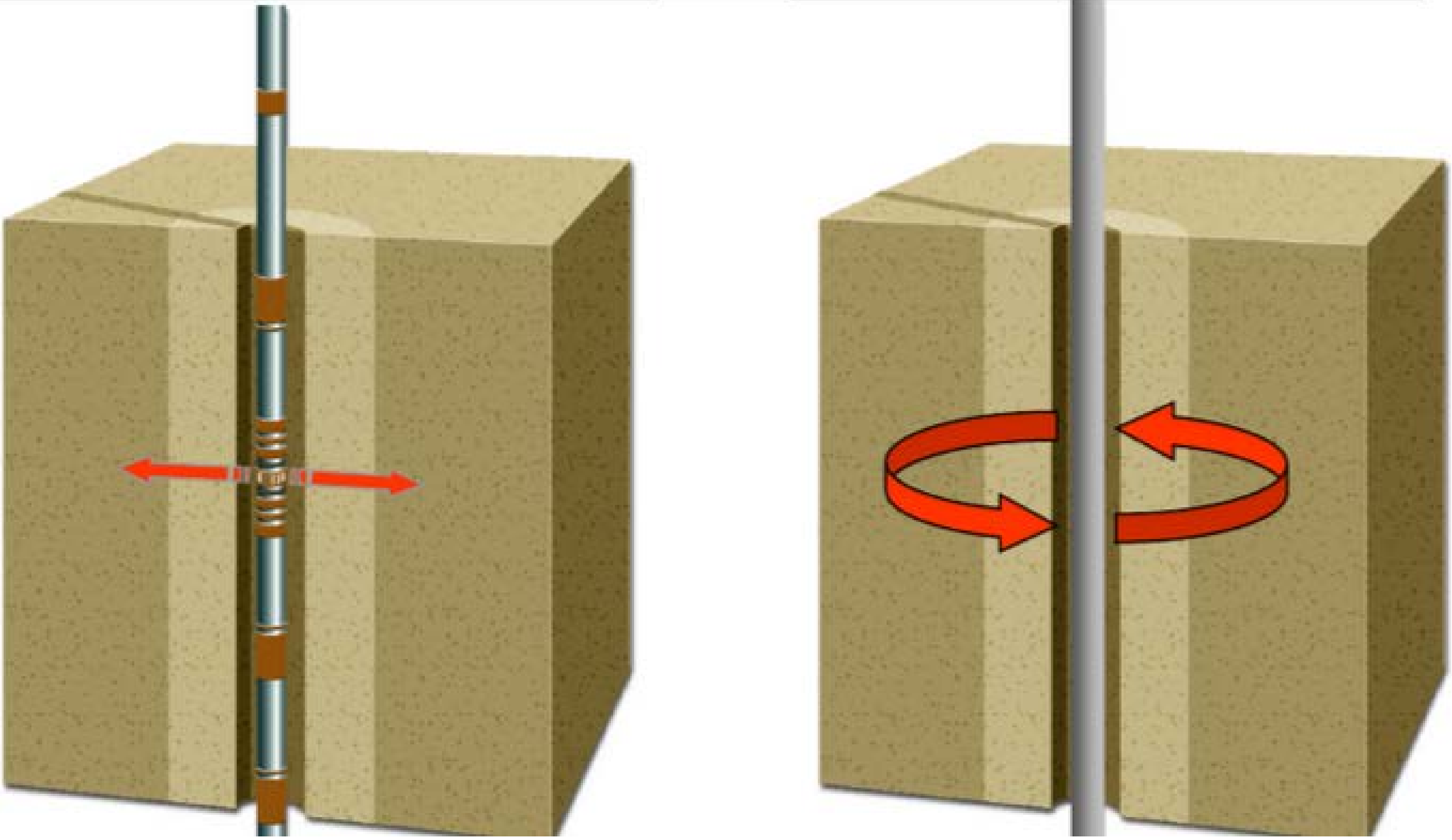

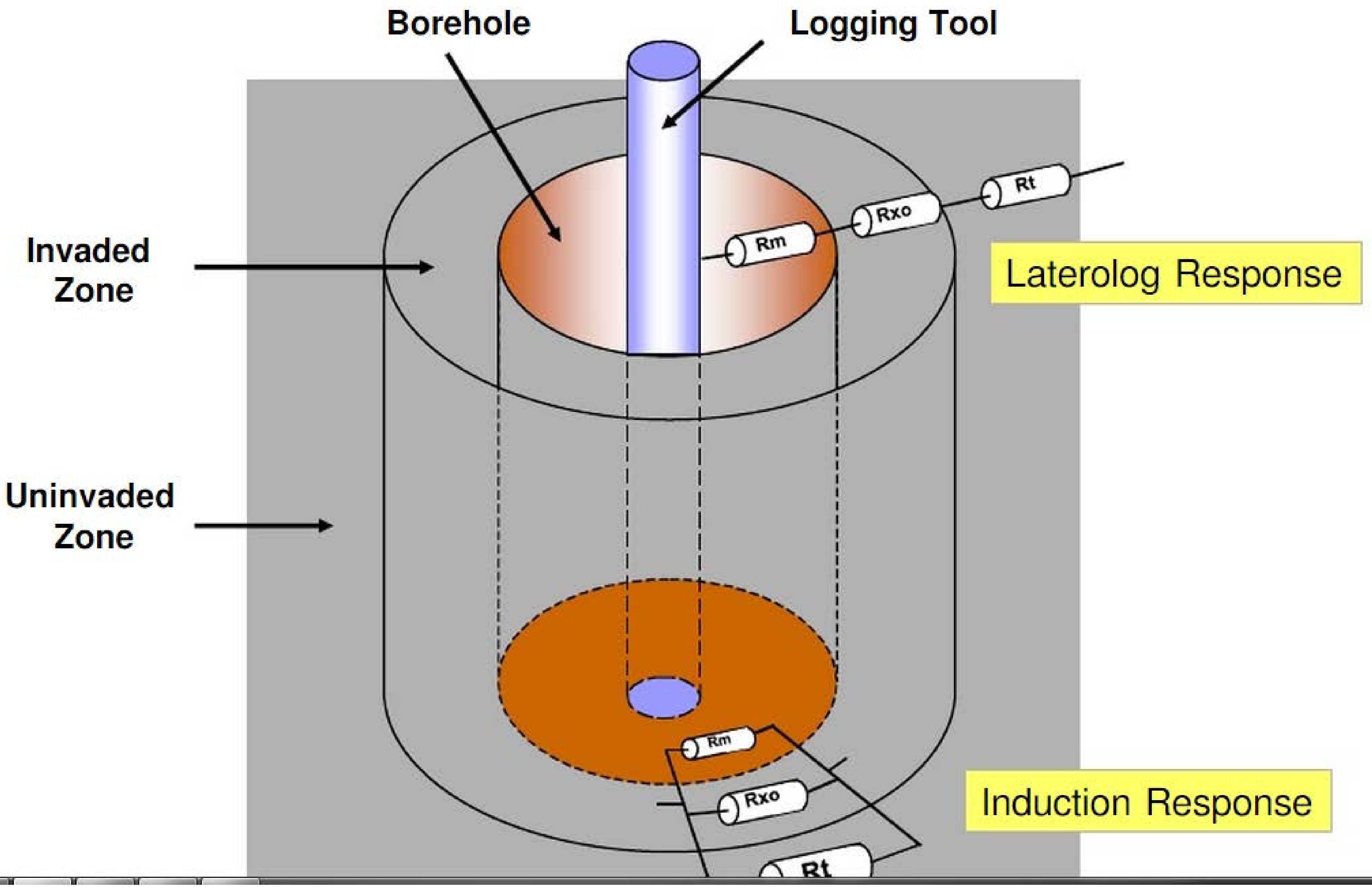

Borehole
Logging Tool
Invaded Zone
Uninvaded Zone
Rm
Rxo
Rt
Laterolog Response
Rm
Rxo
Rt
Induction Response

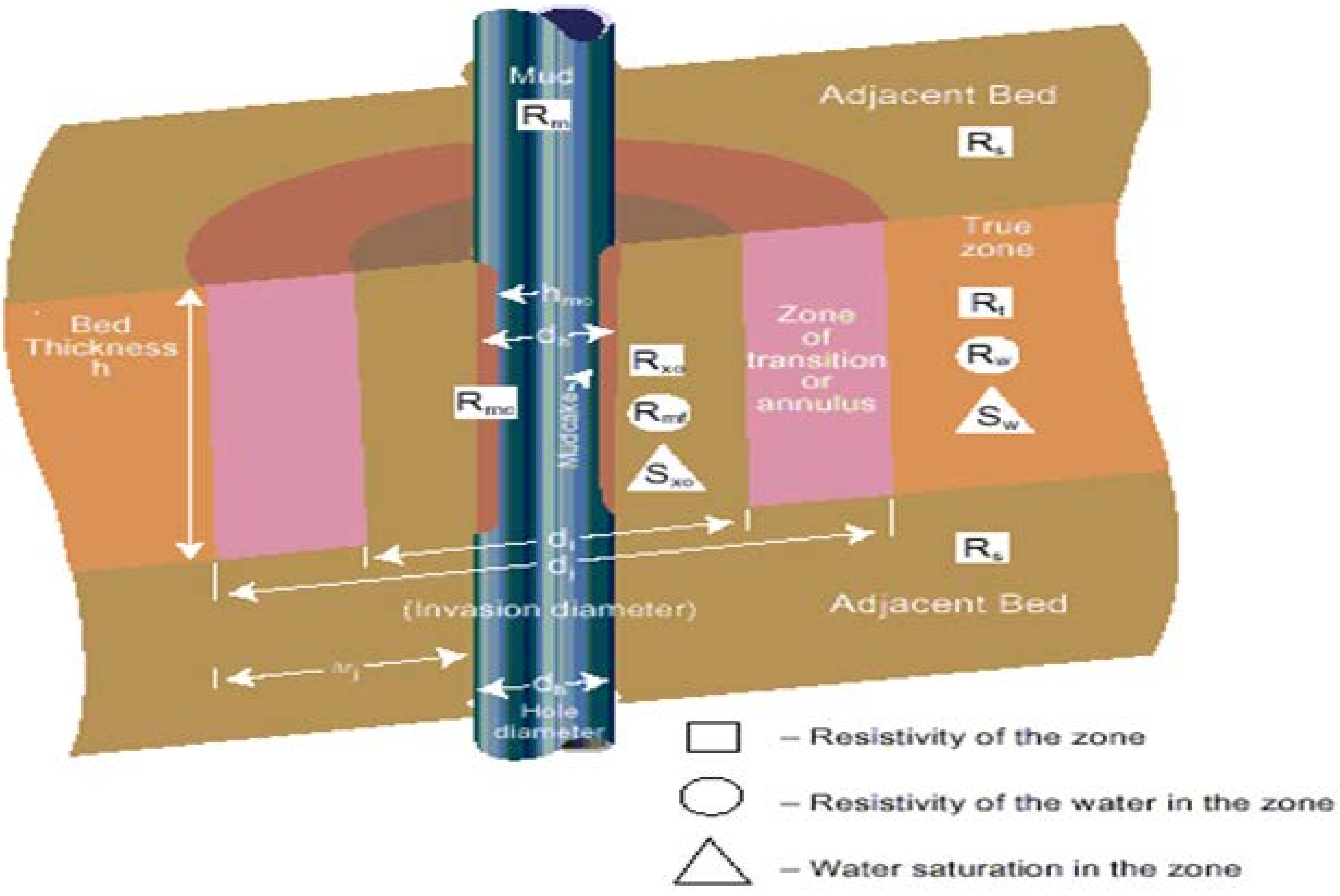
Mud
R_m
Adjacent Bed
R_s
True zone
R_t
R_w
S_w
Bed Thickness h
h_{mc}
d_h
Mudcake
R_{mc}
R_{xo}
R_{mf}
S_{xo}
Zone of transition or annulus
d_i
d_j
(Invasion diameter)
R_s
Adjacent Bed
d_h
Hole diameter
– Resistivity of the zone
– Resistivity of the water in the zone
– Water saturation in the zone

Rt – True Formation Resistivity

- R_t is the True Resistivity of the formation
- Client performs reservoir analysis using R_t
- Incorrect R_t = Incorrect Analysis = Incorrect production decision
- Symbols: R_w, R_m, R_t, R_{xo}, R_{mc}, R_o

  S_w, S_{xo}

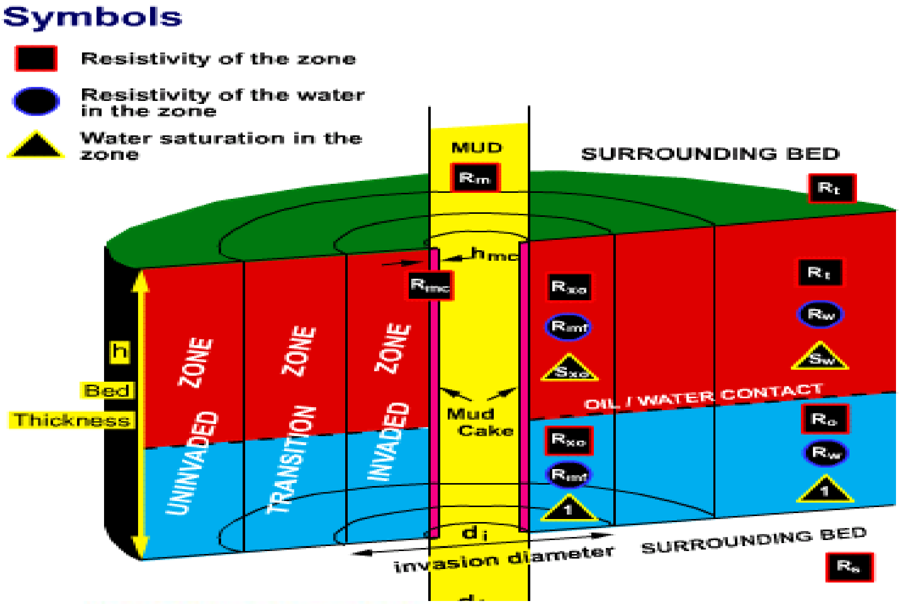

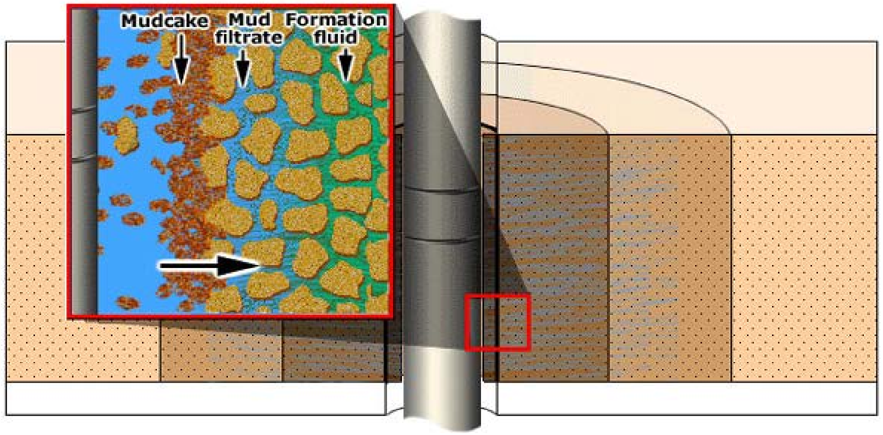

Resistivity : Laterolog

Current is forced through the mud into the formation

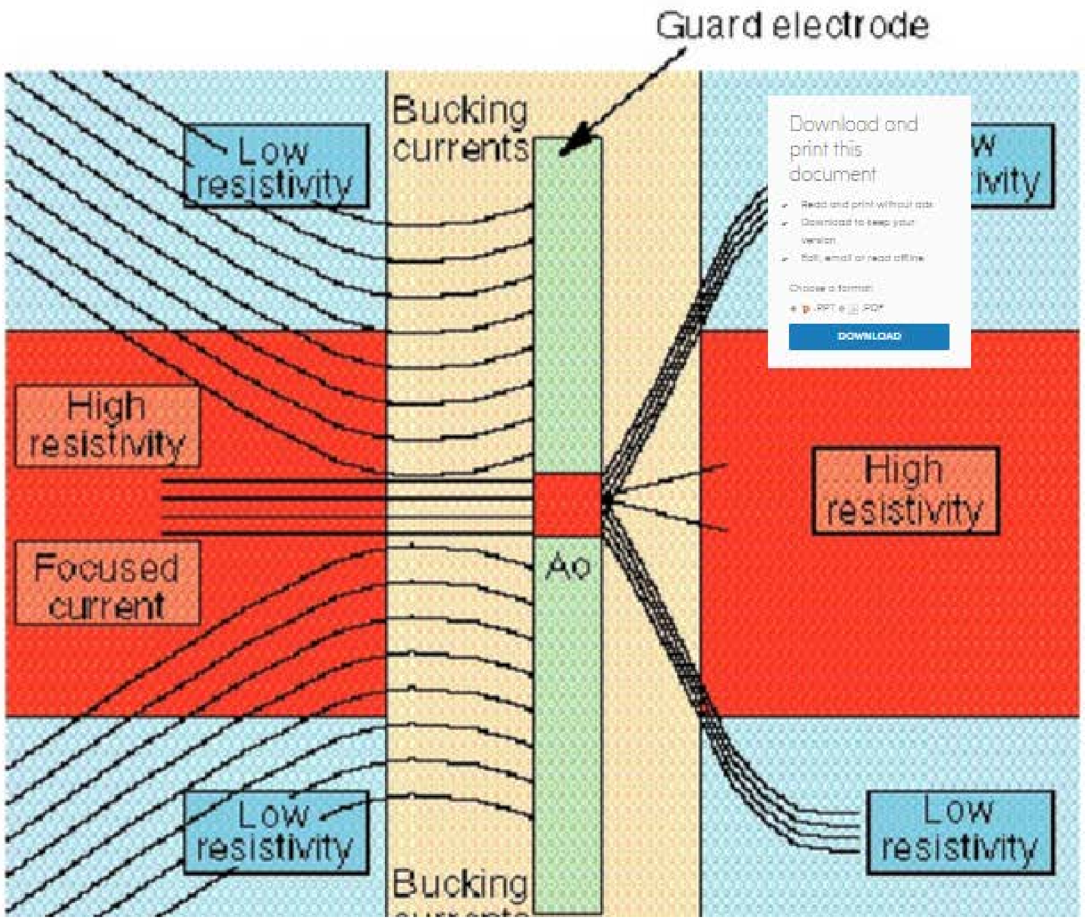

Dual Laterolog Measurement

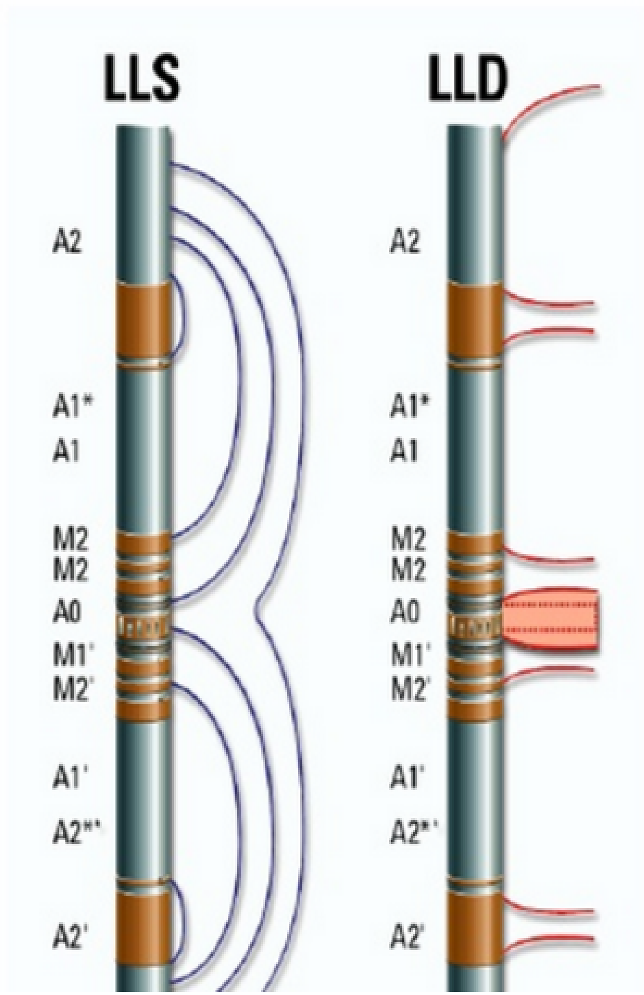

LLD: deep measurement, currect returns to surface.

LLS: shallow measurement, current returns to the tool itself.

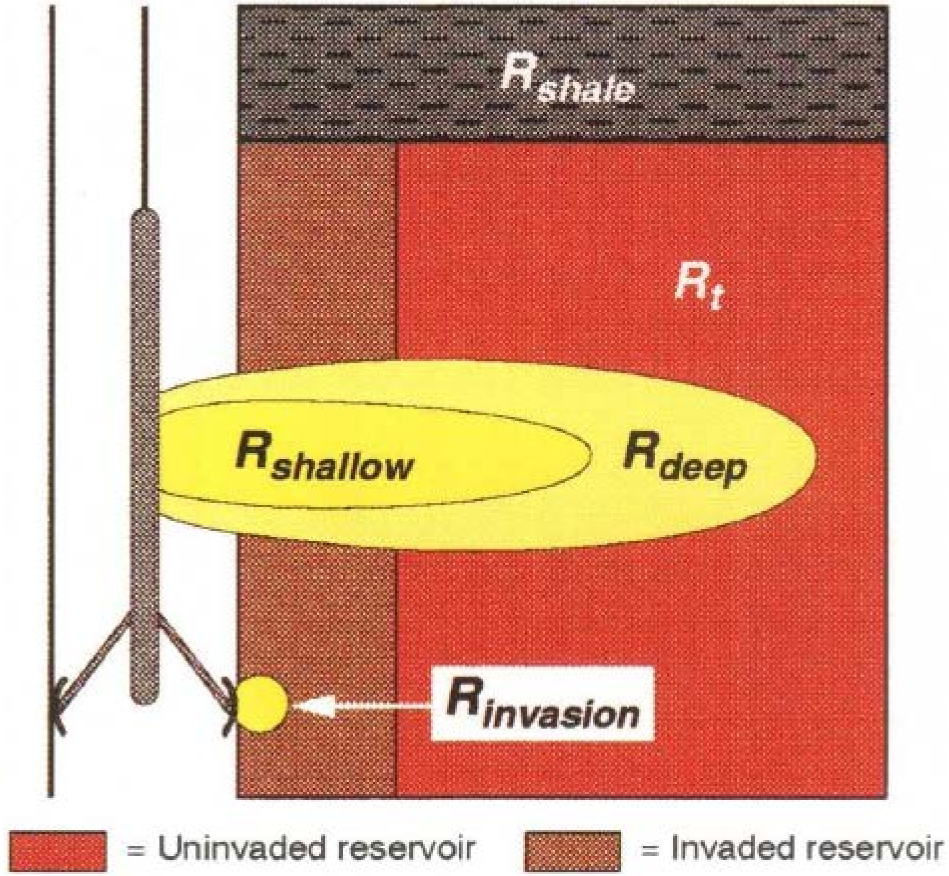

(after van Ditzhuijzen, 1994)

Resistivity : Laterolog Shallow (LLS)

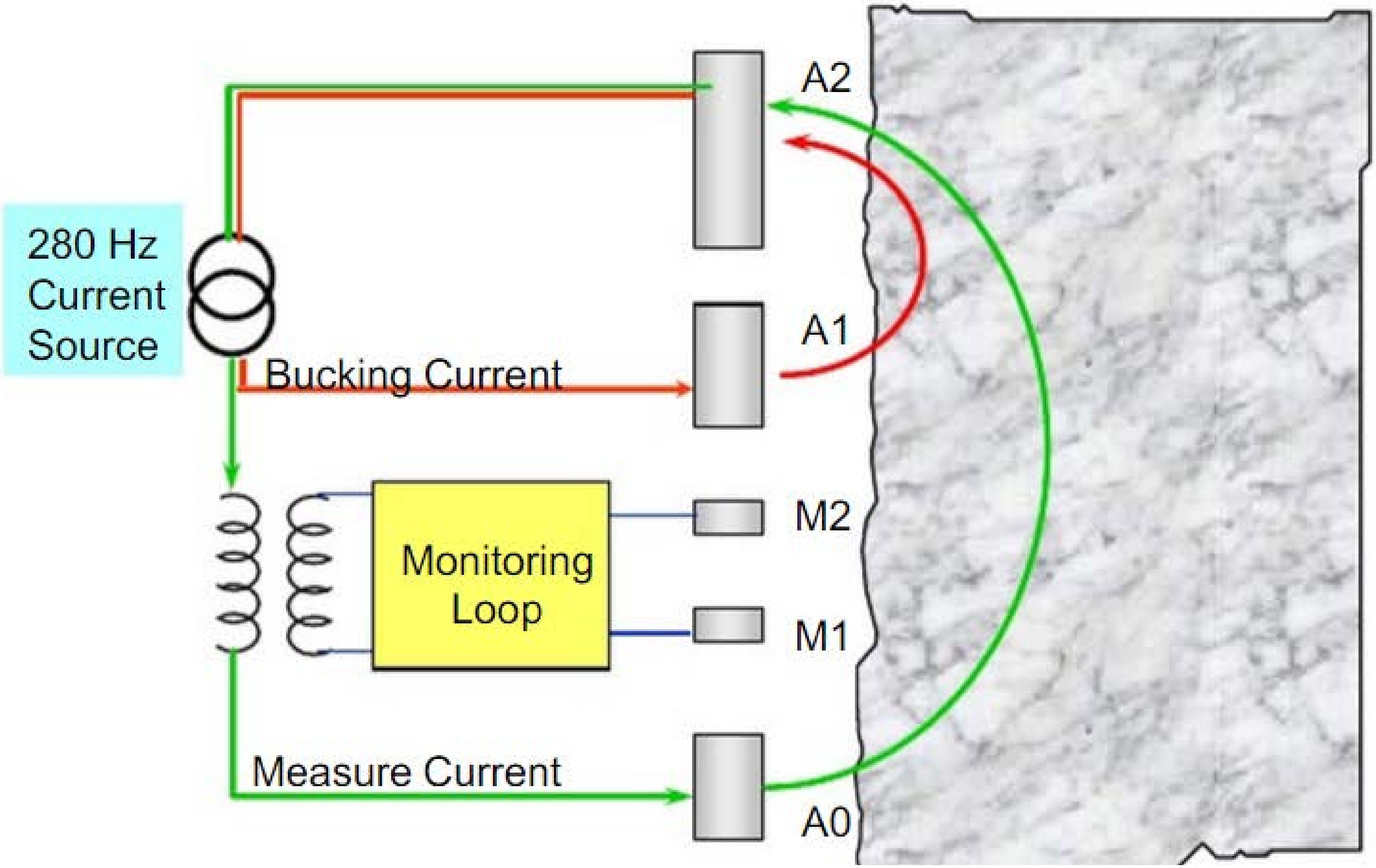

Resistivity :
Laterolog Deep (LLD)

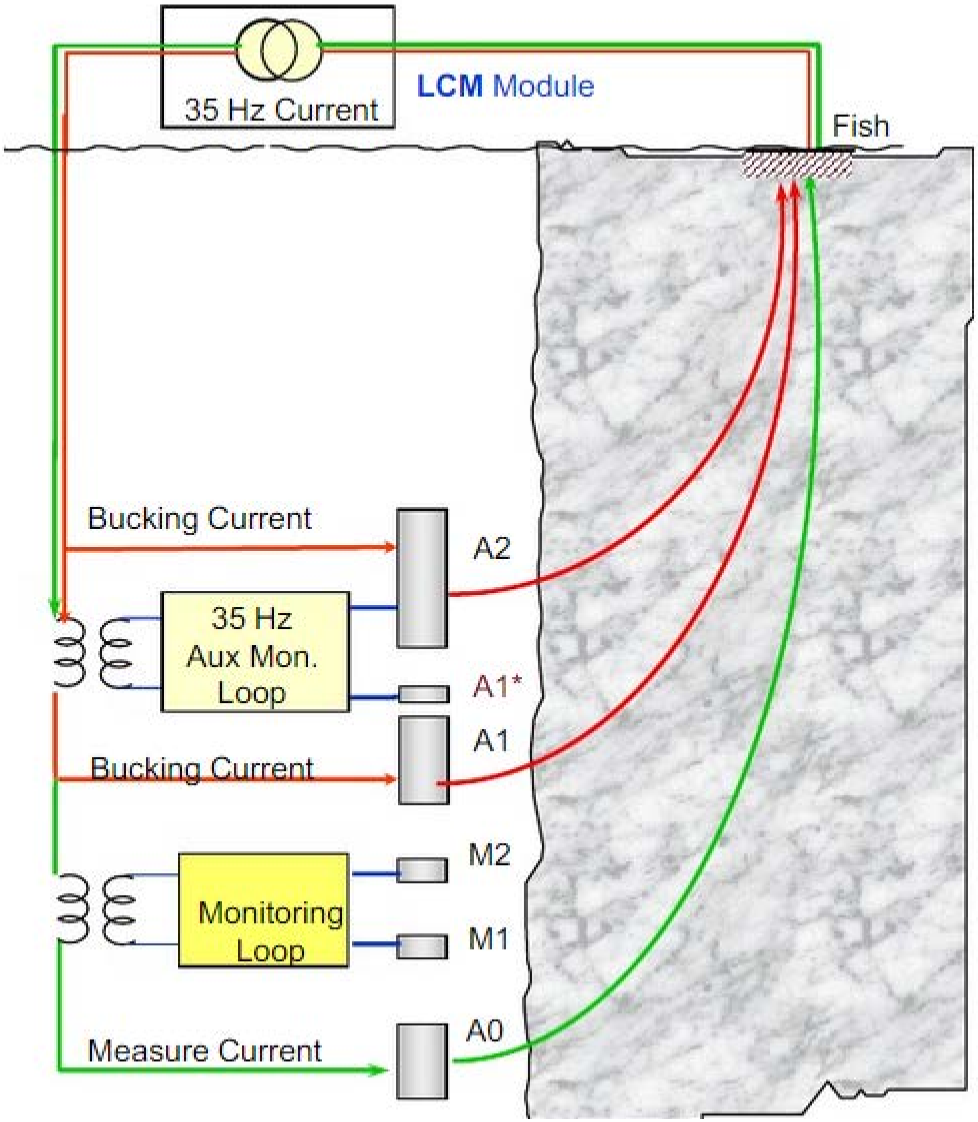

Resistivity : Laterolog invasion effects

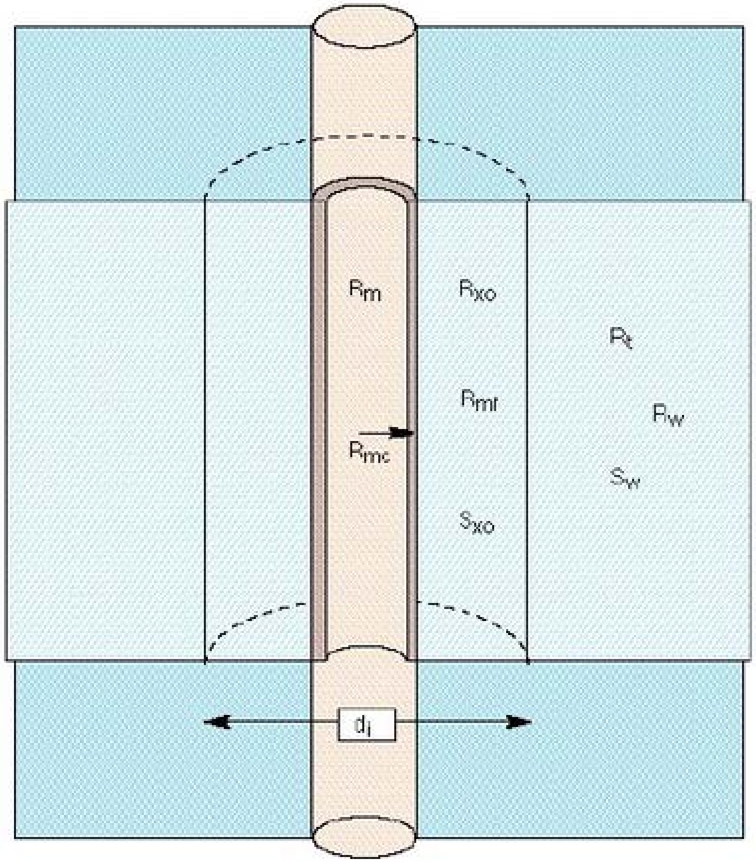

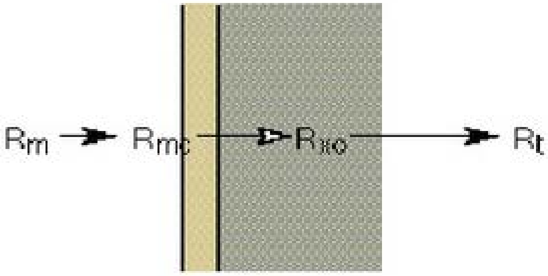

RLL = Vm Rm + Vmc Rmc + Vxo Rxo + (1-Vm-Vmc-Vxo) Rt

Resistivity : Laterolog

TLD Tool Components

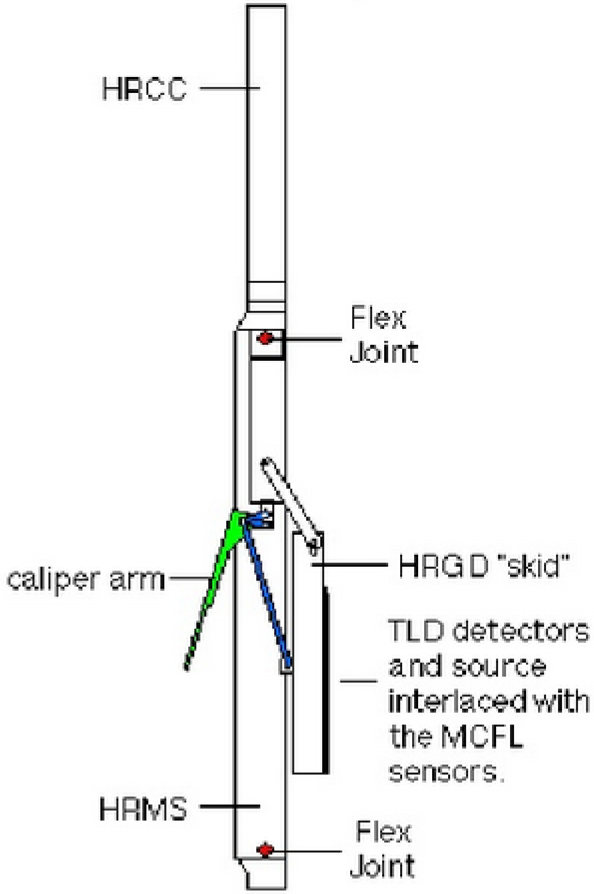

High - Resolution Skid

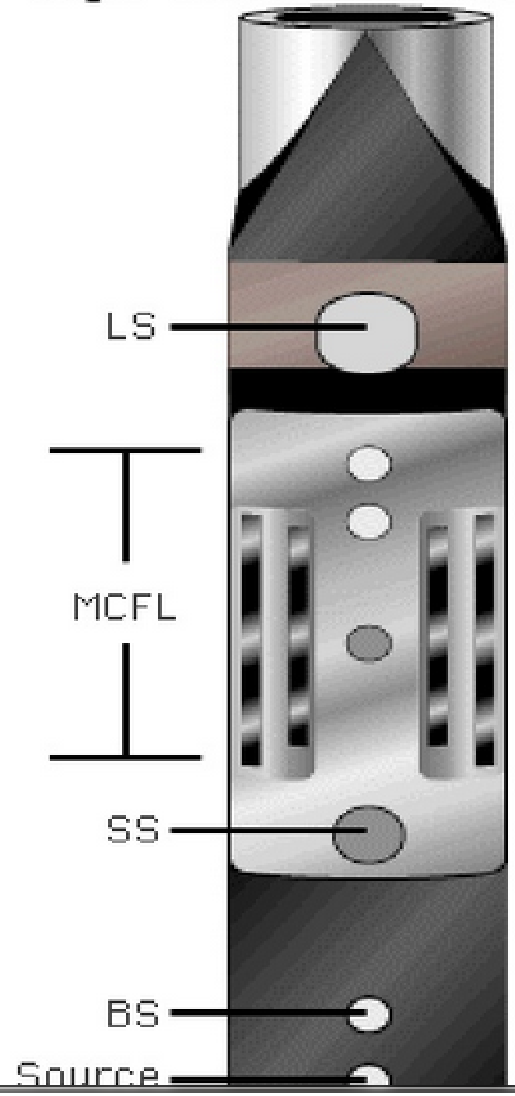

Resistivity : Laterolog invasion effects

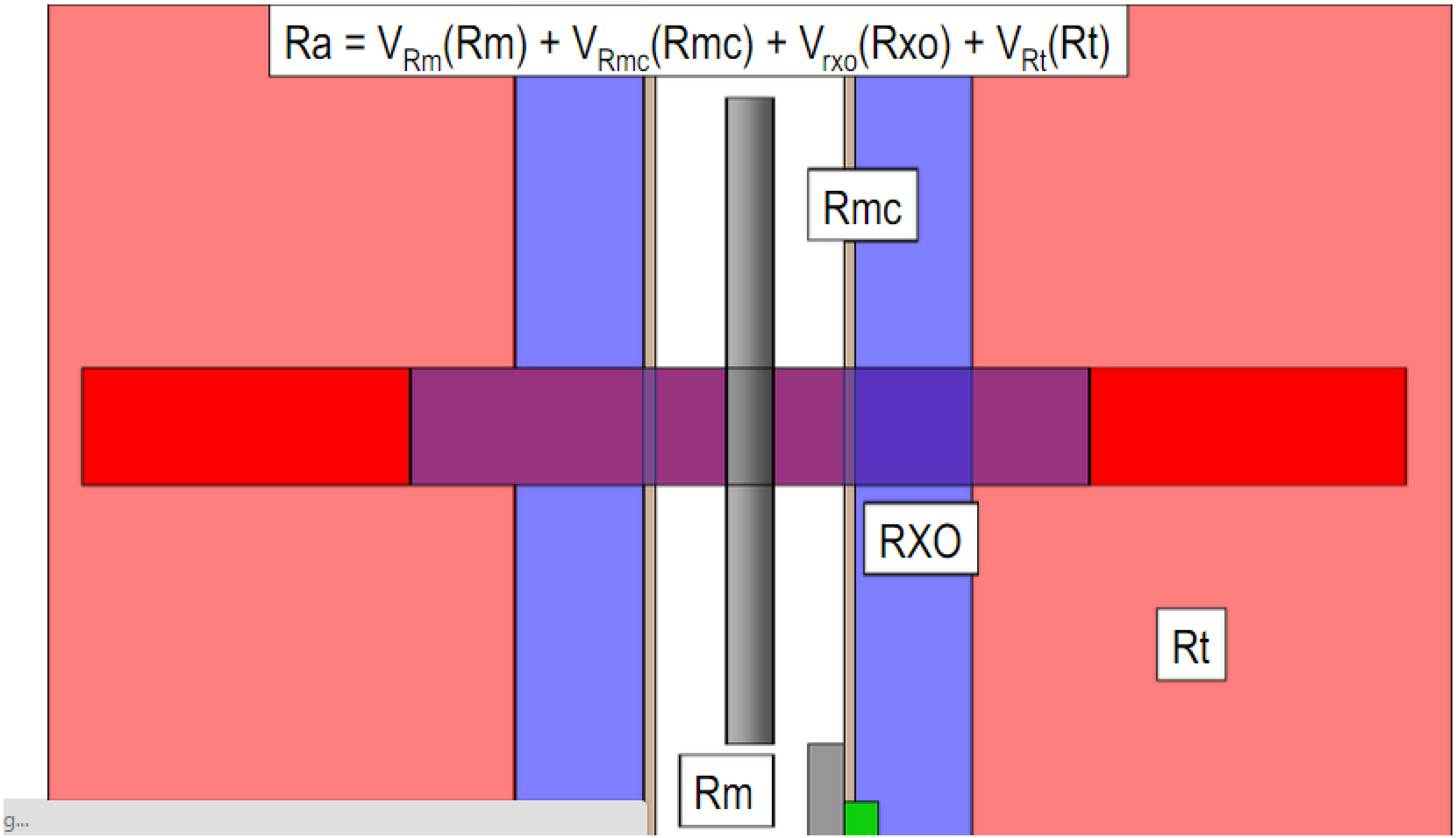

Resistivity : Laterolog invasion effects

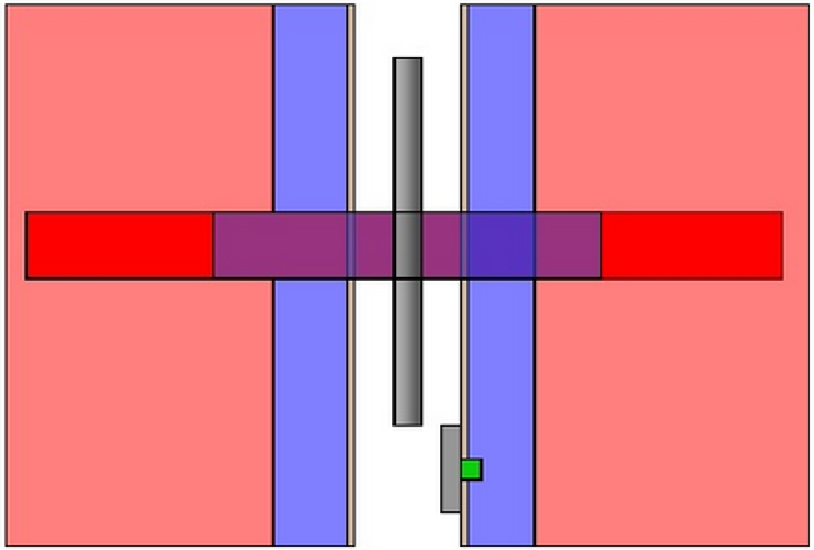

If Rmf < Rw then Rxo < LLS < LLD < Rt
If Rmf > Rw then Rxo > LLS > LLD > Rt

Using Rxo, LLS & LLD, Rt and Di can be computed

Resistivity : Laterolog invasion effects

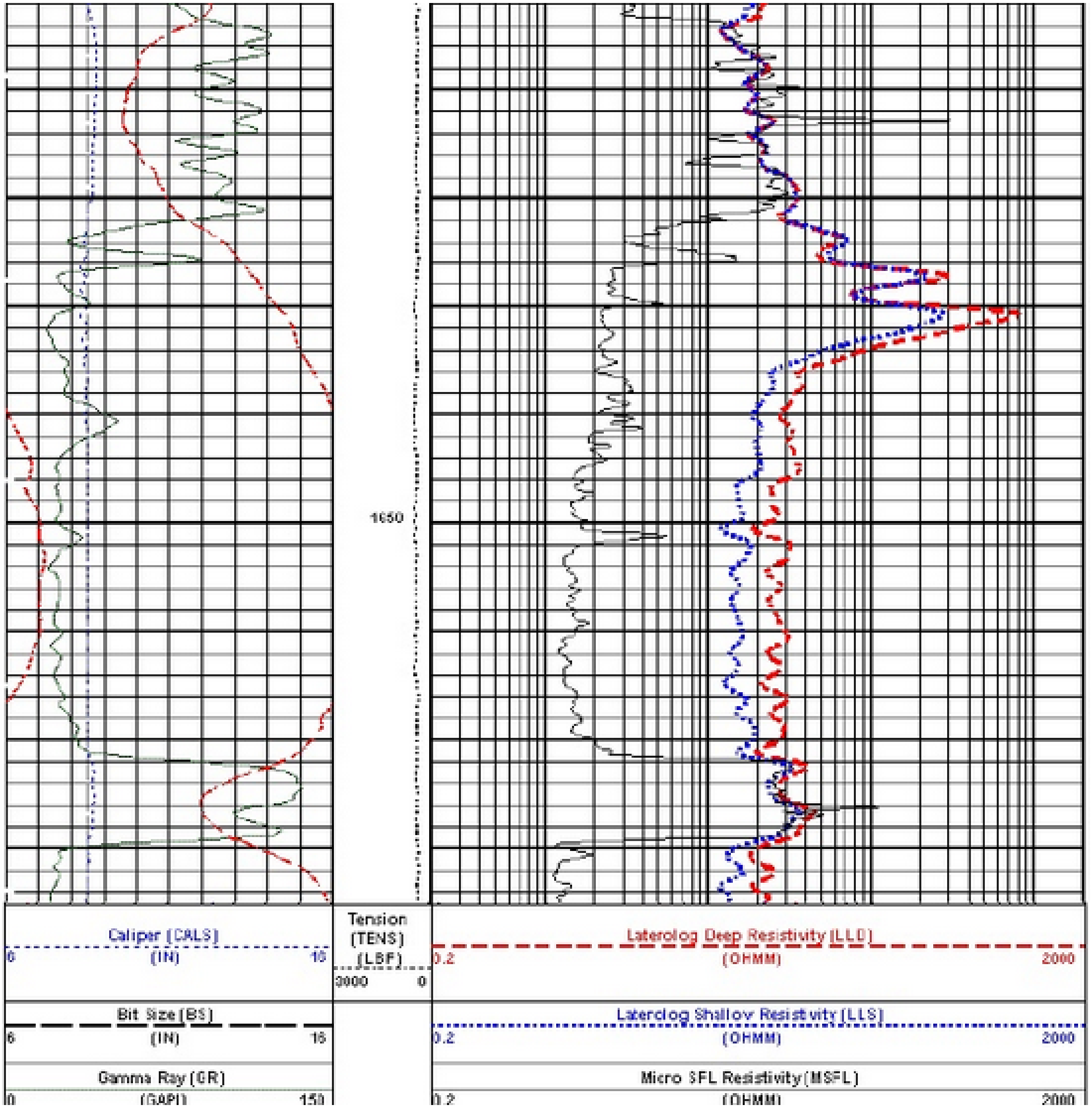

Groningen Effect

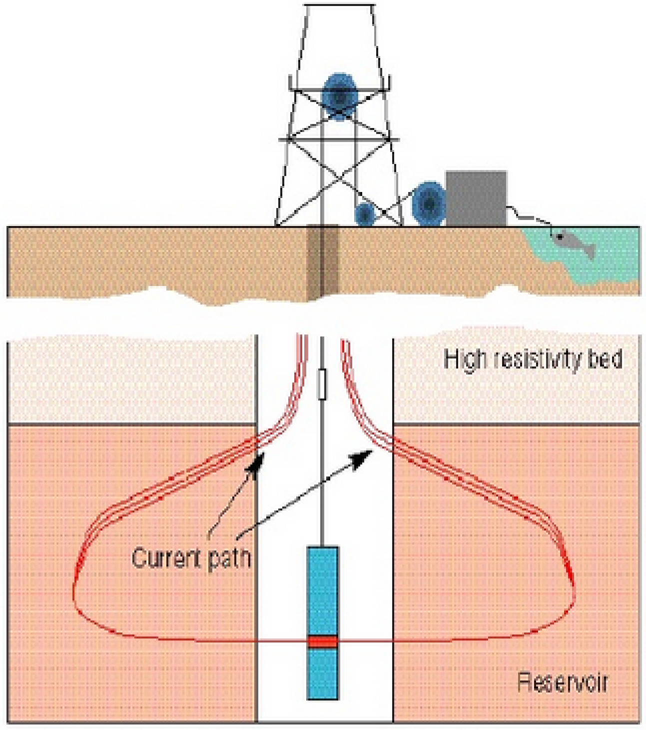

- Caused by highly resistive beds overlying the formation that is being measured.
- This forces the deep current into the mud column.
- This is caused by the voltage reference (cable-torpedo) becoming non-zero.
- LLd reads too high
- More pronounced at low resistivity

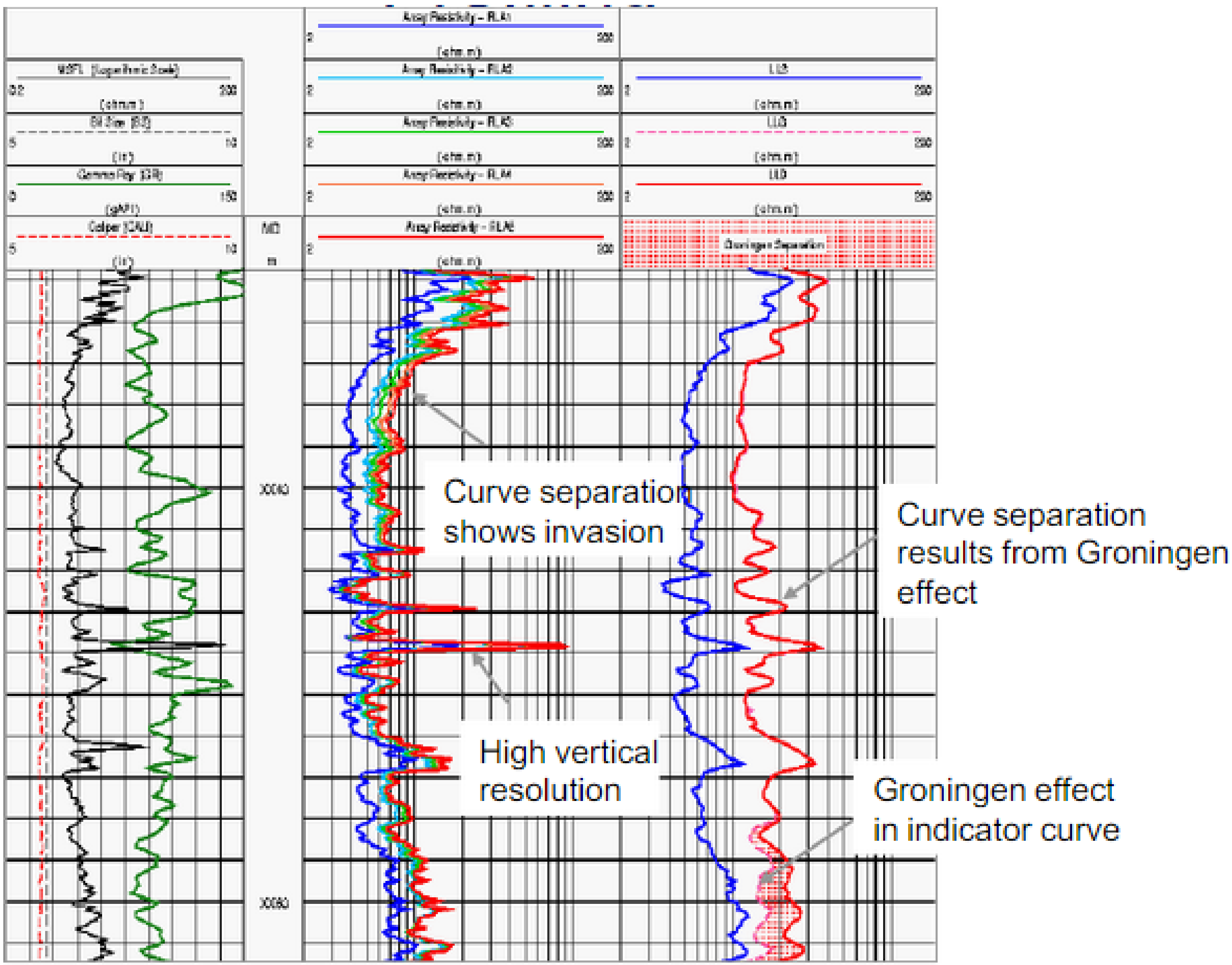

HRLA tool **DLL tool**

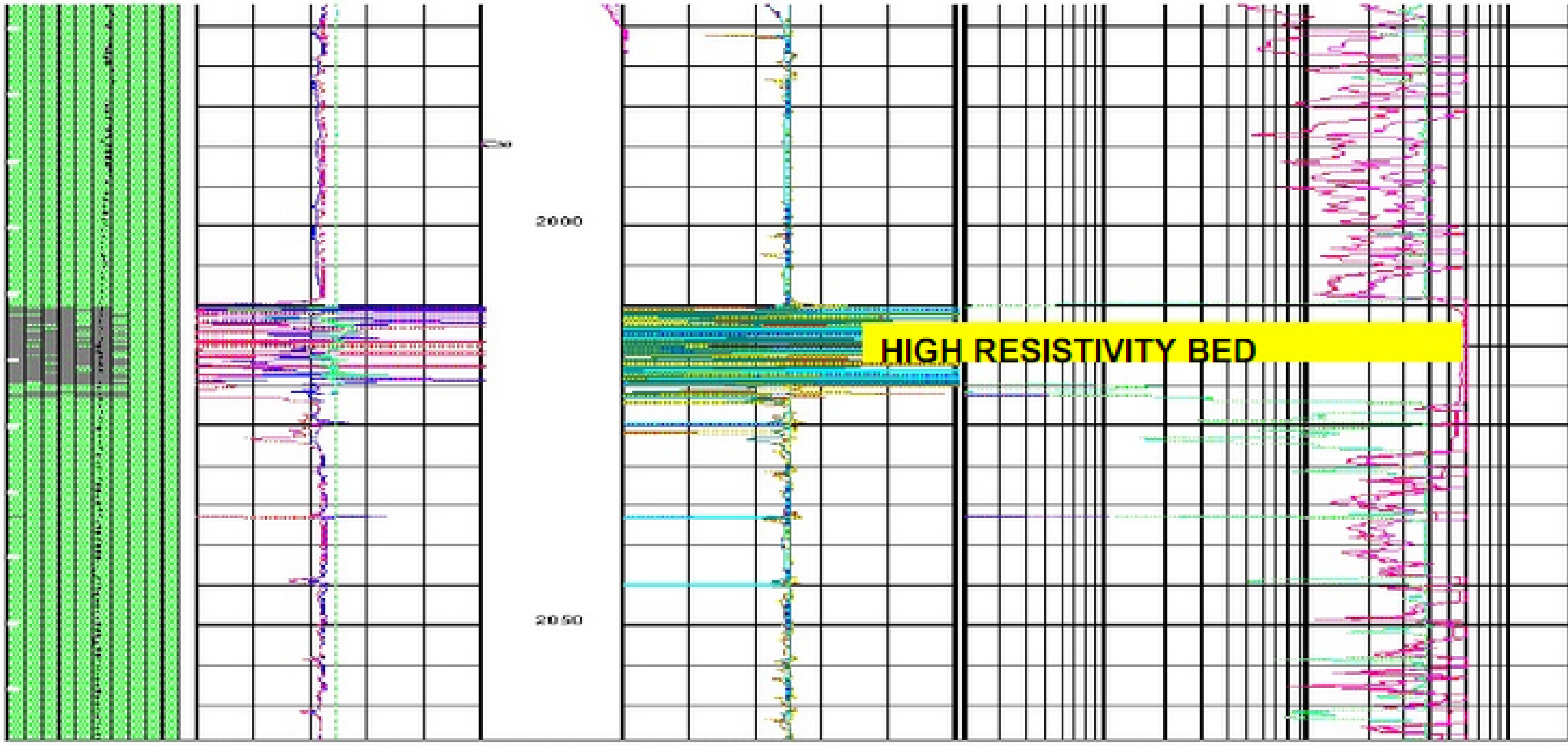
2000
2050
HIGH RESISTIVITY BED

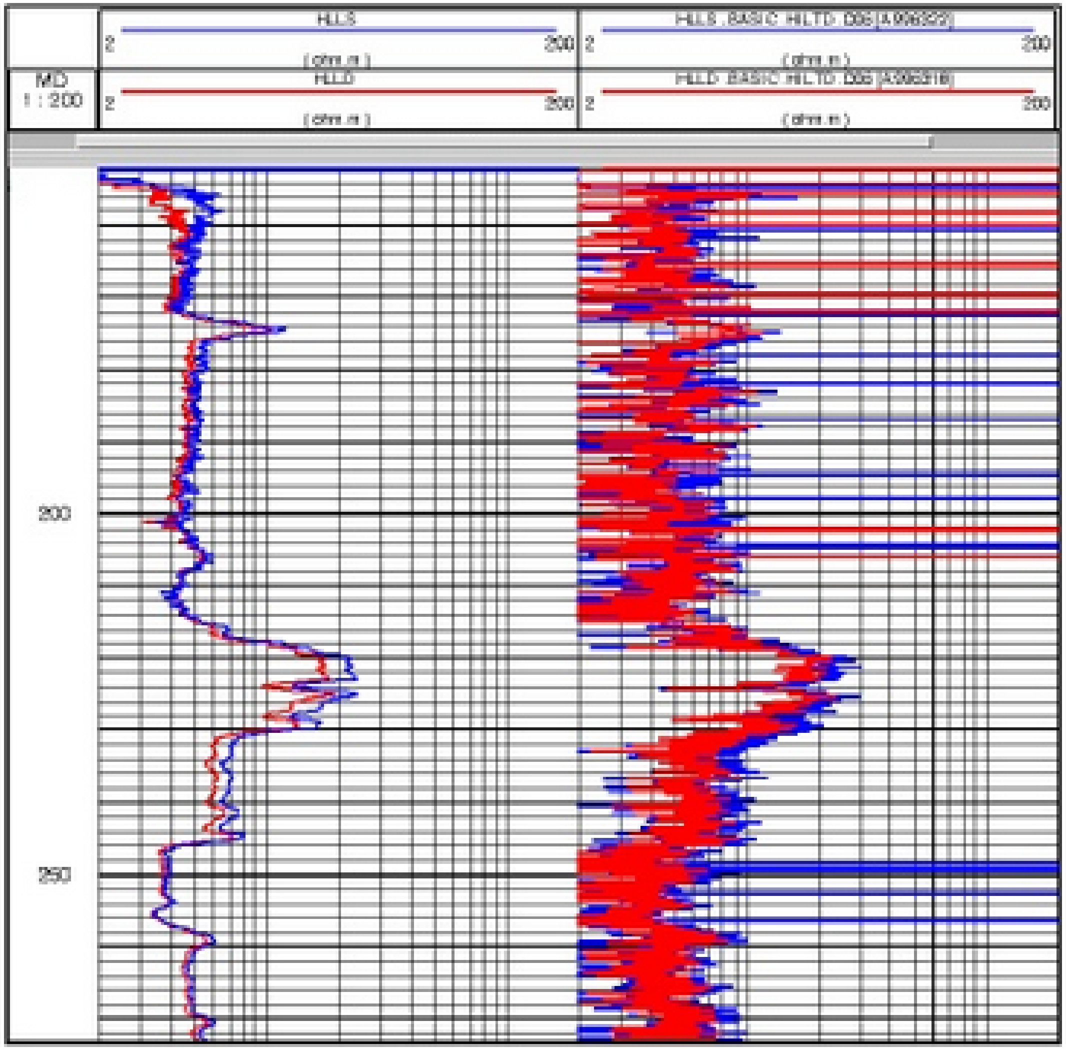

Rig Generator OFF Rig Generator ON

$$S_w = \sqrt[n]{\frac{aR_w}{\varphi_{eff}^{m} R_t}}$$

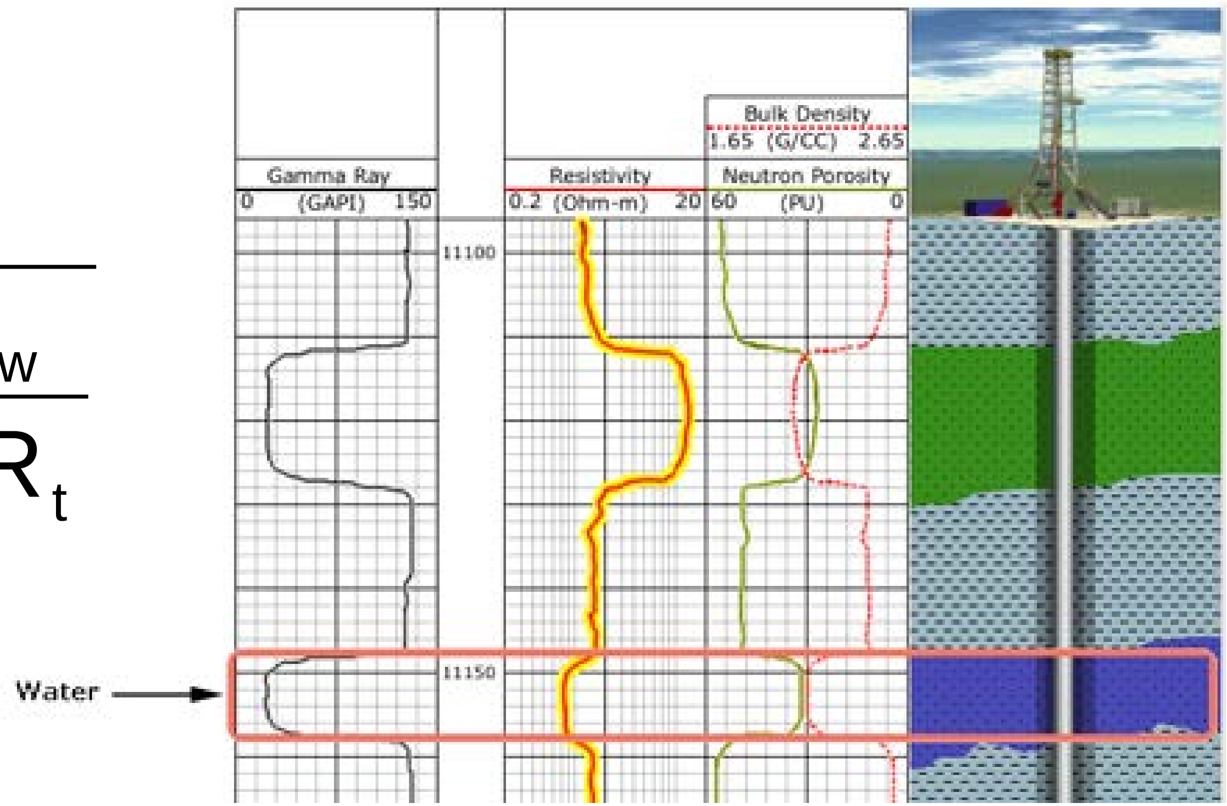

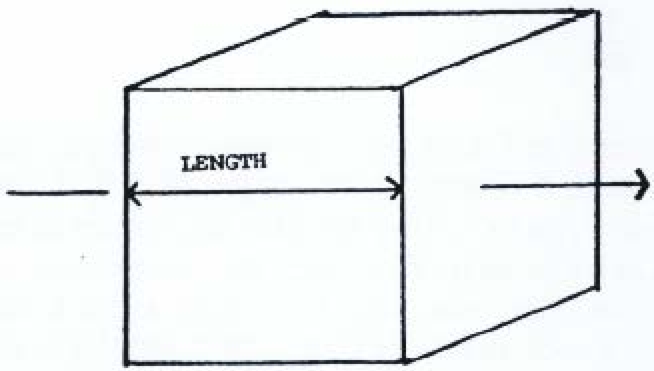

$$r = \frac{R \times L}{A}$$

Figure 4-12. Illustration of ionic current through an unimpeded path.

where R = resistivity of the water
r = resistance of the cube
L = length of the cube
A = area of the cube perpendicular to the direction of measurement, L

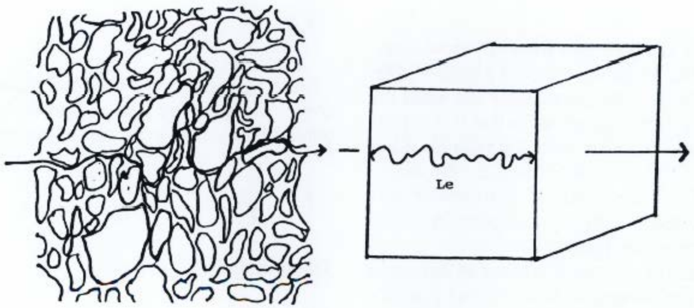

Figure 4-13. Illustration of ionic current through a formation.

If R has a value of 0.05 ohm-meters and L and A are 1 meter, then the resistance of the sample is 0.05 ohms.

If we replaced some of the water with a cubic meter of rock composed of straight capillary tubes, the resistivity of the water and the length of the sample would not change. The rock matrix takes no active part in the conduction of ionic current, being for all practical purposes an insulator, so the total conducting

We see that reducing the conductive area of the sample's face effectively increases its resistance. The exposed conductive area of the sample just discussed is proportional to the porosity of the rock, and for our cubic meter, the equation may be restated as:

$$r = \frac{R \times L}{\Phi}$$

Formation factor =

$$\frac{\text{resistivity of rock saturated with fluid}}{\text{resistivity of the saturating fluid}}$$

or

$$F = \frac{R_o}{R_w}$$

R_o, the resistivity of the fluid saturated rock, was given by the expression:

$$r = \frac{R \times L_e}{\Phi}$$

and R_w, the resistivity of the saturating fluid, was given by:

$$r = \frac{R \times L}{A}$$

Thus

$$F = r \times L_e/\Phi/r \times L/A = \frac{A \times L_e}{\Phi \times L}$$

The area of the cube is one meter, so our expression for F now becomes:

$$F = \frac{(L_e/L)}{\Phi}$$

Porosity can also be expressed in terms of formation factor. By plotting formation factor versus porosity determined from laboratory data for many different rocks and reducing to equations the curves generated on such graphs, a general relationship was found of the form:

$$F = \frac{a}{\Phi^m}$$

The values a and m in this expression relate porosity to F in much the same manner as the ratio (L_e/L) related resistivity to F. They describe the texture of the rock. The value m is often called the cementation exponent, since its value tends to increase as the extent to which a rock is cemented increases, but this is not the only factor controlling its value. Both a and m depend upon properties of the original sediment, and upon whatever processes converted the sediment to rock. The values of a and m will vary from one rock to the next.

This is the so-called *Archie Equation*, named after G.E. Archie, an early pioneering analyst. It works well in carbonate reservoirs, whose porosity and permeability are mainly secondary.

$$F = \frac{0.62}{\Phi^{2.15}}$$

The *Humble Equation*, mainly the work of W.O. Winsauer and his colleagues, adequately describes sandstones and other granular structures whose porosity is mainly primary. Because of earlier calculating tools incapable of handling the complex power of the Humble Equation, a simple version of it yields similar values. This is the *Tixier Relationship*:

$$F = \frac{.81}{\Phi^2}$$

To relate these rather idealized models to the resistivities measured by well logs of real rock/fluid systems, let us return to an earlier expression:

$$F = \frac{R_o}{R_w}$$

Transposing it:

$$R_o = FR_w$$

as R_{wa}, or apparent water resistivity. We may now state:

$$R_t = FR_{wa}$$

where R_t = the system resistivity recorded by the log

Hydrocarbon presence in the rock pores serves to increase the measured value of R_t by increasing the length L_e of the ionic path. Oil and gas behave exactly as the rock matrix does in their effect on conductivities, i.e., they are insulators. Normally hydrocarbons exist in the rock pores as suspended droplets, acting like fine grains of rock inserted in the spaces between the larger grains. The apparent resistivity of the water in the pore space increases, as it has been shown that F is independent of fluid resistivities.

Calculating Water Saturation

Earlier we sought to calculate water saturation by comparing the resistivity of a zone to an idealized resistivity of the same rock containing only water. This poses certain difficulties, as logs do not directly measure R_o. Short of actually sampling the rock and its fluids some means must be found to determine R_o from the logs. Recalling two of our earlier statements:

$$S_w \propto \frac{R_o}{R_t} \text{ and } R_o = FR_w$$

By substituting:

$$S_w \propto \frac{FR_w}{R_t}$$

F may be found from a porosity log and the appropriate F-Φ relationship. R_w may be obtained by measuring produced samples or calculating it from the SP. R_t, of course, is directly measured by the logging instruments. We have a workable means of calculating the ratio R_o/R_t. But in what way is it proportional to S_w? Archie showed that the constant of proportionality, for resistivity comparisons, is a power of S_w by reducing graphs of measured laboratory data to equations. The relationship becomes:

$$S_w^n = \frac{FR_w}{R_t}$$

where n, the constant of proportionality, is the resistivity index exponent, commonly referred to as the saturation exponent.

In totally oil wet rocks, n can have a value as high as 3.0, 4.0, or greater. Such rocks are extremely rare. In water-wet rocks, n has a value of 2.0. In shaly uncompacted coastal sands, it has a value of 1.8. These two values will suffice for virtually all situations.

The use of n as a basis of comparison works equally well for other resistivity contrasts. Since we know that $R_o = FR_w$ and $R_t = FR_{wa}$, substituting these expressions for R_o and R_t enables us to say:

$$S_w^n = \frac{R_w}{R_{wa}}$$

The quantity R_{wa}, although not directly measured, is commonly computed by the surface computer and printed directly on the log as an auxiliary curve. It is computed using the equation:

$$R_{wa} = \frac{R_t\Phi^m}{a}$$

Obviously, we must have both a resistivity and a porosity log in addition to some feel for the appropriate values of a and m in order to perform the computation.

The contrasts R_o/R_t and R_w/R_{wa} are useful in the field as a quick-look interpretation method for reducing the number of zones to consider. Clean salt water zones generally exhibit R_t and R_{wa} values lower than those found in shales. These R_t and R_{wa} values, when read in a water-bearing zone near the zone of interest, are arbitrarily assumed to be R_o and R_w. It is easily observed that when R_t and R_{wa} exceed three times the values of R_o and R_w, the calculated water saturations will be less than 60%. This is usually considered to be the upper limit of commercial producibility. Chapter 6 will cover the technique in greater detail.

- All water saturation determinations from resistivity logs in clean (nonshaly) formations with homogeneous intergranular porosity are based on Archie's water saturation equation, or variations thereof. The equation is

$$S_w^n = \frac{F R_w}{R_t} \text{ ....(1)}$$

- Rw is the formation water resistivity, Rt is the true formation resistivity, and F is the formation resistivity factor. F is usually obtained from the measured porosity of the formation through the relationship

$$F = a / \phi^m \text{ ....(2)}$$

- For Sxo, the water saturation in the flushed zone, a similar expression exists:

$$S_{xo}^n = \frac{F R_{mf}}{R_{xo}}, \text{ ....(3)}$$

- where Rmf is the mud filtrate resistivity and Rxo is the flushed zone resistivity.

$$S_w = \sqrt[n]{\frac{aR_w}{\varphi_{eff}^{m} R_t}}$$

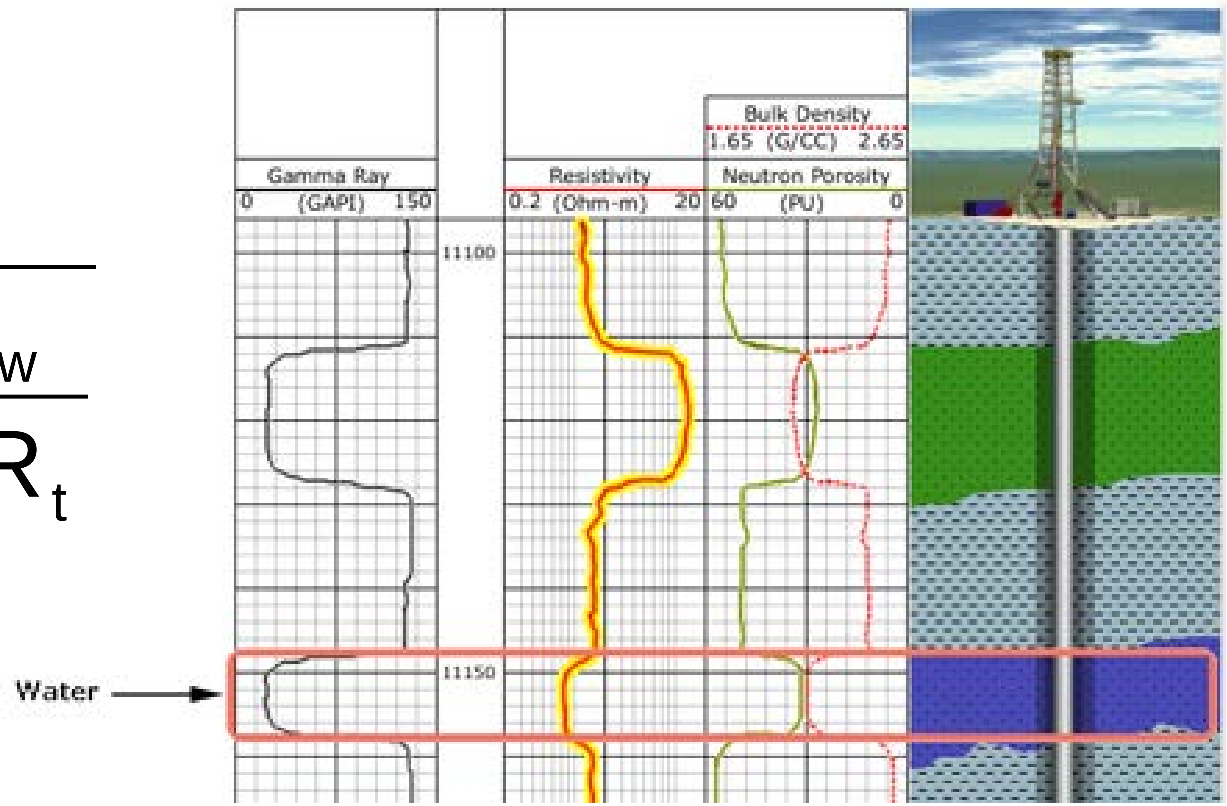

Why Do We Need to Know This?

- Determining R_t is not simple
- Many things prevent our tool from reading R_t:
  - Wellbore effects
  - Tool physics effects
  - Formation effects
- Curve separation can help us to determine R_t if we understand why the curves are reading different values.

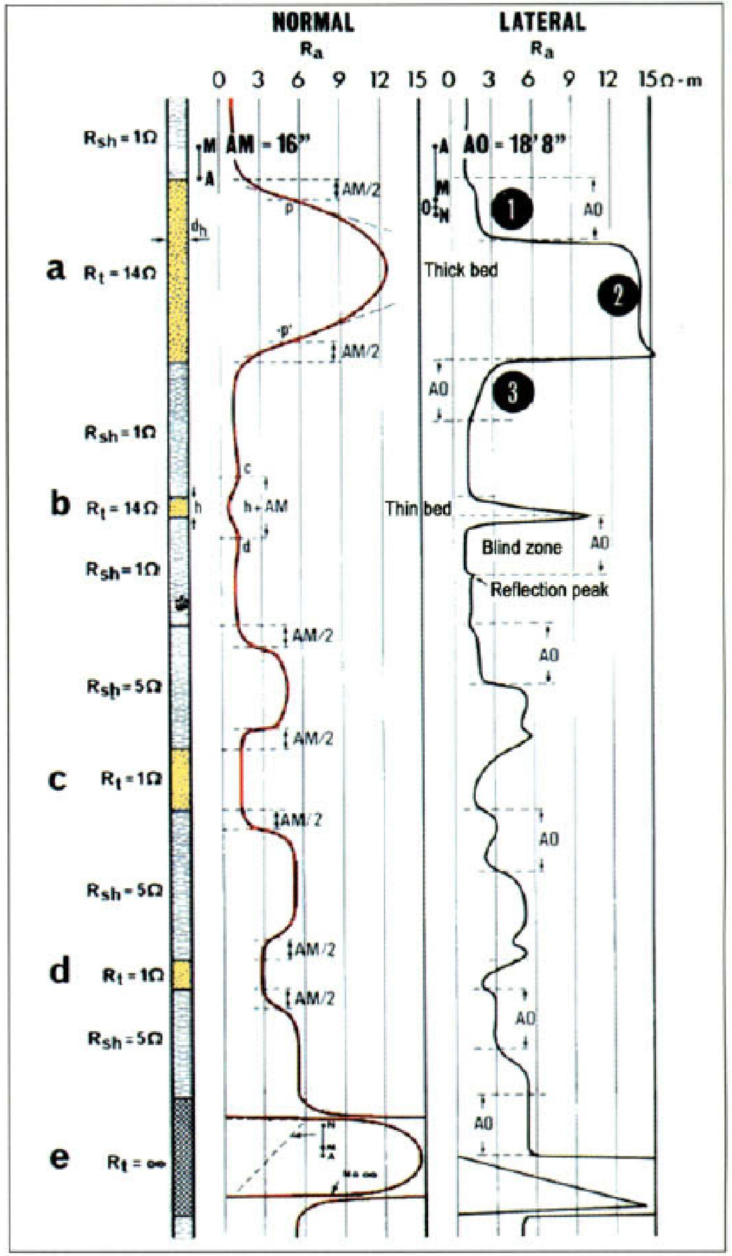

Figure 4-8 - The influence of bed-thickness and resistivities on the shapes of the lateral and normal responses.

چند نکته در نمودار مقاومت

1. در گل حفاری آب شیرین, مقاومت مخصوص گل حفاری بیشتر از آب سازند است. در زون آبدار مقاومت مخصوص ناحیه شسته شده نیز بیشتر از اب سازند است. با نزدیک شدن به ناحیه بکر مقاومت کاهش می یابد.

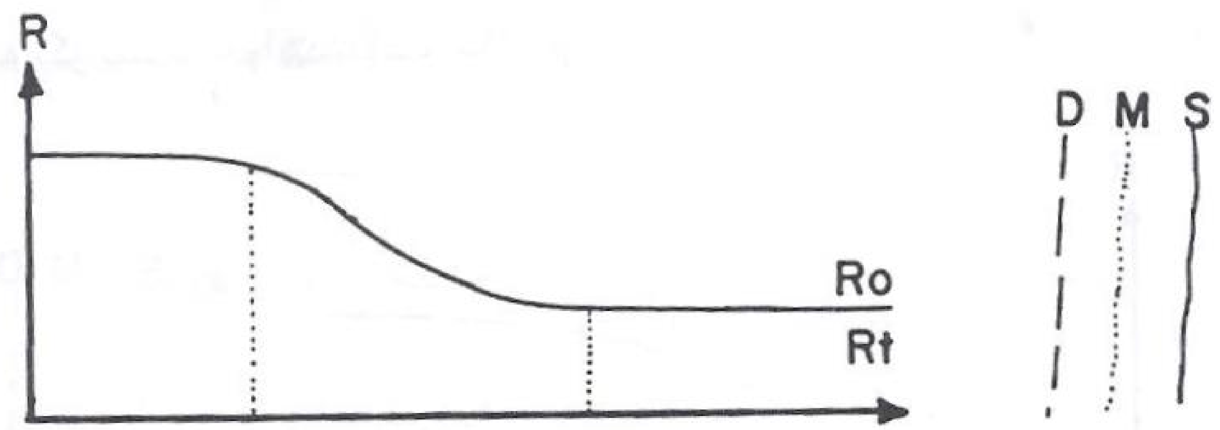

2. در زون هیدروکربور دار که با گل شیرین حفاری شده است, مقاومت مخصوص پشت زون شسته شده (ناحیه عبوری و بکر) ممکن است بیشتر یا کمتر باشد که بستگی به اشباع آب و مقاومت مخصوص آب سازند دارد.

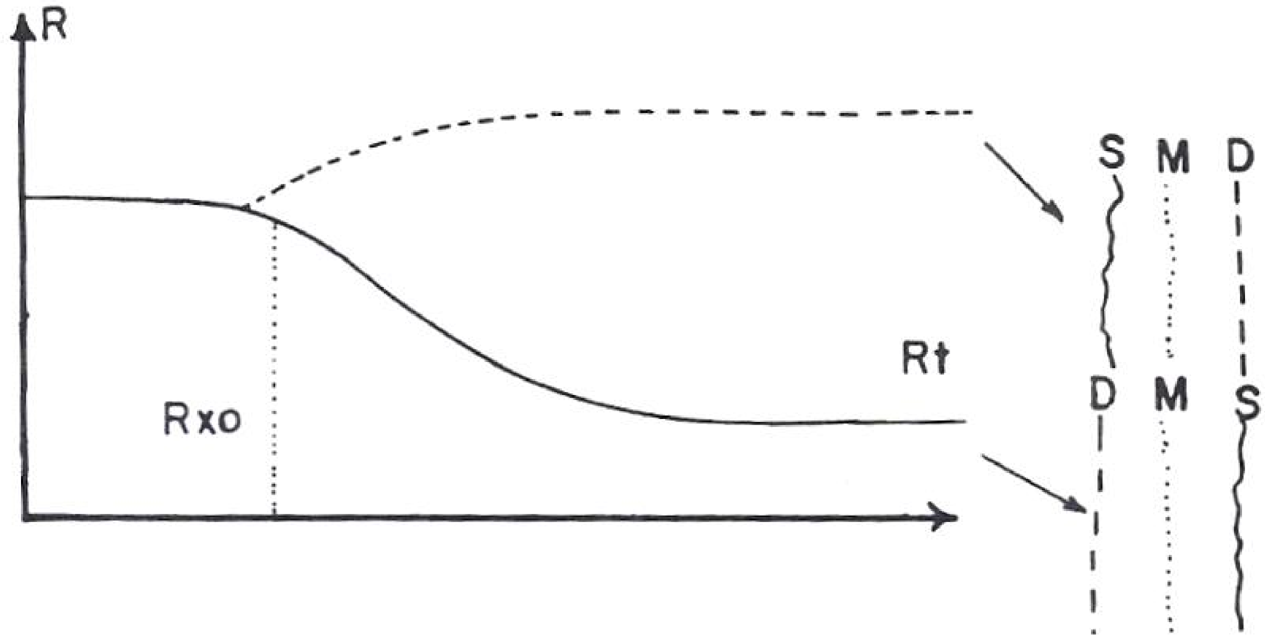

3. اگر با گل حفاری شور حفاری شده باشد. ناحیه شسته شده دارای مقاومت مخصوص کمتری از سایر قسمت ها می باشد. اگر سازند دارای آب باشد و مقاومت مخصوص آن نیز بیشتر از گل باشد در این صورت مقاومت مخصوص ناحیه بکر یا مساوی یا بیشتر از ناحیه شسته شده خواهد بود. در حالت دیگر اگر سازند دارای هیدروکربور باشد مقاومت ناحیه بکر بیشتر خواهد بود.

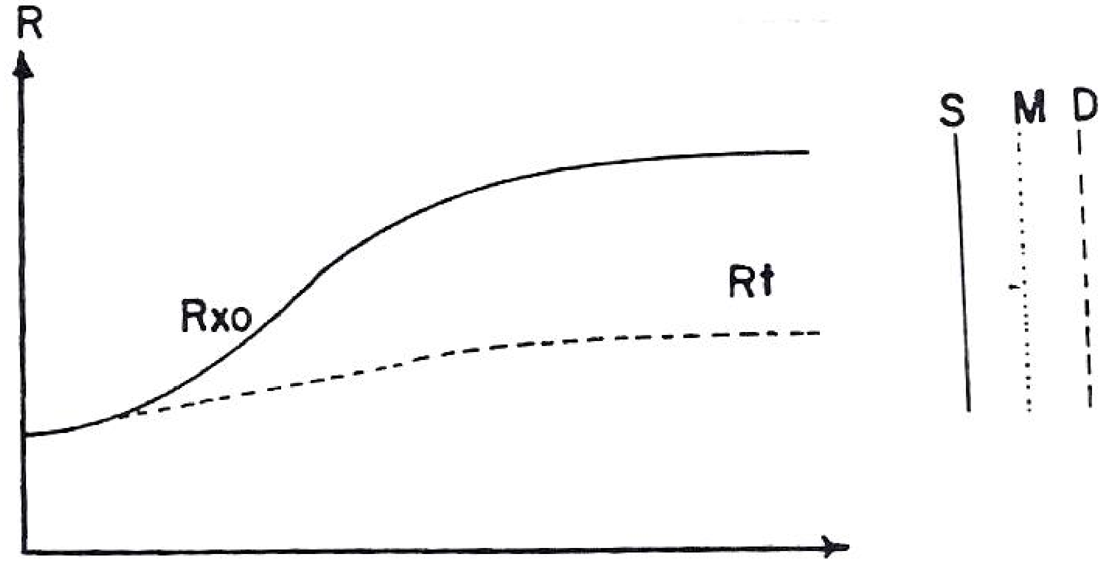

- تفسیر منحنی ها در حالتی سازند دارای هیدروکربور باشد (مقاومت مخصوص سیال سازند بیشتر از گل حفاری باشد) حالت های زیر قابل تفسیر است.

1. عدم نفوذ تراویده گل و یا نفوذ بسیار سطحی

قطر نفوذ < قطر چاه + ۲ اینچ

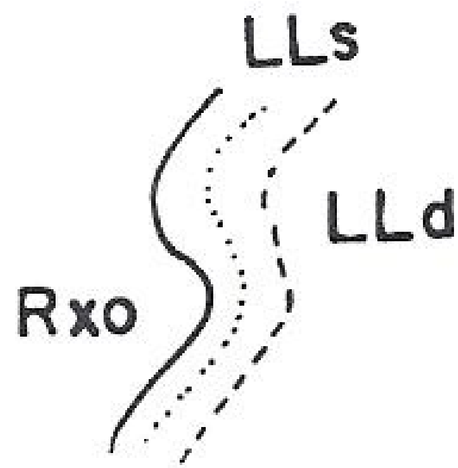

2. نفوذ متوسط تراویده گل به درون سازند

قطر چاه + ۲ اینچ < قطر نفوذ < ۴۰ اینچ

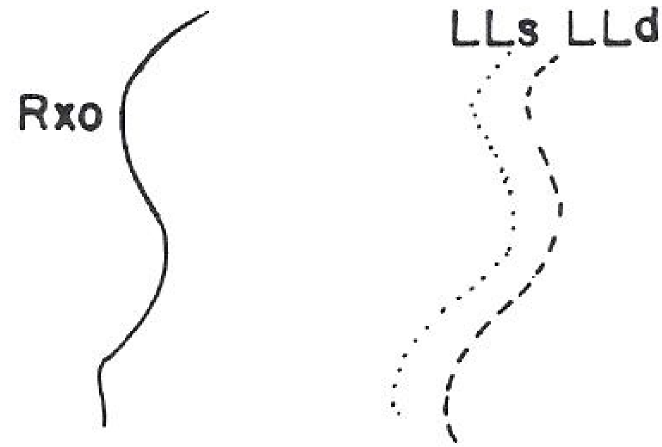

3. نفوذ عمیق تراویده گل به دورن سازند

۶۰ اینچ > قطر نفوذ > ۴۰ اینچ

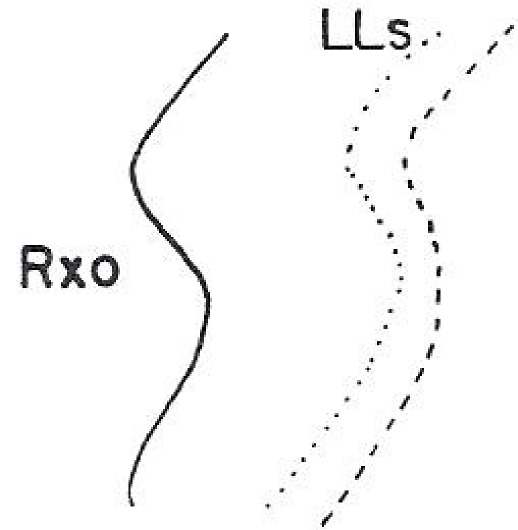

4. نفوذ بسیار عمق تراویده گل به درون سازند

۶۰ اینچ < قطر نفوذ

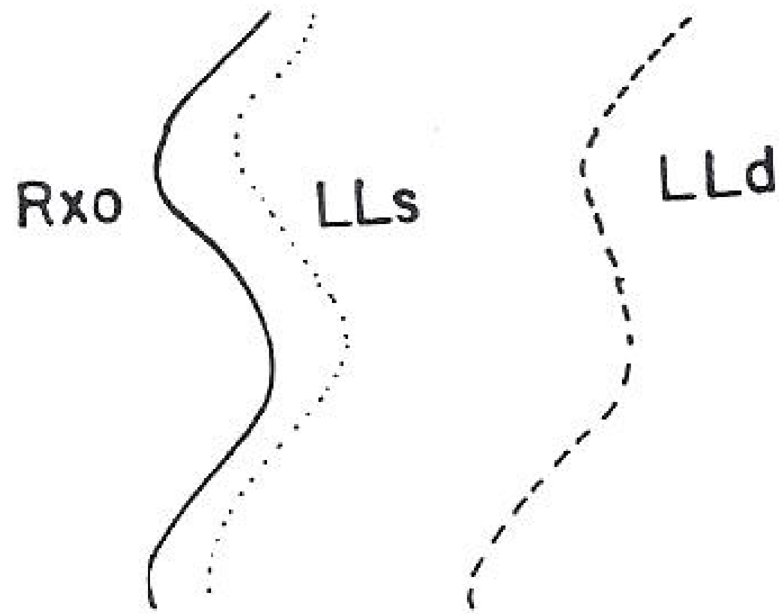

Induction Log

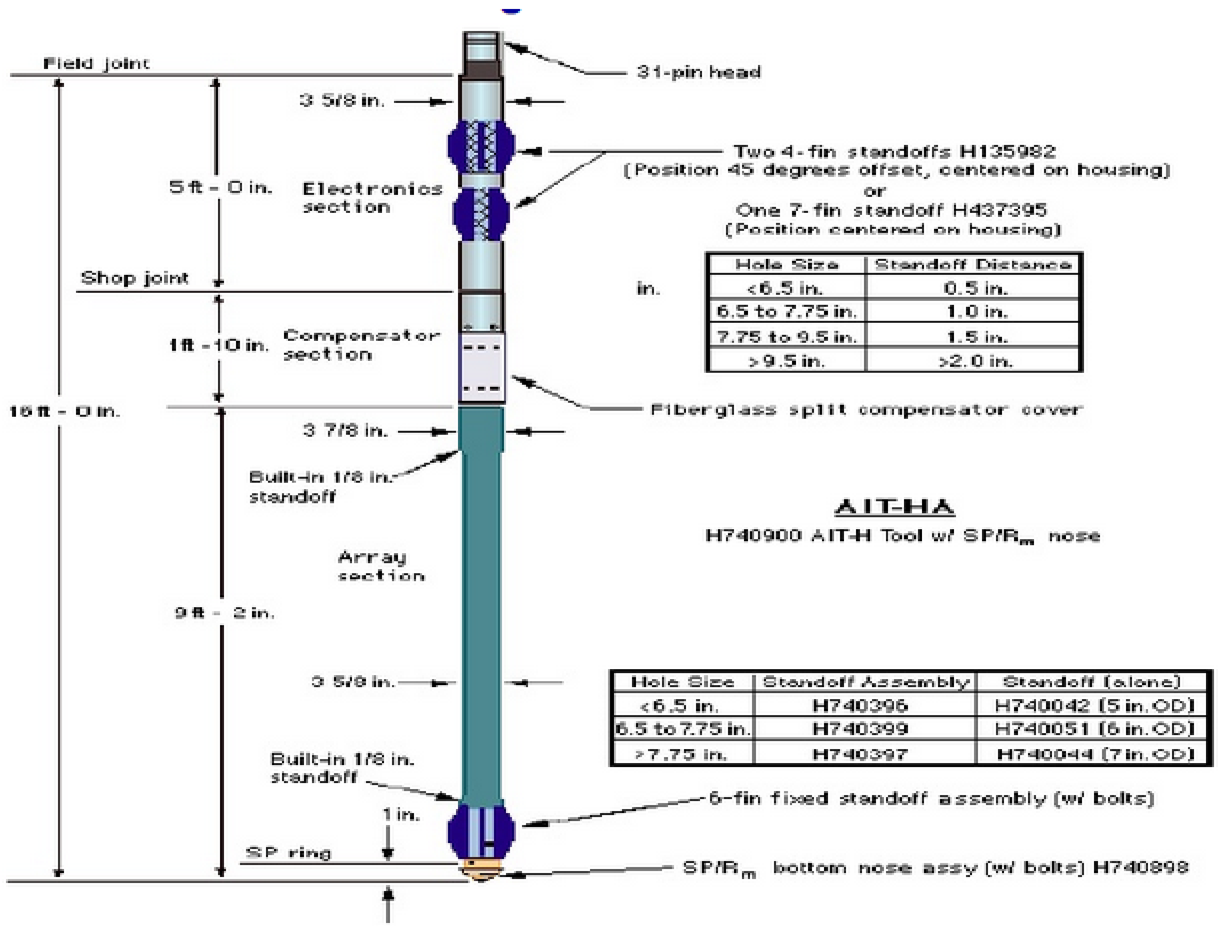

Hole Size	Standoff Distance
<6.5 in.	0.5 in.
6.5 to 7.75 in.	1.0 in.
7.75 to 9.5 in.	1.5 in.
>9.5 in.	>2.0 in.

Hole Size	Standoff Assembly	Standoff (alone)
<6.5 in.	H740396	H740042 (5 in. OD)
6.5 to 7.75 in.	H740399	H740051 (6 in. OD)
>7.75 in.	H740397	H740044 (7 in. OD)

Induction tools are based on principles of electromagnetic induction. A magnetic field is generated by an AC electrical current flowing in a continuous loop/transmitter coil. The magnetic field from the transmitter coil induces ground loop currents in the formation. These ground current loops will in turn have an associated alternating magnetic field which will induce a voltage in the receiver coil, the magnitude of which is proportional to the formation conductivity.

- It works in oil based muds and air filled holes where latero tool fails.
- Tool accuracy is excellent for formations having low to moderate resistivity (up to ~100 Ohm.m.
- The Dual Induction Latero (DIL) tool records three resistivity curves having different depths of investigation (ILD,ILM & LL3)

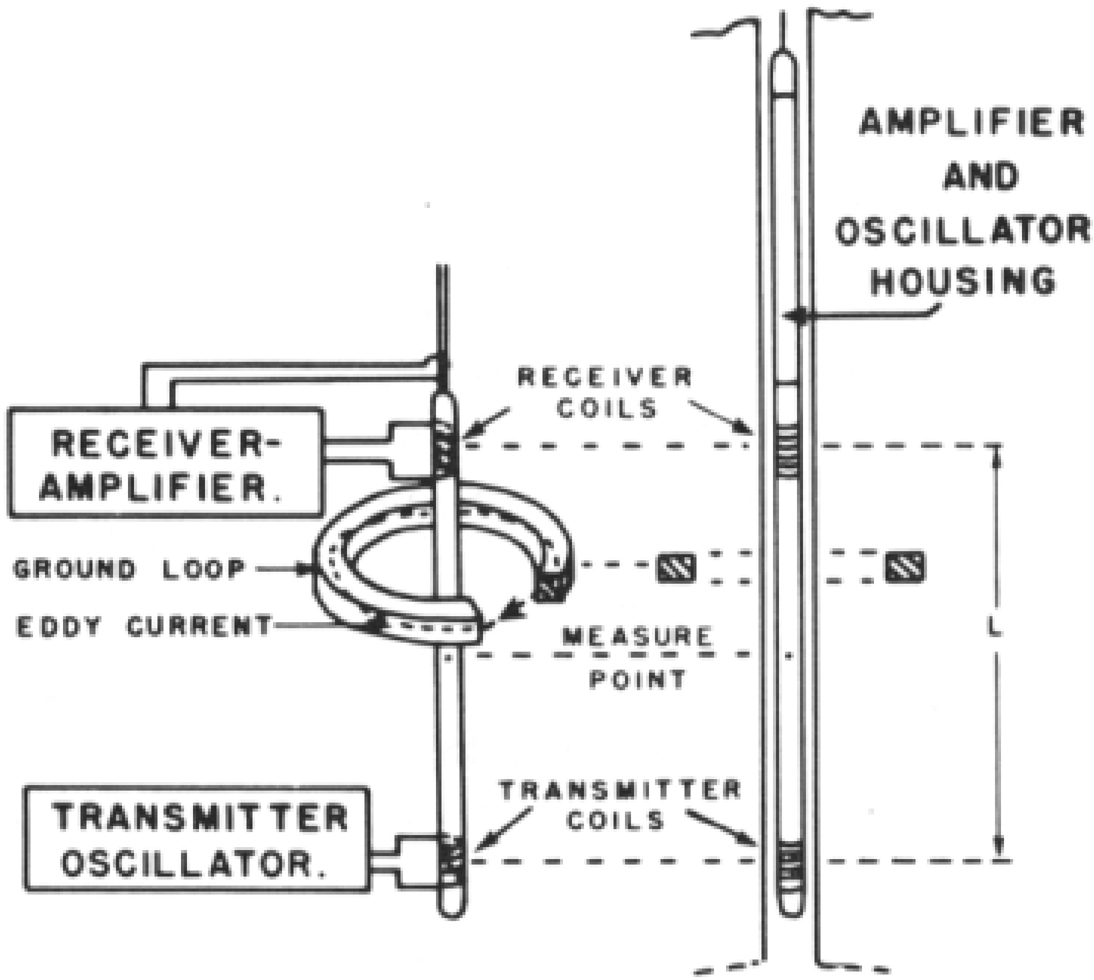

Induction Log Equipment

(Courtesy of Schlumberger)

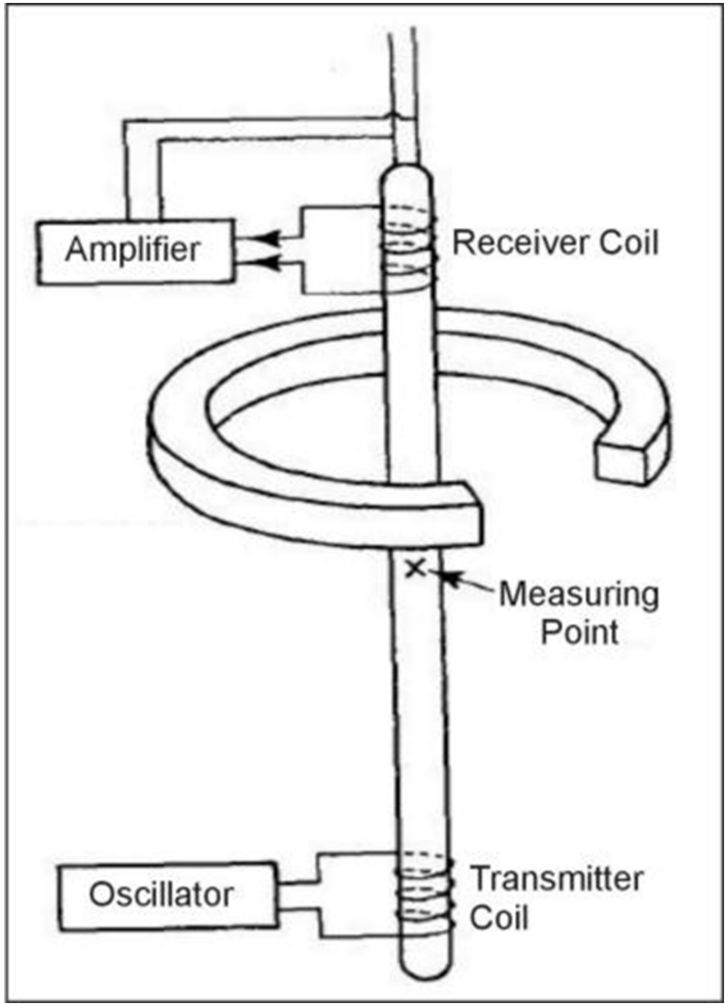

Amplifier
Receiver Coil
Measuring
Point
Oscillator
Transmitter
Coil

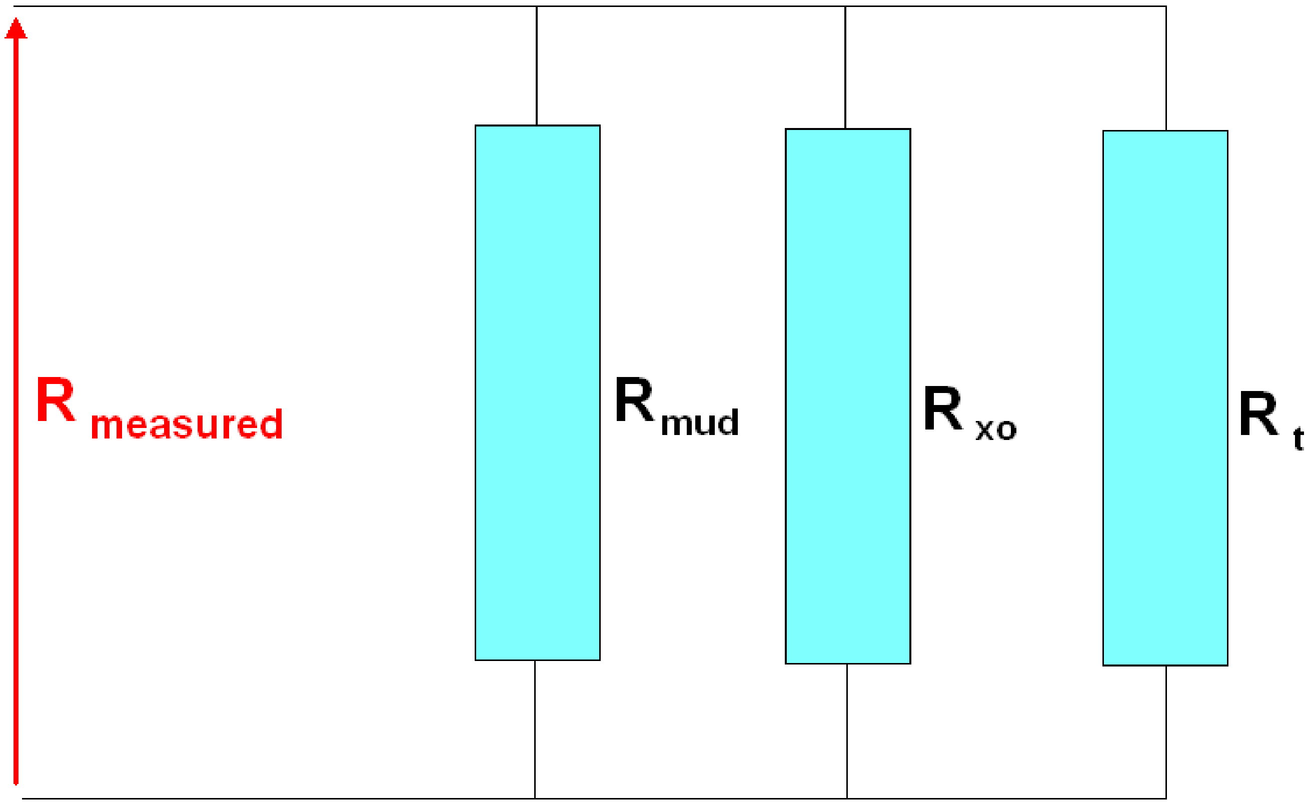

$$\frac{1}{R_{measured}} = \frac{1}{R_{mud}} + \frac{1}{R_{xo}} + \frac{1}{R_t}$$

Operating Range

- 0.1 to 2000 ohmm
- Moderate Rxo < Rt
- Rt/Rm <100 (with hole diameter considered)
- Large diameter holes with moderate Rt/Rm and moderate Rt

$$1/Ra = 1/(V_{Rm}(Rm)) + 1/(V_{Rmc}(Rmc)) + 1/(V_{rxo}(Rxo)) + 1/(V_{Rt}(Rt))$$

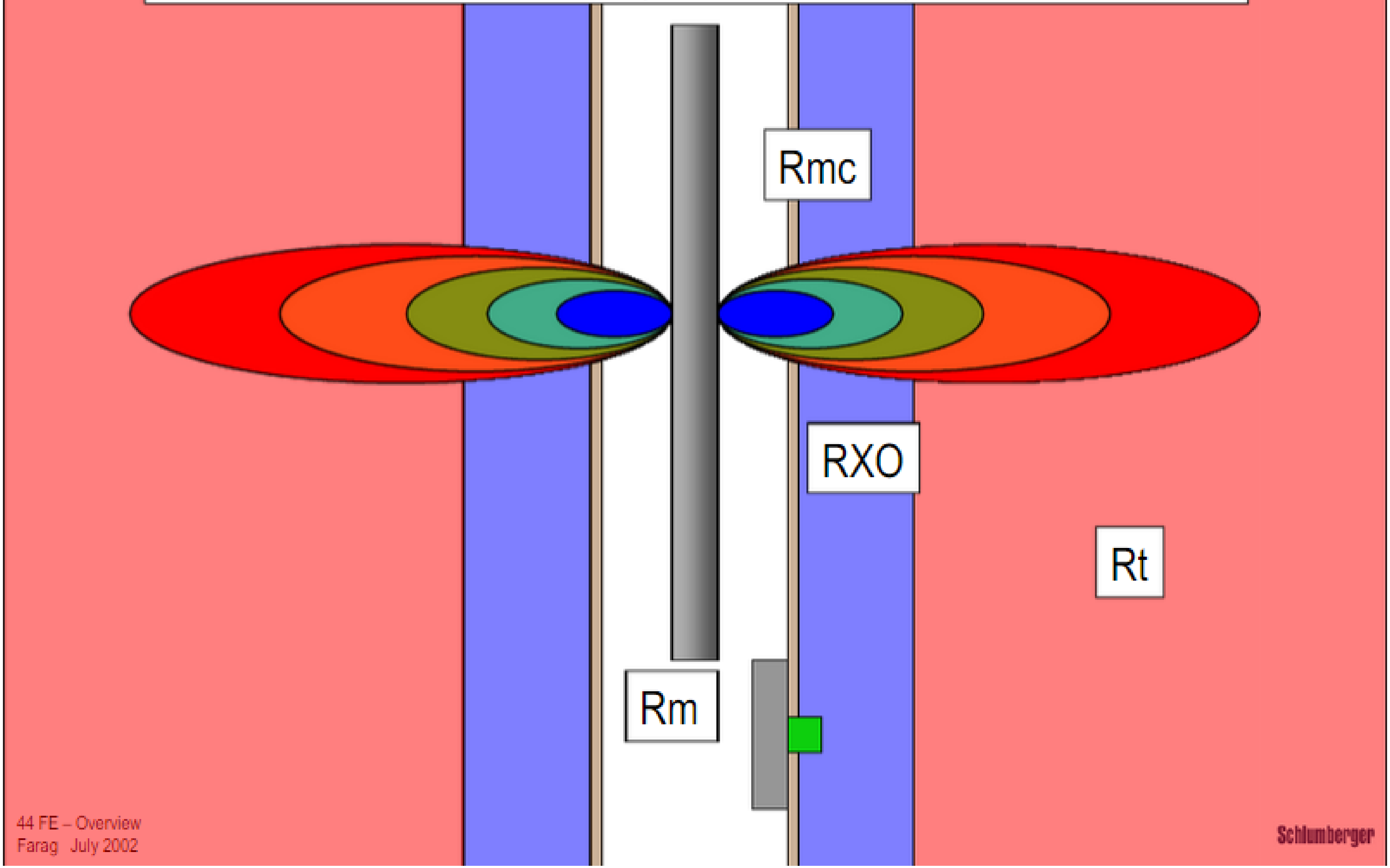

Resistivity : Induction

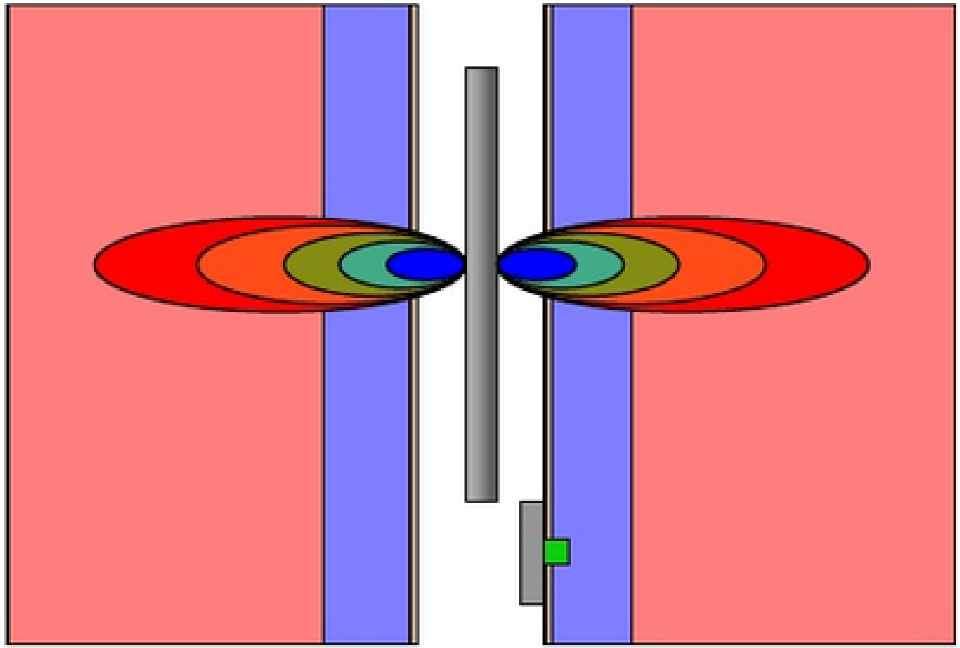

If Rmf < Rw, AT10 < 20 < 30 < 60 < 90
If Rmf > Rw, AT10 > 20 > 30 > 60 > 90

From the 5 curves Rt can be computed

Resistivity : Induction Focusing

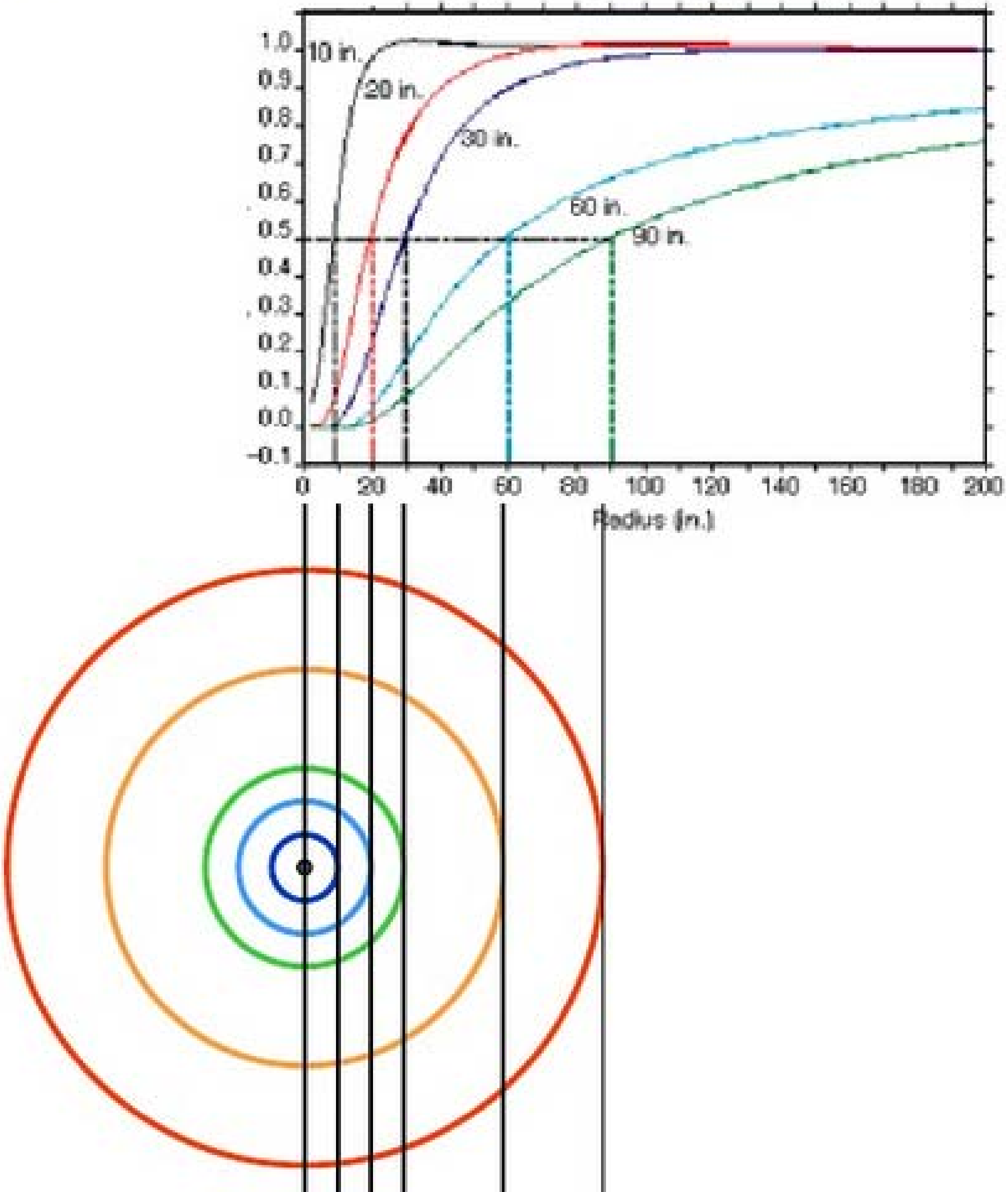

Resistivity : Induction

Hole size and shape

Uncertainty in hole size or mud resistivity can cause large errors on the shallow curves but much smaller errors on the deeper measurements

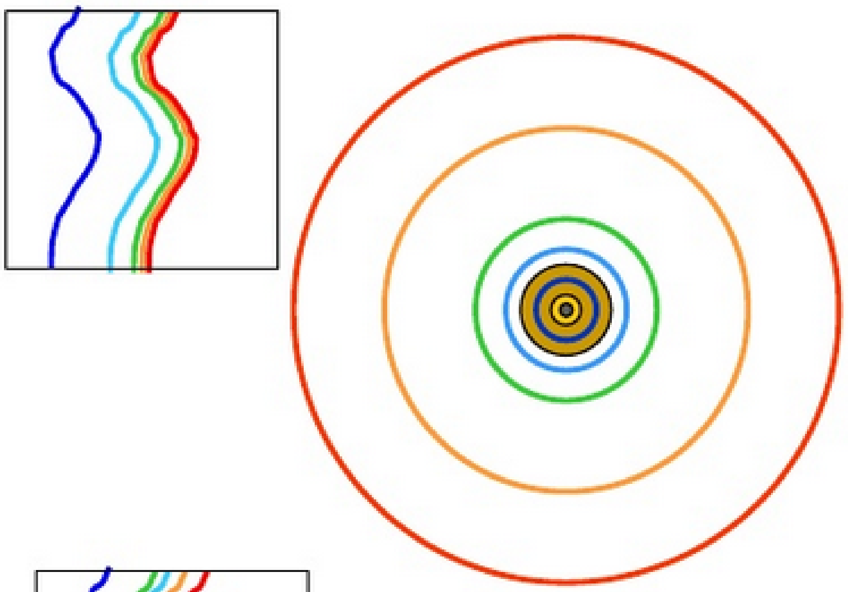

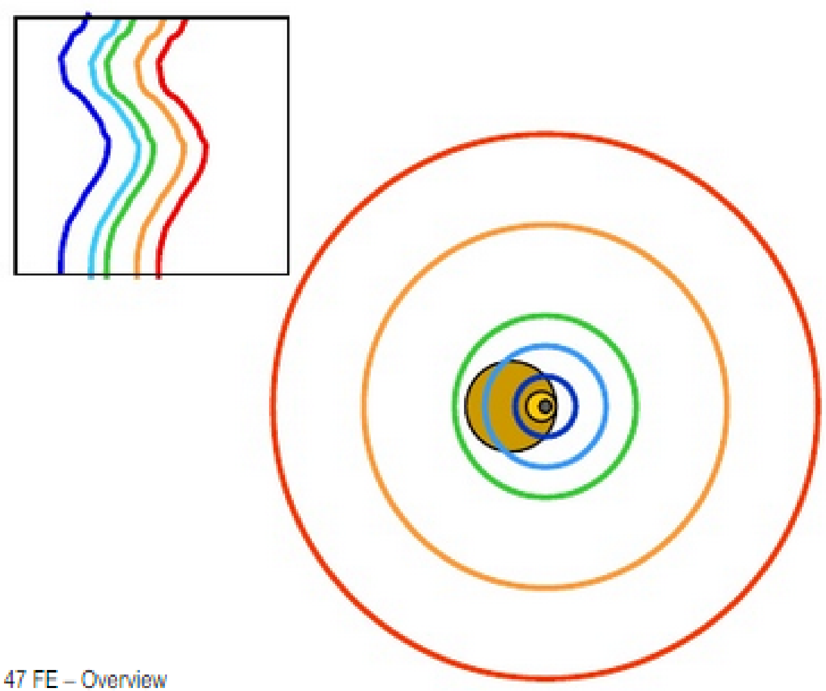

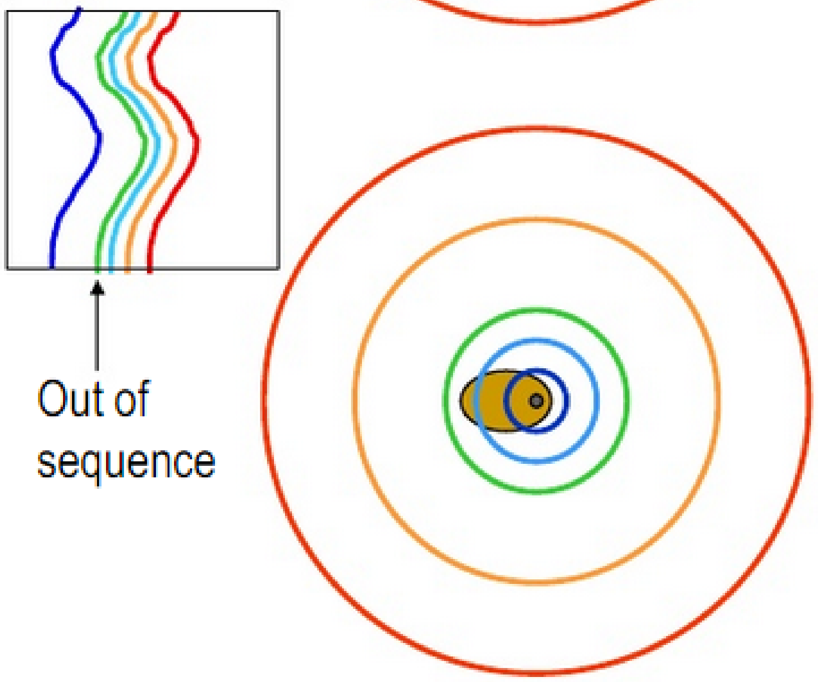

Resistivity : Induction Invasion

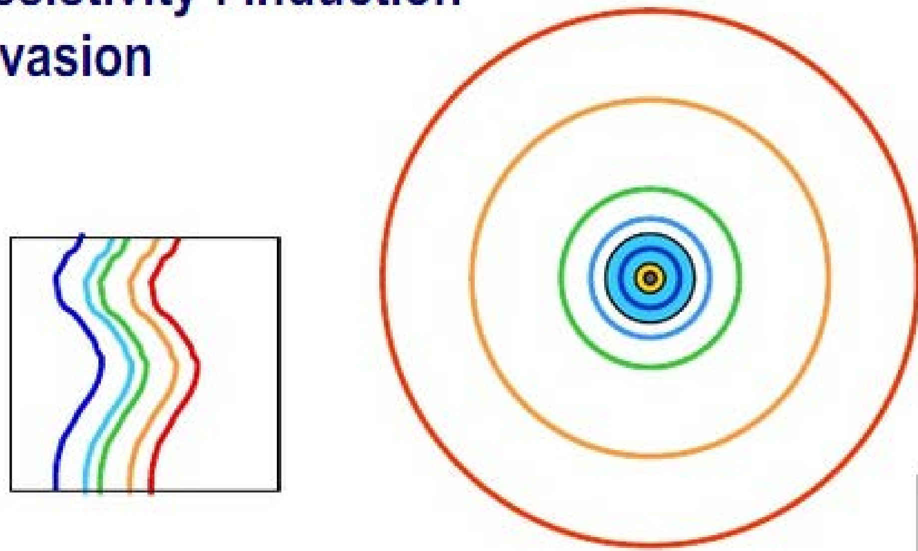

Very deep invasion can affect even the deepest measurements, non-cylindrical invasion may affect the Rt computation

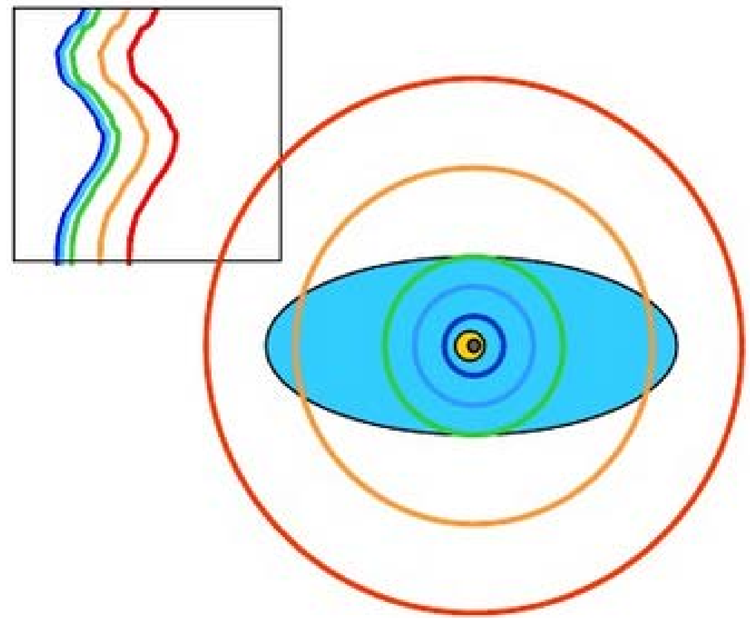

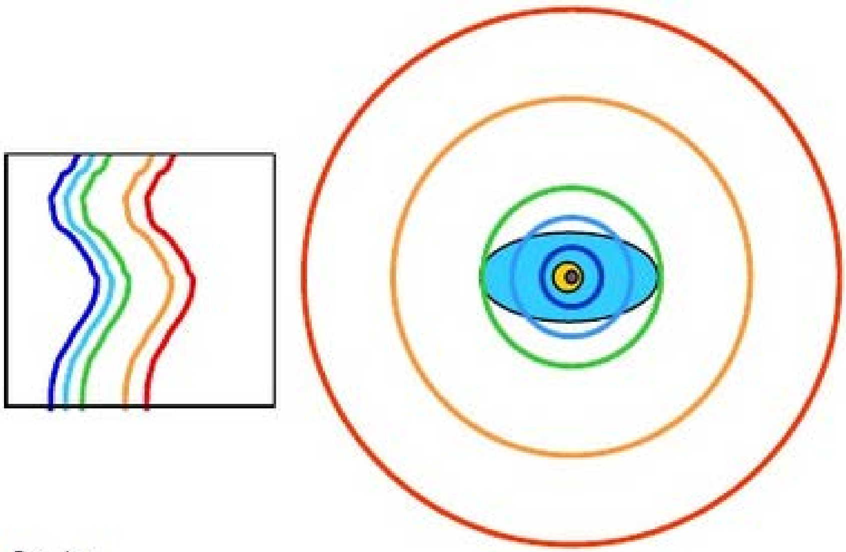

Induction Resistivity in Deviated Wells

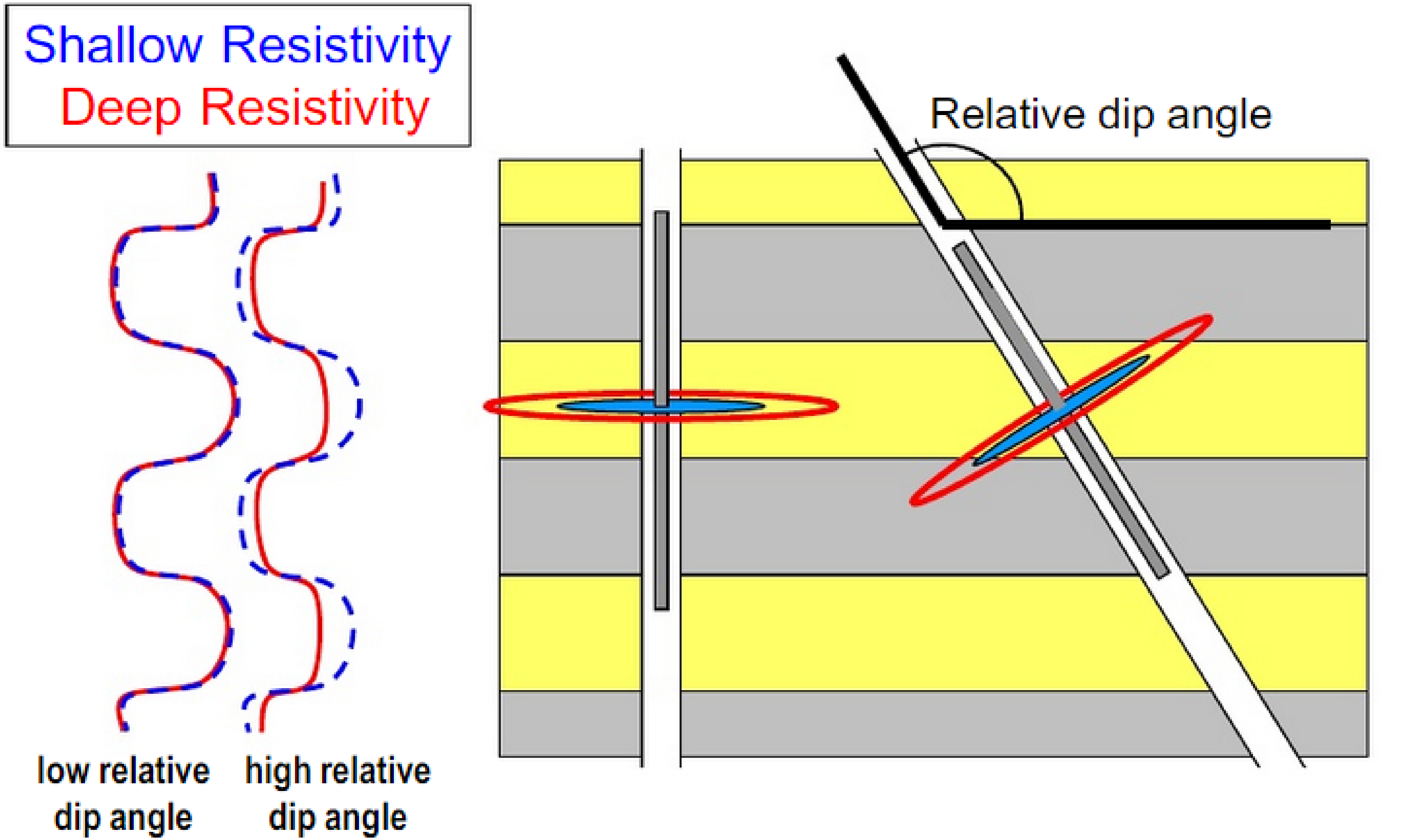

BS = 8”

Rt = 200

Rxo = 30

Rm = 0.1

S/O = 1.5”

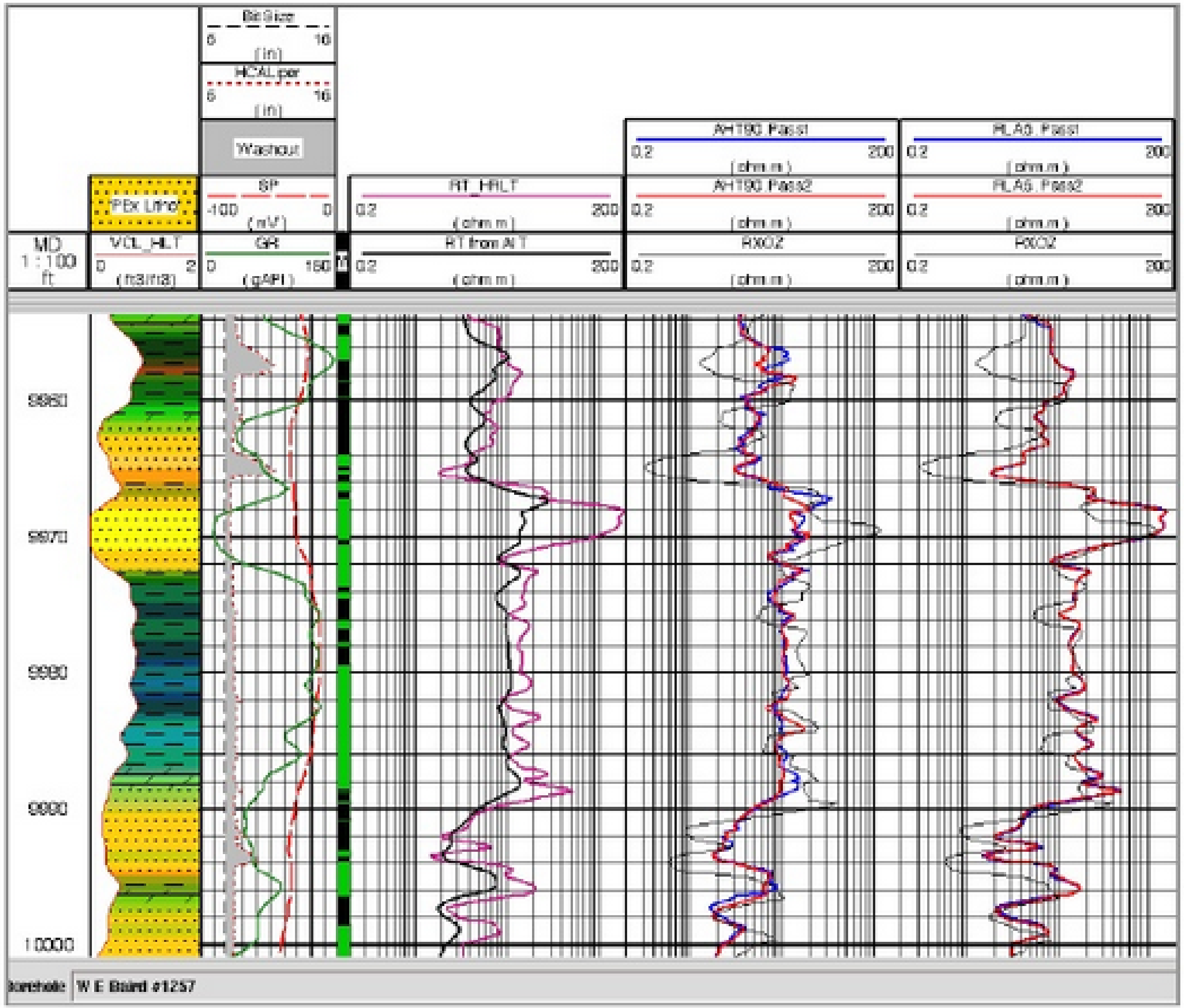

Well seismic surveying

مقدمه

- در لرزه نگاري معمولي ، فرستنده و گيرنده هردو در سطح زمين قرار دارند و اطلاعات مربوط به ساختار زمين را به اين وسيله شناسايي مي شود ، اما در لرزه نگاري درون چاهي منبع يا گيرنده و يا هردوي آنها در داخل چاه قرار مي گيرند و داده ها به اين روش بدست مي آيند.
- استفاده از لرزه نگاري درون چاهي اين امكان را به ما مي دهد كه يك فهم دقيق تري از مخزن در حين عمليات اكتشاف بدست آوريم.
- در زير انواع لرزه نگاري درون چاهي را مشاهده مي كنيد.

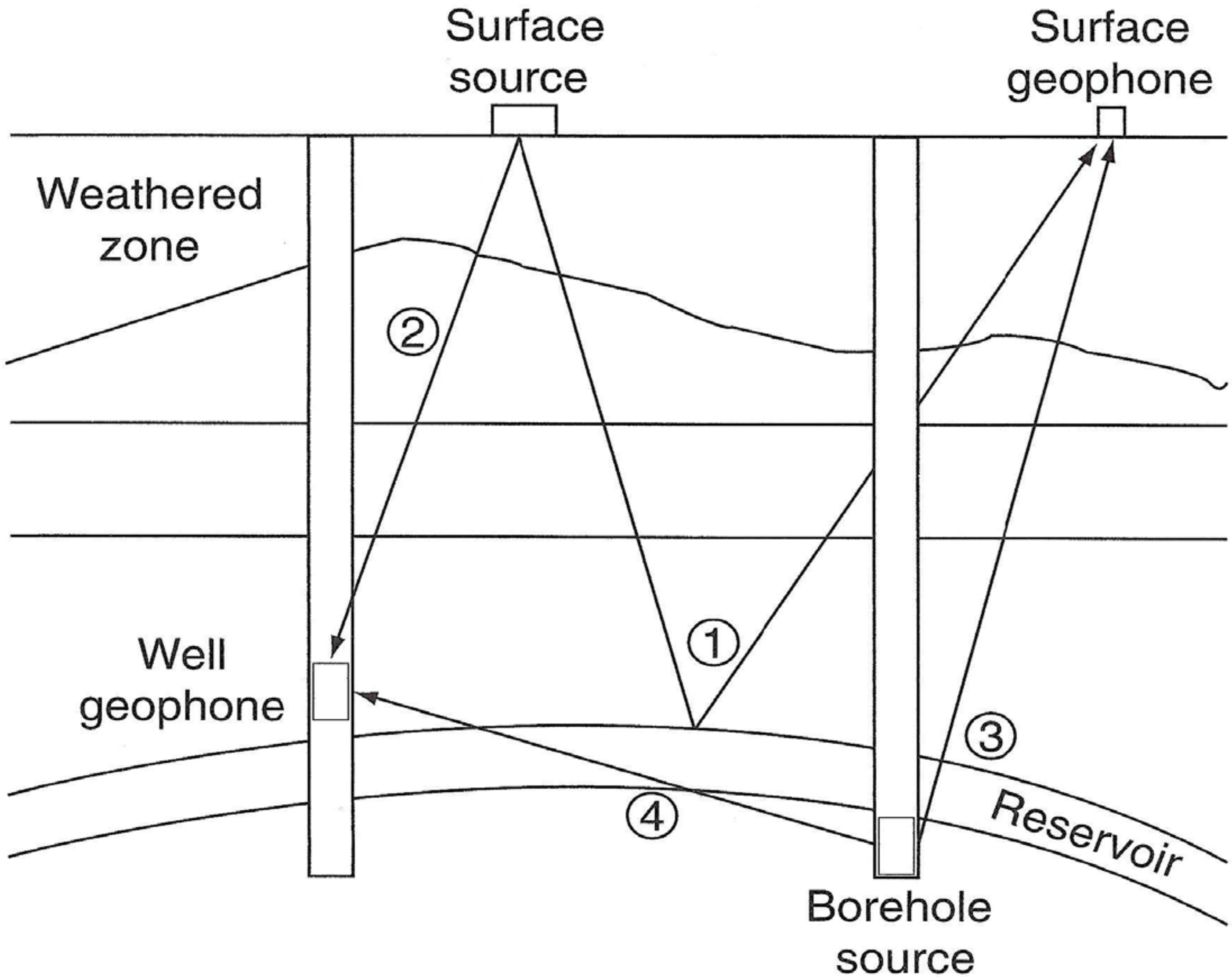
Surface
source
Surface
geophone
Weathered
zone
2
1
3
4
Well
geophone
Reservoir
Borehole
source

- در شکل قبل سه نوع لرزه نگاري درون چاهي را مشاهده مي كنيد كه عبارتند از:

1. شات در سطح و برداشت در چاه
2. شات در چاه و برداشت در سطح
3. شات در چاه و برداشت در چاه ديگر

Surface shot

- يك نوع از اين عمليات vertical seismic profile(VSP) مي باشد.
- در شكل اسلايد بعد مي توان يك نمونه از برداشت هاي VSP را مشاهده كرد ، در اين برداشت ها محور افقي ژئوفون ها در اعماق مختلف بوده و محور قائم زمان است.
- در VSP فاصله ي دو ژئوفون در چاه معمولا بين 3 تا 23 متر است.
- در VSP براي اين كه بتوان مساحت جانبي بيشتري را مورد بررسي قرار داد ، مي توان تعدادي شات با offsetهاي مختلف انجام داد و با افزايش offset ميزان جستجوي جانبي نيز افزايش مي يابد.

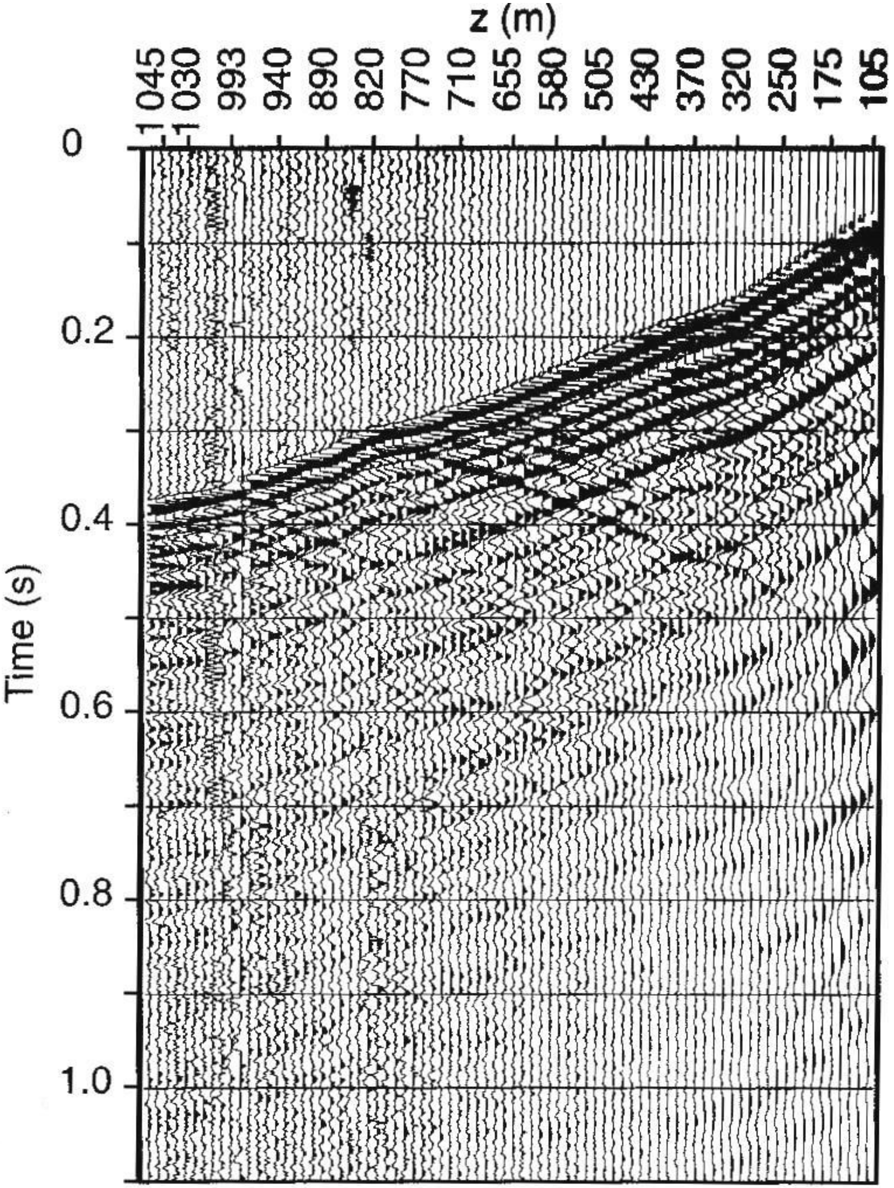
z (m)
1045
1030
993
940
890
820
770
710
655
580
505
430
370
320
250
175
105
Time (s)
0
0.2
0.4
0.6
0.8
1.0

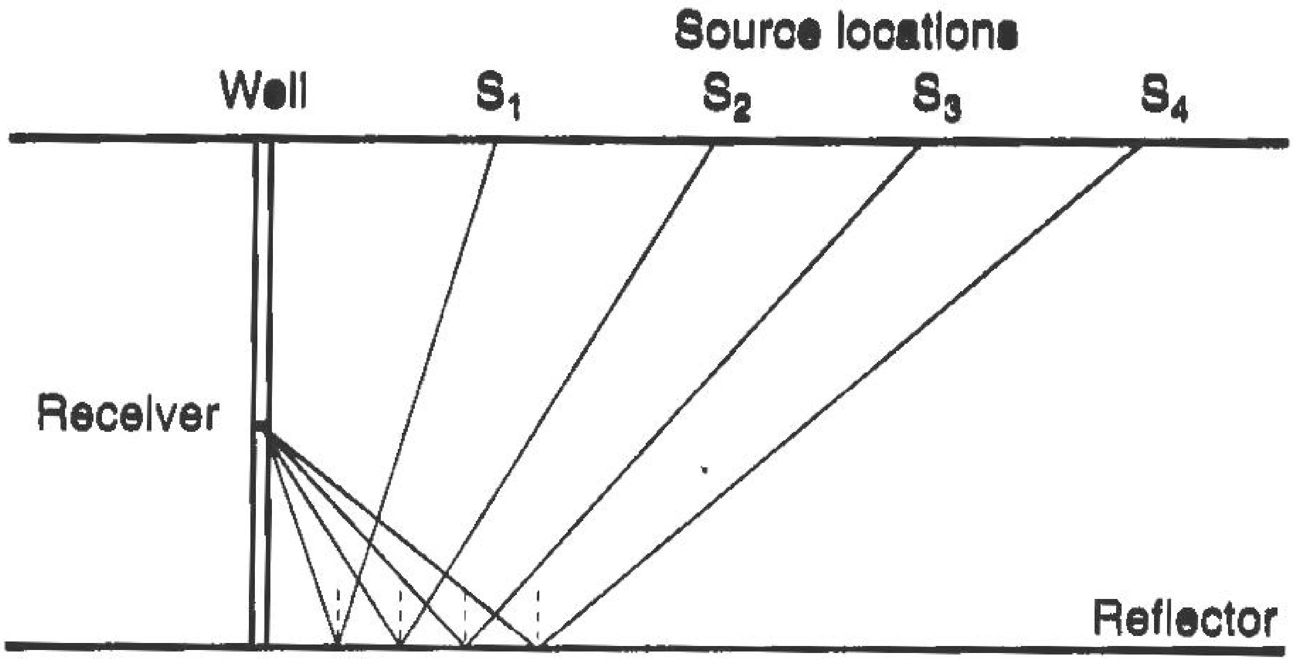
Source locations
Well
S_1
S_2
S_3
S_4
Receiver
Reflector

Shot in the well

- مسير شماره 3 در شكل زير مي باشد.

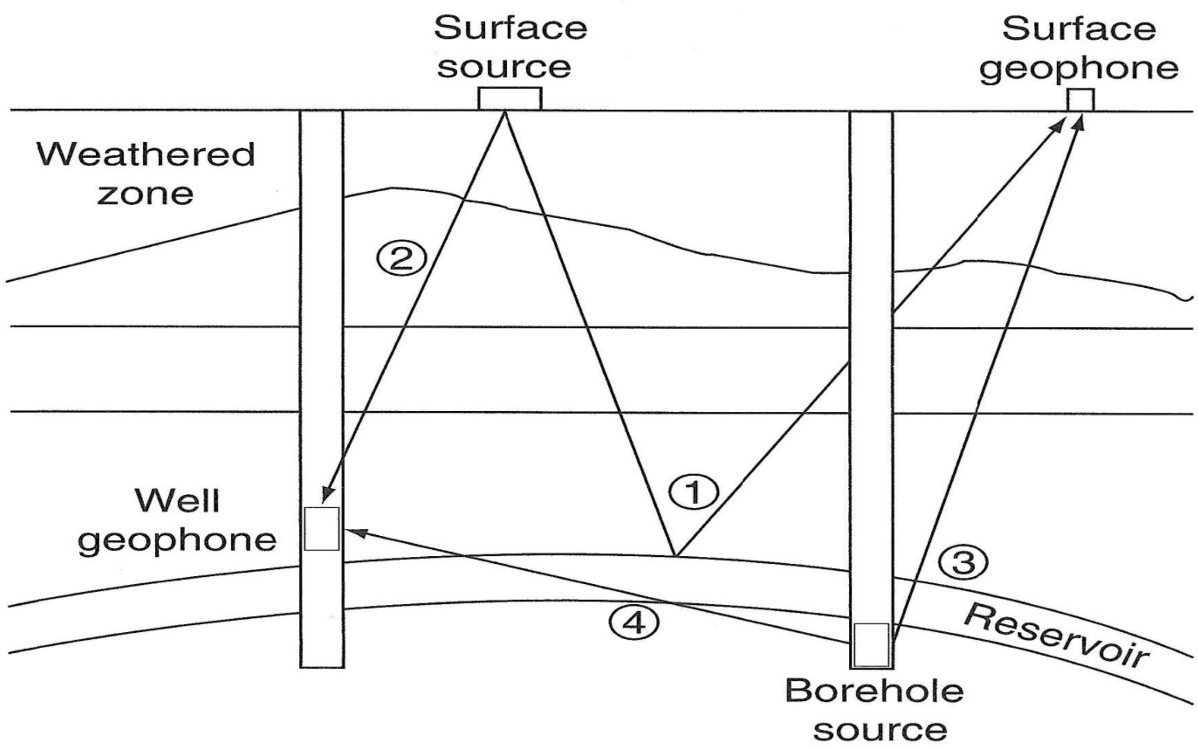

- در اين روش به يك منبع در داخل چاه نياز داريم و دريافت كننده ها بر اساس آرايشي كه از قبل انتخاب شده است در سطح قرار مي گيرند.
- يك سري از Seismic while drilling(SWD)ها از اين نوع مي باشد كه از امواج توليدي از مته را به عنوان منبع استفاده مي كنند.

Well – to – well seismic

- استفاده از این روش به علت وجود امواج بازتابي زیاد نسبت به دو روش دیگر تفسیرش مشکل تر و پر هزینه تر مي باشد.

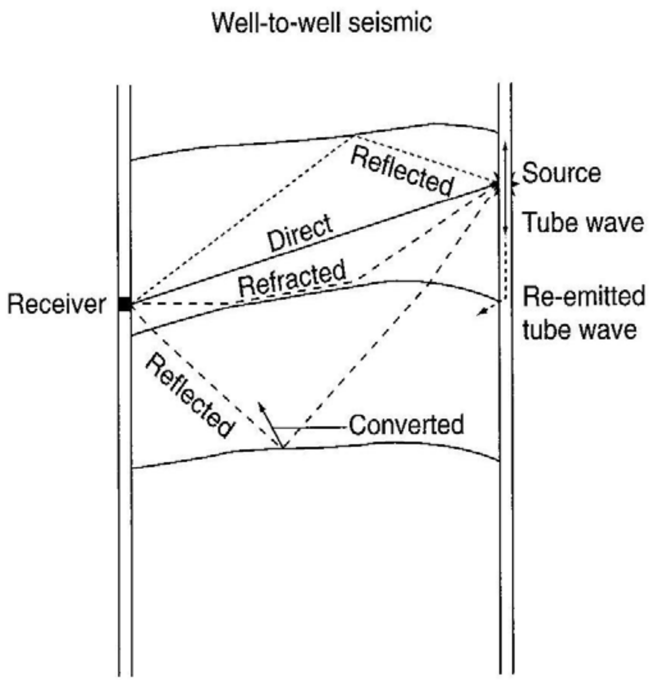

- این روش معمولا در عملیات عمراني و یا معدن استفاده مي شود اما در بررسي مخازن با عمق کم هم قابل استفاده است.

- این روش منجر به بدست آوردن يك section از لایه هاي بين دو چاه مي شود.

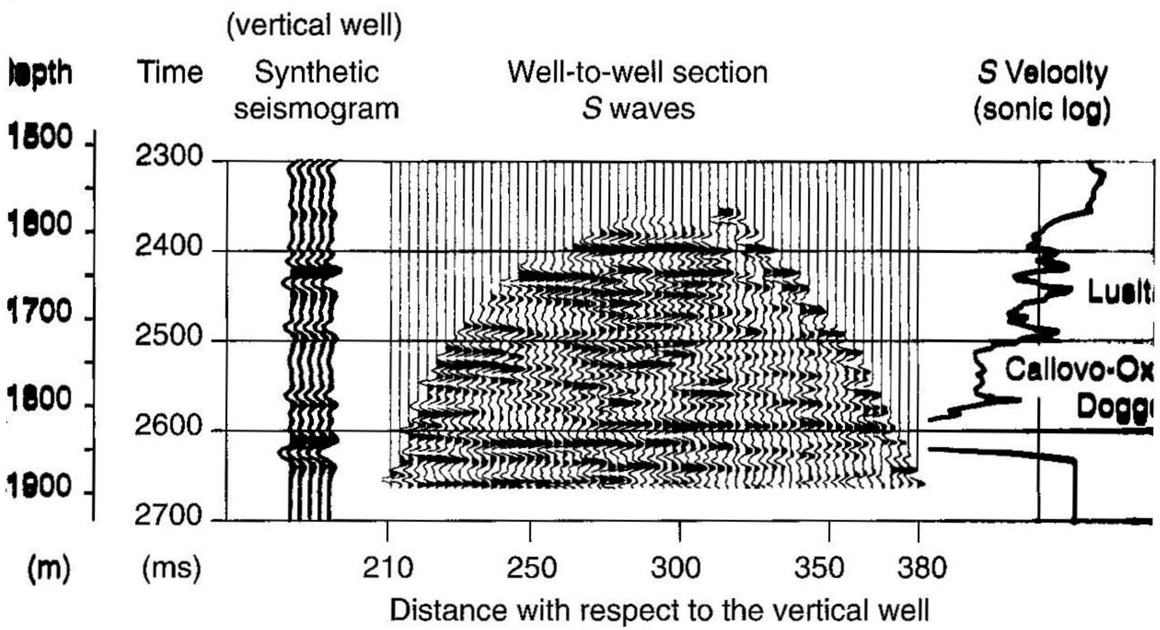

- در زير مثالي از كاربرد اين روش در مهندسي عمران را مشاهده مي كنيد.

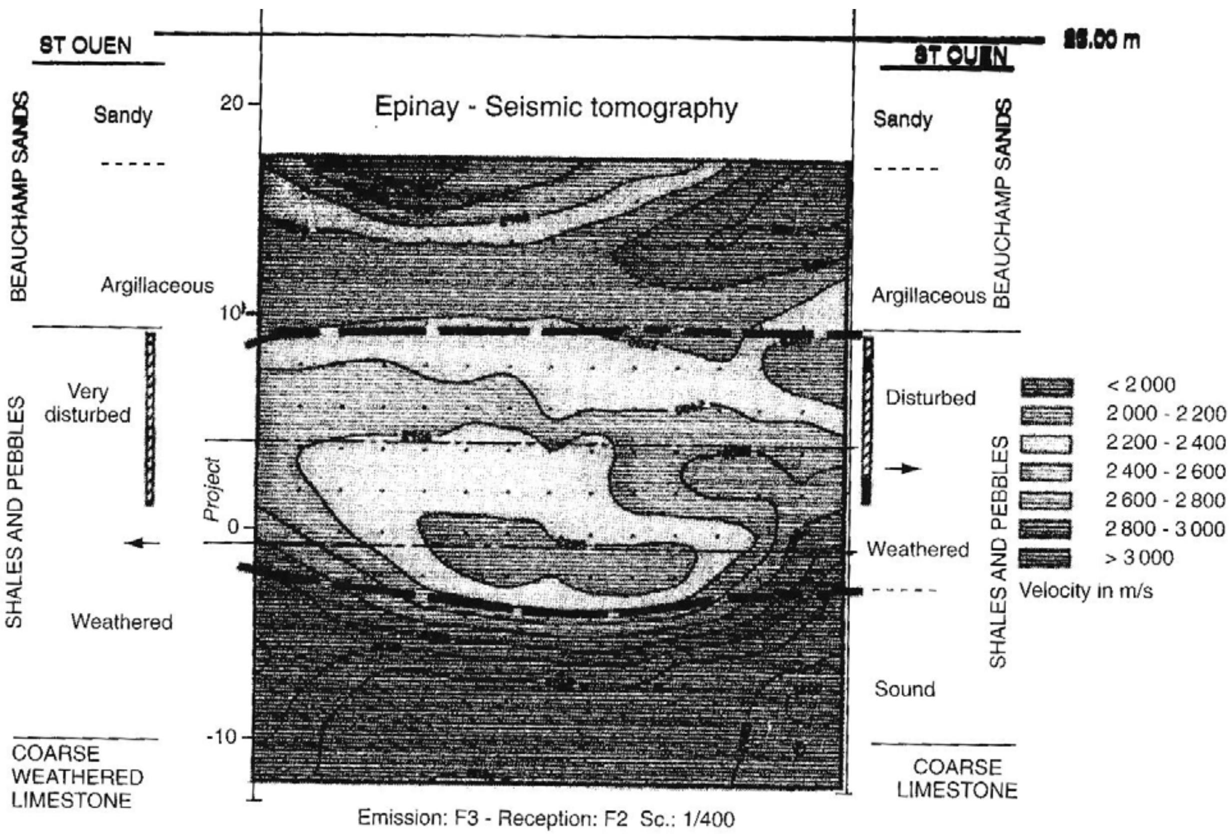

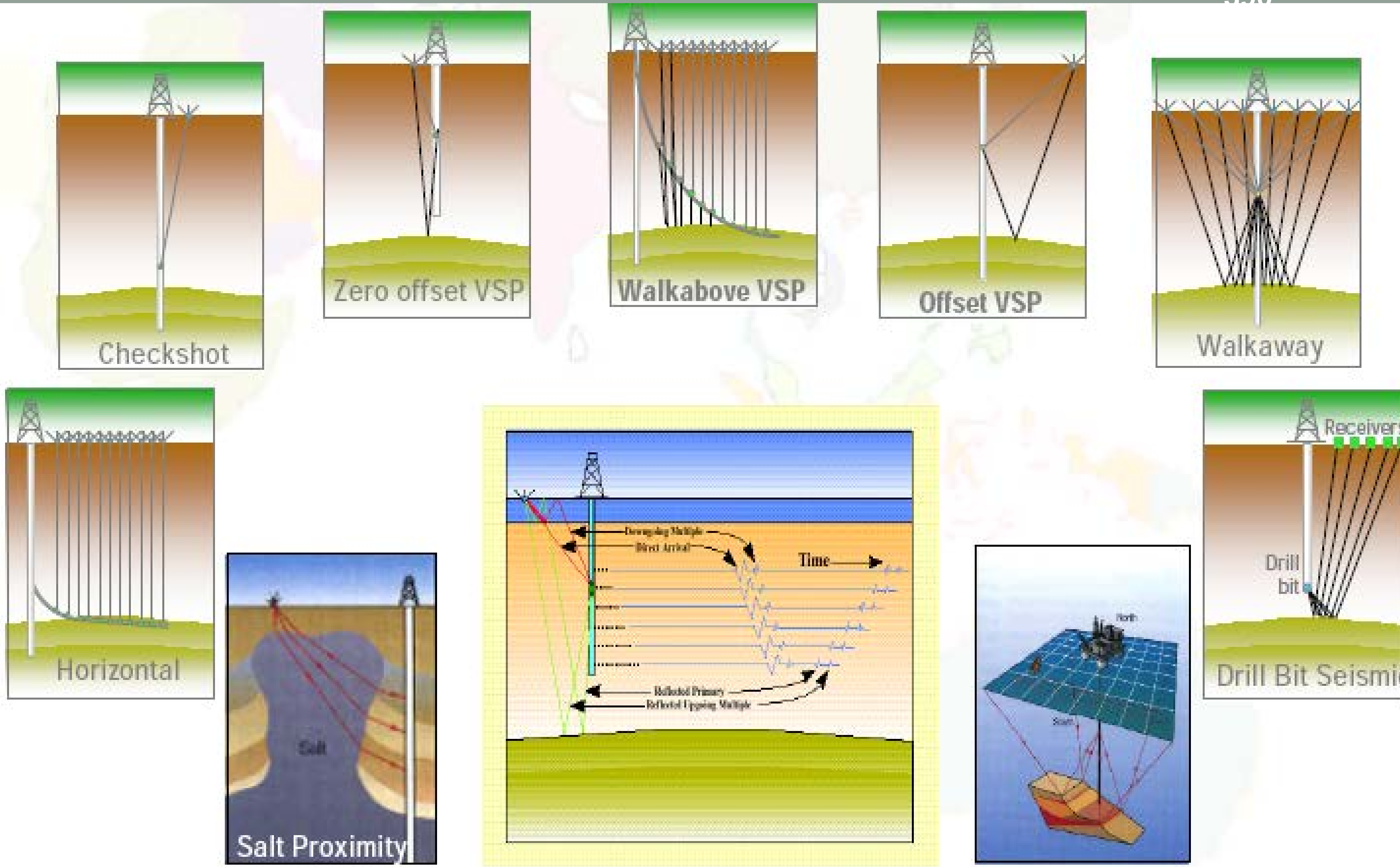
Checkshot
Zero offset VSP
Walkabove VSP
Offset VSP
Walkaway
Horizontal
Salt Proximity
Time
Receivers
Drill
bit
Drill Bit Seismic

VSP

- وقتي در عمليات VSP شات مي كنيم ، امواج از فرستنده در تمام جهات پراكنده مي شوند ، در نتيجه يكسري از امواج مستقيما به ژئوفون ها موجود در چاه مي رسد ، اما يكسري امواج بعد از چندين انعكاس به گيرنده مي رسند(Multiple).
- در تفاسير VSP سطح مبنا را انتهاي لايه ي هوازده در نظر مي گيريم.

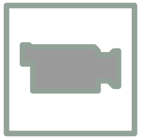

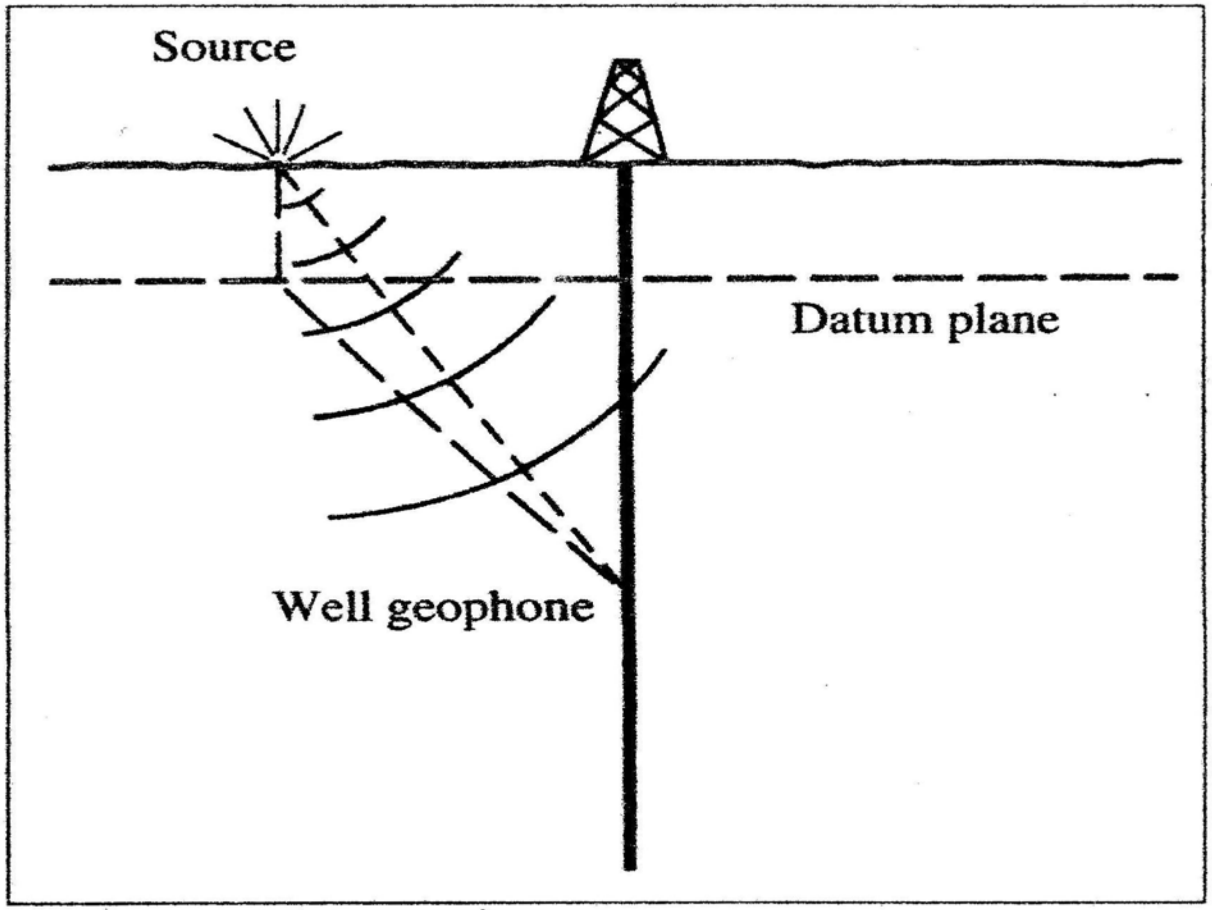

Implementation of seismic well velocity survey.

- در شکل بعد مي توان اختلاف بين VSP و horizontal Seismic profile را مي توان مشاهده کرد.

- VSP همانند velocity survey مي باشد اما دو تفاوت عمده دارد:

1. فاصله ي ژئوفون ها در VSP حداکثر 23 متر است ولي در velocity survey فاصله به چند صد متر هم مي رسد.
2. در velocity survey اولين موج رسيده براي ما اهميت دارد و ثبت مي شود اما در VSP از امواج بعدي هم استفاده مي شود.

VSP concept

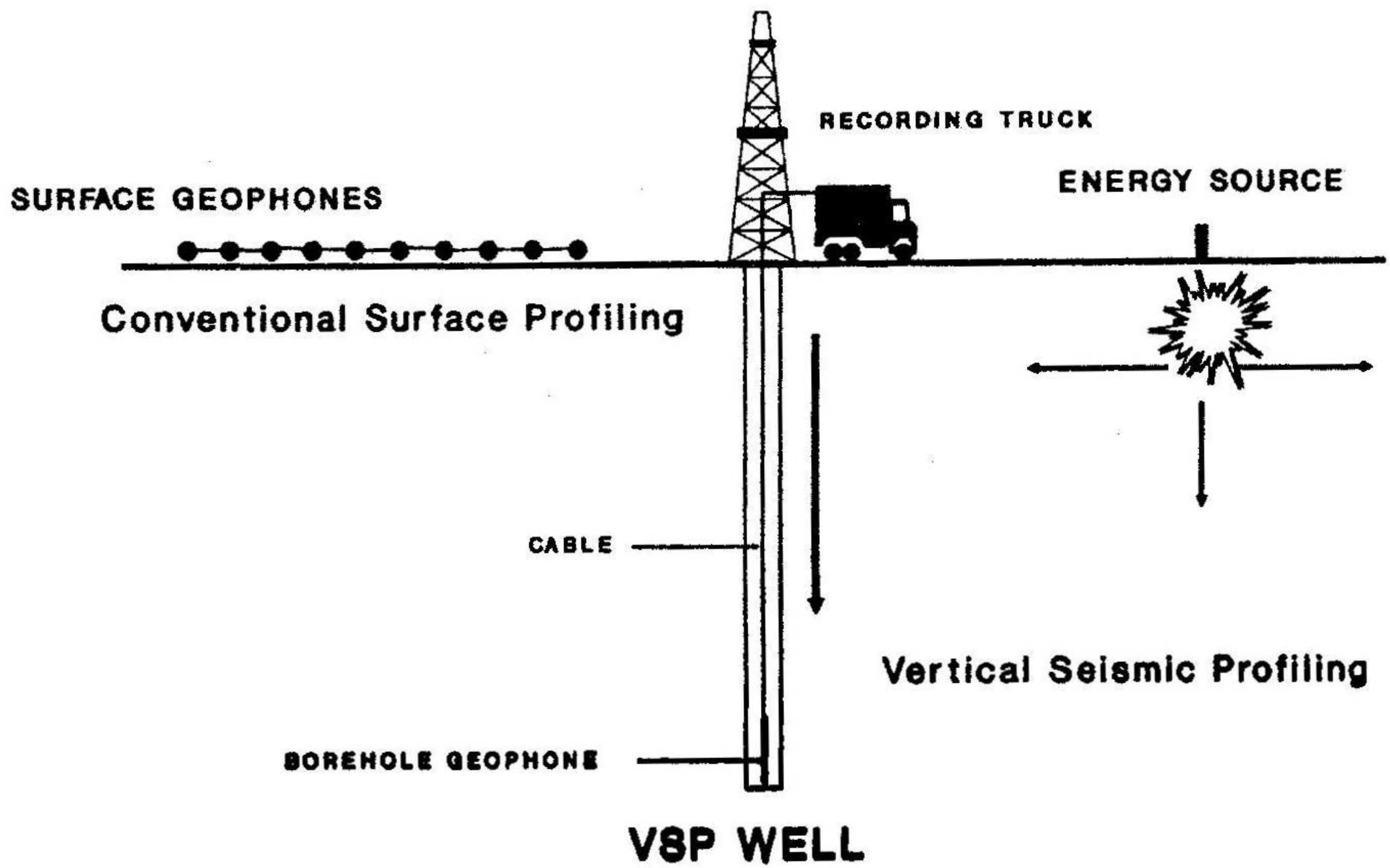
RECORDING TRUCK
ENERGY SOURCE
SURFACE GEOPHONES
Conventional Surface Profiling
CABLE
Vertical Seismic Profiling
BOREHOLE GEOPHONE
VSP WELL

- در عملیات VSP باید مراحل زیر را طي کنیم:

1. چك كردن عمق ابزارها در چاه.
2. گیر دادن ابزارها به دیواره و شل كردن كابل
3. ثبت امواج لرزه اي
4. مشخص كردن اولین امواج رسیده
5. محكم كردن كابل
6. آزاد كردن ابزارها

- حاصل عملیات بالا يك نمودار زمان انتشار در مقابل عمق است($t=f(z)$).

- در عمليات VSP اگر چاه قائم باشد معمولا در يك نقطه شات مي كنيم ، اما اگر چاه مايل باشد بايد تعداد زيادي شات داشته باشيم.

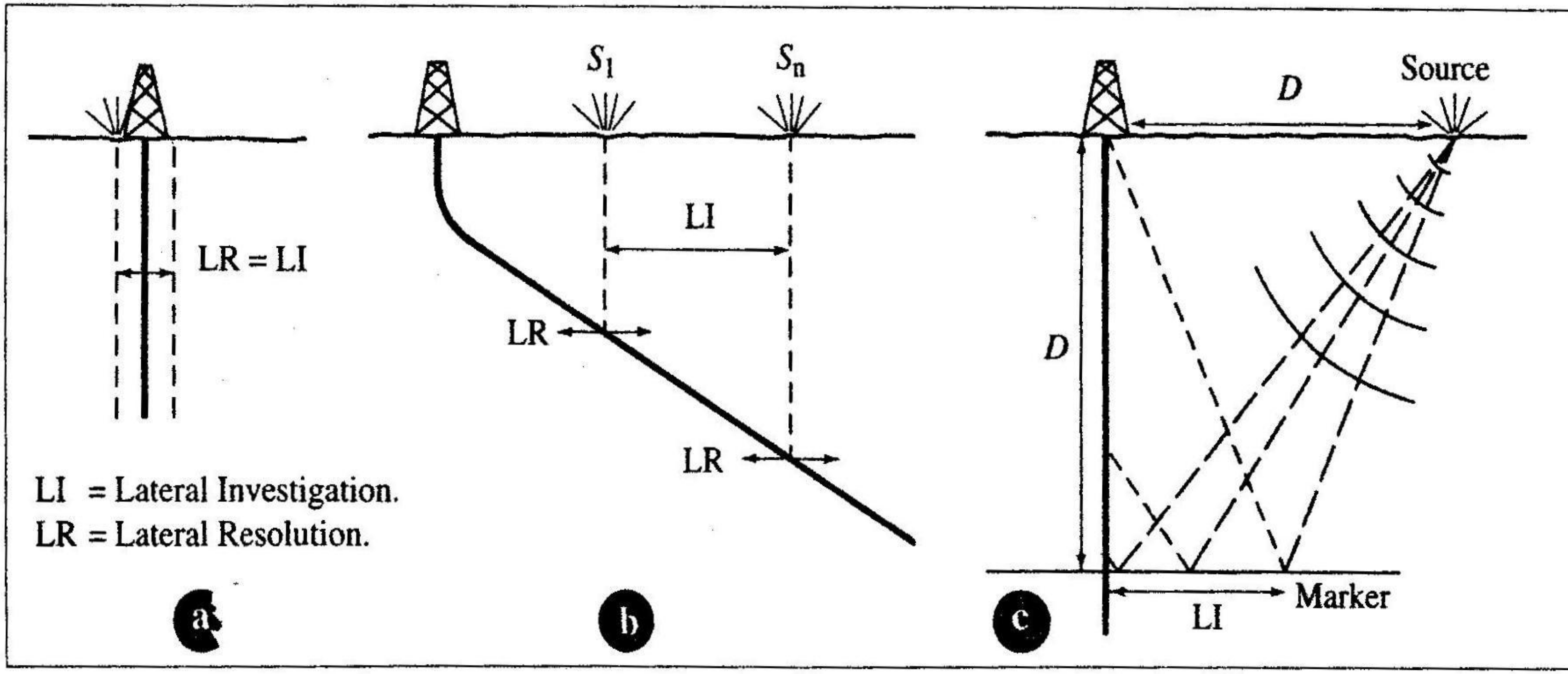

Lateral range of investigation (LI) and lateral resolution (LR) in a vertical seismic profile.

- همانطور که در شکل بالا مشاهده شد، در چاه قائم مقدار Lateral investigation برابر lateral resolution است ، اما در چاه مایل این دو مقدار با هم متفاوت است(بخش b).
- يك راه براي افزايش LI استفاده از offset بيشتري است(بخش c).
- در VSP offset مقدار LI حدودا نصف offset مي باشد.

- در VSP مقدار فاصله ي ماكزيمم(Δz_{max}) بستگي به حداقل سرعت لايه ها (V_{min}) و ماكزيمم فركانس لايه ها (F_{max}) دارد و داريم:

$$\Delta Z_{max} = V_{min} /2F_{max}$$

- به عنوان مثال اگر سرعت حداقل برابر 150 متر بر ثانيه و فركانس بيشينه برابر 150 هرتس باشد بيشترين فاصله مجاز ژئوفون ها برابر 5 متر است.

Separation upgoing & downgoing wave

- در دو شکل زیر مي توان ايده ي خوبي از امواج بالا رونده و پايين رونده بدست آوريم.

Upgoing primaries and multiples

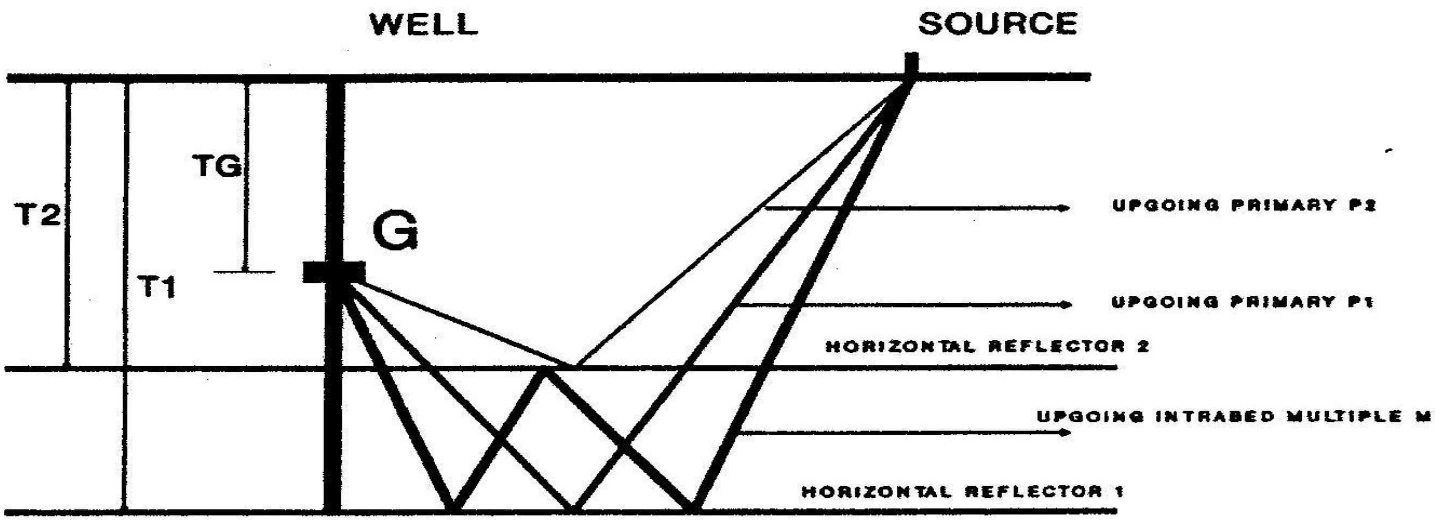

T1,T2,TG are one way vertical travel time to reflectors 1,2 and geophone G. Large offset is assumed for better visual clarity. Reflectors 1,2 are assumed to be horizontal.

t1:Upgoing travel time from reflector 1 to geophone.

$t1=T1+(T1-TG)=2T1-TG$

t2:Upgoing travel time from reflector 2 to geophone.

$t2=T2+(T2-TG)=2T2-TG.$

tM:Upgoing multiple travel time from reflector 1 to geophone

$tM=T1+3(T1-T2)+T2-TG \quad =2T1+2(T1-T2)-TG.$

Downgoing surface and intrabed multiples

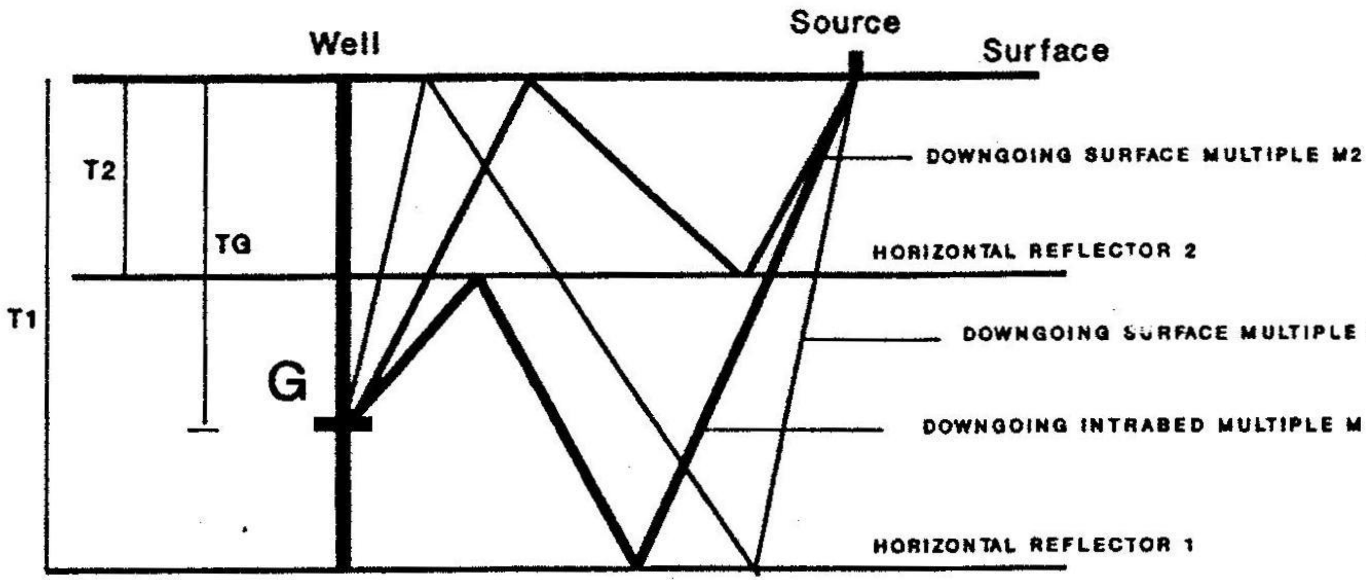

RAYPATHS DESCRIBING THE DOWNGOING SURFACE MULTIPLES AND INTRABED MULTIPLES THAT ARRIVE AT THE VSP GEOPHONE. ASSUME THAT REFLECTORS 1, 2 ARE HORIZONTAL

$t1 = 2T1 + TG$

$t2 = 2T2 + TG$

$$tM = T1 + (T1-T2) + (TG-T2)$$
$$= T1 + T1 - T2 + TG - T2$$

$$tM = 2(T1-T2) + TG$$

- در شكل بعد trace هاي كلي مربوط به يك عمليات VSP كه داراي دو بازتاب كننده ي A و B و 5 گيرنده در اعماق مختلف مي باشد را مشاهده مي كنيد.
- در اين شكل 7 سري موج رسيده را مشخص كرده ايم.

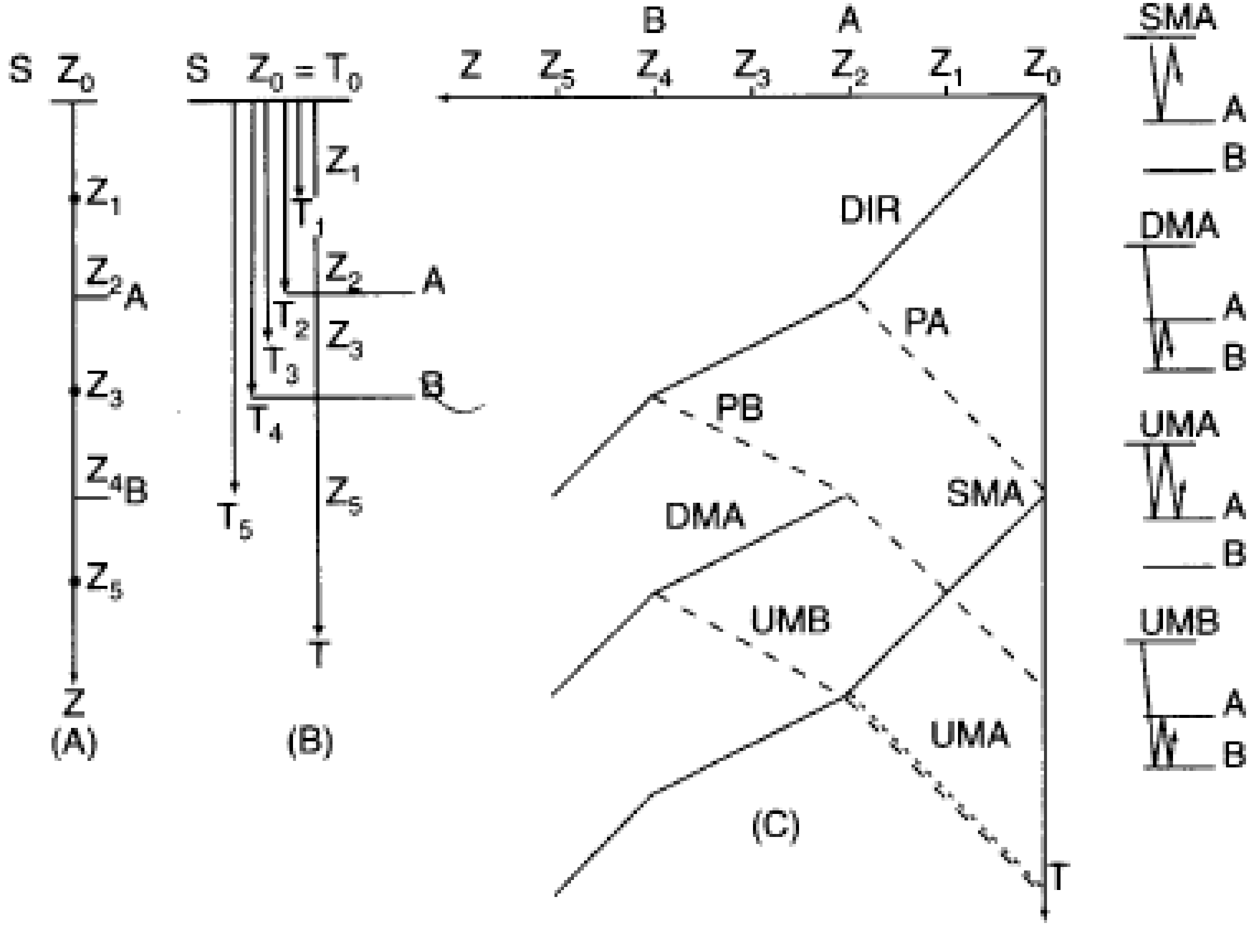
S
Z_0
Z_1
Z_2 A
Z_3
Z_4 B
Z_5
Z
(A)
S
$Z_0 = T_0$
Z_1
T_1
Z_2
A
T_2
Z_3
T_3
B
T_4
T_5
Z_5
T
(B)
B
A
Z
Z_5
Z_4
Z_3
Z_2
Z_1
Z_0
DIR
PA
PB
SMA
DMA
UMB
UMA
T
(C)
SMA
A
B
DMA
A
B
UMA
A
B
UMB
A
B

- در ادامه مي خواهيم به بررسي هفت سري موج مشخص شده در بالا بپردازيم.

1. Direct arrival(DIR): اين ها امواجي هستند كه به طور مستقيم به هر كدام از گيرنده ها مي رسد ، در شكل مشاهده مي شود كه با افزايش عمق زمان رسيدن نيز افزايش مي شود و هر بازتاب كننده باعث ايجاد يك شكستگي در روي نمودار مي شود. اين سري از امواج را توسط هر 5 گيرنده دريافت مي كنيم.

2. Primary reflection on horizon A (PA): اين امواج عبارتند از امواج بازتابي از سطح A كه به گيرنده هاي بالاي اين سطح مي رسد. زمان رسيدن اين امواج را مي توان از رابطه ي زير بدست آورد.

$$T_A = T_4 + (T_2 - T_i)$$

- در رابطه ي بالا i بين 0 تا 2 است.
- زمان T_A با افزايش عمق كاهش مي يابد ، به عنوان مثال اين زمان براي گيرنده اي در سطح برابر $2T_2$ مي باشد.

3. Primary reflection on horizon B(PB): این امواج عبارتند از امواج بازتابي از سطح B که توسط گیرنده هاي اول تا چهارم ثبت مي شود(گیرنده هاي بالاي سطح B).

- زمان رسیدن این امواج را مي توان از فرمول مقابل بدست آورد.

$$T_B = T_4 + (T_4 - T_i)$$

- در رابطه ي بالا i بین 0 تا 4 است.

4. Surface multiple after reflection on horizon A (SMA):

همانطور كه مي دانيم امواج بازتابي از سطح A به سمت بالا حركت مي كنند اما در سطح بين اين لايه با هوا به علت اختلاف آمپيدانس زياد اين موج مجدد به سمت پايين بازتاب مي كند و باعث ايجاد Multiple هايي در تمام ژئوفون ها مي شود. اثر اين امواج بر روي نمودار x-t همانند امواج DIR مي باشد با اين تفاوت كه يك انتقال زماني به اندازه ي زمان سير از سطح A تا سطح زمين نيز دارد.

- زمان رسيدن اين امواج تقريبا برابر با $2T_2 + T_i$ مي باشد كه i بين 0 تا 5 مي باشد.

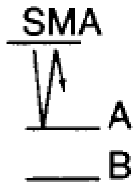

5. Downgoing multiple creat by horizon A after reflection on horizon B (DMA): اين امواج عبارتند از امواج حاصله از بازتاب مجدد امواج بازتابيده از سطح بالايي افق B توسط سطح پاييني A .

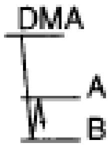

- اين امواج توسط گيرنده ي 2 به بعد ثبت مي شود و با افزايش عمق زمان آن نيز زياد مي شود.
- زمان رسيدن اين امواج برابر است با:

$$T = T_4 + (T_4 - T_2) + (T_i - T_2)$$

- اثر اين امواج مشابه امواج DIR مي باشد با اين تفاوت كه از گيرنده ي دوم به بعد ثبت شده و داراي انتقال زماني برابر $2(T_4 - T_2)$ مي باشد.

6. Upgoing multiple created by horizon A after reflection at the surface (UMA): اين امواج را مي توان بازتابي از امواج SMA توسط سطح A دانست و يا به عبارت ديگر امواج دوبار بازتاب شده بين سطح و افق A هستند.

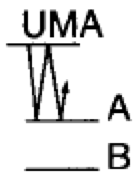

- اين امواج در گيرنده هاي بالاي سطح A اثر دارد همانند امواج PA.
- زمان رسيدن اين امواج برابر است با :

$$T = 3T_2 + (T_2 - T_i)$$

- در اين رابطه i بين 0 تا 2 مي باشد.

7. Upgoing multiple created by horizon B after reflection on horizon A (UMB): این امواج عبارتند از امواجي که از بازتاب امواج DMA توسط سطح B و یا به عبارت دیگر امواج دوبار بازتاب شده بین سطح A و B مي باشند.

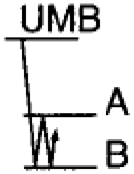

- زمان رسیدن این امواج با کاهش عمق افزایش مي یابد و تنها توسط گیرنده هاي بالاي سطح B ثبت مي شوند.
- زمان رسیدن این امواج برابر است با:

$$T = T_4 + 2(T_4 - T_2) + (T_4 - T_i)$$

- در این رابطه i بین 0 تا 4 مي باشد.

چند نكته

- با داشتن زمان رسيدن اوليه (first arrival time) براي هر دو گيرنده ي متوالي (i و i+1) مي توان سرعت متوسط را بين اين دو گيرنده از رابطه ي زير بدست آورد.

$$V_{i,i+1} = (Z_{i+1} - Z_i)/(T_{i+1} - T_i)$$

- در صورتي كه بدانيم دو گيرنده در يك لايه قرار دارند مي توان تخميني از سرعت در آن لايه را با فرمول بالا بدست آورد.

- امواج رسيده به گيرنده هارا مي توان دو دسته تقسيم بندي كرد:

1. امواج پايين رونده(downgoing): عبارتند از ، DMA,SMA,DIR كه بوسيله ي خطوط پر رنگ در شكل مشخص شده و با افزايش عمق زمان هم زياد مي شود.
2. امواج بالا رونده (upgoing): عبارتند از: PA,PB,UMA,UMB كه توسط خطوط نقطه چين در شكل مشخص شده اند و با كاهش عمق زمان آنها زياد مي شود.

در عمليات VSP اگر امواج upgoing را مورد بررسي قرار دهيم مي توان با استفاده از يك انتقال زماني براي هر كدام از ژئوفون ها در عمقهاي مختلف پروفيل لرزه نگاري درون چاهي را به پروفيل لرزه اي سطحي تبديل كرد ، مقدار انتقال زماني برابر است با:

$$T = T_S - T_i$$

- در اين رابطه T برابر است با زماني كه ژئوفون ها موج را دريافت كرده و T_S برابر است با زماني كه اگر ژئوفون در امتداد مسير امواج به سطح انتقال داده شود لازم است كه اين زمان به آن اضافه شود.
- T_i هم برابر است با زمان رسيدن اولين موج مستقيم به ژئوفون ها (زمان مربوط به DIR).
- با اين روش مي توان پروفيل هاي لرزه اي درون چاهي را با پروفيل هاي لرزه اي سطحي مقايسه كرد و هر دو را با هم مورد بررسي قرار داد.

- اگر در نمودار x-t به جاي مكان ژئوفون ها از زمان رسيدن موج به آنها استفاده كنيم ، تمام سرعت ها در مسير يكسان مي شود با اين تفاوت كه شيب امواج بالا رونده برابر 1- و شيب امواج پايين رونده برابر با 1 مي شود.

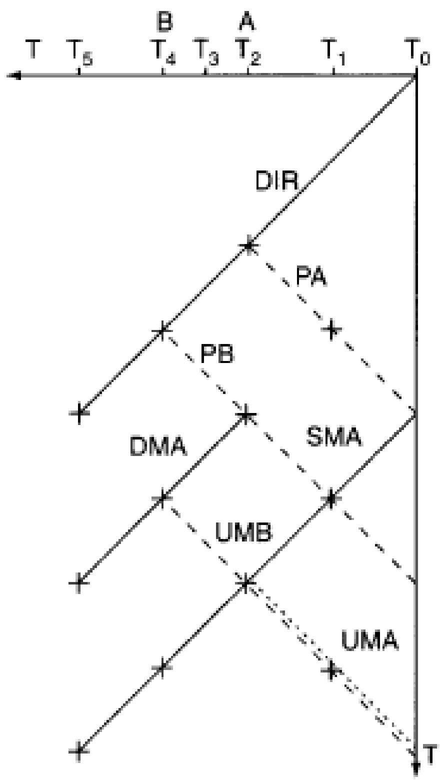

- از محاسن اين روش اين مي باشد كه مي توان امتداد اثرهاي بدست آمده را امتداد داد (بدون داشتن خطا زيرا خط راست را امتداد مي دهيم) و در جاهايي كه اطلاعات بدست نيامده اطلاعات بدست آوريم.
- با اين روش مي توان به راحتي افق ها را مشخص كرد ، به عنوان نمونه محل برخورد PA با DIR نشان دهنده ي افق A مي باشد و يا محل برخورد PBبا DIR هم نشان دهنده ي افقB مي باشد.
- اگر ما يك ناحيه ي ريزش كرده در ديواره چاه داشته باشيم ، نمي توان از آنجا اطلاعاتي بدست آورد ولي با اين روش مي توان امتداد امواج گذرنده از اين ناحيه را رسم كرد و سطح لايه را بدست آورد.
- در شكل بعد نمونه اي از اين امتداد دادن را مشاهده مي كنيد.

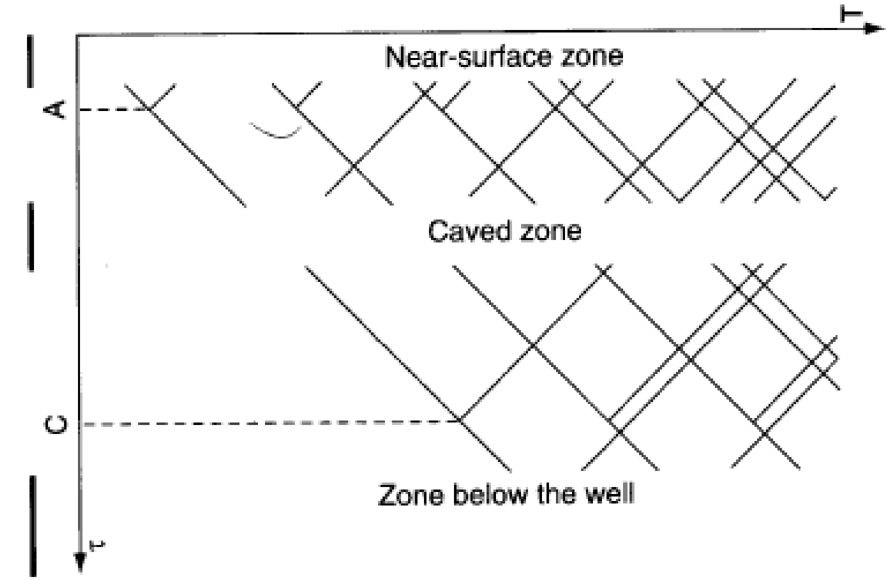
T
Near-surface zone
A
Caved zone
C
Zone below the well
τ

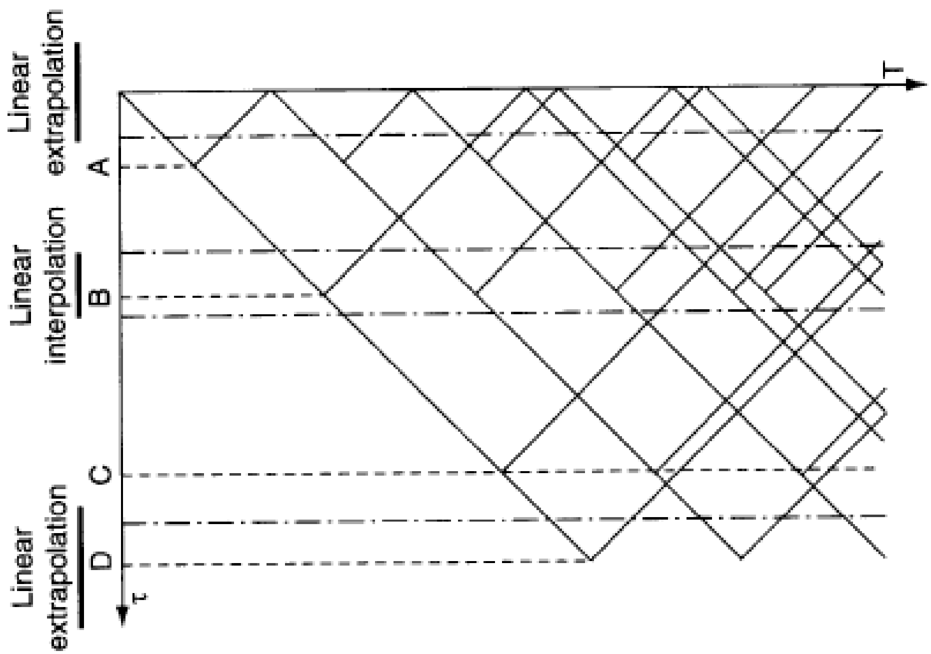
Linear extrapolation
A
Linear interpolation
B
C
Linear extrapolation
D
T
τ

Noise

- Randome noise: ممكن است حركت سيال در پشت لوله جداريي كه خوب سيمان نشده و يا حركت سيال داخل چاه يك سري نويز در برداشت ها ايجاد مي كند.
- Geophone coupling: در لرزه نگاري سطحي يك سري نويز هاي ناشي از بد قرار گرفتن ژئوفون ها در سطح زمين ايجاد مي شود ، اما در ژئوفون هاي درون چاهي بد وصل شدن آنها به يكديگر و نامناسب بودن اتصال آنها به ديواره باعث ايجاد يك سري نويز بعد از رسيدن جبهه ي اصلي به ژئوفون مي شود ، اين امواج باعث حركت ژئوفون شده و اين نويزها توليد مي شود.

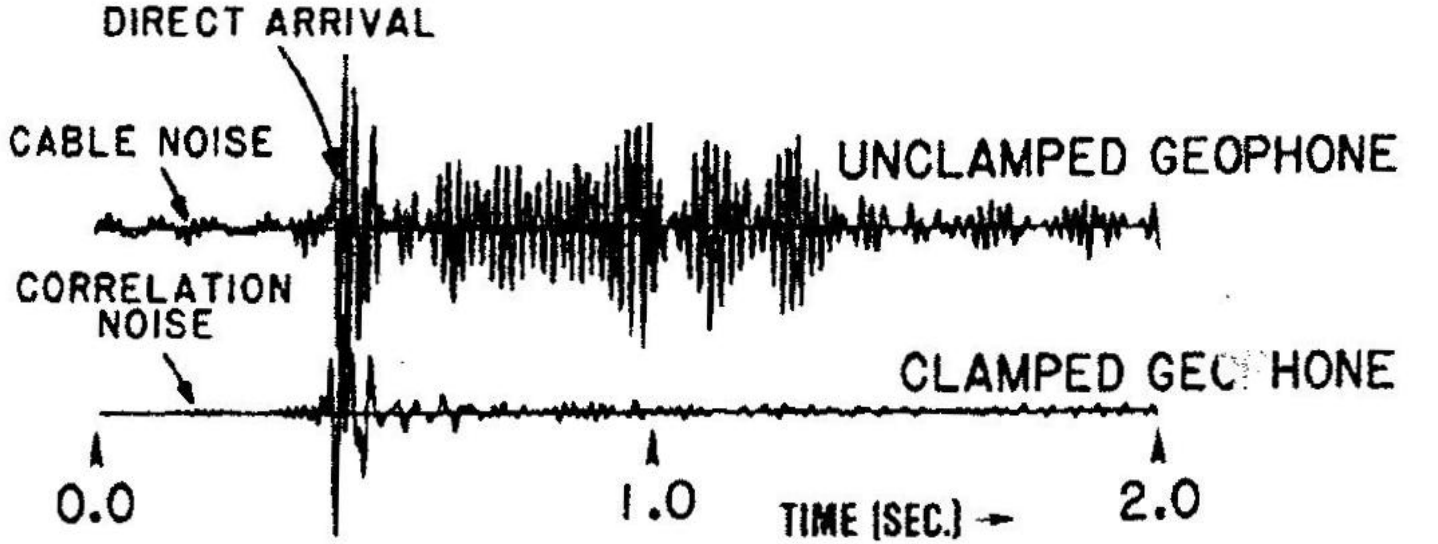

GEOPHONE DEPTH – 1295 METERS
SOURCE OFFSET – 209 METERS

EFFECT OF GEOPHONE CLAMPING ON SIGNAL RESPONSE.

- Cable wave: انتشار موج در امتداد کابل نيز امکان دارد ، سرعت انتشار اين امواج بستگي به دانسيته ي کابل دارد.
- سرعت انتشار امواج در امتداد کابل بين 2500 تا 3500 متر بر ثانيه است.
- در چاه هاي کم عمق يا لايه هاي زمين شناسي کم سرعت ، امواج رسيده از کابل مي تواند اولين موج رسيده باشد(همانند شکل قبل).
- براي رفع اين مشکل بايد طناب را از حالت کشش خارج کرد و آن را شل کرد(slacking)، به اين گونه که بعد از اينکه از اين ژئوفون ها به عمق مناسب رسيدند و به طور محکم در ديوار مستقر شدند طناب را مقداري آزاد مي کنيم ، اثر slacking را در اسايد بعد مشاهده مي کنيد.

Effect of cable slack on geophone signal (courtesy Geophysical Press, from Hardage, B.A.: "Vertical Seismic Profiling, Part A: Principles," 1983)

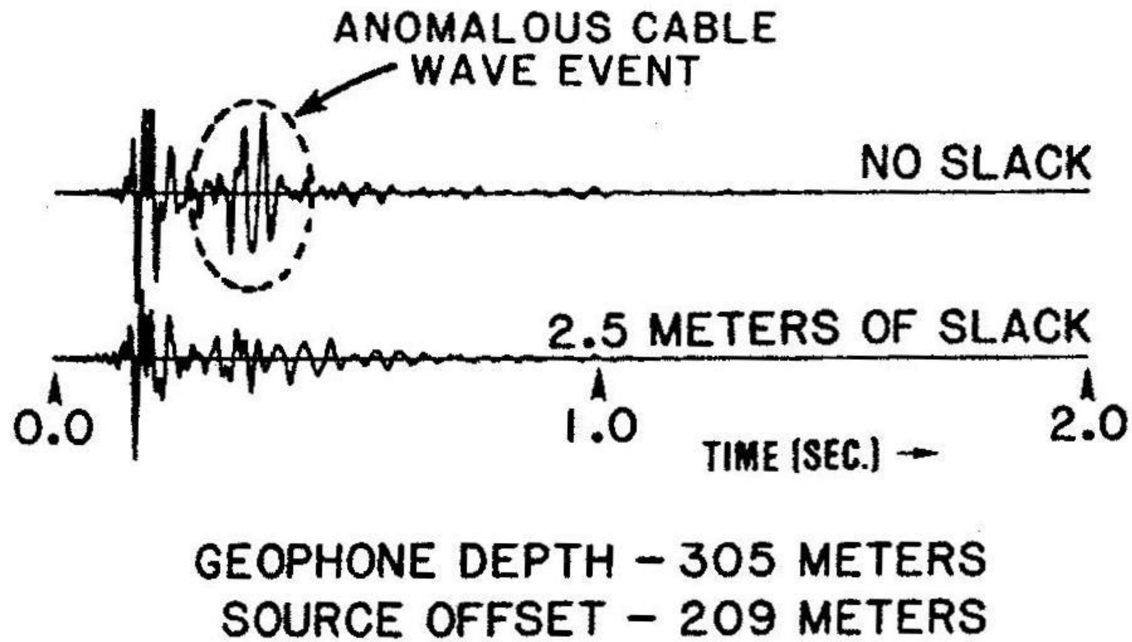

- Surface wave: در اكتشاف لرزه اي سطحي امواج ريلي و لاو را در نزديكي سطح داريم و اين امواج در ژئوفون هاي سطحي ثبت مي شود ، با افزايش عمق اثر اين امواج ازبين مي رود.
- اما در VSP چون عمق ژئوفون ها زياد است امواج سطحي توانايي رسيدن به آن نقطه را ندارند.
- Unbounded casing: لوله ي جداري سيمان نشده باعث كاهش شديد انرژي و دامنه ي امواج مي شود و كيفيت داده ها را از بين مي برد.

- Tube wave: يك چاه پر شده از مايع باعث ايجاد يك محيط براي انتشار موج هاي ناخواسته اي به نام امواج لوله اي مي شود.
- شكل شماتيك زير گسترش اين امواج را مشاهده مي كنيد.
- اين امواج يكي از مخربترين الگوهاي نويز مي باشد ، زيرا اين امواج همدوس بوده و با عمل stacking نه تنها نمي توان اثر آنها را كاهش داد بلكه اثر آنها تقويت مي كند.
- اين امواج براي شناسايي بعضي از ساختارها مانند لايه هاي تراوا يا شكستگي ها مي تواند كمك كند.

Tube wave (modified from Hardage, 1983)

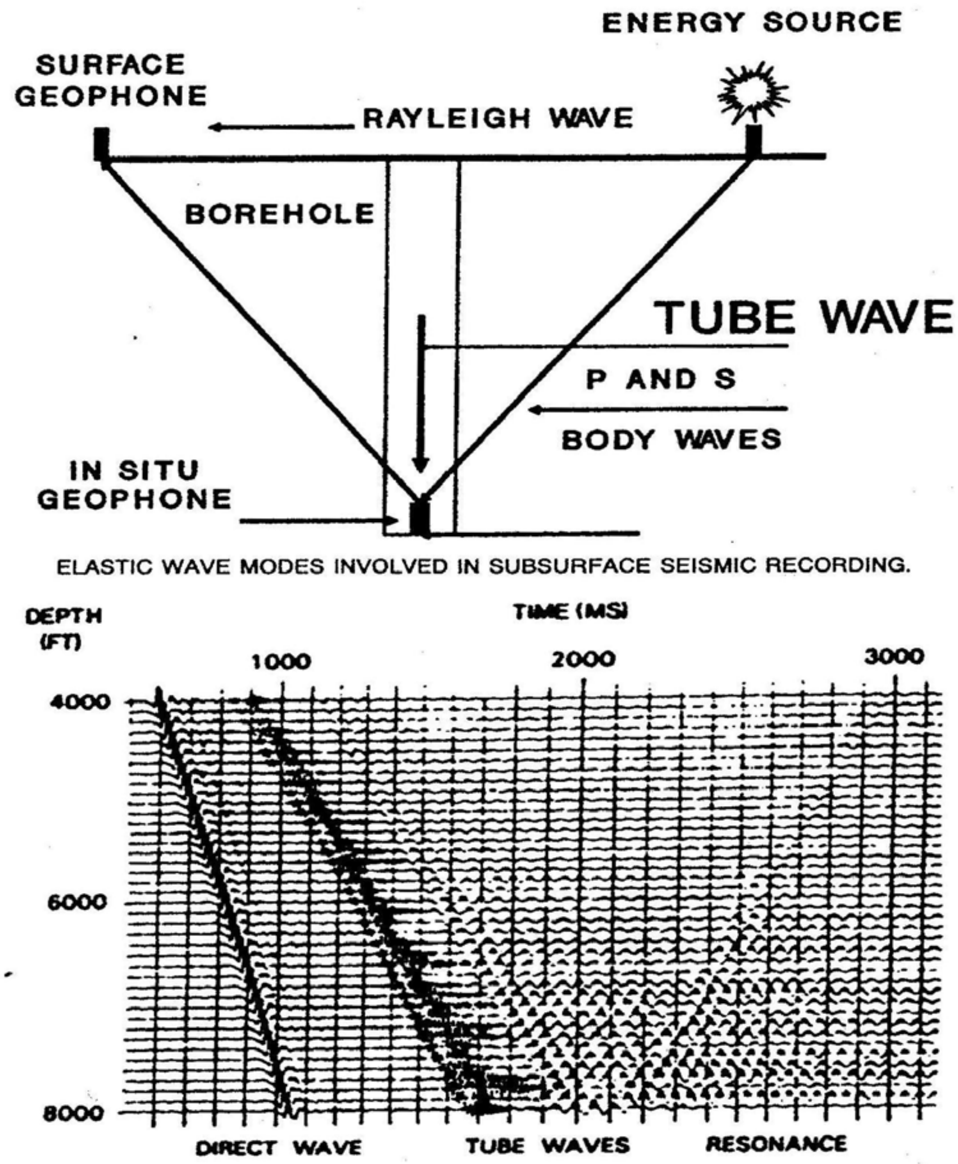

- امواج لوله اي وقتي حاصل مي شوند كه ذرات موجود در ستون گل كه حفره ي چاه را پر كرده اند به حركت در آيند.
- امواج سطحي(امواج rayleigh) كه به حفره چاه مي رسند تبديل به امواج لوله اي شده و در امتداد چاه حركت مي كنند.
- امواج لوله اي به سمت بالا و پايين چاه حركت كرده و با تغيير آمپيدانس در بالاي ستون گل و يا ته چاه و يا هر تغيير در قطر چاه امواج لوله اي ثانويه را توليد مي كنند.

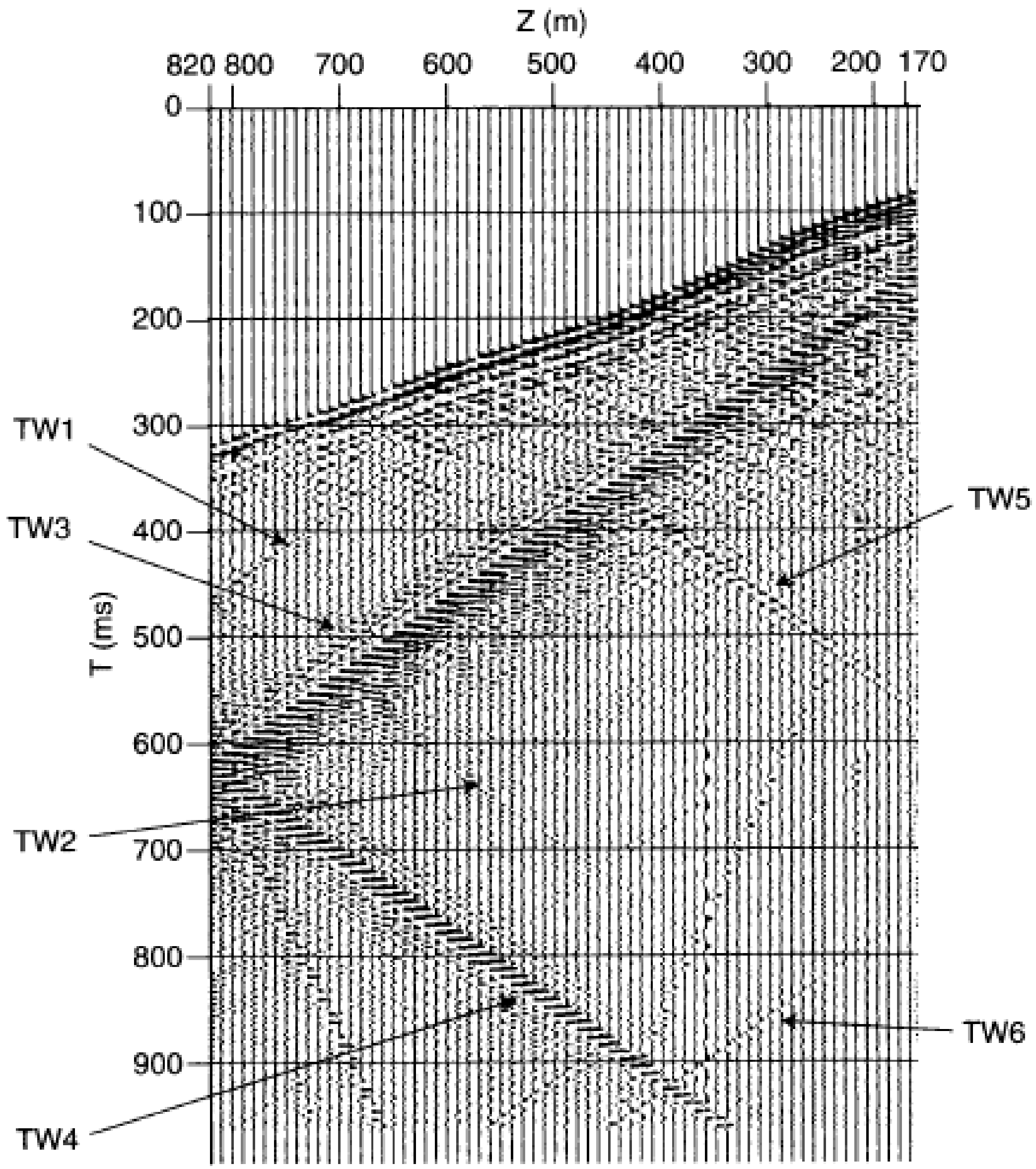
Z (m)
820 800 700 600 500 400 300 200 170
0
100
200
300
400
500
600
700
800
900
T (ms)
TW1
TW3
TW2
TW4
TW5
TW6

- يك راه براي كاهش امواج لوله اي اين است كه چون اين امواج از امواج سطحي توليد مي شوند مي توان با كاهش سطح گل در چاه مانع از نفوذ نويزهاي سطحي به داخل سيال چاه شده و مقدار امواج لوله اي را كاهش داد.
- اين راه حل به شرطي قابل اجرا است كه عواملي مانند فشار چاه اجازه ي خارج كردن مقدار از گل حفاري را بدهد.

- Surface caltural noise: علت ایجاد این امواج حرکت افراد و ماشین آلات در نزديكي سایت VSP مي باشد.
- نحوه ي كاهش و حذف این نویز ها ایجاد محیط ساکت و آرام در حین عملیات مي باشد.

VSP applications

- كاربرد هاي VSP را مي توان در دو گروه كلي زير جاي داد:

a. Exploration application

b. Reservoir engineering & drilling application

a. Exploration application:

- Determining reflection
- Identification of seismic coefficients
- Comparison of VSP with synthetic seismogram
- Fresnel zone and VSP horizontal resolution
- Seismic amplitude studies
- Determining physical properties of the rocks
- Seismic wave attenuation
- Thin bed stratigraphy

b. Reservoir engineering & drilling application:

- Predicting depth of seismic reflectors
- Predicting rock condition ahead of the bit
- Defining reservoir boundaries
- Locating faults
- Monitoring secondary recovery processes
- Seismic tomography & reservoir description
- Predicting high – pressure zone ahead of the bit
- Detection of man – made fractures

Reflection coefficient

- امواج صوتي از سطحي که آمپيدانس صوتي تغيير کند بازتاب مي شوند.
- پلاريته ، دامنه و خاصيت فازي (phase characteristics) موجك ها توسط reflection coefficient در مرزها تعين مي شود.
- امواج بالارونده نسبت به امواج پايين رونده اطلاعات بيشتري از اعماق مي دهند چون از بازتاب کننده ي عميق تر بازتابيده شده اند.
- دانستن اين ضريب وقتي اهميت پيدا مي کند که بخواهيم داده هاي VSP را تفسير کنيم ، چون اين داده ها شامل داده هاي بالارونده و پايين رونده مي باشنده که هم از سطح بالايي و هم از سطح پاييني بازتابيده شده اند.

- مقدار reflection coefficient برابر است با:

$$R = (\rho_2 v_2 - \rho_1 v_1)/(\rho_1 v_1 + \rho_2 v_2)$$

- اين پارامتر وقتي كه اطلاعات stratigraphic و lithological را در تفاسير VSP وارد كنيم بسيار اهميت پيدا مي كند.

Identification of a seismic reflector

- يك تفسير خوب تلاشي است كه براي ارتباط داده هاي بدست آمده با ساختار چينه شناسي طبقات و رخساره هاي رسوبي.
- در صورت داشتن اطلاعات خوب VSP قادر هستيم كه عمق هر لايه (رخساره) را در نزديكي چاه توسط امواج بالارونده اوليه مشخص كنيم.
- در نتيجه با استفاده از VSP مي توان نقشه هاي ساختاري بدست آمده از لرزه نگاري سطحي را اصلاح كرد.

- با استفاده از يك برداشت VSP با مقدار S/N(signal to noise ratio) پايين مي توان به سوالات زير پاسخ داد.

1. بازتاب كننده ي ثبت شده توسط روش هاي ديگر آيا مرز لايه است يا يك ناپيوستگي مي باشد؟
2. كدام مرز سنگ ها را مي توان توسط داده هاي لرزه نگاري سطحي تشخيص داد و كدام را نه!

- در شكل زير مي توان يك نمونه از تعين بازتاب كننده ها را مشاهده كرد.

Identification of a seismic reflector (courtesy Geophysical Press, from Hardage, B.A.: "Vertical Seismic Profiling, Part A: Principles," 1983, adapted from Balch et al., 1981)

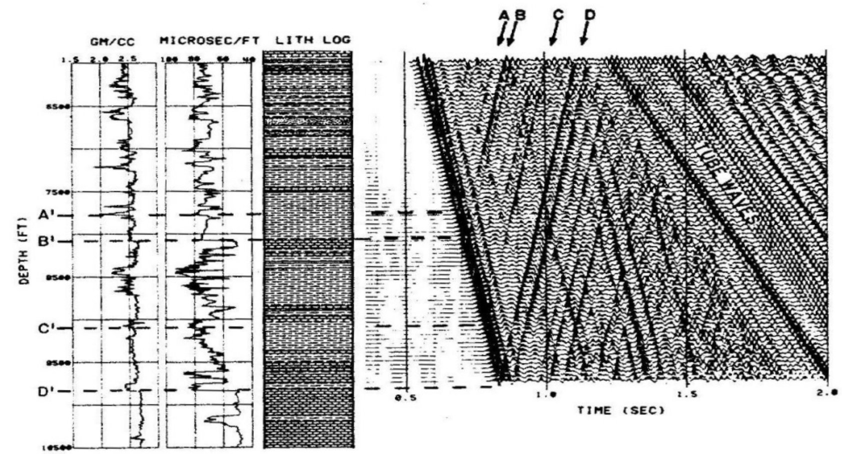

AN EXAMPLE OF THE RELIABILITY WITH WHICH VSP DATA CAN OFTEN IDENTIFY PRIMARY SEISMIC REFLECTORS. FOUR UPGOING PRIMARY REFLECTIONS ARE SHOWN BY THE LINEUP OF BLACK PEAKS LABELED A, B, C, D. THE SUBSURFACE DEPTH OF THE INTERFACE(S) THAT GENERATED EACH REFLECTION CAN BE DEFINED BY EXTRAPOLATING THE APICES OF THE BLACK PEAKS DOWNWARD UNTIL THEY INTERSECT THE FIRST BREAK LOCI OF THE DOWNGOING COMPRESSIONAL EVENT. THESE DEPTHS ARE LABELED A', B', C', D'. THESE ARE RAW FIELD DATA. NO PROCESSING HAS BEEN DONE OTHER THAN A NUMERICAL AGC FUNCTION HAS BEEN APPLIED TO EQUALIZE ALL AMPLITUDES.

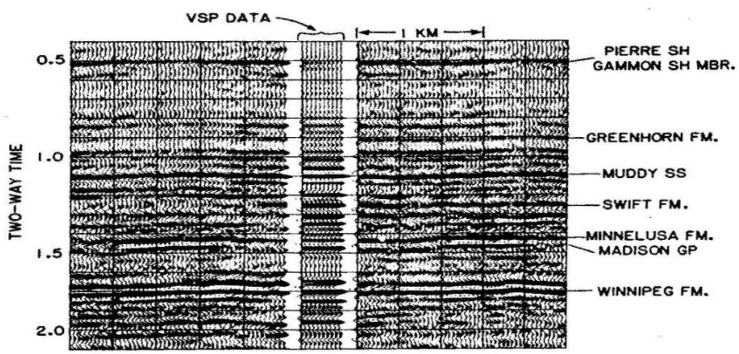

COMPARISON BETWEEN SURFACE-RECORDED REFLECTION DATA AND PROCESSED VSP DATA AT THE USGS MADISON LIMESTONE TEST WELL NO. 2. (ALTERED FROM BALCH ET AL., 1981B).

Predicting interval velocity

- يكي ديگر از داده هاي بدست آمده از آناليز داده هاي VSP نمودار آمپيدانس صوتي در مقابل عمق است.
- مقدار تغييرات دانسيته نسبت به تغييرات سرعت در رسوبات تقريبا ناچيز است بنابراين مي توان از تغييرات دانسيته نسبت به سرعت صرف نظر كرد
- شكل زير يك نمونه از اين نمودار است.

Predicting velocity ahead of the bit (courtesy of Seismograph Service Corporation)

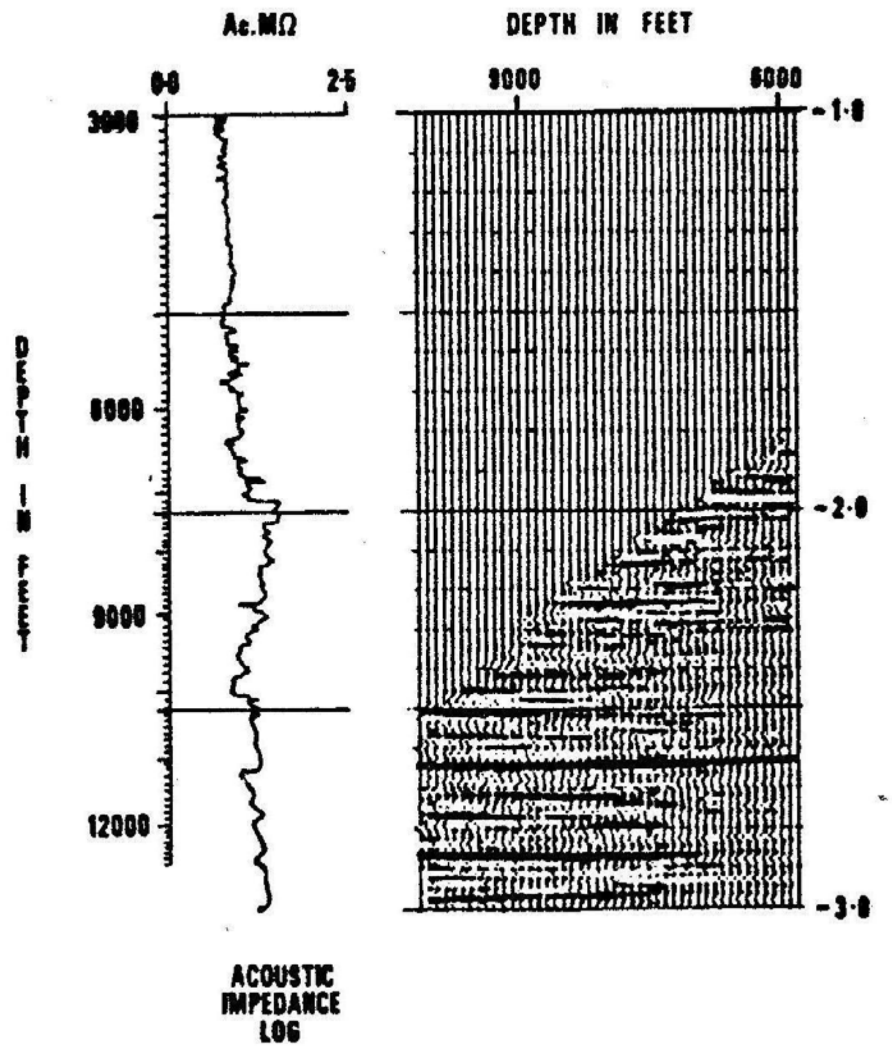

Predicting depth of seismic reflector

- دانستن عمق سر سازندها در حين حفاري و عمليات بعد از آن بسيار با اهميت است ، مشخص كردن سرسازندها را مي توان با استفاده از لرزه نگاري سطحي هم بدست آورد ولي در مناطقي كه چاه اكتشافي مي خواهيم حفر كنيم ، استفاده از اطلاعات سطحي با عدم قطعيت بالايي همراه است. بنابراين از اطلاعات VSP استفاده مي كنيم.
- از مزاياي استفاده از VSP به جاي لرزه نگاري سطحي در تعيين سر سازندها اين مي باشد كه چون ژئوفون ها در عمق است كمتر تحت تاثير نويزهاي سطحي قرار مي گيرند و تحليل آنها راحت تر است.
- شكل بعد يك مثال از يافتن سرسازندها است ، در اينجا براي مشخص كردن سرسازند ها محل برخورد امواج بالارونده با پايين رونده را مشخص كرده ، اين محل برخورد سطح بازتاب كننده مي باشد كه در اين شكل در عمق 9850 فوتي قرار دارد.

Predicting depth of a seismic reflector (courtesy Geophysical Press, from Hardage, B.A.: "Vertical Seismic Profiling, Part A: Principles," 1983)

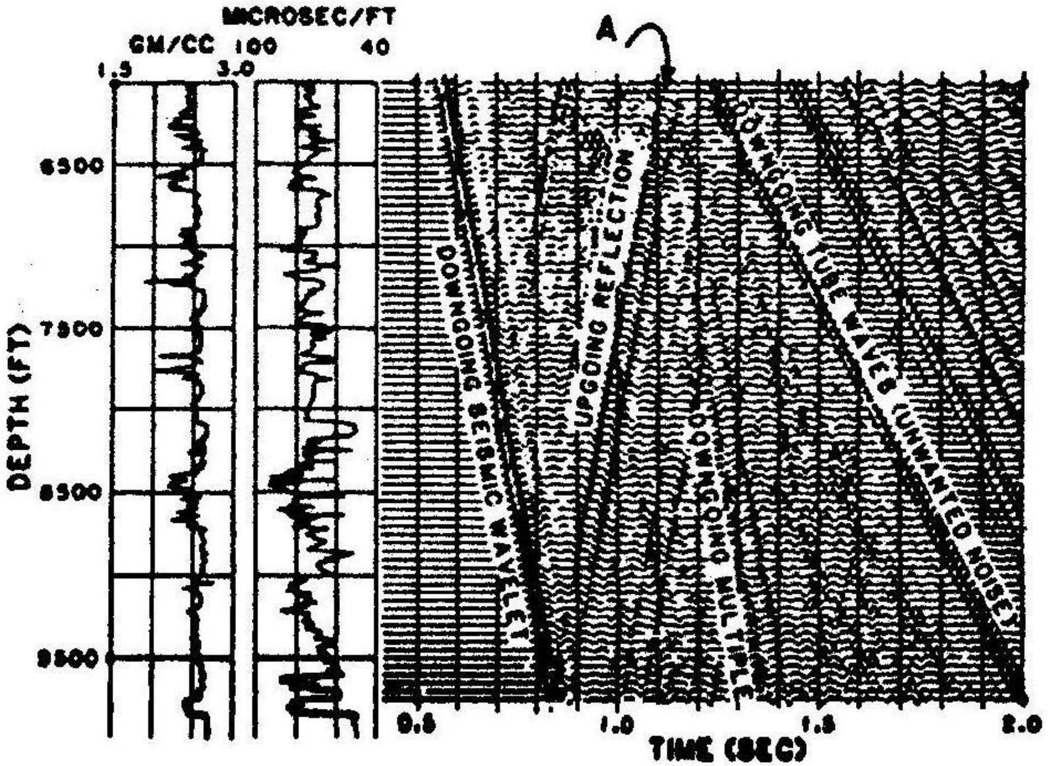

VSP DATA SHOWING A STRONG REFLECTOR, "A", ORIGINATING AT A DEPTH OF 9,850 FEET

Looking ahead of the bit

- از دیگر استفاده هاي VSP پیش بیني فاصله اي است كه مانده و باید حفاري شود تا به سرسازند مورد نظر برسیم.
- بر این اساس مي توان آمادگي لازم براي وارد شدن به آن لایه را از قبل داشت و در نتیجه عواملي مثل وزن گل را به مقدار لازم برسانیم.
- در اسلاید بعد تا عمق 8000 فوتي حفاري شده است و سپس داده هاي VSP برداشت شده ، سپس براي مشخص كردن محل سرسازند موجك هاي حاصل از امواج بالارونده و پایین رونده را امتداد داده و محل برخوردشان محل سرسازند را مشخص مي كند.

Looking ahead of the bit (courtesy Geophysical Press, from Hardage, B.A.: "Vertical Seismic Profiling, Part A: Principles," 1983)

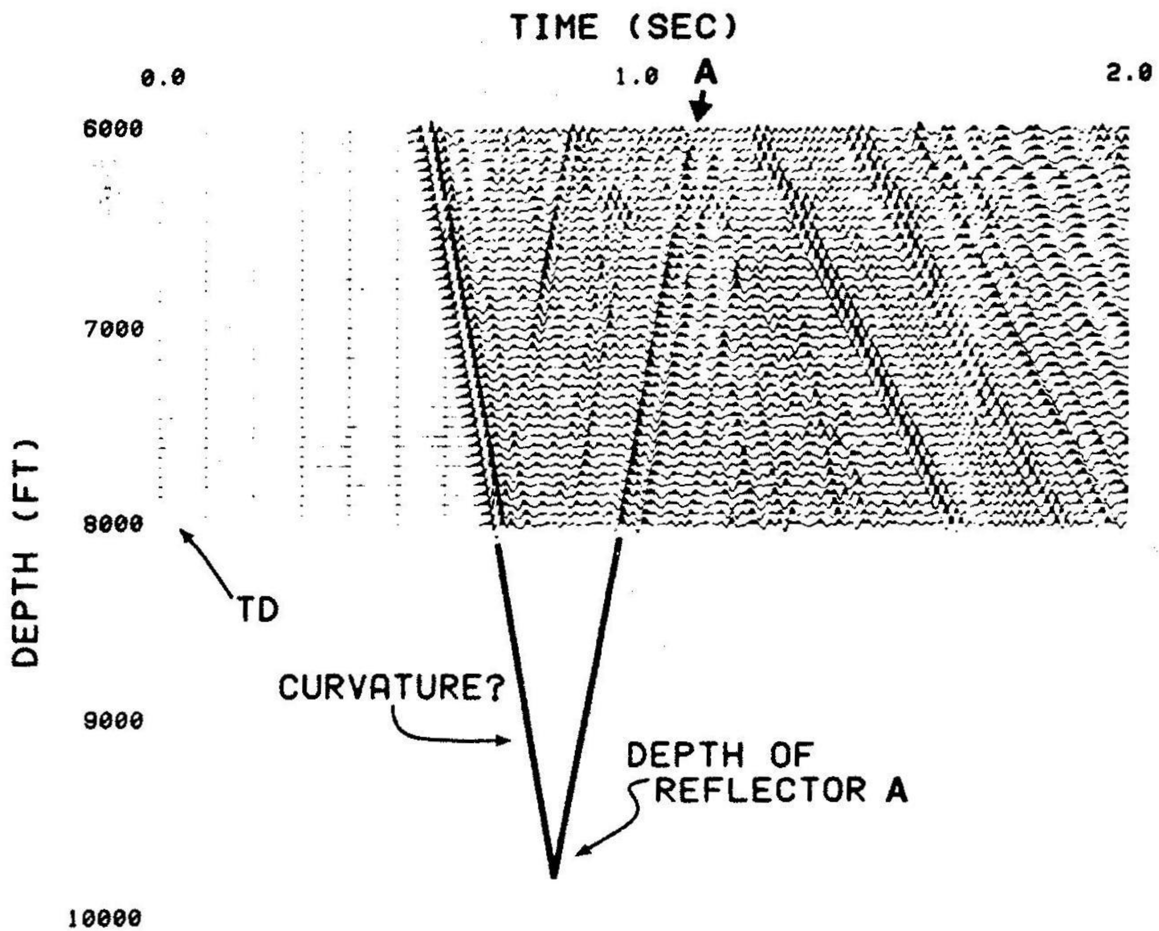

Predicting pore pressure & porosity ahead of the bit

- يكي ديگر از كاربردهاي جالب VSP اين مي باشد كه شرايط زير مته را مي توان توسط آن پيش بيني كرد.
- Stone و همكاران از VSP براي محاسبه ي سرعت نفوذ و عمق مته استفاده كردند و با تلفيق آن با اطلاعات پتروفيزيكي توانستند pore pressure و تخلخل را به طور دقيقي مشخص كنند.

مشخص كردن لايه با تراوايي بالا و ناحيه شكافدار

- امواج لوله اي علاوه بر توليد توسط موارد گفته شده مي توانند توسط امواج فشاري گذرنده از يك لايه با تراوايي بالا نيز توليد شده(شكستگي ها هم يك بخش با تراوايي بالا محسوب مي شوند) و به سمت بالا و پايين چاه حركت كنند.

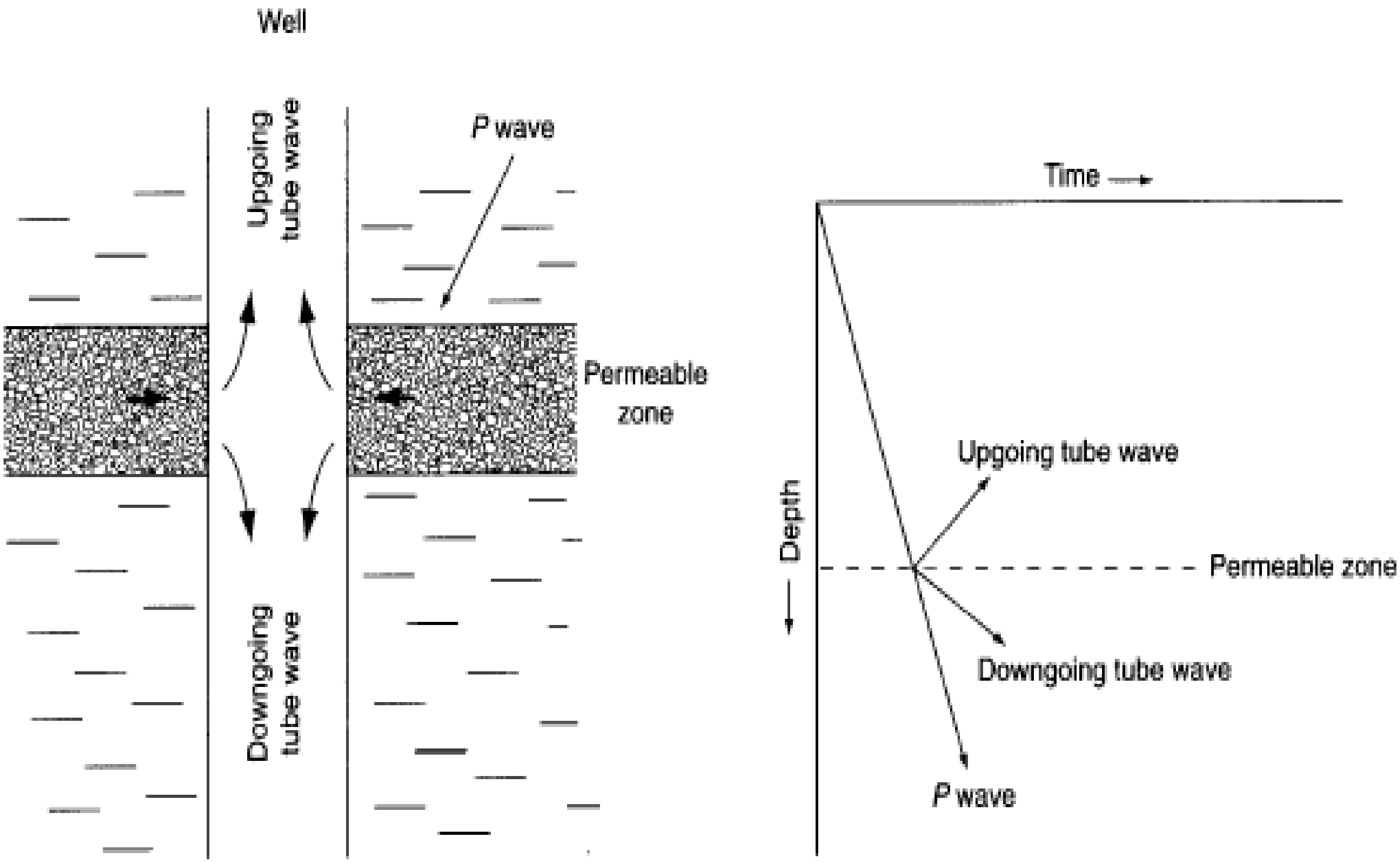
Well
Upgoing tube wave
P wave
Permeable zone
Downgoing tube wave
Time
Depth
Upgoing tube wave
Permeable zone
Downgoing tube wave
P wave

- همانطور که گفته شد امواج لوله اي در امتداد چاه حرکت کرده و در برخورد با نقطه اي که آمپيدانس صوتي تغيير کند امواج لوله اي ثانويه را ايجاد مي کنند.

- شکل زير يك نمونه ي خوبي از امواج لوله اي مي باشد.

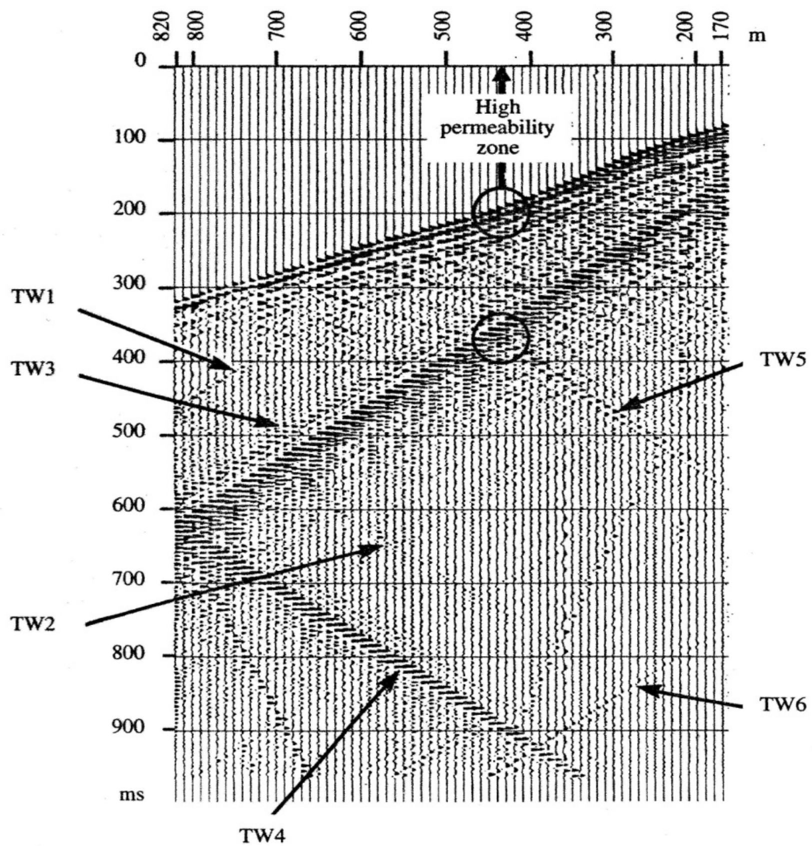

Tube waves (TW1 to TW6).
(Courtesy of Gaz de France-IFP)

- در اين شكل احتمال مي رود كه در عمقي حدود 440 متري يك لايه با تراوايي بالا وجود داشته باشد.
- در توجيه گفته ي بالا مي توان گفت كه:

1. امواج فشاري در عمقي حدود 440 متر يك سري امواج لوله اي توليد كرده كه به سمت پايين در حركت است به نام TW_1.
2. امواج TW_3 امواج لوله اي حاصل از امواج سطحي مي باشند زيرا از اعماق كم شروع شده و به سمت اعماق زياد ميروند ، اما اين امواج در عمق در حدود 440 متري امواج لوله اي ثانويه به نام TW_5 را به علت تغيير آمپيدانس بازتابانده به سمت بالا.

- امواج TW_4 نيز امواج بازتابانده است و TW_2 و TW_6 نيز امواج لوله اي پايين رونده هستند.

- در ادامه به بررسي يك Case stuy در مورد تعيين شيب لايه ها با استفاده از VSP در منطقه ي AUZANCE مي پردازيم.

- در اين مطالعه بعد از برداشت داده ها ، پردازش هاي اوليه زير را روي آنها انجام داده ايم.

1. اصلاحات مربوط به استفاده از يك vertical vibrator با sampling rate برابر 2 ميلي ثانيه.
2. Stack كردن سيگنال هاي خوانده شده.
3. اصلاحات مربوط به جهت هاي هر ژئوفون.
4. Despike كردن داده ها ي بدست آمده.

• در شكل زير مي توان لرزه نگاشت مربوط به امواج برشي و فشاري را مشاهده كرد.

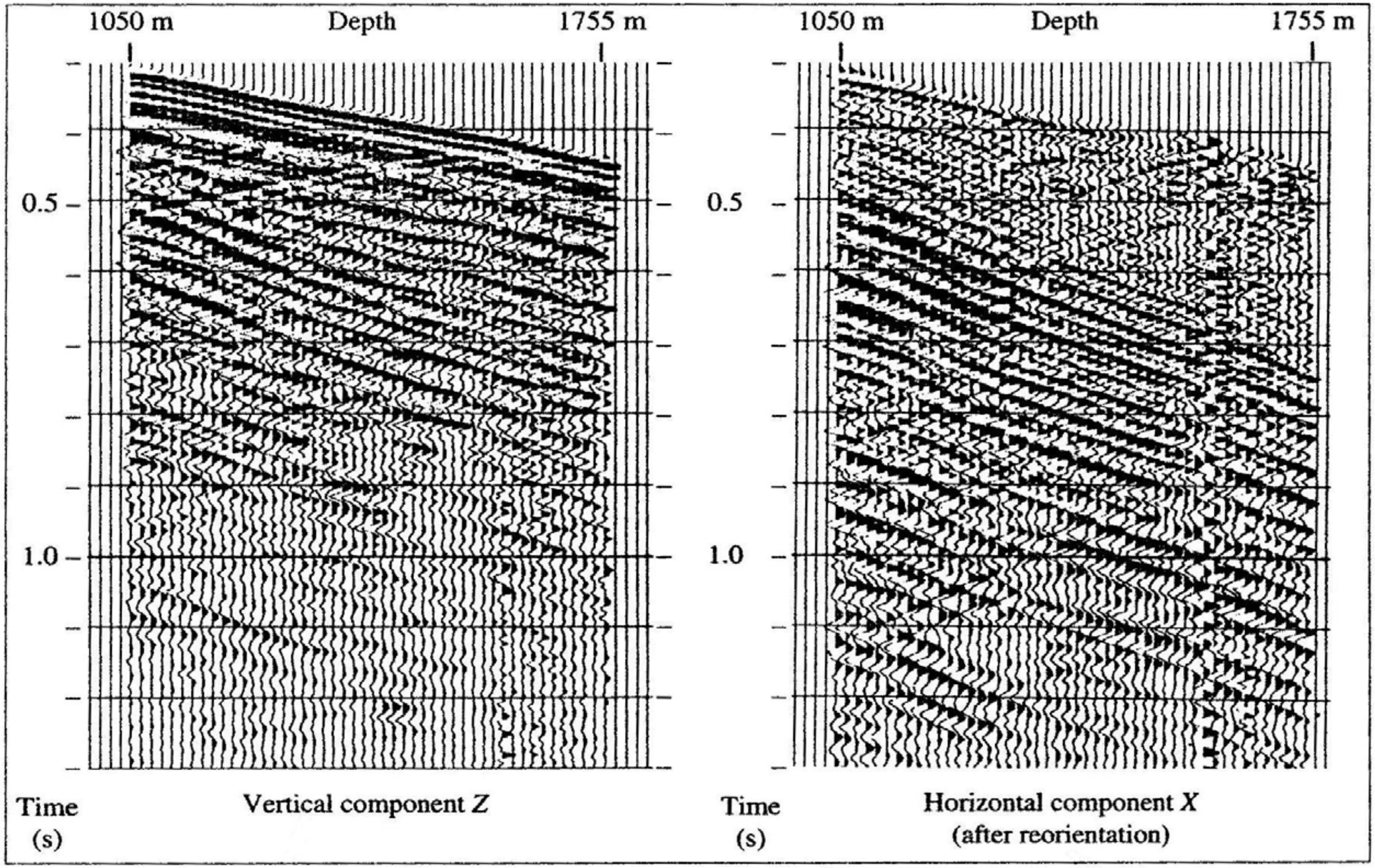

Horizontal and vertical components of VSP (well AZ 08).

- در اين مطالعه الگوريتمي كه براي جداسازي امواج به كار رفته ، الگوريتمي ابتكاري است كه توسط Mari & Gavin در سال 1990 پيشنهاد شده و تركيبي از فيلتر سرعت و فيلتر پلاريزان مي باشد.
- نهايتا با استفاده از داده هاي first arrival downgoing مقدار سرعت ها بدست آمده و بر اساس الگوهاي متقاطع مشخص شد كه 3 بازتاب كننده داريم كه در اسلايد بعد آن را مشاهده مي كنيد.

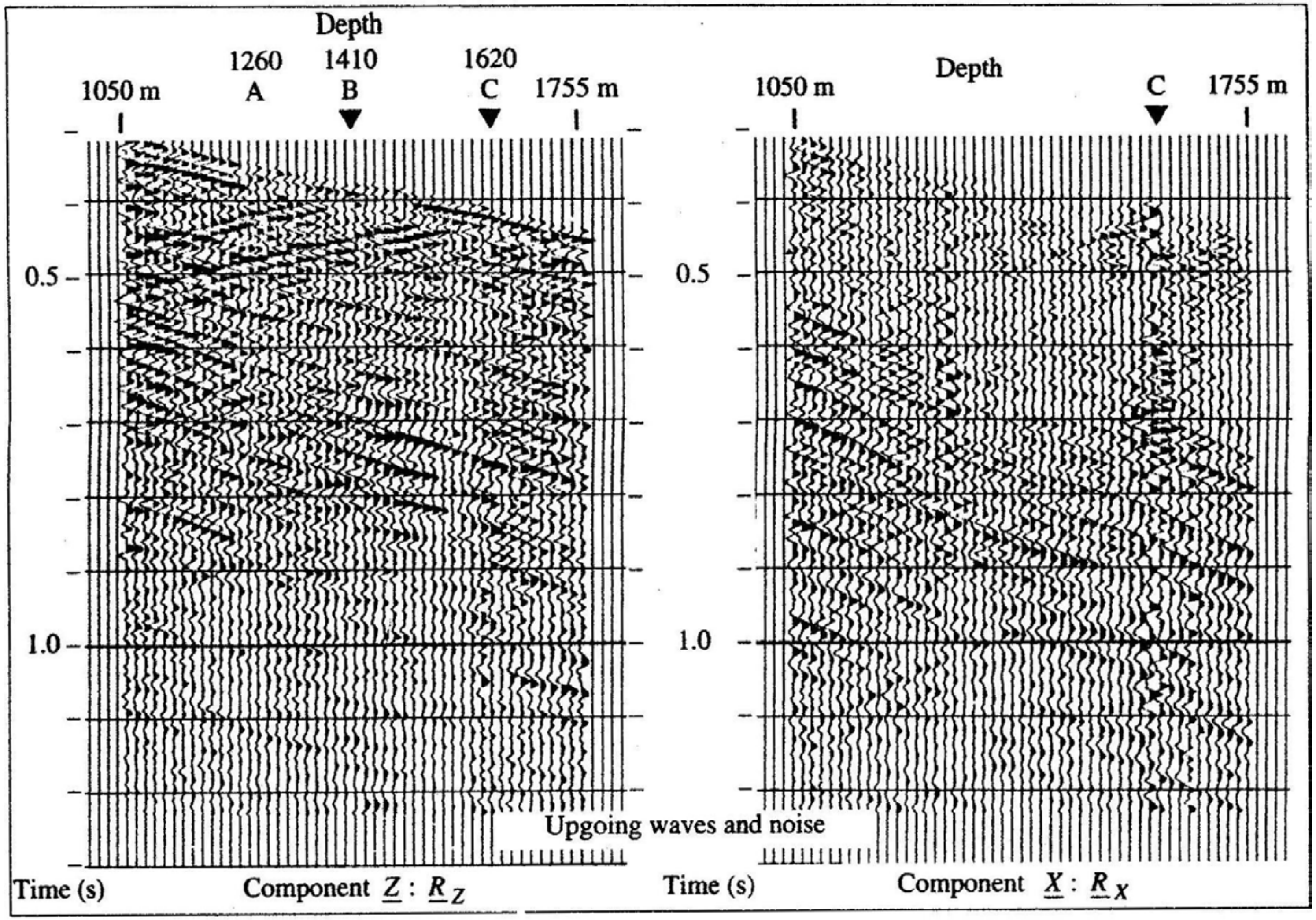

Residual VSP sections.

- شكل بالا سه بازتاب كننده A,B,C كه به ترتيب در اعماق 1753 ، 1410 و 1260 است مشخص شده است.
- حال براي بدست آوردن شيب لايه ها از cross plot داده هاي عمق بر حسب transmit time استفاده مي كنيم(cross plotمورد استفاده ابتكاري است كه در سال 1991 توسط Mari Gavin , پيشنهاد شده است).
- به عنوان نمونه در اسلايد بعد اين cross plot را براي بازتاب كننده ي C مشاهده مي كنيد.
- بر اساس اين cross plot شيب بازتاب كننده بين 20 تا 25 درجه بدست مي آيد.

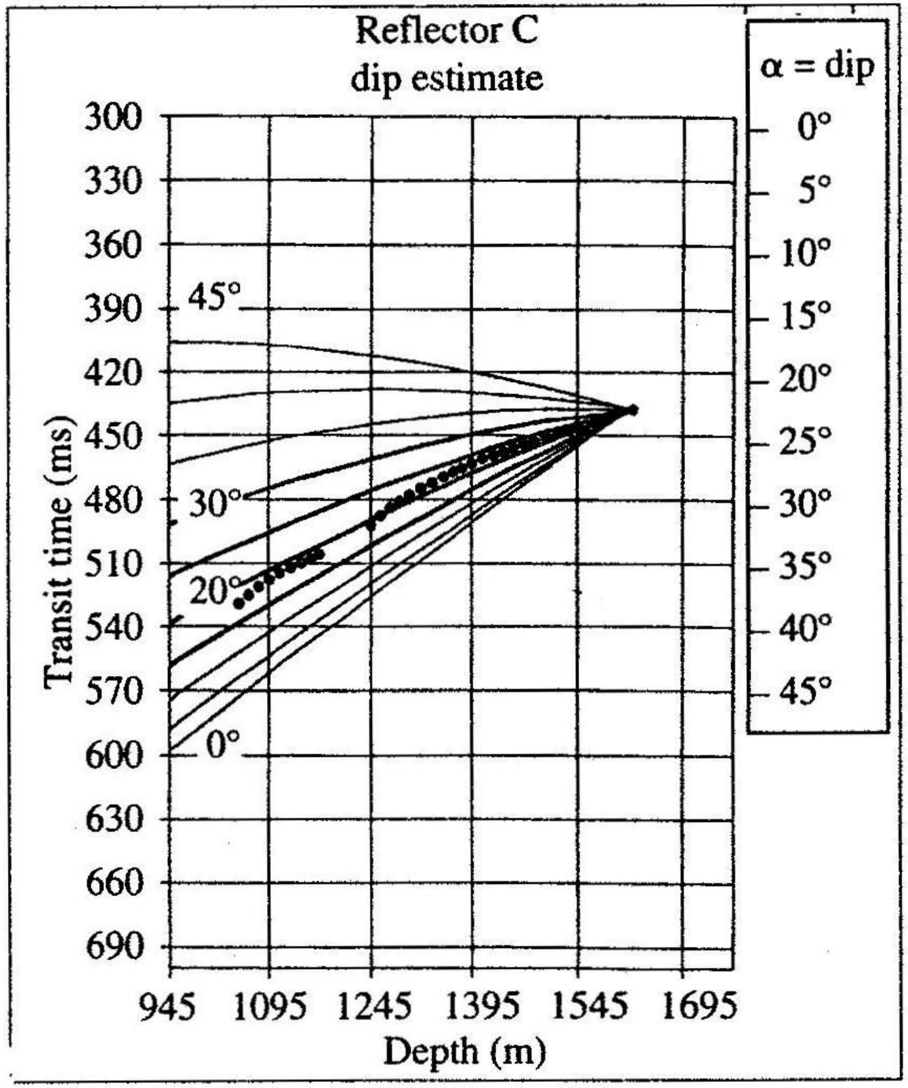

Chart used to estimate dip of reflector C.

- در جدول زير مي توان داده هاي بدست آمده براي هر سه سطح بازتاب كننده را مشاهده مي كنيد.

Marker	Depth(m)	Velocity(m/s)	Seismic dip(degrees)
A	1260	3750	10
B	1410	3800	10 To 15
C	1620	4000	20 To 25

- براي نشان دادن صحت اين روش نتايج را با نتايج حاصل از نمودار dipmeter مقايسه مي كنيم و به اين نتيجه مي رسيم كه دقت كار VSP در حدود 5 درجه اختلاف با نتايج نمودار شيب سنج دارد.

- داده هاي شيب سنج برابر است با:

A $\longrightarrow$ 10 – 20

B $\longrightarrow$ 14 – 18

C $\longrightarrow$ 20 - 30

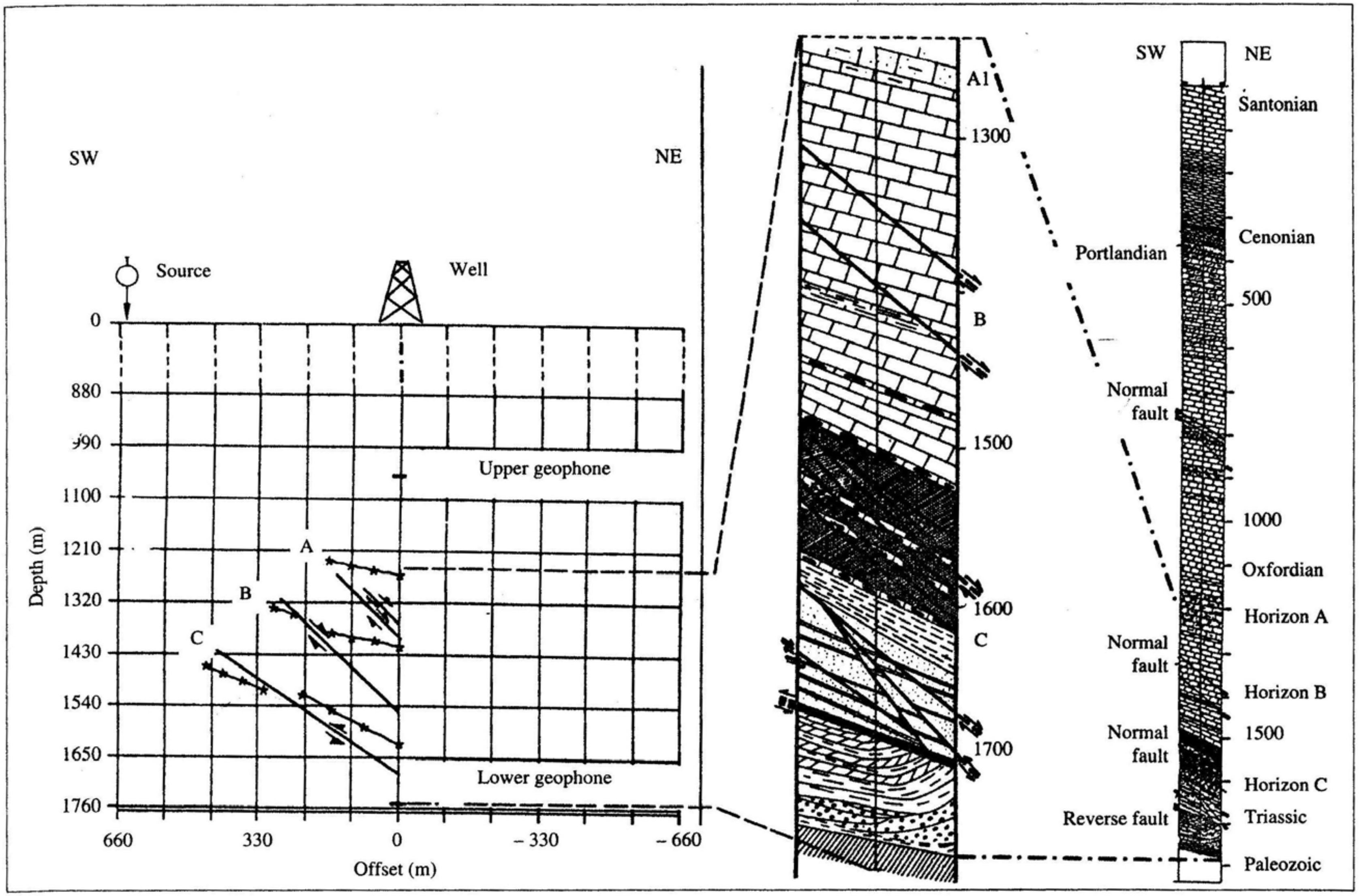

Geological model of the Auzance structure based on VSP survey and dipmeter logging. *(Courtesy of Gaz de France)*

- ابزار مورد نیاز در VSP عبارتند از:

1. حفره چاه
2. منبع انرژي
3. ژئوفون درون چاهي
4. سیستم جمع آوري اطلاعات

Borehole

- فاكتورهاي اثر گذار درمورد چاه عبارتند از:

a) Hole deviation:

- برداشت در چاه قائم اقتصادي تر و تفسير آن راحت تر مي باشد.
- در چاه كج ، داراي يك عدم قطعيت در مورد محل ژئوفون ها مي باشيم.
- چاه كج داراي اين حسن مي باشد كه در صورتي كه از يك سكوي دريايي چندين چاه كج حفر كرده باشيم مي توان با داده هاي بدست آمده يك مدل بسيار عالي از لايه ها و مخزن بسازيم.

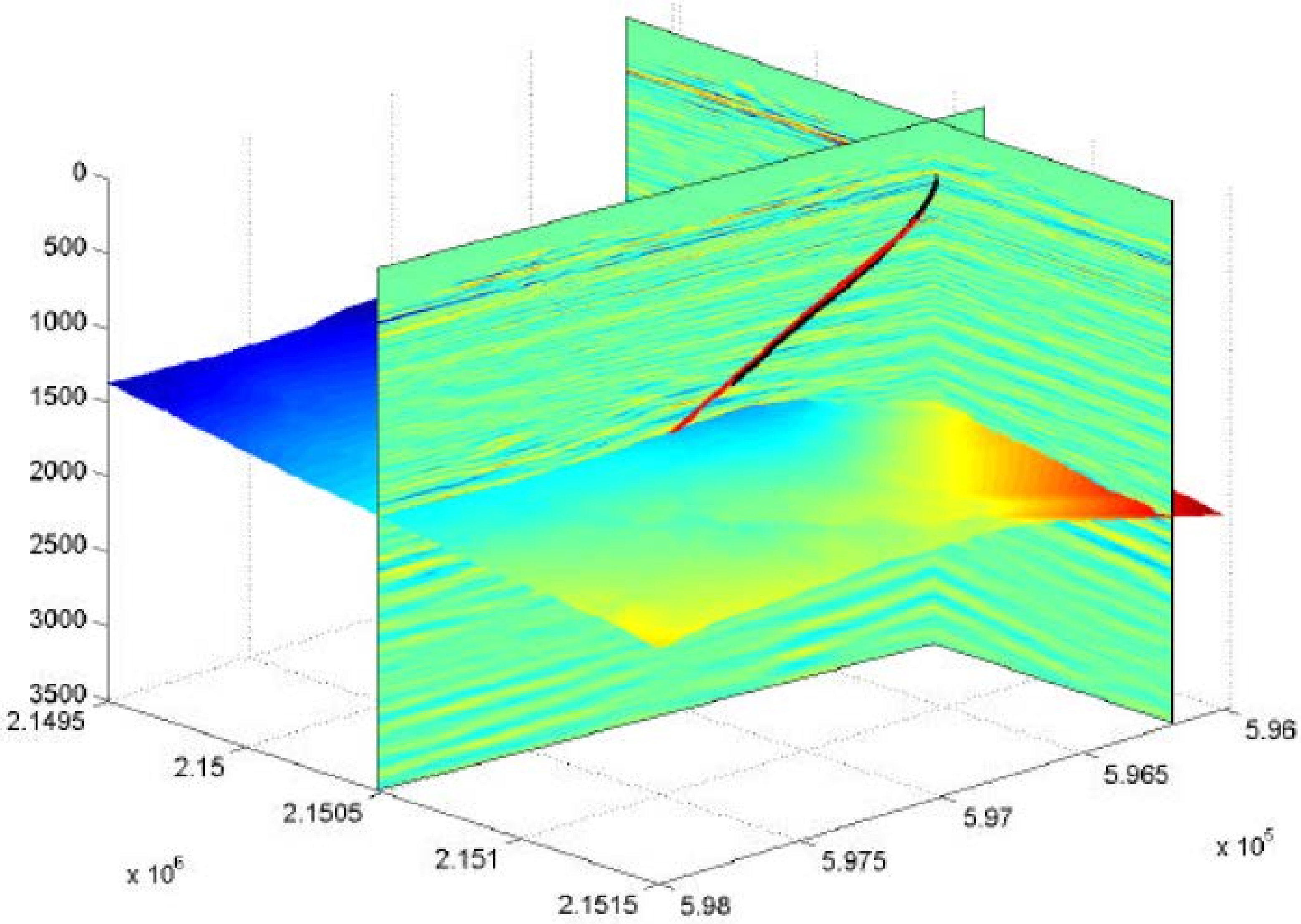
0
500
1000
1500
2000
2500
3000
3500
2.1495
2.15
2.1505
2.151
2.1515
x 10^6
5.96
5.965
5.97
5.975
5.98
x 10^5

b) لوله ي جداري و سيمان كاري:

- انجام عمليات VSP در يك چاه داراي لوله جداري ترجيح داده مي شود ، چون مشكلاتي نظير گير كردن ابزار ، وجود انحناي ناخواسته در ديواره و ... وجود ندارد.
- در جايي كه لوله جداري وجود دارد بايد پشت آن حتما سيمان شده باشد تا اينكه يك محيط كه توانايي انتقال انرژي صوتي را دارد ايجاد شود.

- در كل ژئوفون ها ممكن است در 4 محيط مختلف قرار گيرند كه عبارت است از:

1. يك لوله جداري كه به تنهايي سيمان شده است
2. بدون لوله جداري(open hole)
3. يك لوله جداري بدون سيمان شدگي ولي قديمي به گونه اي كه گل و مواد همراه گل در پشت لوله جداري به شكل جامد درآيند.
4. يك لوله جداري جديد كه هنوز سيمان نشده است.

c) شعاع چاه:

- در يك چاه uncased، ناهمواري هاي ديواره چاه مي تواند روي چسبانده شدن ژئوفون به ديواره مشكل ايجاد كند به خصوص در مناطقي كه washout شده باشد، بر همين اساس بايد قبل از انتخاب محل قرار گيري ژئوفون ها نمودارcaliper گرفته شود و بر اين اساس محل ژئوفون ها مشخص شود.

- Blair در سال 1982 نشان داد كه به شرطي كه طول موج امواج بيش از 10 برابر قطر چاه باشد مي توان ژئوفون ها را در هر سمت از ديواره چاه قرار داد و در صورتي كه طول موج كوچكتر از 10 برابر قطر چاه باشد بايد از دو ژئوفون در دو سمت مقابل استفاده كرد ، به اين آرايش waveshadow مي گويند.

d. موانع موجود در چاه:

- در چاه هاي casing شده ممكن است موانعي مانند packer و يا هر وسيله اي ديگري در در چاه وجود داشته باشد كه در مسير ژئوفون ها ايجاد ممانعت كند براي همين ما قبل از انجام عمليات VSP بايد به وسيله ي يك tools ارزان كه از نظر قطر با قطر ژئوفون ها يكسان باشد را در چاه راند و مشخص كرد كه مانعي در سر راه ژئوفون ها وجود ندارد و سپس شروع به عمليات VSP كنيم.
- ترجيح بر اين است كه ما ژئوفون ها را در عمق هايي قرار دهيم كه بيشترين اطلاعات پتروفيزيكي را از آن نقطه داريم ، به خصوص نمودار CBL كه مشخص مي كند پشت لوله جداري سيمان است يا نه!

VSP energy source

- منبع بايد يك جبهه موج استوار و قابل تكرار ايجاد كند.
- مقدار انرژي منبع بايد با دقت مشخص شده و يك مقدار optimum انتخاب شود ، زيرا "بيشترين انرژي منبع ، بهترين نتايج را نمي دهد".
- ابزاري كه از آنها به عنوان منبع ايجاد مي شود عبارتند از:
- 1- ديناميت 2- mechanical impulse source 3- vibrator 4- air guns

Seismic source

- مي توان منبع انرژي را به دو گروه خشكي و دريايي تقسيم كرد.
- منبع انرژي دريايـي اصلي عبارتند از:

1. Air gun
2. Water gun

- منبع انرژي خشکی اصلي عبارتند از:

1. Vertical vibrator or horizontal vibrator
2. Weight – droppers
3. با حفر يك گودال آب از air gun استفاده کنیم.

ديناميت

- ديناميت دفن شده مقدار ضريب كاهش دامنه اي برابر 2 دارد اما ديناميت معلق در هوا ضريب كاهشي برابر 30 دارد.
- استفاده از ديناميت براي اين كه بخواهيم چند شات داشته باشيم كه جبهه ي يكساني داشته باشد مشكل است.
- در استفاده از ديناميت قطر و عمق گمانه انفجار بايد به دقت مشخص شود و اين عمق بايد زير لايه هوازده باشد ، ونيز ديواره گمانه بايد casing گذاري شده باشد تا سازند به داخل نريزد.
- مي توان داخل گمانه محل انفجار را پر از آب كرد تا ضريب كاهش دامنه را كم كنيم.

Shot hole design for repeatable wavelet (modified from Hardage, 1983)

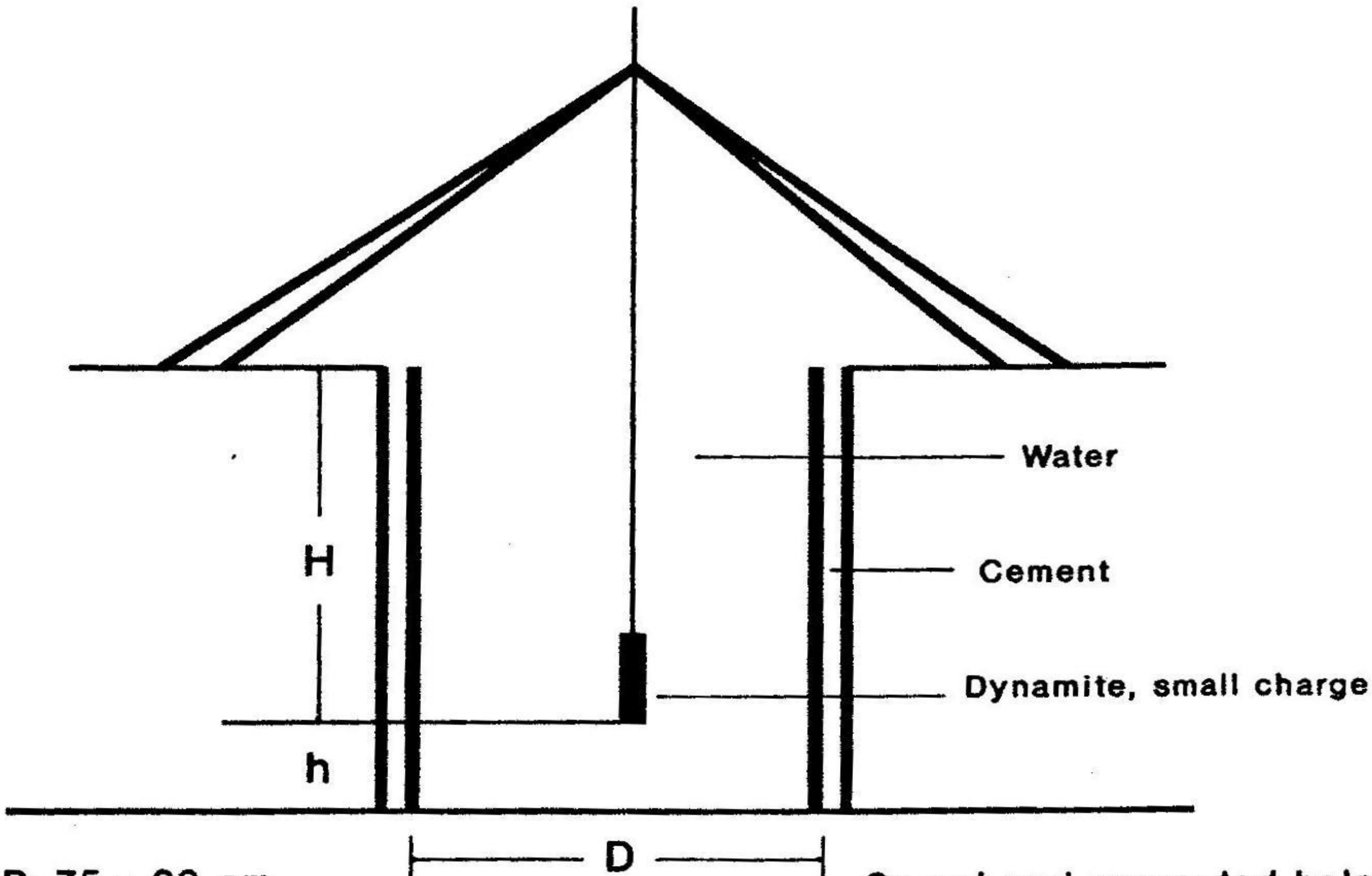

D: 75 - 90 cm
H: 12-15 meters
h: 3 meters

Cased and cemented hole
Charge size: .5-1.5 Kg

Mechanical impulse source

- استفاده از این منبع براي عملیات VSP بسیار مناسب است ، اما باید قبل از انجام کار محل عملیات براي امکان استفاده از این روش تست شود.

Mixed P- and S-wave impulse source: Soursile (IFP).

Vibrators

- این وسیله چون قابل حمل است این امکان را مي دهد که در نقاط مختلف شات داشته باشیم.
- Vibrator بهترین انتخاب براي عملیات VSP مي باشد چون مي تواند یك جبهه موج مناسب و تکرار پذیر را ایجاد کند.

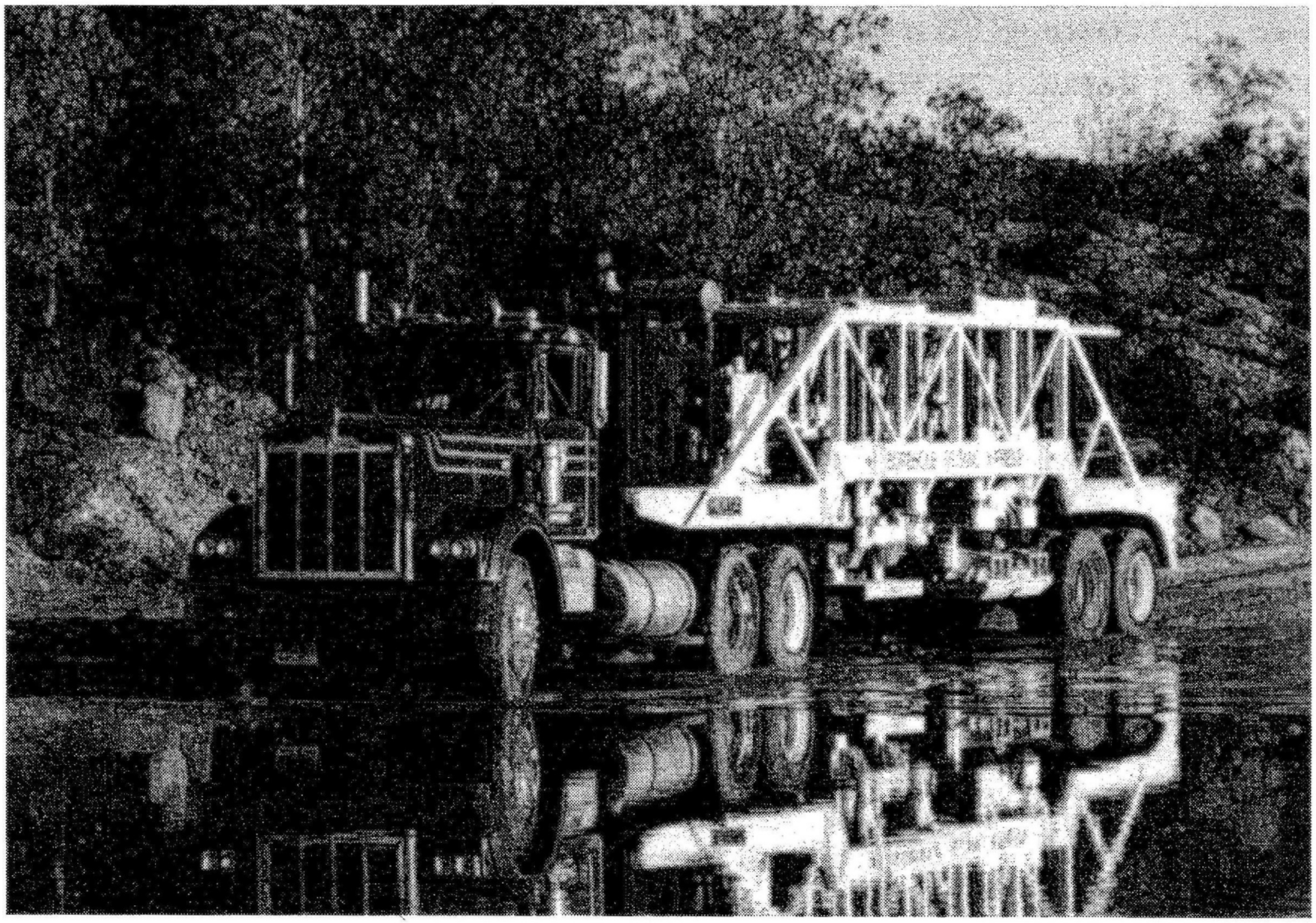

Mixed *P*- and *S*-wave vibrator source specially designed for well seismic acquisition (Mertz).

Air gun

- عمليات با air gun خيلي راحت است.
- Air gunوسيله اي ايمن است.
- Air gun را مي توان مطابق شكل زير در خشكي هم استفاده كرد

Using a marine air gun as an onshore VSP energy source (modified from Hardage, 1983)

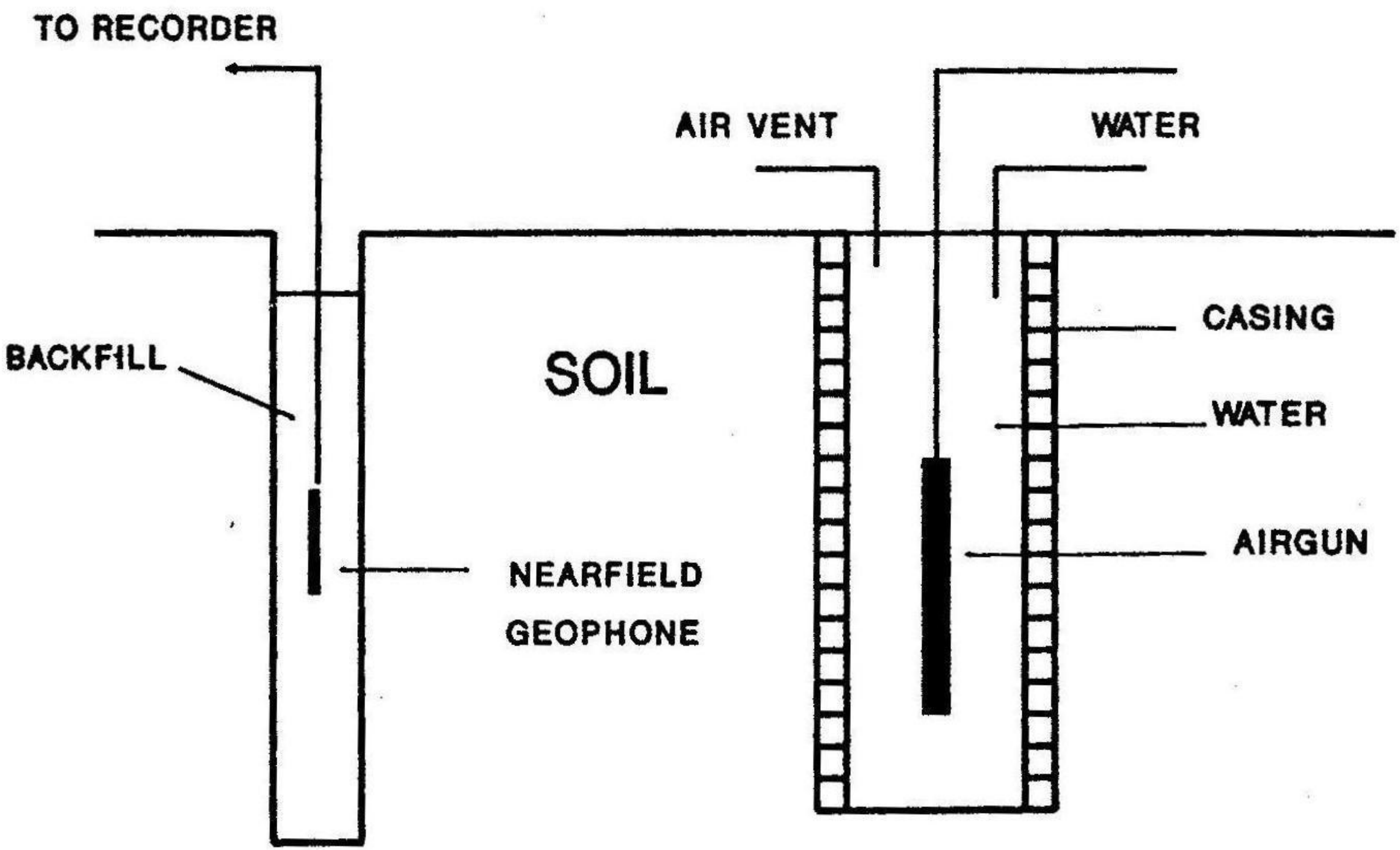

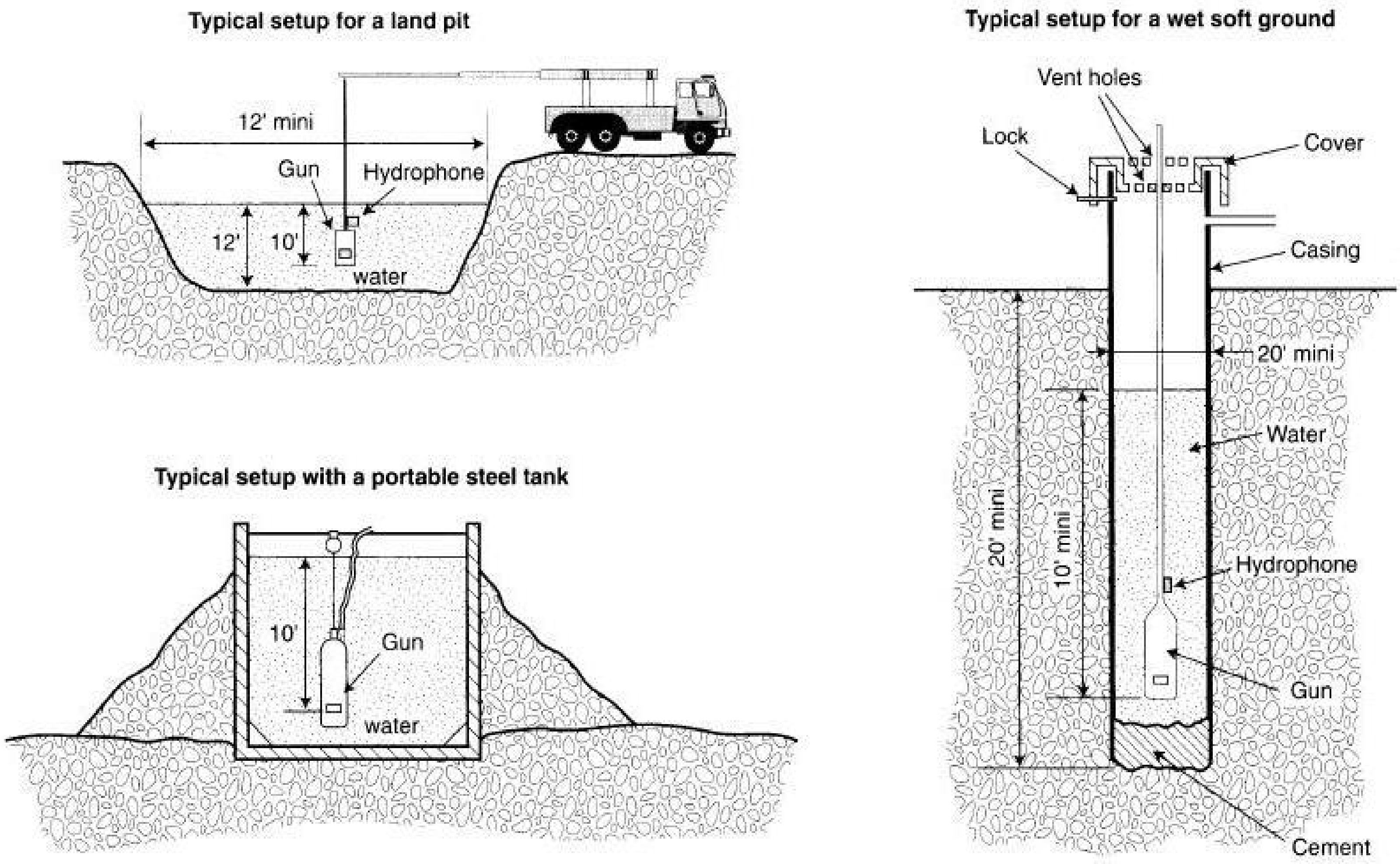

Possible implementations of marine sources in onshore well seismic acquisition (Schlumberger).

Energy in put

- مقدار انرژي velocity survey و VSP survey كاملا با هم متفاوت است حتي مي توان گفت كه مقابل هم مي باشند.
- در velocity survey فقط مي خواهيم اولين موج رسيده را مورد بررسي قرار دهيم ولي در VSPعلاوه بر اولين موج رسيده به امواج بالارونده و پايين رونده را هم نياز داريم.
- بنابراين در عمليات VSP نياز به انرژي بيشتري داريم زيرا موج بايد بعد از بازتاب در بازتاب كننده اي در عمق ، در ژئوفوني در فاصله ي بسيار بالاتر از آن ثبت شود براي همين انرژي بيشتري نياز داريم.

cable

- در عمليات VSP كابل كلاس 7 به كار مي رود كه توسط Well – logger ها به كار مي رود.

The downhole geophone

- در شكل زير مي توان تفاوت ظاهري ژئوفون هاي سطحي را با درون چاهي مشاهده كرد.
- ژئوفون هاي درون چاهي قابليت تحمل دما و فشار بالا را دارند و توسط يك arm به ديواره مي چسبد.

A typical land geophone and a VSP geophone (modified from Hardage, 1983)

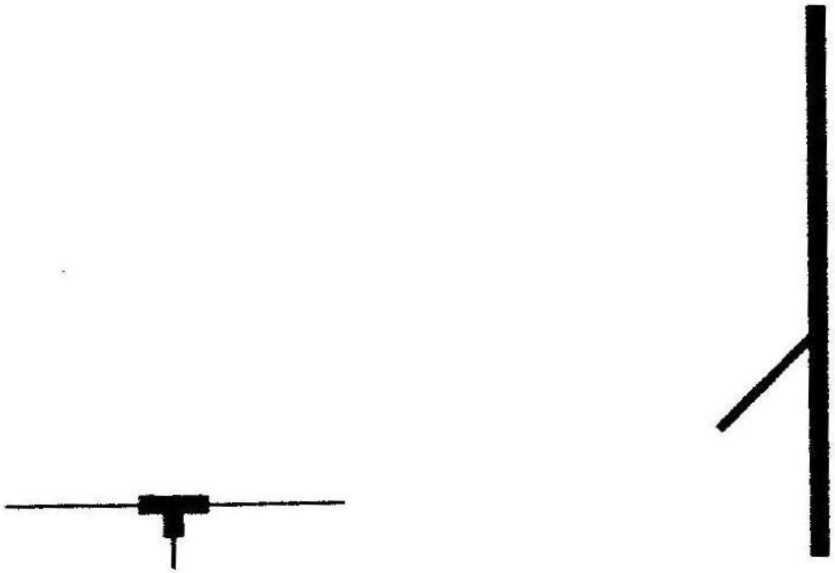

Spike-planted land geophone

Downhole VSP geophone

Parameters

Spike-planted land geophone	Downhole VSP geophone
Length: 10 cm (4 Inches)	Length: 3 m (9.8 Feet)
Diameter: 3 cm (one Inch)	Diameter: 10 cm (4 Inches)
Weight: 200 gm (.45 Pound)	Weight: 100 Kg (225 pounds)

- گيرنده بايد داراي دو خاصيت باشد:

1. حداقل اثر را از امواج لوله اي بگيرد.
2. به بهترين وجه به سازند بچسبد.

- براي رسيدن به هدف اول بايد ابزار حداقل سايز و قطر را داشته باشد.
- براي رسيدن به هدف دوم بايد حداقل وزن و بيشترين سطح تماس را با چاه داشته باشد.

- ژئوفون ها درون چاهي امروزه داراي سه بخش هستند.

1. ژئوفون
2. هيدروفون
3. Inclinometer

- ژئوفون ها نسل جديد داراي يك گيرنده گاماري نيز مي باشند که نتايج بدست آمده از آن را با نمودار گاماي بدست آمده از عمليات logging مقايسه کرده و براي تصحيح عمق VSP به کار برده مي شود.

A

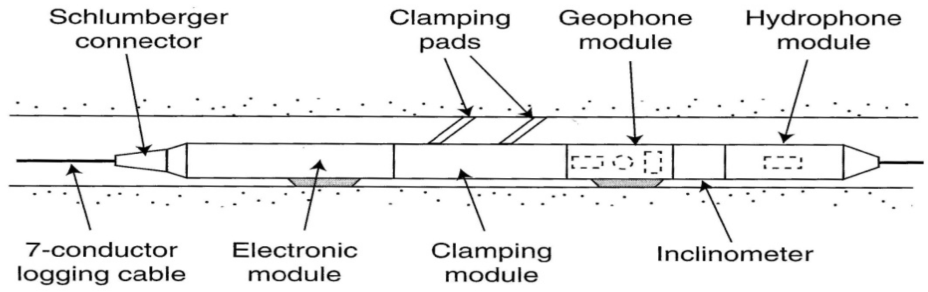

B

CGG-IFP ARTEP SPH well-logging tool (IFP). Length: 2.36 m; diameter: 10 cm; weight: 94 kg; temperature and pressure limits: 180°C and 1 200 bars; seismic equipment: 3-component geophone, hydrophone, inclinometer. **A**. Schematic. **B**. Picture.

THE CSI* TOOL: A new design architecture

A New Architecture

The CSI tool is a new-generation three-axis borehole seismic tool. It is designed for superior performance and combinability with itself, an array of sensors, and with other tools such as:
- Gamma Ray for accurate depth control
- Inclinometry tool for accurate spatial orientation
- Auxiliary measurement sonde for safety

Features

- Sensor module decoupled from sonde body
- Combinability
- Coupling quantified through shaker responses
- Powerful downhole electronics
- Gimbal-mounted geophones with locking system
- In-situ geophones and electronic calibration

Design Objectives

- **Acoustic quality of the system**
  Cartridge, sonde, module, gimbal and sensors have been designed and tested to ensure a system response identical to that of a single geophone.
- **Acoustic quality optimized in the borehole**
  Sensor module decoupling, points of contact design and explicit measurement of the coupling quality through shaker activation, all contribute to enhance signal quality.
- **Signal processing quality**
  All electronic and mechanical parameters affecting signal reproduction are measured by in-situ tests.
- **Efficiency through combination**
  The new receiver architecture has brought combination capability without compromising signal quality.

Tool Schematic

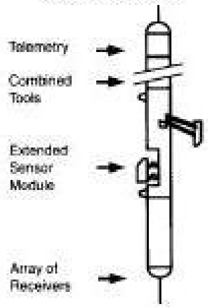

Sensor Module

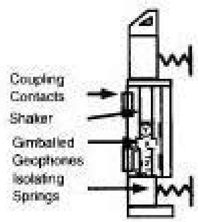

Combinable Seismic Imager

* Mark of Schlumberger

SPECIFICATIONS

General

Length (1 tool)	5340 mm	214 in.
Weight (1 tool)	123 kg	271 lbs
Diameter*	117 mm	4-5/8 in.
Maximum opening**	483 mm	19 in.
Anchoring force: 5 in.	280 da N	630 lbs
10 in.	320 daN	719 lbs
19 in.	500 da N	1124 lbs
Gimbal tilt range	0 to 90°	

* 4 in. without stand-off
** 22 in. with pad extension

Environmental ratings

Pressure rating	1400 bars	20,000 psi
Temperature rating	175°C	350°F

Measurements

Sampling rate	2 KHz
Selectable output sampling rates:	0.5, 1, 2 and 4 ms
Analog-to-digital conversion with autoranger: 16 bits	
Preamplifier gain:	30 dB
Amplifier gain:	6-72 dB in 6 dB steps; selectable per channel
Analog filter:	
Low-cut frequency (- 3 dB)	2.5 Hz
Low-cut slope	+ 12 dB/octave
High-cut frequency (- 3 dB)	300 Hz
High-cut slope	-36 dB/octave
Digital filter rejection at Nyquist	>70 dB
Synchronization	±45 µs after calibration
Tool transfer function flat below geophone spurious frequency	
Gimbal deviation	±1° after calibration
Gimbal relative bearing	±1° after calibration
Caliper	±0.1" after calibration
In-situ calibration tests	
Multiplexer for logging, seismic and auxiliary channels	
Sonde control and safety in absence of telemetry	

Combinations

Example of open hole combination

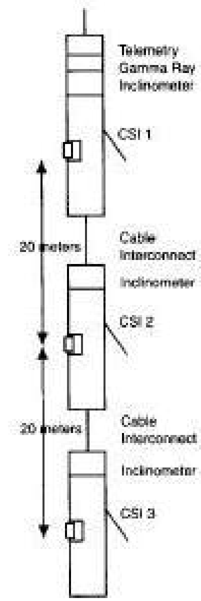

Maximum recommended combinations:
3 tools in open hole
4 tools in cased hole

Combinable Seismic Imager

* Mark of Schlumberger

Characteristics of the CSI tool (Schlumberger).

Downhole Geophone Array Specifications

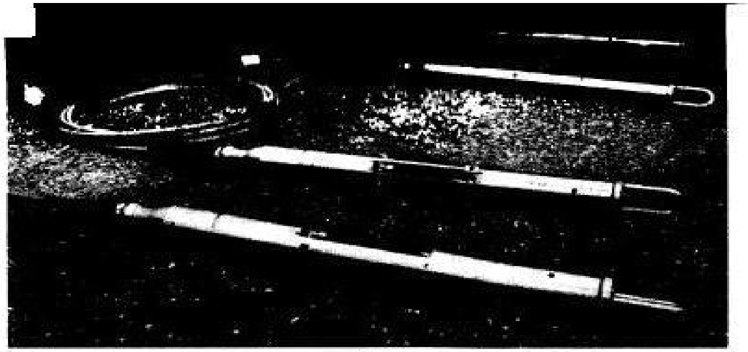

TOOL CONFIGURATION

(a.)	Master Unit comprising:	
	Tension Compression Unit	TCU
	Seismic Telemetry Unit	STU
	Hydraulic Power Unit	HPU
	Hydraulic Clamping Unit	HCU
(b.)	Up to 12 individual receivers or Hydraulic Seismic Unit	HSU
(c.)	Weight Unit (incorporates motion sensor)	WU

TENSION COMPRESSION UNIT (TCU)

Accuracy	+/- 10 daN	
	+/- 22 lbf	
Tension max	+/- 5000 daN	
	+/- 11,250 lbf	
Temperature max	180°C	356°F
Pressure max	1,200 bar	17,600 psi

SEISMIC TELEMETRY UNIT (STU)

Temperature max	150°C	300°F
Pressure max	1,200 bar	17,600 psi
Uplink telemetry rate	512 kbaud	

HYDRAULIC POWER/CLAMPING UNIT (HPU/HCU)

Temperature max	180°C	356°F
Pressure max	1,200 bar	17,600 psi
Pump motor voltage	220 V	(270V at surface on wireline)
Pump motor current (max)	700 mA	(torque limiter acts at c.800mA)
Over pressure relief valve	155 bar +/- 5 bar	2,280 psi +/- 70 psi
Tension safety valve	850 daN	1,900 lbf
Hydraulic oil capacity	c. 10 litres	c.2.2 gals
Hydraulic oil type	Univis J13	

All specifications subject to change without notice

HYDRAULIC SEISMIC UNIT (HSU)

Temperature max	150°C	300°F
Pressure max	1,200 bar	17,600 psi
Locking force	140 daN max. 300 lbf max	
Weak links	Graduated decreasing values with depth down sting	
Hydraulic oil capacity	1 litre	0.22 gals
Digitisers	24 bit delta-sigma	
Sample rate & alias filter	2,1, 0.5, 0.25 ms, 187.5,375,750,1500 Hz	
Dynamic range	> 110 dB	
Distortion	< 0.1 %	
DC offset	< 0.1 µV (self calibrating)	
Geophone pre-amp gain	54 dB	
Receivers	- 3 orthogonal SMC1850 10 Hz gimballed geophones. or 3 orthogonal SMC1850 10 Hz fixed geophones or 3 orthogonal SMC1850 30 Hz fixed geophones -1 down-hole hydrophone, sensitivity -88 dB re 1V / µbar	

1998 CGG

SURFACE CONTROLE PANEL (SCP)

Operating temperature max	40 deg C
Mains voltage	230 V AC
Current max	5 A
Size	19" 6U chassis
Features	Telemetry receiver with dedicated FFT processor card and cable equalisation Graphical display of motor current vs. time. Software control of Parameters and settings

ACQUISITION SURFACE PANEL (ASP)

Operating temperature max	40 deg °C
Mains Voltage	90-260V AC
Current max	5 A
Size	19" 6U chassis
Features	48 seismic + 4 auxiliary digital channels via data link from SCP 8 analogue channels (24 bit delta-sigma as in SST500 HSUs) Source controller interfaces Control and data link to PC recording system

WEIGHT AND DIMENSIONS

Complete Tool String	12 level 10m int.	6 level 10m int.	6 level 20m int.	8 level 15m int.
Tool string length overall	132.7m (435.4ft)	72.7m (238.4ft)	132.7m (435.4ft)	132.7m (435.4ft)
Length below HCU depth zero point	128.2m (420.6ft)	68.2m (223.7ft)	128.2m (420.6ft)	128.2m (420.6ft)
Tool string weight in air	630kg (1390lbs)	450kg (993lbs)	542kg (1196lbs)	588kg (1298lbs)

LOCKING RANGES

	Maximum tool o/d		Minimum Locking dia		Max Locking dia	
7"arm kit	92mm	(3 5/8")	102mm	(4")	183mm	(7.2")
9 5/8" arm kit	103mm	(4")	108.6mm	(4.27")	231 mm	(9.1 ")
13" arm kit	155mm	(6.1 ")	165mm	(6.5")	330mm	(13.0")
16" arm kit	155mm	(6.1 ")	T.B.A	(T.B.A)	408mm	(16.1 ")

INTER-RECEIVER INTERVALS

Selectable at:	10 metre	15 metre	20 metre

All specifications subject to change without notice

1998 CGG

Characteristics of the SST-500 tool (CGG).

- در زير ابزار جديد schlumberger مي باشد كه نام آن MAST است و ويژگي هاي آن را در اسلايد بعد مشاهده مي كنيد.

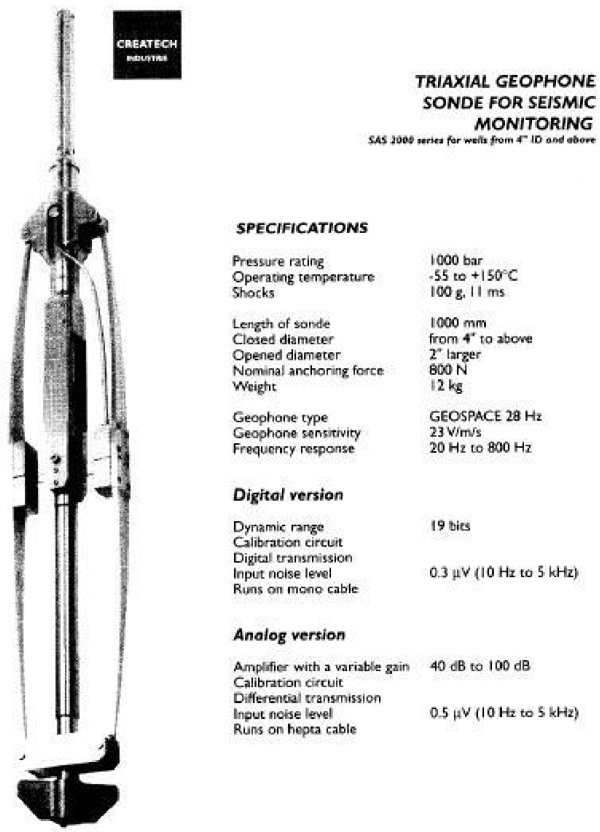
CREATECH INDUSTRIE

TRIAXIAL GEOPHONE SONDE FOR SEISMIC MONITORING

SAS 2000 series for wells from 4" ID and above

SPECIFICATIONS

Pressure rating	1000 bar
Operating temperature	-55 to +150°C
Shocks	100 g, 11 ms
Length of sonde	1000 mm
Closed diameter	from 4" to above
Opened diameter	2" larger
Nominal anchoring force	800 N
Weight	12 kg
Geophone type	GEOSPACE 28 Hz
Geophone sensitivity	23 V/m/s
Frequency response	20 Hz to 800 Hz

Digital version

Dynamic range	19 bits
Calibration circuit	
Digital transmission	
Input noise level	0.3 µV (10 Hz to 5 kHz)
Runs on mono cable	

Analog version

Amplifier with a variable gain	40 dB to 100 dB
Calibration circuit	
Differential transmission	
Input noise level	0.5 µV (10 Hz to 5 kHz)
Runs on hepta cable	

Example of monitoring tool (Createch).

Clamping type	mechanical arm
Clamping force	165 lbs
Tool Weight	10 kg/22 lbs (shuttle)
Tool Length	5 ft (shuttle)
Tool Type	array
Simultaneous levels	up to 8
Spacing	variable
Combinability	GR
Sensor Type	GAC* (3-200 Hz)
Diameter	48 mm / 1 7/8"
Min Operating Diameter	59 mm / 2 5/16"
Max Operating Diameter	270 mm / 10.6"
(using different arm)	450 mm / 17.7"
Max Deviation	no limit
Downhole AD conversion	16 bits
Downhole Dynamic Range	152 dB
Sample rate	0.5, 1, 2, 4 ms
Time between shots	15 s (4 s/1 ms/24 channels)
Max Temperature	140°C/285°F
Max Pressure	10000 psi
Recording System	Standalone (PC)
Logging Cable	Mono/Heptacable

Technical characteristics of the MSAT system (*Modular Seismic Array Tool*) (Schlumberger).

VSP در چاه کج

- در شکل زیر انواع برداشت VSP در چاه کج را مشاهده مي کنيد.

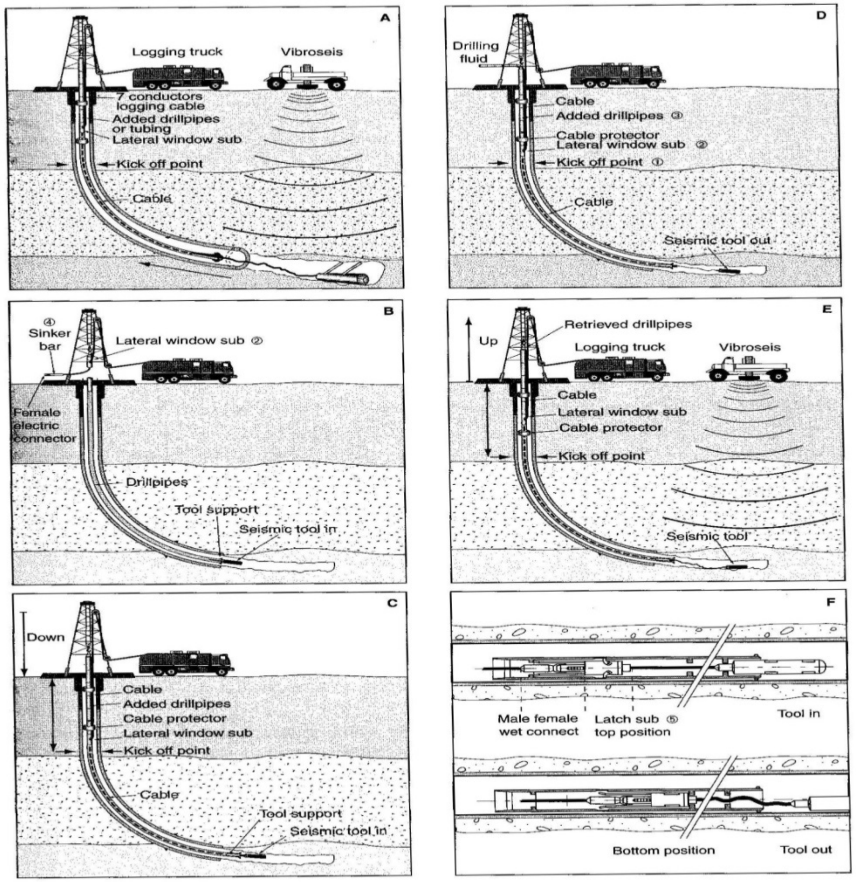

Description of the Horseis method (IFP patented) used to lower a sensor in a deviated or horizontal well. **A.** Setup during seismic recording. **B.** Lowering of the tool via the drillpipe. **C.** Connection of the tool with the cable. **D.** Expulsion of the tool out of its protecting sleeve. **E.** Clamping of the tool to the formation. **F.** Schematic of the connector and of the tool protecting sleeve [after Mari, Wittrisch et al., 1990].

VSP field procedures

- قبل از انجام عملیات و بعد از آن باید کل سیستم را تست کنیم و مطمئن شویم که سیستم ثبت داده ها یکسري از سیگنال ها را به طور ناخواسته حذف نکند.

SEISMIC WHILE DRILLING (SWD)

- استفاده از VSPمعمولي اطلاعات بسياري را به ما مي دهد اما براي انجام آن نياز است حفاري متوقف شود ، رشته ي حفاري از چاه خارج شود ، ژئوفون هاي درون چاهي به داخل چاه رانده شود تا عمليات شروع شود و نهايتا دوباره رشته حفاري به داخل چاه رانده شود تا عمليات حفاري شروع شود و اين باعث افزايش زمان و صرف هزينه ي زيادي مي شود.
- علاوه بر افزايش زماني ، خطراتي هم مانند Sticking و يا fishشدن ابزار VSP هم وجود دارد كه ممكن است بر مشكل بيفزايد.
- همچنين چون VSP در هر لحظه انجام نمي شود نمي توان محل دقيق مته را در هر زمان مشخص كرد.

Seismic while drilling

- SWD را مي توان به دو گروه تقسيم كرد:
  - Reverse ray path همانند drill bit seismic
  - Normal ray path همانند VSP – WD

SWD

- Drill bit - SWDعبارت است از استفاده از انرژي مته هاي 3 – CONE به عنوان منبع انرژي در حين حفاري براي يافتن time – to – depth و look – ahead information.

- در سال 2000 توسط شركت schlumberger ابزار vertical seismic profile while drilling(VSP-WD) ارائه شد كه در اين روش امواج در سطح توسط يك منبع توليد مي شود و توسط ژئوفون مخصوصي در بالاي مته برداشت مي شود ، در اين روش اطلاعات يا ذخيره شده يا توسط ابزار MWD به سطح منتقل مي شود(اين عمل در هنگامي كه پمپ ها خاموش است انجام مي شود تا S/N افزايش يابد).

- SWD باعث مي شود كارآيي و ايمني حفاري به مقدار زياد افزايش يابد.
- با SWD مي توان محل دقيق قرار گيري لوله ي جداري و يا محل core گيري را با دقت مشخص كرد.
- مي توان با SWD وضعيت سازندهاي پيش رو را مشخص كرد و وزن گل مناسب را تعيين كرد.
- با SWDمي توان محل دقيق مته را مشخص كرد.
- با SWD مي توان مشخص كرد كه در ادامه و در مقابل مته چه سازندي را خواهيم داشت.
- با استفاده از SWD مي توان به درستي به سمت محلي كه مي خواهيم به آن برسيم حركت كنيم.

تاریخچه SWD

- ايده SWD به سال 1930 برمي گردد ، زماني كه حفاري ضربه اي رايج بود.
- اولين تلاش براي استفاده از سيگنال هاي توليد توسط مته در سال 1968 توسط يكي از ژئوفيزستهاي IFP بر مي گردد.
- در گذشته نمي توانست از مته هاي PDC به عنوان منبع استفاده كرد ، زيرا ميزان امواج صوتي آنها كم بود.
- استفاده از مته هاي roller – cone هم محدوديت هايي دارد مانند اين كه سازند بايد hard to medium hard باشد ، دندانه هاي مته بايد به اندازه ي كافي بلند باشد و ....

- در دهه ي 90 تلاش هاي بسياري براي پيشرفت اين روش انجام شد و نهايتا در سال 2000 شركت schlumberger ابزار خود را معرفي كرد كه مي تواند بالاي مته بسته شود و توسط يك منبع در سطح امواج را ايجاد كرد و توسط ابزار جديد ثبت كنيم و نهايتا توسط MWD اطلاعات ثبت شده به سطح منتقل مي شود.
- اخيرا ابزاري با نام swept impulse hydraulic به بازار آمده كه استفاده از مته هاي PDC را نيز ممكن كرده و محدوديت هاي استفاده از roller cone را هم رفع كرده است.

- عمليات SWD داراي دو مرحله است:

- Planning
- Operation

- مراحل planning شامل مواردزير مي باشد:

- Ray trace modeling
- Real time processing
- Acquisition density
- Site survey
- Rig setup
- Drilling personnel training

- مراحل Operation شامل مواردزير مي باشد:

- Source handling
- Network/application performance
- Decision making process/resources

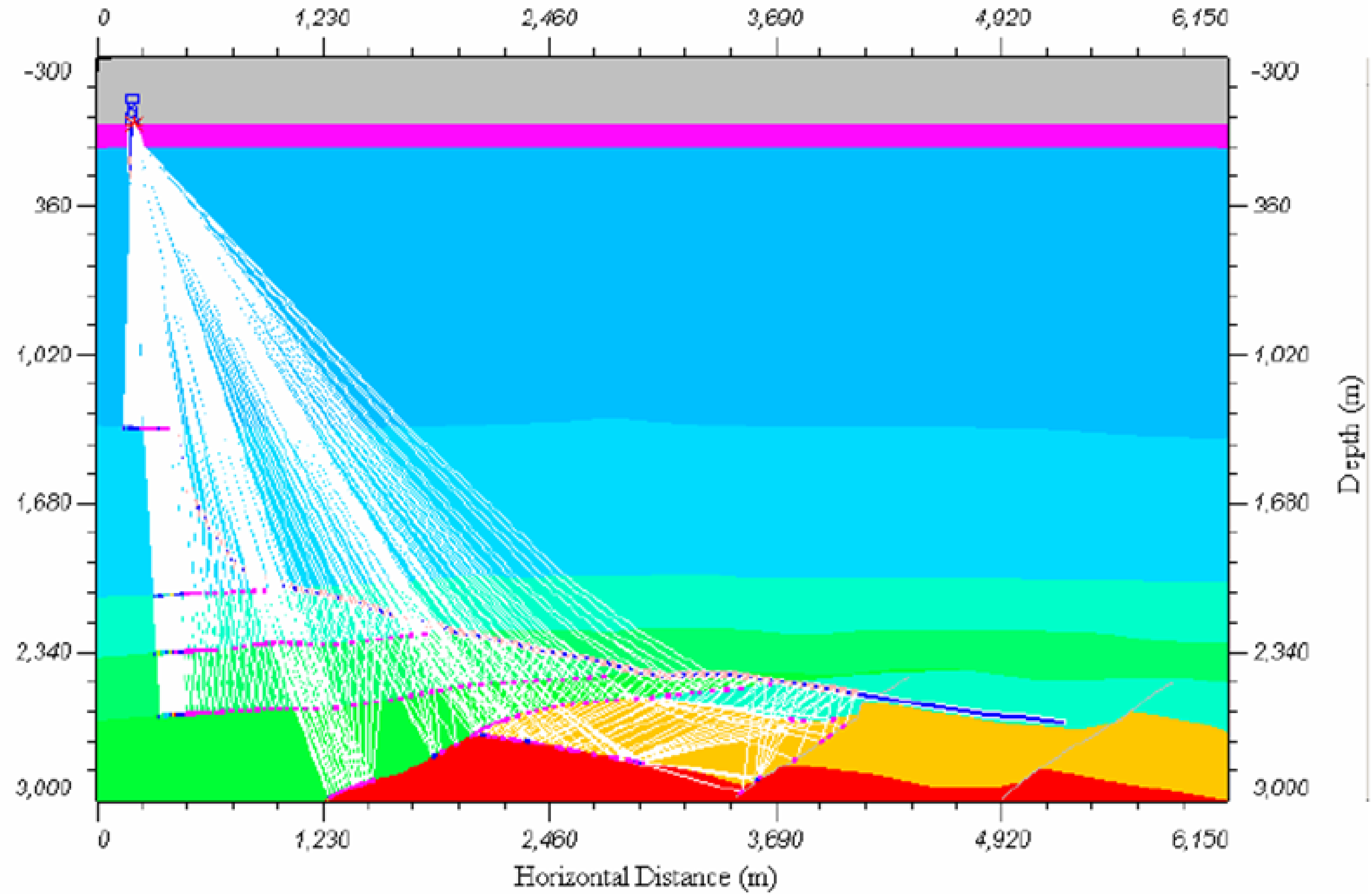

Rig-source raypath analysis

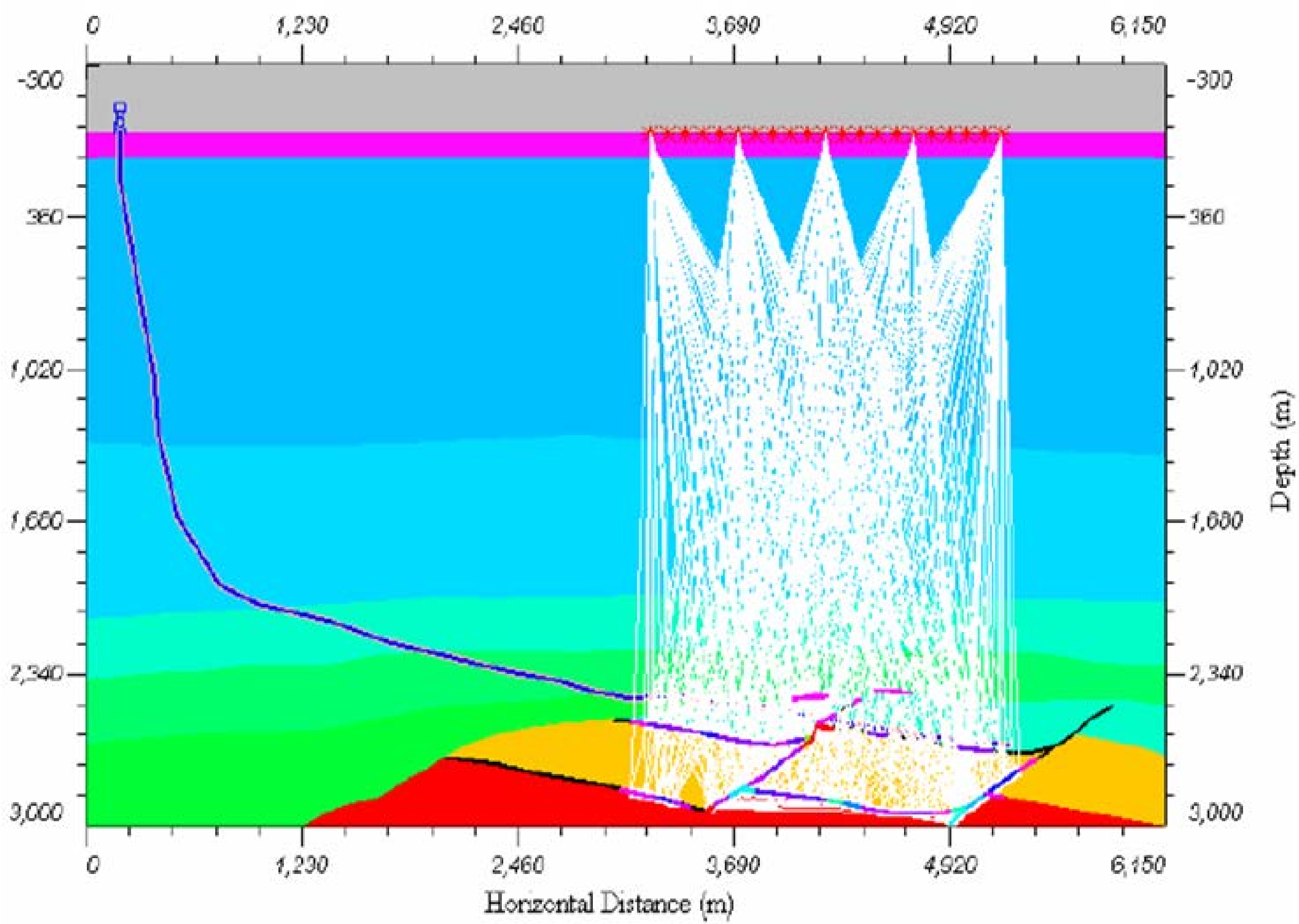

Vertical incidence ray path analysis

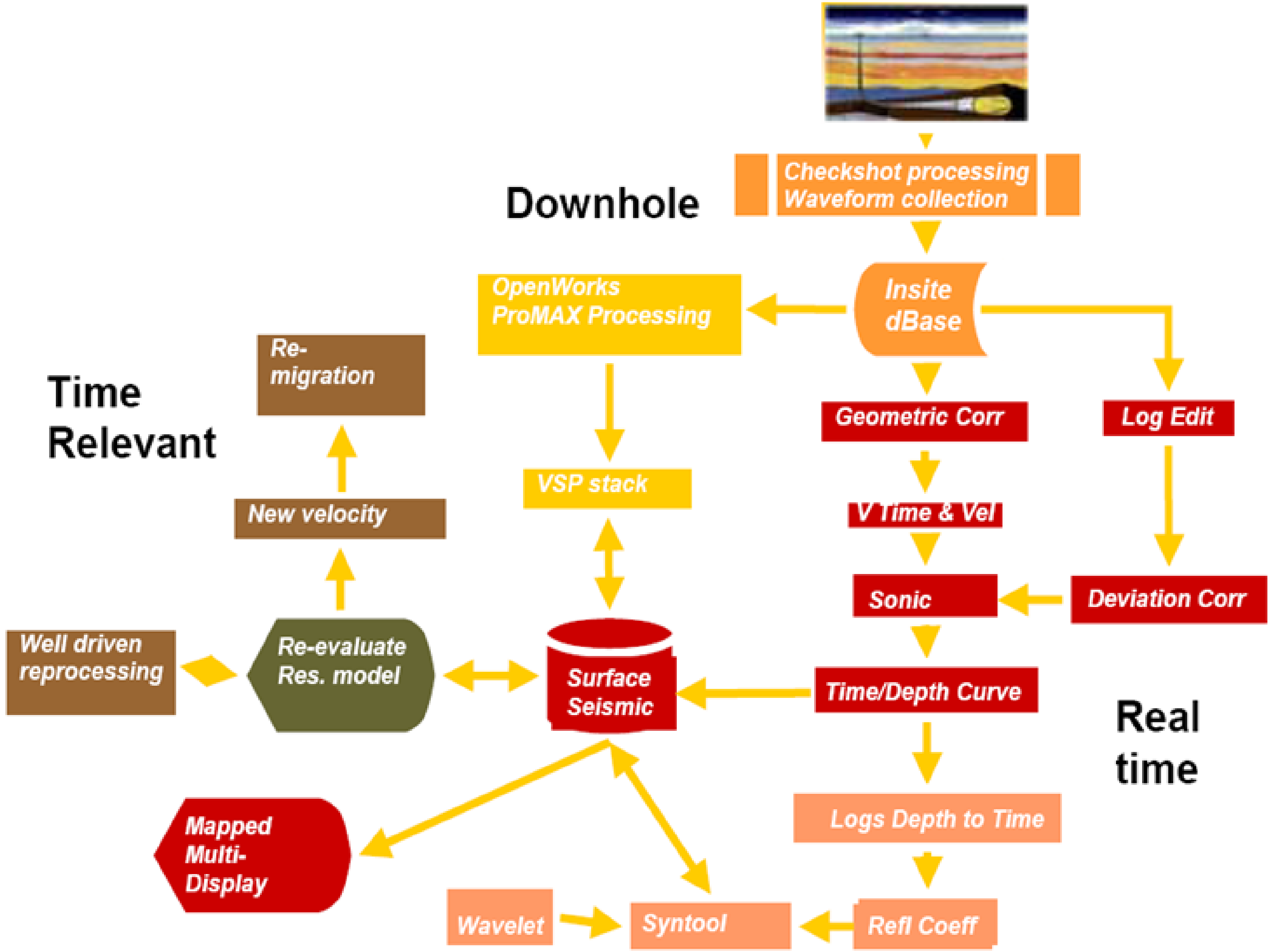

SWD processing flow

Drill bit seismic

- Drill bit seismic را با نام seismic guided drilling هم مي شناسند.
- در اين روش منبع مته اي است كه در حال ويران كردن سازند ته چاه مي باشد.

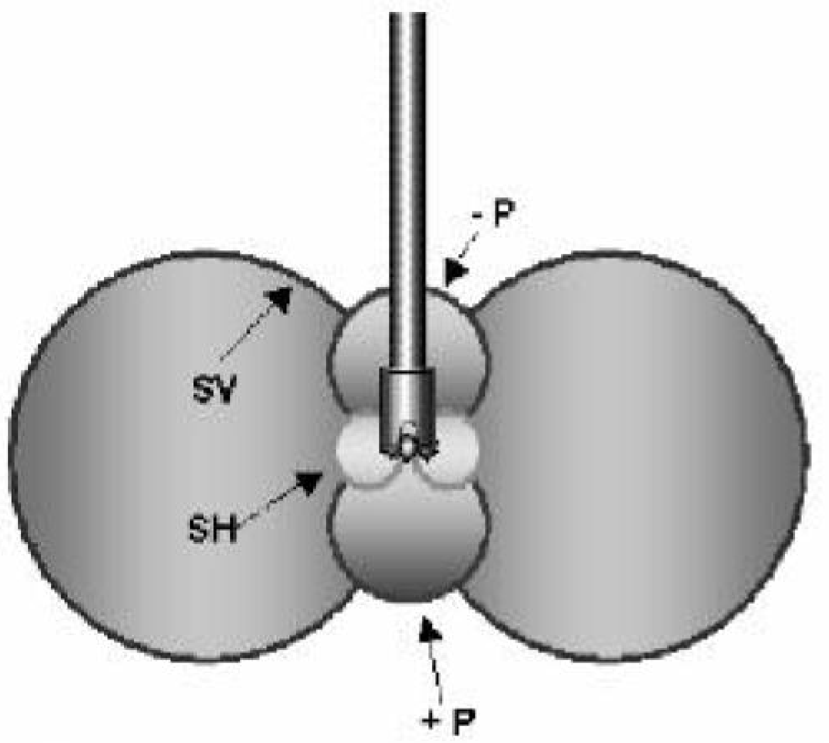

Accoustic Radiation Pattern of a Tri-Cone Bit.

- وقتي دندانه هاي مته در سازند نفوذ مي كنند باعث ايجاد يك ارتعاش محوري در رشته ي حفاري مي شود.
- علاوه بر اين امواج ، امواج فشاري هم در جهت مخالف در سازند ايجاد مي شود كه اين امواج نهايتا توسط ژئوفون در سطح برداشت مي شود.
- امواج لرزه اي محوري هم كه در امتداد رشته حفاري گسترش يافته اند نيز مي توان توسط accelerometer كه در روي top drive و يا swivel قرار مي گيرد مشخص مي شود.

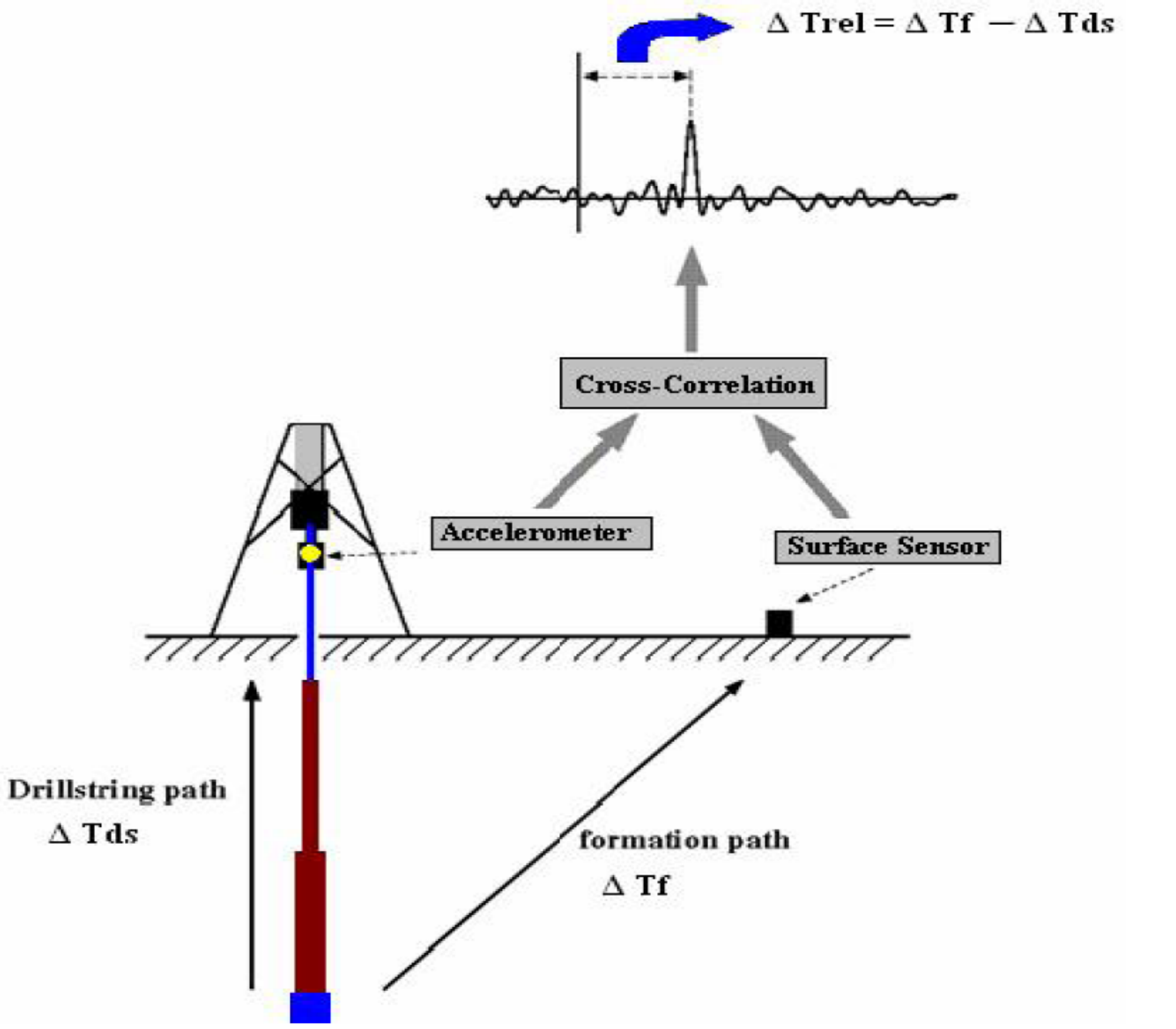

Cross correlating the accelerometer signal and the surface sensor signal gives a relative time difference (ΔT_{rel}). Once the relative time difference is determined (ΔT_{rel}), the time taken along the axial string (ΔT_{ds}) could be determined and from both these information the travel time along the formation path (ΔT_f) can be calculated.

- در شكل بالا همانطور كه مشاهده شد و زمان ثبت مي شود يكي Δt_{ds} كه مربوط به accelerometer بوده و ناشي از انتشار امواج در امتداد رشته ي حفاري است ، دوم Δt_f كه حاصل انتشار امواج در سازند مي باشد.
- براي اين كه بتوان مقايسه اي بين Δt_f و Δt_{ds} كرد بايد داده هاي Δt_{ds} را يك انتقال زماني بدهيم.
- براي محاسبه ي اين انتقال زماني ، مته را مقداري از سطح بالا كشيده و رها مي كنيم و يك پيك شاخص را در accelerometer بدست مي آوريم و مطابق شكل Δt_{rel} را يكبار حساب مي كنيم.

- حال با توجه به اينكه در حين حفاري داده هاي مربوط به acclerometer داراي صحت بيشتري نسبت به داده هاي ژئوفون مي باشد ، مي آيم تمام داده هاي حاصل از accelerometer را به اندازه ي Δt_{rel} انتقال مي دهيم. سپس Δt_f را بدست آورده و مورد آناليز قرار مي دهيم.
- حال اگر مته وارد ناحيه ي جديدي شد مراحل بالا را مجدد تكرار كرده و Δt_{rel} را حساب كرده و مانند مراحل بالا دوباره تكرار مي كنيم.

- در این روش دو سري گیرنده داریم:

1. اندازه گیري لرزش محوري توسط یك Accelerometer كه روي top drive ویا swivel قرار دارد.
2. یك آرایه از ژئوفون ها در نزدیكي چاه ، روي زمین ، كه شامل 12 تا 36 عدد ژئوفون مي باشد(در این روش فاصله ي ژئوفون ها حدود 20 تا 30 متر از well head مي باشد).

- در سري دوم گیرنده ها توصیه مي شود كه ژئوفون ها در یك چاله دفن شوند تا اثر امواج سطحي كمتر شود.
- لایه هوازده در دو جا مشكل ایجاد مي كند.

1. اگر سازند مورد حفاري سخت باشد امواج قوي تولید مي شود و در نتیجه امواج سطحي قوي توسط این لایه تولید مي شود و كیفیت برداشت از بین مي رود.
2. اگر سازند مورد حفاري نرم باشد امواج تولیدي ضعیف است و در لایه هوازده جذب مي شود.

Acquisition system

- در شكل زير يك شماي كلي از سيستم جمع آوري اطلاعات را مشاهده مي كنيد.

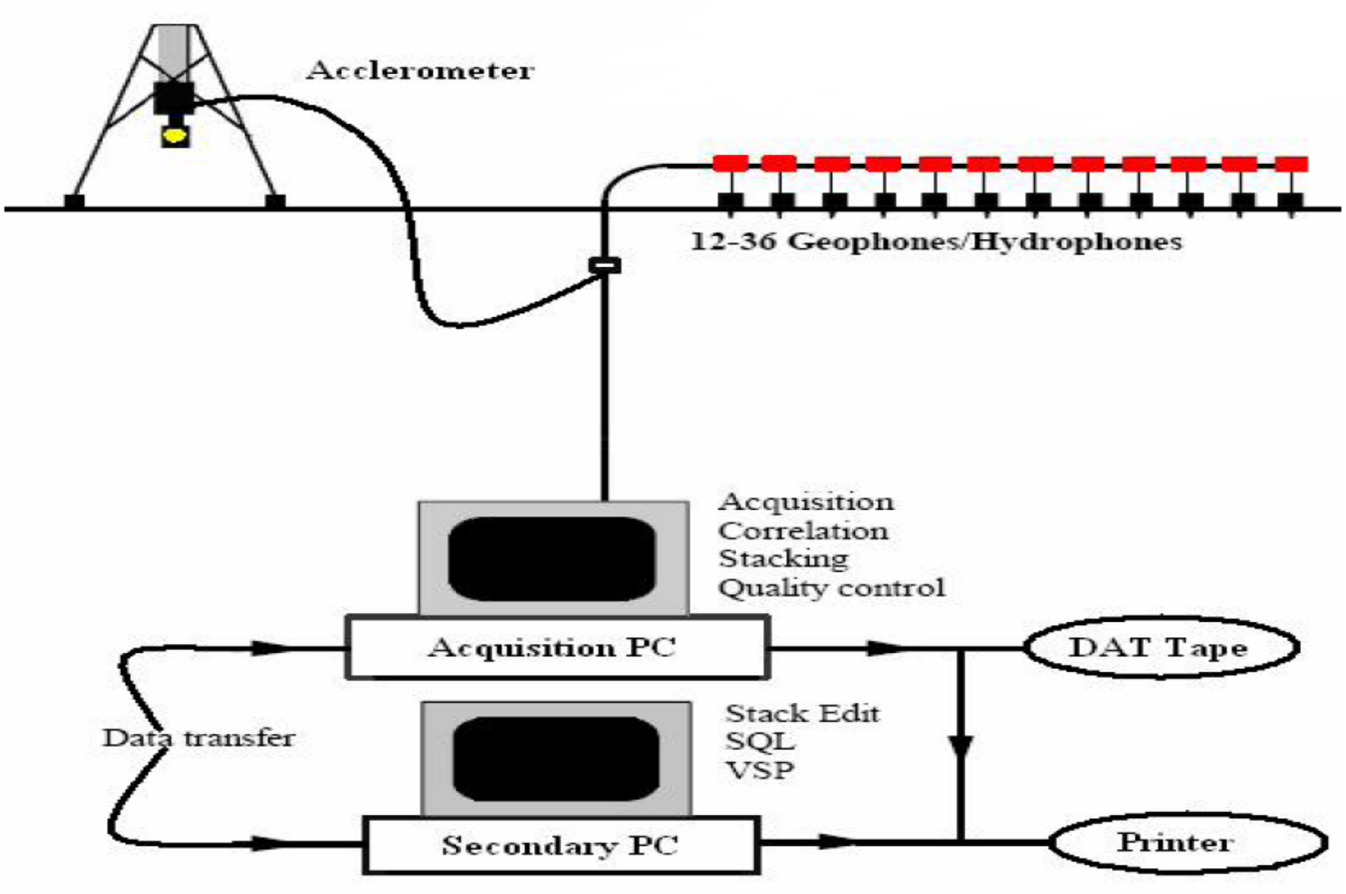

Schematic of Data Acquisition Process.

- شكل بالا داراي دو Pc بوده كه يكي براي جمع آوري داده ها و ديگري براي پردازش داده ها مي باشد.
- در برداشت هاي عادي براي جمع آوري داده هاي ژئوفون ها از single chanel استفاده مي كنند كه تمامي خروجي هاي ژئوفون ها به آن وصل است و به اين طريق نويزها كاهش مي يابد.
- اما در SWD مقدار نويزهاي حاصل از محيط و امواج سطحي خيلي بيش از اين مي باشد كه با اين روش بتوان اثر آنها را كم كرد. براي همين هر ژئوفون را به صورت جداگانه برداشت مي كنيم و با استفاده از يك Pc تمام داده ها را جمع كرده و سپس براي پردازش از كامپيوتر ديگري استفاده مي كنيم.
- در جايي كه داده ها به طور جداگانه برداشت شود مي توان تصحيحات آماري و NMO را راحت تر از حالتي كه تمام داده ها با هم جمع مي شود انجام داد.

Overview of signal processing

- نمودار time – depth را با داشتن زمان سير موج در امتداد رشته ي حفاري مي توان بدست آورد.
- زمان عبور موج را مي توان با استفاده از دانستن سرعت موج در هر قطعه از رشته ي حفاري و دانستن طول آن قطعه مشخص كرد.
- براي محاسبه ي اين زمان مي توان سرعت امواج در لوله هاي حفاري را با استفاده از فرمول زير محاسبه كرد.

$V = \sqrt{(E/D)}$

E: young's modulus

D: density

- سرعت در رشته ي حفاري تقريبا برابر 5150 متر بر ثانيه مي باشد.
- در صورتي كه در داخل لوله ها و بين لوله ها و ديواره گل باشد سرعت عبور موج تا 10% مي تواند كاهش يابد.
- راه ديگر مشخص كردن traveling time در رشته ي حفاري ، ايجاد ضربه توسط مته به تنهايي و محاسبه ي زمان رسيدن اين ضربه به سطح و مشخص كردن آن توسط accelerometer مي باشد.

Noise removal

- ابزاري مانند پمپ ها و موتورهاي ديزل باعث ايجاد نويز شديد مي شوند.
- گاهي اوقات امواج ضعيف حاصل از مته در بين اين نويزها كاملا محو مي شود.
- معمولا حذف نويزها در حفاري خشكي سخت تر از حذف نويزهاي حفاري دريايي است.
- يكسري از نويزها هم توسط حركت سيال در ديواره چاه ايجاد مي شود.
- با stack كردن مي توان مقدار زيادي از اين نويزها را حذف كرد.
- نويزها ايجاد شده توسط دكل حفاري معمولا با استفاده از digital filter حذف مي شود.
- وقتي امواج در امتداد رشته ي حفاري حركت مي كنند ممكن است به علت تغيير آمپيدانس در طول رشته ي حفاري(مانند تغيير قطر لوله ها) يك سري multiple ها ايجاد شده كه توسط accelerometer مشخص مي شوند و براي حذف اين ها از drill string image processing استفاده مي كنيم.

- در دريا وقتي امواج توليد شده توسط مته به بستر دريا مي رسد و وارد آب مي شود ، اما در سطح دريا چون مقدار ضريب بازتاب بسيار بالا است و دوباره به سمت بستر بازتاب مي كند و باعث ايجاد multiple هايي مي شود.

- براي غلبه بر اين مشكل در برداشت دريايي هم از هيدروفون استفاده مي شود و هم از ژئوفون و امواج هم در سطح دريا و هم در بستر دريا ثبت مي شود و با انطباق مناسب نتايج اين دو مي توان اين multiple ها را حذف كرد.

Drill bit seismic with shock absorber & EMWD

- به جاي IFP كه accelerometer بيرون چاه روي top drive قرار مي گرفت از down hole accelerometer استفاده كرد و براي انتقال داده هاي آن به سطح از MWD بهره جست.
- سپس مشاهده كرد كه down hole accelerometer هم مانند قبل مقدار زيادي multiple در يافت مي كند اما مقدار فركانس آن بالاتر مي باشد.
- سپس ژئوفيزيست هاي IFP متوجه شدند كه اگر بالاي مته يك vibro seismic قرار دهند مقدار multiple ها به شدت كاهش مي يابد كه اين ابزار را به نام shock absorber ناميدند.
- امروزه استفاده از shock absorber به شدت رايج شده و با اين روش توانسته اند S/N را به مقدار زيادي بهبود بخشند.

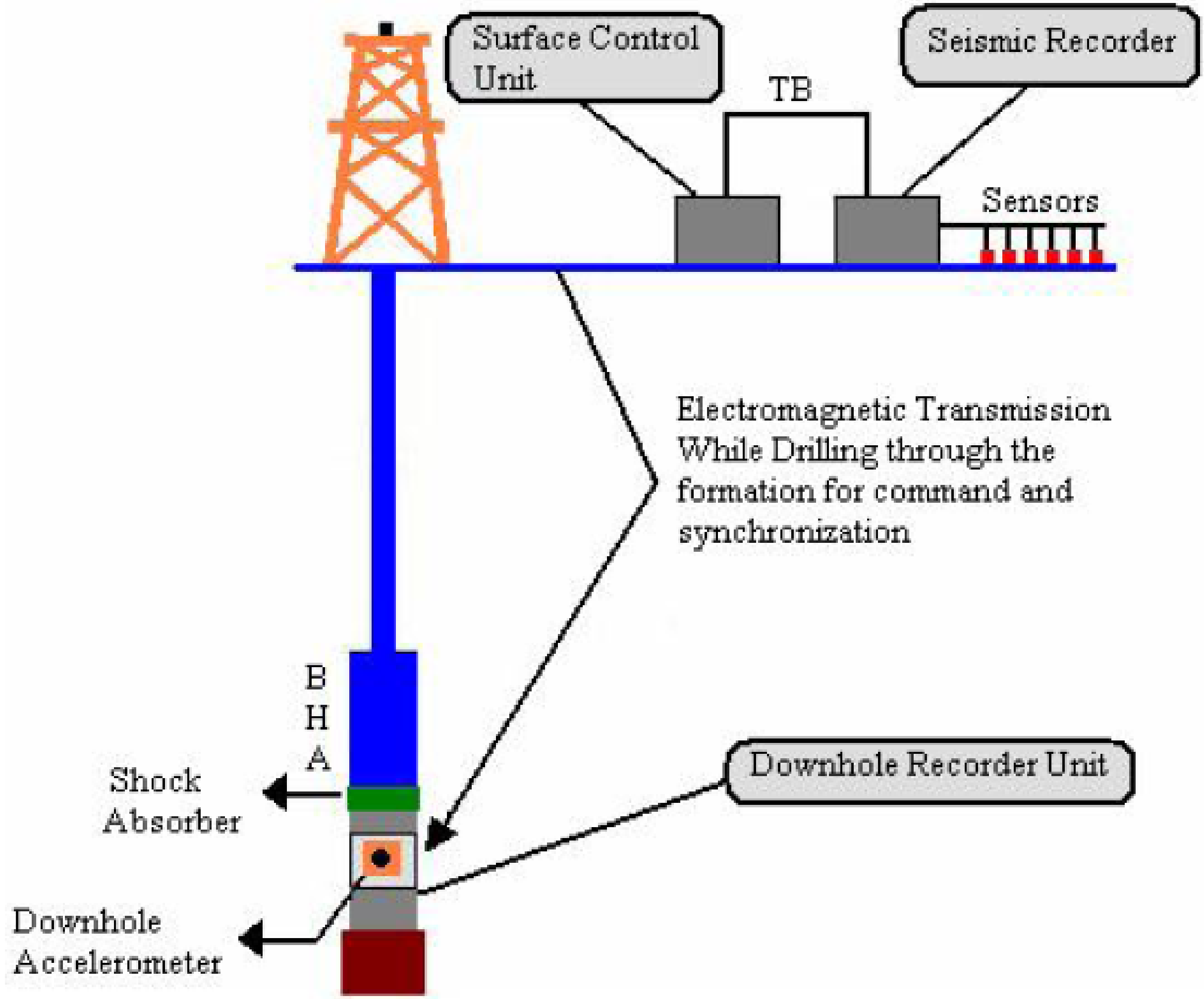

A sketch of Drill-Bit EM-SWD recoding chain

- استفاده از MWD داراي يکسري مشکل است ، از جمله نياز به نگهداري فراوان دارد ، اما شرکت Geoservices ابزاري با نام electromagnetic measurement while drilling(EMWD) را پيشنهاد کرد که مشکلات MWD را از ميان بر مي داشت.

- کاربردهاي Drill bit – SWD عبارت است از:

1. Salt proximity survey.
2. Predicting Pore pressure ahead of the Bit.
3. Creating a Look Ahead Image.
4. Locating the Drill-Bit.
5. Optimizing casing/coring point.
6. Drilling hazard risk reductions.

Salt proximity survey

- Drill-Bit seismic salt proximity survey, where drill bit act as a source at different depths with geophone array at the surface above the salt domes .Seismic travel time are recorded and are combined with other information such as exact location of both source and receiver and the velocity of signal in salt and surrounding rock and distance of the top of the salt domes helps in construction of salt dome profile. Vertical and lateral variation observed on both the drill-bit seismic and wireline VSP can be used to update the geological model. This survey reduced the cost of an additional sidetrack and saved more than $ 100000 in case of a well like Qarn Nihayda-1 of North Oman.

Predicting Pore pressure ahead of the Bit

- Pore pressure can be predicted from the amalgamation of seismic while- Drilling velocities and other drilling parameters in association with various modeling techniques. Accuracy in predicted pore pressure helps to predict the optimum mud weight to be used.

Creating a Look Ahead Image

- Seismic Image of the formation ahead of the Bit can be generated on a real time basis which can be correlated with the surface seismic section to make up any time difference. This helps in correcting the position of horizons as seen on the surface seismic sections.

Locating the Drill-Bit

- The time to depth information obtained on a real time basis help to locate the position of the bit on the surface seismic section with the progress in drilling activities. This information could be successfully used to guide the well trajectories and assigning accurate target.

Optimizing casing/coring point

- With the help of Look- Ahead image and position of the drill bit the position of casing and coring points could be determined with precision .Thus, by elimination of planned casing in some cases7 save enormous money.

Drilling hazard risk reductions

- An abrupt increase in formation pressure could lead to significant drilling hazard, particularly if the depth of hazard is not known to a high degree of accuracy prior to drilling. When combined with intermediate VSP's the while drilling technique can provide a look ahead to potential deviations from a normal pressure regime. Deviations from the trend often indicate onset of overpressure, and they can be seen in seismic while drilling results hundreds of meters ahead of the bit, in time to take action to drill ahead safely.

مزاياي استفاده از Drill bit SWD

1. كاهش ريسك حفاري
2. كاهش هزينه هاي حفاري
3. افزايش كارآيي حفاري به مقدار زياد
4. كنترل چاه را به مقدار زيادي بهبود مي بخشد
5. باعث افزايش توليد مي شود ، با هدايت كردن دقيق چاه به محل مخزن

محدوديت هاي Drill bit SWD

1. اين تكنولوژي در سازند هاي نرم و يا خيلي عميق نمي توان استفاده كرد.
2. در چاه هاي كه زاويه انحراف آنها زياد باشد نيز نمي توان از اين تكنولوژي استفاده كرد ، چون مقدار جذب و ضعيف شدن امواج بسيار زياد مي شود.
3. از اين روش زماني كه مته roller cone باشد مي توان استفاده كرد ، به اين دليل نمي توان از مته هاي PDC استفاده كرد زيرا لرزش محوري آنها كم است.

- توجه: محدوديت هاي 1 و 2 با ابزار MWD كه اندازه گيري را در نزديكي مته انجام مي دهد رفع مي شود. و مشكل 3 با ابزار جديدي كه به تازگي به بازار عرضه شده برطرف مي شود.

Vertical seismic profiling while drilling(VSP – WD)

- VSP معمولي داراي كيفيت بالاي داده مي باشد ولي محدوديت هاي بسياري باعث مي شود كه استفاده از آن را محدود مي كند ، از جمله محدوديت ها مي توان به موارد زير اشاره كرد.
  - اتلاف بيش از حد زمان
  - افزايش خطرات حفاري
  - در چاه هاي high – deviated به روش معمول قابل استفاده نيست ،در صورت اجبار هم نياز به ابزار tough logging equipment دارد كه هزينه و پيچيدگي كار را افزايش مي دهد.
- براي غلبه بر محدوديت هاي ياد شده ابزار VSP – WD ابداع شد كه در ادامه به بررسي آن مي پردازيم.

- VSP و VSP – WD از نظر source و sensor فرقي ندارد، فقط در VSP – WD به جاي کابل از فرستنده ي ويژه اي استفاده مي کنند که در شکل زير آن را مشاهده مي کنيد.
- VSP – WD در زماني که حفاري به عللي متوقف شده باشد انجام مي شود تا مقدار نويزها به حداقل برسد.
- در VSP – WD، first break time توسط mud pulstelemetry به سطح فرستاده مي شود و اطلاعات full – wave form در حافظه ي دستگاه مي ماند و در حين trip مي توان آن را بدست آورد.

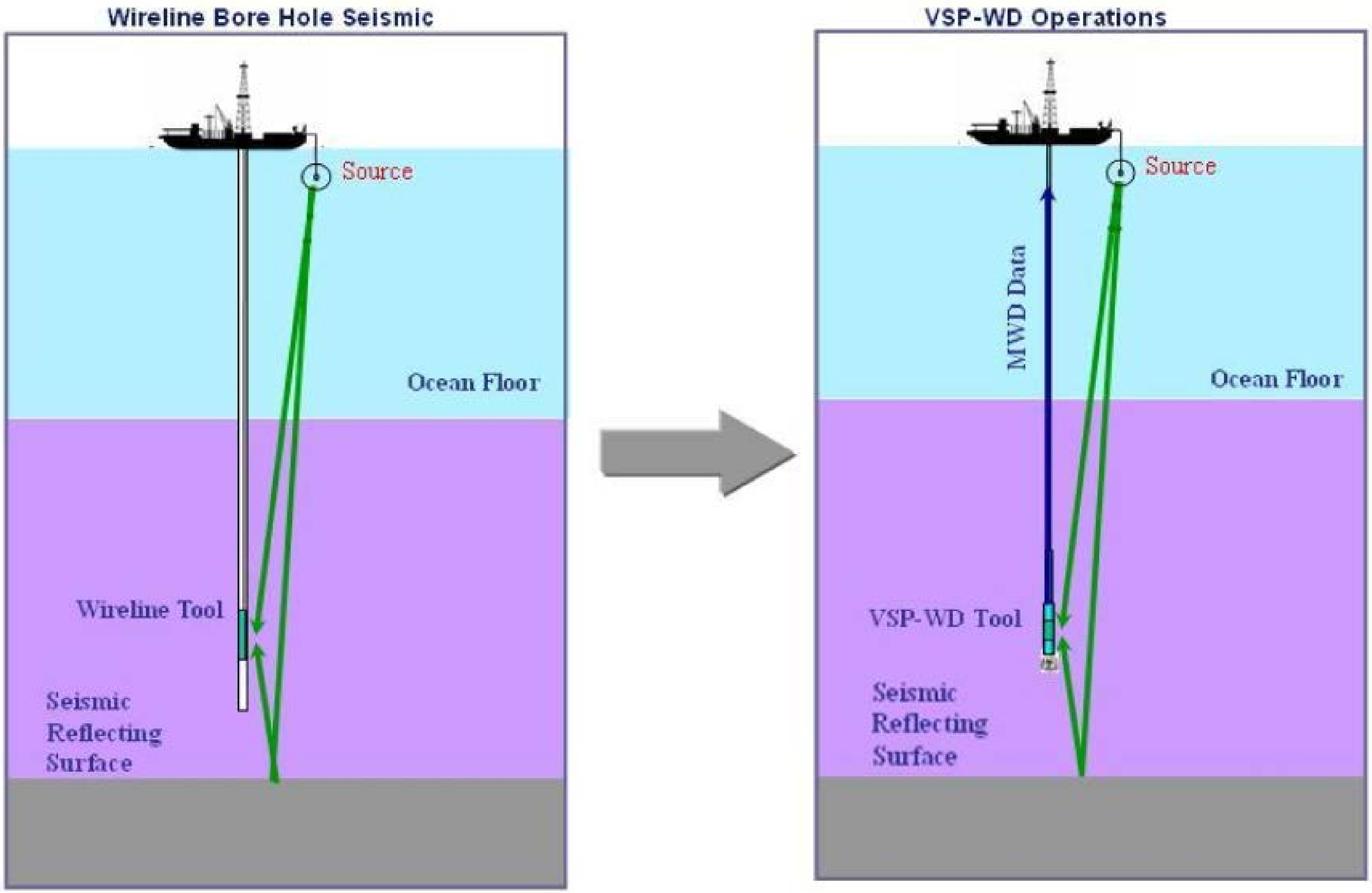

Transfer of Wireline seismic Technology to Drilling Operations

- مراحل کار VSP – WD را در شکل زیر مشاهده مي کنيد.

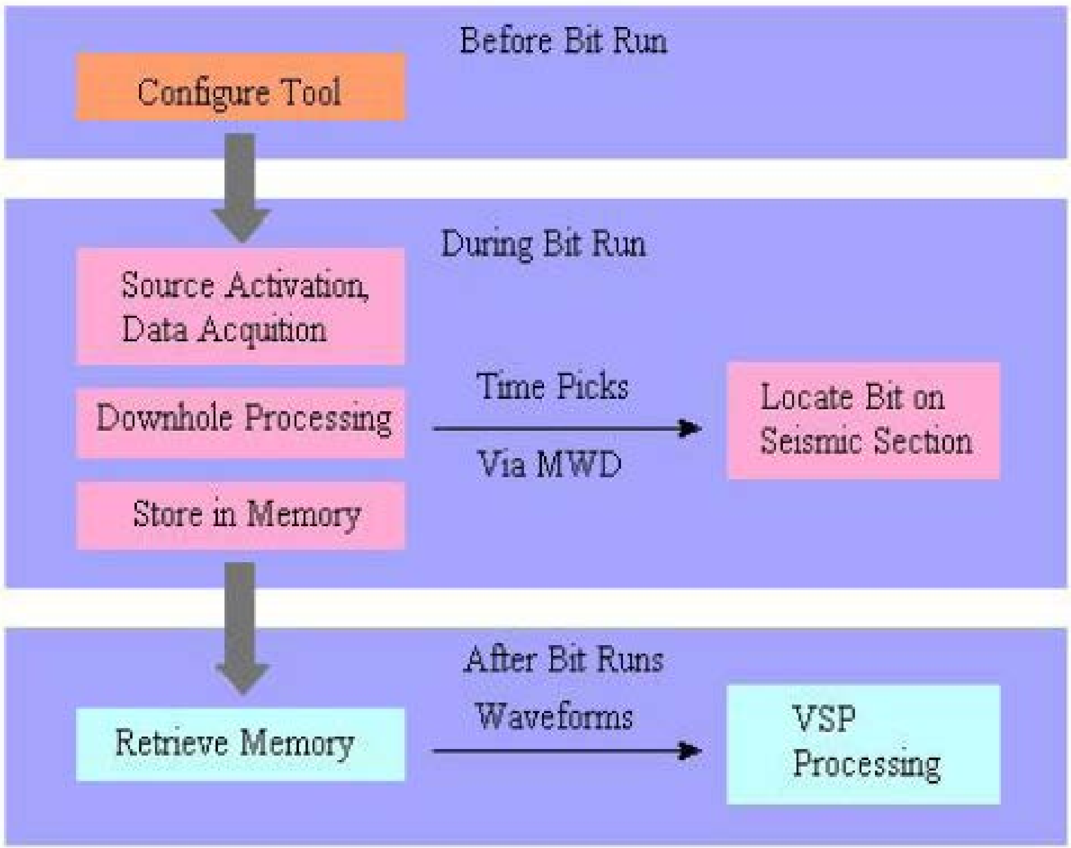

General operating procedures for VSP-WD surveys

- در هنگام بالا كشيدن رشته ي حفاري اين امكان وجود دارد كه منبع مرتب فعال باشد و ما در هر عمقي كه گيرنده قرار مي گيرد يك برداشت داشته باشيم همانند VSP معمولي.
- VSP – WD شديدا به ژئومتري چاه و محل منبع وابسته است.
- استفاده از اين ابزار در چاه هاي قائم با zero offset source بهترين نتيجه را مي دهد.

- وسايل لازم براي اين عمليات عبارتند از:
  - Air gun system
  - كامپيوتر براي تهيه timing information و process data
  - يك منبع هوا با فشار بالا(حدود 3000 psi)
  - سيستم GPS براي مشخص كردن محل دقيق منبع به خصوص در offset source
  - Processing software براي QC اوليه و آناليز اوليه
  - Tap tester براي تست كردن ساعت هاي ابزارها

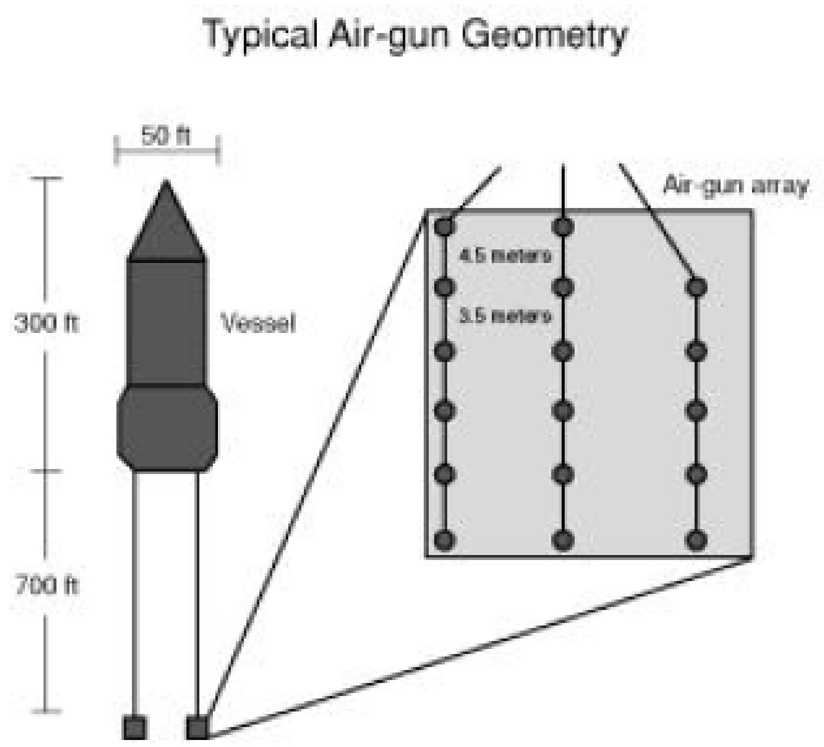

The schematic diagram shows an air-gun array towed several hundred meters behind a seismic vessel to provide an energy source for the acquisition of marine seismic data.

The surface system

The Source Equipment

Seismic Navigation and Processing system.

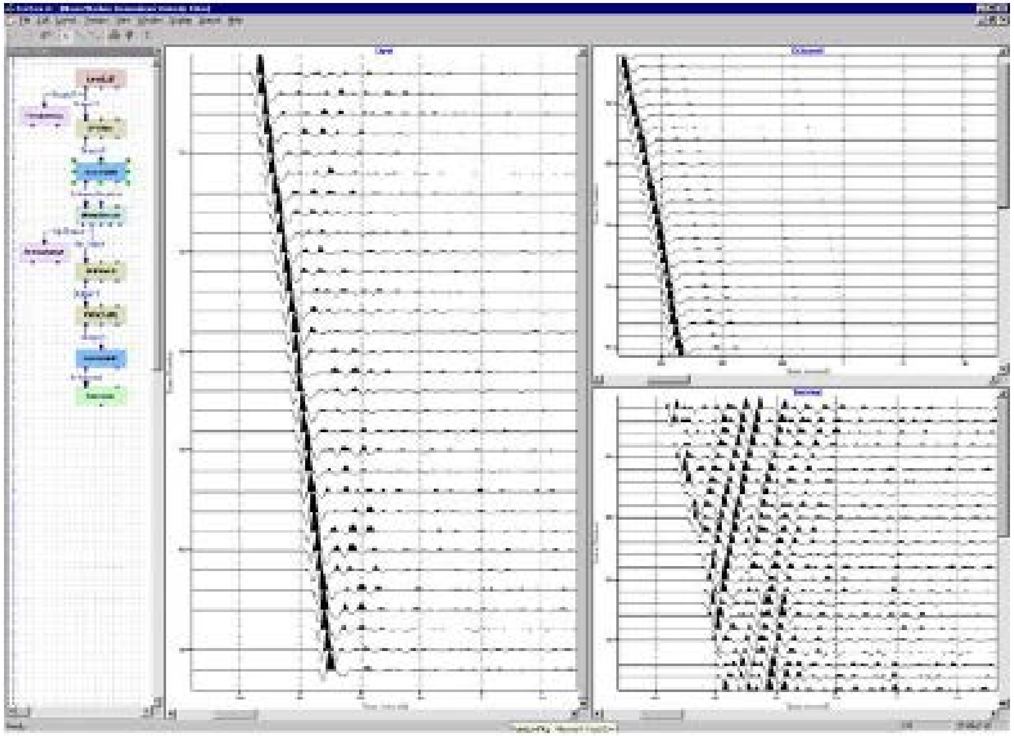

Seismic Processing Software with highly configurable interface.

Synchronization check of the clock and the entire system during a shallow hole test prior to running in the hole.

- در VSP – WD براي اينكه بتوان داده ها را با هم مقايسه كرد بايد از ابزار درون چاهي و ابزار سرچاهي كه هر 15 ثانيه يكبار با هم همزمان شود استفاده كرد(براي اين هر 15 ثانيه چون منبع هر 15 ثانيه يكبار مي تواند شات كند)

- دستگاه به طور خودكار هر سه شات كه در يك مكان انجام مي شود(زمان اضافه كردن هر stand حدود 45 ثانيه است كه مي توان سه شات در اين زمان كرد)را با هم stack كرده و نتايج را توسط mud telemetery به سطح مي فرستد.

Real time processing

- يك بخش هر نرم افزار به تهيه real time visualization اختصاص دارد. در زير يك نمونه را مشاهده مي كنيد.

Time-depth curve and depth prediction

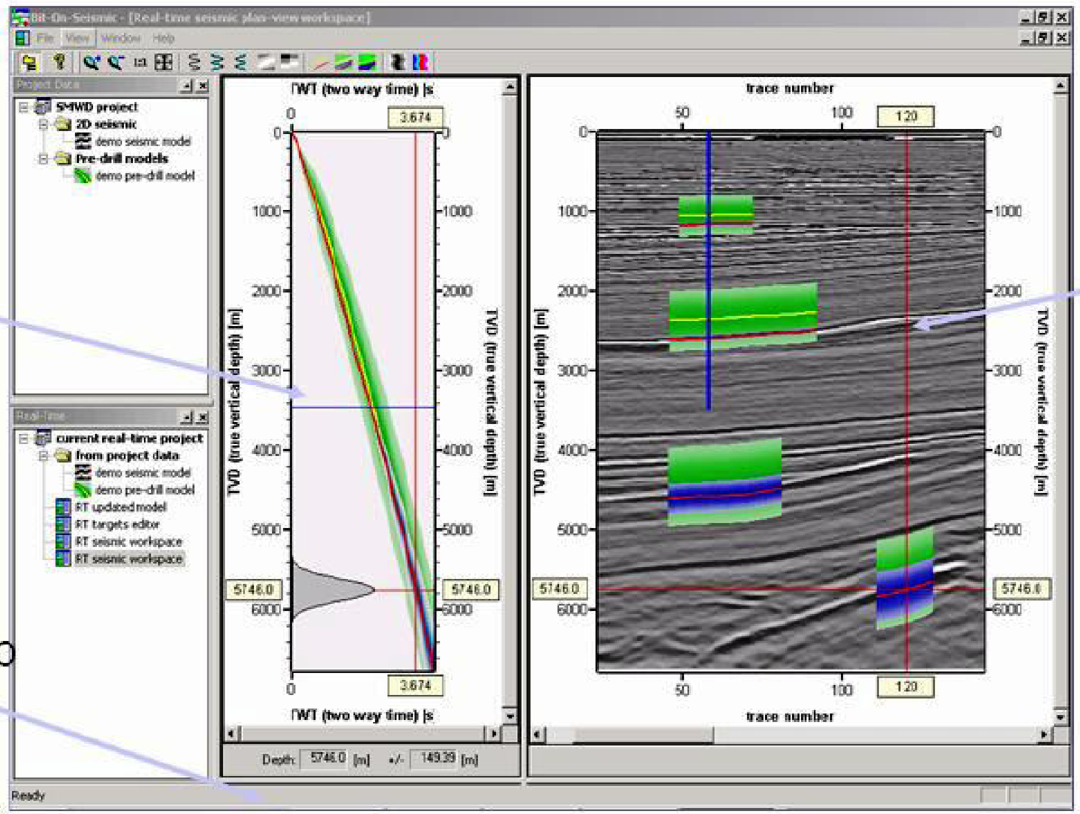

Surface seismic in depth

Distance to target and remaining uncertainty

Figure shows a snapshot of Realtime Processing software. VSP-WD tool's time-depth/ velocity information is used to continuously update the bit position on the surface seismic. This real-time information minimizes uncertainty when drilling towards target horizons.

- Real – time باعث ايجاد ارتباط مستقيم بين حفارها و ژئوفيزيست ها مي شود و مي توان مسير حفاري را به دقت مشخص كرد.
- نرم افزار دو seismic section را تهيه مي كند.
  - يكي برحسب زمان براي ژئوفيزيست ها
  - ديگري برحسب عمق براي حفاران كه محل دقيق مته را مشخص كنند.

مزاياي VSP - WD

1. تنها روشي است كه مي توان در چاه هاي افقي هم اطلاعات VSP را بدست آورد.
2. حفارها مي توانند محل دقيق مته را مشاهده كرده و لايه هاي پيش رو را مشخص كنند.
3. توسط اين روش چون لايه ها به طور كامل مشخص مي شود مي توان محلي كه مي خواهيم core بگيريم را به راحتي مشخص كرد و نيازي به كم كردن سرعت حفاري براي مشخص كردن لايه حفر شده از روي cutting ها نداريم.
4. با مشخص شدن محل دقيق core گيري از coreگيري بيش از حد ممانعت مي كند.

5. در اين روش نياز به نگه داري عمل حفاري نيست و به طور متوسط $ 420000 صرفه جويي مي شود.

6. ناپيوستگي ها به راحتي مشخص مي شود.

7. محل قرار گيري لوله ي جداري به راحتي و با سرعت و دقت مشخص مي شود.

8. مي توان pore pressure را پيش بيني كرد و وزن گل لازم را مشخص كرد.

VSP - WD محدوديت هاي

1. It is claimed that it provides look-ahead imaging, however the range and accuracy of this capability is still not accurately known.
2. Mud Pulse telemetry of processed velocity is planned but not presently commercial.
3. The biggest limitation of VSP-WD services is to ensure a good mechanical coupling of the VSP seismic sensor with the borehole and high precision required on downhole clock.

Image Log

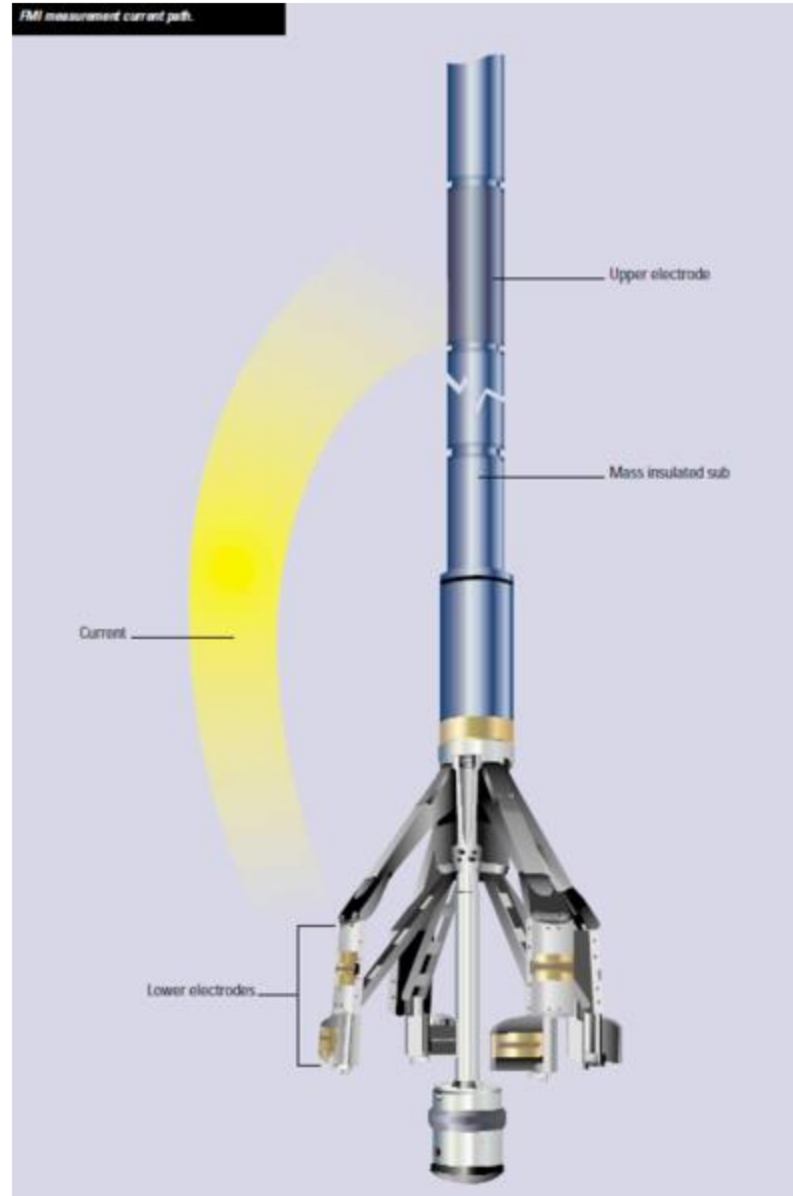
FMI measurement current path.
Upper electrode
Mass insulated sub
Current
Lower electrodes

Reservoir scale deformation

- Small scale faults and fractures plus the internal structure of faults revealed by core and image logs

Core orientation

Core marked to show 'way-up'

Up

L R

Recognition of natural fractures

- Cementation
- No geometric relationship with core
- Shear offset
- Planar
- Propagation along bedding not down core
- Multiple sets

Faults in core

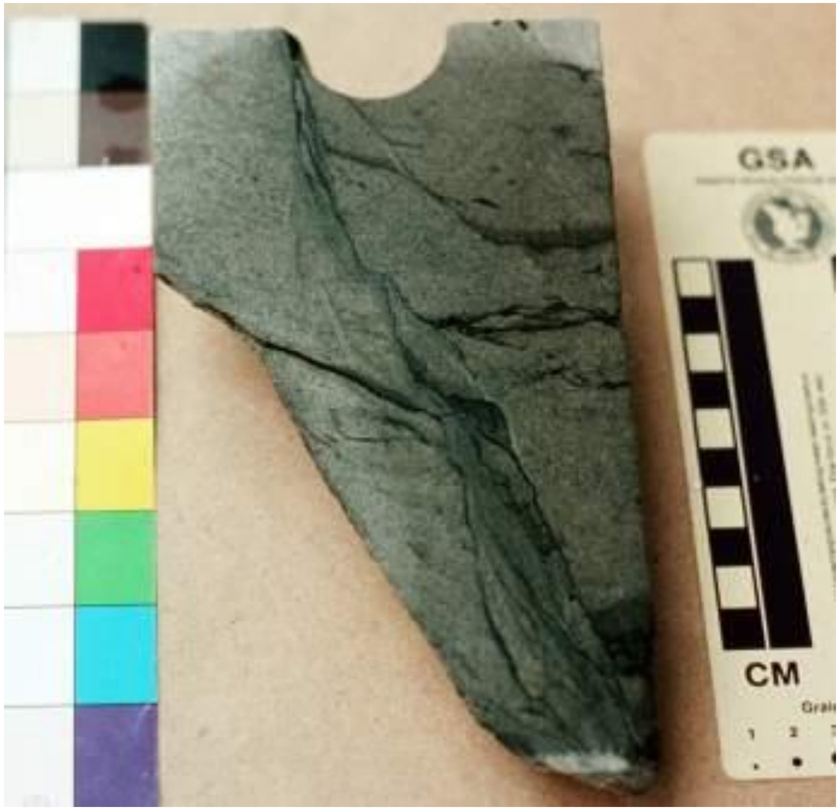

Natural fractures

Fracture spacing and layer boundaries in Chalk core

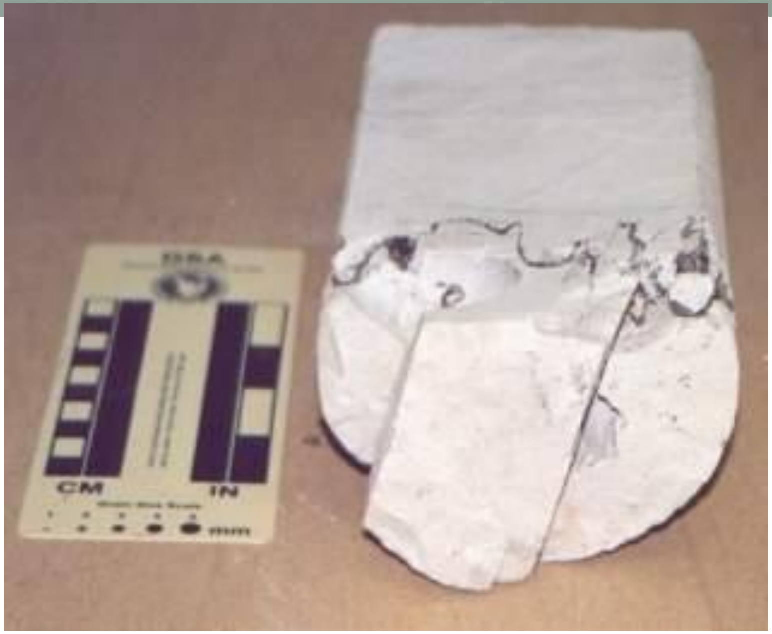

Fracture spacing

$$\text{Spacing} = \frac{\text{Core slab surface area}}{\text{Total fracture height in core}}$$

Fracture Spacing in Miss. Madison Ls

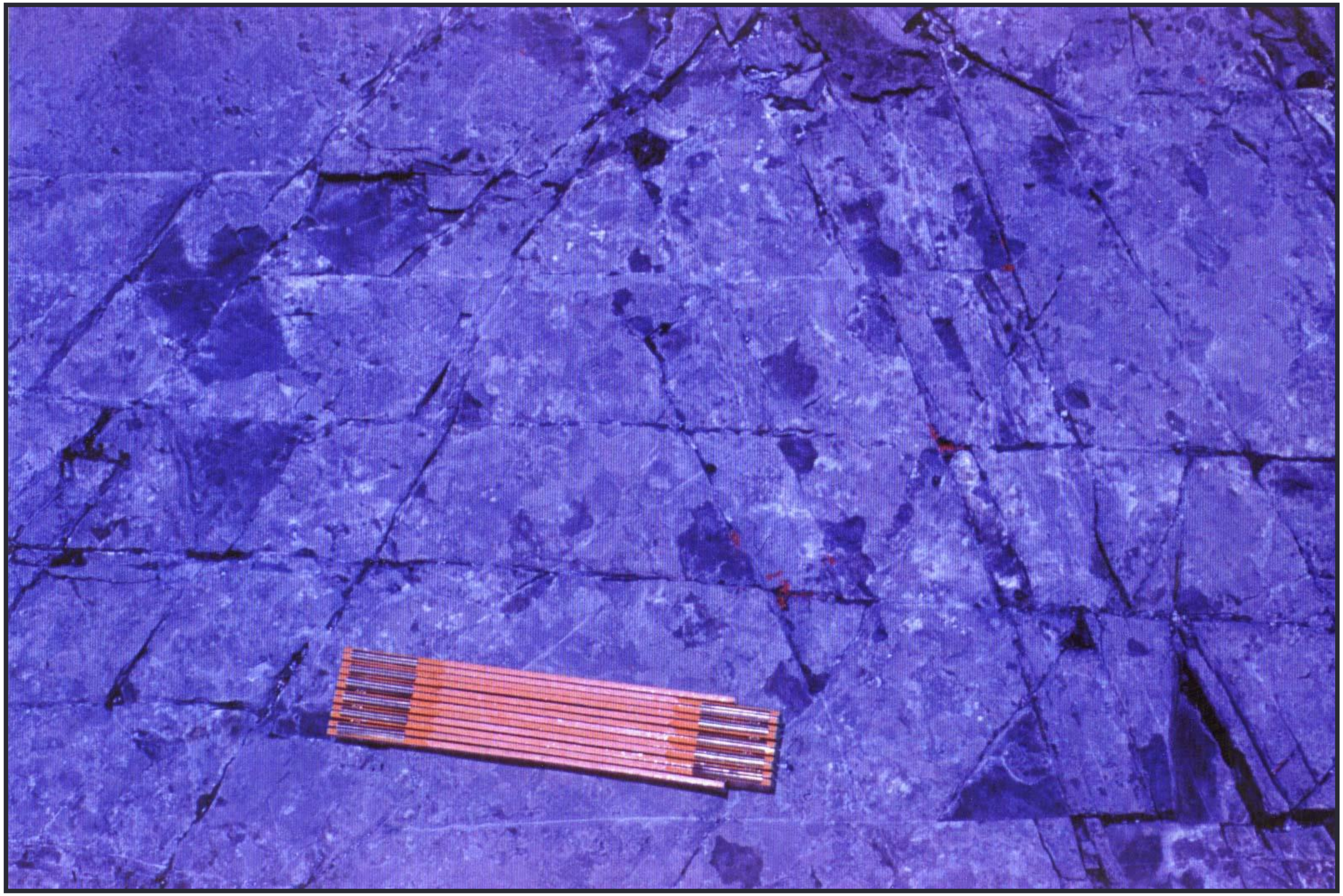

Coring induced fractures

- Can be mistaken for natural uncemented fractures and so influence identification of productive zones
- Types recognized using characteristic fracture surface morphology or fracture geometry:
  - Centreline fractures
  - Petal fractures
  - Torsional fractures
  - Scribe-knife related
  - Core-plug related
  - Unloading

Fracture surface morphology

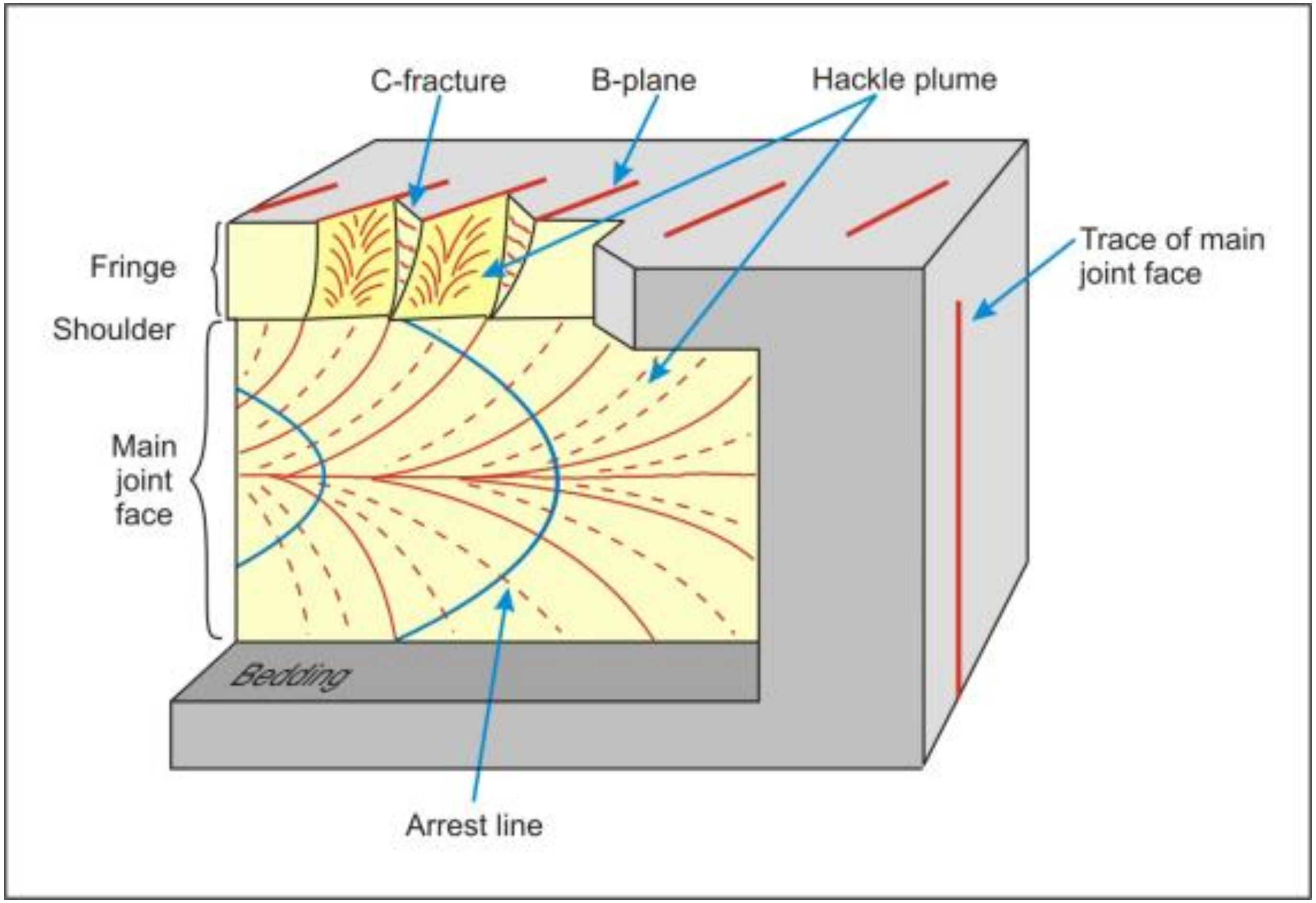

Arrest lines indicating Propagation down core

Petal-centreline fractures

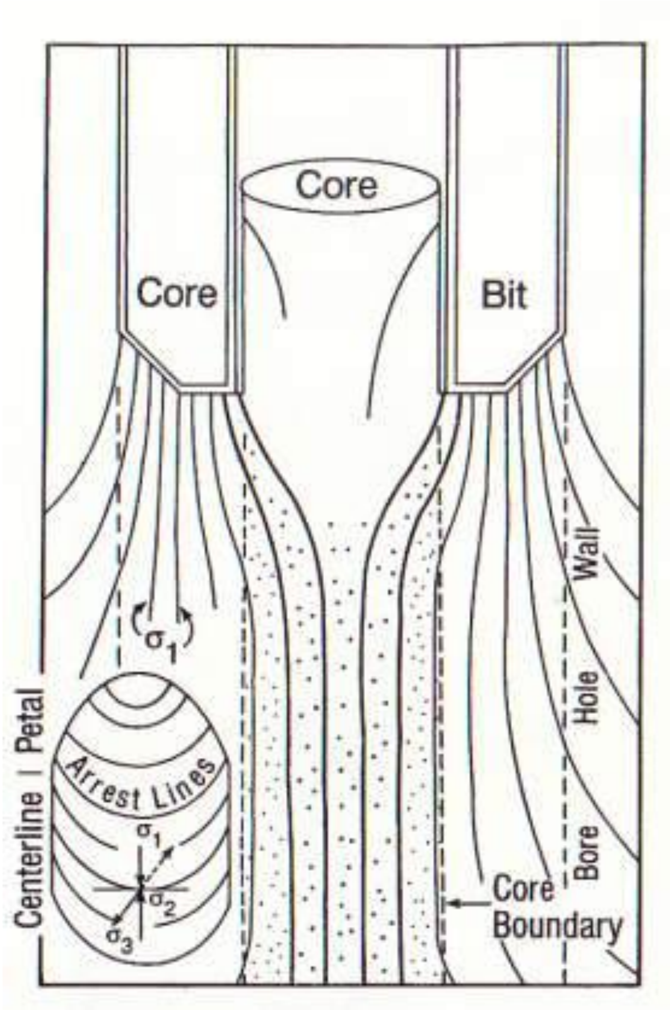

Petal-centreline fractures

Scribe knife damage

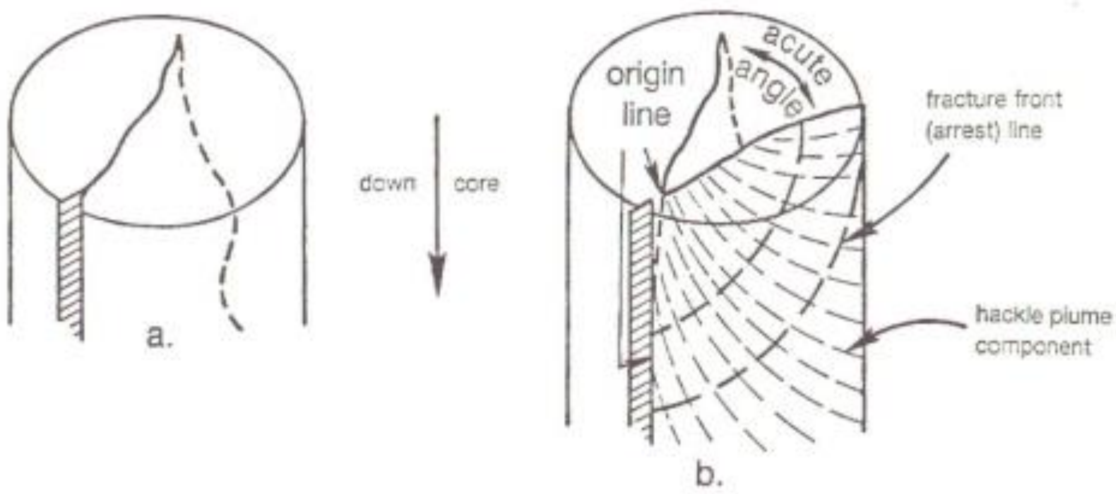

Scribe knife damage

Core discs

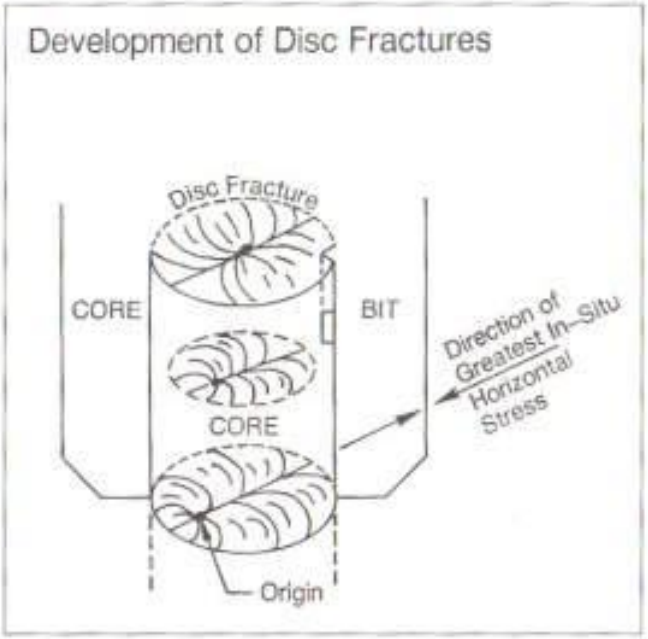
Development of Disc Fractures
Disc Fracture
CORE
BIT
CORE
Direction of Greatest In-Situ Horizontal Stress
Origin

Core discs

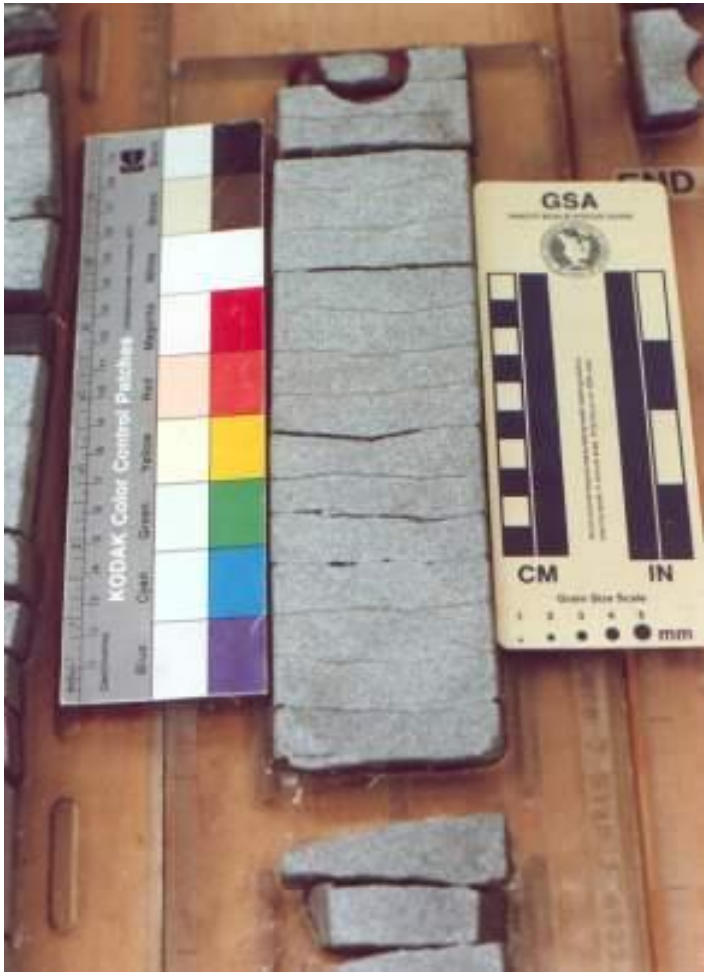

Core disc

Torsional fractures

Core spin

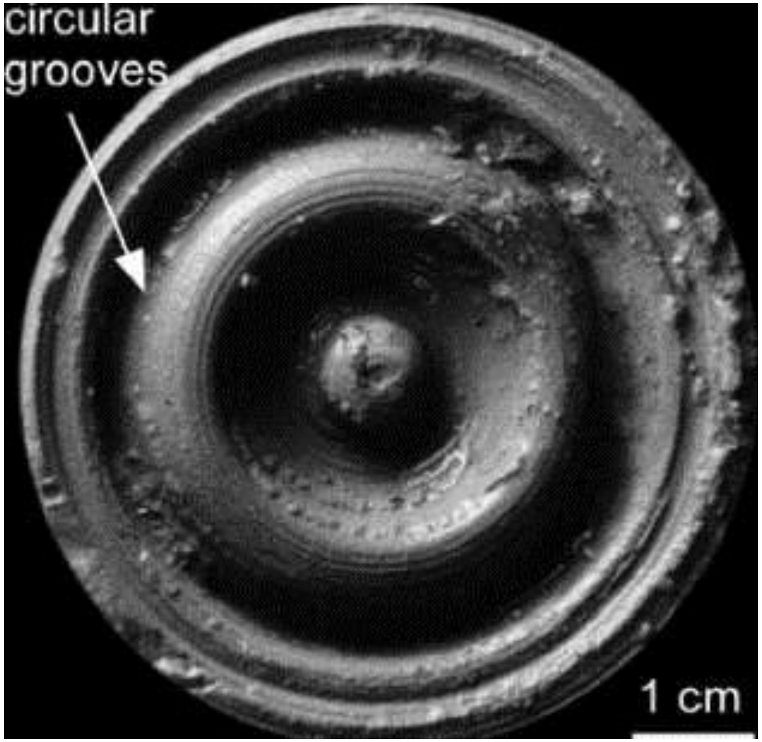

From Paulsen *et al*. (2002)

Rubble zones in core

- Induced
- Often at base of a core
- Can develop where lithologies change

Types of downhole image tools

- Electrical Resistivity: FMS (Formation MicroScanner),
  FMI (Formation MicroImager),
  RAB (Resistivity-At-Bit), etc

- Ultrasonic: UBI (Ultrasonic Borehole Imager),
  BHTV (BoreHole TeleViewer), etc

- Video.

Downhole video

Clear drilling fluid is required for downhole video - not often the case.

J. Nelson, COLOG

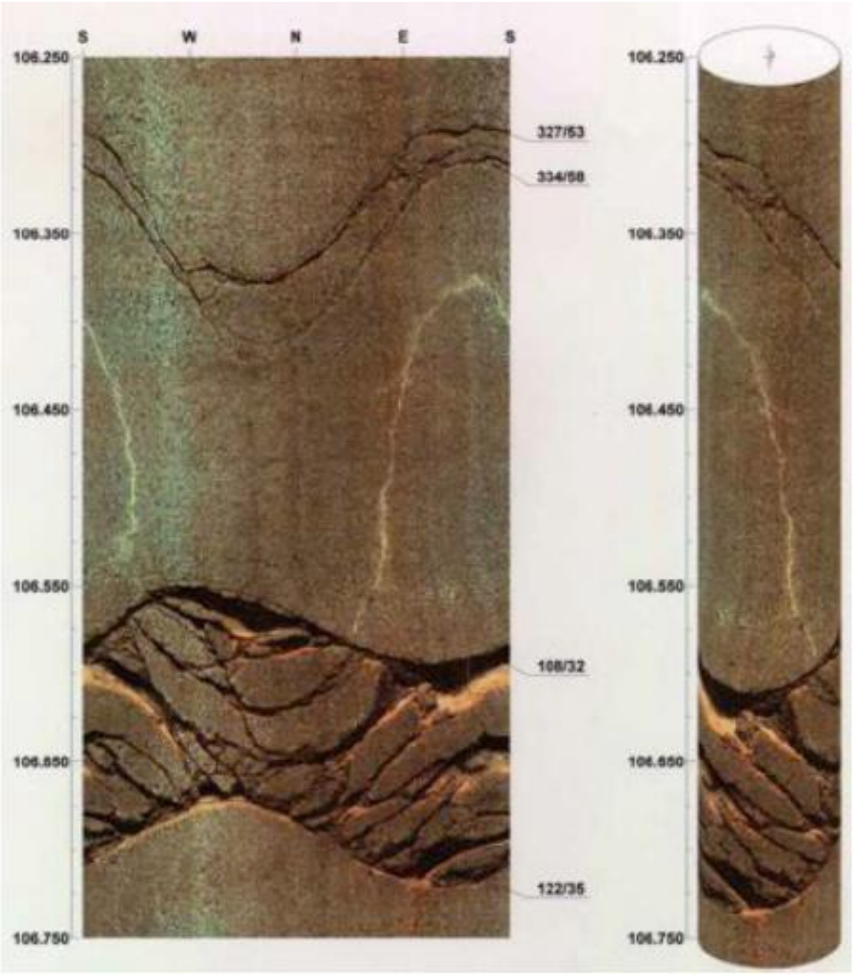

The first downhole images?

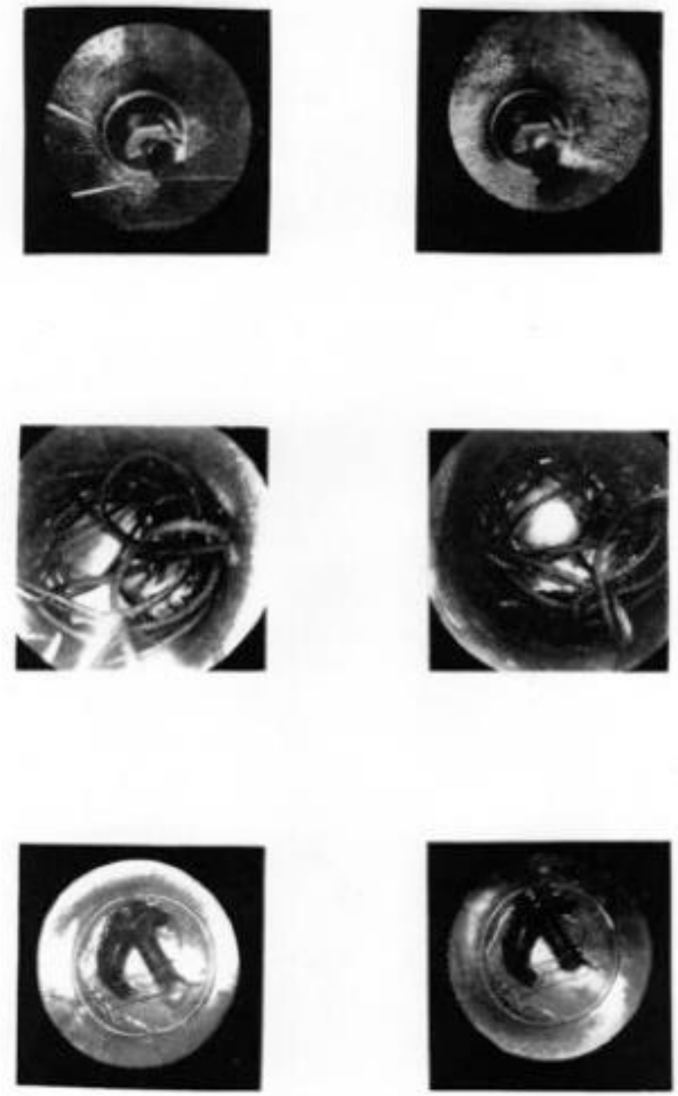

Fig. 39.—Photographs of Lost Articles in Baku Oil Wells.

Thompson / Loran 1904,

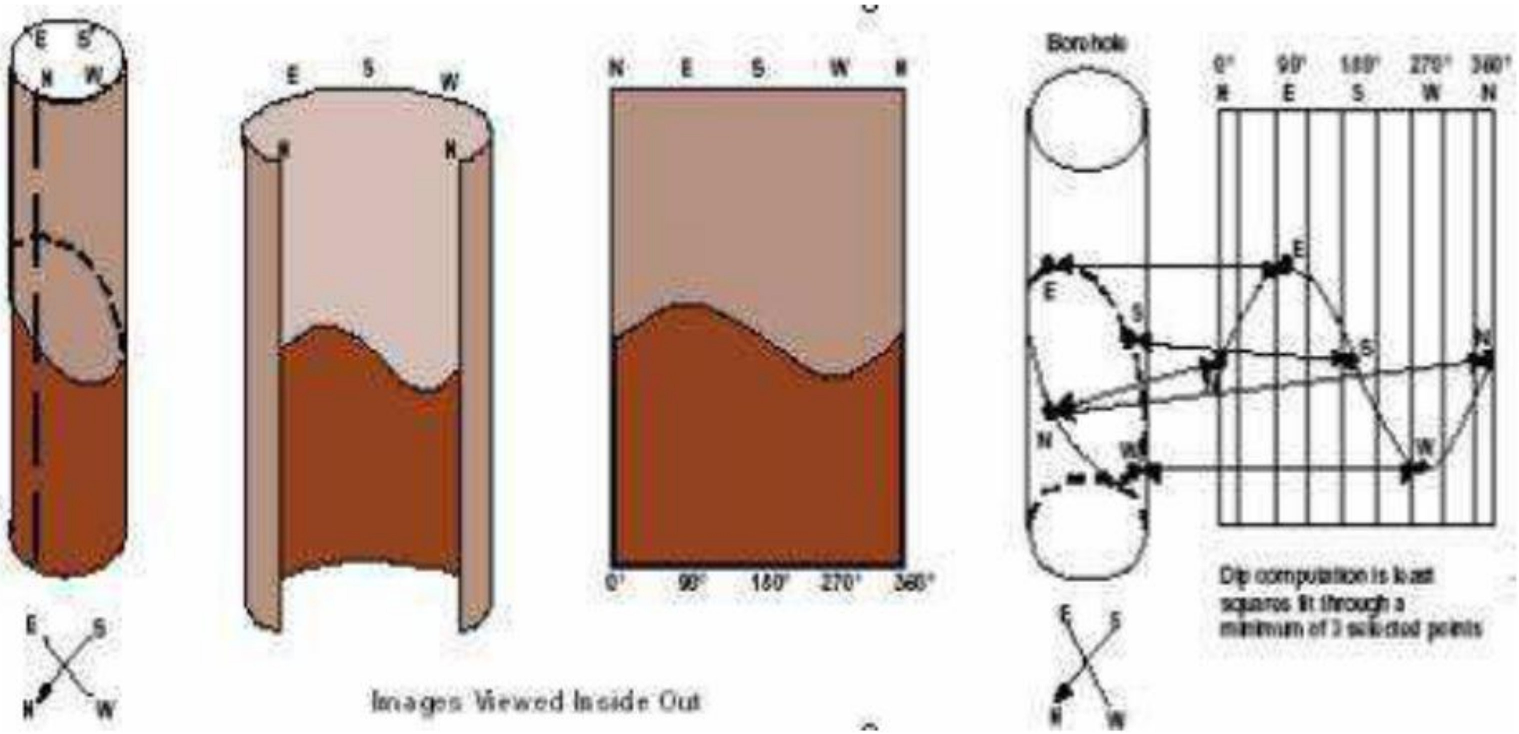

Images Viewed Inside Out
Borehole
0° 90° 180° 270° 360°
N E S W N
Dip computation is least squares fit through a minimum of 3 selected points

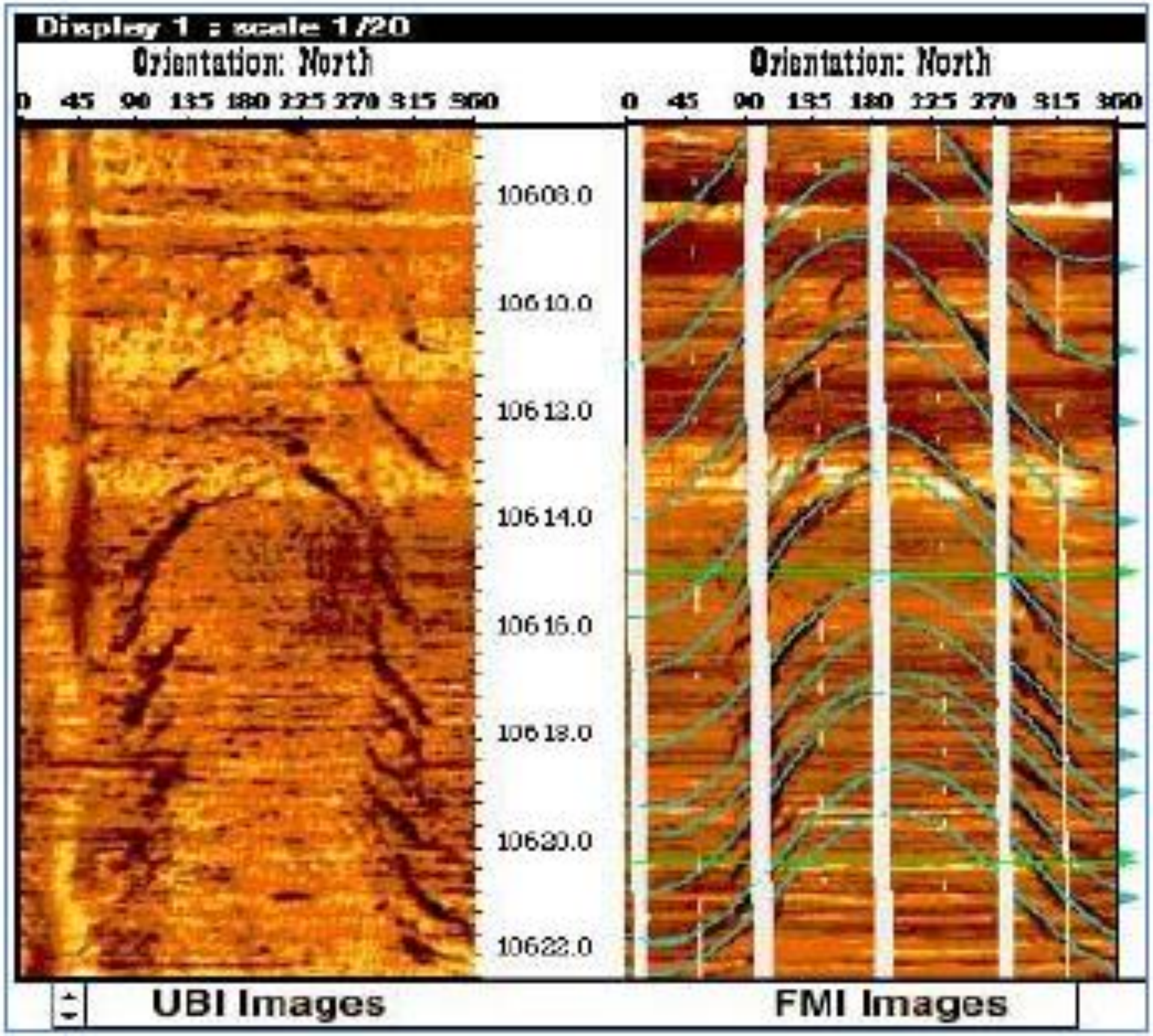

Display 1 : scale 1/20
Orientation: North
0 45 90 135 180 225 270 315 360
Orientation: North
0 45 90 135 180 225 270 315 360
10608.0
10610.0
10612.0
10614.0
10616.0
10618.0
10620.0
10622.0
UBI Images
FMI Images

Table 1. Baker Hughes imaging tools summaries

Service Company	Tools	Mud in Borehole	Tools characteristics and capabilities
Baker Hughes	**STAR Imager** Service	conductive /water based mud	Pads with 24 sensors mounted on each of the six articulated arms, giving a total of 144 microresistivity measurements with a vertical and azimuthal resolution of 0.2 in (~5 mm). Operates alone or in combination with the Baker Hughes CBIL imaging. Able to log images in vertical, horizontal, highly deviated, and rugose wells.
	Earth Imager Service	Non-conductive /oil based mud	Allows simultaneous acquisition of high-resolution microresistivity and acoustic borehole image data. Has an articulated six-arm carrier. Ability to log images in vertical, horizontal, highly deviated, and rugose wells.
	Circumferential Borehole Imaging Log (CBIL)	All type of muds	High-resolution borehole acoustic images in difficult conditions, including high-porosity, unconsolidated formations. Suitable for fracture and fault analysis. Can be used for interpretation of the near-wellbore stress field from borehole breakouts and drilling-induced fractures. 250-kHz operating frequency enables good performance in larger holes and heavier muds. Full 360-deg. borehole imaging tool operating in the pulse-echo mode. Generates sharp images and boundary delineation. Its small size of 3.625 in. (92 mm) allows for operation in slim holes as well as large-diameter holes.
	Ultrasonic Xplorer Imaging Service	All type of muds	High-resolution borehole acoustic images in difficult wellbore conditions, including OBM and large boreholes. Attains full 360° image coverage providing sharp images and boundary delineation. The lower operating frequency (250 kHz), along with downhole digital signal processing (DSP), allows for better performance in larger boreholes and in highly attenuating muds. Quite effective in horizontal wells. Its small size 3.625 in. (92 mm) allows for operation in slim holes, as well as large-diameter holes up to 16 in. (406 mm). Provides an acoustic amplitude image and a travel-time image. By calibrating the travel-time image, it is possible to provide a high-resolution borehole shape.

Baker Hughes	**GeoXplorer Imaging** Service	Non-conductive /oil based mud	Provides high-resolution formation microresistivity imaging in low-resistivity formations drilled with nonconductive mud systems. The high-resolution images allow for near-wellbore geological and petrophysical reservoir evaluation. 10 sensors mounted on six articulated arms to provide 60 microresistivity measurements, with a vertical resolution of 0.8 in (20 mm), and 79% borehole coverage in an 8.0” borehole. Operates in highly deviated boreholes. Determines an accurate net-pay even in thinly bedded intervals. Allows accurate positioning of fluid sampling or sidewall coring tools. The simultaneous acquisition of GeoXplorer and UltrasonicXplorer provides a more complete picture for accurate fracture evaluation, particularly in shale gas or fractured basement evaluation.

Table 2. Schlumberger imaging tools summaries

Service Company	Tools	Mud in Borehole	Tools characteristics and capabilities
Schlumberger	**FMI Fullbore Formation MicroImager**	conductive /water based mud	Provides real-time microresistivity formation images and dip with 80% borehole coverage in 8-in boreholes and 0.2-in image resolution in the vertical and azimuthal directions. Used for determining net pay in laminated sediments of fluvial and turbidite depositional environments, visualize sedimentary features to understand structure specially in not cored intervals, provide high quality of bedding dip data in highly deviated wells which improves the structural interpretation of seismic sections and computation of the true stratigraphic thickness. Improve modeling outputs, by supporting stochastic modeling of the sand-shale distribution. Define channel heights in amalgamated units, and others such as the channel width and channel sinuosity, can be estimated using geological analogs, based on detailed sedimentological analysis of FMI image data. Improve mechanical earth models for optimizing well planning. Better understanding of borehole stability.

Schlumberger	**Ultrasonic Borehole Imager (UBI)**	All type of muds	Analyze fractures, drilling-induced fractures and the stress regime and conduct borehole stability studies, with 100% borehole coverage, and structural interpretations. Two operating frequencies (measure both amplitude and transit time) modes of image resolution are available; standard and the higher resolution which deliver an accurate borehole cross section for deriving borehole stability and breakout information. The UBI processing technique avoids cycle skips and reduces echo losses. Image resolution is selected to correspond to the logging environment, such as mud type and density. The higher frequency yields higher image resolution. The lower standard frequency gives a robust measurement in highly dispersive muds. UBI tool measures attributes of ultrasonic waves reflected at the borehole wall and the rugosity of the borehole wall can dominate the reflection amplitude. UBI images are strongly sensitive to surface variations in the borehole wall but not to variations in lithology. Formation changes are normally seen on UBI images only if corresponding borehole surface effects, such as changes in rugosity or hole diameter, are present.
	Oil-Base MicroImager (OBMI)	Non-conductive /oil based mud	OBMI microresistivity imaging tool with four pads acquires five potential difference measurements that are used to quantitatively determine the resistivity of the invaded zone., see structural, stratigraphic, and anisotropic features as small as 0.4 in [1 cm], giving high-resolution azimuthal information. The sensitivity of the OBMI measurement delivers computed dips that are highly accurate even in formations with little resistivity contrast.

Table 3. Halliburton imaging tools summaries

Service Company	Tools	Mud in Borehole	Tools characteristics and capabilities
Halliburton	**Electrical Micro Imaging Service (EMI^{SM})**	Conductive/ water based mud	Six independent, articulating arms, each outfitted with 25 small electrodes on pad. Maintains optimum pad contact with a minimum of pad pressure, even in rugose, washed-out, or non-circular bore holes. An electrical current flows from the pads into the rock then upward in the wellbore to return at the top of the tool. Microresistivity contrast in the rock layers sampled 120 times per foot. Images are used to examine bed thicknesses ranging from a fraction of an inch to several feet; and accurately calculate sand thickness counts. Image enhancement techniques help further identify the precise characteristics of the formation reservoir. Identifies individual fault event and orientation. Detailed images of sedimentary features allow descriptions of bed boundaries, internal bed characteristics, textural changes, and laminated sand/shale sequences. Images can be presented in 2D and 3D formats.
	Oil-Based Micro-Imager Tool (OMRI^{SM})	Non-conductive/oil based mud	Six resistivity measurements per pad, each with a vertical resolution of 1 in. depth of investigation of about 3 in, data of 120 samples per foot with a proprietary signal acquisition scheme optimized for rugose hole conditions. The pads are mounted on six independent caliper arms. The sensor pads are mounted on the caliper arms with unique two-axis of articulation to improve pad contact in less ideal hole conditions which shows widest possible range of logging conditions. Used to analyze thin bed pay, structural and stratigraphic dips, sedimentary geometry and texture, borehole stresses, lithologic unit thickness, permeability barriers, sand attributes, clasts, vugs.
	X-Tended Range Micro Imager Tool (XRMI™)	Conductive/ water based mud	Coverage is 67% in 8.5 in. hole with 120 samples/ft. Good quality images even in high Rt:Rm environments. Has 32 bit digital signal acquisition architecture. S/N ratio by a factor of up to five, and the dynamic range expanded by a factor of up to three. The resulting images offer good reliability even in highly resistive formations ($Rt > 2000$ ohmm) or relatively salty borehole fluids ($Rm < 0.1$ ohmm). Pads mounted on six independently articulated arms help to maintain pad contact in rugose, washed-out, elliptical, or highly deviated boreholes.

Halliburton	**Circumferential Acoustic Scanning Tool-Visualization (CAST-V™)**	All type of muds	A high-frequency acoustic transducer to provide a full hole image. A second acoustic transducer is mounted in the scanner housing to measure characteristics of the borehole fluid. A directional sub is provided to orient images. Run primarily in open hole, 200 points horizontally by 40 samples/ft vertically. It is designed to operate in conjunction with other sonic tools but must be run centralized in fluid filled boreholes. Provides structural, stratigraphic, and sedimentological analyses for optimized offset well placement, completion design, and hydrocarbon depletion efficiency, thin bed delineation and improved net pay estimations, 2D and 3D borehole geometry and breakout presentations.

FMI

Fullbore Formation MicroImager Log.

Topics

- Applications
- Tool History
- Current Tool Theory
- Factors Affecting Log Results
- Log Quality
- Tool Setup & Operations
- Tool Maintenance

Applications

- Azimuthal Micro-Resistivities for dip, bed and fracture analysis
- Dip calculation data is a major input in reservoir modeling and interpretation
- Inclinometry for directional surveys.
- Borehole geometry from calipers.
- Hole volume

Tool History

- SHDT (Stratagraphic High-Resolution Dipmeter Tool)
- FMS/MEST (Fullbore Micro-Scanner)
- FMI/FBST (Fullbore Scanning Tool)
- OBDT (Oil Based Dipmeter Tool)

Slim - FMS (MEST-B)

- MEST-B (Above) is the slimhole version of the FMS. Two rows of 8 buttons on 4 pads.
- MEST-B 3 3/8” closing diameter.
- MEST-C 5” closing diameter.
- CTS telemetry.
- Bottom only

FMI

- 4 pads, 4 flippers
- DTS telemetry
- 5” closing diameter

PADS & FLIPPERS?

- Pads are connected to the calipers.
- Flippers are hinged to the pads, and are not hydraulically controlled
- Pad pressure can be hydraulically increased.

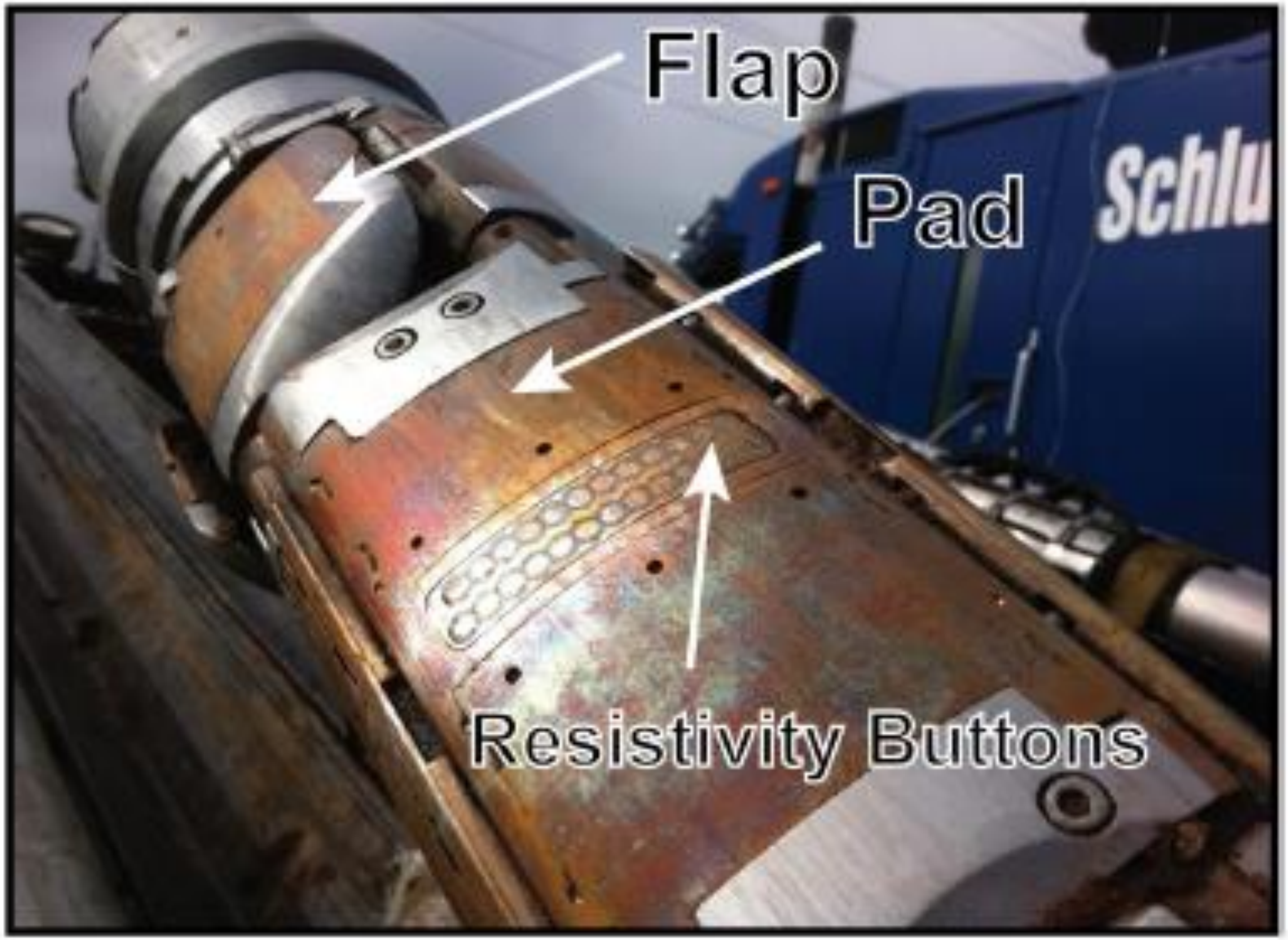
Flap
Pad
Schlu
Resistivity Buttons

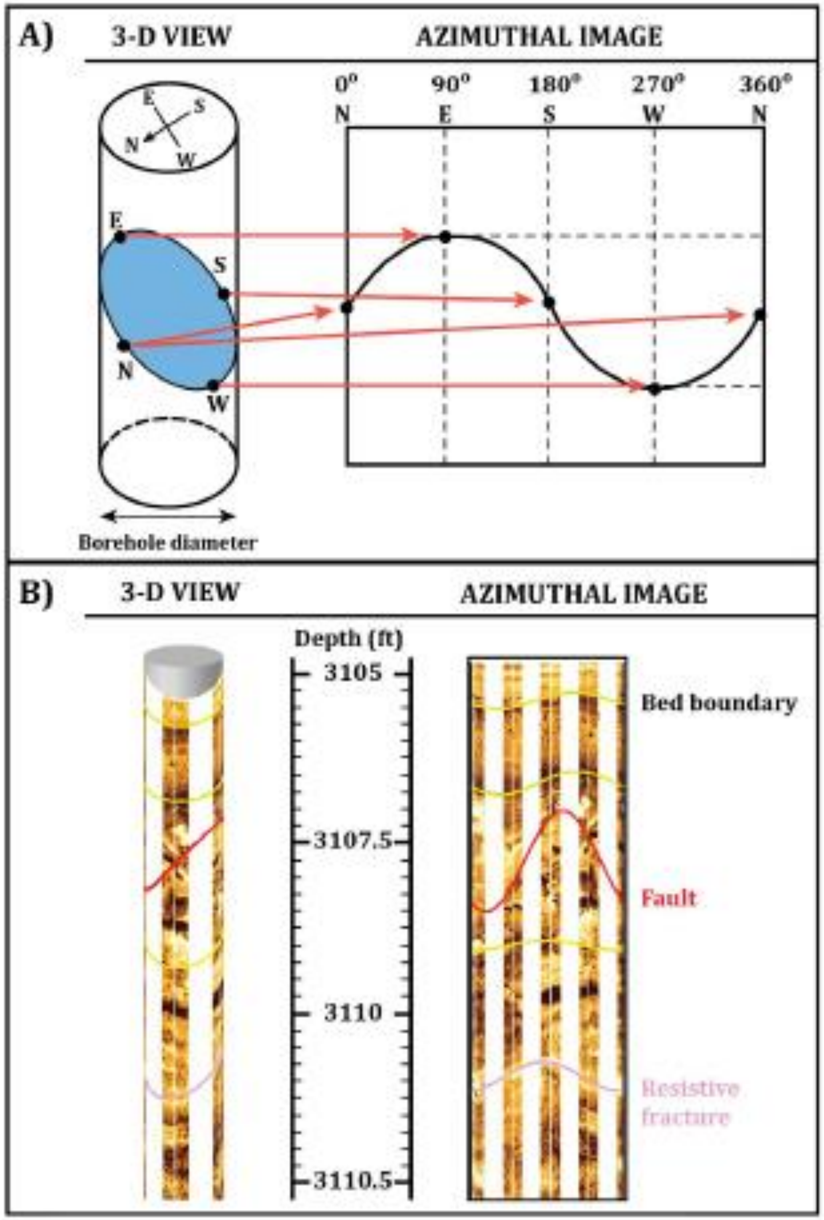

A)
3-D VIEW
AZIMUTHAL IMAGE
0° N
90° E
180° S
270° W
360° N
E
S
N
W
Borehole diameter
B)
3-D VIEW
AZIMUTHAL IMAGE
Depth (ft)
3105
3107.5
3110
3110.5
Bed boundary
Fault
Resistive fracture

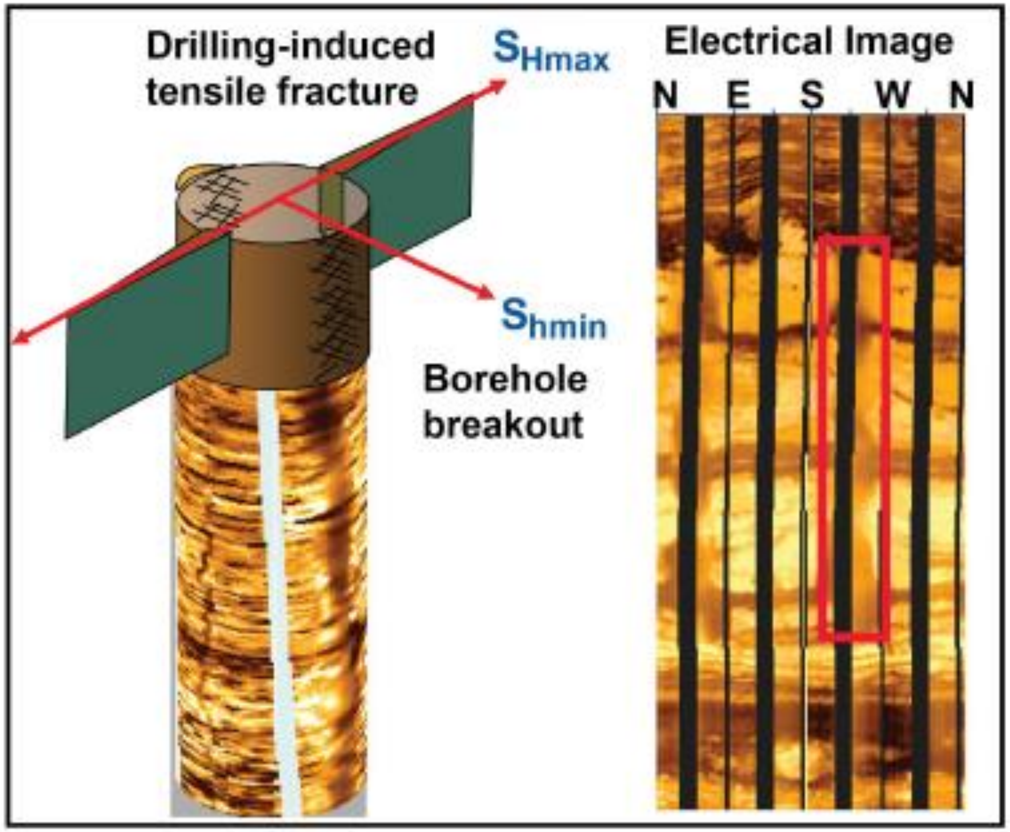
Drilling-induced
tensile fracture
S_{Hmax}
S_{hmin}
Borehole
breakout
Electrical Image
N E S W N

Resolution

- Samples: 62.5 Hz
- 5mm resolution (Button Size)
- Logging Speed must be less than 1800 fph

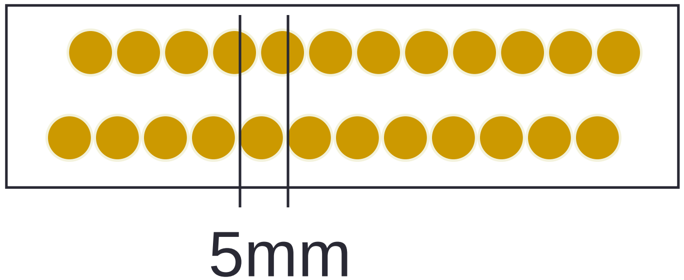

FMI PADs Have Guts Too!

- Button signals are multiplexed at the pads to reduce noise.
- Don’t hit them with hammers!

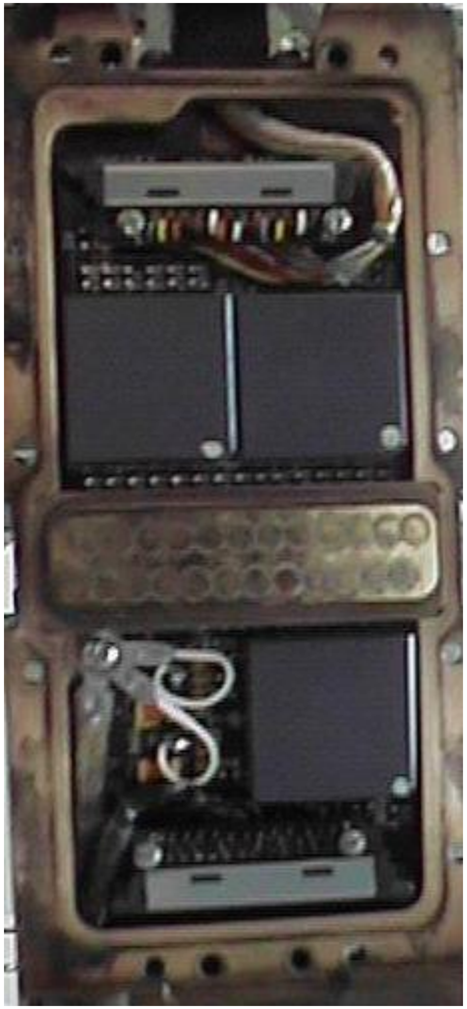

- Uphole power supply
- Phantommed on lines 1 and 4 to tool.
- Magnitude and Gain controlled either automatically (changes with formation) or manually.

Passive Focusing

- As opposed to Active Focusing (Dual-Laterolog).
- Simple but has limited functionality.
- Current is emitted from buttons and pads, creating an equipotential surface parallel to the borehole wall. The current returns to the cartridge.

Passive Focusing

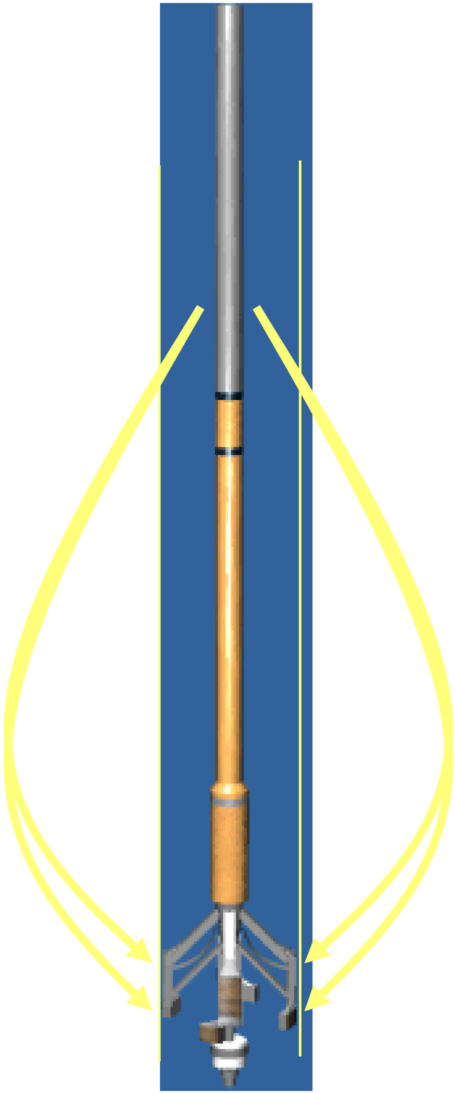

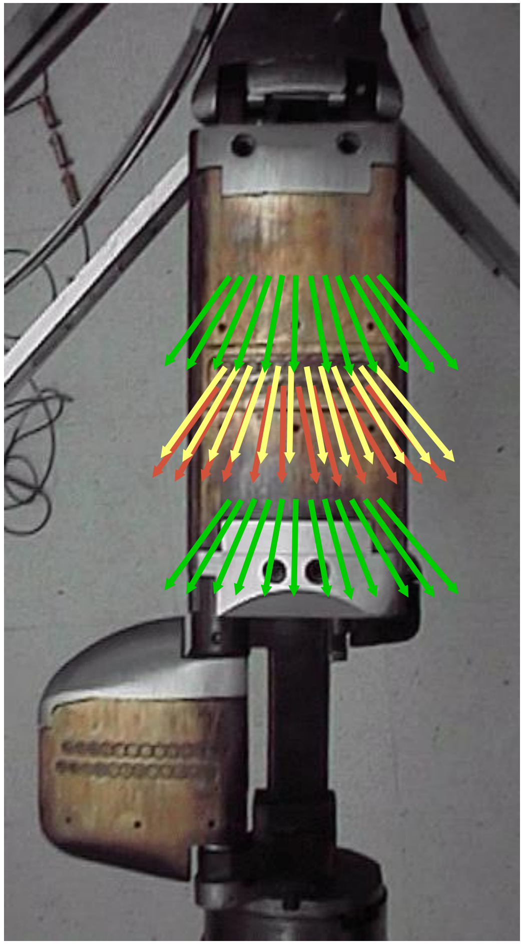

Dips

- Dips show up as sinusoidal features on an FMI Image
- Colors represent different micro-resistivities

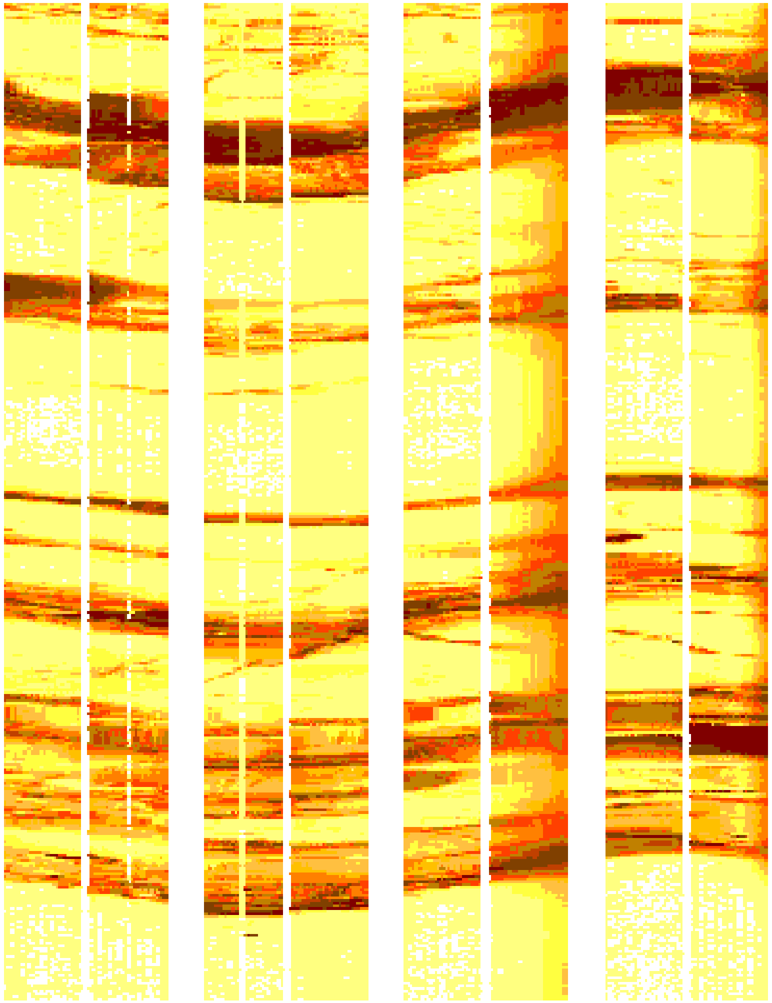

Dips

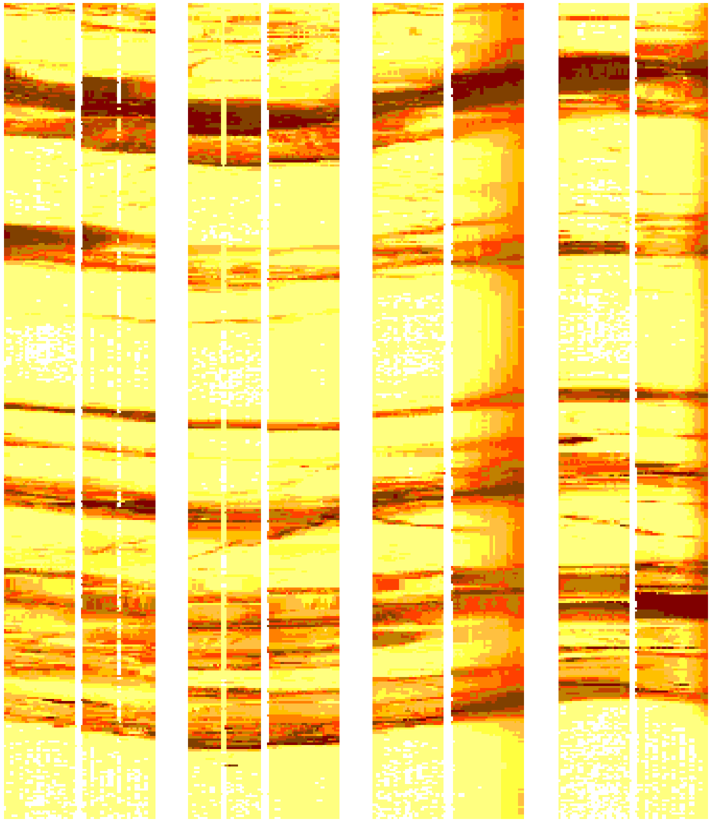

Dips

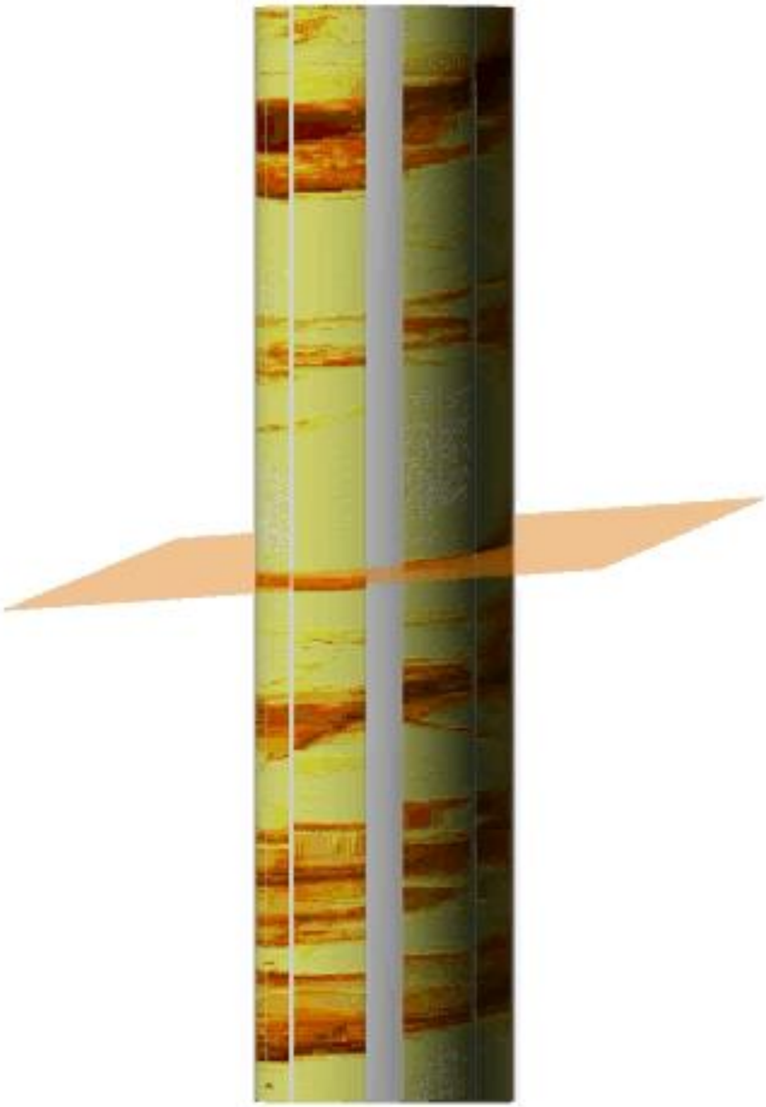

Dip Calculation

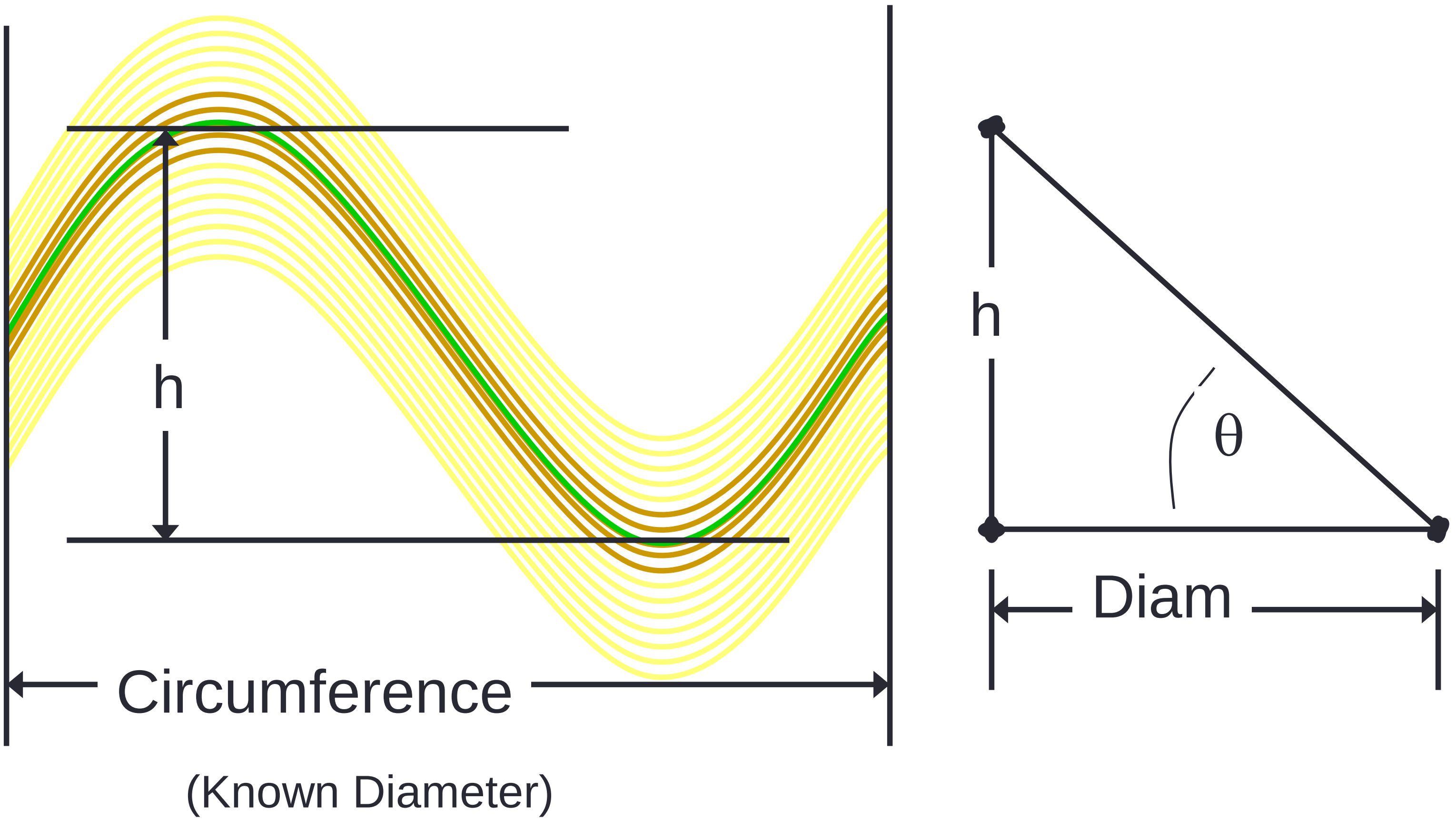

θ = ATan (h / Diam)

= Dip Angle

- به طور کلی، در نمودارهای تصویری، صفحات لایه بندی و شکستگی هایی که با دیواره چاه برخورد کرده است، به صورت منحنی های سینوسی با رابطه کلی زیر استنباط می شوند

$$y = A \sin(x+B) + C$$

$$A = R \tan \varphi$$

$$B = \frac{\pi}{2} - \beta$$

- R شعاع چاه، φشیب، βآزیموت و C موقعیت منحنی سینوسی در تصویر است. صفحات لایه بندی، اغلب دارای شیب و امتداد کم و بیش ثابت بوده و شیب آنها کمتر از ۴۵ درجه می باشد.

Geographic Features

Tool Rotation

- Since the tool will rotate during the log, we must know "HOW" it is rotating.
- If we don't know the rotational position of the dipmeter tool, then we will not know which direction the dip is.

With Orientation

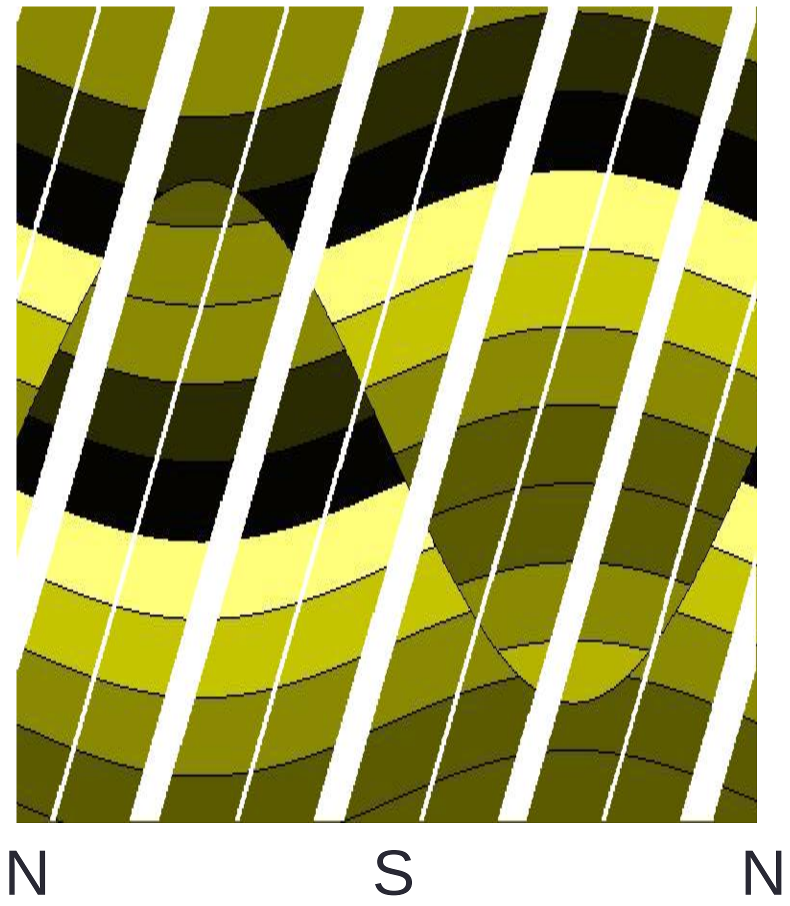

No Orientation

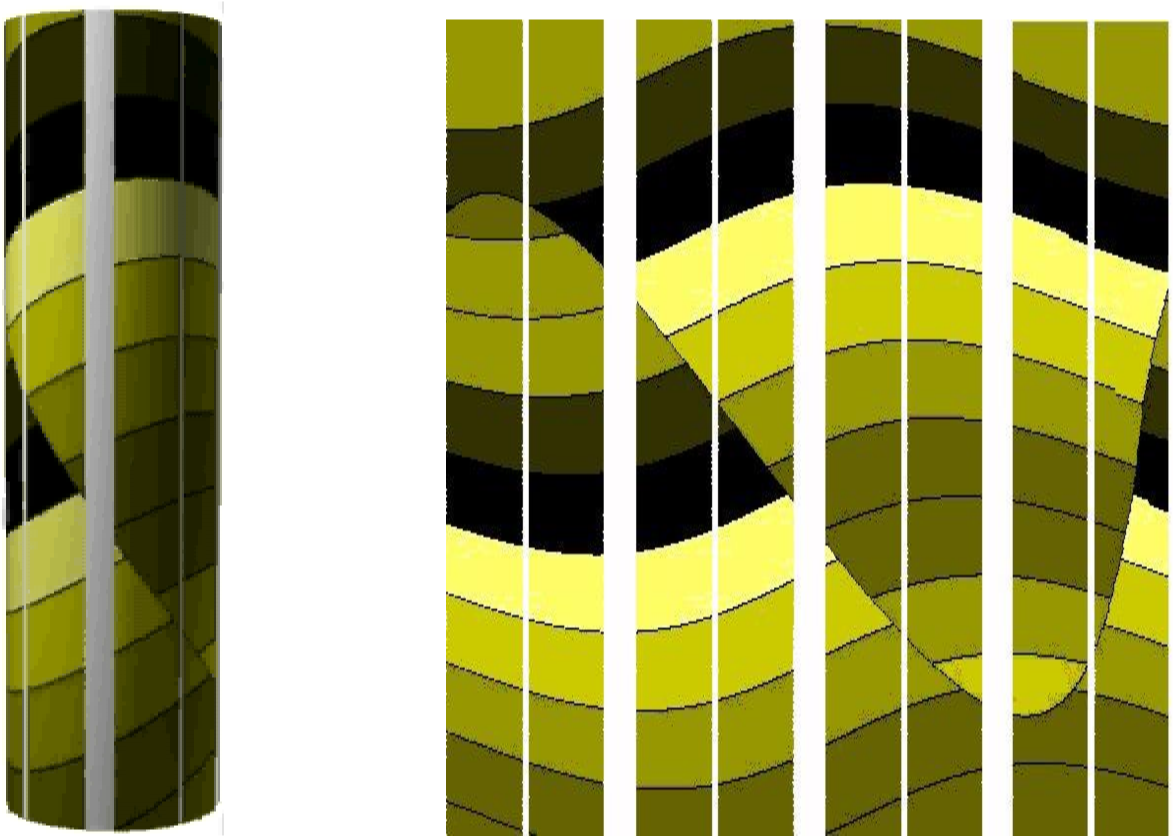

Inclinometry

- “Where” the data came from is as important as the data itself.
  - Images can be oriented with respect to North or to the top of the borehole.
- Compare it to taking a core or sample but not knowing what depth it came from.
- For this reason, and inclinometry tool is required: GPIT

Inclinometry, GPIT

- The GPIT is located inside the FMI sonde (FBSS).
- It can be removed and placed into its own housing.

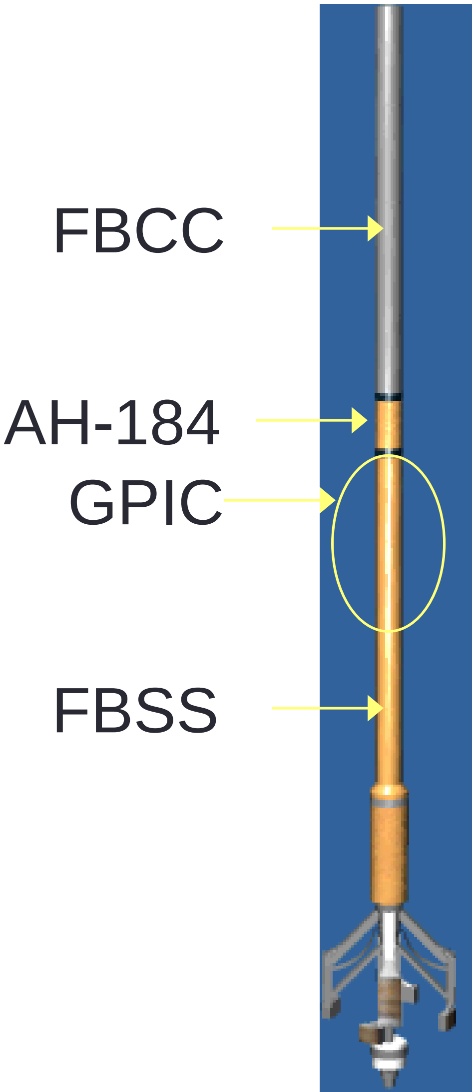

GPIT Block Diagram

- GPIC-AC : DTB
- GPIC-C : FTB

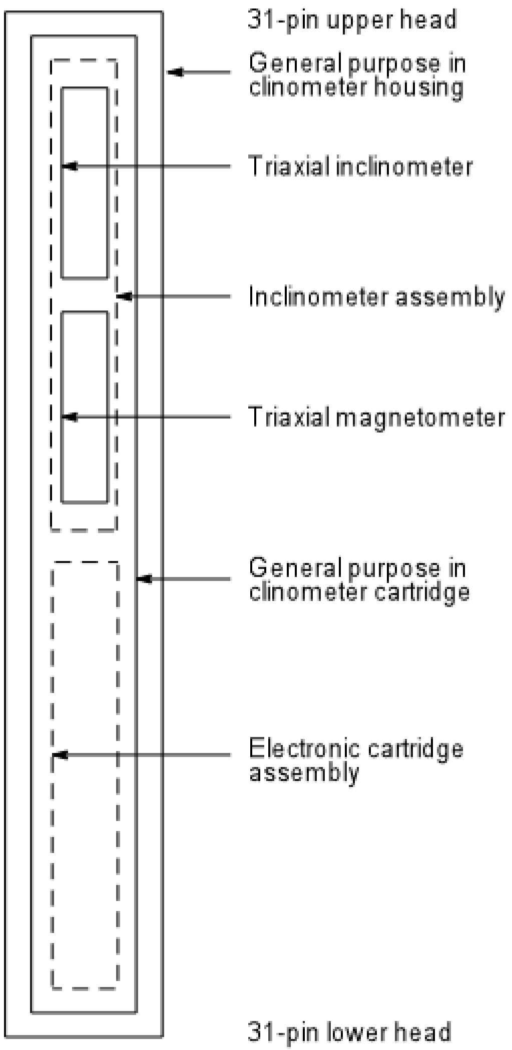

Magnetic Field Strength

- A Triaxial magnetometer (three single axis magnetometers) are used to determine the rotational position of the tool, relative to the Earth's magnetic field. (Magnetic North)
- $F_{NOR} = \sqrt{(F_X^2 + F_Y^2 + F_Z^2)}$
- F_{NOR} = Depends on where you are.

Flux Gate Magnetometer

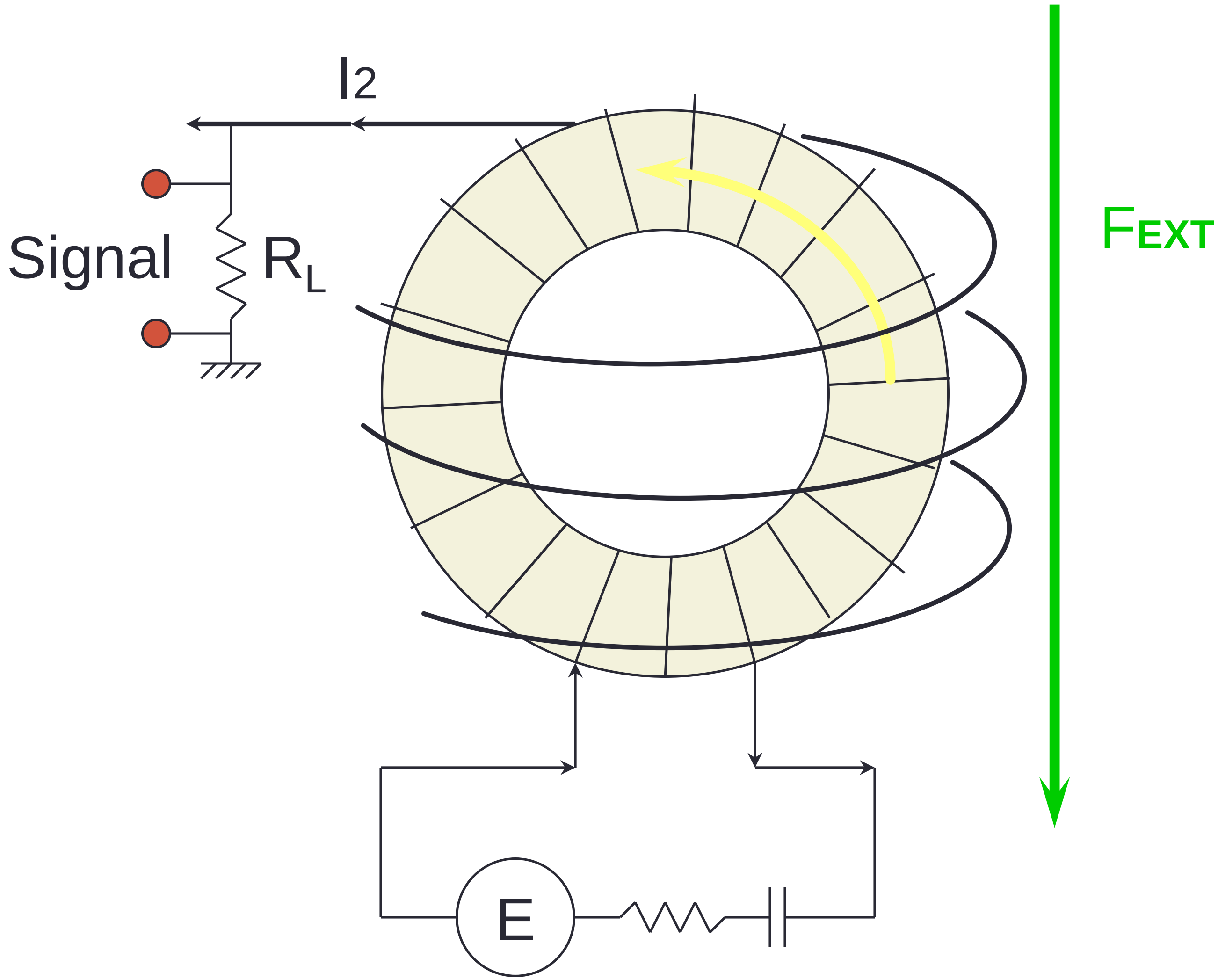

Inclinometry, P1AZ

- Pad 1 Azimuth

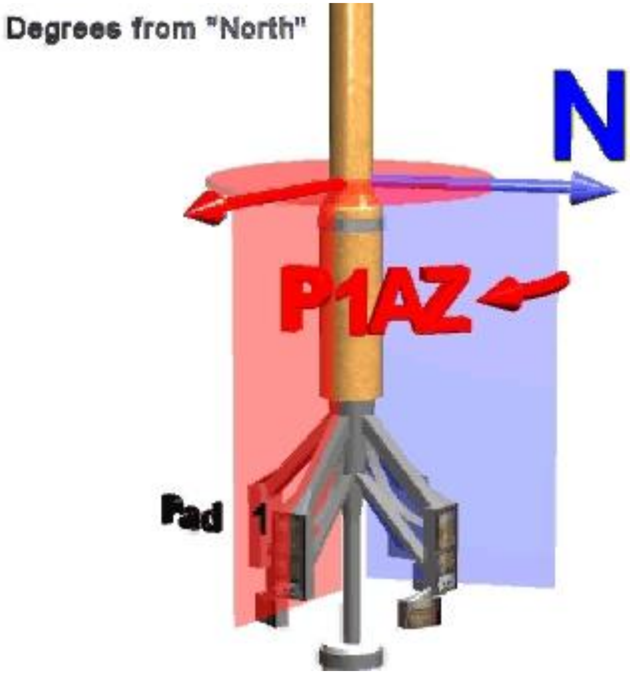

- Degrees from Magnetic north on a horizontal plane.
- I.e.: P1AZ = 180 means Pad 1 is south.

Longitude / Latitude

- LATD: Latitude (in degrees)
- LOND: Longitude (in degrees)

Inclinometry, RB

- Relative Bearing

- Degrees from “UP” on a vertical plane
- i.e. RB = 180 means Pad 1 is down.

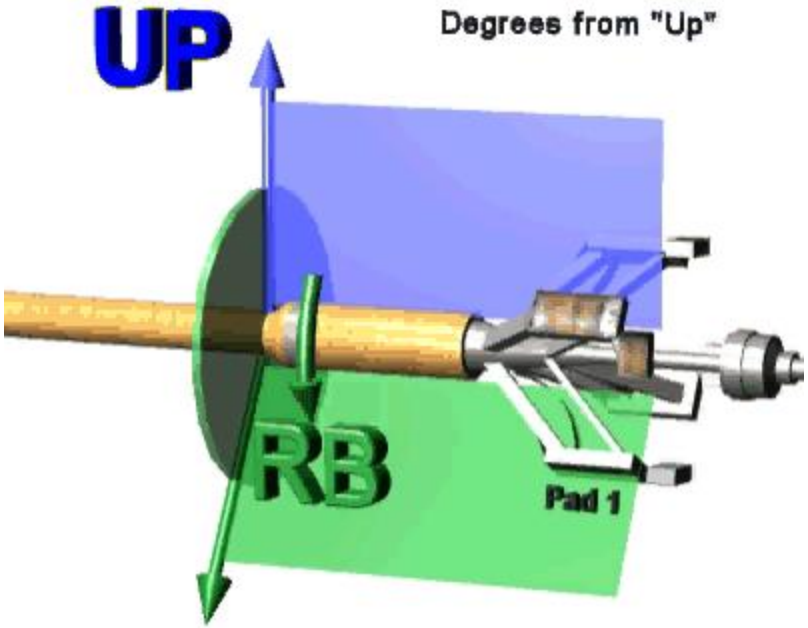

Inclinometry, Deviated Well

- Relative Bearing & P1AZ Track each other

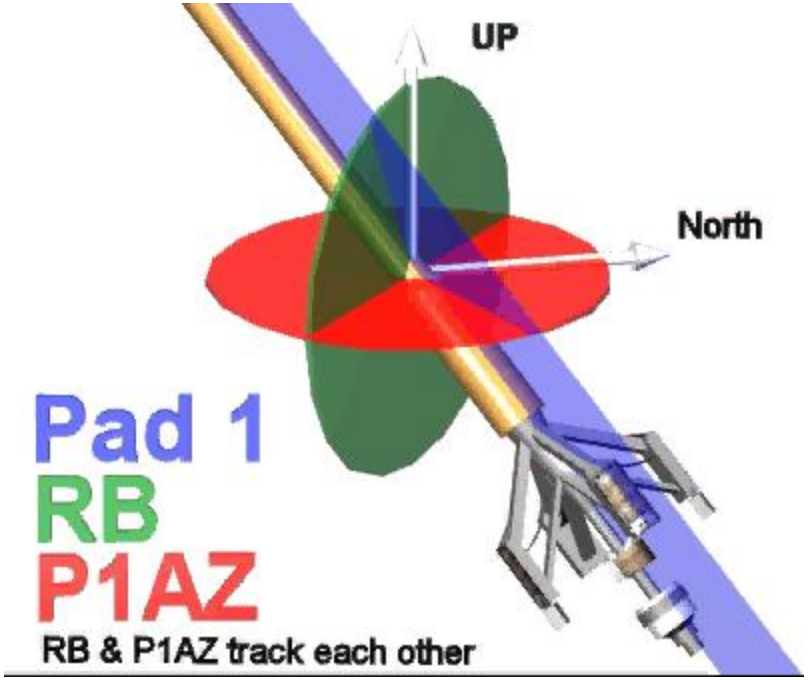

- In deviated wells, both can be used to orient images

Inclinometry

- HAZI
  - Direction the hole is travelling (N,S,E,W)
- DEVI
  - Deviation of the hole (From Vertical)
  - i.e.:
    Vertical well = 0 deg deviated
    Horizontal well = 90 deg deviated

Worst Case

- In the event of the failure of one (**and only one**) of the GPIT accelerometer in the Ax or Ay or magnetometer channels, the job can still be rescued in a computing center. If the accelerometer along the z-axis fails, speed correction can no longer be performed.

Repeatabliltiy

- AZIM ± 2°
- DEVI ± 0.2°
- CALI ± 0.25 in.

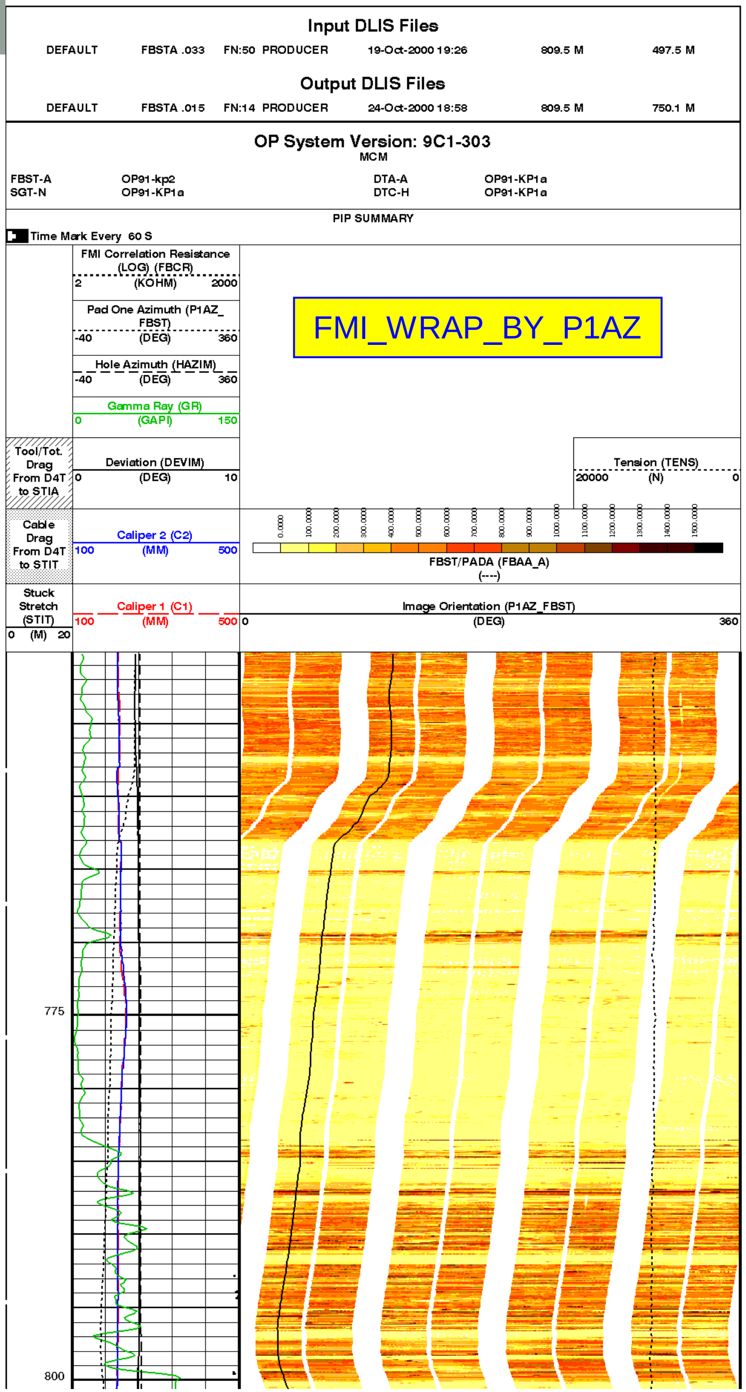
Input DLIS Files
DEFAULT FBSTA .033 FN:50 PRODUCER 19-Oct-2000 19:26 809.5 M 497.5 M
Output DLIS Files
DEFAULT FBSTA .015 FN:14 PRODUCER 24-Oct-2000 18:58 809.5 M 750.1 M
OP System Version: 9C1-303
MCM
FBST-A OP91-kp2 DTA-A OP91-KP1a
SGT-N OP91-KP1a DTC-H OP91-KP1a
PIP SUMMARY
Time Mark Every 60 S
FMI Correlation Resistance (LOG) (FBCR)
2 (KOHM) 2000
Pad One Azimuth (P1AZ_FBST)
-40 (DEG) 360
Hole Azimuth (HAZIM)
-40 (DEG) 360
Gamma Ray (GR)
0 (GAPI) 150
FMI_WRAP_BY_P1AZ
Tool/Tot. Drag From D4T to STIA
Deviation (DEVIM)
0 (DEG) 10
Tension (TENS)
20000 (N) 0
Cable Drag From D4T to STIT
Caliper 2 (C2)
100 (MM) 500
FBST/PADA (FBAA_A)
(----)
Stuck Stretch (STIT)
0 (M) 20
Caliper 1 (C1)
100 (MM) 500
Image Orientation (P1AZ_FBST)
0 (DEG) 360
775
800

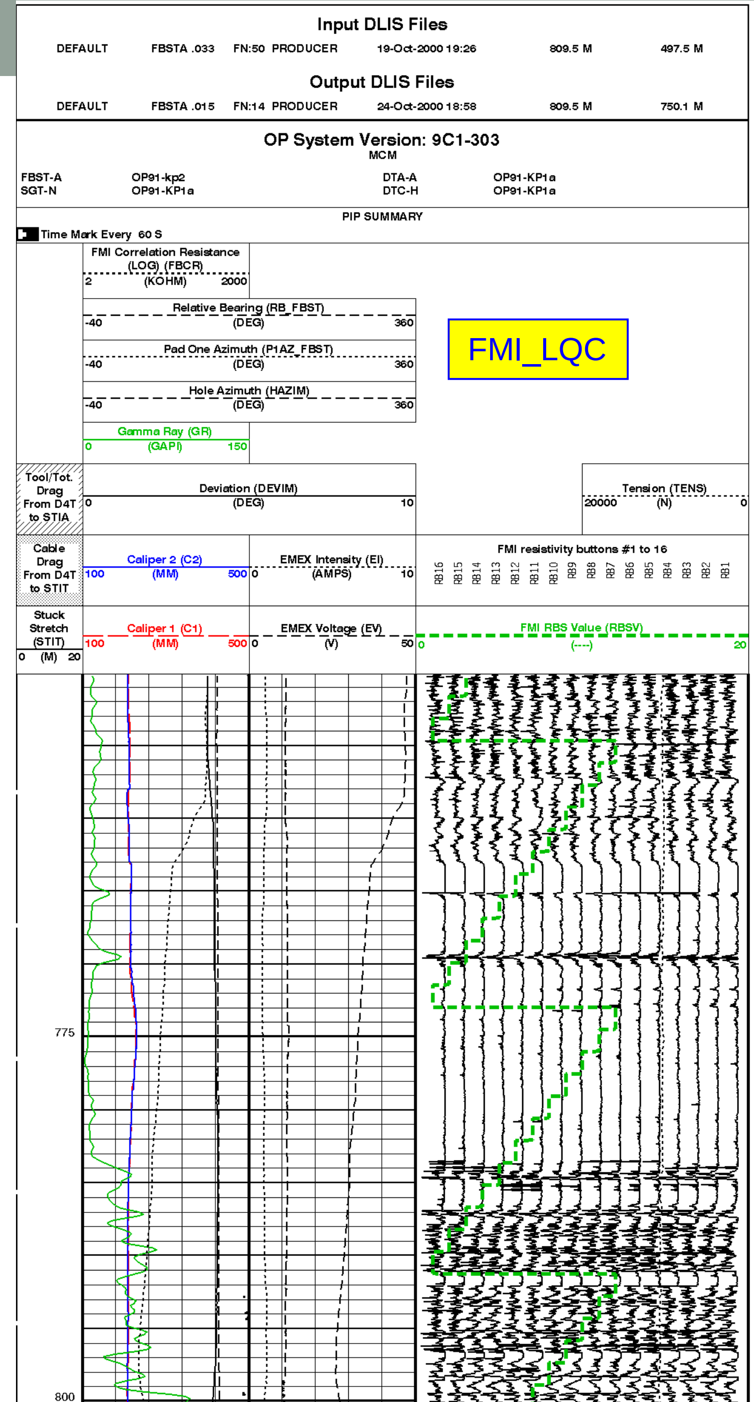
Input DLIS Files
DEFAULT FBSTA .033 FN:50 PRODUCER 19-Oct-2000 19:26 809.5 M 497.5 M
Output DLIS Files
DEFAULT FBSTA .015 FN:14 PRODUCER 24-Oct-2000 18:58 809.5 M 750.1 M
OP System Version: 9C1-303
MCM
FBST-A OP91-kp2 DTA-A OP91-KP1a
SGT-N OP91-KP1a DTC-H OP91-KP1a
PIP SUMMARY
Time Mark Every 60 S
FMI Correlation Resistance (LOG) (FBCR)
2 (KOHM) 2000
Relative Bearing (RB_FBST)
-40 (DEG) 360
Pad One Azimuth (P1AZ_FBST)
-40 (DEG) 360
Hole Azimuth (HAZIM)
-40 (DEG) 360
Gamma Ray (GR)
0 (GAPI) 150
FMI_LQC
Tool/Tot. Drag From D4T to STIA
Deviation (DEVIM)
0 (DEG) 10
Tension (TENS)
20000 (N) 0
Cable Drag From D4T to STIT
Caliper 2 (C2)
100 (MM) 500
EMEX Intensity (EI)
0 (AMPS) 10
FMI resistivity buttons #1 to 16
Stuck Stretch (STIT)
0 (M) 20
Caliper 1 (C1)
100 (MM) 500
EMEX Voltage (EV)
0 (V) 50
FMI RBS Value (RBSV)
0 (----) 20
775
800

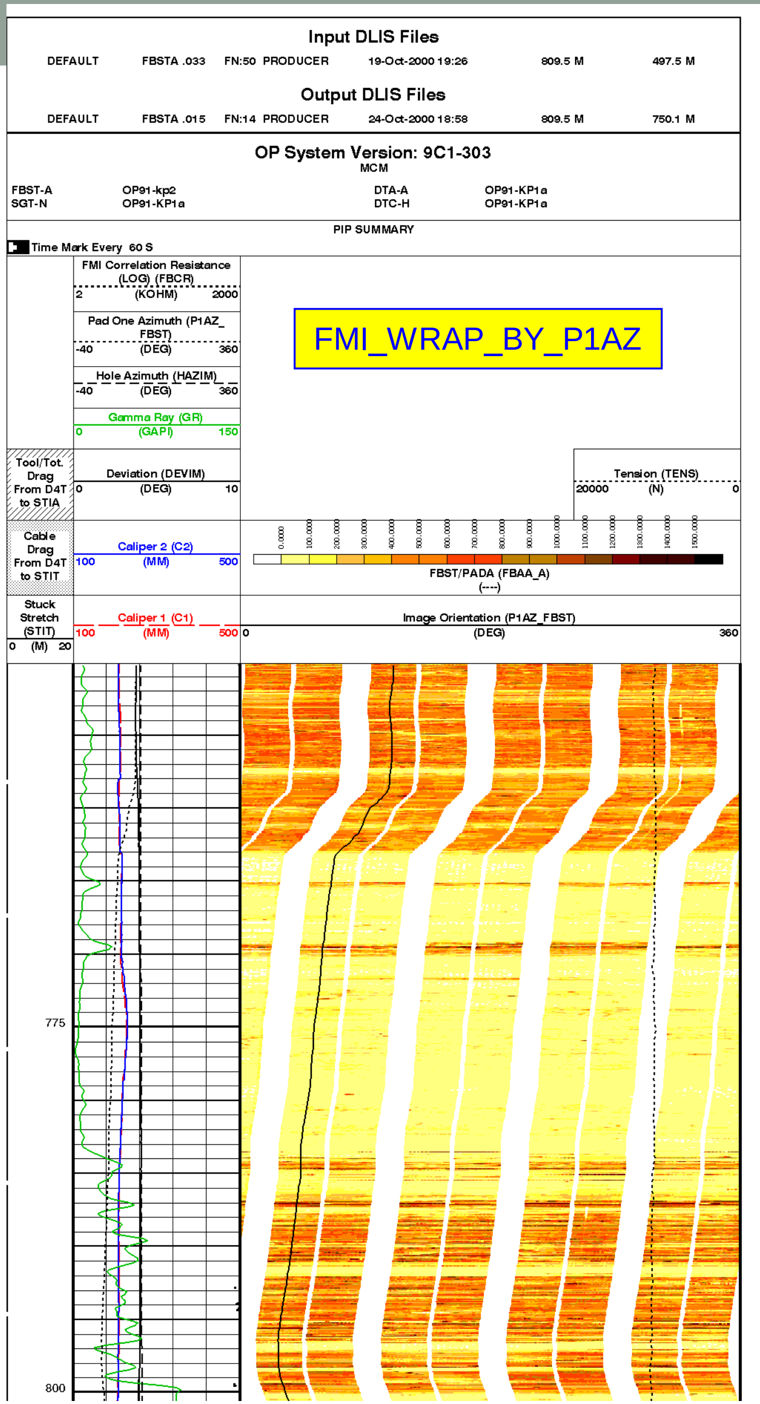

Input DLIS Files
DEFAULT FBSTA .033 FN:50 PRODUCER 19-Oct-2000 19:26 809.5 M 497.5 M
Output DLIS Files
DEFAULT FBSTA .015 FN:14 PRODUCER 24-Oct-2000 18:58 809.5 M 750.1 M
OP System Version: 9C1-303
MCM
FBST-A OP91-kp2 DTA-A OP91-KP1a
SGT-N OP91-KP1a DTC-H OP91-KP1a
PIP SUMMARY
Time Mark Every 60 S
FMI Correlation Resistance (LOG) (FBCR)
2 (KOHM) 2000
Pad One Azimuth (P1AZ_FBST)
-40 (DEG) 360
Hole Azimuth (HAZIM)
-40 (DEG) 360
Gamma Ray (GR)
0 (GAPI) 150
FMI_WRAP_BY_P1AZ
Tool/Tot. Drag From D4T to STIA
Deviation (DEVIM)
0 (DEG) 10
Tension (TENS)
20000 (N) 0
Cable Drag From D4T to STIT
Caliper 2 (C2)
100 (MM) 500
FBST/PADA (FBAA_A)
(----)
Stuck Stretch (STIT)
0 (M) 20
Caliper 1 (C1)
100 (MM) 500
Image Orientation (P1AZ_FBST)
0 (DEG) 360
775
800

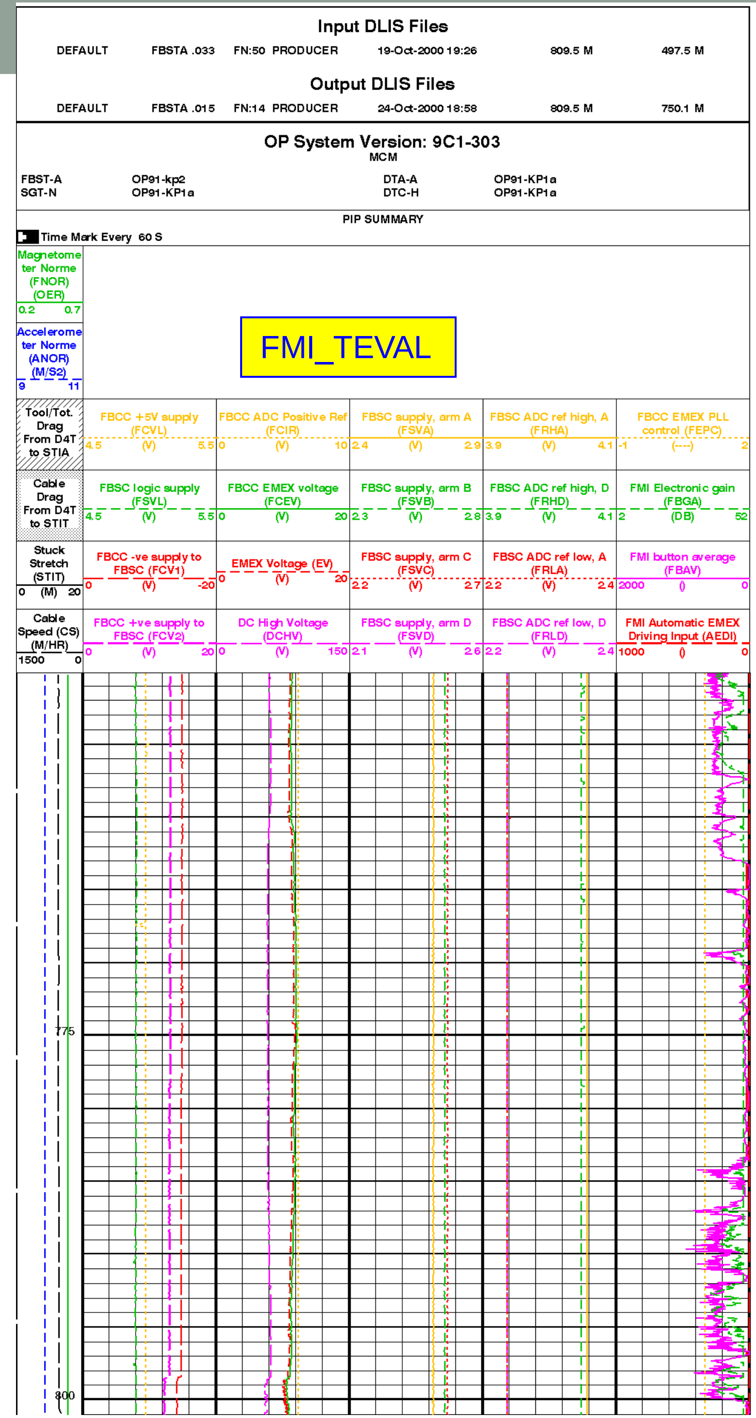

Input DLIS Files
DEFAULT FBSTA .033 FN:50 PRODUCER 19-Oct-2000 19:26 809.5 M 497.5 M
Output DLIS Files
DEFAULT FBSTA .015 FN:14 PRODUCER 24-Oct-2000 18:58 809.5 M 750.1 M
OP System Version: 9C1-303
MCM
FBST-A OP91-kp2 DTA-A OP91-KP1a
SGT-N OP91-KP1a DTC-H OP91-KP1a
PIP SUMMARY
Time Mark Every 60 S
Magnetometer Norme (FNOR) (OER)
0.2 0.7
Accelerometer Norme (ANOR) (M/S2)
9 11
FMI_TEVAL
Tool/Tot. Drag From D4T to STIA
FBCC +5V supply (FCVL) 4.5 (V) 5.5
FBCC ADC Positive Ref (FCIR) 0 (V) 10
FBSC supply, arm A (FSVA) 2.4 (V) 2.9
FBSC ADC ref high, A (FRHA) 3.9 (V) 4.1
FBCC EMEX PLL control (FEPC) -1 (----) 2
Cable Drag From D4T to STIT
FBSC logic supply (FSVL) 4.5 (V) 5.5
FBCC EMEX voltage (FCEV) 0 (V) 20
FBSC supply, arm B (FSVB) 2.3 (V) 2.8
FBSC ADC ref high, D (FRHD) 3.9 (V) 4.1
FMI Electronic gain (FBGA) 2 (DB) 52
Stuck Stretch (STIT) 0 (M) 20
FBCC -ve supply to FBSC (FCV1) 0 (V) -20
EMEX Voltage (EV) 0 (V) 20
FBSC supply, arm C (FSVC) 2.2 (V) 2.7
FBSC ADC ref low, A (FRLA) 2.2 (V) 2.4
FMI button average (FBAV) 2000 () 0
Cable Speed (CS) (M/HR) 1500 0
FBCC +ve supply to FBSC (FCV2) 0 (V) 20
DC High Voltage (DCHV) 0 (V) 150
FBSC supply, arm D (FSVD) 2.1 (V) 2.6
FBSC ADC ref low, D (FRLD) 2.2 (V) 2.4
FMI Automatic EMEX Driving Input (AEDI) 1000 () 0
775
800

Input DLIS Files

DEFAULT	FBSTA .033	FN:50	PRODUCER	19-Oct-2000 19:26	809.5 M	497.5 M

Output DLIS Files

DEFAULT	FBSTA .015	FN:14	PRODUCER	24-Oct-2000 18:58	809.5 M	750.1 M

OP System Version: 9C1-303

MCM

FBST-A	OP91-kp2	DTA-A	OP91-KP1a
SGT-N	OP91-KP1a	DTC-H	OP91-KP1a

PIP SUMMARY

Time Mark Every 60 S

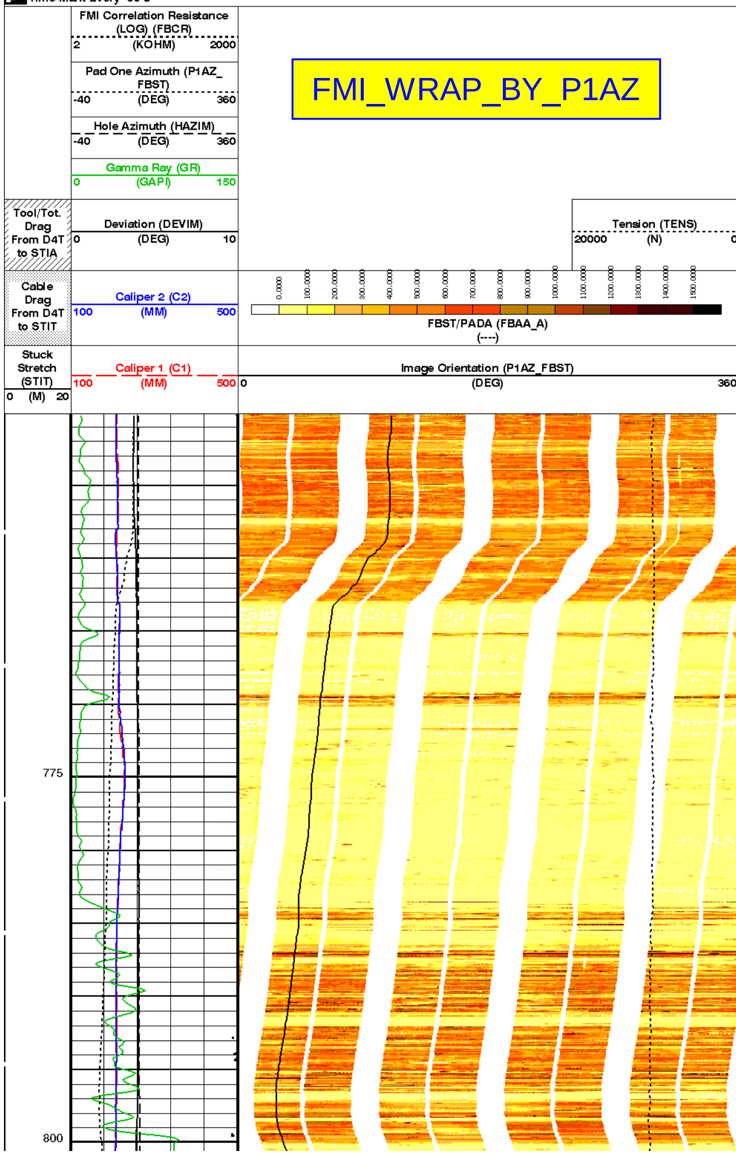

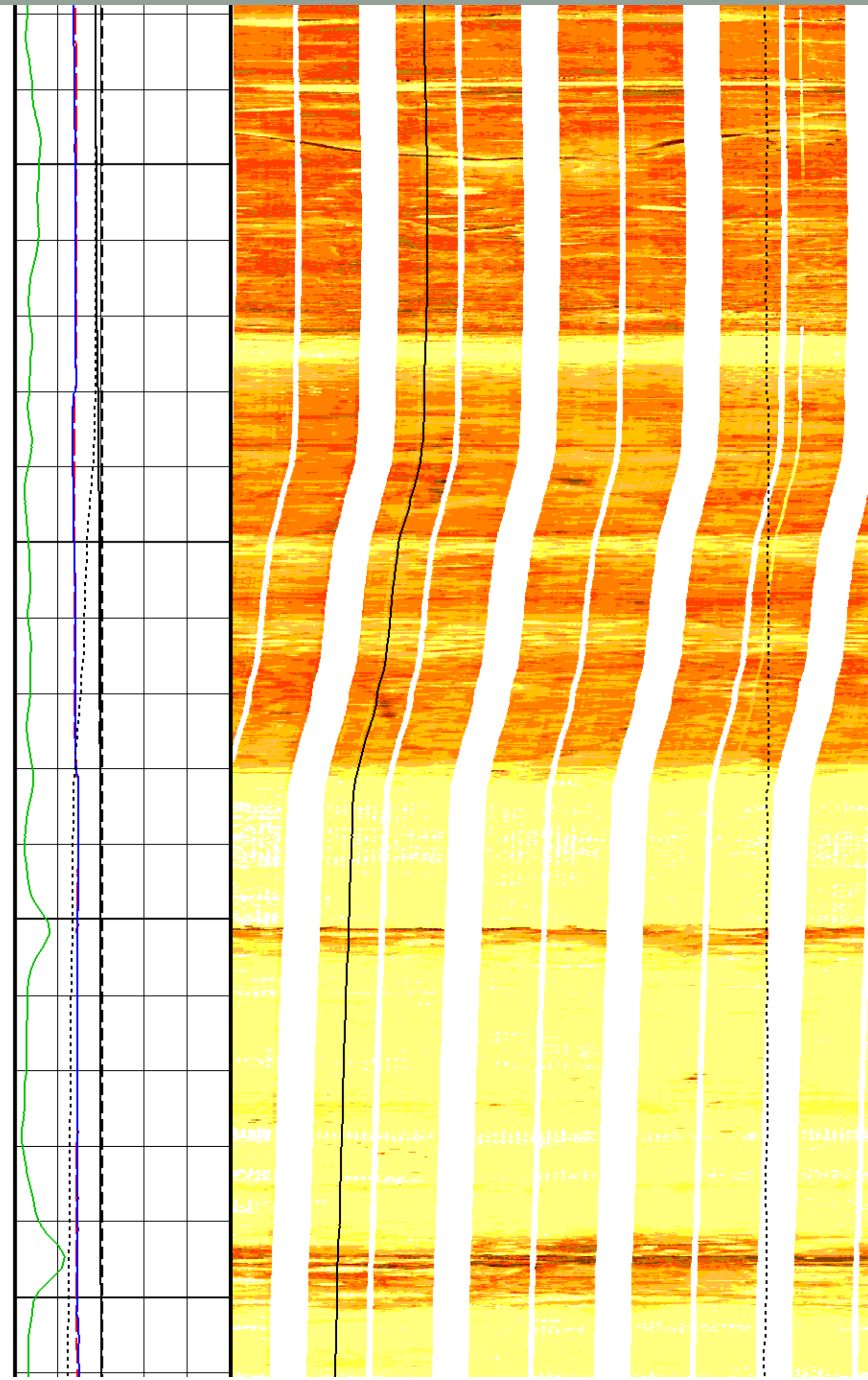

- To visualize the image logs, two different types of color normalization are done on the data; Static and Dynamic normalization
- Static normalized images have the same color scaling over the entire logged interval and thus show large-scale resistivity variations related to lithology changes and structural events (faults, fractures unconformities, etc…). Dynamic normalized images are color scaled on a 2- ft- sliding window, thus maximizing rock fabric detail (texture) and bedding information.n.

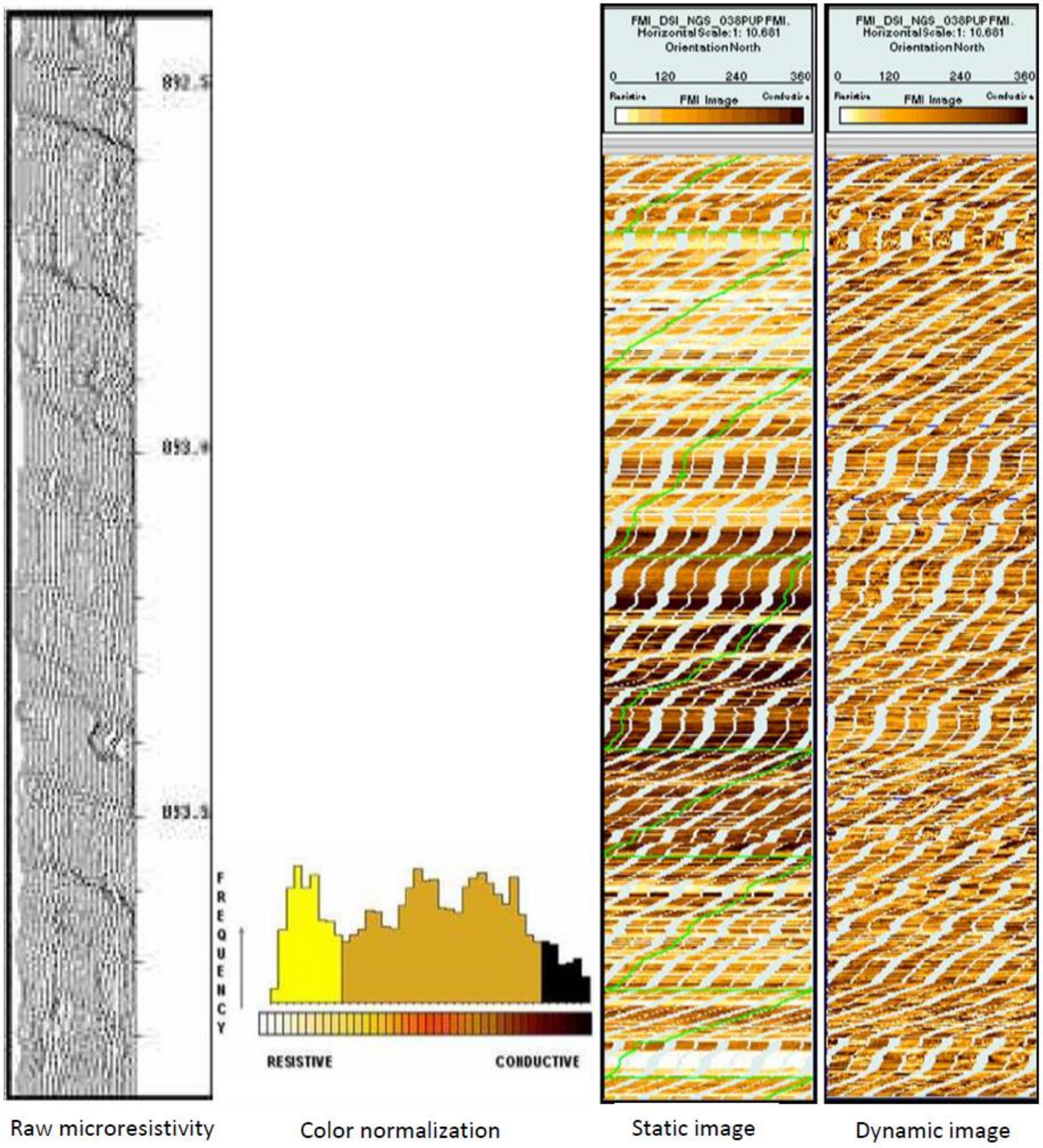

Figure 9. FMI log data from raw to static and dynamic normalized images, (Schlumberger)

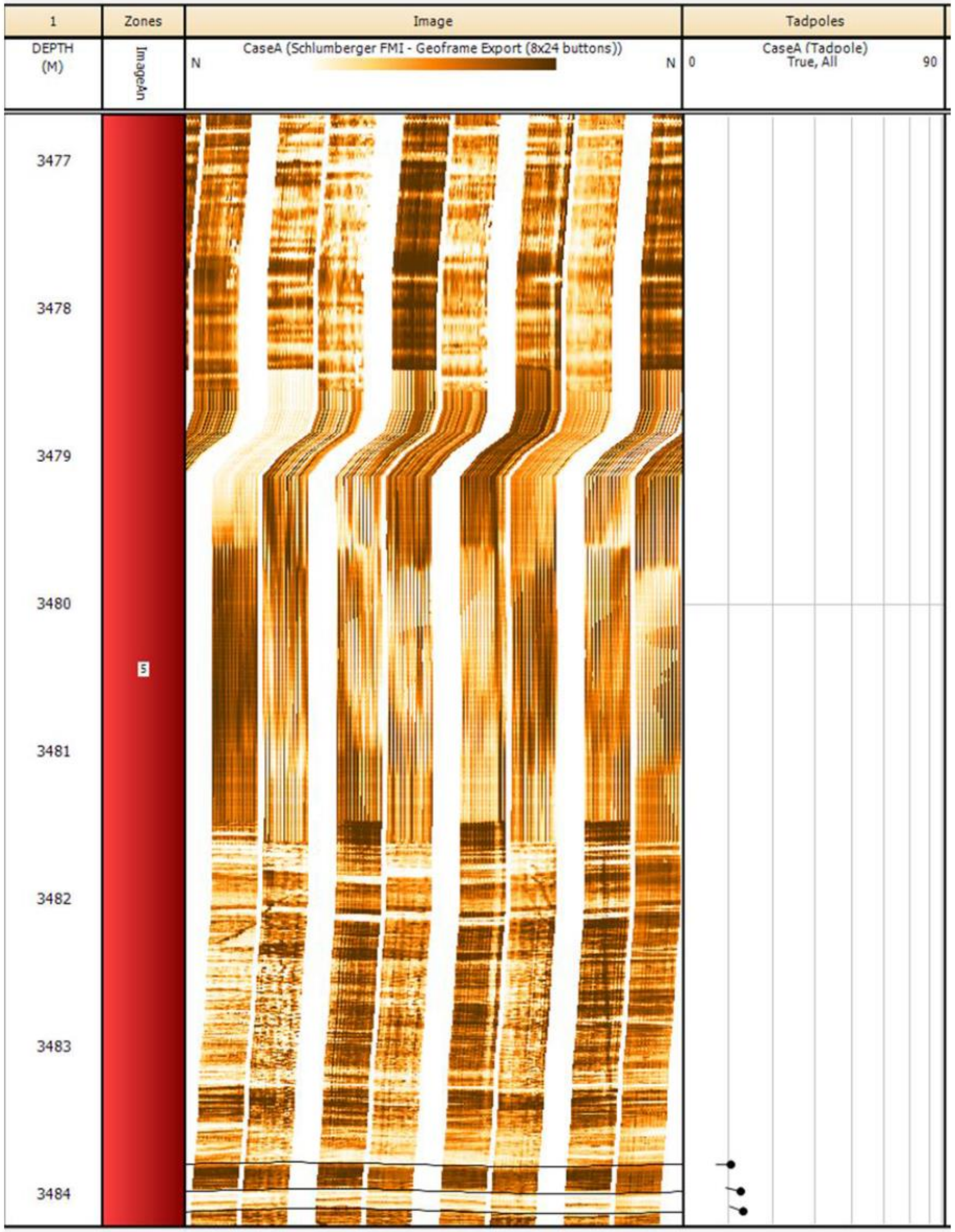

Figure 14. Bad hole image data due to tool stuck and release over the 3 meter interval. (Scale 1/20)

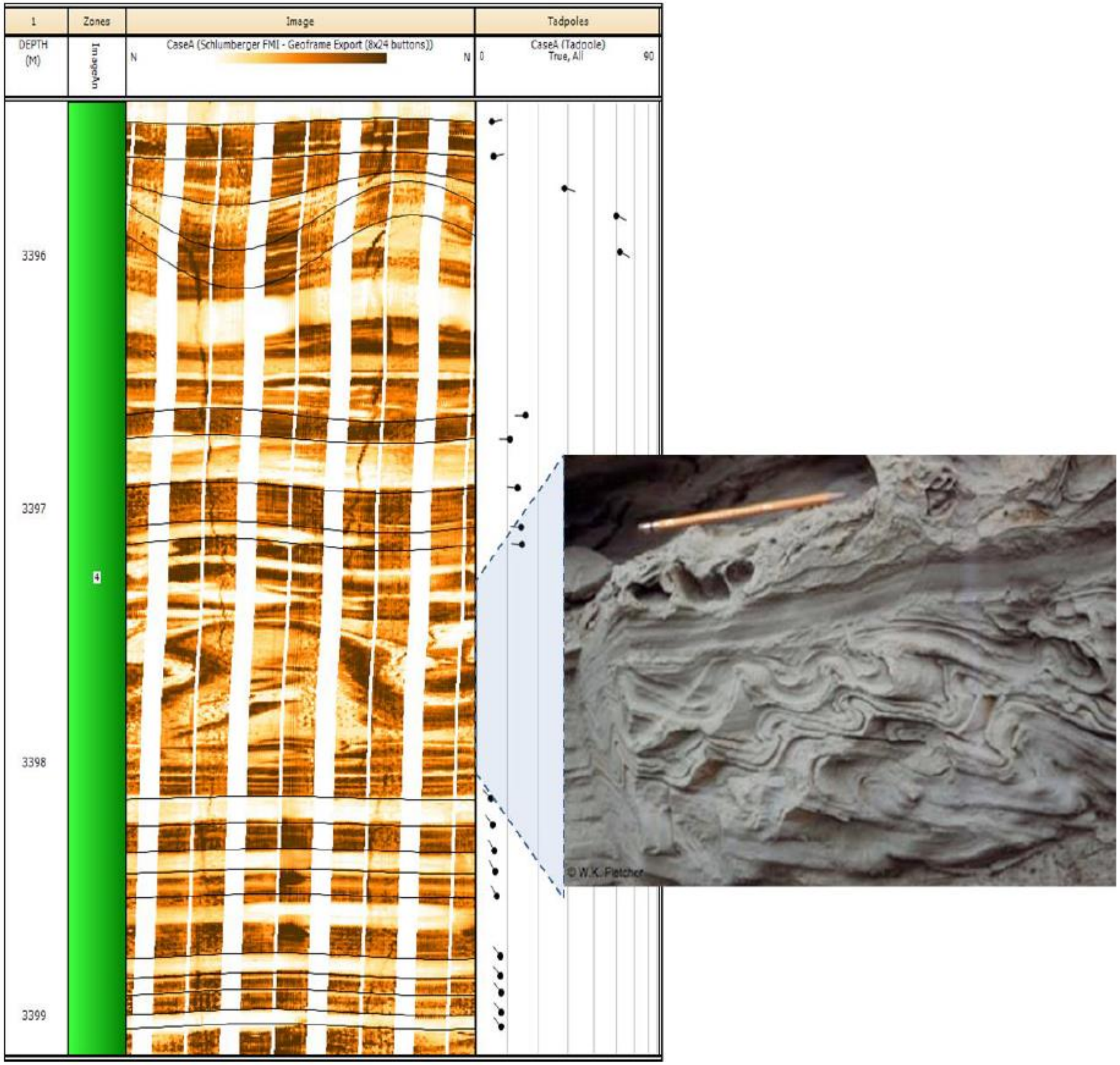

Figure 15. Deformation of soft sediment leading to convolute bedding (slump), suggesting intense structural deformation of the turbidity flow deposits. (Slump photo from GEOL342: Sedimentation and Stratigraphy Spring 2013). (Image log scale 1/20)

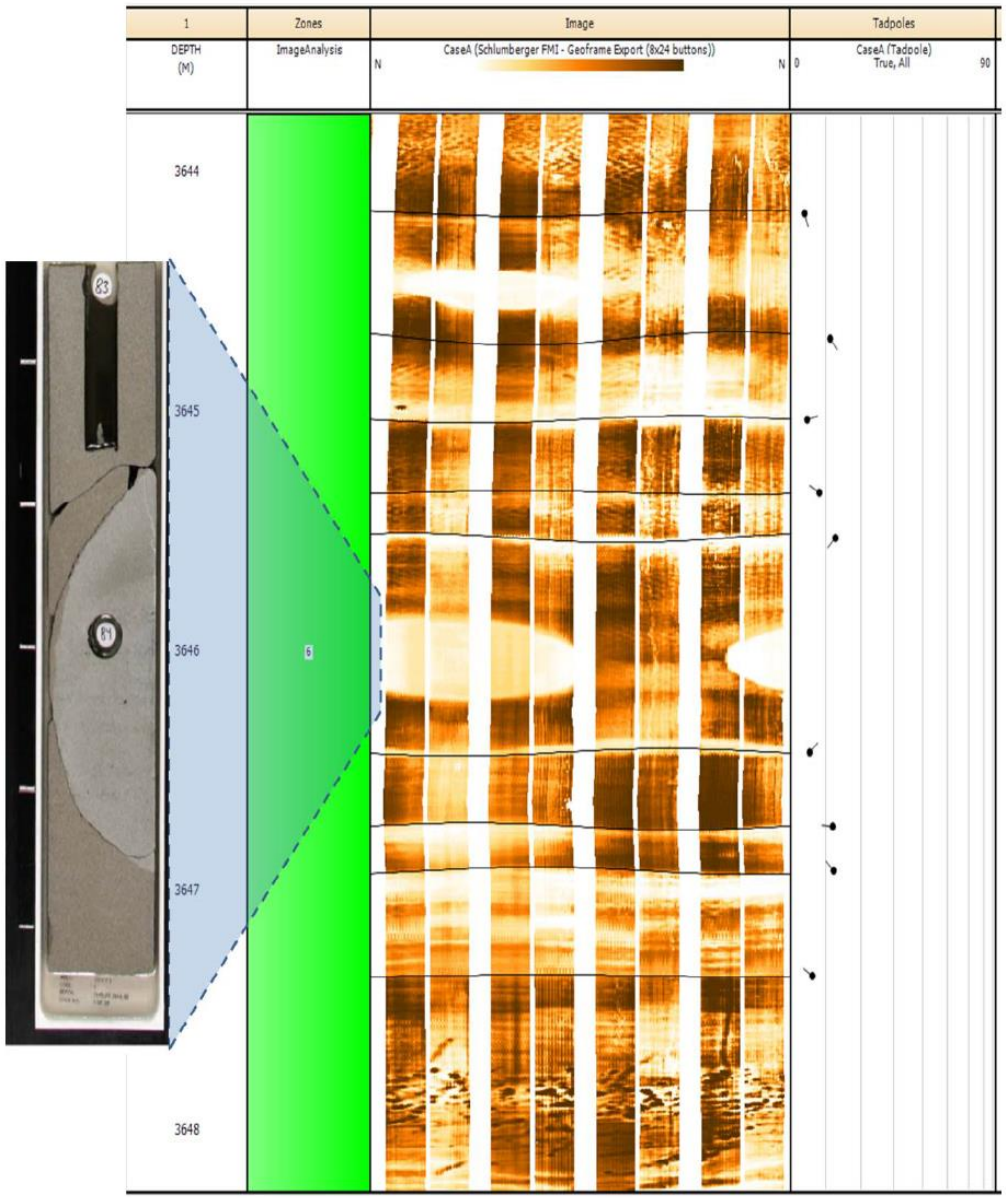

Figure 19. FMI image log with calcite cemented nodule. Image log shows that the nodule has not been detected by all image tool pads as can also be seen in the core photo. Note the possible bioturbation pattern in the bottom of the image log. (Core photo unit is 10cm and image log scale 1/20)

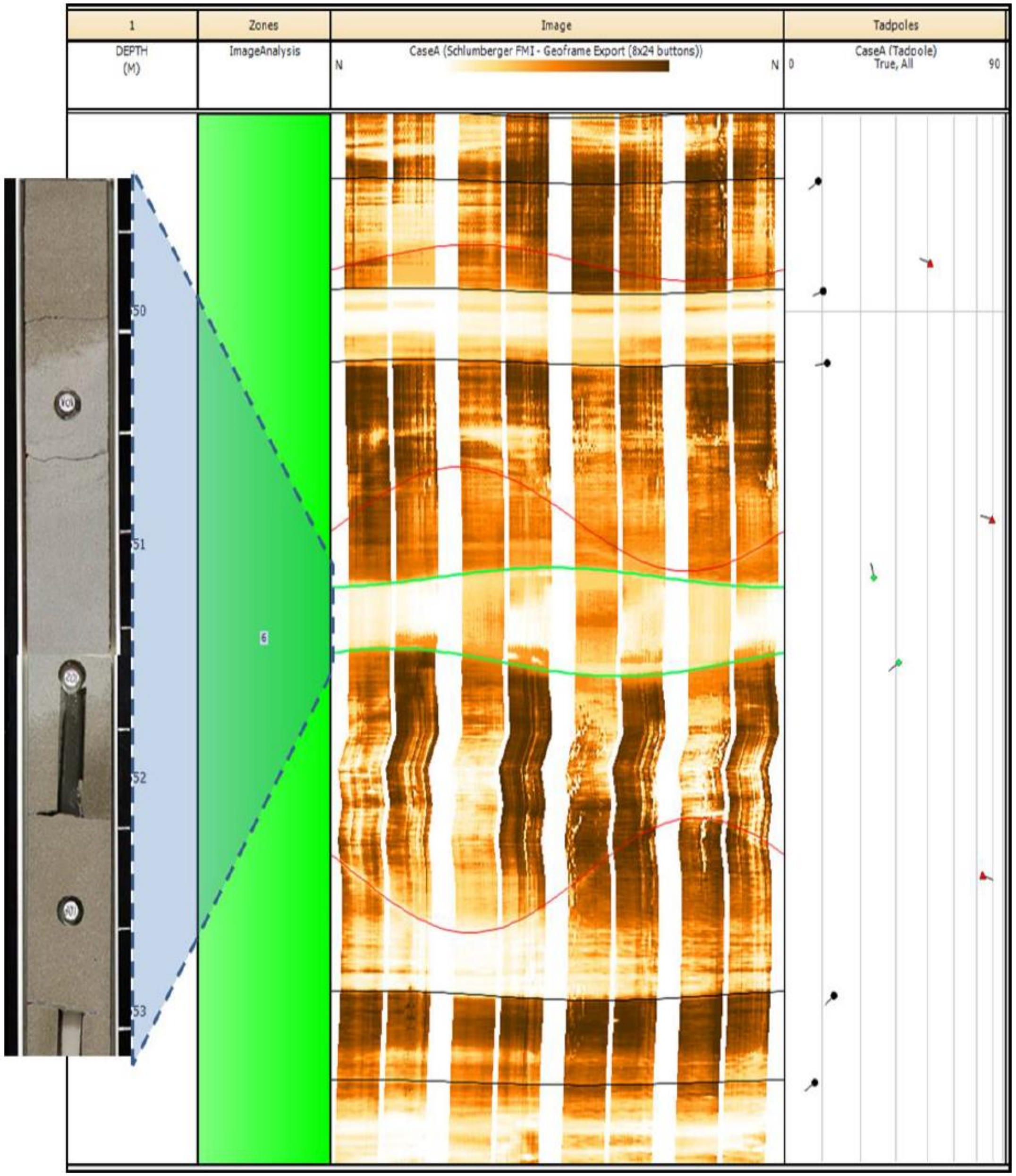

Figure 20. FMI image log with three conductive fractures and one diffusive calcite cemented zone. (Core photo unit is 10cm and image log scale 1/20)

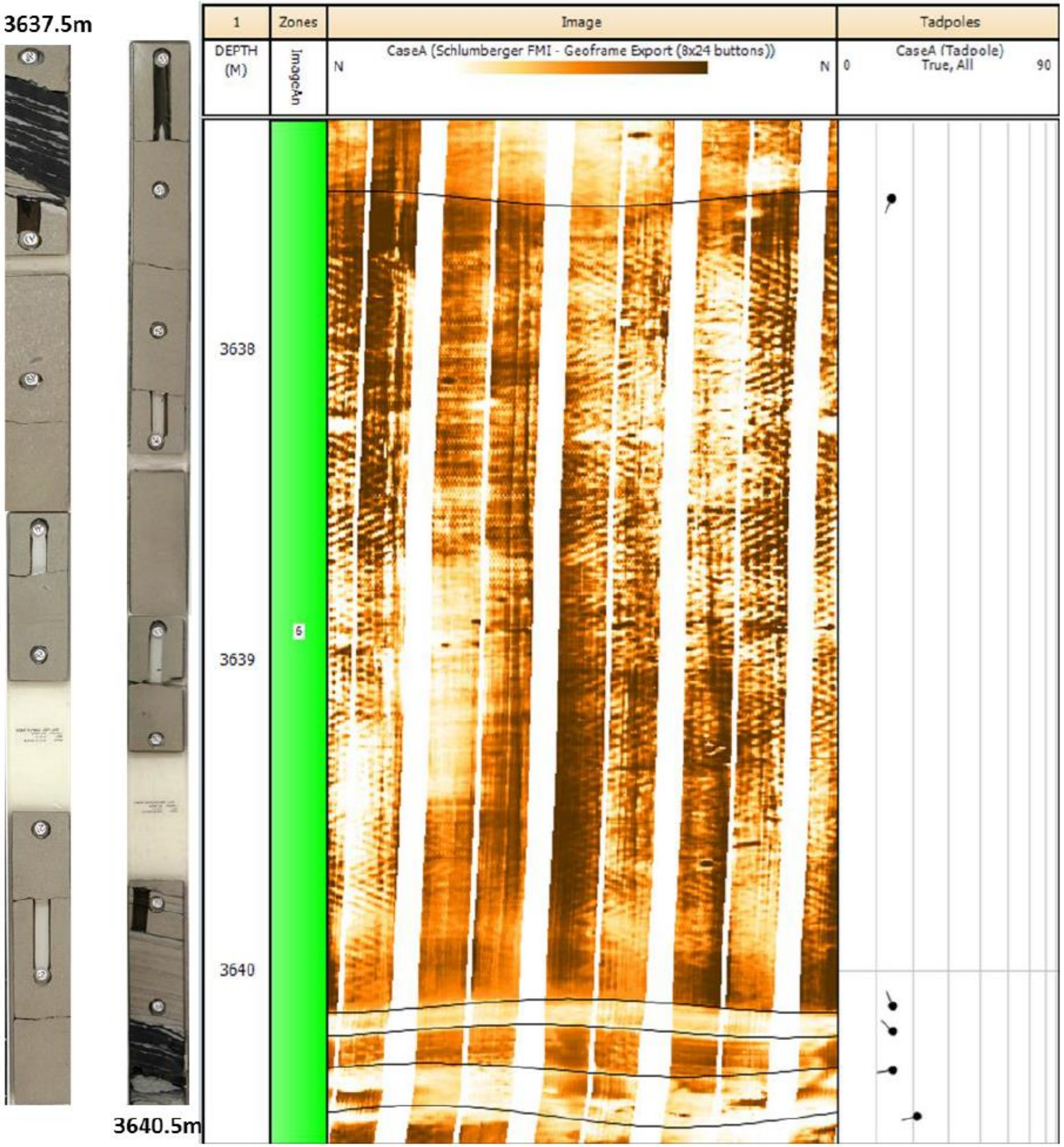

Figure 21. FMI image of 2.5m thick homogeneous sandstone layer without identifiable dip angle/azimuth in the sand. Few resistive mixtures of tight shales and calcite cement are identified at the top and bottom of the interval. (Every core column is 1.5m and image log scale is 1/20)

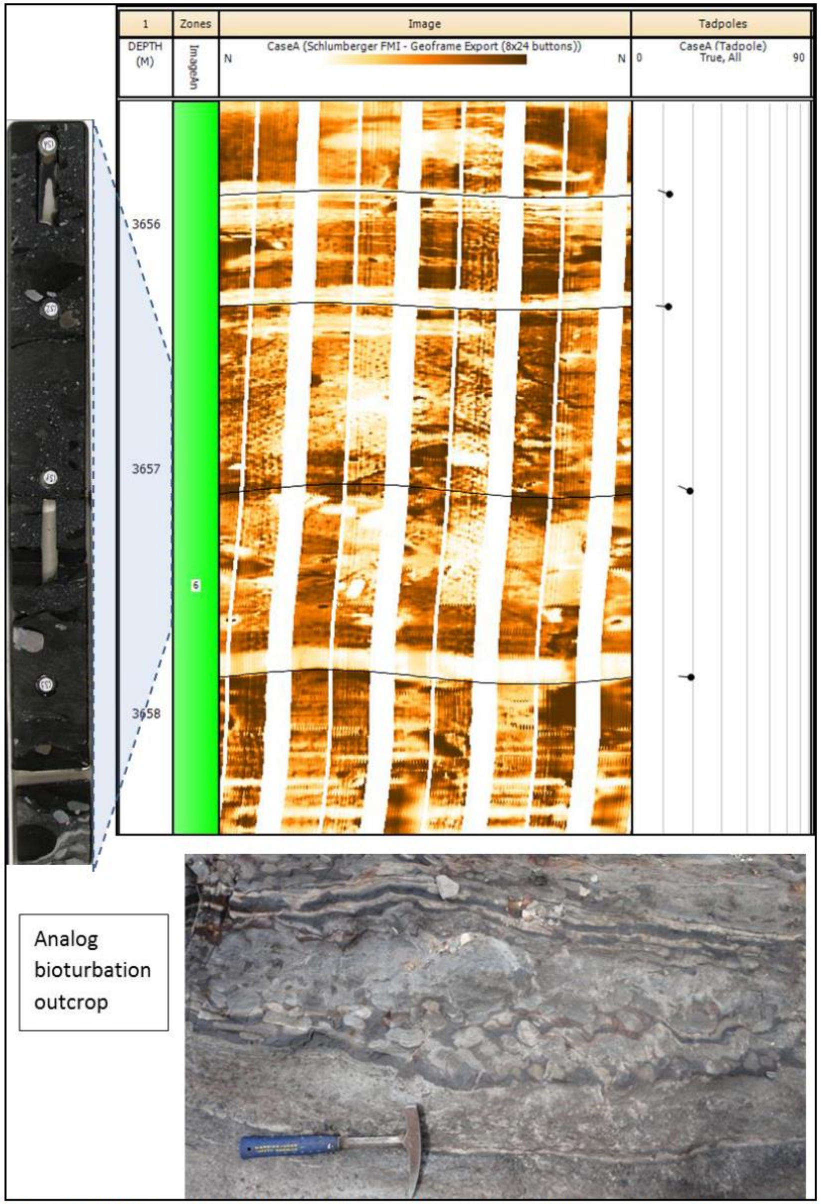

Figure 22. FMI image log of bioturbated zone with core photo of the zone. An analog outcrop of bioturbation is shown below the figure. (Core scale is 1m and image log scale is 1/20)

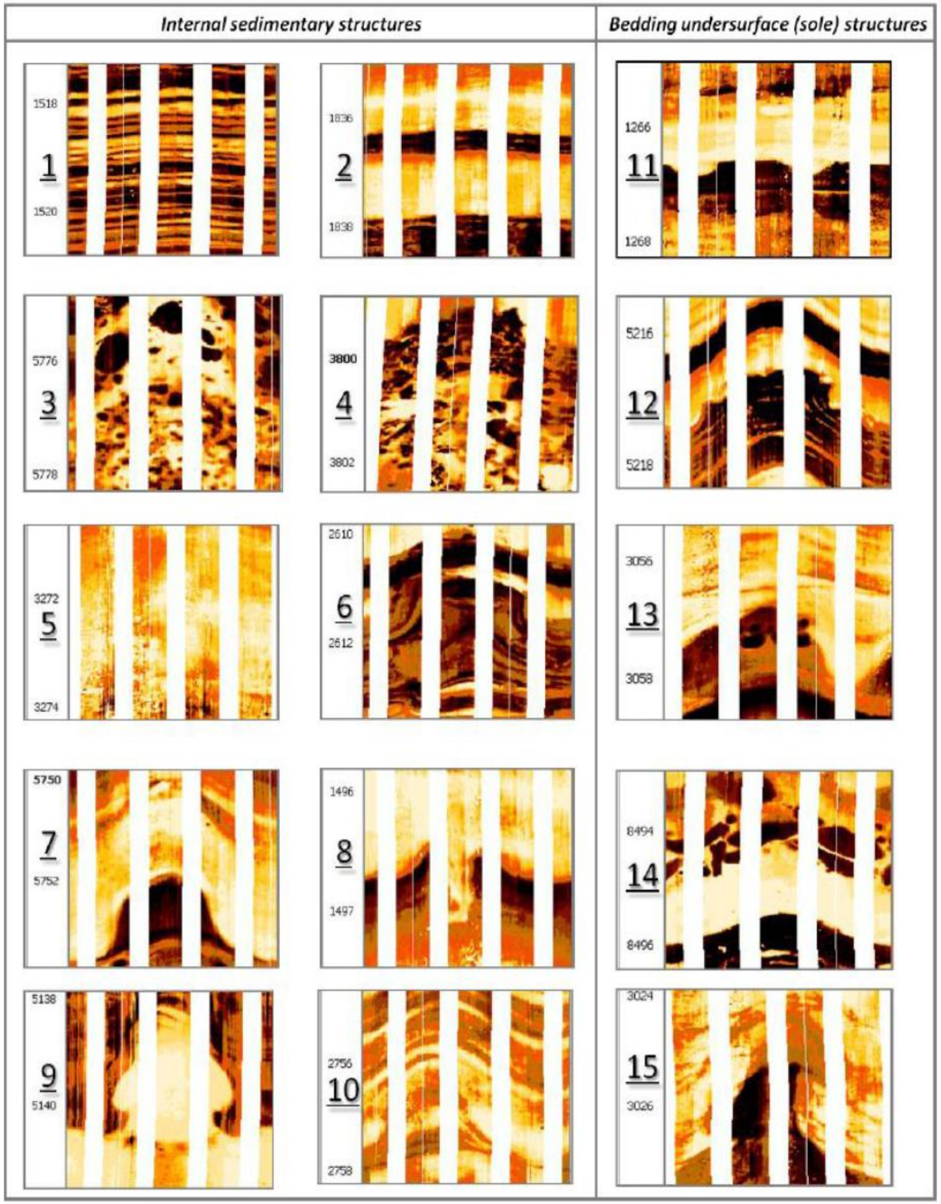

Figure 3. Sedimentary structures observed on the high-resolution borehole image logs. (depth in feet): 1,lamination ; 2,bedding; 3, inverse/reverse grading; 4, conglomerates; 5,massive bed; 6, convolute bedding (slump); 7, sediment deformation ; 8, water escape structure; 9, sand injection; 10, cross-bedding; 11,groove cast; 12 load cast; 13, small-scale scour surface; 14, erosional channel base with lag ;15 ,flame structure (Amer et. al., 2011).

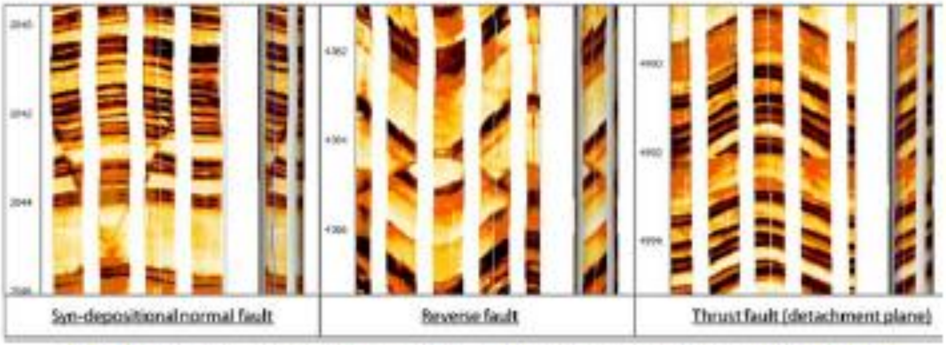

Figure 4. Normal, reverse and thrust faults as observed on high-resolution image logs (Amer et. al., 2011).

Faults on FMI log

- Offsets visible although throw is difficult to measure
- Dip changes may be visible
- Core to log

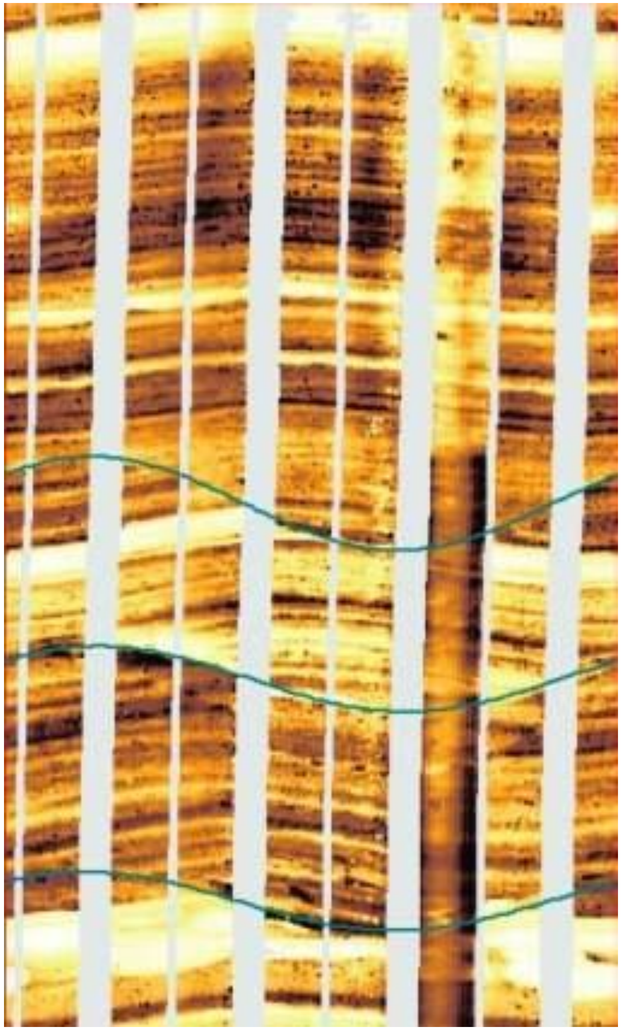

High resolution image logs allow identification of minor, narrow-aperture fractures when calibrated against core

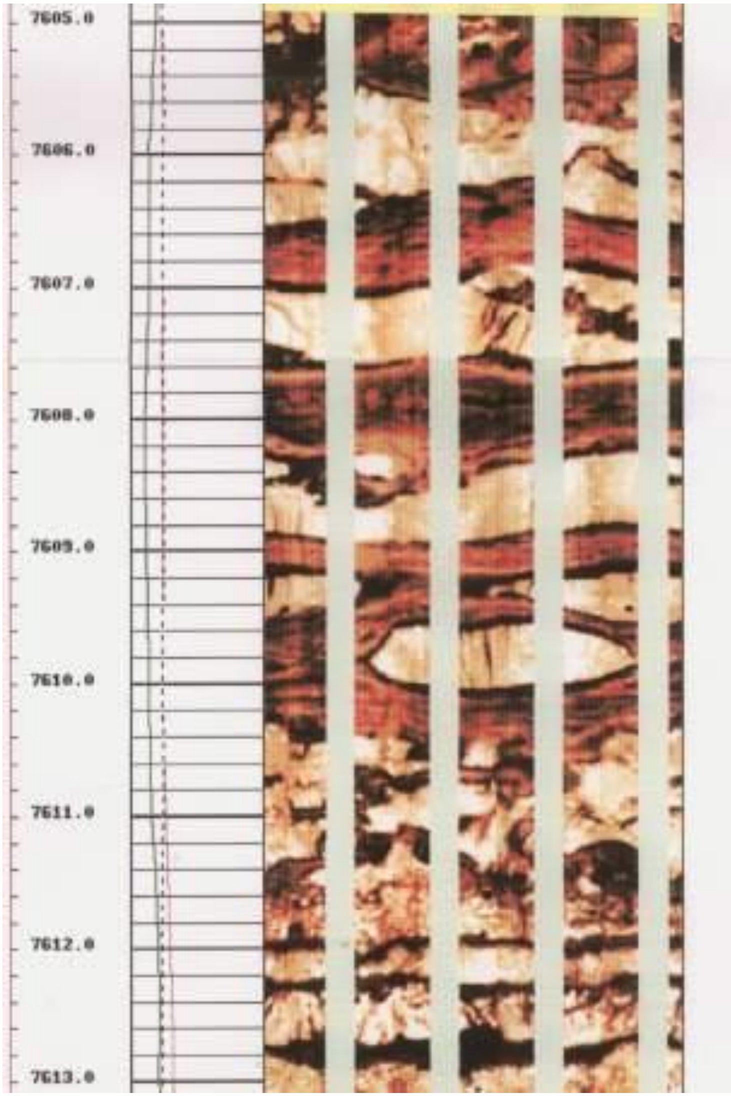

Log Characterization

- Acoustic & electrical imaging logs and their interpretative workstations are becoming the *subsurface standard* for data acquisition, rapidly replacing core.
- Dipole sonic logs are attempting to quantify fracture occurrence and *fracture porosity*.

Quantitative Fracture Analysis

- Planar features are expressed by ellipses on borehole walls which are expressed as sine waves
- Steepness of ellipses reflect the dip magnitude and orientation
- Apparent strike and dip relate to amplitudes and inflections in sine waves

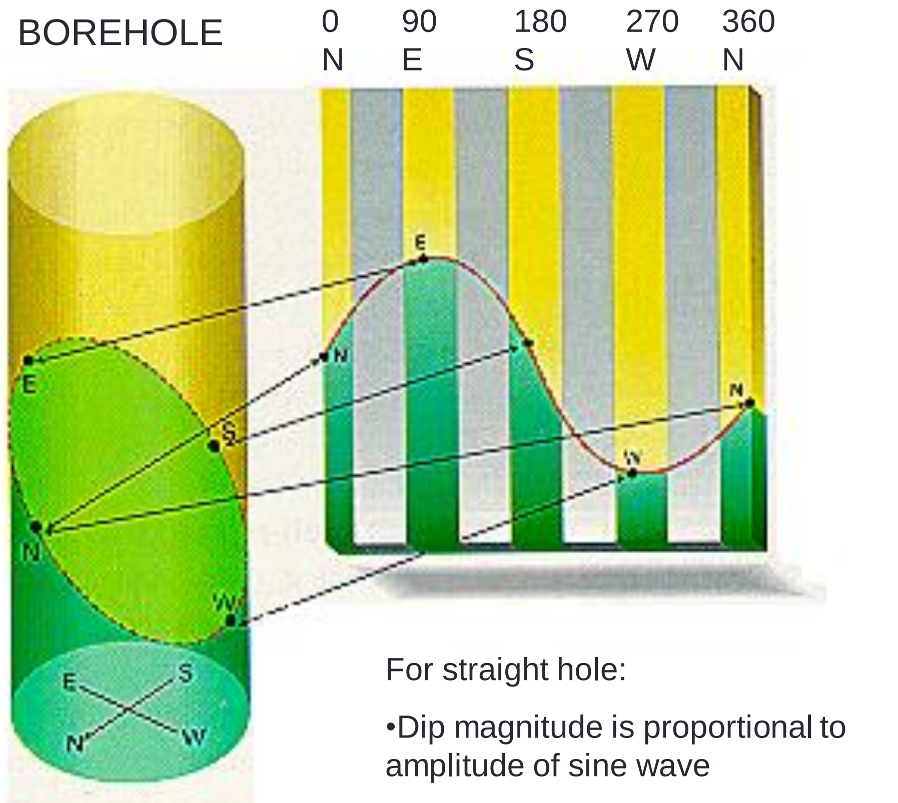

For straight hole:

•Dip magnitude is proportional to amplitude of sine wave

•Dip azimuth is located at minimum of sine wave

TD: 53□ / 270□ W

David Spain (1998)

Faults on FMI

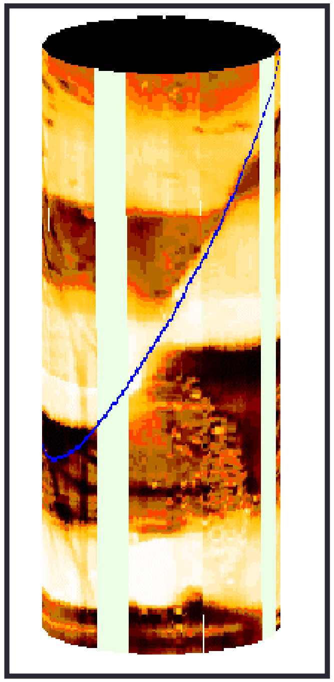

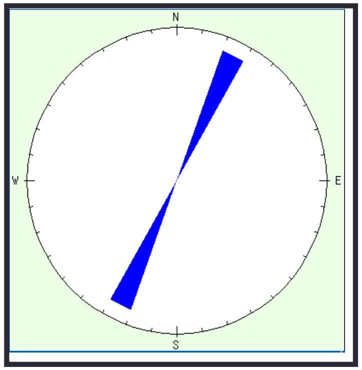

Normal fault

Striking: N25E-S25W

Down to WNW

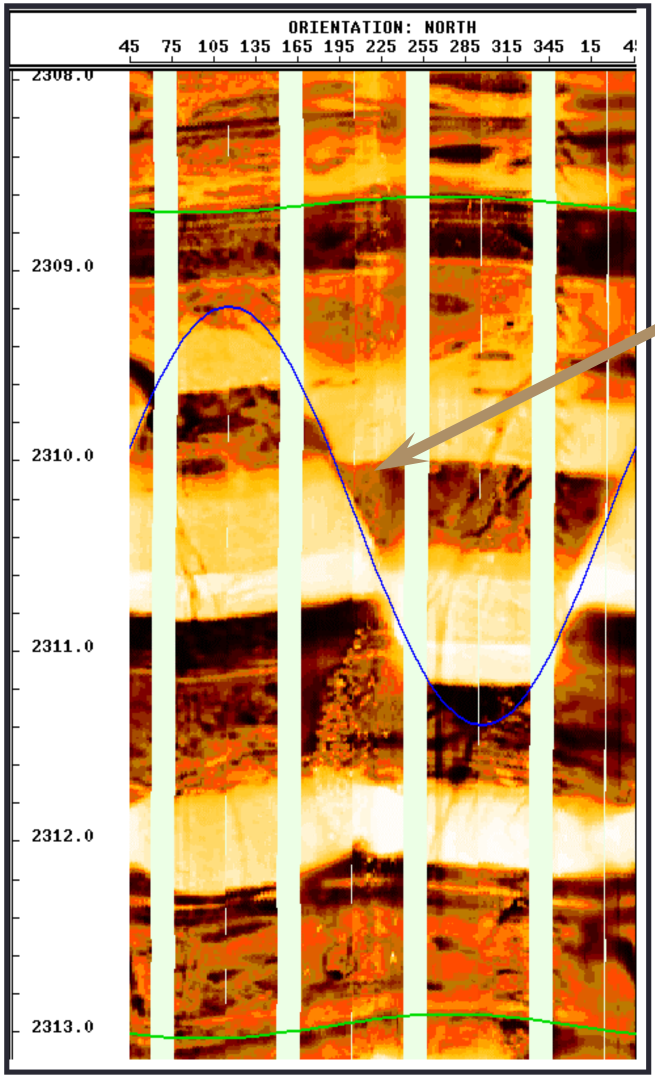

Fracture Trace

TD: 62/304

Oil well in granite.

:

Open fractures are black

Green fracture is filled with somewhat hard, resistive, slightly erodible material.

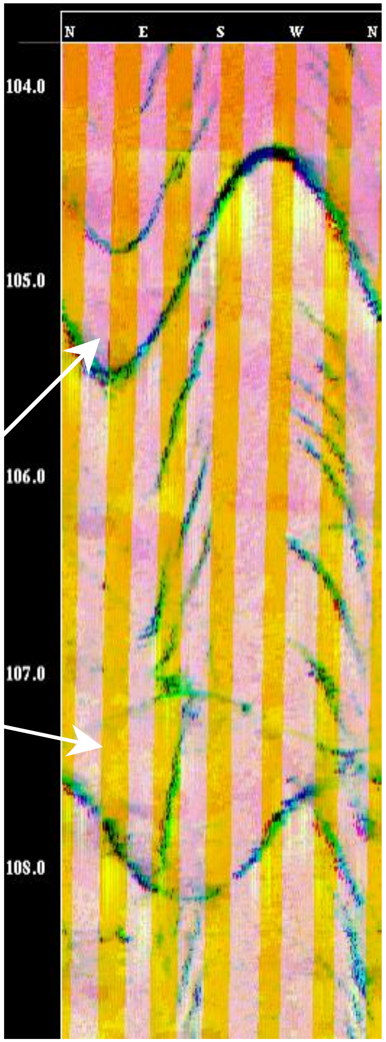

Different fracture types are different colors in multivariate images.

Examples	Amplitude	Microtopography	Resistivity
Open	Dark	Dark	Dark
Vein	Bright	Bright	Bright
Fault gouge *Soft* *Hard*	 Moderate Bright	 Variable *Depends on drilling erosion*	 *Permeable:* Dark *Impermeable:* Bright

Fracture Zone Identification

Seismic attributes

- Single
- Multiple

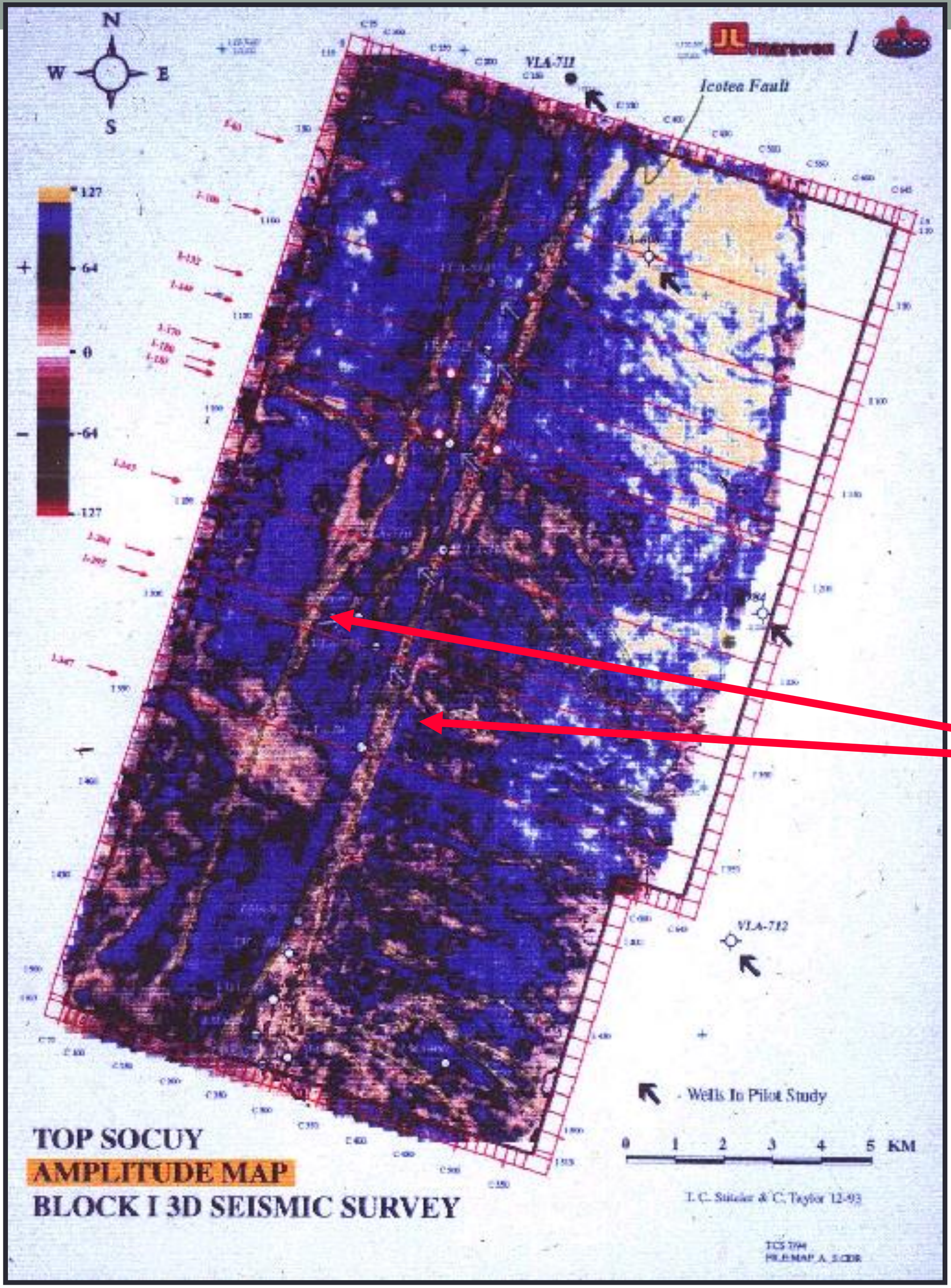

Amplitude Map
Top Socuy

Lake Maravaibo,
Venezuela

Note Fault Traces

3-D Seismic data coherency :

delineating faults and fractures

(Courtesy of Robert Humphreys)

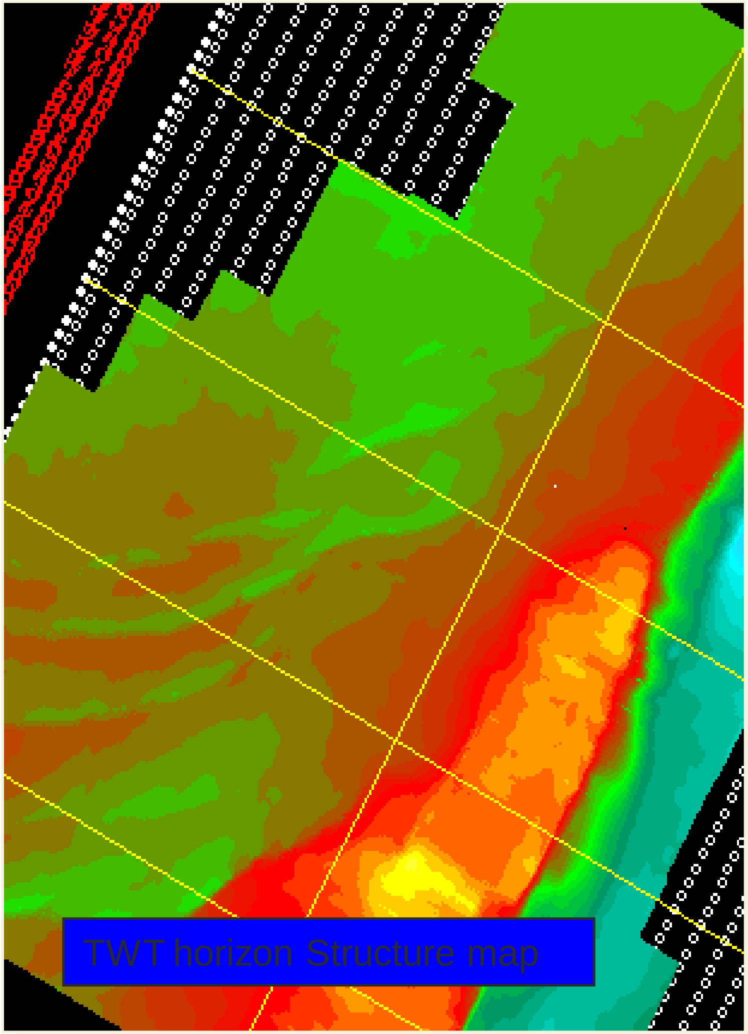

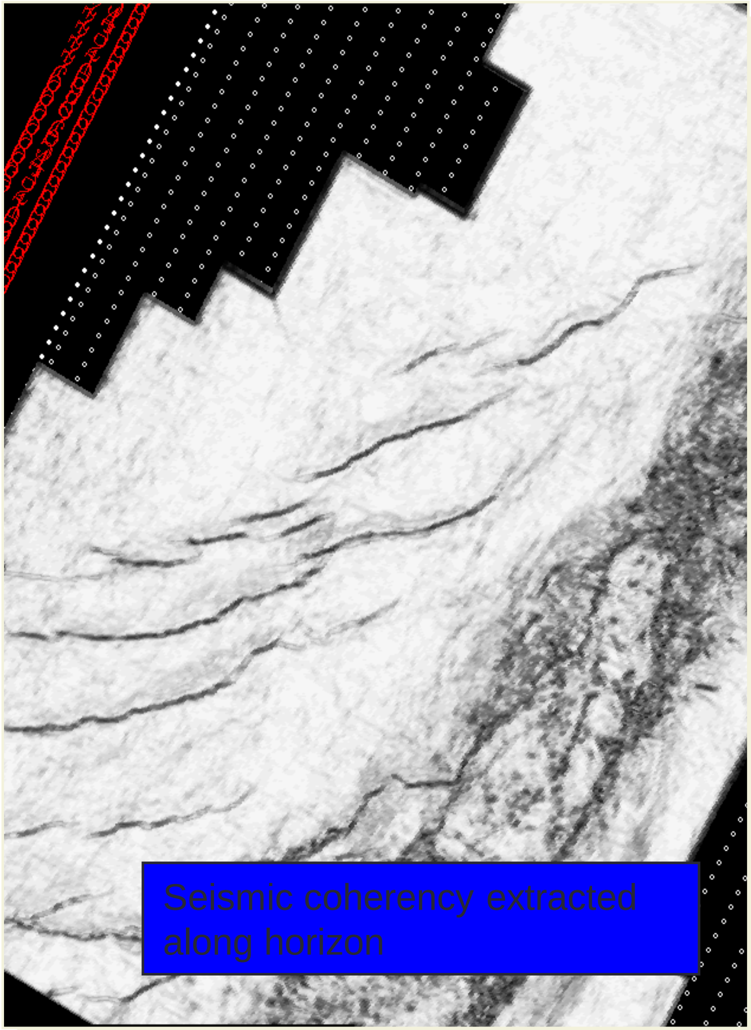

Sum of Absolute Amplitudes Over Normal Fault Segments Linked by Relay Zone

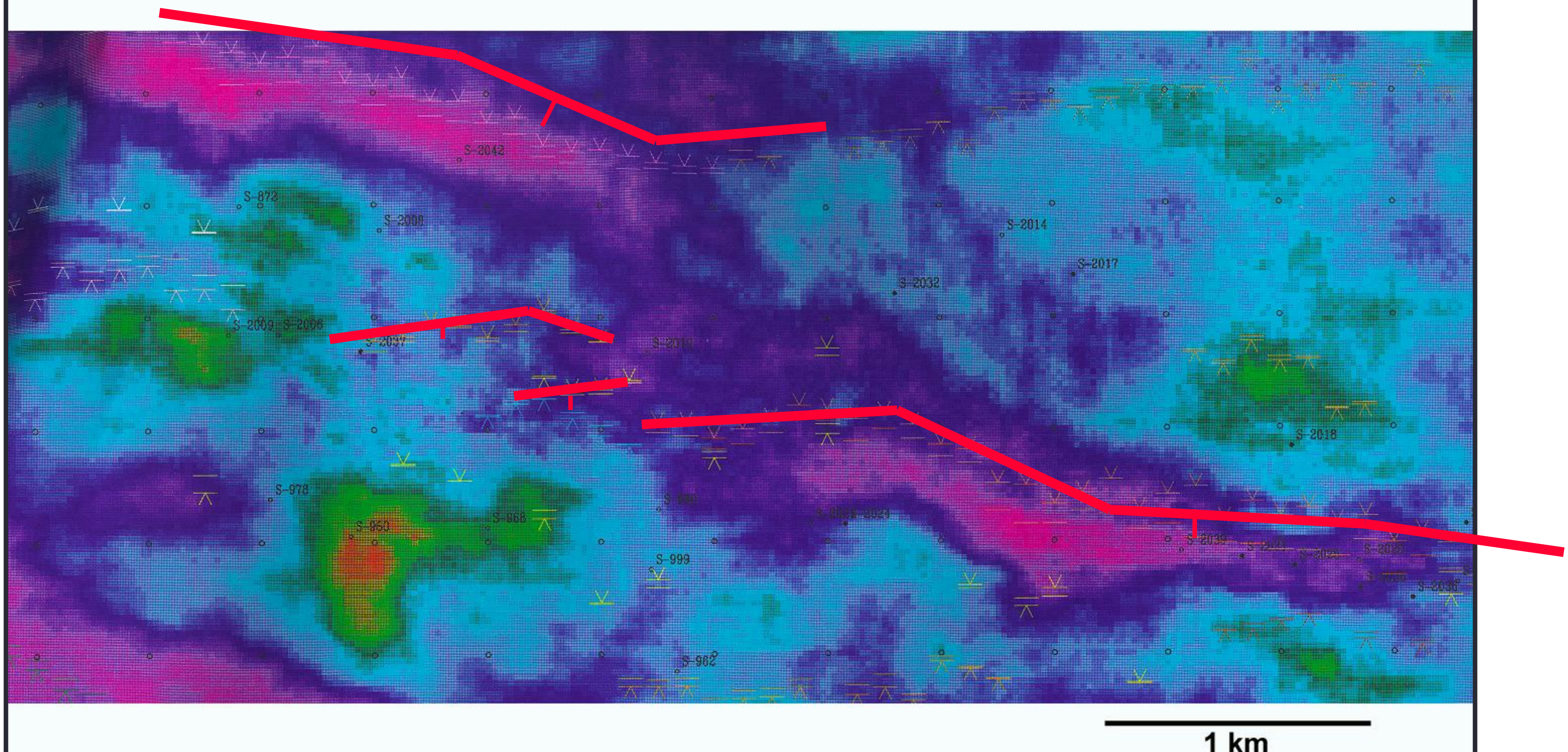

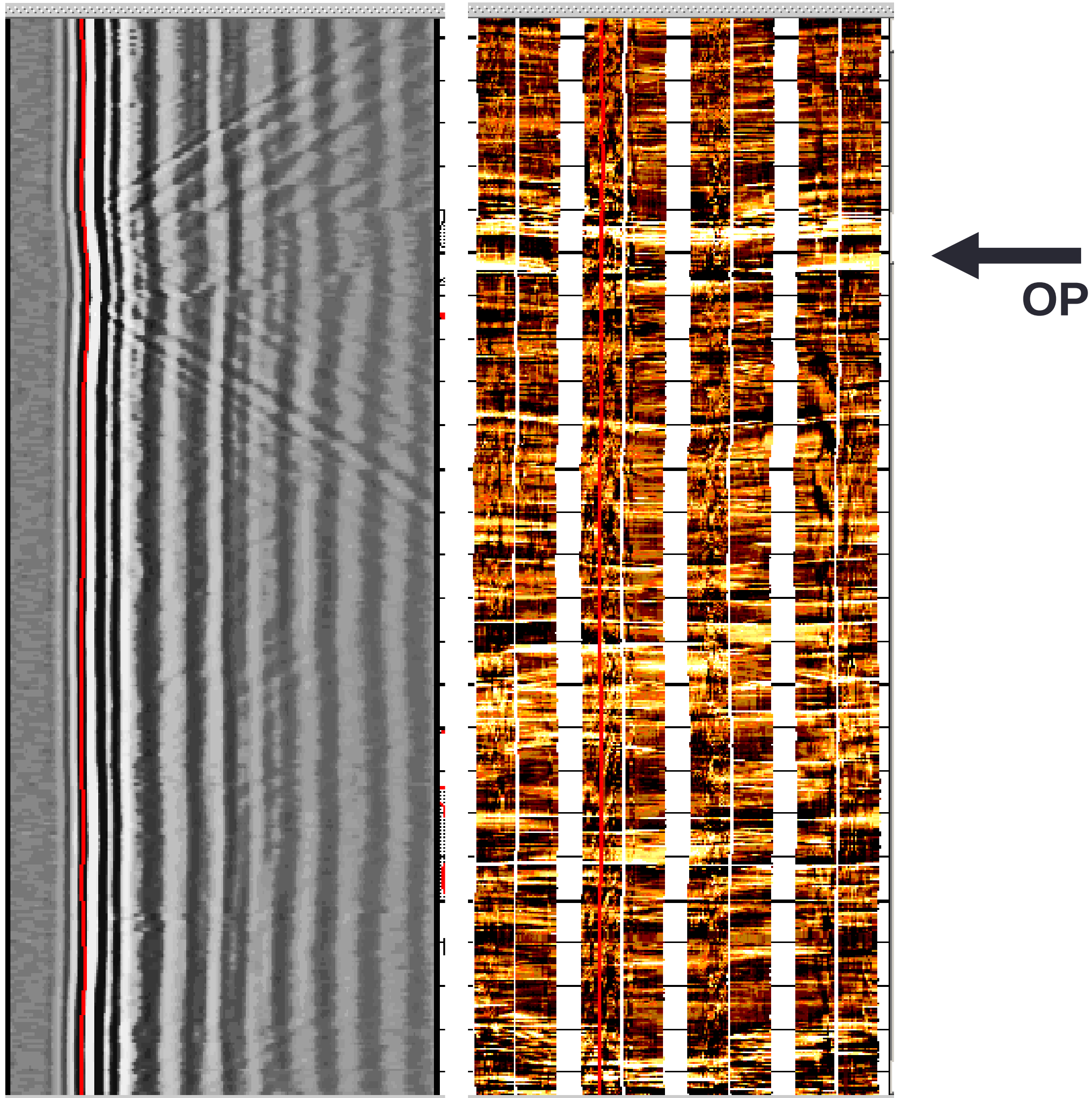

OPEN FRACTURE

Stoneley wave generation at open fracture

Image Logs -
Image facies and depositional environment reconstruction

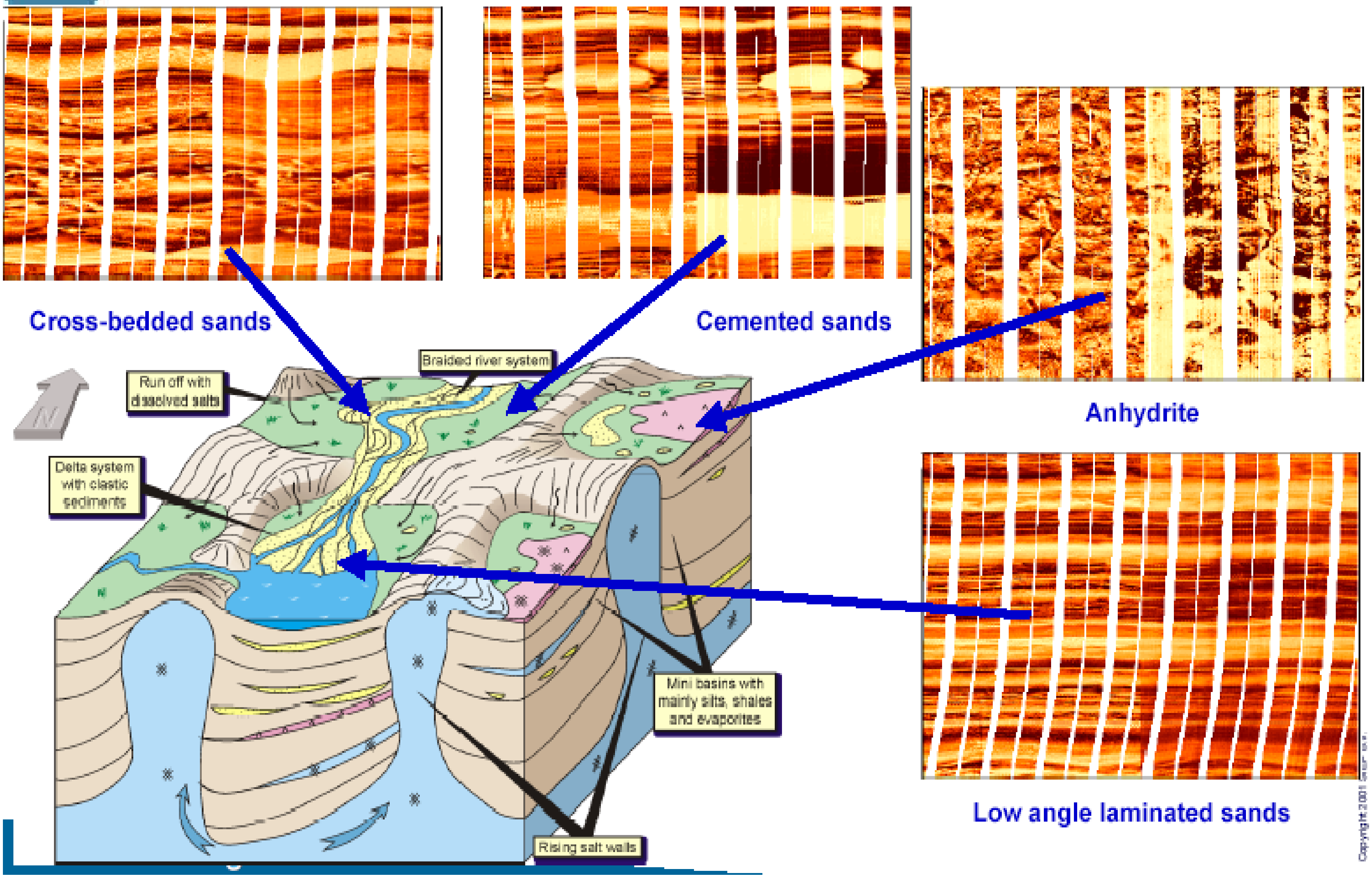

Different Rock Fabrics from FMI log

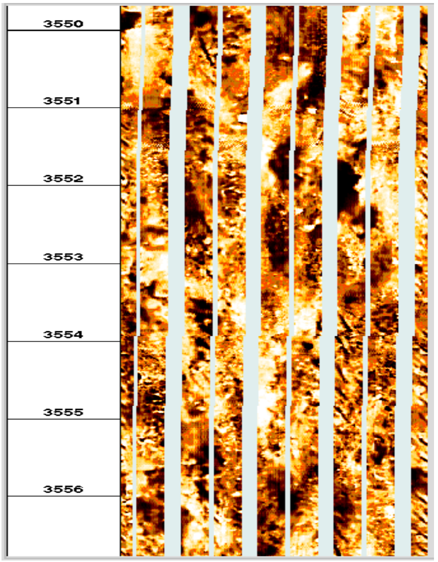

Inter-particle

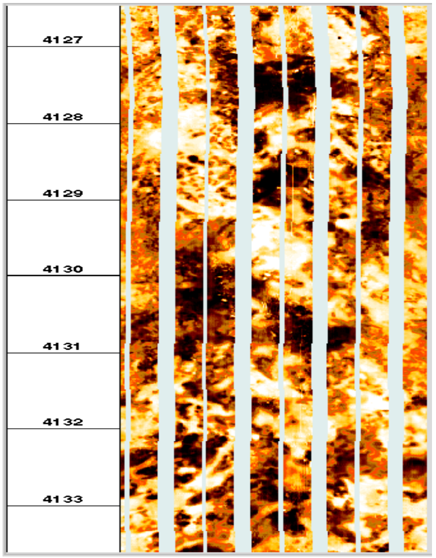

Patchy

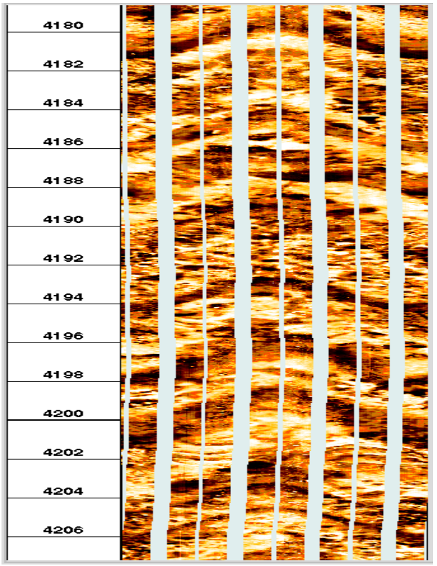

Layered

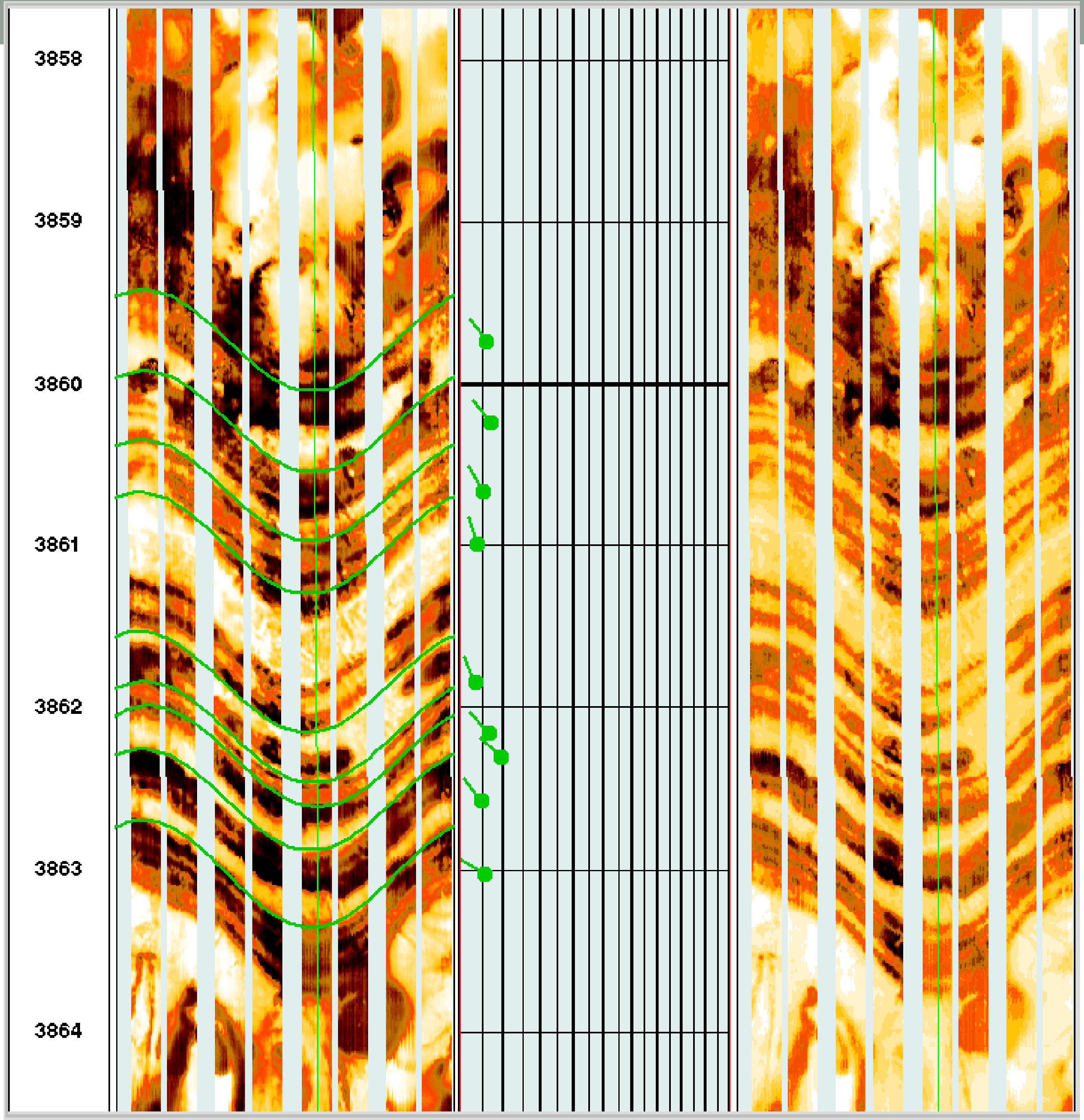
3858
3859
3860
3861
3862
3863
3864

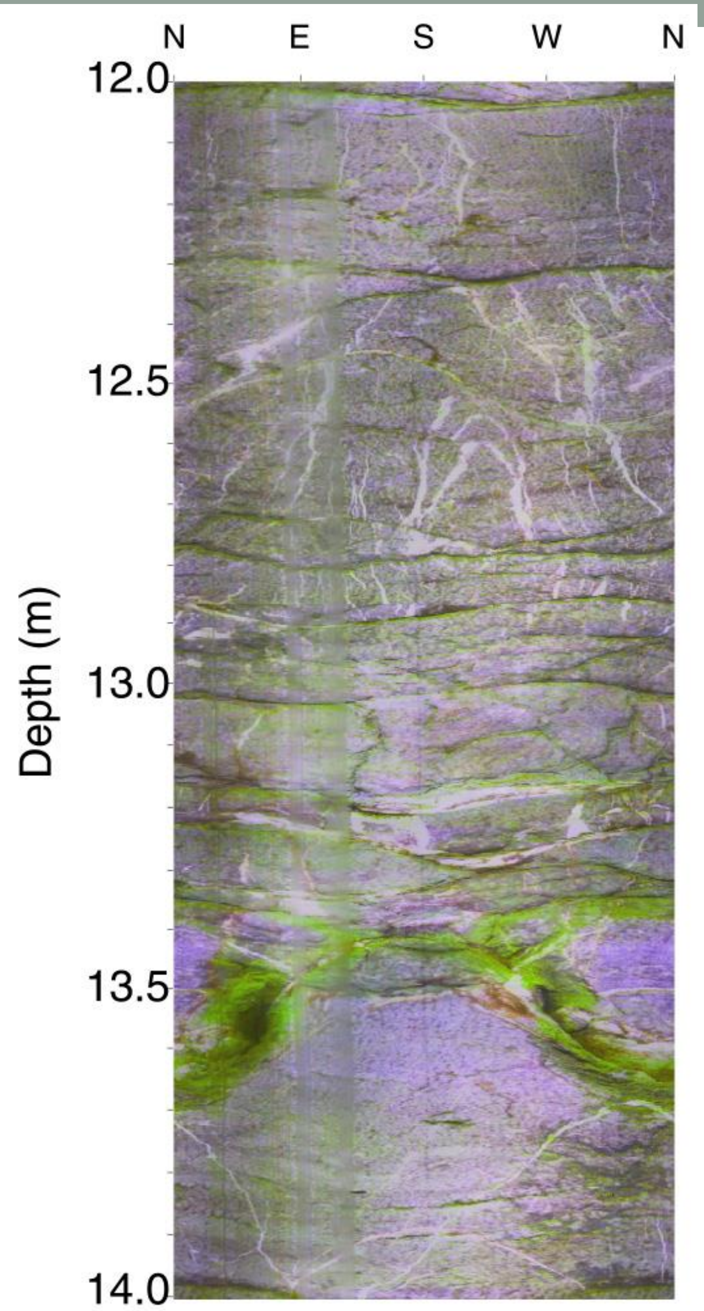
N
E
S
W
N
12.0
12.5
13.0
13.5
14.0
Depth (m)

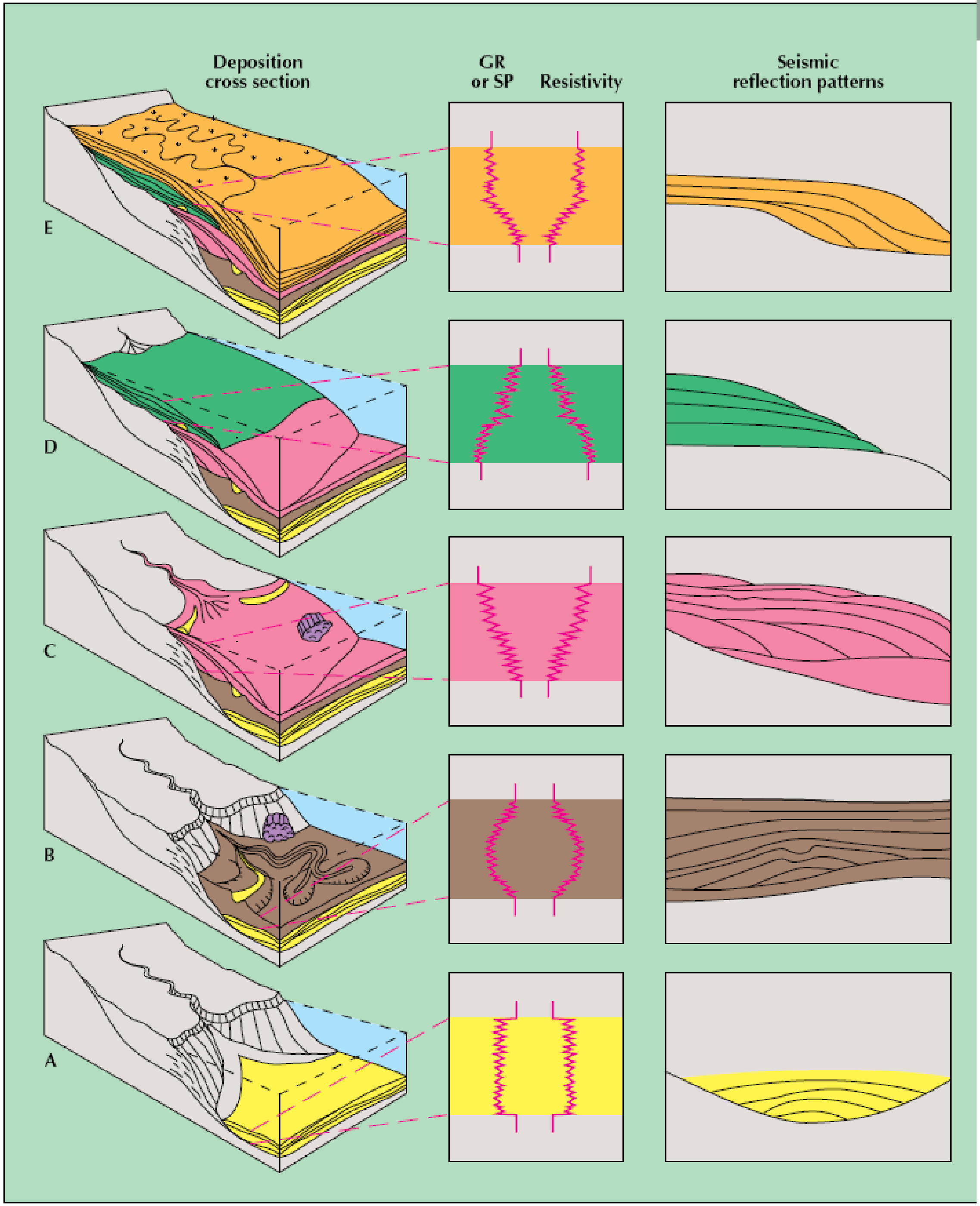
Deposition
cross section
GR
or SP
Resistivity
Seismic
reflection patterns
E
D
C
B
A

UBI image of open fractures

- Fractures make a sinusoidal trace on the borehole wall
- Data on type and orientation
- Acoustic show open fractures
- Resistivity show open and cemented fractures/faults

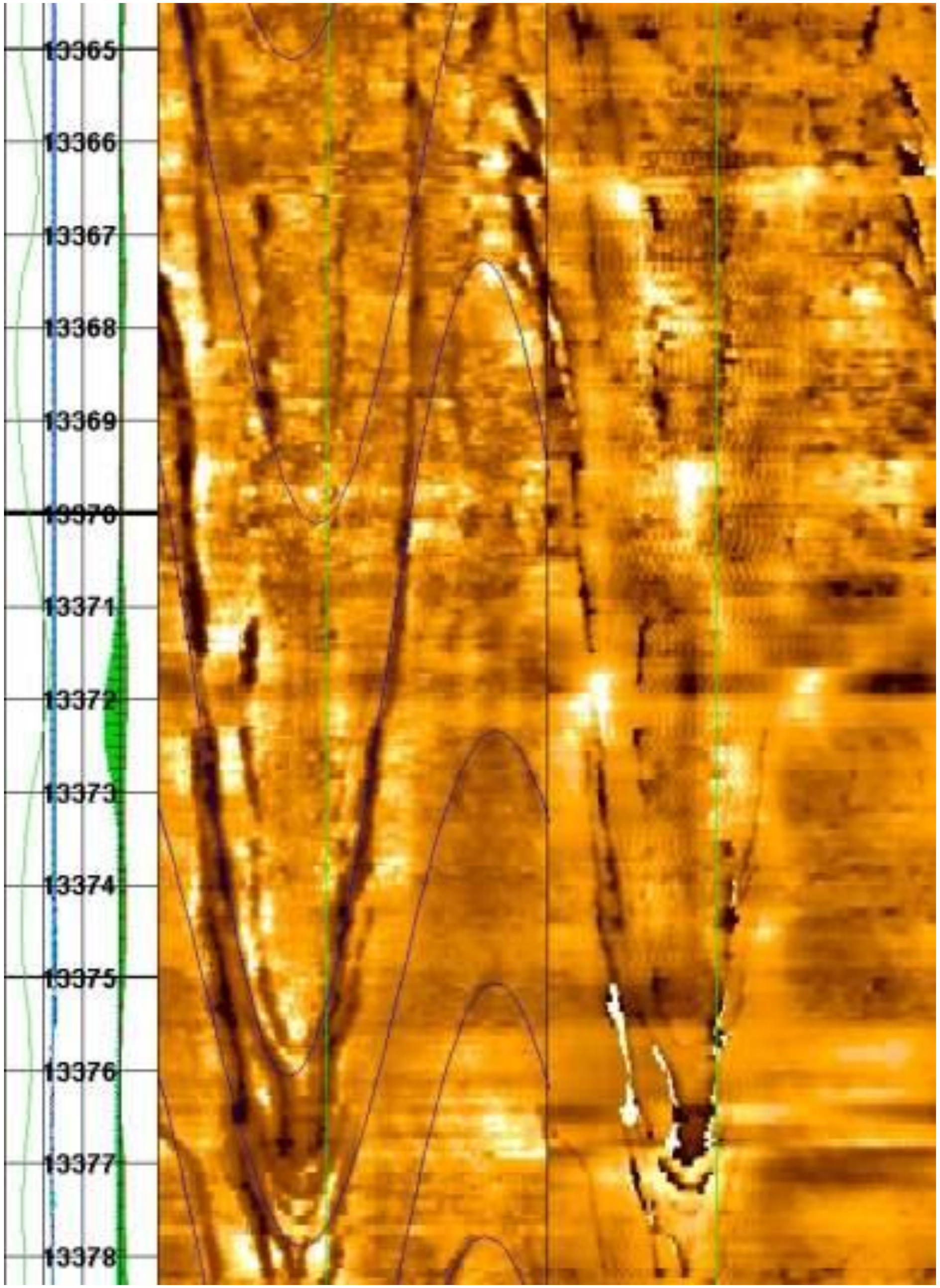

Ultrasonic Borehole Imager

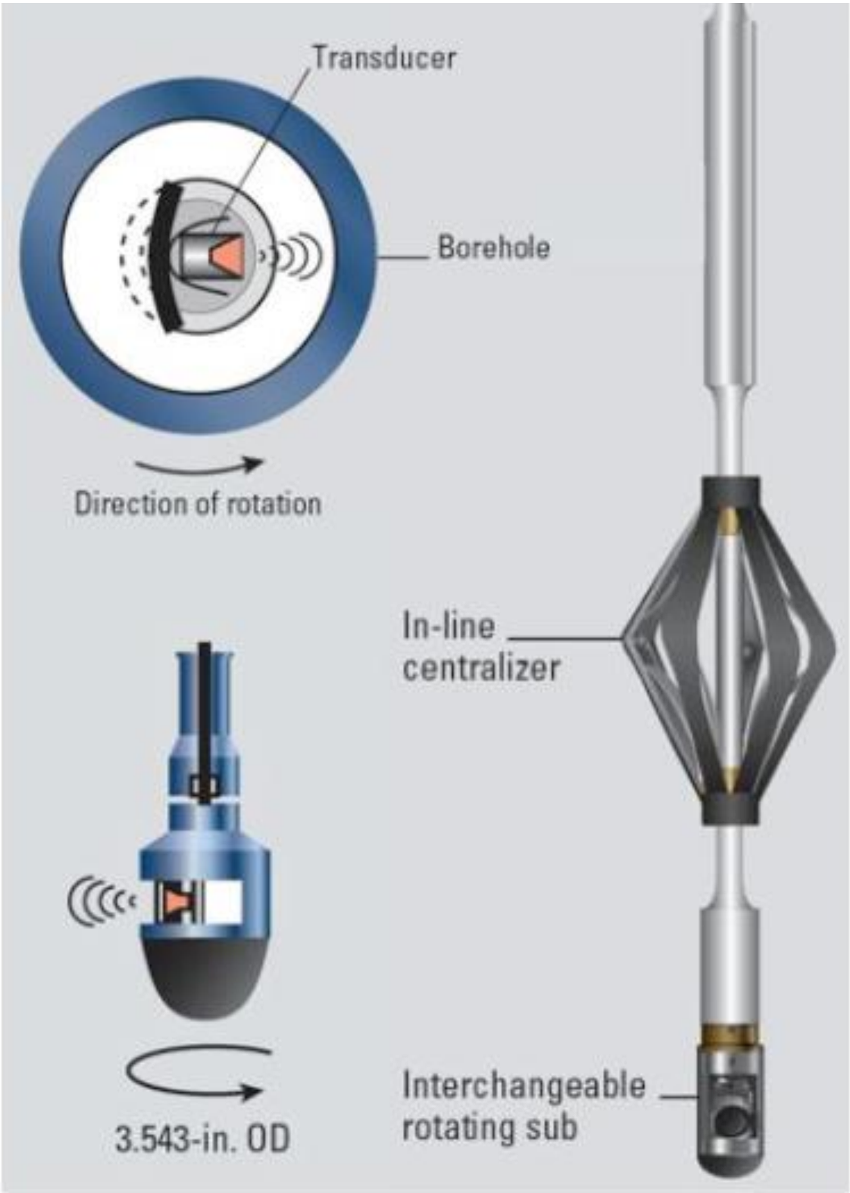

UBI images

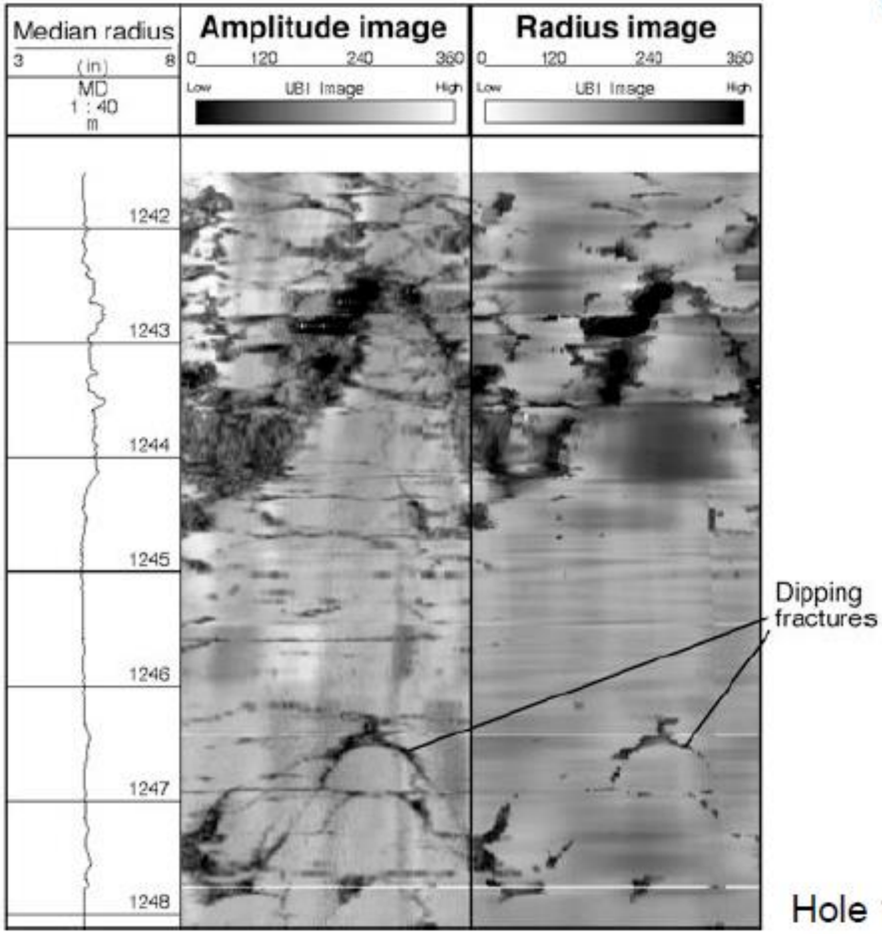

Hole 1

UBI and FMS comparison

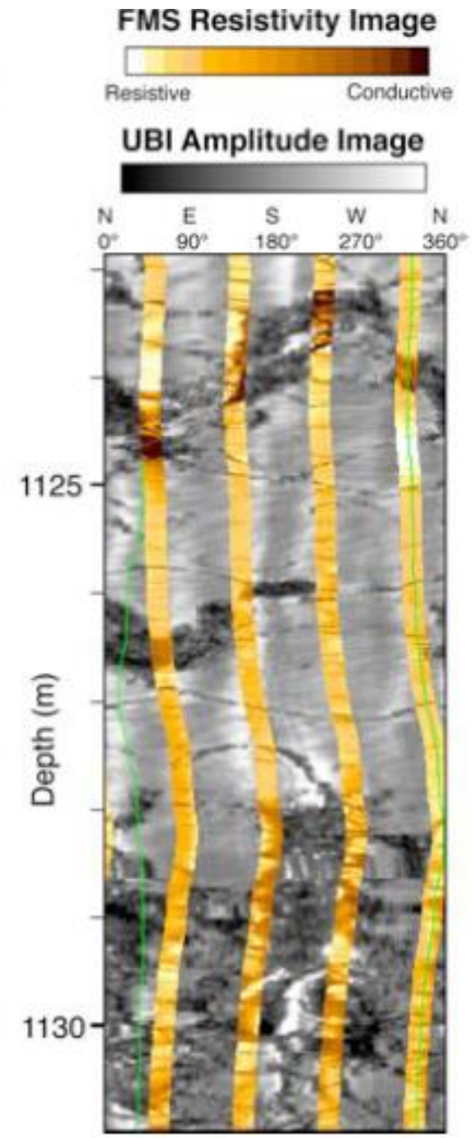

Borehole Breakouts

Mark the minimum stress direction

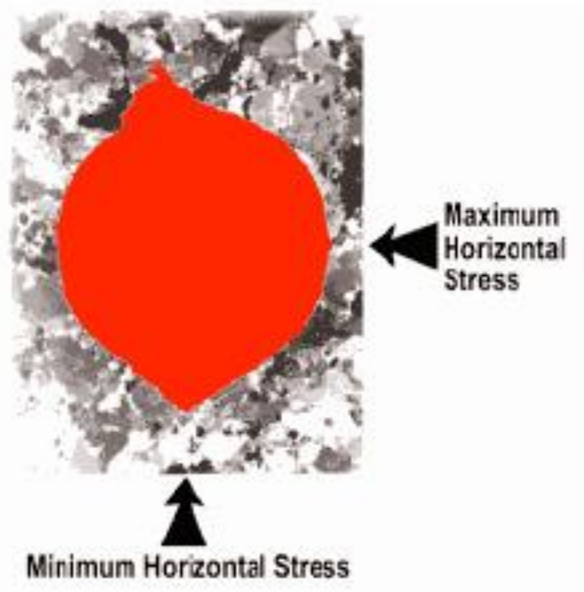

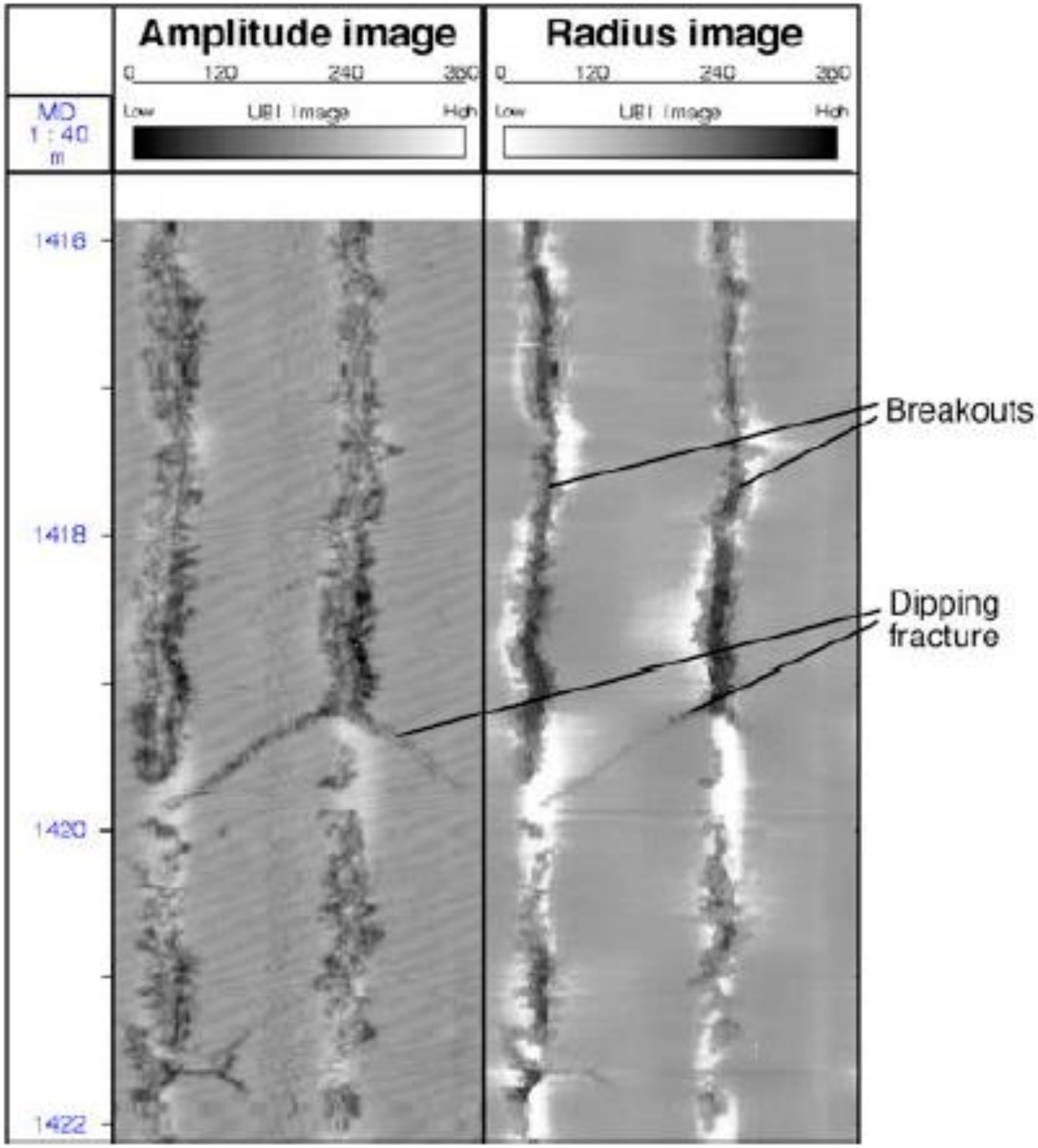

Core orientation